Interdisciplinary approach for the hydrogeological characterization of the Chalk aquifer: application on perchlorate transfer in the Champagne Chalk

Feifei Cao

▶ **To cite this version:**

Feifei Cao. Interdisciplinary approach for the hydrogeological characterization of the Chalk aquifer: application on perchlorate transfer in the Champagne Chalk. Geochemistry. Université de Reims Champagne-Ardenne (URCA), 2020. English. NNT : 2020REIMS013 . tel-02861884

HAL Id: tel-02861884
https://hal.science/tel-02861884

Submitted on 9 Jun 2020

HAL is a multi-disciplinary open access archive for the deposit and dissemination of scientific research documents, whether they are published or not. The documents may come from teaching and research institutions in France or abroad, or from public or private research centers.

L'archive ouverte pluridisciplinaire **HAL**, est destinée au dépôt et à la diffusion de documents scientifiques de niveau recherche, publiés ou non, émanant des établissements d'enseignement et de recherche français ou étrangers, des laboratoires publics ou privés.

Ecole doctorale ABIES

GEGENAA

Université de Reims Champagne-Ardenne

Thèse présentée et soutenue publiquement par

Feifei CAO

Le 5 Mars 2020

En vue de l'obtention du grade de **Docteur de l'Université de Reims Champagne-Ardenne**

Discipline : Géochimie de l'Environnement

Approche interdisciplinaire pour la caractérisation hydrogéologique du milieu crayeux : application au transfert de perchlorates dans la craie de Champagne

Composition du jury

Patrick Höhener,	Professeur,	Aix-Marseille Université,	**Président**
Alain Dassargues,	Professeur,	Université de Liège (Belgique),	**Rapporteur**
Laurent Charlet,	Professeur,	Université Grenoble Alpes,	**Rapporteur**
Danièle Valdes,	Maître de Conférences,	Sorbonne Université,	**Examinatrice**
Neil Sturchio,	Professeur,	University of Delaware (United States),	**Invité**
Vincent Barbin,	Professeur,	Université de Reims Champagne-Ardenne,	**Directeur**
Jessy Jaunat,	Maître de Conférences,	Université de Reims Champagne-Ardenne,	**Co-encadrant**
Patrick Ollivier,	PhD, chercheur,	BRGM Orléans,	**Co-encadrant**

Résumé

Des analyses ont mis en évidence la présence de perchlorate (ClO_4^-, suspecté d'être un perturbateur endocrinien) dans des captages d'eau potable de Champagne-Ardenne. Deux sources sont suspectées : une source militaire liée à la Grande Guerre et une source agricole liée à l'utilisation passée de nitrates chiliens. Les objectifs de l'étude sont de déterminer l'origine et le comportement des ClO_4^- dans les eaux souterraines de la craie de Champagne et d'expliquer les hétérogénéités observées en précisant le fonctionnement de la nappe.

La zone d'étude se trouve à l'est de Reims, où une étude historique, hydrologique, géochimique et isotopique est réalisée. Une forte hétérogénéité géochimique des eaux de la nappe est observée. Un modèle conceptuel du fonctionnement de la nappe est proposé, mettant en évidence les facteurs contrôlant la géochimie des eaux souterraines. Les teneurs élevées en ClO_4^- (> 4 $\mu g \cdot L^{-1}$) sont détectées principalement en aval des Monts de Champagnes, où de grandes quantités de munitions ont été utilisées, stockées et détruites pendant et après la Grande Guerre. Une origine militaire post-conflit est mise en évidence par l'analyse isotopique des ClO_4^- et la détermination de l'âge des eaux. L'évolution spatio-temporelle des concentrations est discutée sur la base des teneurs en ClO_4^-, du fonctionnement de la nappe et des informations historiques, permettant de préciser les sources (e.g. munitions non explosés et sites de destruction des munitions) et les mécanismes de transfert des ClO_4^-. La contamination en ClO_4^- de l'aquifère de la craie de Champagne ne semble pas diminuer à court et moyen termes en raison de la forte persistance des sources de ClO_4^-.

Mots clés : Perchlorate, Nappe de la Craie, Isotopes, Temps de séjour, Grand Guerre

UNIVERSITÉ DE REIMS CHAMPAGNE-ARDENNE

Ecole doctorale ABIES

GEGENAA

Université de Reims Champagne-Ardenne

Thesis presented and defensed by

Feifei CAO

Mars 5, 2020

For the degree of **Doctor in University of Reims Champagne-Ardenne**

Discipline: Environmental Geochemistry

Interdisciplinary approach for the hydrogeological characterization of the Chalk aquifer: application on perchlorate transfer in the Champagne Chalk

Composition of the Commitee

Patrick Höhener,	Professor,	Aix-Marseille Université,	**President**
Alain Dassargues,	Professor,	Université de Liège (Belgique),	**Reviewer**
Laurent Charlet,	Professor,	Université Grenoble Alpes,	**Reviewer**
Danièle Valdes,	Assistant professor,	Sorbonne Université,	**Examiner**
Neil Sturchio,	Professor,	University of Delaware (United States),	**Invited**
Vincent Barbin,	Professor,	Université de Reims Champagne-Ardenne,	**Thesis director**
Jessy Jaunat,	Assistant professor,	Université de Reims Champagne-Ardenne,	**Supervisor**
Patrick Ollivier,	PhD, Research scientist,	BRGM Orléans,	**Supervisor**

Abstract

Perchlorate (ClO_4^-) has frequently been detected in groundwater at concentrations relevant to human health. Analyzes in Champagne-Ardenne have highlighted the presence of ClO_4^- in groundwater for drinking water supply. The ClO_4^- has two suspected sources: a military source related to World War I (WWI) and an agricultural source related to past use of Chilean nitrate fertilizers. The objectives of the study are to determine the sources and behavior of ClO_4^- in the Champagne Chalk aquifer and to explain the heterogeneities observed by specifying the aquifer functioning.

The study area is located east of Reims. A methodology involving historical, hydrodynamic, geochemistry, groundwater dating and isotope analysis has been developed. High spatio-temporal heterogeneities are observed in the Chalk aquifer. A conceptual model of aquifer functioning is proposed, highlighting main factors governing the Chalk groundwater geochemistry. ClO_4^- is detected throughout the area with high concentrations (> 4 $\mu g \cdot L^{-1}$) detected mainly downgradient the Champagne Mounts, where large quantities of ammunition were used, stored and destroyed during and after WWI. A post-WWI military origin of ClO_4^- is inferred from isotopic analysis and groundwater ages. Different tendencies of ClO_4^- variation are observed and interpreted by a combination of ClO_4^- concentrations, aquifer functioning and historical investigations, revealing major sources of ClO_4^- (e.g., unexploded ammunitions, ammunition destruction sites) and its transfer mechanisms in the aquifer. ClO_4^- contamination in the Champagne Chalk seems unlikely to decrease in the short- to medium-term due to the long persistence time of major sources.

Key words: Perchlorate, Chalk aquifer, Isotope analysis, Groundwater dating, World War I

Remerciements

Le temps est venu de remercier toutes les personnes qui ont contribué de près ou de loin à la réalisation de ce travail tout au long de ces trois années extrêmement enrichissantes.

Cette thèse a été menée au sein du laboratoire GEGENAA, et n'aurait pu aboutir sans les supports financiers du BRGM, de l'Agence de l'Eau Seine-Normandie, du Grand Reims, de la Région Grand-Est, et de l'ARS Grand-Est.

Je tiens tout d'abord à faire part de ma plus profonde reconnaissance à Jessy Jaunat et Patrick Ollivier, les deux encadrants de cette thèse, pour leur implication dans cette étude, leur grande disponibilité, leur gentillesse et leurs nombreux conseils. Merci de m'avoir fait partager vos connaissances et vos expériences, et surtout de m'avoir donné le courage et la motivation d'aller au bout de cette aventure !

Je remercie Vincent Barbin, directeur de thèse, pour m'avoir donné la possibilité et les moyens de réaliser les travaux de cette thèse. Merci pour l'ensemble de vos supports et remarques.

Je tiens également à exprimer toutes mes gratitudes envers les membres du jury pour l'intérêt qu'ils ont porté à mon travail en acceptant d'évaluer cette thèse : Patrick Höhener, professeur au sein du Laboratoire Chimie Environnement de Aix-Marseille Université, en tant que président de ce jury en plus de sa qualité d'examinateur ; Alain Dassargues, professeur au département d'Hydrogéologie & Géologie de l'environnement de l'Université de Liège, et Laurent Charlet, professeur à l'Institut des sciences de la Terre (Isterre) de l'Université Grenoble Alpes , en tant que rapporteurs ; et Daniele Valdes, Maître de Conférence de Sorbonne Université en tant que examinatrice de ces travaux.

J'adresse un grand merci à Neil Sturchio, professeur au département de Géologie de l'Université du Delaware aux Etats-Unis, qui m'a accueilli durant un mois au sein de son laboratoire et formé sur l'extraction et la purification des perchlorates et l'analyse isotopique des ions perchlorate. Merci de m'avoir donné de nombreux conseils sur l'interprétation des résultats d'analyses, et surtout de m'avoir fait l'honneur de se déplacer depuis l'autre bout du monde à Reims en tant qu'invité de la soutenance de ces travaux.

Merci à Luc Aquilina et Virginie Vergnaud de l'OSUR, Géoscience Rennes de l'Université Rennes 1, pour les analyses permettant la datation des eaux souterraines et pour les nombreux conseils et les précieuses discussions autour de l'interprétation des résultats d'analyses. Merci à Luc Aquilina d'avoir accepté de devenir membre de mon comité de thèse et pour les nombreux commentaires ayant permis l'aboutissement de ces travaux de recherche. Merci à Virginie Vergnaud pour sa gentillesse et sa disponibilité lors de nos échanges par mail et téléphone pour répondre à mes nombreuses questions concernant l'âge des eaux souterraines.

Je remercie également Emilie Garel du Laboratoire des Sciences Pour l'Environnement de l'Université de Corse Pascal Paoli d'avoir accepté d'être membre de mon comité de thèse, et de m'avoir donné de nombreux conseils et propositions sur les aspects de ma thèse portant sur l'hydrogéologie.

Les résultats acquis au cours de cette étude étant en une grande partie issue de prélèvements et mesures sur le terrain, ces travaux n'auraient pas été réalisable sans la collaboration des propriétaires des piézomètres et des stations de pompages. Je tiens à remercie en particulier l'Aérodrome de Reims-Prunay, Veolia et Cristal Union Sillery pour leurs autorisations d'accès aux forages et leur support sur le terrain lors des prélèvements. Merci également à Monsieur et Madame Baudart et Monsieur Rannou de m'avoir donné l'accès à leurs forages privés.

Les campagnes de prélèvement mensuelles pendant plus de 2 ans n'auraient pas été réalisées sans l'aide précieuses et la participation active d'Alexandra, Julien et bien sûr Jessy. Je les remercie de m'avoir accompagné sur site, sous la pluie, sous le soleil et quelques fois sous la neige. Je n'oublie pas notamment les rencontres avec des moustiques, des bêtes, des rats, un petit serpent au bord de l'eau, une munition à côté d'un pied de Julien et aussi des repas agréables au restaurant Au Soleil d'Or (mon restaurant préféré du terrain !). Tous ces moments passé ensemble avec vous resteront de précieux souvenir de ma vie.

Un grand merci à tous les autres membres de GEGENAA pour leur accueil chaleureux, leur présence, les discussions sérieuses mais aussi celle qui le sont moins. Merci à Pauline de m'avoir réveillée en frappant « doucement » à notre porte chaque fois j'étais endormie devant mon écran. Merci à Alain pour les discussions hydrologiques et historiques concernant la Grande Guerre. Merci à tous les collègues du GEGENAA avec qui j'ai partagé de bons moments pendant les déjeuners, les pots : Benjamin, Maxime, Xavier, Stéphanie, Marie, Béatrice, Céline, Norman et Sébastien.

Je remercie les collègues du BRGM pour leur aide et support, particulièrement Christine (merci beaucoup pour la réalisation des nombreux ordres de missions lors de mes déplacements à Orléans, les congrès, les colloques et la mobilité aux US), Pierre et Murielle pour leur sollicitude et leur implication dans ce projet, Anne qui m'a accompagnée sur le terrain, ainsi que Aziza au BRGM d'Orléans pour son accueil chaleureux pendant mes déplacements.

Je voudrais également remercier mes camarades thésards et les stagiaires avec qui j'ai partagé des moments inoubliables : Soizic qui m'a donnés de nombreux conseils sur les formations de l'Ecole Doctorale et les informations utiles au laboratoire, Son Si Tong, Khairat, Bachirou, Pierre, Thibaud, Quynh, sans oublier Anne qui avait passé la soutenance juste avant moi, Arthur, Déborah, Sarah et Alexis, les stagiaires de Master qui ont su apporter de nouvelles ambiances au bureau, et bien sûr Emilie et Thomas pour les partages de la vie doctorante, les discussions quotidiennes intéressants ainsi que les déjeuners animés au RU.

Enfin et surtout, je pense à mes proches et ma famille. Je remercie mes parents pour leurs supports mentaux malgré la distance France-Chine ainsi que la confiance en mes choix. Mes remerciements s'adressent en particulier à Yang, pour ses encouragements constants, ses douces attentions et sa présence réconfortante à mes côtés pendant les moments les plus durs de cette thèse.

Contents

List of figures

List of tables

Introduction

▪ General background

Perchlorate (ClO_4^-) in an environmental pollutant of growing concern due to its widespread occurrence in water and its adverse health effects by interfering with thyroid uptake of iodine and production of hormones (e.g., Brabant et al., 1992; Braverman et al., 2005; Greer et al., 2002). It is an inorganic anion and powerful oxidizer with high solubility and mobility in water. Under typical surface water and groundwater conditions, ClO_4^- may persist for many years, possibly decades or more in the aquatic environment (Sturchio et al., 2014). Perchlorate salts are widely used as an oxidizer in solid rocket fuels and explosives (Urbansky, 1998). In addition, natural ClO_4^- can form atmospherically and accumulate by dry and wet deposition in vadose soils in arid and semi-arid environments such as the Atacama Desert (Chile) and the southwestern United States (Jackson et al., 2015, 2016; Lybrand et al., 2016; Rao et al., 2007). The nitrate deposits in Atacama Desert (Chilean nitrate), with ClO_4^- as a minor component, have been refined and distributed worldwide for use as NO_3^- fertilizer during the first half of the 20th century, representing a potential widespread source of ClO_4^- contamination (Ericksen, 1983; Rajagopalan et al., 2006). Drinking water is likely to be the largest source of ClO_4^- exposure (Steinmaus, 2016). Over the last two decades, ClO_4^- contamination has been reported from many countries including the USA, Canada, Chile, China, India, UK and France, related to various origins (e.g., Cao et al., 2019a, 2018; Furdui et al., 2018; Jackson et al., 2005; Kannan et al., 2009; McLaughlin et al., 2011; Qin et al., 2014; Sturchio et al., 2014; Vega et al., 2018).

In France, the interest of research on ClO_4^- has increased since 2011 because of the discovery of ClO_4^- contamination in several drinking water resources in SW France, in the Paris basin and in NE France (Lopez et al., 2015). Advisory levels of ClO_4^- in drinking water were issued in 2011 by the French Agency for Food, Environmental and Occupational Health & Safety (ANSES): 15 $\mu g \cdot L^{-1}$ for adults and 4 $\mu g \cdot L^{-1}$ for children under 6 months (ANSES, 2011). In 2018, the advisory value was reduced from 15 to 5 $\mu g \cdot L^{-1}$ for adults (ANSES, 2018). In the Champagne-Ardenne region (NE France), the measurement campaigns carried out by the Regional Health Agency (ARS) in 2014 have demonstrated high levels of ClO_4^- ions (> 15 $\mu g \cdot L^{-1}$) in water resources intended for human consumption. The large extent of ClO_4^- contamination has two suspected sources: military and agricultural. Indeed, the Champagne region was highly marked by the events of World War I (WWI). Related military activities may have emitted large quantities of ClO_4^- in the environment, as both synthetic ClO_4^- and Chilean nitrates were used for ammunition manufacturing during WWI. Thus, there is a potential link between high ClO_4^- concentrations in groundwater and the position of trench areas between 1914 and 1918. An agricultural source was also suspected, as large quantities of Chilean nitrate was used as fertilizer in France (including the Champagne region) between 1880 and 1950 (Lopez et al., 2015). For a better management of water resources in Champagne-Ardenne, it is now necessary to clarify the sources of ClO_4^- (military and/or agricultural) and to understand its behavior in groundwater.

The selected study area with multiple potential sources of ClO_4^- is located east of the Reims city in the Champagne region, where several drinking water catchments are impacted by ClO_4^- contamination with concentrations > 15 $\mu g \cdot L^{-1}$ (ARS, 2013). As the migration of ClO_4^- ions follows groundwater flow due to its high solubility and stability in water, knowledge of aquifer function is a fundamental prerequisite for understanding the sources and environmental behavior of ClO_4^- ions in groundwater.

The aquifer of the study area is the unconfined Champagne Chalk aquifer, which is a crucial water resource of the region. Indeed, the Chalk aquifer is one of the most important aquifers throughout much of northern Europe, as it is intensively exploited for human use with a large proportion reserved for drinking water. In France, the Chalk aquifer covers about 20 % of the metropolitan territory and provides approximately 12 billion $m^3 \cdot year^{-1}$ of water, which accounts for 70% of the drinking water consumed in the north of France (Lallahem, 2002). The hydraulic properties of the Chalk are complex resulting from a combination of matrix and fracture properties (Allen et al., 1997). Recharge of the Chalk aquifer through the unsaturated zone (UZ) can occur very rapidly in fractures or slowly in matrix, making the Chalk aquifer, especially the outcrop area, vulnerable to contamination. In recent decades, there has been growing evidence of the deterioration of the European Chalk groundwater quality due to human activities (e.g., Baran et al., 2008; Barhoum, 2014; Chen et al., 2019; Longstaff et al., 1992). Therefore, a comprehensive understanding of the hydrogeological functioning of the unconfined Champagne Chalk aquifer is of great interest, not only for the study of ClO_4^- contamination in groundwater but also for better protection and management of this important water resource in a more universal way.

▪ Research objectives

Under the above context, the research work of this thesis is realized in two parts: ClO_4^- contamination and Chalk aquifer function. The main objectives of the ClO_4^- contamination part are:

- to assess the extent of ClO_4^- contamination and its spatial-temporal evolution in the Chalk aquifer
- to identify the sources of ClO_4^- contamination (diffuse and/or point sources) and establish links between ClO_4^- occurrence and the type of human activity (military and/or agricultural)
- to understand the mechanism of transport and predict the evolution of ClO_4^- in groundwater in the short- to medium-term.

The main objectives of the Chalk aquifer function part are:

- to specify the flow patterns and mineralization processes of the unconfined Chalk aquifer,
- to explain the heterogeneities observed in groundwater geochemistry.

To acquire the knowledge on Chalk aquifer function, a methodology involving hydrodynamic, hydrogeochemical, and groundwater dating tools has been applied. Research in historical archives has been performed, providing information on historical activities and sites (e.g. WWI, uses of Chilean nitrates, industrial activities) potentially emitting ClO_4^-. Also, isotopic analysis of ClO_4^- has been realized, providing a direct approach for ClO_4^- source apportionment. An approach that combines continuous monitoring of ClO_4^- concentrations, isotopic composition measurements, hydrogeological and historical investigations has been used, allowing better clarification of the sources and behavior of ClO_4^- in the unconfined Champagne Chalk aquifer.

▪ Thesis outline

Part I is a literature review regarding ClO_4^- in waters and general characteristics of the Chalk aquifer. The first section provides a summary of the worldwide occurrence and origin of ClO_4^- in waters, and gives details about water contamination of ClO_4^- in France including the distribution of ClO_4^- in drinking waters and the suspected sources of contamination. The reduction and treatment technologies of ClO_4^- contamination in water are also briefly presented. In the second section, general characteristics of the Chalk formation and properties of the Chalk aquifer are introduced.

Part II presents in detail the study area and the materials and methods used to conduct this thesis research. The selected study area with multiple potential sources of ClO_4^- is described first, including its location and topography, geological and hydrogeological context, climate conditions, land use information, and potential sources of ClO_4^- contamination. Next, the strategy of research and the different approaches and tools used are described. The sampling network established in the study area for the continuous monitoring of hydrogeochemistry and ClO_4^- contamination is presented and the protocols used for measurement and analysis are detailed.

Part III characterizes the hydrogeological function of the unconfined Champagne Chalk aquifer. The mode of recharge and the related response of the Chalk aquifer are presented in the first section, as these aspects are essential prerequisites for the study of groundwater flow and geochemistry. Next, the results of *in situ* continuous monitoring of groundwater level, temperature, and electrical conductivity (EC) are given, which documents the seasonal and annual variation of groundwater level and allows examination of the response of the Chalk groundwater table to precipitation events and exploitation activities. In the second section, the principles and results of groundwater dating using ^3H, CFCs and SF_6 are illustrated, providing information not only on groundwater residence time but also on mixing processes and flow mechanisms within the Chalk aquifer. The groundwater geochemistry is described in detail in the final section. The observed spatio-temporal variation of groundwater geochemistry is presented and interpreted in the context of hydrogeological setting, residence time, and land use information. A conceptual model is proposed based on results presented in this part, which summarizes the hydrogeological functioning of unconfined Chalk aquifers.

Part IV presents results and interpretations regarding the sources and evolution of ClO_4^- in the Champagne Chalk aquifer based on a combination of continuously monitored ClO_4^- concentrations and isotopic analyses of ClO_4^- and NO_3^- as well as the historical and hydrogeological investigations presented in the previous parts. The results of isotopic analyses of ClO_4^- and NO_3^- are presented as evidence of ClO_4^- origin (synthetic and/or natural). Different tendencies of ClO_4^- evolution are discussed and compared with groundwater levels and major solute ions, highlighting major sources of ClO_4^- and the main factors governing the spatio-temporal variations of ClO_4^- in the Chalk aquifer.

Part V illustrates a case study of ClO_4^- contamination in the drinking water catchment of Couraux (an intensive groundwater exploitation site which supplied drinking water for the Reims city with complex hydrogeological properties on a small scale). First, the general characteristics of the geological and hydrogeological context of this water catchment are summarized. Next, the results of ClO_4^- concentration and isotopic analyses in groundwater are presented. The spatio-temporal variation of ClO_4^- is then discussed, providing information on sources and evolution of ClO_4^-. Finally, recommendations for better management of water resources in the water catchment of Couraux are proposed.

Part VI provided a summary of the conclusions and findings of the thesis research, followed by limits of the study and perspectives for future work.

Part I. Literature review

This part summarizes knowledge available in the literature related to perchlorate in waters and general characteristics of the Chalk aquifer, which allows to provide an overview of key concepts in these fields and a solid background for the further investigations of the thesis research.

In chapter 1, the content of the first section has been published as a review article regarding the worldwide occurrence and origin of perchlorate ion in waters (Cao et al., 2019). General properties, sources and major uses of perchlorate are introduced at first. Then, the occurrence of perchlorate in waters on a worldwide scale is presented. Assessment of perchlorate origin using isotopic analysis is described, with a summary of all published ranges of isotopic composition of perchlorate. The situation in France is briefly introduced as an example of case study. In the second section, water contamination of perchlorate in France is detailed (distribution in drinking water and suspected sources), as a supplement of the French case presented in the review article. In the last section, perchlorate reduction and treatment technologies are briefly introduced.

In chapter 2, general characteristics of the Chalk formation (physical and chemical composition of the Chalk and its distribution in France and Europe) and the properties of the Chalk aquifer (hydrodynamic parameters, groundwater flow and geochemistry) are presented.

1. Perchlorate in waters

1.1. Worldwide occurrence and origin of perchlorate ion in waters: a review

This work has been published in the journal "Science of the Total Environment" with the following reference: Cao, F., Jaunat, J., Sturchio, N., Cancès, B., Morvan, X., Devos, A., Barbin, V., Ollivier, P., 2019. Worldwide occurrence and origin of perchlorate ion in waters: A review. Sci. Total Environ. 661, 737–749. https://.org/10.1016/j.sciv.2019.01.107 (see Appendix 1 for the complete version).

Science of the Total Environment 661 (2019) 737–749

Contents lists available at ScienceDirect

Science of the Total Environment

journal homepage: www.elsevier.com/locate/scitotenv

Review

Worldwide occurrence and origin of perchlorate ion in waters: A review

Feifei Cao [a,*], Jessy Jaunat [a], Neil Sturchio [b], Benjamin Cancès [a], Xavier Morvan [a], Alain Devos [a], Vincent Barbin [a], Patrick Ollivier [c]

[a] Université de Reims Champagne-Ardenne – GEGENAA – EA 3795, 2 esplanade Roland Garros, 51100 Reims, France
[b] Department of Geological Sciences, University of Delaware, 255 Academy Street/103 Penny Hall, Newark, DE 19716, United States
[c] BRGM, 3 av. C. Guillemin, BP 36009, 45060 Orléans Cedex 2, France

HIGHLIGHTS

- ClO_4^- is a water contaminant of concern due to its toxicity and widespread presence.
- Both natural and anthropogenic process could contribute to ClO_4^- contamination.
- Stable and radiogenic isotopes analysis of ClO_4^- distinguishes different ClO_4^- origins.
- The French case illustrates the growing recognition of ClO_4^- contamination in water.

GRAPHICAL ABSTRACT

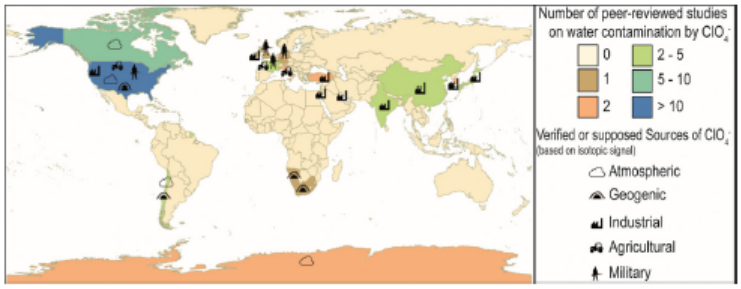

ARTICLE INFO

Article history:
Received 14 November 2018
Received in revised form 9 January 2019
Accepted 10 January 2019
Available online 14 January 2019

Editor: Damia Barcelo

Keywords:
ClO_4^-
Chilean nitrates
Military contamination
Isotope analysis
Forensics

ABSTRACT

Perchlorate (ClO_4^-) is a persistent water soluble oxyanion of growing environmental interest. Perchlorate contamination can be a health concern due to its ability to disrupt the use of iodine by the thyroid gland and the production of metabolic hormones. Its widespread presence in surface water and groundwater makes the aquatic environment a potential source of perchlorate exposure. However, the amount of published data on perchlorate origins and water contamination worldwide remains spatially limited. Here, we present an overview of research on perchlorate origins and occurrences in water, and the methodology to distinguish the different perchlorate sources based on isotope analysis. All published ranges of isotopic content in perchlorate from different sources are presented, including naturally occurring and man-made perchlorate source types, as well as the effects of isotope fractionation that accompanies biodegradation processes. An example of a case study in France is presented to emphasize the need for further research on this topic.

© 2019 Elsevier B.V. All rights reserved.

1.1.1. Introduction

Perchlorate (ClO_4^-) is a chemically stable anion and a powerful oxidizer, and inorganic perchlorate salts are extremely soluble in water (Urbansky, 1998). The high water solubility and the poor adsorption of ClO_4^- to typical soil minerals and organic carbon make this oxyanion highly mobile in the environment (Brown and Gu, 2006), especially in surface water and groundwater.

As the ClO_4^- ion is similar to iodine in both charge and ionic radius, it is known to disrupt the uptake of iodine in the thyroid, potentially affecting thyroid function (Clark, 2000; Urbansky, 2002; Wolff, 1998). The ingestion of ClO_4^- can alter birth outcomes and result in mental retardation and thyroid tumors (e.g., Brabant et al., 1992; Serrano-Nascimento et al., 2018). Also, independent of traditional risk factors, an increased prevalence of diabetes mellitus has been associated with high urinary ClO_4^- levels (Liu et al., 2017).

The concern of ClO_4^- in waters appeared in the second half of the 1990s, with the discovery of important concentrations in ground- and surface waters in several western states in the USA, including the Colorado River which is extensively used for irrigation and human consumption. Concentrations ranging from 8 $\mu g \cdot L^{-1}$ to 3.7 $g \cdot L^{-1}$ have been measured (Urbansky, 1998). Due to suspected toxicity of ClO_4^- and its presence in the environment, analytical techniques for determining low concentrations of ClO_4^- in water have been improved, particularly since the late 1990s. During the period between 1993 and 2005, the detection limit of ClO_4^- was reduced from approximately 400 $\mu g \cdot L^{-1}$ to 0.022 $\mu g \cdot L^{-1}$ (e.g., Burns et al., 1997; Hauser et al., 1994; Jackson et al., 2000; Nann and Pretsch, 1994; Pontius et al., 2000; Sellers et al., 2006; Trumpolt et al., 2005; Tsui et al., 2000; Urbansky, 2000). Today, the detection limit is as low as 5 $ng \cdot L^{-1}$ using LC-ESI-MS/MS method (liquid chromatography-electrospray ionization-tandem mass spectrometry) (Iannece et al., 2013). The current concern and the knowledge base regarding the environmental occurrences and sources of contamination have expanded as the ability to routinely measure low ClO_4^- concentrations in water has increased.

Drinking water is likely to be the largest source of ClO_4^- exposure (Steinmaus, 2016). The United States Environmental Protection Agency (US EPA) has placed ClO_4^- on the drinking water contaminant candidate list in 1998. Consequently, various states have implemented guidelines or goals ranging from 1 $\mu g \cdot L^{-1}$ (Maryland, Massachusetts and New Mexico) to 18 $\mu g \cdot L^{-1}$ (Nevada and Texas) for ClO_4^- in drinking water (Srinivasan and Viraraghavan, 2009). In 2009, the US EPA set a recommended value of 15 $\mu g \cdot L^{-1}$ for drinking water (US EPA, 2006, 2009). In Canada, according to the Canadian Environmental Protection Act (CEPA, 2005), a drinking water guidance value of 6 $\mu g \cdot L^{-1}$ for perchlorate has been developed. The European Food Safety Authority (EFSA) established a tolerable daily intake of 0.3 $\mu g \cdot L^{-1}$ of body weight and defined reference values for perchlorate in different foods (EFSA CONTAM Panel, 2014).

However, in Europe, ClO_4^- is not yet on the list of priority water contaminants and is not routinely measured during sanitary inspection of drinking water. In France, high concentrations of ClO_4^- (> 15 $\mu g \cdot L^{-1}$) have been measured in several drinking waters, leading authorities to issue related health recommendations: tap water should not be consumed by pregnant and nursing women or be used to prepare baby bottles if ClO_4^- concentrations are higher than 4 $\mu g \cdot L^{-1}$ and should not be consumed by adults if concentrations are higher than 15 $\mu g \cdot L^{-1}$ (ANSES, 2011). In 2017, the World Health Organization (WHO) issued an addendum to its fourth edition of the 2011 Guidelines for Drinking Water Quality (GDWQ), which includes a new guideline for ClO_4^- (0.07 $mg \cdot L^{-1}$; WHO, 2017).To our knowledge, there are no standards concerning ClO_4^- concentration in drinking water outside the North America and Europe. This can be explained by the paucity of studies conducted outside these areas.

During the last two decades, case studies on origins and occurrence of ClO_4^- in the environment have been published, focusing mainly on North America (e.g., Clausen et al., 2004; Dasgupta et al., 2005; Fram and Belitz, 2011; Izbicki et al., 2014; Jackson et al., 2005, 2010; Parker et al., 2008; Plummer et al., 2006; Rao et al., 2007; Susarla et al., 1999; Urbansky, 2002; Urbansky et al., 2001a). In recent years, increasing number of studies on ClO_4^- contamination in waters from China, South Korea, India, Japan, Italy, UK, Germany, France and Chile have been published (Anupama et al., 2012; Asami et al., 2009; Calderón et al., 2014; Iannece et al., 2013; Kosaka et al., 2007; McLaughlin et al., 2011; Nadaraja et al., 2015; Qin et al., 2014; Quiñones et al., 2007; Scheytt et al., 2011; Vega et al., 2018; Vigreux-Besret et al., 2015; Wu et al., 2010). A few review papers have been published, providing summaries of case studies on ClO_4^- occurrence in waters from different regions in the world (e.g., Calderon et al., 2017; Kumarathilaka et al., 2016; Srinivasan and Viraraghavan, 2009; Xie et al., 2018; Ye et al. 2012). However, none of these studies provided a comprehensive and detailed review focusing on ClO_4^- contamination in waters on a worldwide scale.

Here we present a review of ClO_4^- occurrence measured in each compartment of the water cycle, including surface water, groundwater and rainwater in a worldwide scale. The natural and anthropogenic origins of ClO_4^- in the environment are described, including the theory of origin of natural ClO_4^-, accumulation mechanism in arid and semi-arid environments, the manufacturing and the use of synthetic ClO_4^-. Measured ClO_4^- concentrations related to natural and synthetic sources from different case studies are presented in detail, intending to provide a comprehensive perspective of research status on ClO_4^- occurrence in waters. The French case study is presented due to the high occurrence of ClO_4^- in waters at large scale and the potential multiple sources (e.g., military, agriculture, industrial). The methodology to distinguish these sources is discussed, which is mostly based on the isotopic composition of ClO_4^-. A summary of all published ranges of isotopic composition of ClO_4^- from different sources in the world including terrestrial ClO_4^- from different regions (e.g., Atacama, southwestern United States) and synthetic ClO_4^- is presented, aiming to provide a comprehensive perspective on isotopic signature of ClO_4^- and its use for future forensic studies.

1.1.2. Sources and uses of perchlorate

1.1.2.1. Natural perchlorate

- **The atmospheric origin of natural perchlorate**

The atmospheric production of natural ClO_4^- is a well-known process. Photochemical reactions between inorganic chlorine and ozone can create ClO_4^- (Trumpolt et al., 2005). UV-mediated photo-oxidation may also play a role in the creation of ClO_4^- (Dasgupta et al., 2005; Jackson et al., 2010). Volcanic eruptions were proposed as another natural source of increased atmospheric ClO_4^- (Furdui et al., 2018; Jaeglé et al., 1996). Also, natural organic chlorine species such as methyl chlorine can be converted to inorganic species (e.g., HCl, $ClONO_2$, ClO) in the atmosphere and can thus contribute to the formation of ClO_4^- in stratosphere (Brown and Gu, 2006; Fabian et al., 1981; Von Clarmann, 2013). Production of ClO_4^- in the atmosphere may also be related to anthropogenic contaminants. Recently, Furdui et al. (2018) suggested that the atmospheric input of chlorinated solvents (e.g., methyl chloroform) from anthropogenic activities could contribute to ClO_4^- sources.

- **Arid and semi-arid deserts**

Following atmospheric production, ClO_4^- is deposited at the earth's surface by dry and wet deposition (Andraski et al., 2014; Rajagopalan et al., 2009). However, given its high solubility and poor sorption properties, it is readily transported to surface water or groundwater through runoff and infiltration of precipitation (Rajagopalan et al., 2009; Rao et al., 2007). This may explain why most natural ClO_4^- occurrences are confined to arid and semi-arid environments, as the evapotranspiration is strong and the amount of atmospheric deposition exceeds the rate of dissolution by ongoing precipitation (Jackson et al., 2015; Rajagopalan et al., 2006; Rao et al., 2007). Terrestrial soil ClO_4^- has been measured in the Atacama Desert (Chile), southwestern United States, southern Africa, United Arab Emirates, northwestern China and Antarctica at concentrations ranging from 10^{-1} to 10^6 $\mu g \cdot kg^{-1}$ (Jackson et al., 2015; Lybrand et al., 2016; Rao et al., 2007). The ClO_4^- accumulation in soils/caliche depends not only on its deposition rate but also on site-specific geologic, hydrologic and biogeochemical conditions.

Generally, the ClO_4^- concentration increases with aridity index and the duration of arid conditions (Jackson et al., 2015). The Atacama Desert is known as the driest desert in the world receiving < 5 $mm \cdot yr^{-1}$ of rain. ClO_4^- has possibly accumulated in this region over 6-10 million years under such hyper-arid conditions (Lybrand et al., 2016; Rao et al., 2007). ClO_4^- concentrations were 1-2 orders of magnitude higher in the Atacama Desert (average concentration of 2×10^5 $\mu g \cdot kg^{-1}$) than in other arid and semi-arid deserts such as the southwestern United States (Death Valley) and the northwestern China (Kumtag Desert) with a shorter duration of arid conditions (Pleistocene and Holocene aged deposits) (Jackson et al., 2015; Lybrant et al., 2016; Qin et al. 2012; Rao et al., 2007).

Despite the shorter accumulation time, a "bottom-up" mechanism in contrast to the primarily "top-down" mechanism in Atacama Desert was proposed for the ClO_4^- accumulation in the Death Valley and the Kumtag Desert: salts were deposited in strata through geological time and have since been redistributed and eva-concentrated into the upper soil horizons by capillary rise (Lybrant et al., 2013, 2016; Qin et al., 2012). The type of soil may also play an important role in ClO_4^- accumulation. For example, in the Death Valley, the clay-rich soil that swell during episodic rain events prevents the leaching of underlying salts, including ClO_4^- (Noble and Mansfield, 1922; Ericksen et al., 1988).

Furthermore, site-specific biological activities (e.g., plants or bacteria) can also influence ClO_4^- accumulation. Despite its high persistence in oxic environments due to large activation energies (Urbansky, 1998), ClO_4^- could be used by microorganisms as an electron acceptor under anoxic conditions; such microorganisms are ubiquitous in the environment (Coates et al., 1999; Xu et al., 2003). Perchlorate-reducing microbes are mostly facultative anaerobes, many of which appear to preferentially reduce nitrate, which generally co-occurs with ClO_4^- in soil/caliche of arid and semi-arid regions (Nozawa-Inoue et al., 2005; Jackson et al., 2015). Perchlorate could also accumulate in some plants (Andraski et al., 2014; Jackson et al., 2005a).

In Atacama Desert, vegetation is absent in the majority of the area and the microbes in soils are generally several orders of magnitude less than in soils of milder deserts (Ericksen, 1981). The very low level of biological activity could be neglected and has been essential to the preservation of nitrate and perchlorate in Atacama Desert. However, in regions with more active biological processes, their influence on natural ClO_4^- concentrations cannot be neglected. In unsaturated zones of the Death Valley, losses of natural ClO_4^- have been observed and attributed to bacteria reduction and plant accumulation (Rao et al., 2007). In 2014, Andraski et al. showed that in a desert-shrub landscape of southwestern United States (Amargosa Desert), selective plant uptake and bioaccumulation were evidenced by leaf ClO_4^- concentrations and Cl^-/ClO_4^- molar ratios that were respectively about 8,000 times greater and 40 times less than soil values. The authors also proposed a ClO_4^- cycle which is hypothesized to include atmospheric deposition, selective plant uptake, leaf bioaccumulation and leaf drop to the soil surface resulting in soil ClO_4^- enrichment and recycling. The topography-soil-plant-water interactions can thus locally influence the distribution of natural ClO_4^- concentrations in a desert-shrub landscape (Andraski et al., 2014).

- **Environmental release of natural perchlorate by human activities**

Paleogeochemical deposits of the Atacama Desert are a rich source of naturally occurring sodium nitrate and perchlorate. These deposits have been intensively mined and exported for agricultural and industrial use. As a result, ClO_4^- present in these deposits has been widely dispersed in the environment. The first recorded exports of Chilean nitrate took place in 1830 to the USA, France, and England. In 1900, Chile provided two thirds of the fertilizer nitrogen used around the world. Afterwards, the breakout of the First World War transformed the consumption of Chilean nitrate from agricultural use toward large-scale production of gunpowder and explosives. Consequently, the production of Chilean nitrate strongly increased, with a peak production of almost 3 million tons in 1916. During the war, European countries (especially Great Britain and Germany) and the USA accounted for more than 97% of the Chilean nitrate market (Ericksen, 1981; Wisniak, 2001). In the early 1930s, with the development of industrial processes for nitrogen fixation, the production of Chilean nitrate was greatly reduced and was surpassed by synthetic nitrogen compounds. By 1950 and 1980, Chilean nitrate accounted for only 15% and 0.14% , respectively, of the world market for fixed nitrogen (Ericksen, 1983; Fram and Belitz, 2011; Rajagopalan et al., 2006). Thus, ClO_4^- contamination related to the utilization of Chilean nitrate has declined in recent decades.

In 1960, damage to crops was attributed to the ClO_4^- naturally present in Chilean saltpeter (Schumacher, 1960). In fact, ClO_4^- levels in Chilean caliche are high enough to adversely affect sensitive crops (Hunter, 2001; Susarla et al., 1999; Urbansky, 2000). In 2001, measurements showed that sodium nitrate fertilizers derived from Chilean caliche commercialized in United States contained approximately 0.5 to 2 $mg \cdot g^{-1}$ of ClO_4^- (E. T. Urbansky et al., 2001). In 2005, a median value about 1 $mg \cdot g^{-1}$ was proposed (Dasgupta et al., 2005). In the 1990s, the refining process of Atacama fertilizers was modified to reduce ClO_4^- concentrations in NO_3^- fertilizer product to 0.1 $mg \cdot g^{-1}$ (Renner, 1999; Urbansky et al., 2001). Nowadays, some Chilean nitrate is still imported to the United States for limited use in organic farming of cotton, tobacco, citrus, and some vegetable crops (Aziz et al., 2006; Sanchez et al., 2006; Urbansky et al., 2001).

Despite the agricultural and industrial use of Chilean nitrates, natural ClO_4^- accumulating in unsaturated area can be readily flushed and mobilized by introduced percolation, especially in arid and semi-arid regions with intensive agriculture. In southwestern United States, continuous irrigation has displaced accumulated salts to depth of several meters and flushed perchlorate from unsaturated zone to groundwater (Rao et al., 2007; Scanlon et al, 2008, 2010). The influence of irrigation on the ClO_4^- groundwater contamination is fully discussed in Part I.1.1.4.1.

1.1.2.2. Synthetic perchlorate

Numerous industrial processes exist for synthetic ClO_4^- production, and among them the electrolytic method using sodium chloride as feedstock is the most used (Brown and Gu, 2006; Schilt, 1979). Synthetic ClO_4^- was firstly manufactured in commercial quantities in Masebo, Sweden in the 1890s (Trumpolt et al., 2005).

The production of synthetic ClO_4^- has been a substantial industry in the United States and Europe. This industry was linked to the emergence of solid rocket fuel using NH_4ClO_4 as a propellant (Mendiratta et al., 1996). Because of its useful properties, ClO_4^- is today widely used in solid propellants, fireworks, explosives, safety flares, matches, electroplating solutions, and a few medical applications. Fireworks used by both pyrotechnic professionals and individual customers contain up to 70% potassium or NH_4ClO_4. Safety flares are used in emergency situations such as road-side accidents. The Santa Clara Valley Water District in California (USA) analyzed the contents of an unburned safety flare and it contained 50,000 $mg \cdot kg^{-1}$ of ClO_4^- and 450,000 $mg \cdot kg^{-1}$ of nitrate (Silva, 2003). The number of industrial uses of ClO_4^- may continue to expand as our understanding and awareness of its usage matures (Trumpolt et al., 2005).

ClO_4^- can also be found in numerous products as impurities. For example, it is present in sodium hypochlorite as a breakdown product and in sodium chlorate as a manufacturing by-product (Aziz et al., 2006). Sodium hypochlorite (NaOCl) is used on a large scale for surface purification, bleaching, odor removal and water disinfection. Hypochlorite solutions contain trace amounts of ClO_4^- that forms during and after manufacture (Stanford et al., 2011). Asami et al. (2009) showed that ClO_4^- concentrations in purchased sodium hypochlorite solutions ranged from 0.17 to 33,000 $\mu g \cdot L^{-1}$. Dasgupta et al. (2006) measured that freshly bought 5% and 10% hypochlorite solutions contain low levels of ClO_4^-, around 10 $\mu g \cdot L^{-1}$. However, after 6 months of aging, ClO_4^- concentration of the 5% hypochlorite solution was 3,000 $\mu g \cdot L^{-1}$ and that of the 10% hypochlorite solution was twice as high. Munster et al. (2008) measured in a fresh container of household bleach a ClO_4^- concentration of 390 $\mu g \cdot L^{-1}$ and it increased to 8,000 $\mu g \cdot L^{-1}$ after two years. Thus, the ClO_4^- concentration in bleach increases with age during storage and this depends on both the initial concentration of sodium hypochlorite and the storage temperature. It has been proposed that sodium hypochlorite breaks down to form ClO_4^- most probably by the formation of chlorate from hypochlorite and then by the formation of ClO_4^- from ClO_3^- (Stanford et al., 2011). Sodium chlorate is largely used in bleaching processes at pulp and paper mills and also as defoliant/herbicide. Electrochemical production of sodium chlorate can generate ClO_4^- impurities at 50-230 $mg \cdot kg^{-1}$ ClO_3^- (Aziz et al., 2006).

1.1.3. Behavior of perchlorate in waters

Once the chemical element is released into natural water systems, its fate depends on both the chemical and physical properties of the aqueous system. Perchlorate salts are characterized by high solubility in water, and the ClO_4^- ion is commonly observed to be stable in the environment, although it may undergo biodegradation by perchlorate-degrading anaerobic bacteria in specific environments in which significant levels of organic carbon are present and electron donors such as oxygen and nitrate are depleted (Trumpolt et al., 2005).

The movement of ClO_4^- in soil is largely dependent on the presence and circulation of water. ClO_4^- does not bind to soil particles. If sufficient infiltration occurs, the ClO_4^- may be completely leached from the soil (Trumpolt et al., 2005). Otherwise, in arid and semi-arid regions, ClO_4^- may accumulate at various horizons in the soil due to evaporation of infiltrating rainfall that leached ClO_4^- from shallower depths.

In dilute concentrations typically found in groundwater, ClO_4^- ions will migrate along the groundwater gradient toward discharge points (Clausen et al., 2004). In addition, longitudinal dispersion results in a faster moving velocity of the contaminant front than the average groundwater velocity. These observations demonstrate that the knowledge about water flow paths and aquifer properties are essential prerequisites to understanding groundwater ClO_4^- contamination.

1.1.4. Occurrence of perchlorate in natural waters

1.1.4.1. Occurrence of perchlorate due to natural sources

- **Wet and dry deposition inputs**

Concentrations of ClO_4^- in rainwater have been reported in a few studies. A total of 1,578 precipitation samples were collected weekly at 16 NADP sites (National Atmospheric Deposition Program) across the United States over a 3-year period from October 2004 to October 2007, indicating a range of ClO_4^- concentration in precipitation from <5 to 102 $ng \cdot L^{-1}$ (Rajagopalan et al., 2009, Table I-1). In 2004, 70% of 25 precipitation samples collected in Lubbock, Texas showed the presence of ClO_4^- (Dasgupta et al., 2005, Table I-1). Extreme events, especially lightning, can lead to higher concentrations. (Parker et al., 2008, Table I-1).

Various concentrations of ClO_4^- have also been detected in rain samples collected in Ireland and China (Barron et al., 2006; Qin et al., 2014; Table I-1). In 2005, Qin et al. also showed that ClO_4^- concentrations observed at sampling sites of urban areas were higher than those observed in rural areas, possibly due to the air pollution which is more severe and more difficult to diffuse in urban areas than in rural areas.

Furthermore, where the water in the surface environment is mostly contributed by precipitation, rainwater may be an important source of ClO_4^- in surface water (Qin et al., 2014).

Measurements by Backus et al. (2005) and Poghosyan et al. (2014) demonstrated that ClO_4^- is present throughout the water of all the Great Lakes (Canada and United Sates) at low concentrations . Isotopic measurements indicated that ClO_4^- in the Great Lakes is dominantly of atmospheric origin (Poghosyan et al., 2014).

Other studies have estimated long-term average concentrations of ClO_4^- in wet deposition. Plummer et al. (2006) predicted ClO_4^- concentrations in precipitation ranging from 19 to 93 $ng \cdot L^{-1}$ based on evapotranspiration-adjusted Holocene groundwater ClO_4^- levels. Rao et al. (2007) estimated ClO_4^- concentrations in precipitation ranging from 3 to 23 $ng \cdot L^{-1}$ with an overall mean of 9 $ng \cdot L^{-1}$ based on natural ClO_4^- reservoirs present in unsaturated zones of the arid and semi-arid southwestern United States.

- **Arid and semi-arid deserts**

The perchlorate-rich geological formations could lead to enrichment of ClO_4^- in surface water and in groundwater during infiltration. Crump et al. (2000) reported ClO_4^- concentrations in groundwater near nitrate deposits in the Atacama Desert at high concentrations up to 10 $mg \cdot L^{-1}$ (Table I-1). ClO_4^- concentrations in tap water from several cities in Chile were also measured, indicating levels much higher than the US EPA or European recommendations for potable water (Crump et al., 2000; Vega et al., 2018; Table I-1). In northern Chile (Atacama desert), high levels of ClO_4^- in surface water were attributed to natural nitrate deposits (Calderón et al., 2014, Table I-1).

Unsaturated zones of the arid and semi-arid southwestern United States are an important source of ClO_4^- contamination in groundwater (Jackson et al., 2005b; Parker et al., 2008; Rajagopalan et al., 2006; Rao et al., 2007). ClO_4^- has been measured in pre-anthropogenic groundwater from upstream parts in the Middle Rio Grande Basin of North-Central New Mexico and attributed to be from natural deposition (Plummer et al., 2006; Table I-1). Geographically extensive elevated ClO_4^- has also been reported in groundwater in the High Plains of Texas, New Mexico, which has been attributed mainly to atmospheric ClO_4^- accumulation in the unsaturated zone (Rajagopalan et al., 2006; Table I-1). Natural occurrence of ClO_4^- has also been reported in some other parts of the Southwest United States (Rao et al., 2007; Table I-1).

Table I-1 : Perchlorate occurrence in waters due to natural sources (ET = Evapotranspiration)

Water type	Location	Measured ClO_4^- concentrations	ClO_4^- source	References
Rainwater	USA	1578 samples (16 sites) from <5 to 102 $ng \cdot L^{-1}$ mean value = 14.1 $ng \cdot L^{-1}$ Site mean value from 7.3 $ng \cdot L^{-1}$ to 21.9 $ng \cdot L^{-1}$	Atmospheric deposition	Rajagopalan et al., 2009; Dasgupta et al., 2006
Rainwater	Texas, USA	25 samples 70% contained measurable ClO_4^- (>10 $ng \cdot L^{-1}$) max value = 1.6 $\mu g \cdot L^{-1}$	Atmospheric deposition	Dasgupta et al., 2005
Rainwater (thunderstorms)	USA	Max value = 24.4 $\mu g \cdot L^{-1}$	Atmospheric deposition	Parker et al., 2008
Rainwater	Ireland	10 samples from <250 $ng \cdot L^{-1}$ to 2.8 $\mu g \cdot L^{-1}$	Atmospheric deposition	Barron et al., 2006
Rainwater	China	from 0.35 to 27.3 $\mu g \cdot L^{-1}$ mean value = 6.37 $\mu g \cdot L^{-1}$	Atmospheric deposition	Qin et al., 2014
Surface water	Great Lakes, USA and Canada	from 0.05 to 0.13 $\mu g \cdot L^{-1}$	Atmospheric deposition	Backus et al., 2005; Poghosyan et al., 2014
Groundwater for industrial use	Atacama Desert, Chile	from 1 to 10 $mg \cdot L^{-1}$	Arid and semi-arid deserts	Jackson et al., 2010
Groundwater for human consumption	Atacama Desert, Chile	from 50 to 150 $\mu g \cdot L^{-1}$	Arid and semi-arid deserts	Jackson et al., 2010
Tap water	Taltal, Chile	from 110 to 120 $\mu g \cdot L^{-1}$	Arid and semi-arid deserts	Crump et al., 2000; Vega et al., 2018
Surface water	Atacama Desert, Chile	from 744 to 1,480 $\mu g \cdot L^{-1}$	Arid and semi-arid deserts	Calderón et al., 2014
Groundwater	Middle Rio Grande Basin, New Mexico, USA	from 0.12 to 1.8 $\mu g \cdot L^{-1}$	Arid and semi-arid deserts	Plummer et al., 2006
Groundwater	Southern High Plains, USA	Max value = 200 $\mu g \cdot L^{-1}$	Atmospheric deposition and ET enrichment / Irrigation	Böhlke et al., 2005; Jackson et al., 2005b; Rajagopalan et al., 2006; Rao et al., 2007; Scanlon et al., 2010

1.1.4.2. Water contamination by anthropogenic activities

- **Chilean nitrate fertilizer**

As noted above, Chilean nitrate fertilizer can contain high quantities of ClO_4^-. It was intensively used in agriculture, leading to the dissemination of natural ClO_4^- in the environment. A metric ton of imported Chilean nitrate could yield as much as $150 \cdot 10^6$ to $1{,}300 \cdot 10^6$ L of water with 6 $\mu g \cdot L^{-1}$ of ClO_4^- (Böhlke et al., 2005).

In 2005, ClO_4^- contamination detected in groundwater of southern California (up to 12 $\mu g \cdot L^{-1}$) and northern New Jersey (25.9 $\mu g \cdot L^{-1}$) with similar isotopic composition to Atacama ClO_4^- was suspected to be derived from the use of Chilean nitrate fertilizer (Böhlke et al., 2005).

ClO_4^- in groundwater from the southern High Plains in west Texas was attributed to either a natural source that is isotopically distinct from Atacama ClO_4^-, or mixture of synthetic (~90%) and Atacama (~10%) ClO_4^- that had been substantially biodegraded (Böhlke et al., 2005). ClO_4^- contamination of groundwater from some agricultural areas in Long Island has also been attributed to Chilean fertilizer use (Böhlke et al., 2009). ClO_4^- contamination in groundwater of southeastern San Bernardino Basin in southern California, with concentrations ranging from 2.5 to 99 $\mu g \cdot L^{-1}$ was partly attributed to Chilean fertilizer along with a likely component of indigenous natural ClO_4^- (Sturchio et al., 2012). Evaluation of mixing proportions of ClO_4^- present in groundwater of Pomona, California (from 2.5 to 11 $\mu g \cdot L^{-1}$) indicated that contamination is dominantly (85-89%) Atacama ClO_4^- derived from the past use of imported Chilean nitrate fertilizer in citrus cultivation (Sturchio et al., 2014).

Recent research carried out by Mastrocicco et al. (2017) indicates ClO_4^- contamination in groundwater of the Po River Delta plain in Italy, which the authors supposed to be derived from Chilean nitrate fertilizer. Moreover, chlorate detected in same water samples was suggested to be a result of ClO_4^- degradation by anaerobic bacteria under low oxygen reduction potential (ORP) conditions in groundwater.

- **<u>Solid propellant and military usages</u>**

Water contamination from solid propellant is often linked with military activities. ClO_4^- diffusion in water from this usage can be related to the manufacturing of the products as well as their use in training sites or in conflict areas.

Camp Edwards located within the Massachusetts Military Reservation near Falmouth (USA) is a good example of ClO_4^- contamination owning to military activities (Table I-2). Training activities at Camp Edwards are typical of most military ranges, and it can be used as a model for future military ranges studies (Clausen et al., 2004). The impact area contains artillery and mortar targets that have been used for training activities since 1911, with the highest frequency of use during World War II. ClO_4^- is largely present at the site scale, with concentrations up to 174 $\mu g \cdot L^{-1}$. The conceptual model realized in the hydrological system of Camp Edwards shows that ClO_4^- is principally found at burn and detonation sites (Clausen et al., 2004). There is also evidence that the use of artillery and mortar spotting charges containing ClO_4^- can contribute to groundwater contamination.

The First World War battlefields of Verdun (France) served as the destruction site of German ammunition deposits in the 1920s. Groundwater at this site has elevated ClO_4^-, and concentrations up to 800 $\mu g \cdot L^{-1}$ have been measured in leachate samples (Bausinger et al., 2007; Ricour, 2013; Table I-2). Widespread ClO_4^- contamination of groundwater related to the First World War is suspected in France at regional scale along or near the former front line, which is probably linked with perchlorate-bearing explosives left on battlefields and/or on ammunition destruction sites (Hubé, 2017).

ClO_4^- present in ammunition during the First World War could be derived from either Chilean nitrate or synthetic ClO_4^-. Further research is being conducted to confirm the sources of ClO_4^- and to assess the related environmental and human health risks (Cao et al., 2018).

- **Fireworks and road flares**

ClO_4^- salts of potassium and ammonium are the primary oxidants in pyrotechnic mixtures, and there have been numerous studies of the contamination of surface and groundwater by ClO_4^- residue from firework displays, especially those launched near or over surface waters (Table I-2). ClO_4^- contamination in surface water samples in Harbour (Canada) was measured 4 days after a firework display (Backus et al., 2005). At the same site, ClO_4^- was not detected a week later. A fireworks display at a lake in Oklahoma (USA) led to ClO_4^- concentrations in surface water ranging from 24 to 1,028 times the mean baseline value, with a maximum concentration of 44.2 $\mu g \cdot L^{-1}$ following the July 4th event in 2006 (Wilkin et al., 2007). Authors observed a rapid disappearance of ClO_4^- in the lake waters following the fireworks display, with return to the baseline value after 10 to over 70 days, due to biodegradation and dilution. From 2008 to 2010, the fate of ClO_4^- in a man-made reflecting pond in New York (USA) was monitored following a firework display. ClO_4^- levels in pond water increased significantly, with concentrations ranging from 0.11 to 519 $\mu g \cdot L^{-1}$ following the fireworks display. ClO_4^- concentrations in pond water then decreased with an average half-life of 29 days (Wu et al., 2011).

In addition to surface water contamination, Munster et al. (2009) showed that total atmospheric deposition can strongly increase following a fireworks display (Table I-2), with measured concentrations of ClO_4^- in precipitation after the July 4th fireworks 18 times above the background level on Long Island in the United States. In China, a seasonal study of ClO_4^- concentrations in snow and surface soil concluded that the contamination comes mainly from the fireworks display of an annual festival (Ye et al., 2013; Table I-2). In Malta, Vella et al. (2015) detected ClO_4^- in 108 of 153 samples of dust fall (71%) and in 28 of 37 indoor dust samples (76%) with concentrations ranging from 0.52 to 561 $\mu g \cdot L^{-1}$, derived exclusively from fireworks. A recent review of environmental ClO_4^- occurrence from fireworks identified the use of fireworks as one of the main contributors of ClO_4^- contamination and focused on the lack of knowledge on this issue (Sijimol and Mohan, 2014 ; Table I-2).

Preliminary research on road flares of the Santa Clara Valley Water District (USA) suggested that each unburned and burned flare could leach 3.6 g and 1.9 mg of ClO_4^-, respectively (Silva, 2003). It is estimated that the ClO_4^- leached from a single unburned, damaged road flare can potentially contaminate approximately 2,700 m^3 of drinking water with concentrations above 4 $\mu g \cdot L^{-1}$ (Silva, 2003). The role of road flares, especially partially burnt ones, in ClO_4^- contamination of water has also been highlighted by Munster and Hanson (2009). In areas with high occurrence of traffic incidents, 10 % of the road runoff samples have ClO_4^- concentration above 5 $\mu g \cdot L^{-1}$ (Table I-2).

- **Domestic detergents and water - wastewater treatment**

Hypochlorite solutions are known to contain trace amounts of ClO_4^-, therefore when hypochlorite is used in the water treatment process ClO_4^- may subsequently be found in drinking water. Aranda-Rodriguez et al. (2017) detected ClO_4^- (between 0.06 and 5.7 $\mu g \cdot L^{-1}$) in treated water from Canadian drinking water treatment plants that use hypochlorite as a disinfectant.

Qin et al. (2014) observed ClO_4^- concentrations ranging from <0.09 to 1.05 $\mu g \cdot L^{-1}$ in treated wastewater effluent in China (Table I-2). Shi et al. (2007) sampled 31 sewage sludges from different sewage plants in across China. ClO_4^- was detected in all samples with concentrations up to 379.9 $\mu g \cdot kg^{-1}$ and an average concentration about 21.7 $\mu g \cdot kg^{-1}$. Her et al. (2011) also measured ClO_4^- in coastal water samples in South Korea with concentrations up to 6.11 $\mu g \cdot L^{-1}$, attributed to runoff of wastewater effluents.

- **Manufactory**

The contamination of water linked to the use of ClO_4^- containing products is of high importance, but past and present manufacturing sites of these products are also sources of strong environmental risks. Tan et al. (2005) reported ClO_4^- contamination of groundwater, stream water (up to 400 $\mu g \cdot L^{-1}$), and sediment pore water (up to 30 $\mu g \cdot L^{-1}$) in Texas (USA), attributed to a solid fuel rocket motor manufacture that closed in 1995 (Table I-2). Several streams far from this study site have been contaminated by groundwater or seepages containing ClO_4^- from the plant. In South India, ClO_4^- concentrations in groundwater, surface water, and tap water have been measured (up to 7.7 $\mu g \cdot L^{-1}$, 30.2 $\mu g \cdot L^{-1}$ and 0.4 $\mu g \cdot L^{-1}$, respectively) in and around a fireworks factory (Isobe et al., 2013; Table I-2). These authors demonstrated that the fireworks industry is the principal source of the water contamination. In China, Wu et al. (2010) measured ClO_4^- concentrations as high as 54.4 $\mu g \cdot L^{-1}$ in surface water samples around a fireworks manufacturing site. Another example is a plant in Israel that has manufactured NH_4ClO_4 for 25 years (Gal et al., 2009). Untreated wastewater was disposed in four infiltration ponds, causing extensive contamination of the underlying aquifer with measured ClO_4^- concentrations up to 35,000 $mg \cdot L^{-1}$ for pore water and up to 412 $mg \cdot L^{-1}$ for groundwater. In France, Negrel et al. (2017) showed high concentrations of ClO_4^- (> 400 $mg \cdot L^{-1}$) in groundwater at an industrial site used for electrochemical production of ClO_3^- and ClO_4^-. Stable isotope analyses of water gave evidence of leakage from end-product storage and the accumulation and release of ClO_4^- from soil.

Although ClO_4^- is highly soluble and mobile in waters, Flowers and Hunt (2007) showed that a point source release of highly concentrated brine solutions can influence ClO_4^- concentrations in groundwater for a long period (>100 years). Indeed, because of the density of the brine, it may move vertically in groundwater. On the top of confining layers, ClO_4^- may physically migrate into low permeability layers from where it may be continuously released to the groundwater by diffusion. This type of release may occur at industrial sites where ClO_4^- is handled in concentrated brines.

- **Irrigation impact**

The natural geochemical cycle of ClO_4^- can be strongly affected by irrigation activities, especially in agricultural areas located in semi-arid or arid regions. If there is substantial accumulation of natural ClO_4^- in the unsaturated zone, ClO_4^- concentration may rapidly increase in groundwater where artificial recharge from irrigation exceeds that from precipitation.

This impact can be summarized in terms of three major components: 1) irrigation can lead to the flushing of atmospherically deposited ClO_4^- from the unsaturated zone into groundwater (Fram and Belitz, 2011; Rajagopalan et al., 2006); 2) in case of an intensively used aquifer, the volume of groundwater impacts the capacity to dilute or assimilate salts introduced from the unsaturated zone, with salinity increasing linearly as aquifer saturated thickness decreases (Scanlon et al., 2010); and 3) the evaporative concentration effect can be strongly increased due to multiple irrigation and return flow cycles which will heighten the annual enrichment factor (Rajagopalan et al., 2006; Rao et al., 2007).

In arid and semi-arid regions, in the case of a closed-basin aquifer used for irrigation, the groundwater quality is expected to degrade over time if the water inflows are mainly by irrigation pumping. For example, in the High Plains of Texas, total dissolved solids are projected to increase in coming decades by an additional 2,200 $mg \cdot L^{-1}$, SO_4^{2-} by 880 $mg \cdot L^{-1}$, NO_3^- by 230 $mg \cdot L^{-1}$ and ClO_4^- by 21 $\mu g \cdot L^{-1}$ (Scanlon et al., 2010).

Table I-2 : Principal water contamination from anthropogenic activities

Uses	Compounds	Reported risk	References
Chilean nitrates used as natural fertilizer in agriculture	$NaClO_4$ $KClO_4$	Use	Böhlke et al., 2005, 2009; Cao et al., 2018; Hatzinger et al., 2018; Jackson et al., 2005b; Mastrocicco et al., 2017; Sturchio et al., 2012, 2014
Solid propellant and military usages / Aerospace industry / commercial explosives	$NaClO_4$, NH_4ClO_4, $KClO_4$	Manufacturing, disposal, missile recycling, historical buried rockets	Bausinger et al., 2007; Böhlke et al., 2005; Clausen et al., 2004; Hubé, 2014, 2017; Hatzinger et al., 2018; Hubé and Bausinger, 2013; Izbicki et al., 2014; Mass DEP, 2005; Mohr, 2007; Ricour, 2013; Sturchio et al., 2012; Tan et al., 2005b
Fireworks and emergency and Signal Flares	$KClO_4$, NH_4ClO_4	Manufacturing, use	Aziz et al., 2006; Backus et al., 2005; Isobe et al., 2013; Mass DEP, 2005; Munster and Hanson, 2009; Munster et al., 2009; Sijimol and Mohan, 2014; Silva, 2003; Vella et al., 2015; Wilkin et al., 2007; Wu et al., 2011; Ye et al., 2013
Industrial manufacturing and uses (airbag inflators, additives in oils, electroplating, tuber manufacturing…)	$NaClO_4$, NH_4ClO_4, $KClO_4$, $HClO_4$	Manufacturing, disposal, use	Böhlke et al., 2005; Fram and Belitz, 2011; Gal et al., 2009; Izbicki et al., 2014
Water and Wastewater treatment and domestic detergents	ClO_4 derived from NaOCl	Storage, use	Aranda-Rodriguez et al., 2017; Her et al., 2011; Mass DEP, 2005; Qin et al., 2014; Shi et al., 2007

1.1.5. Assessment of perchlorate origin

1.1.5.1. Stable isotopic composition of perchlorate

Since the early 2000s, methods of stable isotope analysis have been developed to differentiate natural and synthetic ClO_4^-. ClO_4^- is a non-labile oxyanion and once formed, its oxygen atoms do not exchange with those of the ambient environment over many decades. Therefore, the isotopic composition obtained when the ClO_4^- ion forms is retained as it is transported through the environment. Oxygen isotope ratios are reported as follows:

$$\delta^{18}O(‰) = [(^{18}O/^{16}O)_{\text{sample}} - (^{18}O/^{16}O)_{\text{VSMOW}} - 1] \text{ x } 1000 \quad \text{(I-1)}$$

$$\delta^{17}O(‰) = [(^{17}O/^{16}O)_{\text{sample}} - (^{17}O/^{16}O)_{\text{VSMOW}} - 1] \text{ x } 1000 \quad \text{(I-2)}$$

where VSMOW is the Vienna Standard Mean Ocean Water isotopic reference material. For normal terrestrial oxygen, $\delta^{18}O$ and $\delta^{17}O$ values are correlated according to the following mass-dependent relationship (Young et al., 2002):

$$\delta^{17}O \approx 0.52 \times \delta^{18}O \quad \text{(I-3)}$$

Based on this relation, natural and synthetic ClO_4^- may be differentiated through the calculation of the deviation of $\delta^{17}O$ value from the terrestrial fractionation line (eq. I-3) by:

$$\Delta^{17}O = \delta^{17}O - 0.52 \times \delta^{18}O \quad \text{(I-4)}$$

Several authors have reported isotopic compositions of natural ClO_4^-, and all have significantly positive $\Delta^{17}O$ values. The first measurements of the isotopic composition of oxygen in synthetic and Atacama ClO_4^- were reported by Bao and Gu (2004), who found that $\delta^{18}O$ values of synthetic ClO_4^- were -18.4 ± 1.2 ‰, whereas those of Atacama Desert ClO_4^- ranged from -24.8 ‰ to -4.5 ‰, and Atacama ClO_4^- is enriched in ^{17}O (+4.2 ‰ < $\Delta^{17}O$ < +10.5 ‰, Figure I-1). The ^{17}O enrichment observed in Atacama ClO_4^- was attributed to its production in the upper atmosphere by reactions involving ozone (Bao and Gu, 2004).

Other stable isotope data for oxygen in synthetic ClO_4^- have been published subsequently, showing that values of $\delta^{18}O$ in synthetic ClO_4^- range from -24.8 ‰ to -12.3 ‰ and its $\Delta^{17}O$ value is always 0.0 ± 0.2 ‰ (Böhlke et al., 2005; Sturchio et al., 2006, 2011; Figure I-1). Oxygen in synthetic ClO_4^- is derived from the water used in its production by an electrochemical process, which results in mass-dependent fractionation with $\Delta^{17}O$ ~ 0 (Böhlke et al., 2017; Sturchio et al., 2006; Figure I-1).

Systematic differences in Cl stable isotope ratios of synthetic and natural ClO_4^- are also observed. The $\delta^{37}Cl$ values of synthetic ClO_4^- were first reported by Ader et al. (2001), Böhlke et al. (2005), and Sturchio et al. (2006), ranging from -5.0 to +2.3 ‰. In natural ClO_4^- from Chilean Atacama Desert, reported $\delta^{37}Cl$ values are extremely negative, ranging from -14.5 ‰ to -9.2 ‰ (Böhlke et al, 2005; Sturchio et al., 2006; Jackson et al., 2010).

Other than natural ClO_4^- from the Atacama Desert, which is as a well-known natural occurrence of this ion, other indigenous natural deposits of ClO_4^- have been observed especially in the arid southwestern United States, including the Southern High Plains (Texas) and near Death Valley (California) (Jackson et al., 2005b; Plummer et al., 2006; Rajagopalan et al., 2006; Rao et al., 2007). While the Atacama Desert ClO_4^- has a relatively well documented isotopic composition, relatively few studies have been done to discriminate other indigenous natural ClO_4^- sources through isotopic measurements because of the difficulties involved in sample collection and processing (Sturchio et al., 2011). ClO_4^- from the Southern High Plains has $\Delta^{17}O$ values ranging from +0.2 ‰ to +2.6 ‰, $\delta^{18}O$ values from +0.5 ‰ to +5.1 ‰. The isotopic composition of the Death Valley ClO_4^- is somewhat different with $\Delta^{17}O$, $\delta^{18}O$ and $\delta^{37}Cl$ values ranging from +8.6 ‰ to +18.4 ‰, +2.9 to +26.1 ‰ and -3.1 ‰ to -0.8 ‰ respectively (Figure I-1).

The reason for such a wide range values of $\delta^{37}Cl$ in natural ClO_4^- is still not well understood, but it may be related to regional or hemispheric differences in the source of atmospheric Cl^- or to the mechanism involved in ClO_4^- production. The range of $\Delta^{17}O$ values in natural ClO_4^- could be explained by regional differences in climate and the mode of ClO_4^- formation, as well as possible slow oxygen isotope exchange or abiotic degradation, as the values for Southern High Plains are mostly from groundwater samples and those from Death Valley are from unsaturated zone (Sturchio et al., 2011). Samples from the Great Lakes waters have similar ClO_4^- isotopic compositions to those of SW United States groundwaters, which may indicate that this is a typical isotopic composition of indigenous natural ClO_4^- across midcontinent North America. Despite such remaining uncertainty, forensics studies have successfully used ClO_4^- isotopic date to identify the sources of contamination and mixing fractions in mixed ClO_4^- plumes (Böhlke et al., 2005, 2009; Hatzinger et al., 2018; Jackson et al., 2010; Poghosyan et al., 2014; Sturchio et al., 2011, 2012, 2014).

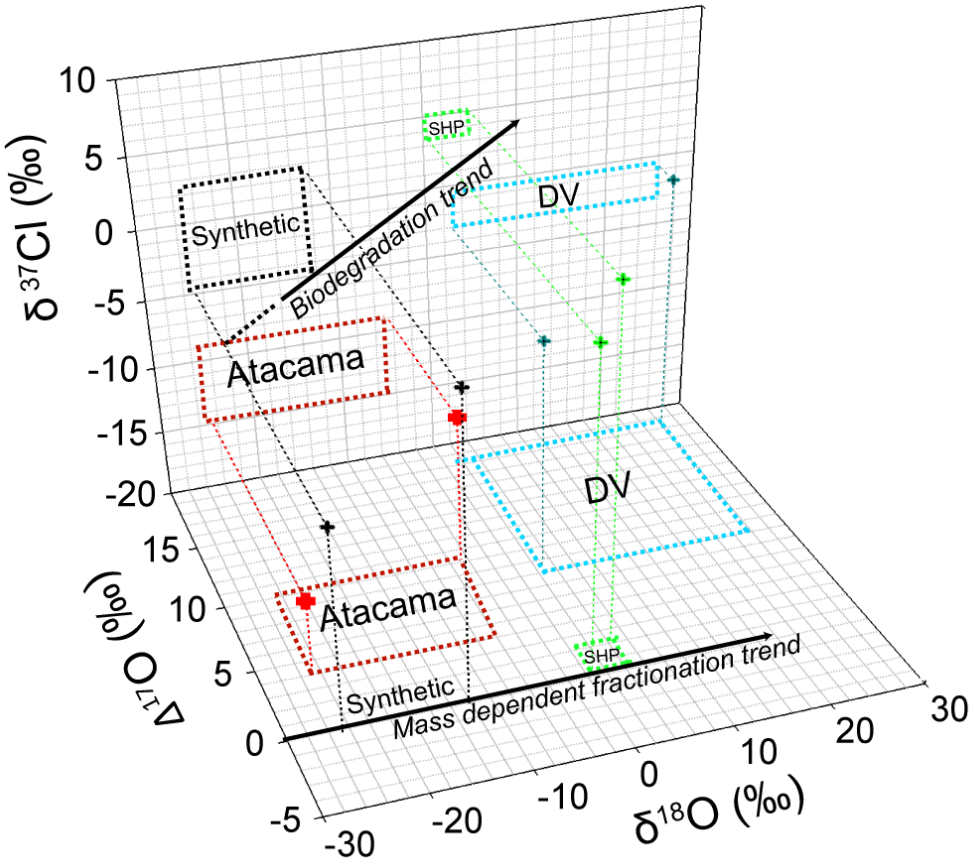

Figure I-1 : Diagram showing the isotopic signature ($\delta^{37}Cl$, $\Delta^{17}O$ and $\delta^{18}O$) of ClO_4^- in synthetic, Atacama, Death Valley (California) (DV) and Southern High Plain (Texas) (SHP) samples from data published in peer-reviewed literature. Arrow in the $\delta^{37}Cl$ vs $\delta^{18}O$ graph represent the direction of biodegradation ($\delta^{37}Cl = 0.4\ \delta^{18}O$) and arrow in the $\Delta^{17}O$ vs $\delta^{18}O$ graph represent the direction of mass dependent fractionation. Dashed boxes represent the maximum range of isotopic signature of the different sources, established through all the data published. (Ader et al., 2001 ; Bao and Gu, 2004 ; Böhlke et al., 2005, 2009 ; Jackson et al., 2005b, 2010 ; Parker et al., 2008 ; Plummer et al., 2006 ; Rajagopalan et al., 2006 ; Rao et al., 2007 ; Sturchio et al., 2007, 2011)

1.1.5.2. Isotopic fractionation during biodegradation

Numerous studies have demonstrated that ClO_4^- can be metabolized by perchlorate-reducing bacteria (PCRB) (Ader et al., 2008; Attaway and Smith, 1993; Coates et al., 1999; Coates and Achenbach, 2004; Hatzinger et al., 2009; Stroo et al., 2009; Wallace et al., 1996; Xu et al., 2015). These organisms could be responsible for ClO_4^- degradation in natural waters using ClO_4^- as an electron acceptor in anoxic environments. They present a high potential for *in situ* bioremediation of ClO_4^- contaminated sites. Numerous laboratory and field studies show isotopic fractionation of ClO_4^- during its degradation.

The first studies on the kinetic isotopic fractionation of Cl in ClO_4^- resulting from microbial respiration were those of Coleman et al. (2003) and Sturchio et al. (2003). Beside demonstrating temperature-dependent degradation kinetics (the ClO_4^- reduction was nearly complete in about 90 min at 37 °C and in 5.5 h to 18 days at 22°C), they showed that $^{35}Cl_{ClO_4^-}$ reduction was faster than that of $^{37}Cl_{ClO_4^-}$.

Reported isotopic fractionation factors for chloride relative to ClO_4^- were between -16.6 ‰ and -12.9 ‰ at 22 °C (Sturchio et al., 2003) and between -15.8 ± 0.4 ‰ and -14.8 ± 0.7 ‰ at 37 °C (Coleman et al., 2003). A statistical re-evaluation of the Coleman et al. (2003) experimental data set of $\delta^{37}Cl$ values of chloride gave a value of Cl isotopic fractionation factor of -14.94 ± 0.15 ‰ during biodegradation, with fractionation factor remaining constant during the reaction (Ader et al., 2008). These studies also indicate that fractionation is not sensitive to the ClO_4^- concentration in the basal medium, nor to the rate of ClO_4^- reduction. The relationship between chloride concentration and Cl isotope ratio follows a Rayleigh distillation model (Ader et al., 2008). Subsequent studies produced data on both oxygen and chlorine isotopic fractionation during ClO_4^- biodegradation, using two different bacterial genera in cultures at temperatures of 22°C and 10°C (Sturchio et al., 2007). The data obtained from these laboratory experiments showed Cl and O fractionation factors of -13.2 ± 0.5 ‰ and -33.1 ± 1.2 ‰ respectively, with no evidence of dependence on bacterial strain or temperature. This work also showed negligible O isotope exchange between ClO_4^- and water during microbial reduction and a fractionation factor ratio ($\varepsilon^{18}O/\varepsilon^{37}Cl$) with a constant value about 2.50 ± 0.04 (Figure I-1). This last result was confirmed in a field study where biodegradation of a groundwater ClO_4^- plume was enhanced by injection of emulsified soybean oil and the isotopic compositions of partly reduced ClO_4^- yielded a $\varepsilon^{18}O/\varepsilon^{37}Cl$ ratio of ~2.63 (Hatzinger et al., 2009). Knowledge of the isotope effects of ClO_4^- biodegradation is of primary importance in forensic studies of ClO_4^- origin and behavior in the environment, as it can provide a test of the microbial reduction hypothesis in field-based ClO_4^- isotopic data sets as well as setting a constraint on the initial isotopic composition of partially biodegraded ClO_4^- (Jackson et al., 2010; Poghosyan et al., 2014; Sturchio et al., 2014).

1.1.5.3. ^{36}Cl as an additional tracer

Radioactive ^{36}Cl (half-life = 301,000 years) is an additional tracer that can be used for distinguishing ClO_4^- sources. Natural atmospheric production of ^{36}Cl occurs due to activation of atmospheric Ar by cosmic-ray spallation reactions and is deposited at Earth's surface as dry fallout or in precipitation (Lehmann et al., 1993). It is also produced in situ by cosmic-ray induced reactions of ^{35}Cl, K and Ca within the upper few meters of the land surface (Clark and Fritz, 1997). Natural ^{36}Cl production and fallout varies with latitude from close to 20 atoms.m^{-2} at mid latitudes to less than 5 atoms.m^{-2} near the equator and poles (Clark and Fritz, 1997). Testing of thermonuclear bombs at oceanic sites in the 1950s also injected a large amount of ^{36}Cl into the stratosphere, resulting in worldwide fallout for several years after (Phillips, 2000). The presence of this bomb pulse ^{36}Cl in dissolved chloride of water may be identified from its anomalously high $^{36}Cl/Cl$ ratio and its association with relatively high ^{3}H activity. Consequently, ^{36}Cl isotopic abundance can be used to identify modern groundwater, analogous to the way elevated ^{3}H is used as an indicator of post-bomb recharge. The washing out of atmospheric Cl^- has brought $^{36}Cl/Cl$ ratios in precipitation back to near-natural levels since about 1980.

In 2009, ^{36}Cl abundance and $^{36}Cl/Cl$ ratio were measured in ClO_4^- of 35 samples chosen to represent the principal known sources of ClO_4^- in the environment: synthetic, natural from Atacama Desert and natural from southwestern United States (Sturchio et al., 2009). The ranges of $^{36}Cl/Cl$ ratio and $\delta^{37}Cl$ from this study are summarized in Table I-3.

Table I-3 : $^{36}Cl/Cl$ ratio and $\delta^{37}Cl$ in synthetic and natural (from Atacama and SW United States) perchlorates (Sturchio et al., 2009)

	$^{36}Cl/Cl$ ($\times 10^{-5}$)		$\delta^{37}Cl$ (‰)	
	Min	**Max**	**Min**	**Max**
synthetic reagents (n = 16)	0	40	-5	2.3
Atacama (n = 10)	0.9	590	-14.5	-9.2
United States (n= 8)	3130	28800	-3.1	5.1

Synthetic ClO_4^- samples have the lowest $^{36}Cl/Cl$ ratios, reflecting the NaCl sources used in the manufacturing process. Conversely, SW United States samples have extremely high $^{36}Cl/Cl$ ratios. The presence of 1950s nuclear ^{36}Cl may be present in the ClO_4^- extracted from some of these groundwater samples. Nevertheless, the absence of tritium in most of these groundwaters indicates pre-bomb recharge. Thus, a largely stratospheric source of ClO_4^- was indicated (Sturchio et al., 2009), because there is no other viable explanation for the elevated ^{36}Cl abundance, and it is also consistent with the elevated ^{17}O abundance found in natural ClO_4^-. Atacama ClO_4^- samples have intermediate ranges of $^{36}Cl/Cl$ ratios, which may be interpreted as initially high $^{36}Cl/Cl$ ratios (similar to those from the SW United States) that decreased by radioactive decay (Sturchio et al., 2009).

Chlorine-36 as a tracer of the source of ClO_4^- in the environment has been applied in the waters of the Great Lakes (United States and Canada), as well as in groundwater around the large Rialto-Colton ClO_4^- plume in SE San Bernardino County, CA. In addition to $\delta^{18}O$, $\Delta^{17}O$ and $\delta^{37}Cl$, the ^{36}Cl abundances of ClO_4^- from Great Lakes water samples were used to trace ClO_4^- (0.05 $\mu g \cdot L^{-1}$ to 0.13 $\mu g \cdot L^{-1}$) origin in these hydrological systems (Poghosyan et al., 2014). This multitracer study indicated that the principal source of ClO_4^- in the Great Lakes is natural ClO_4^- origin from atmospheric deposition and identified a substantial fraction of ClO_4^- in these lakes was deposited during the peak of atmospheric ^{36}Cl abundance following the Pacific thermonuclear bomb tests in the 1950s.

Additional data are still needed and a better knowledge and comprehension of ^{36}Cl natural formation and behavior will be useful for the interpretation of $^{36}Cl/Cl$ ratios of ClO_4^-. Nevertheless, the isotopic abundance of ^{36}Cl in ClO_4^- appears to be a promising supplementary tracer than can greatly improve forensics studies on the origin of ClO_4^-. It is a particularly sensitive indicator of the presence of trace amounts of indigenous natural ClO_4^- in the case of mixed-source samples (e.g., Hatzinger et al., 2018).

1.1.5.4. Limits of perchlorate isotope forensics

Over the past few decades, the evolution of research on stable and radiogenic isotopes of ClO_4^- has provided important tools for studying ClO_4^- origin. Despite progress in methodology and increase in available data on the isotopic composition of ClO_4^-, some limits still need to be considered.

The first is related to the paucity of ClO_4^- isotope studies from different sources, including natural and synthetic ones. Due to the existence of natural ClO_4^- around the world, further studies on these occurrences and their isotopic compositions are recommended. The full range of natural ClO_4^- sources may not be represented in Figure I-1. Fractionation that occurs during biodegradation could lead to misinterpretation of analytical results. The article, comments, and reply published by Sturchio et al. (2014), Bennett (2015), and Sturchio (2015) illustrated the limitations of isotope forensics analysis for ClO_4^- origin determination. Based on isotopic analyses of ClO_4^-, hydrogeological background, numerical modeling, and aerial photography archives, Sturchio et al. (2014) and Sturchio (2015) explained the ClO_4^- occurrence in groundwater of Ponoma (California) to be a result mainly of the past use of imported Chilean nitrate fertilizer in citrus groves. However, Bennett (2015) argued that indigenous natural sources might explain the ClO_4^- concentration in Ponoma groundwater, and that more isotopic data on indigenous ClO_4^- of this region are needed to conclude whether the groundwater ClO_4^- is mainly from Chilean nitrate fertilizer or if it could be mainly indigenous natural ClO_4^-. Bennett (2015) specifically suggested measuring ^{36}Cl as a means by which to resolve the question in this case. In response, Sturchio (2015) presented archived ^{36}Cl data obtained for ClO_4^- from one of the Pomona wells, and from another well in the adjacent city, that were both consistent with a Chilean fertilizer source. This discussion emphasizes that in forensic analysis of ClO_4^- origin based on isotopic analysis, knowledge of hydrological settings and historical land-use data are necessary but not always sufficient to give indisputable conclusions. Multiple isotope ratio measurements of ClO_4^- are needed to best resolve its origin, geographic distribution, and possible mixing relationships or biodegradation. In the future, more geographically widespread isotopic analyses of indigenous natural ClO_4^- may lead to more robust forensic results.

1.1.6. Perchlorate contamination of water: a worldwide phenomenon

1.1.6.1. Example of the French case

The French case illustrates the growing recognition of ClO_4^- contamination in groundwater. In 2009 and 2010, some aquifers of SW and NE France showed ClO_4^- contamination of municipal water supplies at concentrations exceeding 4 $\mu g \cdot L^{-1}$. Based on these observations, a national sampling campaign was conducted by the Regional Health Agencies (Agences Régionales pour la Santé; ARS), with 300 raw and treated water samples evenly distributed across France supplying 20% to 25% of the population.

In addition, 87 supplementary sites were selected by the Professional Federation of Water Enterprises (Fédération Professionnelle des Entreprises de l'Eau, FP2E). These additional samples were selected for their vulnerability to ClO_4^- contamination considering nearby industrial activities, land use, and past military activities. Of these additional samples, 62% came from groundwater, 37% from surface water and 1% from sea water or mixed water (ANSES, 2013).

Of the more than 300 water samples analyzed to date, 75% had ClO_4^- concentrations < 0.5 $\mu g \cdot L^{-1}$ (limit of detection), 2% were between 4 $\mu g \cdot L^{-1}$ and 15 $\mu g \cdot L^{-1}$, and 1% had concentrations above 15 $\mu g \cdot L^{-1}$ with a maximum of about 22 $\mu g \cdot L^{-1}$.

In France, three potential sources of ClO_4^- contamination are suspected: industrial, military sources related to WWI and agricultural. First, 4,000 t/y of NH_4ClO_4 are produced in southwestern France and numerous French plants use ClO_4^- in their manufacturing processes (fireworks manufacturing, armament material, car safety, construction activities; INERIS, 2014). Since 1977, 65 incidents involving ClO_4^- uses and release of hazardous materials have been recorded in metropolitan France (ARIA Database, n.d.). Second, both Chilean nitrates and synthetic ClO_4^- were used for manufacturing of ammunition during the First World War. During the period from November 1915 to November 1916, 2,940,000 t of Chilean nitrate was used for military purposes throughout 140 manufacturing sites in NE France (Hubé, 2014). Thus, there is a potential link between high ClO_4^- concentrations in groundwater from NE France and the position of the front line in this area between 1914 and 1918. This hypothesis is supported by numerous French reports and national publications (Cao et al., 2018; Hubé, 2016; Hubé and Bausinger, 2013; Hubé and Urban, 2013; Lopez et al., 2014; Ricour, 2013). However, this hypothesis is only based on the geographical similarity between ClO_4^- plume occurrences and historical records of conflict areas. More hydrogeological investigations (hydrodynamic investigations, groundwater age data and numerical modelling) are necessary to confirm this hypothesis. Isotopic analysis on ClO_4^- could also afford a way to distinguish different sources of ClO_4^- present in groundwater of NE France. Finally, between 1875 and 1920, large quantities of Chilean nitrates were used as fertilizers in France, which contributed another potential source of ClO_4^- contamination. In fact, France imported large quantities of Chilean nitrates for use both as fertilizer and for the production of ammunition. In 1899 and 1929, the consumption of Chilean nitrate was 150,000 t and 413,000 t respectively.

1.1.6.2. Evidence and perspectives

Interest in ClO_4^- has increased significantly since the discovery of ClO_4^- contamination in potable water supplies of 7 counties of California and Nevada at levels up to 16 $\mu g \cdot L^{-1}$ in 1997. Since the 1990s, 72 peer-reviewed case studies in the natural environment have been listed (Scopus research conducted in September 2018), including natural occurrences and anthropogenic contamination in waters all over the world. Significant geographic differences are observed (Figure I-2); 43% of these studies were conducted in the USA (51% in USA and Canada).

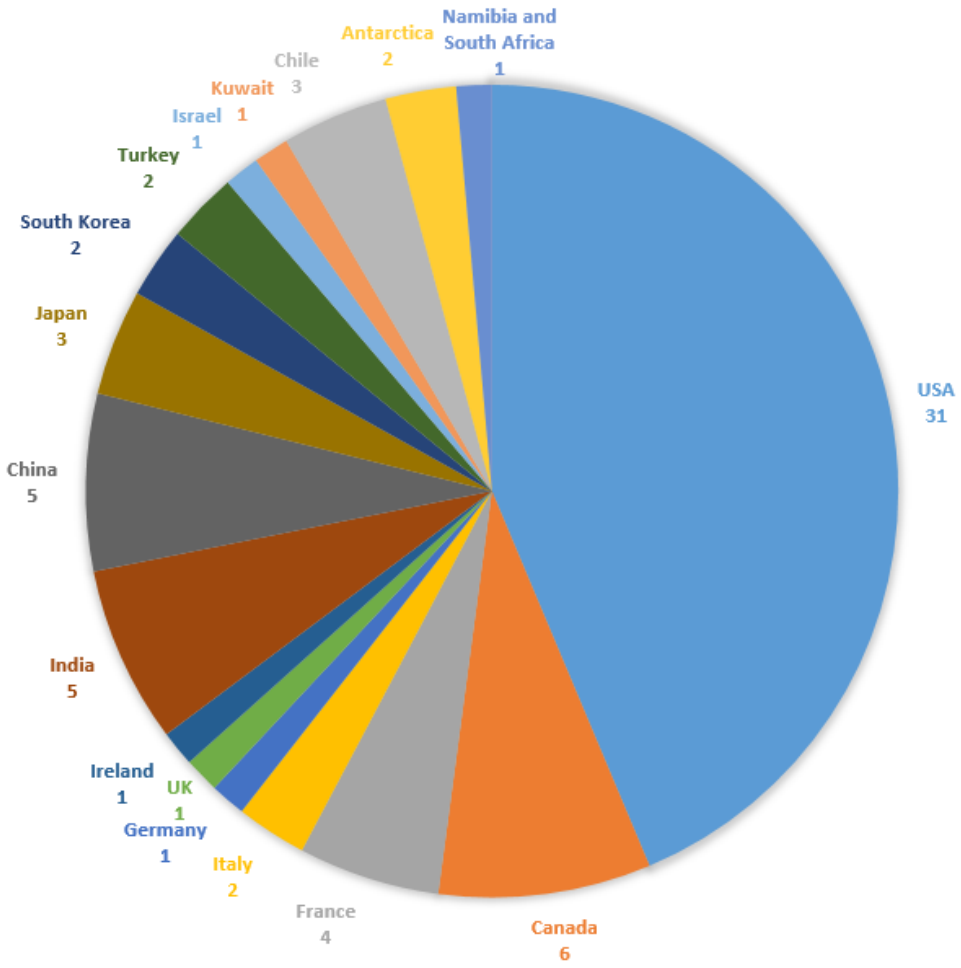

Figure I-2 : Number of peer-reviewed publications (total = 72) dealing with perchlorate contamination of water (occurrence, natural biodegradation, source determination, field remediation) published in international journals, sorted according to the location of the study sites (number of articles is given; UK: United Kingdom)

The lack of scientific research on ClO_4^- occurrence in many parts of the world does not mean that ClO_4^- is absent. Jackson et al. (2015) reported a global survey of ClO_4^- in water and soil samples that included data from Antarctica, Namibia, United Arab Emirates, and South Africa that were thought to be of natural origin based on their elevated concentrations and remote locations in hyper-arid desert environments. Arid environments like those of the Atacama Desert (hyper-arid), Death Valley and the southern High Plains (semi-arid) can be found on all continents and it seems likely that elevated concentrations of natural indigenous ClO_4^- will eventually be found at such locations.

In addition, the industrial production and use of ClO_4^- are expected to increase in decades to come. The current production of ClO_4^- is difficult to estimate because of its strategic status in military and aerospace applications. Regarding the results observed in USA and in Asia, systematic surveys seem essential in areas of past and current production and use. ClO_4^- production plants, fireworks and airbag factories, aerospace testing and launch sites, weapons factories, military installations, and historic battlefields are places where ClO_4^- contamination may occur and should be monitored.

The usefulness of Cl and O perchlorate isotope analysis has been clearly demonstrated in a growing number of studies, primarily in the USA. Further improvement of the forensics methodology for the determination of ClO_4^- sources and their environmental distribution and behavior will benefit large populations in areas where water supplies may be impacted by ClO_4^- contamination. This will require the measurement of many more ClO_4^- isotopic compositions from worldwide sampling of synthetic and natural ClO_4^-.

1.2. Perchlorate contamination of water in France

1.2.1. Advisory values of perchlorate in drinking water

In 2011, following the discovery of perchlorate contamination in some drinking water resources of SW and NE France, the ANSES (French Agency for Food, Environmental and Occupational Health & Safety; in French: Agence nationale de sécurité sanitaire de l'alimentation, de l'environnement et du travail) proposed an advisory value of **15 µg·L^{-1}** for ClO_4^- in drinking water for adults. This advisory value was defined with a RfD (Reference Dose for Chronic Oral Exposure) of 0.7 µg·kg^{-1}·day^{-1} proposed by the US EPA on 2005, with an exposure scenario for an adult weighing 70 kg bw (body weight) consuming two liters of water a day, assuming that the drinking water accounts for 60% of the total ClO_4^- oral intake in adults. An advisory value of **4 µg·L^{-1}** was retained for children under 6 months of age, with an exposure scenario of 0.75 liters of drinking water per day for a body weight of 5 kg (ANSES, 2012).

In 2018, based on the ClO_4^- contamination data in food (produced by the DGCCRF - Direction Générale de la Concurrence, de la Consommation et de la Répression des Fraudes) and in tap water during 2014 to 2017 (produced by the ARS - Agence Régional de Santé), the ANSES re-estimated that the drinking water contributes about 25% of the total ClO_4^- oral intake in adults in France (ANSES, 2018). Based on this estimation and the RfD of 0.7 µg·kg^{-1}·day^{-1} (US EPA, 2005), the ANSES suggested to reduce the advisory value of ClO_4^- in drinking water from 15 to **5 µg·L^{-1}** for adults (ANSES, 2018).

1.2.2. Levels of perchlorate in drinking water

As mentioned above in Part I.1.1.6, the first national campaign for the analysis of ClO_4^- in drinking water was conducted in France between October 2011 and May 2012 by ANSES's Nancy Laboratory for Hydrology (LHN), in response to the first observations of perchlorates in drinking water in SW France. More than 300 pairs of raw water / treated water samples were taken in each French department (ANSES, 2013). Among these samples, about three quarters had ClO_4^- concentrations < 0.5 µg·L^{-1} (limit of quantification) and 2% had concentrations > 4 µg·L^{-1}. No treated drinking water samples had been detected with ClO_4^- concentrations > 15 µg·L^{-1}. Raw groundwater samples collected from three drinking water catchments presented ClO_4^- levels > 15 µg·L^{-1}, representing about 1% of the analyzed water catchments. The maximum value detected was 22 µg·L^{-1} in raw water and 13 µg·L^{-1} in treated water.

According to this national measurement campaign, the distribution of ClO_4^- concentrations in raw water and treated drinking water are presented in Figure I-3. The majority of the sites with high concentrations of ClO_4^- (> 4 µg·L^{-1}) are located in North of France.

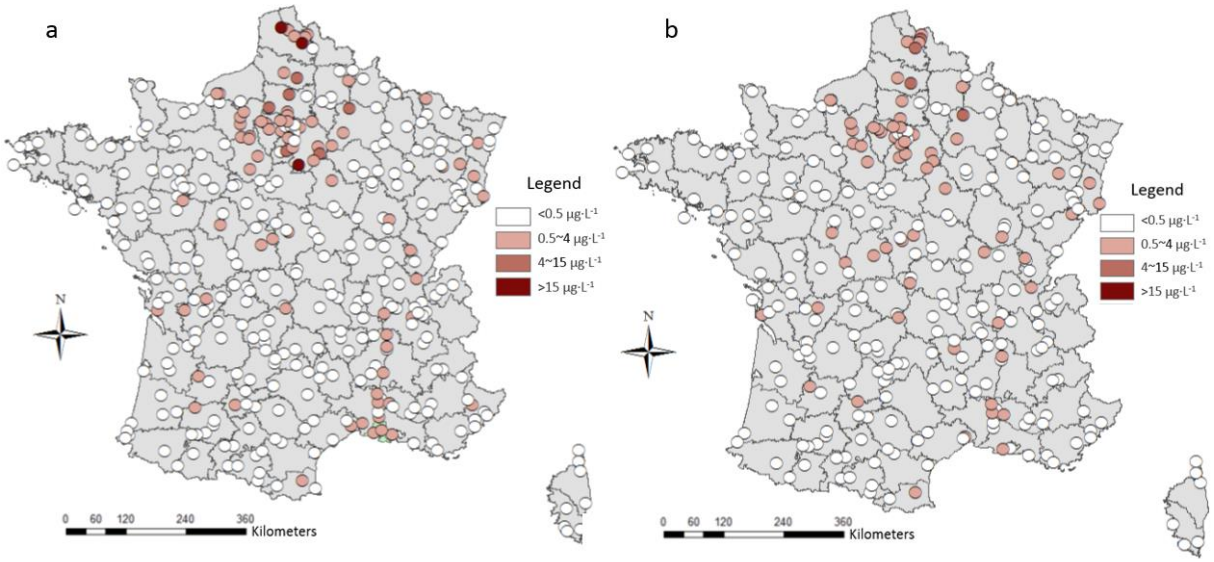

Figure I-3 : Distribution of perchlorate concentrations in raw water (a) and treated water (b) in France (ANSES, 2013)

To better take into account the sites suspected to be contaminated by perchlorate, a second measurement campaign was conducted in 2012 by the Professional Federation of Water Companies (FP2E), as a supplementary to the first national campaign by ANSES. The environmental context of the sampling sites selected by the FP2E can be classified into 6 categories: bombing areas, military sites, mining activities, industrial activities, agricultural activities and other contexts. According to the report of ANSES (2014), 57% of the water samples had ClO_4^- concentrations < 0.5 µg·L^{-1} (limit of quantification) and 6% had concentrations > 4 µg·L^{-1}. No treated or raw water samples had been detected with ClO_4^- concentrations > 15 µg·L^{-1}. The maximum value detected was 7.3 µg·L^{-1} in raw water and 4.1 µg·L^{-1} in treated water. No tendency related to a particular environmental context of the selected sampling sites was evidenced.

In addition to the national campaigns, the France Regional Health Agencies (Agence Régional de Santé, ARS) have conducted perchlorate analysis in water destined for human consumption in NE France since 2011. The results indicated that the regions of Hauts-de-France (Nord, Pas-de-Calais, Somme, Aisne and Oise) and Grand-Est (especially Marne and Ardennes) were significantly marked by perchlorate contamination (Figure I-4). In the region of Hauts-de-France, a total of 1,031 communes showed ClO_4^- concentrations between 4 and 15 µg·L^{-1} and 183 communes showed concentrations > 15 µg·L^{-1}. The department of Pas-de-Calais was the most contaminated with 89 communes showing ClO_4^- concentrations > 15 µg·L^{-1}, while in the departments of Nord, Aisne and Somme the number of communes with ClO_4^- levels > 15 µg·L^{-1} were 30, 31 and 27 respectively. The department of Oise was the least contaminated with only 6 communes presenting ClO_4^- concentrations > 15 µg·L^{-1}. In the departments of Marne and Ardennes, 113 communes showed ClO_4^- concentrations between 4 and 15 µg·L^{-1}; 6 communes and 1 village showed concentrations > 15 µg·L^{-1} (ARS, 2013)

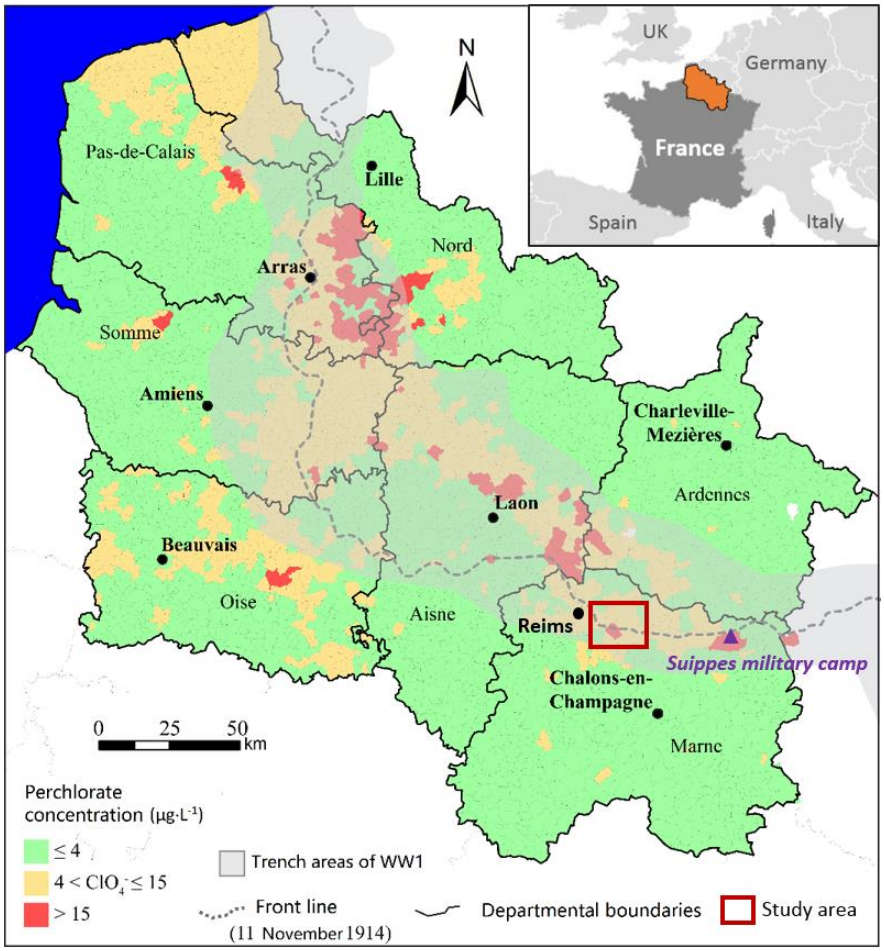

Figure I-4 : Perchlorate concentrations in tap water and position of the trench areas of WWI in NE France (Jaunat et al., 2018, based on 2013 results from ARS Champagne-Ardenne, 2014 results from ARS Nord-Pas-De-Calais and 2013 results from ARS Picardie)

1.2.3. Potential sources of perchlorate contamination in NE France

1.2.3.1. Military source related to WWI

The large extent of ClO_4^- contamination in NE France (Figure I-4) is unlikely to have been caused by point sources related to industrial activities. Indeed, industrial activities involving the use of huge quantities of perchlorate have been absent on this area since the end of WWI (Hubé and Urban, 2013). However, a correspondence can be observed between the spatial distribution of high ClO_4^- concentrations in groundwater and the position of the trench areas between 1914 and 1918 (Figure I-4). On the basis of this correspondence and the fact that large quantities of (per)chlorate explosives were used on the trench areas during the WWI, a military source of perchlorate contamination related to the WWI seems very likely.

Indeed, synthetic ClO_4^- produced industrially by electrolysis was largely used in explosives manufacturing during WWI. According to Hubé (2014), 130,905 T of (per)chlorate explosives were used during the WWI, mainly in grenade and trench artillery. The industrial chlorate contained about 1% - 10% of perchlorate and *vice versa*. The chemical composition of some (per)chlorate explosives used by German and French army during the WWI are presented below (Hubé, 2014):

- Explosive Ch 86/14: NH_4ClO_4 (86%) and Paraffin wax (14%)
- Explosive P: NH_4ClO_4 (71.5%), $NaNO_3$ (Chilean) (20%) and Paraffin wax (8.5%)
- Explosive S: $NaClO_3$ (90%), Paraffin wax (7%) and Vaseline (3%)
- Perchloratite: $KClO_4$ (56%), Dinitrobenzene (32%) and Dinitronaphthalene (12%)
- Pertite: NH_4ClO_4 (72%), $KClO_4$ (10%), Ditrinitrotoluene and TNT (15%) and Sawdust (3%)

In addition, ClO_4^- could also be present in other explosives including black powder (consisting of a mixture of sulfur, charcoal and KNO_3) and nitro group explosives (e.g., TNT, nitroglycerine and nitrocellulose), as Chilean nitrate (with ClO_4^- impurity) was intensively used in the manufacturing of these explosives.

The explosion of these ammunitions during the WWI led to the release of explosives into the soils and underground aquifers. Moreover, after the WWI, countless unused munitions were abandoned on or nearby the trench areas. At the Armistice, in order to reuse the farmlands, the battlefields were cleared and quantities of unused munitions were destroyed. Recent research shows that 2.5–3 million T of ammunition were destroyed in France during the period from 1918 to 1937 (Hubé, 2017). An example of the huge task of ammunition disposal is given for the Aisne department area: from January 1930 to December 1935, 1,450,000 T of projectiles were disposed and 167,000 T, considered as non-transportable, were blown up *in situ*. Despite this, at the end of 1935, 236,794 T of projectiles still remained undestroyed (Hubé, 2017). The munitions exploded on the battlefields during the WWI or exploded / blown up after the WWI can therefore contribute to a rapid and direct release of perchlorate ions into the environment. The destruction sites may constitute areas with “hot-spot” sources of perchlorate contamination, as demonstrated in the USA (Clausen et al., 2004; Martel et al., 2009) and in Germany (Hubé and Bausinger, 2013).

As an important component of ammunition, perchlorate could be released into the environment not only during explosion but also from the unexploded ammunition subsisting in subsoil long time after the war. It was estimated that about 30% of the ammunitions used during the WWI are unexploded. Annually, more than 100 T of ammunition could still be discovered in France (Desailloud and Wemeau, 2016). The envelope of ammunitions could be corroded slowly underground, therefore generate a continuous diffusion of perchlorate into the soil and groundwater.

The ammunitions can be classified into several types according to the degree of detonation, the related dispersion process of explosives are described as following (Hubé, 2014) (Figure I-5):

- Unexploded Ordnance (UXO): unexploded closed ammunition. The release of the explosive charge occurs as a result of the general corrosion of the envelope and / or its perforation. The time required for perforation is variable, depending on the nature and thickness of the envelope as well as the environmental conditions (acidity, oxidation ...). The perforation time was estimated between 250 and 450 years, at a rate of 1 mm / year on average (Parker et al., 2004).
- Low Order Detonated (LOD): partially exploded ammunition. About 1 to 50% of the explosive charge is exploded, with the size of explosive fragments > 1 mm. The explosive residue can persist for more than 100 years in soils.
- High Order Detonated (HOD): fully exploded ammunition. The size of explosive fragments is smaller than 1 mm, accompanied by fragments of metals. The unburned explosive charge is estimated at around 0.01% and can only persist for less than 1 year.
- Sympathetic Detonation (SYDET): unexploded ordnance that detonates partially under the shock of a HOD; same consequence as the LODs.
- Blow-In-Place (BIP): unexploded ordnance destroyed by detonation in a destruction funnel, which is the case for the destruction activities after the WWI. Only part of the explosive charge is exploded (up to 70%), with the size of explosive fragments > 1 mm. At the ammunition destruction sites, the repetition of the detonation causes an accumulation within the same place. The explosive residue can persist for more than 100 years in soils.

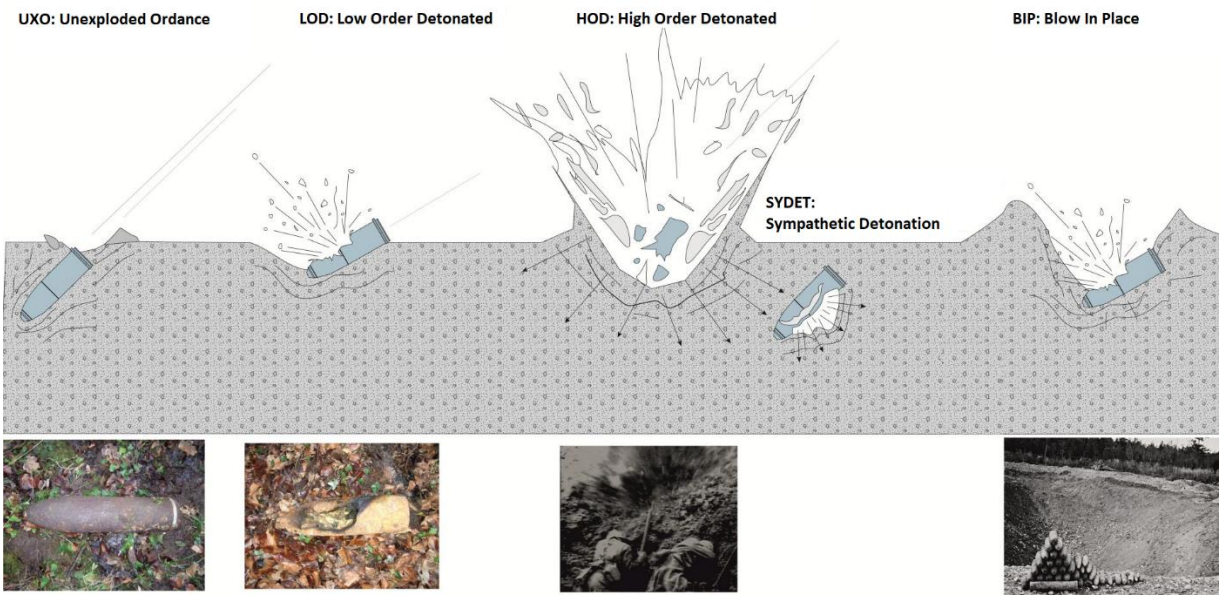

Figure I-5 : Ammunitions under different detonation conditions (adapted from Hubé, 2014)

1.2.3.2. Agricultural source related to Chilean nitrate fertilizer

It should be noted that in certain regions outside the trench areas, high levels of perchlorate have also been detected (e.g., Oise, Pas-de-Calais; Figure I-4). An agriculture source related to the past use of Chilean nitrates is suspected.

Indeed, large quantities of Chilean nitrates which contain high levels of perchlorate as impurity (cf. 1.1.2.1) was imported and used in France between 1880 and 1950 (Lopez et al., 2015). In peacetime, most of the imported nitrates were used in agricultural as natural fertilizer (especially for sugar beet and wheat) (Zimmermann, 1917). It was estimated that around the year 1928, the application quantity of Chilean nitrates to wheat cultivation was between 150 and 400 $kg \cdot ha^{-1}$ and could exceed 800 $kg \cdot ha^{-1}$ to beet cultivation (Lopez et al., 2014). Further studies are needed in order to clarify the perchlorate contaminations sources (military and / or agricultural) in NE France.

1.3. Perchlorate remediation: reduction and treatment

In the last decades, a significant amount of research has been performed to evaluate treatment alternatives for perchlorate remediation in drinking water. Technologies available for perchlorate removal or destruction in water can be classified into physical removal, chemical reduction, biodegradation and integrated technologies. The major technologies are briefly described and discussed in the following sections.

1.3.1. Physical and chemical treatment

1.3.1.1. Ion exchange (IX)

Ion exchange (IX) is one of the most effective and widely used technologies for perchlorate removal from water. Extensive research has focused on developing IX resins that would selectively remove perchlorate when the water contains other competing anions, such as chloride, sulphate, nitrate and bicarbonate, at high concentrations (Srinivasan and Viraraghavan, 2009; Ye et al., 2012). The most commonly used ion exchange media are synthetic, strongly basic, anion exchange resins, with a strong positively charge functional group (Srinivasan and Sorial, 2009), which have proven to be very effective in removing perchlorate from water (Batista et al., 2000). Among these strongly basic anion exchange resins developed, the selective cross-linked-styrene-divinyl benzene resin is one of the most widely used for drinking water contaminated with perchlorate at concentrations from 10 to 100 $\mu g \cdot L^{-1}$ (Chen et al., 2012).

Although ion exchange is a well-tested effective method for perchlorate removal in water, there are still some drawbacks in its practical application such as the high cost of the resins and the disposal of the spent brine which is concentrated in perchlorate.

1.3.1.2. Adsorption

Adsorption can effectively remove many kinds of pollutants in water, so it is widely used in treating drinking water and wastewater. Activated carbon (AC) is the most commonly used adsorbent for the removal of perchlorate, but its adsorption capacity for perchlorate is limited (Chen et al., 2005). It has shown to be competitive for perchlorate adsorption only after appropriate surface modification (Srinivasan and Sorial, 2009; Xie et al., 2018; Ye et al., 2012). However, this process also increases the operational cost and influences the adsorption capacity of the carbon for some of the other contaminants. In addition, the disposal of perchlorate spent carbon and regenerate brine could produce secondary pollution.

1.3.1.3. Membrane

Membrane technologies are based on the principle of employing a semi-permeable membrane that prevents the passage of certain ions thereby treating the water. Technologies such as reverse osmosis (RO), nanofiltration (NF) and ultrafiltration (UF) membranes plays an important role in removing perchlorate from drinking water (Srinivasan and Sorial, 2009; Ye et al., 2012). However, this technology is not suitable for large-scale applications because of fouling issues, costliness and the generation of large volumes of reject streams (Ma et al., 2016). Electrodialysis, being the most effective membrane technology has extremely high operational costs (Srinivasan and Sorial, 2009). Therefore, few studies have explored the use of membrane technology for the removal of perchlorate in recent years and researchers have tended to combine this technology with other technologies to deal with perchlorate contamination in water (Xie et al., 2018).

1.3.1.4. Chemical and electrochemical reduction

Physical removal technologies presented above do not offer a complete solution for perchlorate remediation as they only transfer perchlorate from one stream to another, necessitating further treatment of disposal. A complete reduction of perchlorate in water into harmless chloride can be achieved by the chemical reduction. However, the chemical reduction processes is generally very slow and requires catalysts, most of which are toxic and thus not suitable for the removal of perchlorate in drinking water (Srinivasan and Viraraghavan, 2009; Xie et al., 2018). Electrochemical reduction can convert perchlorate into chloride without catalysts. However, the electrode used is prone to be corrosive and consumes a large amount of electricity (Xie et al., 2018), making this method unsuitable for large-scale applications.

1.3.2. Biodegradation

Although ClO_4^- is highly persistent in oxic environments (Urbansky, 1998), it could be reduced by microorganisms under anoxic conditions (cf. Part I.1.1.2.1); such microorganisms are ubiquitous in the natural environments such as soils, sediments, surface water and groundwater aquifers (Coates et al., 1999; Coates and Achenbach, 2004; Tipton et al., 2003; Waller et al., 2004; Wu et al., 2001). Biodegradation is based on the principle that the special enzymes contained in perchlorate reducing bacteria can lower the activation energy required for perchlorate reduction, thereby using the perchlorate as an electron acceptor for their metabolism (Ye et al., 2012). A widely accepted perchlorate reducing pathway is the following: $ClO_4^- \rightarrow ClO_3^- \rightarrow ClO_2^- \rightarrow Cl^- + O_2$ (Bender et al., 2005). Perchlorate-reducing microbes are mostly facultative anaerobes, many of which appear to preferentially reduce nitrate (Nozawa-Inoue et al., 2005).

Bacterial reduction of perchlorate was observed as early as the 1950s, but most of the research in this area have been conducted only during the past two decades as perchlorate emerged as an environmental contaminant. Microbial treatment process including *ex situ* and *in situ* bioremediation have been extensively explored and worked out in both laboratory and pilot scale bioreactors (Bardiya and Bae, 2011; Sutton, 2006). The conventional bioreactors for *ex situ* treatment are engineered systems that employ either fixed- or fluidized-film reactors with acetate, acetic acid, molasses or ethanol as electron donor (Ye et al., 2012). The *ex situ* treatment process is particularly suitable for the treatment of highly concentrated waste streams originating from the perchlorate manufacturing units or the munition handling facilities (Bardiya and Bae, 2011). However, direct application of the treatment process for the treatment of drinking water is still questionable with the possibly health effects associated with the microorganisms. *In situ* treatment process involves delivery of nutrients such as ethanol, lactate, acetate, citrate, sugars and edible soils to the subsurface to promote the biodegradation of perchlorate by the indigenous bacteria (Srinivasan and Viraraghavan, 2009). The *in situ* bioremediation is particularly suitable for the decontamination of perchlorate from shallow or narrow zones of contamination. This technology is less expensive and significantly lower in maintenance than *ex situ* bioremediation (Bardiya and Bae, 2011; Ye et al., 2012).

1.3.3. Intergraded technologies

Intergraded technologies have been extensively explored for perchlorate removal in water such as microbial reduction supported on granular activated carbon (GAC) media (Choi et al., 2008; Na et al., 2002), iron oxide nanoparticles impregnated on ion-exchange resin (Hristovski et al., 2008), ion-exchange followed by microbial treatment of the brine (Chung Jinwook et al., 2007; Lehman et al., 2008) and microbial reduction on zero-valent iron (ZVI) (Yu et al., 2007). Numerous studies have shown that a combination of technologies could certainly be more effective than any single technology.

In conclusion, ion exchange and biological reduction are two major candidate processes for the removal of perchlorate from drinking water and wastewater. As to the biodegradation, public acceptance has to be considered due to the potential health effects related to these microorganisms if this technology is used for drinking water treatment. All in all, there is no single technology that is perfect for complete perchlorate treatment in water. The intergraded technologies combining one or more of physicochemical and biological process could be more economical and effective for the treatment of perchlorate.

2. Chalk and Chalk aquifer

Chalk groundwater is an important aquifer resource in France and also in much of northwestern Europe as it is intensively exploited for human use, with a large proportion reserved for drinking water. In France, the Chalk aquifer covers about 20% of the metropolitan territory with a total area of 110,000 km^2 (Crampon et al., 1996; Roux, 2018). It accounts for more than 60% of the groundwater used in the regions Hauts-de-France, Normandy, Ile de France, Grand Est and Centre Val-de-Loire (Roux, 2018). However, in recent decades, there is a growing evidence of the deterioration of the Chalk groundwater quality due to human activities (Baran et al., 2008; Barhoum, 2014; Chen et al., 2019; Hakoun et al., 2017; Johnson et al., 2001; Longstaff et al., 1992). Protection of this aquifer requires a sound knowledge of Chalk hydrogeology and groundwater geochemistry.

2.1. The Chalk

The Chalk is a marine sedimentary carbonate rock which was deposited over much of NW Europe during the Cretaceous Period when the area was submerged under the shallow to moderately deep warm sea (Downing et al., 1993). In general, the Chalk is a very fine-grained (less than 10 µm), pure (calcium carbonate formed nearly 98% of its composition), soft, white limestone of high interstitial porosity (~ 40%), that may contain some marl bands and flint (Hancock, 1975). The Chalk matrix (Figure I-6) is composed mainly of skeletal fragments of coccolithophores (planktonic algae), but coarser shell fragments can also be present (Allen et al., 1997).

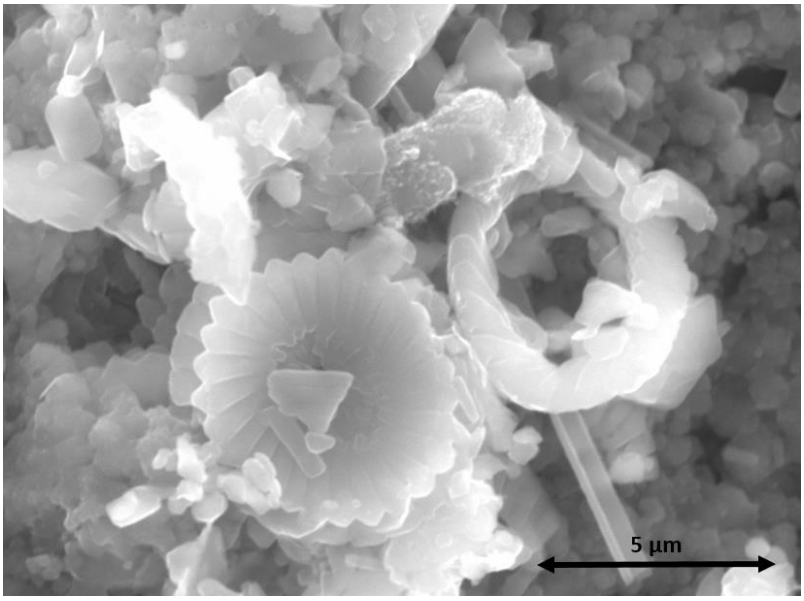

Figure I-6 : Scanning electron photomicrograph of a chalk sample from Estreux (France) showing coccoliths ~5µm wide (adopted from Nguyen, 2009)

Layers of marl can be found within the chalk. They are up to several centimeters thick, some of them being laterally continuous for several hundreds of kilometers. The marl is a calcium carbonate or lime-rich mudstone which contains variable amounts of clay and silt (Allen et al., 1997). The chalk can also contain flints which appear either in the form of continuous thin "sheets" often less than 1 cm in thickness or as layers of discrete irregular nodules between 1 and 30 cm in diameter. The flint was formed from diagenesis of biogenetic silica (Hancock, 1975; Maurice, 2009).

Three basic types of fracture can be recognized in the Chalk: bedding plane fractures, joints and faults (Bloomfield, 1996). Tectonic movements were responsible for the types and orientation of fractures (Allen et al., 1997). Bedding plane fractures are persistent structures that are located at discrete lithological boundaries. In the Chalk bedding plane, fractures may be developed in association with marl seams, flint bands or hardground, or can be localized by abrupt changes in the density of the Chalk (Bloomfield, 1996). Joints and faults are relatively impersistent fractures. Faults are fractures which exhibit a significant shear displacement parallel to the fracture surface and joints are fractures where shear displacement is negligible (Pollard and Aydin, 1988). Price (1987) also defined two types of fractures: 'primary fissures', the original tectonic fracture system usually consisting of orthogonal joints sets and 'secondary fissures' which are 'primary fissures' enlarged by dissolution process.

The Chalk formation is widespread in northwestern Europe covering the large area between the Paris Basin, the London Basin, Denmark and the North West of Germany (Bakalowicz, 2018). Chalk deposits are also present in Poland (Borczak et al., 1990). In France, the Chalk was mainly deposited in the Paris basin consisting of alternating sedimentary beds. The Chalk outcrops over about 70,000 km^2, forming a rim around the central Tertiary outcrop (Figure I-7), with a thickness varying from 100 to 600 m (Crampon et al., 1996).

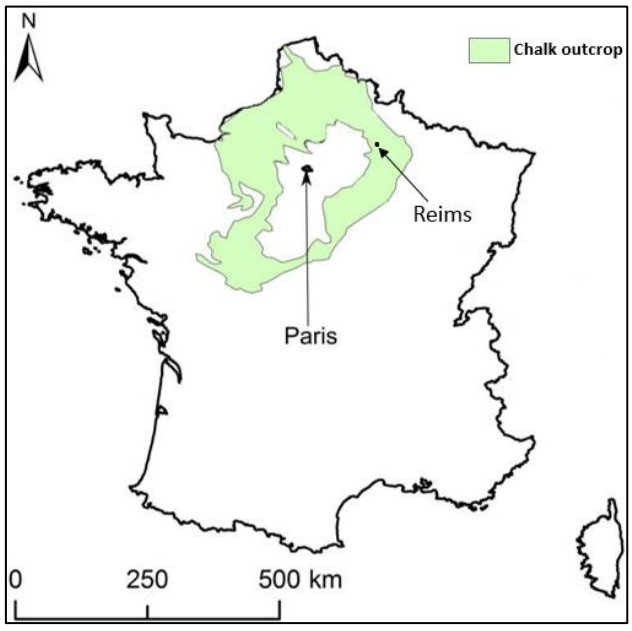

Figure I-7 : Chalk outcrop in France (adapted from Barhoum, 2014)

2.2. The Chalk as an aquifer

2.2.1. Aquifer properties

This section reviews the porosity, permeability and storage characteristics of the Chalk. These hydrodynamic properties show significant regional and stratigraphic variations. Trends in porosity and permeability as well as the typical hydraulic conductivity and transmissivity data are described. The karst behavior of the Chalk aquifer is also presented.

2.2.1.1. Chalk porosity

Rock porosity refers to the fraction of the volume of voids over the total volume (expressed in %). The Chalk has long been recognized as possessing dual porosity (e.g. Foster, 1975; Headworth et al., 1982; Price, 1987): matrix porosity and fracture porosity.

- **Matrix porosity**

The Chalk matrix is characterized by a combination of small grain size, small pore-throat size and high porosity (Whitehead and Lawrence, 2006). The mean porosity of the Chalk matrix ranges from 20% to 40% with a mean pore-throat size of about 0.5 µm (Price, 1987). Although the matrix has a high porosity, small pore throat diameters mean that the pores are not readily drained under gravity (Fitzpatrick, 2011). Only the effective porosity will allow the transfer of water and solute flow. It is estimated between 1 and 4% (Castany, 1982).

Chalk matrix porosity is affected mainly by the degree and nature of diagenesis; it decreases with depth below the surface because of increased compaction (Bloomfield et al., 1995). Two main diagenetic processes occur: mechanical compaction which refers to the physical reorganization of fragments into a denser structure , and chemical compaction which refers to the dissolution and reprecipitation of minerals (Bloomfield, 1997). Chemical compaction processes depend upon pore water chemistry, lithology and clay mineral content and have a more variable effect on Chalk porosity than mechanical compaction (Maurice, 2009).

- **Fracture porosity**

Fractures have a significant role in developing chalk aquifer properties, as without fractures the permeability and specific yield of the Chalk would be nearly negligible (Azeez, 2017). Different types of fractures are defined in the Chalk (cf. Part I.2.1). The fracture porosity is significantly lower than the total porosity: in general, the porosity of the fractures is around 1% of the total volume of porosity (Price et al., 1993).

Fracture distribution in the Chalk is highly heterogeneous. Vertically, fractures are generally only developed towards the top of the aquifer. Deeper within the Chalk, the frequency and aperture of fractures decline due to increasing overburden and a general reduction in circulation groundwater and hence dissolution (Allen et al., 1997). Laterally, frequency of fractures are observed higher in valleys than on the interfluves as the structural weaknesses followed by valleys are more fractured and erosion along valleys favors the opening of horizontal fractures (Allen et al., 1997; Price, 1987; Price et al., 1993).

The heterogeneous distribution of fractures results in variations of permeability in the Chalk, which are described in detail in the following sections.

2.2.1.2. Chalk permeability

Permeability is the capacity of rock to transmit fluids and is determined by the nature and connectivity of voids within the rock (Maurice, 2009). In small scale aquifers, the hydraulic conductivity is normally used as a measure of permeability (Price, 1996). The Chalk aquifer has two components of permeability: the matrix permeability which is low due to the small size of the pore throats and the fracture permeability which dominates.

- **Matrix and fracture permeability**

The Chalk matrix is generally isotropic with respect to permeability, and matrix hydraulic conductivity measured in the laboratory gives values in the range of 10^{-9} to 10^{-7} $m \cdot s^{-1}$ (Price, 1987). These values equate to a transmissivity of about 10^{-7} to 10^{-5} $m^2 \cdot s^{-1}$ for a 100 m thick aquifer. Comparing these values to field measured transmissivities, typically in the range of 5×10^{-3} to 3×10^{-2} $m^2 \cdot s^{-1}$ demonstrates the importance of fractures to the overall transmissivity of the Chalk aquifer (Whitehead and Lawrence, 2006).

As the hydraulic conductivity of the Chalk matrix is negligible with respect to the hydraulic conductivity of Chalk fracture systems, the Chalk permeability can be considered to be dominated by fractures. Fracture permeability is dependent on the aperture and spacing of the fissures and the interconnectedness of the fissure network (Fitzpatrick, 2011). Primary fissures present throughout the Chalk, which have small aperture of typically much less than 1 mm (Worthington, 2003), increases significantly the permeability of the Chalk aquifer compared to the permeability of the Chalk matrix. Price (1987) estimated the transmissivity of primary fissures to be approximately 20 $m^2 \cdot day^{-1}$. However, this value is still much lower compared with the typical field measured values of 500 to 3,000 $m^2 \cdot day^{-1}$ reported in the chalk. Secondary fissures, which refer to the fissures enlarge by dissolution, with apertures of greater than 10 mm (Worthington, 2003), are therefore necessary to account for the high transmissivities in the Chalk aquifer (Fitzpatrick, 2011).

- **Permeability variations with depth**

Zones that have high permeability correspond then to fracture locations. Therefore, the permeability of the Chalk varies significantly with depth and is generally developed towards the top of the aquifer. It has been suggested that there is very little flow deeper than 50 m below the surface, as increased overburden results in fewer open fractures. Consequently, groundwater tends to have longer residence time and are saturated with respect to calcium carbonate thus preventing dissolution (Allen et al., 1997; Whitehead and Lawrence, 2006).

The high permeability zone with dissolution-enhanced fractures corresponds also to the zone of water table fluctuation (e.g., Headworth et al., 1982; Price, 1987). This high permeability zone can have the effect of buffering groundwater levels. When recharge is low, water level falls and the rate of decline diminishes as water level reaches the base of high permeability zone. Conversely, water is discharged quickly from the high permeability zone at times of high recharge, thus not allowing water levels to rise significantly (Allen et al., 1997).

2.2.1.3. Groundwater storage

Specific yield is the ratio of volume of water that drains by gravity to the total volume of the aquifer. The total specific yield of the Chalk is in the range 1% to 3% (Allen et al., 1997; Whitehead and Lawrence, 2006). The relative contribution to groundwater storage from matrix and fractures is difficult to ascertain (Allen et al. 1997). As the matrix porosity of the Chalk is made up of a large number of pores having dimensions of the order of 1 µm, capillary tensions prevailing in the matrix are very high. Therefore, the matrix water content is always close to saturation and relatively difficult to be drained (Brouyère et al., 2004). Consequently, groundwater held in fractures constitutes the largest component of specific yield of the Chalk aquifer. When the groundwater head is lowered within a borehole, the larger fractures will drain initially; the groundwater in smaller fractures moves consequently into the large fractures due to the decrease of head within the aquifer (Allen et al., 1997).

Despite the dominate contribution from fractures to groundwater storage, a matrix storage (about 0.25% of bulk volume) is proposed in the unsaturated zone, due to the drainage and refill over the ranges of capillary fringe related to variation of the moisture content (Lewis et al., 1993; Price et al. 2000). This "additional" unsaturated storage is replenished in winter as recharge reaches the groundwater table and is available in summer, draining slowly downgradient to the water table to contribute to groundwater supplies. It may explain why the Chalk is relatively resilient to drought (Price et al. 2000).

2.2.1.4. The Karstic behavior of the Chalk

Besides the long recognized dual porosity system, the Chalk has also been described as possessing triple porosity with conduit (karst) porosity as the third porosity component at some sites (MacDonald et al., 1998a; Worthington, 2003). Karstic nature of the Chalk has long been recognized and explored, especially in southern England (e.g., Atkinson and Smith, 1974; MacDonald et al., 1998; Maurice et al., 2012; Worthington, 2003) and in Normandy in North of France (e.g. Calba, 1980; El Janyani et al., 2014; Rodet, 1993; Valdes et al., 2005). Small scale karst features are also recognized in the east of the Paris Basin (e.g. in Champagne-Ardenne: Devos et al., 2007, 2006). Karst in the Chalk consist in extensive network of dissolution enlarged channels, through which groundwater flows rapidly. The size of channels can range from several centimeters (conduits) to more than 1 m (caves) (Fitzpatrick, 2011).

Geomorphological evidence of karst characteristics such as dolines, stream sinks, solution pipes and caves are sometimes observed in the Chalk (e.g., Edmonds, 1983; Fagg, 1958; Sperling et al., 1977). In addition, other phenomena can also be related to the karstic nature of the Chalk such as rapid groundwater flow recorded by tracer tests; pumping sand in boreholes and quick response of the water level in boreholes.

2.2.2. Flow and transport in the unsaturated zone

The unsaturated zone (UZ) can be defined as the region of aquifer that lies above the groundwater level. As a consequence of the small pore throat sizes of the Chalk matrix, even in the UZ, the matrix porosity is almost fully saturated (Foster, 1975; Price, 1987; Vachier et al., 1987).

Within the literature, there has been much debate about the significance of flow through fractures compared to the matrix in the UZ. Before 1970, it was believed that the flow in the UZ is entirely through the fissure network, supported by observations of rapid response of the water table after high intensity precipitations (Price et al., 1993). This theory was changed by Smith et al. (1970) and Smith and Richards (1972) with their tracer studies using tritium. They measured the UZ porewater tritium profiles from the Bershire Chalk in England and discovered distinct tritium peaks at 4 and 7 m respectively, which originated from recharge during 1963-1964, years in which tritium levels in rainfall had been exceptionally high due to nuclear bomb tests in 1962-1963. Based on these experimental data, Smith et al. (1970) suggested that the majority (about 85%) of flow in the UZ occurs through the matrix at a mean downward rate of 0.88 $m \cdot year^{-1}$, with some 'bypass flow' through fissures occurring to explain the presence of tritium at depth. Smith et al. (1970) also introduced the concept of 'piston flow', whereby water in the UZ is gradually displaced by new recharge resulting in the deepest groundwater being discharged through the bottom of the system. This explains the rapid water table response to rainfall despite the slow migration of tritium.

Other tracer studies carried out during the last decades also proved the flow dominated through the matrix. At sites with a thick unsaturated zone over a deep water table , an average vertical flow rate of about 1 $m \cdot year^{-1}$ was estimated, with minimum and maximum values of about 0.3 and 2 $m \cdot year^{-1}$ respectively, due to variations in rainfall intensities and physical properties of the Chalk (e.g., Barraclough et al., 1994; Brouyère et al., 2004; Chen et al., 2019; Haria et al., 2003; Van den Daele et al., 2007; Wellings, 1984). However, at shallow groundwater sites the vertical water movement is largely influenced by the effect of capillary fringe. Indeed, the capillary fringe sustains a higher moisture content in the unsaturated zone which reduces the water storage capacity for vertical drainage fluxes. As a result, little water is required to wet the shallow profile before rapid preferential flow events occur, therefore more rapid water potential responses could be observed at shallow groundwater sites than deep groundwater sites (Haria et al., 2003).

Despite a dominant matrix flow in the UZ, rapid flow through fissures have also been demonstrated by artificial tracer testing studies. The rapid flow could temporally or locally be dominant, especially in zones where karstic systems are developed (Ireson et al., 2006; Mathias et al., 2006; Maurice, 2009). Flow rates have been estimated with values ranging from 1 to 20 $km \cdot day^{-1}$ in karstic systems and up to $24 \cdot 10^{-3}$ $km \cdot day^{-1}$ in fissures (Allshorn et al., 2007; Baran et al., 2008; Calba, 1980; Devos et al., 2006; Ireson et al., 2006; Katz et al., 2009; MacDonald et al., 1998a). It should be noted that karst flow usually contribute little to the recharge of Chalk aquifers but can cause punctual problems on groundwater quality such as nitrate and bacterial contaminations (Barhoum, 2014). The preferential recharge by rapid flow could be influenced by multi-factors. Brouyère et al (2004) undertook tracer tests through the Chalk UZ in Belgium and found that where the Chalk is overlain by soils or other deposits, the recharge rate is attenuated and therefore fissure flow is not initiated during high recharge events. Ireson and Butler (2011) also suggested that the characteristics of rainfall events, in terms of duration and intensity, the physical properties of the near surface and the antecedent soil moisture in the near surface can influence the preferential recharge of the Chalk aquifer.

Near surface field measurement of soil moisture content and matrix potential have also been used to investigate recharge mechanisms of Chalk aquifers (e.g., Haria et al., 2003; Wellings, 1984a; Wellings and Bell, 1980). According to these studies, it is generally concluded that flow through the matrix in the UZ is the dominant process, with rapid flow through fractures initiated only when matrix potentials exceed a certain threshold. Wellings and Bell (1980) noted that the movement of solute can be seen steadily downwards during the winter drainage period as a result of high matrix potentials with high soil moisture content, whilst it slows in April/May and then stops throughout the summer. Haria et al. (2003) measured soil water content and matrix potential at an interfluve with a deep UZ and a dry valley with a shallow water table and found that recharge on interfluve was through matrix, whilst recharge at the valley was both through the matrix and by preferential flow through fissures.

In conclusion, recharge is predominately through the Chalk matrix at most of the UZ. Where a connected fracture network exists, near surface rapid flow through fissures can be initiated if the infiltration rate exceeds the hydraulic conductivity of the matrix (Price et al., 2000). Flow through the UZ of the Chalk occurs at three velocity scales: very rapid flow recharge through karstic conduits (~ km·day^{-1}), moderately rapid flow through fissures (~ m·day^{-1}) and slow flow through matrix (~ m·year^{-1}) (Maurice, 2009).

2.2.3. Flow and transport in the saturated zone

Groundwater flow in the saturated zone (SZ) can be illustrated by the Darcy's Law. According to Darcy's Law, the quantity of water flowing through a granular medium is proportional to the hydraulic gradient:

$$q = -K \frac{\partial h}{\partial l} \tag{I.4}$$

Where q is the flow per unit cross-sectional area of the aquifer (the *specific discharge*), K the hydraulic conductivity and $\frac{\partial h}{\partial l}$ the hydraulic gradient.

In multiple-porosity aquifers such as the Chalk, solute transport can be influenced by several processes including advection, diffusion, adsorption and dispersion.

Advection is the term used to describe movement attributed to transport by the flowing groundwater: solutes travel at the same rate as the average linear velocity of the groundwater. Diffusion represents the net movement of solute under a concentration gradient. For the dual-porosity Chalk, Foster (1975) proposed a diffusive exchange mechanism between fissure water and matrix water that could explain the rapid flow through fissures and the slow migration of solutes. He suggested that during wet periods the concentration gradient between the contaminated fractures water and the matrix water would cause diffusion of solute into the matrix, greatly retarding the rate of vertical solute movement. This mechanism has been demonstrated to be of significance for the interpretation of contaminant transport in the UZ of the Chalk (Barker and Foster, 1981; Foster, 1975) and the prediction of the lateral migration rate of pollutants in the SZ of the aquifer (Burgess et al., 2005). The double-porosity diffusive exchange can attenuate contaminant concentrations and significantly extend the duration of contamination (Fitzpatrick, 2011). When the contamination input to the fracture water has ceased, there will be a diffusive flux from the now contaminated matrix water to the fracture water, thus increasing the duration of contamination detected down-gradient. The advection transport in fissures and the diffusive exchange of solutes between fissures and matrix water are two major processes which dominate the solute transport in the Chalk SZ.

Adsorption may also affect the transport of some solutes. Solutes can be attenuated by the process of adsorption during the advective transport of groundwater flow. Adsorption process is influenced by the intrinsic properties of the solutes and most of the surface area of chalk onto which adsorption can take place is within the rock matrix. Dispersion refers to the process of spreading of solutes during transportation. Dispersion arises because of the variations in flow velocity in pores and fractures mainly due to the complex splitting and joining of paths. Dispersion in individual fissures is likely to be small and dependent on the fissure aperture and roughness. At a larger scale, dispersion depends on the interconnectivity of fractures (Grisak and Pickens, 1981, 1980) and the effects of dispersion across fracture networks may become important (Fitzpatrick, 2011).

2.2.4. Geochemistry

The large extent, high conductivity and high water storage of the Chalk aquifer makes this resource essential but vulnerable to pollution (Crampon et al., 1996; Edmunds et al., 1987; Kloppmann et al., 1998; MacDonald et al., 1998b). A good understanding of the Chalk geochemistry is thus fundamental for the environmental management, the monitoring of the eventual anthropogenic impact, the prediction of spatial and temporal variations of groundwater composition and the solutes transport (natural or anthropogenic) (Edmunds et al., 1987; Gillon et al., 2010).

2.2.4.1. Natural baseline geochemistry of Chalk groundwater

The dominant chemical characteristics of Chalk groundwater are acquired during initial percolation through the soil and upper UZ. Since in a Chalk aquifer, the rock matrix is dominated by carbonate minerals, a relative and fast homogeneity of the baseline geochemistry is expected (Edmunds et al., 1987). Beyond the lithological properties of the aquifer, the geochemistry of the groundwater can be influenced by several processes, including atmospheric inputs, water-rock interactions, residence time of the groundwater, mixing of different waters and redox reactions. Spatial and temporal variations in groundwater chemical composition can occur under the influence of these factors.

- **Atmospheric inputs**

Atmospheric inputs through precipitation is mainly determined by the distance of study area to the sea and/or to a source of air pollution (industrial, agricultural, urban etc.) (Barhoum, 2014). Local terrigenous dust consisting of plant debris and rock mineral grains could also influence the chemical composition of precipitation (Celle, 2000). As a result, the type and the concentration of ions in precipitation could be different from one site to another. In the Chalk aquifer, the principal ions contributed by atmospheric inputs are Na^+, Cl^- and SO_4^{2-} (Kloppmann et al., 1994).

- **Water-rock interactions**

Water-rock interactions are major processes that should be taken into account since they control the solute transfer due to the dissolution of primary rock minerals and the precipitation of second phases (Gillon et al., 2010). The calcite content of the Chalk is generally above 95%. Rainwater infiltrating the soil overlying the Chalk becomes quickly saturated with respect to calcite and remains so during passage through the UZ (Edmunds et al., 1987). The molar ratio of Ca^{2+} to HCO_3^- is approximately 1:2 according to the process of dissolution of calcite:

$$CaCO_3(s) + H_2O + CO_2 \Leftrightarrow Ca^{2+} + 2HCO_3^- \quad (I.5)$$

The solubility of carbonates, pH and water alkalinity show a temporal variability, as CO_2 partial pressures varies due to vegetation heterogeneity and seasonal climatic variations (Lee, 1997; Reardon et al., 1980, 1979).

Although the Chalk is generally a very pure carbonate sediment, local variations of the rock mineralogy and its composition could occur, due to presence of dolomitic bodies, clay-rich beds or phosphatic layers (Deconinck et al., 2005; Jarvis, 1980; Richard et al., 2005). Impurities such as Mg and Sr are involved in water-rock interactions. Along the flow path, there is a progressive increase in Mg and Sr concentrations, and more positive $\delta^{13}C$ values indicate that incongruent recrystallization of carbonate is taking place. The comparative gain in Sr is about 3 times greater than Mg, suggesting that Sr is more strongly rejected during recrystallization than Mg (Edmunds et al., 1987; Kloppmann et al., 1998). Mg, Sr along with $\delta^{13}C$ are considered to be a guide of maturity and residence time in the Chalk.

Cation exchange reactions should also be taken into consideration, especially when water flows through clayey deposits. Some increase in Na^+ probably occurs as a result of cation exchange, although this is rather small (Barhoum, 2014).

- **Mixing**

The mixing of waters from different origins could modify the geochemistry of groundwater in a Chalk aquifer. As a double porosity system, waters of different residence times including freshly percolated water, fissure water and matrix porewater tend to mix, thereby influencing the geochemistry (Gillon et al. 2010). The contribution of each water depends on the season, depth, topography etc.

- **Redox reactions**

Redox reactions could influence the geochemistry of Chalk Groundwater, especially when the aquifer is confined below an impermeable overlying clay such as alluvial sediments of rivers. Reducing conditions allow Fe^{2+} concentrations to increase and following the disappearance of oxygen, NO_3^- is quite rapidly reduced (Edmunds et al., 1987).

2.2.4.2. Contamination of the Chalk aquifer

The Chalk soil is often exploited for agricultural use. The agricultural application of fertilizer and pesticide could be flushed into the aquifer during the recharge. These activities could result in the increase of contaminants in groundwater such as NO_3^-, Cl^-, SO_4^{2-} and numerous pesticides (Barhoum, 2014; Kloppmann et al., 1994). Among these contaminants, nitrate is a main indicator of agrichemical pollution. It is persistent where oxygen is present, but it is reduced to N_2 gas either inorganically or bacteriologically under anaerobic conditions of the aquifer. Industrial and urban activities could also contribute to the contamination of Chalk aquifers. The residence time of the aquifer could provide information on the relation between groundwater contamination and related historical activities.

Part II. Study area, materials and methods

This part describes in detail all the materials that have been used as well as the procedures that are undertaken to conduct the thesis research.

In chapter 1, the selected study area with "potential multi-sources" of perchlorate is described. This area, located in NE France, corresponds to a traditional agricultural zone concerned both by military activities related to WWI as well as former use of Chilean nitrate fertilizer. The topography and the geological and hydrogeological context of the study area are presented at first. Then, the climate condition and land use information are described, which is necessary for a better understanding of the aquifer functioning.

In chapter 2, the methodology of research and different approaches/tools used are described firstly. The purpose of the measurement/analyzes realized are described, with the aim to clarify the strategy of the study in a comprehensive view. Then, the sampling network established in the study area consisting of 36 sampling points is presented. The protocol of measurement and analyzes are detailed in the last section. The equipment used, the sampling and analytical method for each parameter are described separately.

1. Description of the study area

1.1. Location and topography

The study area is located east of Reims (NE of France; Figure II-1) and covers approximately 500 km^2 between the Suippe River (as the Northern and Eastern boundary) and the Vesle River (as the Southern boundary). Both the two rivers have several tributaries; the Prosne River (tributary of the Vesle River) is usually dry while others are permanent watercourses (Figure II-1).

The altitude of the study area is relatively low (up to about 260 m NGF; Figure II-1). The lowest altitude is about 80 – 100 m, in the valleys of Vesle River, Suippe River and their tributaries. The Berru Mount and the Champagne Mounts have the highest altitude of more than 240 m NGF.

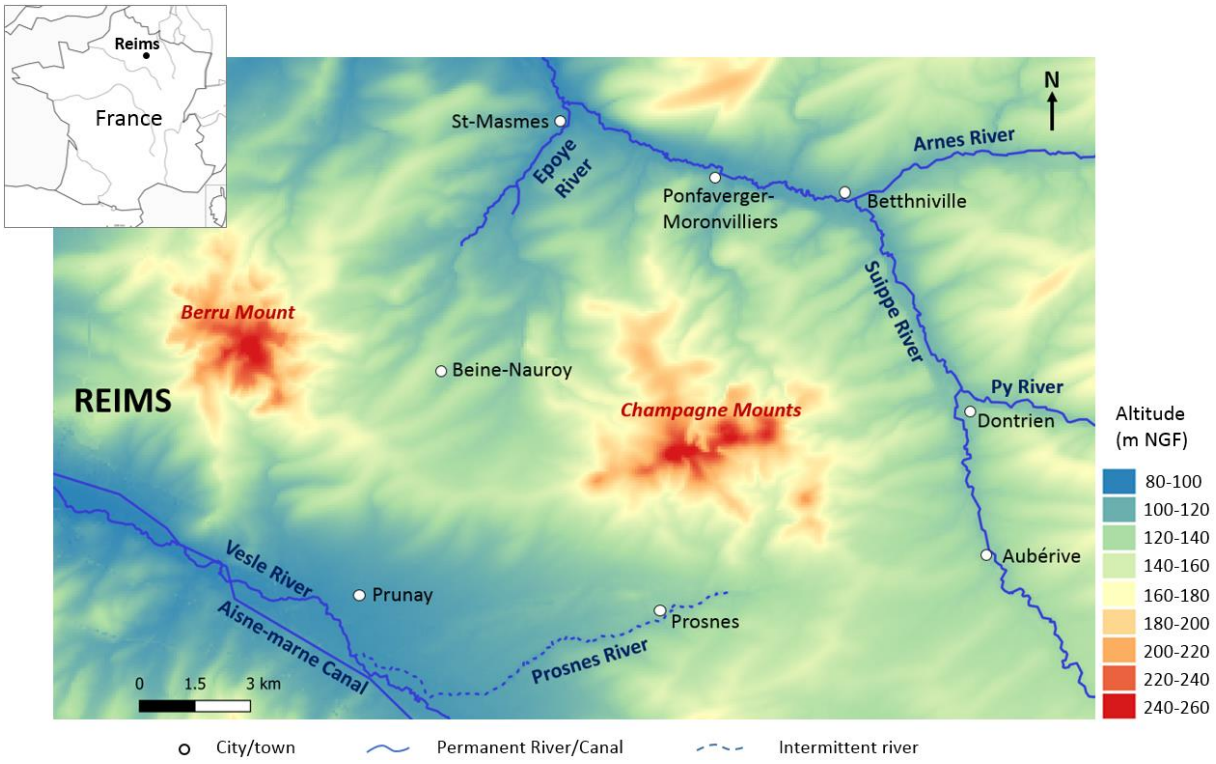

Figure II-1 : Location and topography of the study area

1.2. Geology

The study area is located in the Paris basin (Figure II-2). It is a sedimentary basin with a diameter of about 600 km covering the northern half of France, bordered by the Armorican Massif to the West, the Massif Central to the South, the Massif des Vosges to the East, the Ardennes-Brabant massif to the Northeast and the English Channel to the Northwest. Successive geological deposits from the Triassic to the Tertiary were laid down, the most recent of which are outcropping in the center of the basin (Figure II-2). The Upper Cretaceous formation extends over an area of 70,000 km^2 in the Paris Basin (Hubert et al., 2006).

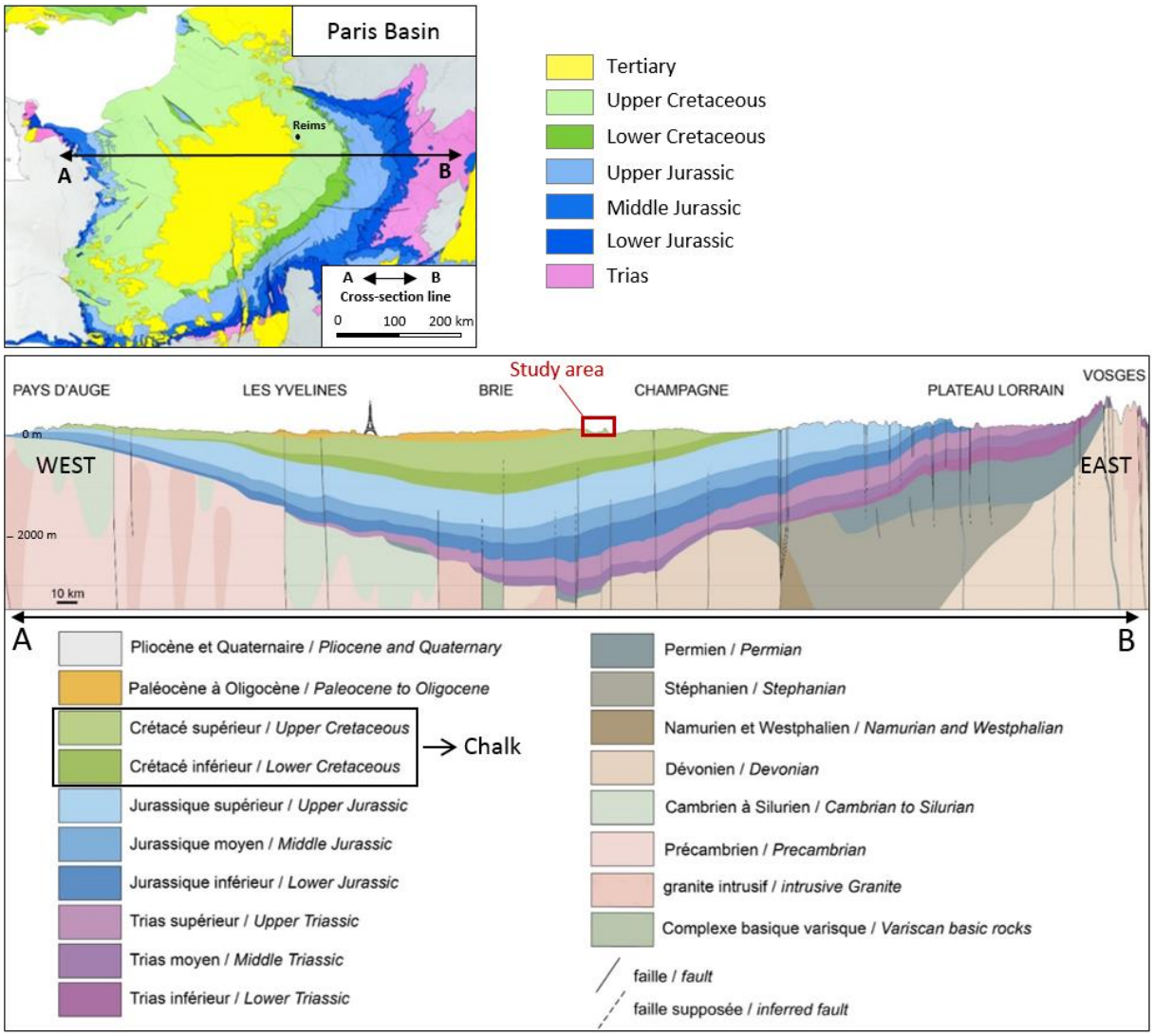

Figure II-2 : Geological map (adopted from Mégnien, 1979) and a geological section of the Paris Basin (cross-section A-B, adopted from Gély and Hanot, 2014)

The study area is located east of the edge of Tertiary formation (Figure II-2). The Upper Cretaceous formation constitutes almost the entire surface, with only a limited surface of Tertiary formation at the Berru Mount (Figure II-3). The Chalk formation is partially covered by Quaternary formations including graveluche (a periglacial formation), colluvium and alluvium (Figure II-3).

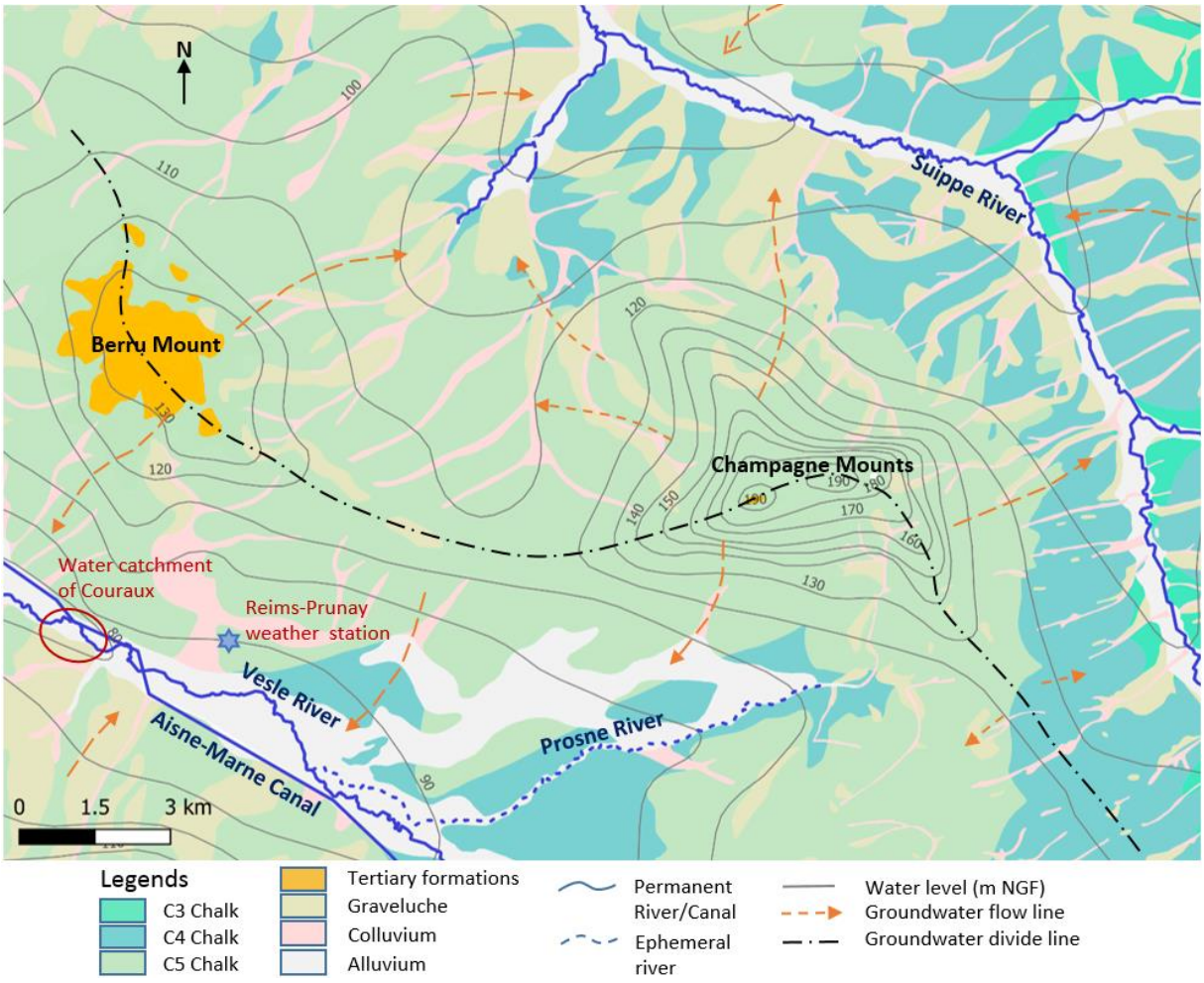

Figure II-3 : Geological and Hydrogeological map of the study area recorded at high water level (source of geological map: Laurain et al., 1981, Allouc and Le Roux., 1995; source of water level data: Rouxel-David et al., 2002a)

1.2.1. Cretaceous

The Cretaceous formations outcropping on the surface of the study area are constituted by Coniacian (C3), Santonian (C4) and Campanian (C5) Chalks (Figure II-3), lying over a base of Turonien and Sénonien Chalks. The Campanian (C5) Chalk outcrops on the majority of the study area, with a thickness of about 85 m (Rouxel-David et al., 2002b). The Santonian (C4) Chalk outcrops mainly along the Vesle River and the Suippe River, with a thickness of 20 to 35 m (Laurain et al., 1981). The Coniacian (C3) Chalk outcropping is rare in the study area (only on the right bank of the Suippe River; Figure II-3) therefore is not discussed here.

Despite the different age of formation, the Santonian (C4) and Campanian (C5) Chalks are very similar to each other, represented by pure white Chalks with a fine (calcite granule with diameter of 5 to 10 µm) and homogeneous structure presenting a conchoidal fracture (Moreau et al., 1985). Stratigraphic differentiation is permitted only by the observation of micro fauna, although this is quite rare (Laurain et al., 1981). The first 10 – 20 meters of the Champagne Chalk are significantly fractured and the fracturing decreases with depth (cf. Part I.2.2.1.1; Mangeret et al., 2012; Vachier et al., 1987).

The chemical compositions of Santonian (C4) and Campanian (C5) Chalks in the Champagne region were measured by Gillon et al. (2010), using a Scanning Electronic Microscope (SEM) in combination with X-ray analysis (Table II-1). The C4 and C5 Chalks are mainly composed of carbonate (>95%) containing impurities such as Si, Al, Mg and Sr (originated from minerals as silicate, quartz, kaolinite and clay; cf. Part I.2.1). The purity of Chalk increased with depth (Gillon et al., 2010).

Table II-1 : Chemical compositions of Santonian (C4) and Campanian (C5) Chalks (adopted from Gillon et al., 2010)

		C4 Chalk mean	**C5 Chalk mean**
	Carbonate (weight %)	98.5	96.6
Element concentrations ($mol \cdot kg^{-1}$)	Ca	9.76	9.62
	Si	0.17	0.28
	Al	0.12	0.16
	Fe	0.021	0.030
	Mg	0.049	0.052
	Sr	0.013	0.014
	Na	<0.064	<0.058
	K	0.010	0.014
	Mn	0.003	0.003
	Ti	0.005	0.006
	P	0.016	0.014
	S	0.015	0.013

1.2.2. Tertiary

The Chalk formation is locally overlain by Tertiary formations at the Berru Mount in the west of the study area (Figure II-3). The generalized stratigraphic series of Tertiary formations can be described as following (Rouxel-David et al., 2002b):

- lying directly on the Chalk, 10 to 15 m of sand from the Thanetian,
- 20 m of clay from the lower Ypresian,
- 10 to 20 m of sand from the upper Ypresian,
- 5 to 25 m of coarse limestone from the Lutetian (marine),
- 30 m of marl from Lutetian (continental),
- 10 m of limestone and marlstone from the Bartonian and the Priabonian,
- a few meters of clay from the Rupelian

Within this succession of permeable (sand and coarse limestone) and deposits with low permability (clay and marl), only a few thin aquifers of limited extent can be developed with some springs flowing from the sand layers (Laurain et al., 1981). As a result, these aquifers are not able to provide enough quantity of water for local exploitation such as drinking water supply.

1.2.3. Quaternary

1.2.3.1. Graveluche

Graveluche refers to a periglacial formation with a maximum thickness of 6 to 10 m (Rouxel-David et al., 2002b). During the Quaternary, the long period of freeze-thaw alternation produced cryoturbation of the Chalk and movement in the terrain (Allouc et al., 1995). Graveluche, resulting from this gelifraction process of the chalk, is a mix of carbonate, clay and sand (Vernhet, 2007). This periglacial formation was formed on the North-East, East and South-East orientated slopes, which were more exposed to the freeze-thaw movements (Allouc et al., 1995). This could explain why this formation is more widely spread in the north (the catchment area of the Suippe River) than in the south of the study area (Figure II-3).

The particle size and mineral composition of the graveluche are very variable depending mainly on the topography. Generally, from top to bottom of the slope were observed the cryoturbated Chalk, the coarse graveluche and fine-grained graveluche with decreasing particle size and increasing clay content (Allouc et al., 1995).

1.2.3.2. Alluvium

Alluvium deposits are located in river valleys, composed mainly by sand, clay and gravel (Vernhet, 2007). Their thickness could reach about 10 m in maximum, with locally accumulated clay layers up to 5 m (Rouxel-David et al., 2002b). At the right bank of the Prosnes River, a large surface of alluvium formation (Figure II-3) implies a much larger extension of this river during the Quaternary (Rouxel-David et al., 2002b).

1.2.3.3. Colluvium

Colluvium is present mainly in dry valleys, with a thickness up to 3 m. They have substantially the same composition as the soils from which they formed, but a higher silt and clay content. The Tertiary formation at the Berru Mount generated a large surface of colluvium (clayey and non-calcareous) between the Berru Mount and the Vesle river, with a thickness of about 0.5 to 1 m (Rouxel-David et al., 2002b).

1.3. Hydrogeology

1.3.1. The unconfined Champagne Chalk aquifer

1.3.1.1. Aquifer description

The unconfined Champagne chalk aquifer is a crucial water resource of the region. It is the only resource used for drinking water and is also largely exploited for agricultural and industrial uses. The total porosity of the Chalk is here about 40% (Crampon et al., 1993), with only 1% related to the effective porosity (Vachier et al., 1987). This means that, on average, 1 m^3 of chalk contains about 400 L of water of which only 10 L can be mobilized. The Champagne Chalk aquifer is not homogeneous, and the availability of water is mainly a function of the Chalk fracturing, which decreases with depth and depends on the proximity of surface drainage valleys and paleo-valleys (cf. Part I.2.2.1). The fractured zone is considered to be the main reservoir of the Chalk aquifer, with an average thickness of 30 m on reliefs and 40 m in valleys (Rouxel-David et al., 2002b).

1.3.1.2. Hydrodynamic properties

The heterogeneous distribution of fracturing network results in a great spatial variation of permeability and storage yield (Table II-2). In the study area, the hydraulic conductivity could reach up to 10^{-2} $m \cdot s^{-1}$ near surface and decreases progressively to less than 10^{-7} $m \cdot s^{-1}$ beyond 40 m deep. The Champagne Mounts constitute the main reliefs where the specific yield ranges from 1% to 2%, while in river valleys these values are much higher, ranging from 3% to 5% (Allouc et al., 2000).

Table II-2 : Average values of hydrodynamic parameters (Allouc et al., 2000)

Location	Hydraulic conductivity ($m \cdot s^{-1}$)	Storage yield (%)
Relief	3×10^{-8} to 3×10^{-7}	1 to 2
Dry valley	3×10^{-7} to 3×10^{-5}	2 to 3
River valley	3×10^{-7} to 0.01	3 to 5

1.3.1.3. Groundwater flow

The study area is divided into two parts by the groundwater divide line across the summit of Berru Mount and the Champagne Mounts, which delimits the Vesle River watershed in the south and the Suippe River watershed in the north (Figure II-3). According to piezometry data of the study area (Rouxel-David et al., 2002a), the chalk aquifer is naturally drained by rivers and dry valleys.

In the UZ of the Champagne Chalk, the transfer velocity of water varies from 0.45 m·year^{-1} under cultivated fields to 0.75 m·year^{-1} under natural vegetation according to tracer studies using tritium (Vachier et al., 1987). Therefore, 90% of the exploitable groundwater in the next years are already in the Chalk aquifer (Rouxel-David et al., 2002b).

In the SZ, the groundwater flow flux can be calculated according to the Darcy's law:

$$V_{Darcy} = K \times i$$

With:

- K : hydraulic conductivity (m·s^{-1})
- i : hydraulic gradient

The hydraulic gradients (i) also vary significantly between reliefs and valleys, ranging from 15 ‰ on the slopes of the Champagne Mounts to about 1 ‰ in the Vesle river valley (Allouc et al., 2000). Assuming the hydraulic conductivity (K) values presented above (Table II-2), it is possible to calculate the Darcy flux in the SZ of the study area. The calculated flow flux varies between 0.16 m·year^{-1} on reliefs and 315 m·year^{-1} in river valleys.

1.3.2. Aquifer-river interactions

In the study area, the aquifer is naturally drained by rivers all along the year. However, groundwater exploitation could locally modify the flow direction, especially during the low water-level period. This is the case for pumping stations for drinking water supply (e.g., water catchment area of Couraux; Figure II-3) along the river bank (Figure II-4). As a result of drawdown of water table caused by intensive pumping, the aquifer is locally recharged by the river water. Therefore, the pumped water is composed of both groundwater from aquifer and river water. The proportion between these two inputs depends mainly on the pumping flow, the distance of the pumping station to the river bank and the permeability of the river bed (Moreau et al., 1985; Rouxel-David and Cordonnier, 2002).

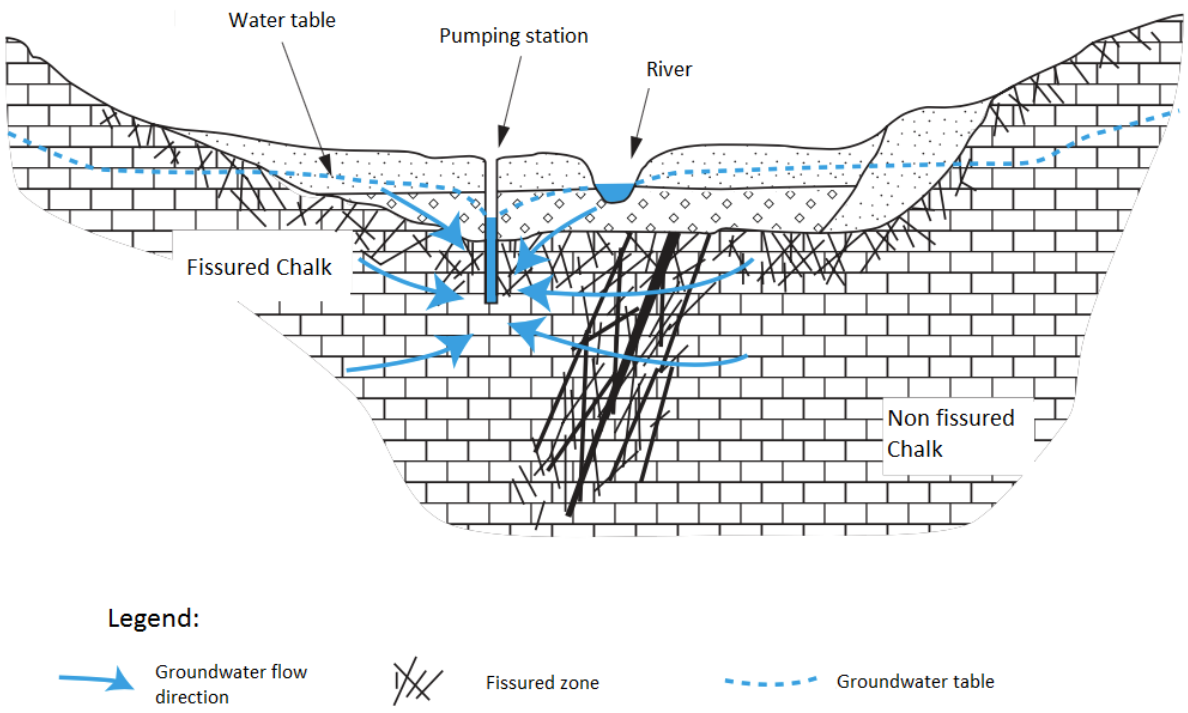

Figure II-4 : Influence of pumping on groundwater flow near the river (adopted from Rouxel-David and Cordonnier, 2002)

The Canal Aisne-Marne, which flows along the Vesle River (Figure II-3), also contributes to the recharge of the Vesle River and the Chalk aquifer. The quantity of leakage varies according to the season, which is much more important during the dry period when the canal banks dry out and fissured more (Moreau et al., 1985).

1.4. Climate

The temperature and precipitation data presented in this chapter come from the database of Météo-France (http://www.infoclimat.fr) and they originate from measurements at the Reims-Prunay weather station (Table II-3 : Description of Reims-Prunay weather station. This station is located in the southwestern part of the study area (Figure II-3) and the historical data between 2012 and 2019 allow to describe the climatic context of the area.

Table II-3 : Description of Reims-Prunay weather station

Station	Météo-France code	Coordinats			Altitude (m NGF)
		WGS84		Lambert 93 (m)	
Reims-Prunay	51449002	X	4°09'18''E	784129	95
		Y	49°12'30''N	6901715	

The precipitation constitutes the main recharge of the Champagne Chalk aquifer and represents the input signal of the hydrological system. According to data from Reims-Prunay station (Table II-4), the average annual rainfall is 566 mm In the study area, with a minimum value of 437 mm·year^{-1} in 2015 and a maximum value of 622 mm·year^{-1} in 2014. In general, it rains relatively regularly throughout the year without significant seasonality observed (Figure II-5 and Table II-4).

Table II-4 : Monthly and annual rainfall (2012-2019) at Reims-Prunay weather station

Year	Monthly rainfall (mm)												Annual rainfall (mm)
	Jan.	Feb.	Mar.	Apr.	May	Jun.	Jul.	Aug.	Sep.	Oct.	Nov.	Dec.	
2012	50	11	23	56	46	101	89	17	48	49	34	85	608
2013	23	22	25	31	114	56	62	35	39	60	69	57	594
2014	57	63	7	4	58	51	115	60	16	79	58	54	622
2015	53	38	28	32	24	14	15	74	66	30	45	19	437
2016	57	46	64	41	106	60	95	12	37	34	37	9	597
2017	28	36	44	3	36	75	59	61	97	29	63	53	583
2018	103	28	52	30	36	56	30	15	14	27	45	56	492
2019	37	41	34	20	71	46	15						
Average	51	36	35	27	61	57	60	39	45	44	50	47	553

Over the same period, the average annual atmospheric temperature is 11.1 °C, with the maximum value of 11.9°C reached in 2018 and the minimum value of 10.1 °C reached in 2013 (Table II-5). The month of July is the hottest with an average temperature of 19.7 °C and February the coldest with an average temperature of 3.7 °C (Figure II-5). The climate of the region is humid temperate oceanic with continental tendencies.

Table II-5 : Monthly and annual average atmospheric temperature (2012-2019), at Reims-Prunay weather station

Year	Monthly Average Temperature (°C)												Annual
	Jan.	Feb.	Mar.	Apr.	May	Jun.	Jul.	Aug.	Sep.	Oct.	Nov.	Dec.	average (°C)
2012	5	0,3	8,7	8,9	15,2	15,8	17,6	19,2	14,2	11,3	6,3	5,4	10,7
2013	2,3	1,4	3,4	9,4	11,4	15,8	20,6	18,1	15,1	13,1	6,1	4,5	10,1
2014	5,6	6,1	7,7	11,1	13,1	16,7	19,3	16,6	16,1	13,3	8,8	4,6	11,6
2015	3,5	3,4	6,6	10	12,7	17	20,1	19,9	14	10,5	9,8	8,4	11,3
2016	4,3	5,5	5,7	9	13,4	17,1	19	19	17,3	9,9	6,3	2,5	10,8
2017	0,2	5,9	8,9	8,6	17,5	18,6	19,6	18,5	14,3	12,6	6,1	5	11,3
2018	6,9	0,9	5,8	12,5	15,5	18,3	22	19,6	15,8	12,5	7,1	5,5	11,9
2019	2,9	5,8	8,4	9,8	11,6	18,3	19,7						
Average	3,8	3,7	6,9	9,9	13,8	17,2	19,7	18,7	15,3	11,9	7,2	5,1	11,1

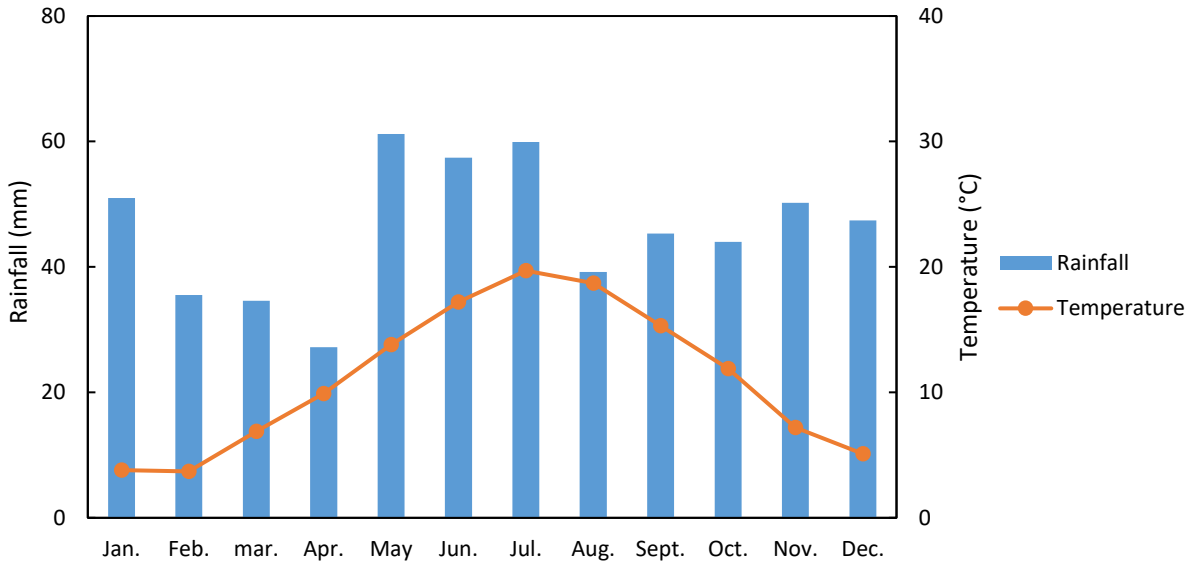

Figure II-5 : Monthly average temperature and rainfall at Reims-Prunay weather station (2012-2019)

1.5. Land use of the study area

The CORINE Land Cover (CLC) geographic database (https://www.statistiques.developpement-durable.gouv.fr/corine-land-cover-0), from which the data presented in this section are derived, is a biophysical inventory of land cover produced under the European Environment Information Coordination Program. The data come from the visual interpretation of satellite images with additional supporting data.

Land use of the study area can be divided into three major types (Figure II-6).

1) Agricultural: this type occupies the majority of the study area. The main crops are wheat, barley, sugar beet and alfalfa (Laurain et al. 1981). Vines are also cultivated with limited surfaces, mainly on slope of the Berru mount. In order to increase the agricultural production, fertilizers (especially nitrogen products) and pesticide are used, the residues of which could enter into the aquifer following infiltration.

2) Forest: this is the second major type of land use which covers in particular the Berru and Champagne Mounts and the riparian areas, representing about 15% of the surface of the study area.

3) Anthropic: this category mainly includes cities, villages and industrial sites, representing about only 3% of the area of the sector. The Moronvilliers military camp is located on the Champagne Mounts (Figure II-6). This military camp was used as ammunition destruction grounds after the WWI. In 1957, a nuclear experimental center attached to the Atomic Energy Comision (CEA) was established on this sector. On this center (also called the Moronvilliers Experimental Polygon), detonation tests for the development of nuclear bombs have been carried out since 1958 (Hubert, 2005). The CEA used various radioactive products during its experiments, such as beryllium, depleted uranium, and tritium. Non-radioactive substances were also used including lead and other chemical explosives whose composition was not detailed. A large landfill site (Veolia Onyx Est) is also situated in middle of the study area, west of the Moronvilliers military camp. A small waste deposit site is located in the west of the landfill (Figure II-6).

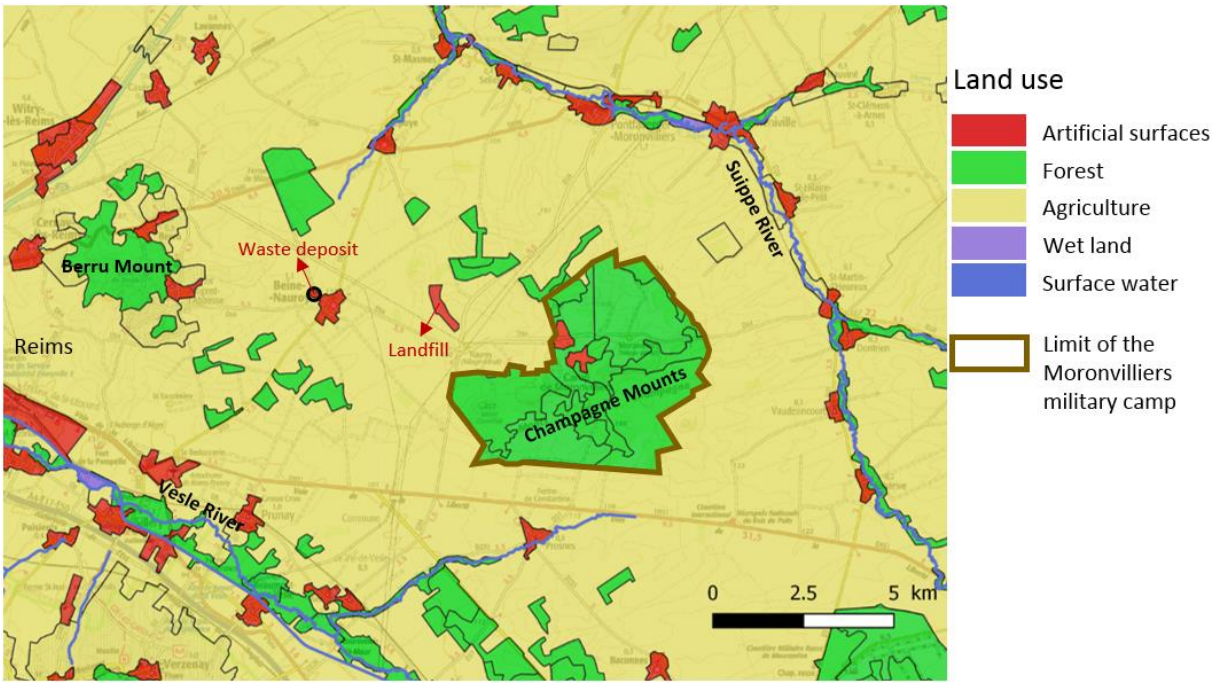

Figure II-6 : Land use information in the study area (data from the CORINE Land Cover database)

2. Sampling and analytical methods

2.1. Methodology of research

A methodology that combined various approaches / tools was applied in this study (Figure II-7). In order to study the sources and behaviors of ClO_4^- ions in the unconfined Chalk aquifer, a continuous monitoring of the groundwater hydrogeochemistry for two years was performed in the study area. An intensive sampling network consisting of 36 sampling points was established.

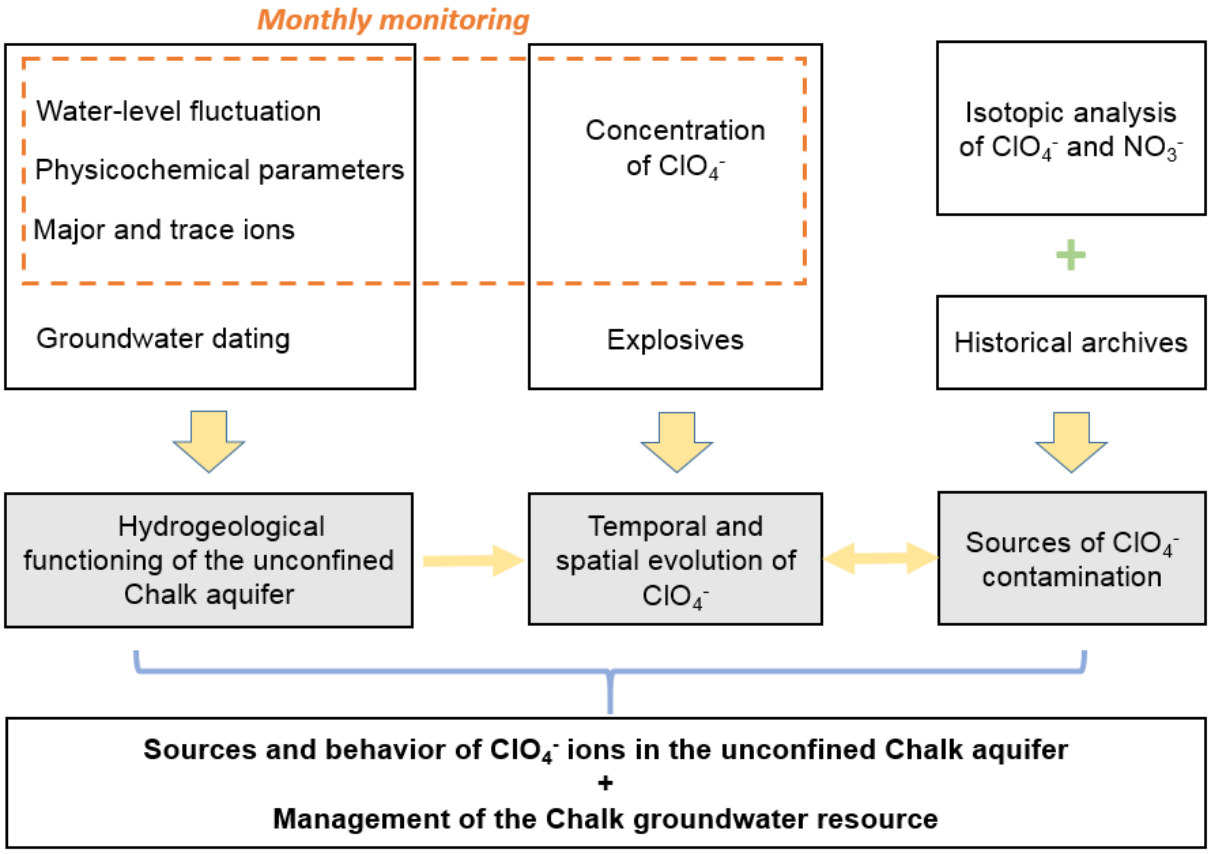

Figure II-7 : Methodology of research and different approaches used in the study

Concentration of ClO_4^- in groundwater was monitored monthly during two hydrological cycles (2017-2019), with the aim to observe its temporal and spatial evolution in the aquifer. Explosives, which could possibly coexist with ClO_4^- were also analyzed. Due to the high solubility and stability of ClO_4^- in water, the migration of ClO_4^- ions follows essentially the flow of groundwater. Therefore, the knowledge about water flow paths and aquifer properties are fundamental prerequisites for understanding the observed evolution of ClO_4^- ions in time and space and predicting the future of contamination. Also, the knowledge of the functioning of this aquifer is essential for the management of groundwater source in the region of Champagne-Ardenne.

To acquire the knowledge of hydrogeological functioning of the unconfined Chalk aquifers, a methodology based on a combination of hydrodynamic, hydrochemistry and groundwater dating tools was developed. Based on the established sampling network in the study area, groundwater level fluctuations and chemical compositions (major ions concentrations) were monitored monthly during two years (2017-2019), allowing to clarify the hydrodynamic and geochemical properties as well as the recharge pathways of the unconfined Champagne Chalk aquifer. Groundwater residence times were also estimated, using multi-tracers including CFCs, SF_6 and ^3H. The combination of these approaches provides a comprehensive understanding of the Chalk aquifer functioning so that a conceptual model of groundwater flow can be proposed. The observed spatio-temporal evolution of ClO_4^- contamination was then interpreted with properties of the aquifer, especially by exploring the relationship with water level fluctuation and groundwater residence time.

In parallel, isotopic analysis of ClO_4^- in water samples collected in the study area was performed. This method allowed to distinguish the origin of ClO_4^-: synthetic and/or natural ClO_4^-. ClO_4^- isotopic analysis was also performed for water samples collected from sites concerned with "pure" military or agricultural contamination. The "pure" isotopic signature was compared with isotopic data measured in the study area to confirm the source of ClO_4^- contamination. Isotopic analysis of NO_3^- was also performed to identify the presence of the traces of Chilean nitrates utilization. In addition, researches in historical archives were performed, providing information on historical activities and sites (e.g. WWI, uses of Chilean nitrates, industrial activities) potentially emitting ClO_4^-. Because they are necessary to understand the historical context of the study area, the results of historical investigations have even been presented in the previous part. Nevertheless, they are an essential part of this work. This information, together with the observed evolution of ClO_4^- and the Chalk aquifer functioning allowed to identify the diffuse and/or punctual sources in the study area, to quantify the source of contamination and to estimate the future evolution of ClO_4^- concentrations in the unconfined aquifer in a short or medium term.

2.2. Sampling locations

In order to study the hydrogeological functioning of the unconfined Chalk aquifer and the origin and behavior of ClO_4^- in groundwater, an intensive sampling network was established in the study area. The first step of the selection of sampling points was the collect of information on available boreholes/wells in the study area from the Infoterre database (http://infoterre.brgm.fr). Over 300 boreholes/wells were spread over the study area, including irrigation boreholes, pumping stations for drinking water supply, industrial boreholes and boreholes for public service, domestic use, heating, etc. A first selection was performed by eliminating closed, abandoned and inaccessible boreholes (geothermal drilling, fire extinguishing, etc.). Then, a second selection was made following several field visits. During the field visit, the location, condition and accessibility of the boreholes were confirmed. Finally, 26 groundwater points with easy accessibility and well distributed over the study area were selected, including 19 boreholes, 3 pumping stations for drinking water supply and 4 springs (Figure II-8; Table II-6). The boreholes and pumping stations have long screen depths which cover at least half of the well depths (Table II-6), thus providing a weighted average of groundwater.

Considering the hydrogeological context of the study area, surface water is here tightly related to groundwater of the Chalk aquifer. In order to take into account the aquifer-river relationships, 10 surface water sampling points were also selected in the Aisne-Marne Canal, Vesle River, Suippe River and their tributaries (Figure II-8; Table II-6). In total, 36 sampling points were selected, forming the monitoring network of this study.

A first screening campaign was carried out in June 2017, which allowed to obtain a chemical map of the study area, especially the situation of perchlorate contamination. 15 sampling points (primarily points with high concentrations of perchlorate, spatially well distributed) were then selected for monthly monitoring over the next two years to observe the spatial and temporal evolution of groundwater geochemistry (Figure II-8; Table II-6). From June 2017 to June 2019, 21 sampling campaigns were carried out at these 15 points. In addition, 4 large sampling campaigns which covered the majority of the 39 sampling points were carried out in June 2017, September 2017, October 2018 (low water level) and March 2019 (high water level) with possibly additional sampling at some points (Table II-6).

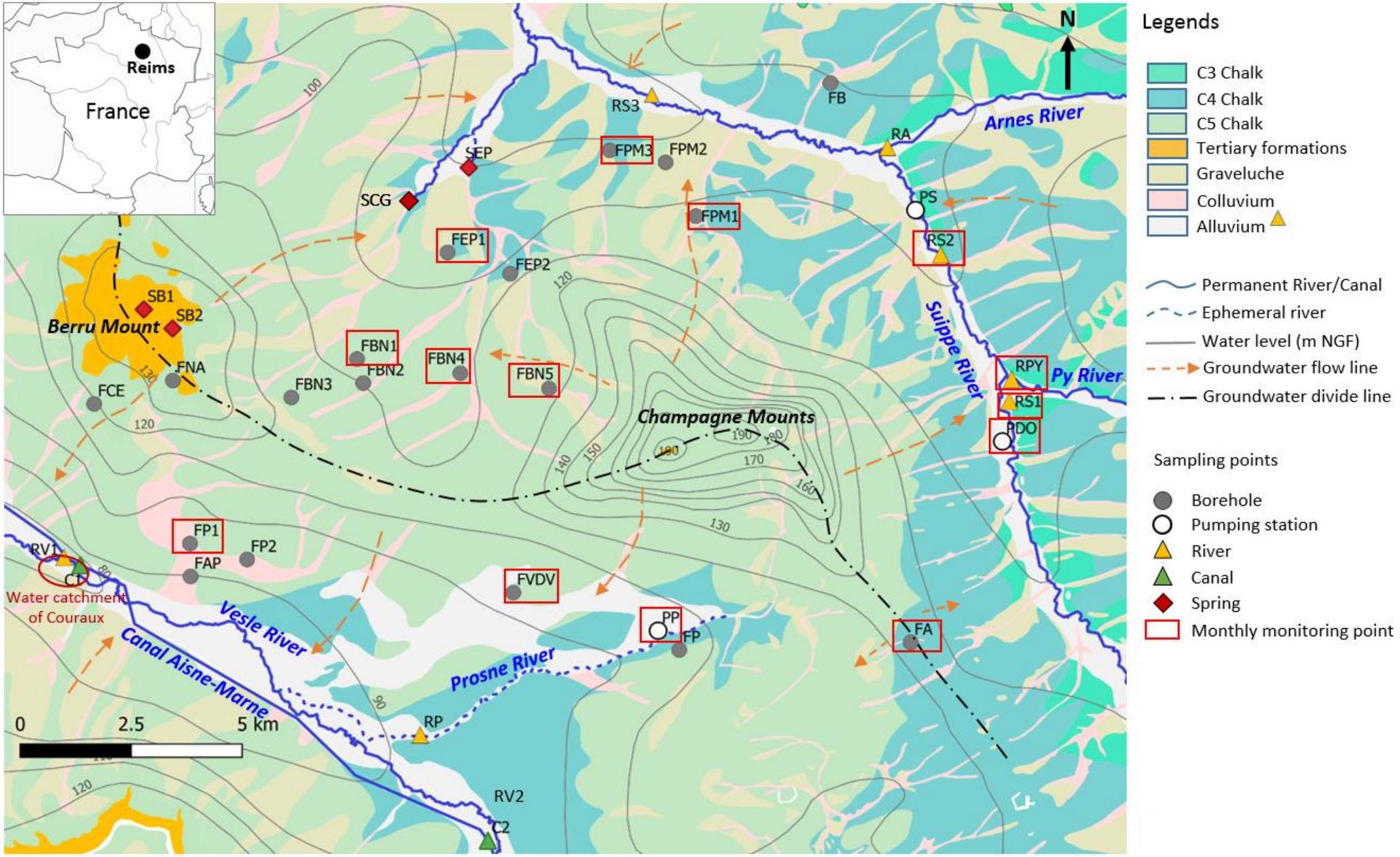

Figure II-8 : Location of the sampling points in the study area

Table II-6 : Properties of the sampling points, sampling frequency and analysis realized (N/A = Not Available; routine analysis including major/trace ions; ClO_4^-)

**The borehole FBN1 is no longer available on the database of Inforterre, therefore the old N°BSS is used.*

Name	Type	N°BSS	Town	Latitude (°N)	Longitude (°E)	Altitude (m NGF)	Depth (m)	Screen depth (m)	Water level logger	Groundwater dating	ClO_4^- isotopic analysis	Nb of routine analysis
FAP	Borehole	BSS000KGEM	Prunay	49,20634	4,15561	89,5	15	6,5 - 15	P / T / EC	2	N	21
FP1	Borehole	BSS000KGDP	Prunay	49,21308	4,15558	95	19	9 - 15	P / T	2	N	21
FBN1	Borehole	01323X0069	Beine-Nauroy	49,25048	4,20809	134	48	4 - 48	P / T	2	N	21
FBN4	Borehole	BSS000KFHS	Beine-Nauroy	49,24725	4,23997	111	28	16 - 28	P / T	2	2	21
FBN5	Borehole	BSS000KFHT	Beine-Nauroy	49,24383	4,26732	140	47	24 - 43	P / T / EC	2	N	21
FEP1	Borehole	BSS000KFKY	Epoye	49,27210	4,23658	107	25	7 - 25	P / T	2	N	21
FPM1	Borehole	BSS000KFHN	Ponfaverger-Moronvilliers	49,27875	4,31364	107	24	N/A	P / T	2	N	21
FPM3	Borehole	BSS000KFLB	Ponfaverger-Moronvilliers	49,29255	4,28730	103	21	7 - 21	P / T	2	N	21
FVDV	Borehole	BSS000KGJZ	Val-de-Vesle	49,20202	4,25525	107	22	12,5 - 20,5	P / T	2	1	21
FA	Borehole	BSS000KGWT	Aubérive	49,19046	4,37777	123	35	3,5 - 30	P / T	2	N	21
PP	Pumping station	BSS000KGJC	Prosnes	49,19371	4,29981	110	80	23 - 80	N	2	N	21
PDO	Pumping station	BSS000KGQX	Dontrien	49,23141	4,40722	111	25	7 - 25	N	2	N	21
FCE	Borehole	BSS000KEYU	Cernay-les-Reims	49,24205	4,12656	175	85	N/A	N	N	N	1
FNA	Borehole	BSS000KFDV	Nogent-l'Abbesse	49,24661	4,15105	165	47	N/A	N	N	N	1
FBN3	Borehole	BSS000KFEQ	Beine-Nauroy	49,24280	4,18759	124,9	56	12 - 56	N	N	N	3
FBN2	Borehole	BSS000KFGP	Beine-Nauroy	49,24554	4,20989	122	32	10 - 32	N	N	N	4
FEP2	Borehole	BSS000KFKZ	Beine-Nauroy	49,26752	4,25589	107	23	N/A	N	N	N	6
FPM2	Borehole	BSS000KFLC	Ponfaverger-Moronvilliers	49,28990	4,30454	121	35	N/A	N	N	N	5
FP2	Borehole	BSS000KGET	Prunay	49,20966	4,17316	97	21	N/A	N	N	N	4
FP	Borehole	BSS000KGLG	Prosnes	49,18969	4,30624	116	23	7 – 22,5	N	N	N	4
FB	Borehole	BSS000KGND	Betheniville	49,30563	4,35599	98	33	N/A	N	N	N	1
PS	Pumping station	BSS000KGPF	Betheniville	49,27923	4,38166	98,5	16	7 - 16	N	N	N	4
SEP	Spring	BSS000KFGV	Epoye	49,28945	4,24359	92			N	N	N	7
SCG	Spring	BSS000KFEE	Epoye	49,28196	4,22426	94			N	N	N	2
SB2	Spring	BSS000KFDW	Nogent-l'Abbesse	49,25732	4,15116	216			N	N	N	1

SB1	Spring	BSS000KFDY	Berru	49,26133	4,14238	225	N	N	N	1
RS1	River	-	Dontrien	49,20934	4,38269		N	N	N	21
RPY	River	-	Dontrien	49,29687	4,39348		N	N	1	21
RS2	River	-	St-Hilaire-le-Petit	49,28406	4,37468		N	N	N	21
RA	River	-	Betheniville	49,29139	4,37188		N	N	N	4
RS3	River	-	St-Masmes	49,29215	4,36657		N	N	N	4
RV1	River	-	Puisieulx	49,19397	4,36776		N	N	N	3
RV2	River	-	Sept-Saulx	49,19762	4,40498		N	N	N	3
RP	River	-	Thuisy	49,19469	4,34720		N	N	N	1
C1	Canal	-	Puisieulx	49,22109	4,40568		N	N	N	1
C2	Canal	-	Sept-Saulx	49,21219	4,40051		N	N	N	1

2.3. In-situ measurement, sampling and analytical methods

2.3.1. In-situ monitoring: water level, temperature and conductivity

From December 2017, the groundwater level and temperature were recorded hourly in 9 unexploited boreholes (Table II-6) using pressure sensors (In-Situ Rugged TROLL 100 Water Level Logger). The water level in boreholes was calculated by barometric compensation, associated with the atmospheric pressure sensor installed at the FAP station (Reims-Prunay aerodrome).

According to the data obtained by in-situ water loggers, the water level of 2 boreholes (FAP and FBN5, Table II-6) seemed to react much faster than the other holes following the rainy events. In order to better understand the behavior of the Chalk aquifer at these two sites, the in-situ water loggers were replaced by the CTD-DIVER water loggers (Schlumberger Water Services) to monitor additionally hourly electrical conductivity (EC) besides the groundwater level and temperature.

The accuracy of measurement for the two water loggers are detailed in Table II-7.

Table II-7 : Accuracy of measurement of In-situ Rugged TROLL 100 Water Level Logger and CTD-DIVER water logger

	Pressure	Temperature	Electrical conductivity
In-situ Rugged TROLL 100	±0.05% of reading	±0.3°C	-
CTD-DIVER	±0.05% of reading	±0.1°C	±1% of reading

2.3.2. Well logging and camera inspection

The information on the monitoring boreholes is incomplete and limited in the Infoterre database (http://www.infoterre.brgm.fr), particularly with regard to the condition of the casing, the screen depth and the physicochemical data. These information are essential for a better understanding of the flow patterns and geochemistry of groundwater in the aquifer. Consequently, additional investigations were carried out in August 2018 within the 9 unexploited boreholes:

- *in-situ* camera inspection to check the status and geometry of the boreholes;
- well-logging to continuously record the physicochemical parameters (temperature, redox potential, dissolved oxygen, pH, electrical conductivity and chloride) through the whole depth of water column. The sensors used for well-logging were IDRONAUT OCEAN SEVEN 303Plus and IDRONAUT OCEAN SEVEN 316Plus.

In each borehole, the well logging was made without pumping, then the inspection camera was passed. In case of high turbidity of water resulting in a very low visibility in the borehole, the camera was passed after a pumping (sometimes during the pumping).

2.3.3. River flow measurement

Water flow in the Suippe River and its tributaries were determined by the cross-section method, which refers to measuring the water depth and velocity at a series of points in a cross-section of the river.

River water velocity was measured using an OTT C2 Small Current Meter. By multiplying the cross-sectional area (width of section × water depth) by the velocity, the water flow of this section of river can be calculated. The water flow of each section was added to determine the total water flow of the river.

2.3.4. Monthly monitoring of groundwater geochemistry

The monthly monitoring of groundwater flow and geochemistry were realized from June 2017 to June 2019 during two complete hydrological cycles. Groundwater from unexploited boreholes were taken by a submerged pump (Grundfos MP1). During pumping, physicochemical parameters (pH, temperature, electrical conductivity and redox potential) were measured. Groundwater samples were collected only when the physicochemical parameters had stabilized. For the exploited boreholes, water samples were collected directly at the tap. Spring and river waters were sampled directly at emergence or in streams.

All collected water samples were analyzed to determine the content of major ions (Ca^{2+}, Mg^{2+}, Na^{+}, K^{+}, Cl^{-}, NO_3^{-}, SO_4^{2-} et HCO_3^{-}) and trace elements (Al, As, Cd, Co, Cr, Cu, Fe, Mn, Ni, Pb, Sb, Sr, Zn), perchlorate.

2.3.4.1. Physical and chemical parameters

Instrument used in the field for *in situ* measurements of physicochemical parameters are:

1) Alkalinity digital titrimeter: HACH AL-DT. In the context of Chalk groundwater, the concentration of CO_3^{2-} is usually negligible and the alkalinity is assimilated to the concentration of HCO_3^{-}.
2) Multi-parameter WTW 3320:
    - pH / temperature meter: pH SenTix 41
    - redox potential meter: SenTix ORP
    - conductivity meter: TétraCon 325

2.3.4.2. Major and trace elements

Water samples for analysis of major elements (Ca^{2+}, Mg^{2+}, Na^{+}, K^{+}, NO_3^{-}, SO_4^{2-}, Cl^{-}) and trace elements (Cu, Fe, Mn, Zn, Al, As, Pb, Cr, Co, Cd, Sb) were collected in two 50 ml polyethylene bottles after filtration through 0.45 µm membranes and acidification with nitric acid for cation analysis, and then stored at 4°C before analysis.

The major cations and trace elements were measured in the GEGENAA laboratory (University of Reims Champagne-Ardenne, Reims) by optical emission spectrometry coupled to ICP (ICAP 6300, THERMO). For each analysis, triplicate measurements were realized, and the average value was calculated as the final result. The anions were measured at GEGENAA and at the University of Corsica by ion chromatography for a small number (DIONEX ICS 2000). The quality of the analysis is controlled by calculating the ion balance. Analyzes with a balance greater than 10% were rejected and the analysis was then redone. The majority of the analytical results in this study show a balance of less than 5%.

2.3.4.3. Perchlorate

For analysis of perchlorate, raw water without filtration was collected in 100 ml polyethylene bottles and stored at 4°C before analysis. Analyzes were carried out at BRGM (Orléans) by ion chromatography (DIONEX ICS 2000).

2.3.5. Explosives

Analyze of explosives in water samples collected from all the 36 sampling points in the study area was realized once on June 2017. Water samples were collected in 1L amber glass bottles and then stored at 4°C before analysis.

The analysis of 39 explosives (see Table II-8) was performed by the company Envilytix GmbH (Wiesbaden, Germany) with an RPHPLC- DAD system. The analytes in water samples were identified by comparison with the retention times and the UV/Vis spectra of commercially available or synthesized reference compounds. The quantitation was carried out by linear calibration curves (r^2 >0.98) recorded for all these compounds (Bausinger et al., 2007).

Table II-8 : List of explosives analyzed in water sample

No.	Compound	Limit of quantification in water ($\mu g \cdot L^{-1}$)
1	2-Amino-4,6-dinitrotoluene	0,10
2	4-Amino-2,6-dinitrotoluene	0,10
3	3,5-Dinitroaniline	0,10
4	2,4-Dinitrotoluene	0,10
5	2,6-Dinitrotoluene	0,10
6	1,3,5-Trinitrobenzene	0,10
7	2,4,6-Trinitrotoluene	0,10
8	1,2-Dinitrobenzene	0,10
9	1,3-Dinitrobenzene	0,10
10	2-Nitroaniline	0,10
11	3-Nitroaniline	0,10
12	1-Nitronaphthalene	0,10
13	2-Nitronaphthalene	0,10
14	1,3-Dinitronaphthalene	0,10
15	1,5-Dinitronaphthalene	0,10
16	1,8-Dinitronaphthalene	0,10
17	1,3,5-Trinitronaphthalene	0,10
18	1,3,8-Trinitronaphthalene	0,10
19	1,4,5-Trinitronaphthalene	0,10
20	Hexogen	0,10
21	Octogen	0,10
22	Tetryl	0,10
23	PETN	0,25
24	Akardit 1	0,10
25	Akardit 2	0,10
26	Centralit 1	0,10
27	Centralit 2	0,10
28	Diphenylamine	0,10
29	2-Amino-4,6-dinitrobenzoic acid	0,10
30	4-Amino-2,6-dinitrobenzoic acid	0,10
31	2,4-Dinitrobenzoic acid	0,10
32	2,6-Dinitrobenzoic acid	0,10
33	2-Nitrophenol	0,10
34	3-Nitrophenol	0,10
35	4-Nitrophenol	0,10
36	2,4-Dinitrophenol	0,10
37	2,6-Dinitrophenol	0,10
38	2,4,6-Trinitrophenol	0,10
39	2,4,6-Trinitrobenzoic acid	0,10

2.3.6. Groundwater dating using CFCs, SF_6 and tritium

Two sampling campaigns for groundwater dating using CFCs and SF_6 were carried out in May 2018 (high water level) and October 2018 (low water level). Waters for CFCs and SF_6 analysis were collected in stainless-steel ampoules after washing through at least three volumes of the ampoule, without any atmospheric contact during sampling to avoid contamination. Waters for noble gases analysis were sampled in 500 mL glass flasks. The bottles were submerged in flowing water, flushed, and capped without headspace to avoid air bubbles.

Analyses of CFCs, SF_6 and noble gases were performed at the Geosciences Laboratory of the University of Rennes 1. CFCs and SF_6 concentrations in water samples were measured by gas chromatography with an electron capture detector after pre-concentration by a "purge and trap" method, described by Aquilina et al. (2006) and Vergnaud-Ayraud et al. (2008). The analytical uncertainty is about 1-3% for CFCs and 5% for SF_6. Noble gases (Ar, Ne) were measured using a micro-gas chromatograph (GC 3000, SRA instruments) with an uncertainty of about 3% for Ne and less than 2% for Ar (Aquilina et al., 2006; Vergnaud-Ayraud et al., 2008). The concentrations of noble gases were used to estimate recharge temperature and excess air contribution, which are essential for determining the solubility of CFCs and SF_6 in Henry's law.

The sampling campaigns for groundwater dating using tritium was carried out in May 2019. Water samples were collected in 1L glass flasks. Analyses of tritium was performed at the laboratory of HYDROSYS LABOR in Budapest, Hungary. The tritium analysis procedure is based on the principal of selective isotopic enrichment using electrolysis. The volume of the water samples was reduced from 250 ml / 800 ml to 14 - 15 ml by electrolytic enrichment. The tritium activity of enriched water samples was counted by liquid scintillation analyzer (LD> 0.2 TU). In view of the enrichment and measurement parameters, the tritium concentration in the original water sample was calculated with customized software (http://www.hydrosyslabor.hu/services.html).

2.3.7. Perchlorate isotopic analysis

In order to discriminate perchlorate sources (natural and/or synthetic), 5 sampling campaigns for isotopic analyzes of perchlorates were carried out in the study area at the following monitoring sites: FBN4 (on high water level and low water level), FVDV, P6 (water catchment of Couraux) and PY (Py river). One sampling campaign was carried out outside the study area, near the Suippes Military camp (RM; Figure I-4) in order to obtain a "pure military isotopic signature" of perchlorate.

A minimum of 10 mg of perchlorate is required to perform the isotopic analysis of perchlorate. Water samples were collected using columns containing perchlorate specific ion exchange resin (IX resin). The recommended flow rates through the column is 0.5 – 2 $L \cdot min^{-1}$. As a result, the minimum volume of water required is 1,000 L for a sample concentration of 10 ppb perchlorate, requiring at least 8 hours of flow. Before entering the ion exchange (IX) columns, a pre-filtration of water is necessary. In practice, a system consisting of a 20 µm filter cartridge and then a 5 µm filter cartridge was installed between the pump outlet and the column (Figure II-9). The flow rate and the physicochemical parameters were checked every 20 minutes (at exit 2) and the filter cartridges were changed every 2 hours in order to avoid clogging. After sampling, the columns were stored at 4 °C before analysis.

The extraction and purification of ClO_4^- was done in the Department of Civil and Environmental Engineering of Texas Tech University (USA) and the key steps were summarized as follows: 1) the resin was washed by deionized water and flushed with 4M HCl to remove NO_3^-, SO_4^{2-}, HCO_3^- and organics; 2) the absorbed ClO_4^- was eluted from the IX resin using a solution of 1M $FeCl_3$ and 4M HCl (Gu et al., 2007, 2001; Gu and Brown, 2006); 3) eluted ClO_4^- was purified by a series of precipitation, liquid-liquid extraction, evaporation, cation exchange processes and crystallized as a ClO_4^- salt for isotopic analysis.

The relative abundances of stable isotopes of chlorine (^{37}Cl and ^{35}Cl) and oxygen (^{18}O, ^{17}O and ^{16}O) in ClO_4^- were measured using isotope mass spectrometry (IRMS) at the Environmental Isotope Geochemistry Laboratory at University of Delaware (USA).

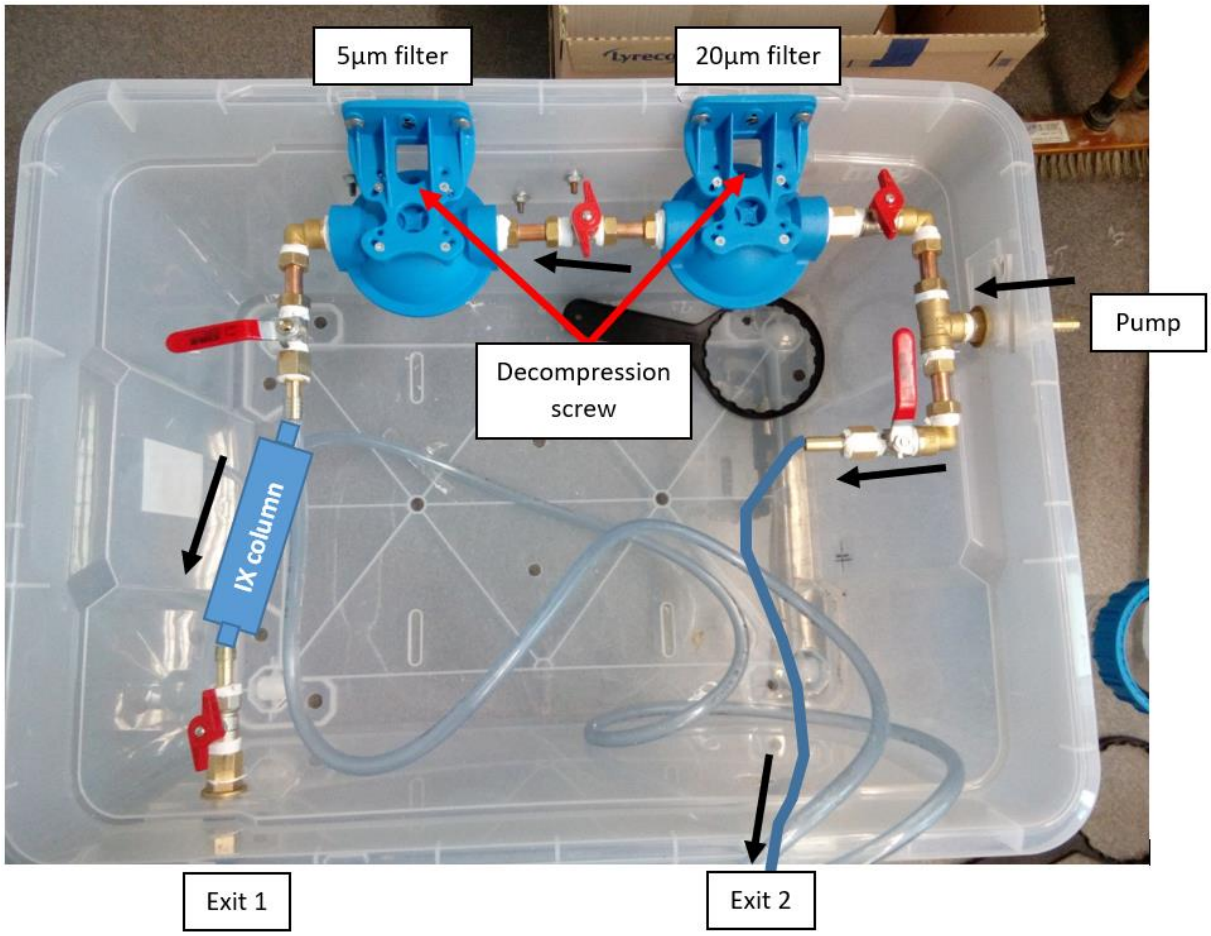

Figure II-9 : Sampling system for perchlorate isotopic analysis with pre-filtration (5µm filter and 20 µm filter cartridge)

2.3.8. Nitrate isotopic analysis

For isotopic analysis of NO_3^-, water samples were collected in 100-mL polyethylene bottles after filtration through 0.45 µm membranes. Nitrogen and oxygen isotope ratios were measured using an automated denitrifier method as described in Morin et al. (2009) and Savarino et al. (2013). This technique uses *Pseudomonas aureofaciens* bacteria to convert NO_3^- to N_2O, which is then analyzed for its isotopic composition after thermal decomposition to O_2 and N_2. Isotopic analysis was performed on a Thermo Finnigan MAT253 equipped with a gas-bench interface at the Laboratoire de Glaciologie et Géophysique de l'Environnement at the University of Joseph Fourier Grenoble (France).

Part III. Characterization of the functioning of the unconfined Champagne Chalk aquifer

This part presents the results regarding the hydrogeological functioning of the unconfined Champagne Chalk aquifer, which are essential for the study of perchlorate contamination and the management of groundwater source of the region.

In chapter 1, the estimation of effective rainfall using the water balance method and the results of *in situ* continuous monitoring of groundwater level, temperature and EC are presented. The hourly data obtained for two years allows to study precisely the response of the Chalk aquifer following precipitation and exploitation activities. In chapter 2, principles and results of groundwater dating using ^{3}H, CFCs and SF_6 are detailed. The estimated apparent ages with the related mixing models (piston flow, the binary or exponential mixing) allow to provide important information regarding mixing process and flow mechanisms within the aquifer. In chapter 3, the temporal and spatial variation of major and trace elements is presented. The origins of the major ions in groundwater are discussed. The observed spatial and temporal variation of groundwater geochemistry is presented and interpreted by a combination of hydrogeological setting, residence time and land use. A conceptual model is proposed in chapter 4 to explain the hydrogeological functioning of unconfined Chalk aquifers.

The results presented in Part III has been published in "Journal of Hydrology" with the following reference:

Cao, F., Jaunat, J., Vergnaud-Ayraud, V., Devau, N., Labasque, T., Guillou, A., Guillaneuf, A., Hubert, J., Aquilina, L., Ollivier, P., 2020. Heterogeneous behavior of unconfined Chalk aquifers infer from combination of groundwater residence time, hydrochemistry and hydrodynamic tools. Journal of Hydrology 581, 124433. https://doi.org/10.1016/j.jhydrol.2019.124433.

The complete version of this article can be found in Appendix 2.

Journal of Hydrology 581 (2020) 124433

Contents lists available at ScienceDirect

Journal of Hydrology

journal homepage: www.elsevier.com/locate/jhydrol

Research papers

Heterogeneous behaviour of unconfined Chalk aquifers infer from combination of groundwater residence time, hydrochemistry and hydrodynamic tools

Feifei Cao[a,*], Jessy Jaunat[a], Virginie Vergnaud-Ayraud[b], Nicolas Devau[c], Thierry Labasque[b], Aurélie Guillou[b], Alexandra Guillaneuf[a], Julien Hubert[a], Luc Aquilina[b], Patrick Ollivier[c]

[a] Université de Reims Champagne-Ardenne – GEGENAA – EA 3795, 2 esplanade Roland Garros, 51100 Reims, France
[b] OSUR, Géosciences Rennes, UMR 6118, CNRS/Université Rennes-1, F-35042 Rennes, France
[c] BRGM, 3 av. C. Guillemin, BP 36009, 45060 Orléans Cedex 2, France

ARTICLE INFO

This manuscript was handled by Huaming Guo, Editor-in-Chief

Keywords:
Chalk aquifer
Groundwater age
Water level
Geochemistry variability
Water resource
Unsaturated zone

ABSTRACT

Chalk groundwater is an important aquifer resource. It is intensively exploited for human use, with a large proportion utilized for drinking water. The improvement of the knowledge on Chalk aquifer hydrogeological functioning is essential for the management of this resource. Here, we developed a methodology based on a combination of hydrodynamic, hydrochemistry and groundwater dating tools. A study site with Chalk outcrops was selected in NE France where groundwater geochemistry and water level were monitored continuously for 2 years from 2017 to 2019 and groundwater residence time was estimated using CFCs and SF_6. Overall, the aquifer has an inertial behaviour with respect to recharge. Nevertheless, a rapid water level response following rainfall events was observed at one site, suggesting the presence of highly developed fracture network at the local scale. According to the mixing process (piston flow, exponential or binary mixing) defined at each sampling site, groundwater dating indicated rather heterogeneous ages ranging from modern to about 50 years. High spatial and temporal heterogeneities were observed and interpreted by a combination of hydrogeological setting, residence time and land use information, highlighting main factors governing the Chalk groundwater geochemistry including water level fluctuation, thickness of the Unsaturated Zone (UZ), superficial formations, distribution of fracture network, aquifer-river relations and human activities. A conceptual model was proposed accordingly to explain the hydrogeological functioning of unconfined Chalk aquifers.

1. Response of the unconfined Champagne Chalk aquifer to recharge

1.1. Aquifer recharge: estimation of effective rainfall

The precipitation (wet) is considered as the input signal of the aquifer. However, not all the water of the precipitation can participate in the recharge of groundwater: a significant part of precipitation may leave the hydrosystem by evapotranspiration and / or by runoff (Figure III-1). Only a reduced portion infiltrates through the UZ to the water table, increasing the quantity of water stored in the aquifer. The amount of rainfall remaining after evapotranspiration which is available for both runoff and groundwater recharge is defined as effective rainfall (ER) (Hiscock, 2009).

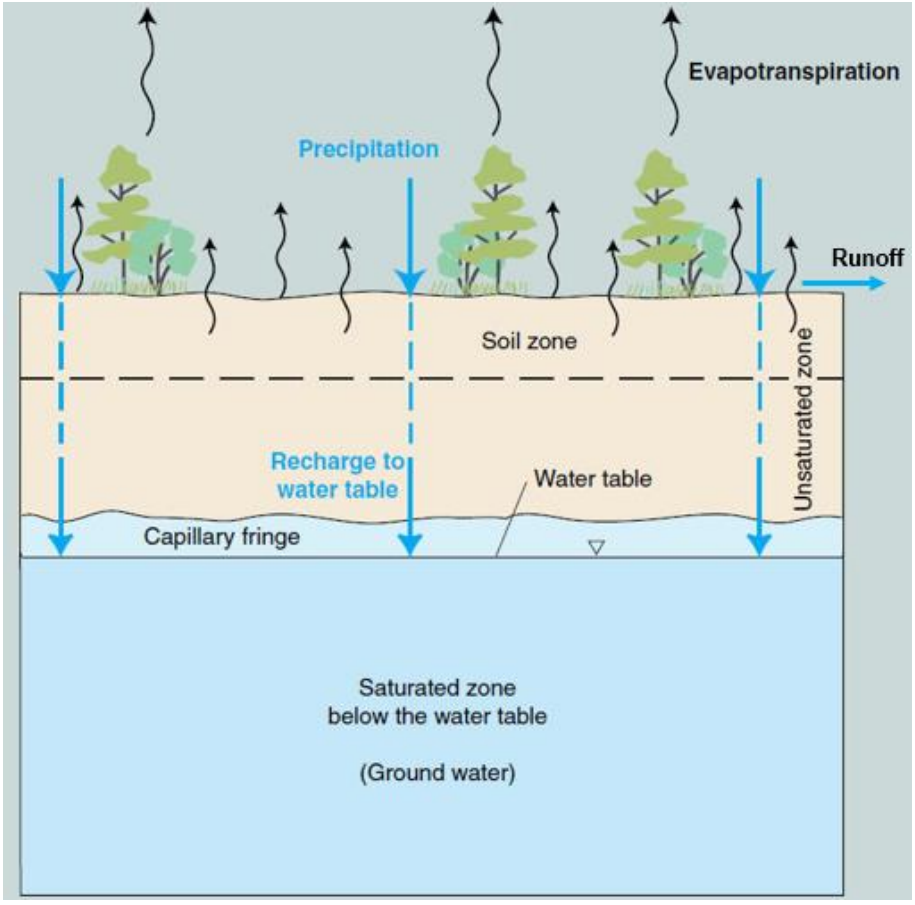

Figure III-1 : Basic visualization of field-scale water cycle (according to https://www.usgs.gov/special-topic/water-science-school/science/groundwater-storage-and-water-cycle)

1.1.1. Water balance method

The effective rainfall was estimated by a method based on the water balance in this study. At the aquifer scale, the water balance can be described as following:

$$P = ER + AET + \Delta S$$

With:

- P: precipitation (total rainfall)
- ER: effective rainfall, which includes the net recharge of aquifer and runoff
- AET: actual evapotranspiration
- ΔS: change in soil water reserve

On unconfined Chalk aquifers, the surface runoff is usually considered as very low (less than 5%) or absent (Chiesi, 1993; Foster, 1975; Mathias et al., 2006). A zero runoff is assumed for the Champagne Chalk aquifer in this study. Therefore, the ER is approximately equal to the recharge of aquifer and can be calculated as following:

$$ER = P - AET - \Delta S$$

The parameters of actual evapotranspiration (AET) and change in soil water reserve (ΔS) cannot be measured directly. Thornthwaite (1948) proposed a method to evaluate the AET and ΔS therefore to determine the ER based on the precipitation (P), the potential evapotranspiration (PET, the potential amount of water that would transpire and evaporate if a sufficient water source was available) and the available water capacity of the soil (AWC, the maximum amount of plant available water a soil can provide). The Thornthwaite method describes the following principles:

If P > PET, then:

- AET = PET
- The excess precipitation (P – PET) first replenishes the soil water reserve and then recharges the aquifer (ER) when the AWC is attained.

If P < PET, then:

- All precipitation is evaporated, the difference between PET and P (PET – P) is drawn from the soil until the AWC is depleted. In this case, the ER equals to zero.

Successive improvements to the Thornthwaite method have been proposed, notably to introduce a progressive emptying of the soil water reserve (e.g., Ahlvin and Smoots, 1988; Carrega, 2013; Dingman, 2002; Liu et al., 2005). In fact, unlike the process of the filling of soil water reserve by rainfalls, the process of emptying is much more progressive. This means that over a certain period of time (daily steps used in this study), only a part of the soil water reserve would be used for the satisfaction of evapotranspiration excess over precipitation. Dingman (2002) proposed a refined formulation to calculate how the soil water reserve is emptied using a decreasing exponential function:

$$\Delta S = S_i - S_{i-1} = S_{i-1} \times (1 - e^{\frac{PET-P}{AWC}})$$

In this study, the Thornthwaite method integrated with Dingman's refined equation was used to calculate the daily ER from 2016 to 2019.

In practice, the ER calculation was realized using ESPERE (acronym for Estimation de la Pluie Efficace et de la Recharge in French, Estimation of effective rainfall and recharge in English), a Microsoft Excel sheet application developed by Lanini et al. in 2015 for estimating aquifer recharge (Santoni et al., 2018).

The daily data of precipitation and PET used for ER calculation was provided by Météo France measured at the Reims-Prunay weather station (located in the study area; Figure II-3). The provided PET data was estimated by the Penman-Monteith method. The AWC, however, is a parameter difficult to evaluate as it depends on numerous factors such as the texture and thickness of soil, the topography, the type of vegetation and the agricultural activities. As a result, the AWC value could be very heterogeneous even on a small scale (Barhoum, 2014). Thiéry (1980) estimated that the AWC value in France ranged mainly from 50 to 150 mm. Lacherez-Bastin (2005) proposed AWC values on chalks ranging from 70 to 150 mm. An average value of 100 mm was proposed for the Champagne Chalk by Chiesi in 1993. In this study, it was decided to use a single average AWC value to represent the entire study area located between the Vesle River and Suippe River. The ER chronic were calculated using **4 AWC values: 50, 70, 100 and 150 mm** and compared to the measured piezometric data (2017 -2019) to determine the most appropriate AWC value for the study area. The calculated ER values are detailed in the following section.

1.1.2. Estimated effective rainfall

The calculated ER values were compared with the monitored groundwater level fluctuation (Figure III-2). The piezometric data measured at the borehole FEP1 is used here to represent the general tendency of groundwater level fluctuation in the study area (for further details of the measured groundwater levels, see Part III.1.2). Average annual ER from 2016 to 2018 estimated with different AWC values were also calculated (Table III-1).

According to the results, smaller AWC values produce larger quantities of ER, representing better infiltration conditions of the soil (Figure III-2 and Table III-1). In 2017 and 2018, the groundwater level started to rise on October and December respectively. Only AWC values of 50 and 70 mm have allowed to produce ER on October 2017 and December 2018, consistent with the observed groundwater level fluctuation in the study area (Figure III-2). According to annual ER values from 1949 to 2001 estimated by the MEDD (Ministre de l'Ecologie et du Développement Durable), the average annual ER in the region of Reims was between 100 and 150 mm (Baran et al., 2008). The AWC value was finally set at 70 mm with an **average annual ER of 137.2 mm** (Table III-1), which best corresponds to the ER values of the study area recorded in the literature.

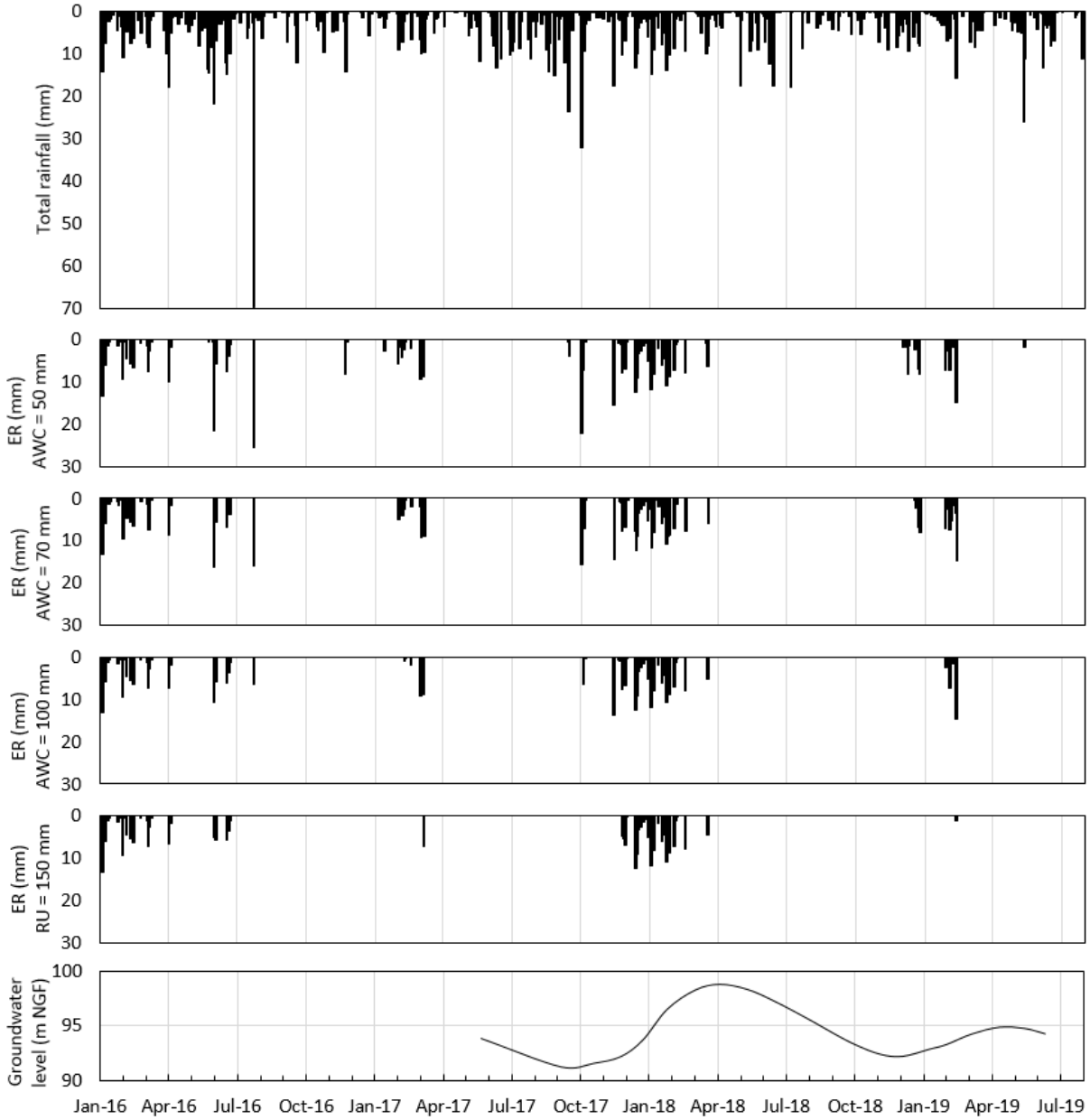

Figure III-2 : Total rainfall (Reims-Prunay weather station) and effective rainfall (ER) calculated with AWC = 50, 70, 100 and 150 mm from 2016 to 2019 compared with measured piezometric data (borehole FEP1) in the study area from 2017 to 2019

Table III-1 : Annual ER values calculated with AWC = 50, 70, 100 and 150 mm from 2016 to 2018

AWC	50 mm	70 mm	100 mm	150 mm
2016	163.1	137.5	120.4	106.8
2017	172.5	156.7	124.2	77.7
2018	135.4	117.4	96	95.3
Mean value	157	137.2	120.7	93.3

According to monthly ER estimated with AWC = 70 mm from 2016 to 2019, two periods can be distinguished during a hydrological cycle: a period from November to March during which large quantities of ER are produced, with the maximum average monthly ER of 34.2 mm in January; a period from April to October during which low to zero ER are produced (Table III-2 and Figure III-3).

Significant annual variations of ER were observed from 2016 to 2019. During the winter months from November 2017 to February 2018, the total amount of ER (181.3 mm) was much more abundant than those of the same period from 2016 to 2017 (20.5 mm) and from 2018 to 2019 (66.2 mm).

Table III-2 : Monthly ER (mm) from January 2016 to June 2019 estimated with AWC = 70 mm

	Jan.	Feb.	Mar.	Apr.	May	Jun.	Jul.	Aug.	Sep.	Oct.	Nov.	Dec.
2016	37.4	21.3	21.3	1.81	21.4	18.2	16.0	0.0	0.0	0.0	0.0	0.0
2017	7.0	13.5	22.4	0.0	0.0	0.0	0.0	0.0	15.6	7.7	43.4	47.0
2018	81.6	9.3	6.1	0.0	0.0	0.0	0.0	0.0	0.0	0.0	0.0	20.5
2019	10.8	35.2	0.0	0.0	0.0	0.0	-	-	-	-	-	-
Mean	34.2	19.8	12.5	0.5	5.4	4.6	5.3	0.0	5.2	2.6	14.5	22.5

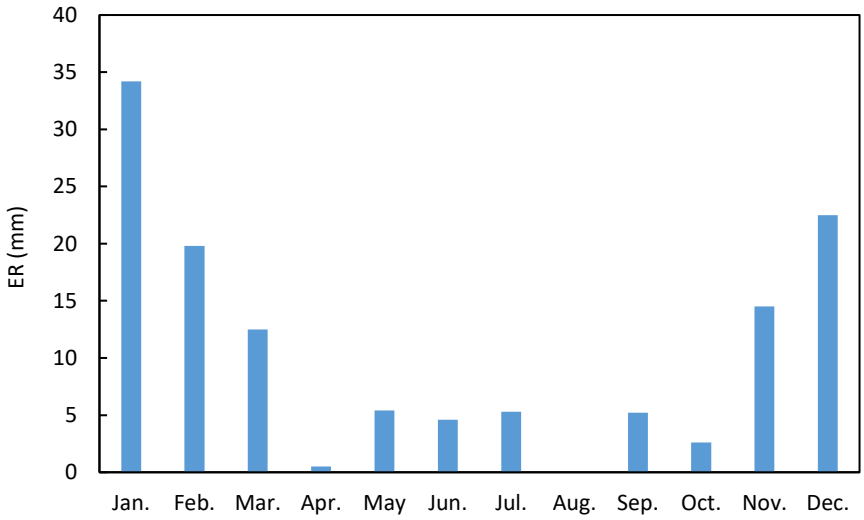

Figure III-3 : Average monthly ER estimated with AWC = 70 mm

1.2. Results of *in situ* continuous monitoring of groundwater level, temperature and EC

The results of *in situ* continuous monitoring (hourly data) of groundwater level and temperature at 9 unexploited boreholes (Table II-6) and EC at FAP and FBN1, from 2017 to 2019, are presented in this section.

1.2.1. Seasonal and annual variation of water level

Chalk groundwater level showed seasonal variations (Figure III-4). The highest water level was reached in March/April following the winter/spring recharge and the lowest level was reached in October/November (Figure III-4). Annual variations were also observed. The water level in March/April 2018 was much higher than that of the same period in 2017 and 2019 due to the larger ER in the winter of 2017 and the spring of 2018 (cf. Part III 1.1.2).

Seasonal water level fluctuations were spatially variable in the study area (Table III-3). The changes in water level between high and low water conditions in 2018 were down to < 5 m near river valley (FAP) but could reach up to 15 m on interfluve (FBN1, FBN4 and FBN5), with the thickness of UZ varying from 2 m (FAP) to 26 m (FBN1) (Table III-3). The rise of water level was not simultaneous in different boreholes (Figure III-4). In 2018, 4 boreholes (FBN4, FEP1, FP1 and FAP) reached their maximum levels in April, 4 boreholes (FA, FBN5, FVDV and FPM3) reached their maximum levels in March and 1 borehole (FBN1) reached its maximum level in February. Moreover, the rise of water level during recharge period was more rapid than the decline of water level during discharge period at all sampling sites. This asymmetry was less evident for boreholes near river valleys (FAP, FP1; Figure III-4).

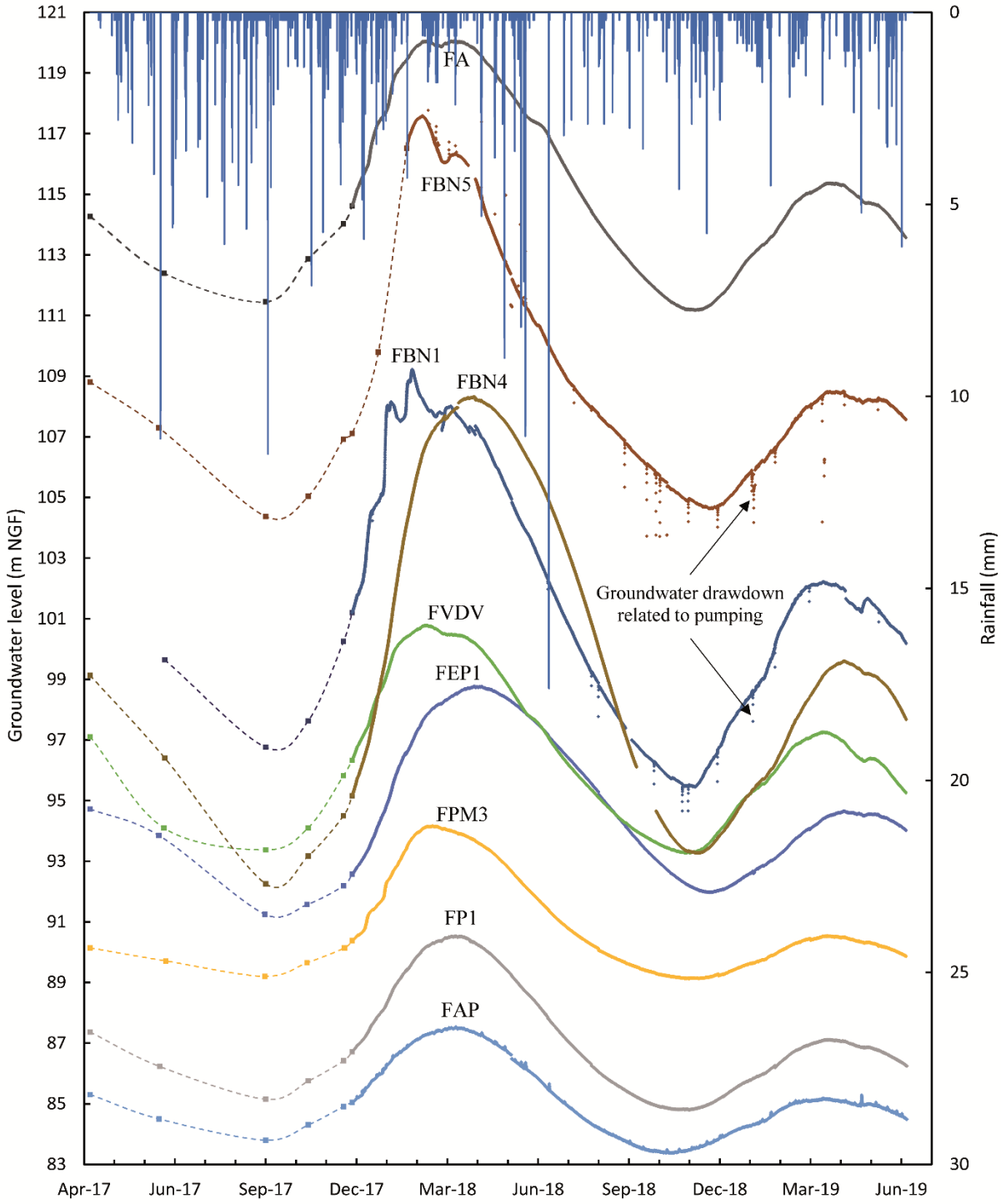

Figure III-4 : Rainfall (hourly data) and groundwater level from April 2017 to June 2019 (solid line: hourly data measured by water-level loggers; dashed line: water level curve drawn by monthly data)

1.2.2. Aquifer responses to rainfall events

1.2.2.1. General situation at the majority of the boreholes

Overall, the Chalk aquifer exhibits a very inertial behavior in our study area: at the majority of the boreholes (except for FAP, FBN1 and FBN5), the curves of groundwater level were smooth with rather gentle slopes (Figure III-4). At these same boreholes, the groundwater temperatures were also very stable in time, ranging from 10.2 to 11.3 °C with standard deviations < 0.1 °C (Table III-3).

Table III-3 : Summary of groundwater temperature and water table fluctuation from December 2017 to June 2019 (hourly data) measured by water-level loggers installed in unexploited boreholes and the minimum unsaturated zone (UZ) thickness (derived from the water level in high water period in 2018)

Name	Altitude (m)	Temperature (°C)					Water level fluctuation (m)	Min thickness of the UZ (m)
		Number of data	Min	Mean	Max	Standard deviation		
FAP	90	11703	8.7	11.5	14.2	0.59	4.0	2.0
FP1	95	11703	10.9	11.1	11.3	0.03	8.5	4.5
FBN1	134	11554	10.6	10.9	11.2	0.07	14.5	26.0
FBN4	111	11192	10.2	10.5	10.8	0.09	15.5	2.5
FBN5	140	7041	10.2	11.2	11.6	0.14	12.5	22.5
FEP1	107	11702	10.4	10.6	10.8	0.04	9.5	7.5
FPM3	103	11695	11.0	11.2	11.4	0.04	9.0	9.0
FVDV	107	11657	10.8	11.1	11.3	0.05	8.0	7.0
FA	123	11699	10.7	11.0	11.3	0.05	9.0	3.0

1.2.2.2. FAP

At FAP, sharp increases of water level (several decimeters) and decreases of EC (up to 300 µs·cm^{-1}) were observed following the rainfall events (Figure III-5). The temperature also reacted quickly after rainfalls and can be divided into two phases: 1) the temperature increased following precipitation (from June 2018 to December 2018); 2) the temperature decreased following precipitation (from December 2017 to June 2018 and from December 2018 to June 2019).

In order to better visualize the aquifer response to rainfalls at FAP, a rainfall events on July 5, 2018 and the related variation of water level, temperature and EC is presented in detail (Figure III-6). The precipitation occurred between 15h and 16h on July 5, with an intensity of 17 mm·h^{-1}. The water level increased about 1 hour after the rainfall and reaches a maximum value after 4 hours. Then it stabilizes gradually to its pre-disturbance level in the following tens of hours (Figure III-6). Water temperature increased about 2h after the rainfall and reached its maximum value about 7h later (11.6 to 12.2°C). EC decreased about 2h after precipitation and reached its minimum value about 9h later (625 to 460 µs·cm^{-1}). The video inspections showed that the tube is in good condition, a direct intrusion of rainwater into this borehole is unlikely.

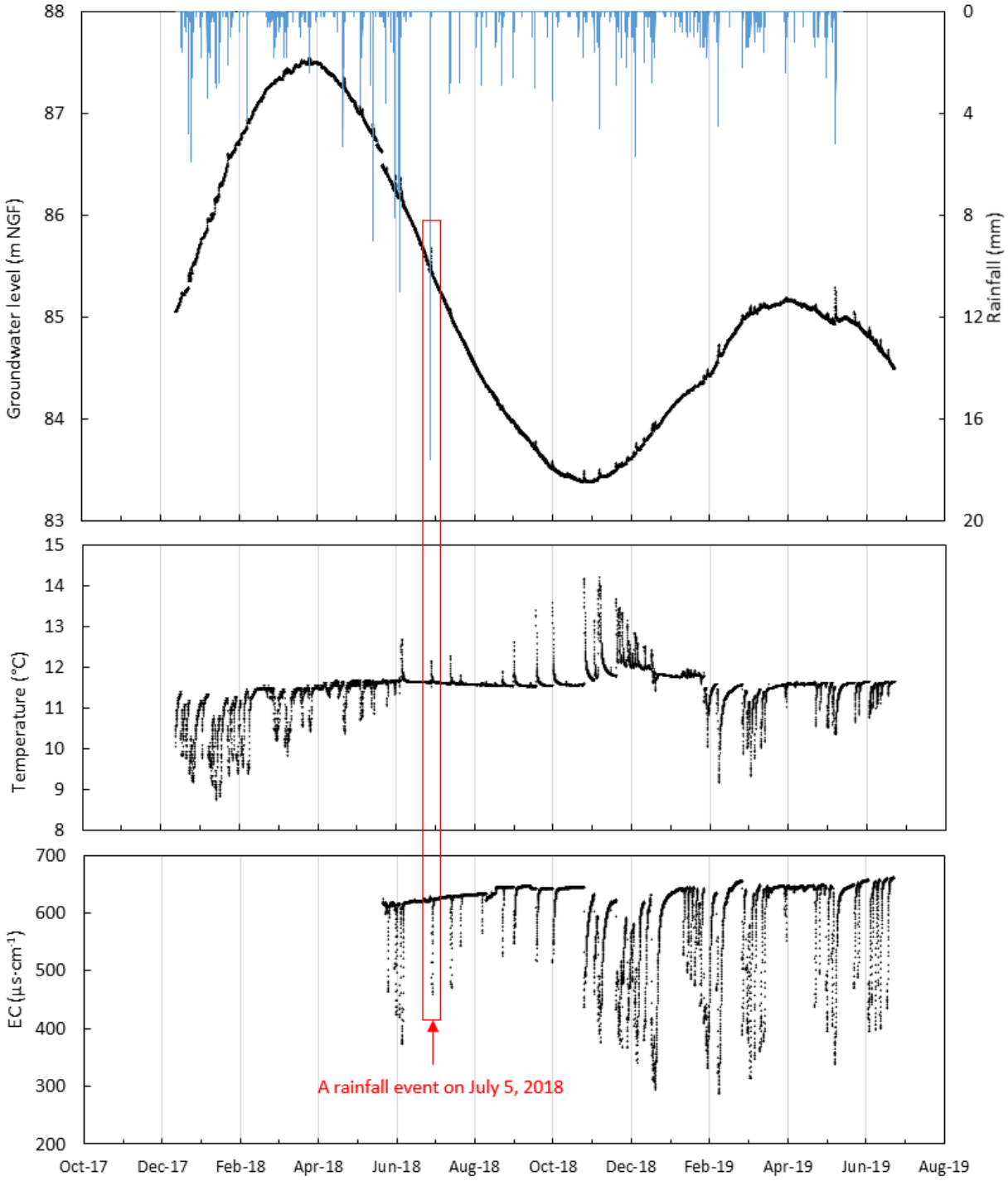

Figure III-5 : Temporal variation of groundwater level, temperature and EC at FAP from December 2017 to June 2019 (the reactivity of the July 5, 2018 event is detailed in Figure III-6)

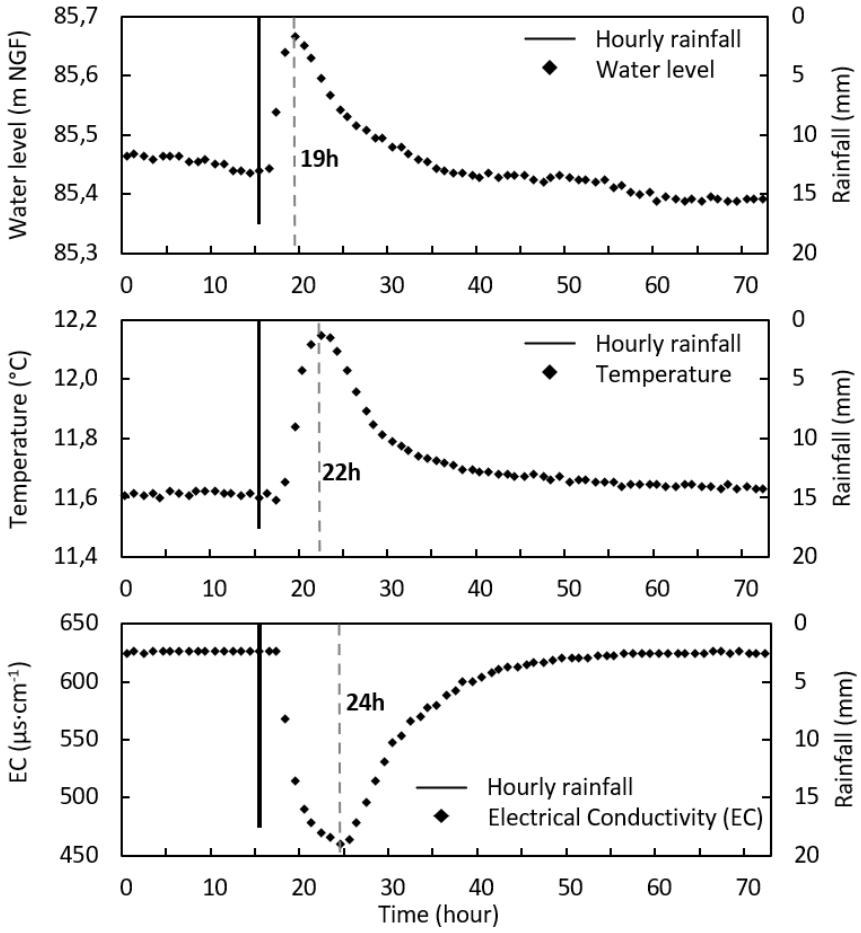

Figure III-6 : Response of groundwater level (hourly data), temperature (hourly data) and conductivity (hourly data) to a rainfall event (17mm at the 15th hour) at FAP from July 5th to July 8th 2018

1.2.2.3. FBN1 and FBN5

At FBN1 and FBN5, large fluctuations in water levels were observed during high water level period, probably related to nearby groundwater exploitation for industrial and agricultural purposes (Figure III-4). In addition, rapid drawdown was observed following pumping for water sampling during low water period (Figure III-4).

At FBN5, the drawdown of water level was also accompanied by slight increases of temperature and EC (Figure III-7). In fact, the borehole FBN5 is relatively deep (47 m) with a low water level (Table II-6). During the water pumping, the submerged pump was placed not far from the bottom of borehole, on which were deposited sediments of minerals, sands or organic particles of plants and microorganisms. Once the pumping is finished, a part of water in the pumping system flowed back into the borehole. Sediments on the bottom stirred up and mixed in water leading to turbidity. Consequently, EC and temperature of water slightly increased after pumping as water near the bottom was more mineralized with sediments and water remained in the pumping system had a higher temperature. After a short period of sedimentation, the monitored parameters stabilized gradually to its pre-disturbance level (Figure III-7).

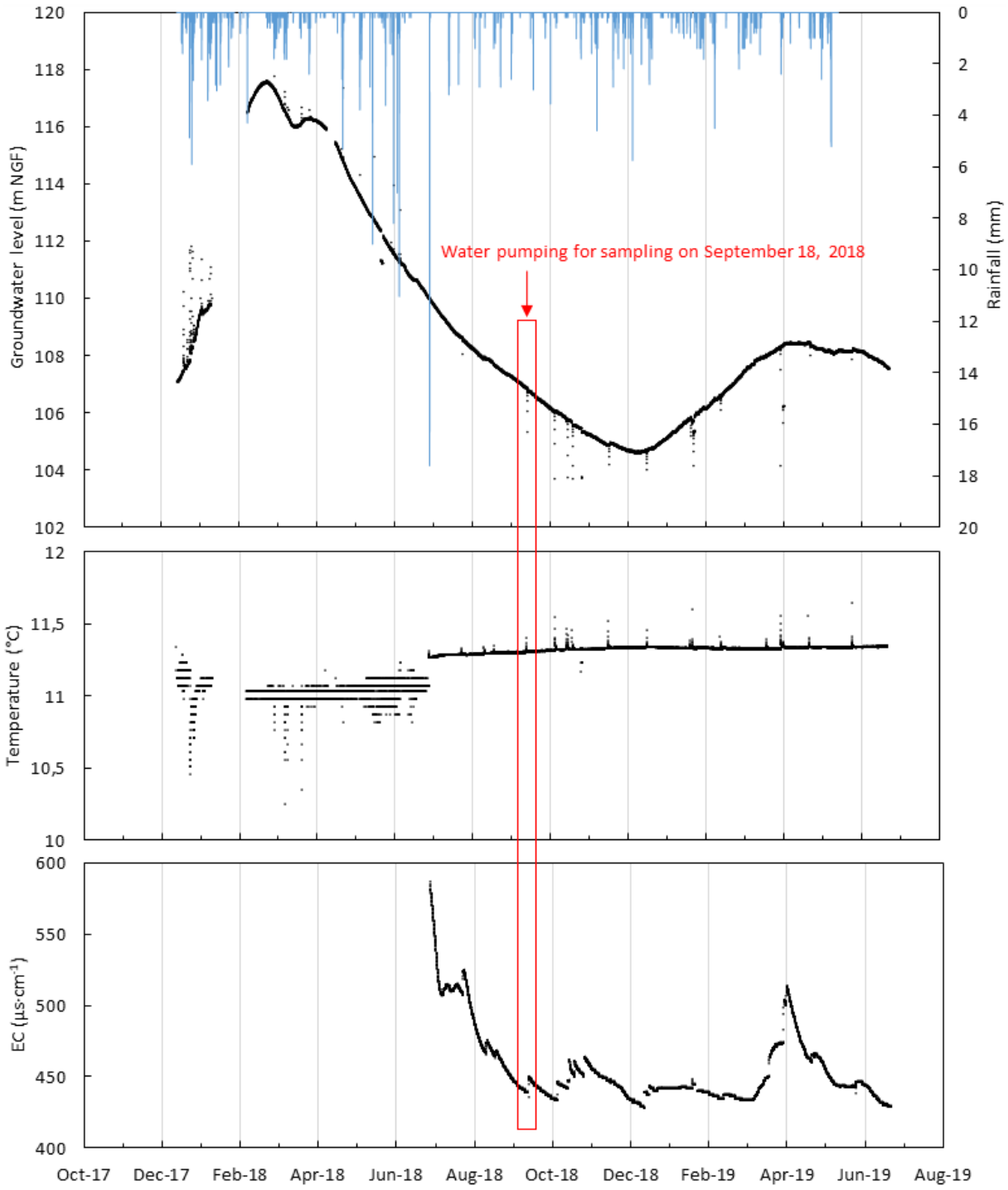

Figure III-7 : Temporal variation of groundwater level, temperature and EC at FBN5 from December 2017 to June 2019

**The measured temperature before July 2018 was slightly lower and more variable, as the In-Situ Rugged TROLL 100 water logger was replaced by the CTD-DIVER water logger in July 2018 and the measurement accuracy of temperature changed consequently from 0.3 to 0.1 °C (Table II-7).*

At FBN5, rapid increases in water level and decreases in temperature were also observed following rainfall events, particularly during high water level period in 2018 (Figure III-7). The range of water level increase in borehole could reach up to 4 m immediately after rainfall, which seemed unlikely to be related to the actual groundwater level in the aquifer. A direct intrusion of rainwater into the borehole during period of high soil moisture and intensive precipitation could explain these variations.

Indeed, *in situ* video inspection showed abnormalities of this borehole tube. At FBN5, the casing set inside the borehole consists of a successive of short PVC pipes. However, notches were observed on the unslotted casing (above the screen position) near the junction part of these PVC pipes (Figure III-8), allowing rainwater to seep into the borehole.

Figure III-8 : Abnormality of casing of borehole FBN5 observed by video inspection

1.2.3. Comparison of the measured water level with the piezometric map of BRGM

The piezometric levels measured *in situ* are compared with the piezometric map produced by BRGM in 2002 (Rouxel-David et al., 2002b). In practice, at each monitored borehole, the piezometric levels estimated from water level contour lines during the high water level period (mid-April) in 2002 are compared with the values measured during the same period (mid-April) in 2018 (Figure III-9). The two series correspond perfectly with each other on all the monitored boreholes (r^2 = 0.98; Figure III-9), indicating that the piezometric map in 2002 is still valid and representative of the current situation.

The number of continuous monitored boreholes in the study area is not sufficient to produce a new piezometric map, therefore the piezometric map of 2002 is used throughout this study.

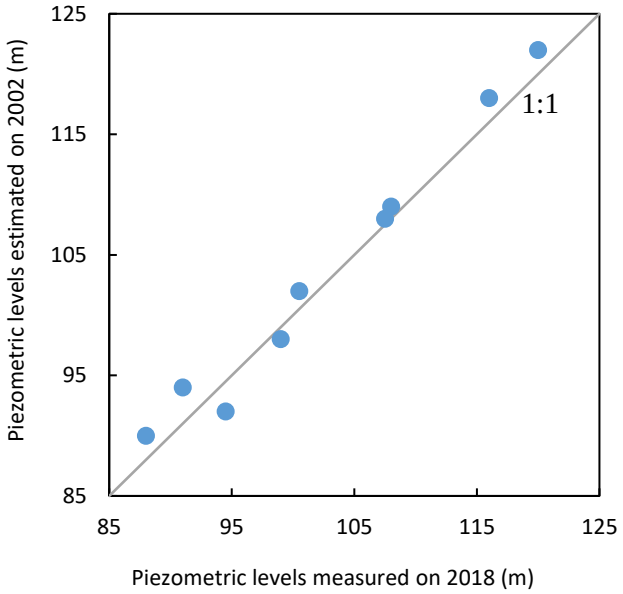

Figure III-9: Comparison of piezometric levels measured in situ with the BRGM piezometric map (Rouxel-David et al., 2002b)

1.3. Discussion on aquifer recharge and hydrological characteristics

According to the estimated ER (Figure III-2 and Figure III-3), the unconfined Champagne Chalk aquifer is mainly recharged from November to March due to excess of rainfall compared to evapotranspiration. The aquifer is discharged from April to September. This recharge mode is consistent with the observed groundwater level fluctuations, whereby the highest water level was reached in March/April and the lowest level reached in October/November (Figure III-4). The annual variations of ER were also consistent with the observed annual variations of groundwater level: the water level in March/April 2018 was much higher than that of the same period in 2017 and 2019 due to the high effective precipitation in the winter of 2017 and the spring of 2018. Indeed, water level during high water season of 2018 was the highest since the last ten years, as demonstrated by piezometric chronicles of two boreholes in Chalk aquifer near the study area monitored since 2008 (ADES database, 2019; **Appendix 3**).

The unconfined Chalk aquifer of the study area possesses highly heterogeneous hydrological characteristics. A higher variation in water levels was observed on interfluves than in river valleys (Figure III-4) attesting differences in transmissivity and storage yield. In river valleys, high density of active fractures are consistently developed, resulting in high permeability of the aquifer (Haria et al., 2003; Ineson, 1962; Price, 1987; Price et al., 1993). At times of high recharge, water is discharged quickly through the fractures toward the river valleys where water levels present low fluctuations, thus not allowing the water levels to rise significantly (Allen et al., 1997; Whitehead and Lawrence, 2006). Conversely, on interfluves, the low permeability and storage yield makes the Chalk aquifer more sensitive to recharge and discharge, resulting in greater and faster water level fluctuations between low water and high water periods (Allen et al., 1997). In general, groundwater reached the maximum level earlier on interfluves than in river valleys, which is reasonable as on interfluves the distance to the groundwater divide line is closer and the time of lateral flow from the recharge zones towards the borehole is shorter.

Rapid drawdown of groundwater level observed at FBN1 and FBN5 implied a low productivity of these two boreholes, which could be explained by the thick UZ (>20 m) and poor permeability of the aquifer, as the density of fractures decreases with depth. Apart from these exceptions, the Chalk aquifer of the study area exhibits a very inertial behavior with respect to recharge, as evidenced by the slow and progressive temporal variations of the water levels and high stability of water temperature (standard deviations < 0.1°C; Table III-3) in boreholes. No impact of individual rainfall events was observed, suggesting a dominant recharge through the Chalk matrix, as demonstrated by numerous studies in Chalk aquifers (e.g., Barhoum, 2014; Haria et al., 2003; Ireson et al., 2006; Mathias et al., 2006; Smith et al., 1970; Wellings and Bell, 1980).

However, differences are observed at FAP. Sharp increases in water level after rainfall events were observed, followed by equally rapid declines. Similar rapid responses within 24h of rainfall were observed in a few previous investigations (Allen et al., 1997; Lee et al., 2006). Allen et al. (2007) suggested that this behavior would be expected only if the large fractures had been replenished (rapid transfer initiated) and subsequently drained during recharge period. The increase and decrease phases of groundwater temperature may be easily explained by the higher atmospheric/soil temperature in summer/autumn and lower atmospheric/soil temperature in winter/spring compared with groundwater temperature. The sharp decrease of EC was a result of dilution by rainwater. The variation of temperature and EC combining with that of water level confirms that the aquifer at FAP testifies to rapid transfers *via* a well-developed fracturing network thus exhibits no longer an inertial behavior. Note that the response of water level was faster than that of temperature and EC, as the water pressure transfer process was faster than the mass transfer and the mixing between rainwater and groundwater. Rapid flows through fractures are added to matrix flows that are still effective as evidenced by the evolution of groundwater levels on an annual scale (Figure III-5).

In conclusion, seasonal and annual fluctuations of groundwater level were observed in the study area as a result of seasonal and annual variations in ER (aquifer recharge). Although the majority of the aquifer has an inertial behavior with respect to recharge, a rapid response following rainfalls can be allowed locally by highly developed fractured network in the Chalk.

2. Groundwater dating by ^{3}H, CFCs and SF_6

2.1. Principle of dating by ^{3}H, CFCs and SF_6

Groundwater dating refers to determining the time difference that a water parcel needs to travel from the groundwater surface (top of the SZ) to the position where the sample is taken (Suckow, 2014). The groundwater time thus determined does not take into account the water transfer time in the UZ (Ayraud, 2005; Vittecoq et al., 2007).

Numerous methods have been developed to estimate the groundwater residence time using different dating tools (^{14}C, ^{39}Ar, ^{81}Kr, ^{32}Si, ^{3}H, CFCs, SF_6, etc.), each of which corresponds to a certain interval of residence time. According to the context of our study, modern groundwater (recharged after the 1950s) dating methods using atmospheric tracers ^{3}H, CFCs and SF6 were selected. In fact, the assumption of relatively young groundwater in the unconfined Champagne aquifer will be confirmed in the following sections.

2.1.1. Dating with ^{3}H

2.1.1.1. General properties and atmospheric concentrations of ^{3}H

Tritium (^{3}H) is one of the most used tracers to identify the presence of young waters. It is a radioactive isotope of hydrogen that has a half-life of 12.43 years (Unterweger et al., 1980). Radioactive decay of ^{3}H produces the noble gas helium (^{3}He).

Tritium is naturally produced by cosmic radiation in the upper atmosphere. Natural tritium concentrations in precipitation were estimated between 0.5 and 20 UT (Clark and Fritz, 1997). In 1954, from samples of vintage wines, Kaufman and Libby determined natural ^{3}H concentrations in precipitation of 3.4 to 6.6 TU in the regions of Naples (Italy), Bordeaux and Rhone (France).

However, a much larger anthropogenic production of ^{3}H has occurred following periods of atmospheric testing of nuclear devices that began in 1952. The temporal and spatial evolution of ^{3}H content in precipitation can be obtained in the GNIP database (the Global Network of Isotopes in Precipitation), a worldwide observation network of hydrogen and oxygen isotopes in precipitation, established by the International Atomic Energy Agency (IAEA) and the World Meteorological Organization (WMO).

Figure III-10 shows monthly ^{3}H concentrations in rainwater measured at Ottawa (Canada, the station with the longest record of observation since 1953) and Stuttgart (Germany, the station with long record of observation near the study area). The sharp increase in concentrations from the beginning of nuclear tests is clearly visible on the Ottawa and Stuttgart curve (Figure III-10). A peak of about 6000 UT was reached in precipitation of the northern hemisphere in 1963-1964 (IAEA, 2008). Concentrations of ^{3}H in precipitation have decreased since the mid-1960s bomb peak, except for some small increases from Chinese and French nuclear tests in the late 1970s (visible on the Stuttgart curve; Figure III-10). Since the 1990s, most of this anthropogenic tritium has disappeared from the atmosphere and the global tritium levels in precipitation are now between 5 and 30 UT in the northern hemisphere, close to the "pre-bomb" natural levels (Figure III-10).

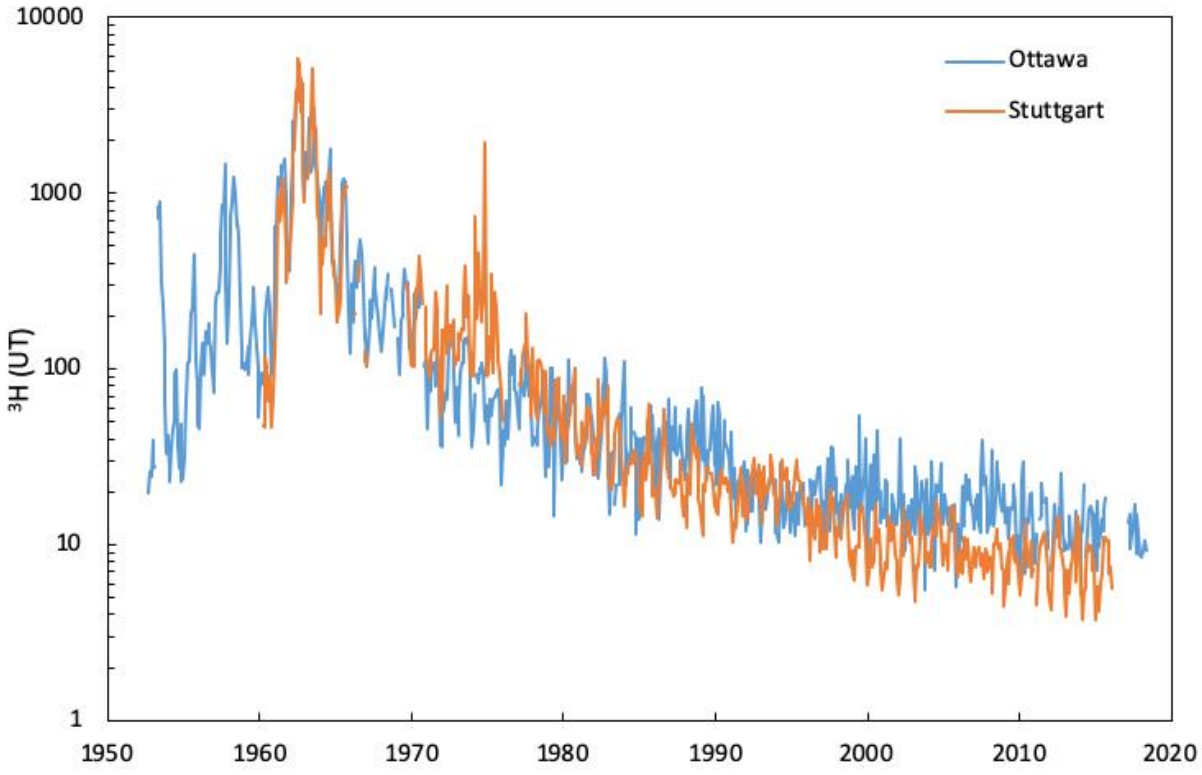

Figure III-10 : ^{3}H concentration in precipitation (monthly data) at Ottawa and Stuttgart (source: GNIP database)

2.1.1.2. Dating method with ^{3}H

As ^{3}H has an inert behavior in groundwater, unaffected by groundwater chemistry and contamination from most anthropogenic sources, ^{3}H dating can be applied to a wide range of hydrologic investigations. Different methods of groundwater dating by ^{3}H can be used (Clark and Fritz, 1997):

- The identification of the atmospheric peak of ^{3}H concentration in groundwater clearly implies the period of aquifer recharge.
- The calculation of the radioactive decay time of ^{3}H, based on a known $^{3}H/^{3}He$ ratio makes it possible to estimate the residence time of groundwater.

- The analysis of ^{3}H concentration time series based on a regular sampling of several years at a specific point makes it possible to observe the passing and decrease of the ^{3}H content peak, allowing to indicate the residence time of water in the system.
- Qualitative interpretation: if concentration of ^{3}H is not detectable, the measured water was recharged before the anthropogenic input of ^{3}H into the atmosphere by the nuclear tests in the 1950s; if low levels of ^{3}H are observed, the measured water came from a recent recharge since the late 1980s; if high levels of ^{3}H are observed (> 30 UT), the measured water was recharged in the 1960s. The value of 30 UT was proposed by Clark and Fritz in 1997 according to the radioactive decay of ^{3}H since the 1960s. Based on the half-life of ^{3}H (12.43 years) and the sampling year of this study (2018), a recharge time in the 1960s can be proposed if the observed levels of ^{3}H are > 15 UT.

The first three methods require the observation of the ^{3}H peak, the known $^{3}H/^{3}He$ ratio and/or the regular sampling for long periods. The last method is applied for this study, as it allows to provide a qualitative estimation of the residence time by using only one single measurement of ^{3}H. A much better accuracy of groundwater dating is provided by CFCs and SF_6.

2.1.2. Dating with CFCs and SF_6

2.1.2.1. General properties and atmospheric concentrations of CFCs and SF_6

- **<u>CFCs</u>**

CFCs or chlorofluorocarbons are more commonly known by their commercial name Freon. The production of CFCs began in the early 1930s as safe alternatives to ammonia and Sulphur dioxide in refrigeration (McCulloch, 1999). They can also be used as propellants, solvents and blowing agents in plastic foams. From the 1950s, CFCs have been widely used in industry and diffused into the atmosphere and the hydrosphere (Vittecoq et al., 2007). Consequently, atmospheric concentrations of these gases have increased dramatically since the 1960s. Since 1974, studies have shown that CFCs can have a destructive effect on the ozone layer (Cicerone et al., 1974; Molina and Rowland, 1974). In 1987, the production and consumption of CFCs were regulated under the Montreal Protocol. After the Montreal Protocol was signed, new data showed worse-than-expected damage to the ozone layer. In 1992, the production and consumption of CFCs were globally banned according to the Copenhagen Amendment to the Montreal Protocol.

The first measurements of CFCs in the atmosphere were realized in 1971 and 1974. Since 1976, systematic monitoring of these gases have been carried out by the NOAA (National Oceanic and Atmospheric Administration, USA). Atmospheric concentrations of CFCs prior to 1970 were estimated from information on CFC production (Mccarthy et al., 1977).

The evolution of the atmospheric concentrations of the three main CFCs (CFC-12, CFC-11 and CFC-113) since 1940 is presented in Figure III-11. The intensive industrial use of CFCs and the discovery of their harmful effects on the environment have led to a characteristic evolution of their atmospheric concentrations: a sharp increase between 1950 and 1990, then a plateau between 1990 and 2000 followed by a slight decrease from the 2000s.

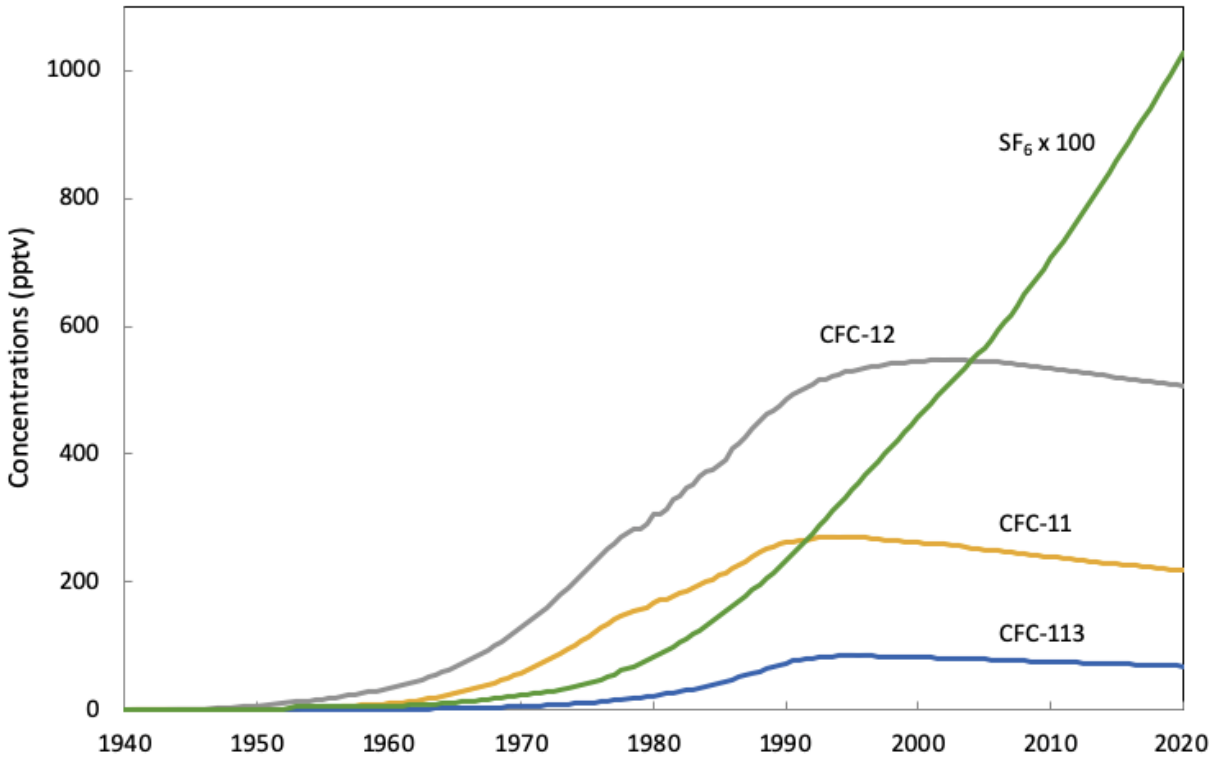

Figure III-11 : Atmospheric concentrations of CFCs et SF_6 in the northern hemisphere (Source: USGS – United States Geological Survey, https://water.usgs.gov/lab/software/air_curve/index.html)

- **SF_6**

Sulfur hexafluoride (SF_6) is used as a gaseous dielectric medium for high-voltage circuit breakers, switchgear, and other electrical equipment in the electrical industry. Significant industrial production of SF_6 began in the 1960s. Unlike CFCs, which come exclusively from anthropogenic sources, SF_6 can also be present naturally in rocks. The major known source of terrigenous SF_6 is found in fluorite and granite; however, significant concentrations of SF6 is also reported in other mineral and rock types such as hydrothermal mineral deposits, halite and dolomite (Busenberg and Plummer, 2000; Harnisch and Eisenhauer, 1998). SF_6 is extremely stable, with an estimated atmospheric lifetime of 800 to 3200 years (Ravishankara et al., 1993).

As a potent greenhouse gas, atmospheric concentrations of SF_6 are also monitored (Figure III-11). The use of SF_6 is still allowed with constant industrial production. As a result, SF_6 atmospheric concentration is still accumulating rapidly in the atmosphere with a current growth rate of about 6.9% per year (Geller et al., 1997).

2.1.2.2. Dating method with CFCs and SF_6

Several basic assumptions and conditions are necessary for groundwater dating based on CFCs and SF_6 (Ayraud, 2005; Katz et al., 1995; L. N. Plummer et al., 2006a). It is first necessary to collect water samples representative of the aquifer, without any contact to the atmosphere or other possible CFCs / SF_6 sources (Busenberg and Plummer, 1992). It is then assumed that the water samples was in solubility equilibrium with the UZ air at time of recharge and that the composition of the UZ air follows that of the atmosphere (L. N. Plummer et al., 2006a).

Groundwater dating with CFCs / SF_6 is based on the historical atmospheric concentrations of these gases recorded during the last 50 years, the Henry's Law solubility and the measurement of CFCs / SF_6 concentrations in groundwater samples. According to Henry's Law, the concentration of a gas dissolved in water in equilibrium with atmosphere is proportional to the partial pressure of the gas in air (p_i):

$$C_i = K_{H_i} p_i \tag{III-1}$$

with C_i the concentration of the i^{th} CFC in water, and K_{H_i} the Henry's Law constant for this gas. The partial pressure of the gas in air (p_i) is defined as following:

$$p_i = x_i \, (P - p_{H_2O}) \tag{III-2}$$

with x_i the dry air mole fraction of i^{th} CFC in air (in pptv, parts per trillion volume), P the total atmospheric pressure and p_{H_2O} the water vapor pressure (Warner and Weiss, 1985). The Henry's Law constant K_H can be calculated with the following equation:

$$\ln K_H = a_1 + a_2 \left(\frac{100}{T}\right) + a_3 \ln\left(\frac{100}{T}\right) + S \left(b_1 + b_2 \left(\frac{T}{100}\right) + b_3 \left(\frac{T}{100}\right)^2 \right) \tag{III-3}$$

with T the temperature in degrees kelvin and S the salinity in parts per thousand by weight (‰). K_H for solubility of CFC-11, CFC-12, CFC-113 and SF_6 have been determined over a range of temperatures and salinities at 1013.25 hPa total atmospheric pressure (Bu and Warner, 1995; Warner and Weiss, 1985). Table III-4 gives the constants for K_H calculation (III-3) valid for temperatures of 273-313 kelvin (0-40°C) and salinities of 0-40‰.

Table III-4 : Constants for calculation of K_H for CFC-11 and CFC-12 (Warner and Weiss, 1985), CFC-113 (Bu and Warner, 1995) and SF_6 (Bullister et al., 2002)

CFC	a_1	a_2	a_3	b_1	b_2	b_3
Solubilities in mol·kg^{-1}·atm^{-1}						
CFC-11	-136.2685	206.1150	57.2805	-0.148598	0.095114	-0.0163396
CFC-12	-124.4395	185.4299	51.6383	-0.149779	0.094668	-0.0160043
CFC-113	-136.129	206.475	55.8957	-0.02754	0.006033	---
SF_6	-98.7264	142.803	38.8746	0.0268696	-0.0334407	0.0070843
Solubilities in mol·L^{-1}·atm^{-1}						
CFC-11	-134.1536	203.2156	56.2320	-0.144449	0.092952	-0.0159977
CFC-12	-122.3246	182.5306	50.5898	-0.145633	0.092509	-0.0156627
CFC-113	-134.243	203.898	54.9583	-0.02632	0.005874	---
SF_6	-96.5975	139.883	37.8193	0.0310693	-0.0356385	0.00743254

According to eq. III-3, the Henry's Law constant K_H must be calculated at the recharge temperature, which is defined as the temperature in the UZ above the water table where air-water equilibrium is carried out (Dunkle et al., 1993). The recharge temperature can be calculated from the concentration of dissolved noble gases, especially Ar and Ne, based on Henry's Law assuming that these gases were equilibrated with the atmosphere at recharge. The solubility of these gases vary differently function of temperature, which makes them very useful in determining recharge temperatures (Weiss, 1970). The Henry's Law constant K_H is also a function of salinity. However, most shallow groundwater is so dilute that corrections for salinity are not necessary (L. N. Plummer et al., 2006a).

The total atmosphere pressure during recharge (P) is usually unknown but can be estimated from the recharge elevation. For elevations less than 3000 m, the following relationship can be used (List, 1949):

$$\ln P = -\frac{H}{8300} \qquad \text{(III-4)}$$

The vapor pressure of water is given by (Weiss and Price, 1980):

$$\ln p_{H_2O} = 24.4543 - 67.4509\left(\frac{100}{T}\right) - 4.8489\ln\left(\frac{100}{T}\right) - 0.000544S \qquad \text{(III-5)}$$

With the equations and parameters presented above, the dry air mole fraction of CFCs or SF_6 (x_i) can therefore be calculated from the concentration measured in groundwater. The recharge date is then determined by comparing the calculated air mixing ratio with historical CFCs/SF_6 concentrations in local air.

2.1.2.3. Effects that can modify apparent groundwater age

- **Recharge temperature**

The recharge temperature is essential for determining the solubility of CFCs and SF_6. In general, the lower the recharge temperature, the higher the solubility. It means that over-estimation of the recharge temperature results in apparent ages too young and under-estimation gives ages too old. An uncertainty in recharge temperature of ± 2°C results in age uncertainties of 3 years or less for water recharged prior to about 1990 (Busenberg et al., 1993). Uncertainty in recharge temperature of ± 2°C leads to uncertainty in apparent CFC ages of 1 year or less for water recharged prior to the mid-1970s. As the CFCs atmospheric concentrations peaked in the mid- and late-1990s, CFCs apparent ages became very sensitive to uncertainties in recharge temperature (Cook et al., 2006).

When the UZ is less than a few meters thick, the recharge temperature responds to seasonal variations (Matthess, 1982). The amplitude of variation decreases with the depth from surface. The UZ temperature is usually constant for depths greater than 5 to 6 m (Williams and Gold, 1976). In such cases, the recharge temperature is usually within about 1°C of the mean annual surface-soil temperature (Andrews and Lee, 1979; Heaton and Vogel, 1981; Herzberg and Mazor, 1979; Mazor, 1972).

- **Excess air**

Excess air arises from the solution of air bubbles trapped by infiltrating water in the UZ (Heaton and Vogel, 1981). During the infiltration in the UZ, small bubbles of air may become trapped in the capillary fringe and then be carried down to below the water table. The trapped gas then partitions into groundwater with increased hydrostatic pressure, making dissolved gas concentrations higher than the concentrations to be expected for atmospheric equilibrium (Cook et al., 2006).

The amount of excess air introduced during infiltration depends mainly on two factors: the physical structure of the UZ and the pattern of rainfall and recharge. Air entrapment will presumably be favored by small pores and narrow capillary channels in fine-grained soil. Soils with wide joints such as coarse gravel should be less favorable for the air entrapment (Heaton and Vogel, 1981). Recharge of the aquifer by intense rainfalls accompanied by a subsequent rapid rise of the water table, may especially favor entrapment and downward transport of air bubbles (Ayraud, 2005; Plummer et al., 2001).

If the excess air is not considered, the apparent groundwater age by CFCs and SF_6 will generally be too young due to the higher concentration. In most studies, excess air could be neglected for the calculation of CFCs apparent ages due to high solubility of these gases. However, the influence of excess air can be important on SF_6, therefore requires correction (IAEA, 2006; Vittecoq et al., 2007).

Excess air can be determined by analysis of the concentration of different noble gases in water samples. The amount of excess air in groundwater ranges from 0 to about 50 ml/L with the majority of values less than 10 ml/L (Wilson and McNeill, 1997). For example, average values of 2.8 ± 1.2 ml/L were found for groundwater abstracted from the chalk aquifer in England (Darling et al., 2012).

- **Contamination**

Local pollutions of CFCs and SF_6 may exist due to the proximity of sources of these trace gases. The concentrations in contaminated water samples often exceed by far the equilibrium concentrations with the atmosphere and no age information can be assigned.

Some commonly recognized sources of CFCs contamination include seepage from septic tanks, landfills (Kjeldsen and Christophersen, 2001), release from polyurethane foam waste (Kjeldsen and Jensen, 2001), leaky sewer lines, leakage from underground storage tanks, infiltration or disposal of industrial wastes and recharge from rivers contaminated with CFCs (Cook et al., 2006). CFCs contamination could also result from agricultural activities. Agricultural application of pesticides may introduce CFCs, particularly CFC-11 to unsaturated air, as CFCs are allowed as inert ingredients in pesticide formulations (N. Plummer et al., 2000). In addition, CFCs can sorb into rubber and polymers; therefore water samples can also be contaminated with CFCs from contact with these materials such as permanently installed submersible pumps in wells with rubber parts (Cook et al., 2006; Dunkle et al., 1993).

SF_6 less commonly reaches contaminated values. Anthropogenic sources of SF_6 include high-voltage electricity supply equipment, Mg and Al melting and landfills (Darling et al., 2012; Santella et al., 2008). Unlike CFCs, which come exclusively from anthropogenic sources, SF_6 can also be present naturally in rocks. The major known source of terrigenous SF_6 is found in fluorite and granite; however, significant concentrations of SF_6 is also reported in other mineral and rock types such as hydrothermal mineral deposits, halite and dolomite (Busenberg and Plummer, 2000; Harnisch and Eisenhauer, 1998).

The contamination of CFCs and SF_6 could be atmospheric or in-ground and tends to affect urban/peri urban and fractured aquifer the most (Morris et al., 2005, 2006). Other ways in which excesses of trace gases can be introduced into water samples include contaminations from sampling equipment, contact with air during sampling and introduction of young and/or contaminated water by pumping (Cook et al., 2006).

In this study, all precautions have been taken during the sampling process in order to avoid contamination. One advantage of measuring concentrations of several trace gases in a single water sample is that it is less impossible that the sample is contaminated with all tracers. Even if the sample is contaminated with one tracer, other tracers can still be used for dating.

- **Unsaturated zone**

Groundwater dating with CFCs and SF_6 is based on the assumption that trace gases concentrations in the soil air above the water table are the same as their atmospheric concentrations. In aquifers with relative thin UZ (< 10 m), the trace gases concentrations of soil air map with that of the atmosphere (Cook et al., 2006; Cook and Solomon, 1995). However, when a thick UZ separates the atmosphere from the water table, there will be a time lag for the transport of CFCs and SF_6. The transport of gases through UZ can occur in the gas and liquid phases. This is a function of diffusion coefficients, soil water content, recharge rate etc. (Cook and Solomon, 1995; Weeks et al., 1982). If this effect is not considered, groundwater residence time obtained with CFCs and SF_6 may overestimate true groundwater ages. It should be noted that the time lag may be much shorter in fractured aquifers (Darling et al., 2005).

In the study area, water level loggers installed in the non-exploited sampling wells (Table II-6) allowed recording groundwater levels every hour. The measured water table fluctuations (Table III-3) showed that 7 of the 9 monitored wells have a water table depth less than 10 m during high water season. Two wells (FBN1 and FBN5) have a water table depth between 20 and 30 m. Considered the fractured chalk aquifer of the study area, the time lag for the transport of CFCs and SF_6 could be relatively short. Therefore, the UZ should not influence significantly the apparent groundwater age in the study area.

- **Biodegradation**

Although CFCs may be considered essentially stable under aerobic conditions, they are subject to degradation processes under anaerobic conditions (Darling et al., 2012; Khalil and Rasmussen, 1989; Oster et al., 1996). This tends to affect CFC-11 and CFC-113 more rapidly than CFC-12, as reported in a number of studies (Hinsby et al., 2007; Horneman et al., 2008; Khalil and Rasmussen, 1989; Sebol et al., 2007). Under aerobic conditions with dissolved oxygen more than 10%, CFCs degradation is unlikely to occur therefore could be neglected.

In the study area, the measured dissolved oxygen in groundwater varied from 24 to 102% (Table III-6), implying aerobic conditions of the aquifer. Therefore, the influence of CFCs degradation on groundwater apparent age was not considered.

- **Other factors**

Other factors such as sorption, hydrodynamic dispersion and groundwater mixtures can also influence groundwater dating by CFCs and SF_6.

Sorption is only likely to be a problem in aquifers where the matrix has a high organic content, such as organic-rich sediment and coal (IAEA, 2006).

Hydrodynamic dispersion is a process whereby CFCs that enter an aquifer at different times or locations can be mixed. Since the variation of atmospheric CFCs and SF_6 concentrations are continuous processes, the effects of dispersion on apparent ages may be rather small (Cook et al., 2006).

In this study, sorption and dispersion have a generally small effect on groundwater dating and are therefore ignored. The effect of groundwater mixture is discussed in the following chapters with different calculation models.

2.2. Calculation models

Groundwater flow is usually accompanied by mixtures according to flow patterns of the aquifer. As a result of mixture, the CFCs concentrations in groundwater change and so does the apparent age. In order to better estimate the groundwater ages, conceptual models of underground water circulation are necessary. Three simplified models are used in this study for the calculation of apparent ages: piston flow model, exponential mixing model and the binary mixing model.

2.2.1. Piston flow model (PFM)

The piston flow is the simplest case of groundwater age distribution (Figure III-12). The model assumes a tracer travels from the inlet position (recharge area) to the outlet position (a well or spring, for example) without any dispersion or mixing (Jurgens et al., 2012; Etcheverry, 2002; Małoszewski and Zuber, 1982). The PFM can be applicable to groundwater flows with low dispersion, high linear velocity or short flow path from recharge to discharge point. Tracers measured from wells in confined aquifers with a small recharge area or shallow, short screened wells in unconfined aquifers can follow piston flow behavior approximately (Jurgens et al., 2012).

2.2.2. Exponential mixing model (EM)

The exponential mixing model (EM) is applicable to simple homogeneous unconfined aquifers of constant thickness with spatially uniform recharge (Cook et al., 2006) (Figure III-12). The EM describes the age distribution of a completely mixed reservoir (Ericksen, 1971). In this model, groundwater age increases logarithmically with the depth but independent on the horizontal location (Appelo and Postma, 2004; Cook et al., 2006). The apparent age calculated from EM are expressed by the mean residence time (MRT), which corresponds to the duration of flow line longer than 2/3 of the flow lines. This model can be appropriate for large screened wells or aquifers that discharge to springs or streams. It assumed mixing occurs within the sampling well or spring rather than in the aquifer (Jurgens et al., 2012).

2.2.3. Binary mixing model (BM)

Binary mixing model (BM) considers a mixing of two different water masses. One of the components could be CFC-free water or recent water (0 to 10 years). The proportion of the two components and the apparent age of one of the two components can be calculated. This model can be appropriate for aquifers with short-circuit pathways that result in age mixtures of significantly mean ages, karstic aquifers or watershed with transmissivity contrasts (Jurgens et al., Katz et al., 2009; Michel, 2004).

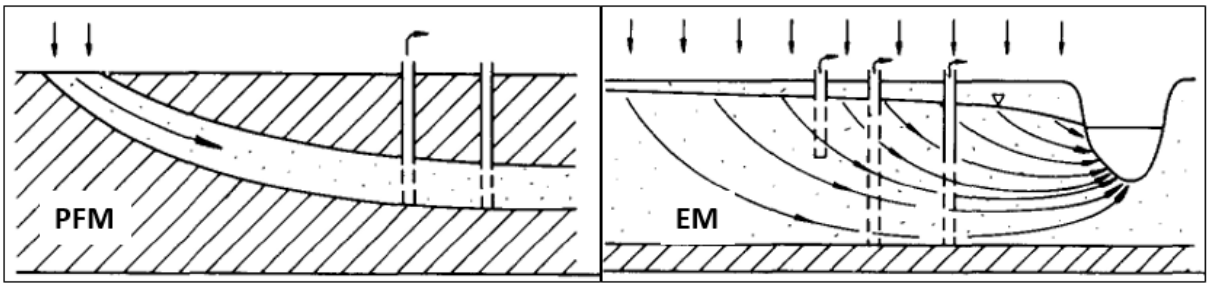

Figure III-12 : Schematic diagram of piston flow model (PFM) and exponential mixing model (EM) (Małoszewski and Zuber, 1982)

In reality, groundwater mixtures are usually complicated processes rather than simple binary mixing or perfect mixing of all inflows. The measurement of CFCs and SF_6 concentrations could provide information on the range of groundwater age rather than an exact age. Application of the different models to water samples collected in the study area are presented in Part III 2.3.2.

2.3. Data interpretation

2.3.1. Results of dating by ^{3}H

The concentrations of ^{3}H measured in groundwater samples are showed in Table III-5. At FBN1 and FEP1, ^{3}H was not detectable (<0.5 UT). Groundwater ages of pre-1950s in the study area are unlikely (for more details see Part III. 2.3.2) and additional measurement is needed to confirm and explain the very low concentrations of ^{3}H at these two sites. At the other sampling points (10 of 12), the observed concentrations varied from 0.7 ± 0.2 UT to 4.9 ± 0.4 UT, with an average value of 2.5 ± 1.3 UT, suggesting relatively young groundwater ages since the late 1980s (Clark and Fritz, 1997).

Table III-5 : Concentrations of tritium (^{3}H) measured in groundwater samples collected in the study area on May 2019

Sample name	Sampling date	Tritium concentration (TU ± σ)
FBN1	2019/05/27	<0.5
FBN4	2019/05/27	4.1 ± 0.3
FBN5	2019/05/27	0.7 ± 0.2
FEP1	2019/05/28	2.2 ± 0.3
FPM3	2019/05/27	<0.5
FP1	2019/05/28	2.0 ± 0.3
FAP	2019/05/27	2.9 ± 0.3
FVDV	2019/05/27	1.7 ± 0.2
FA	2019/05/27	4.9 ± 0.4
PP	2019/05/27	2.1 ± 0.3
PDO	2019/05/27	3.1 ± 0.3
FPM1	2019/05/27	1.2 ± 0.2

2.3.2. Results of dating by CFCs and SF_6

2.3.2.1. Estimation of recharge temperature and excess air

In groundwater samples, Ne and Ar concentrations ranged from $0.84 \cdot 10^{-8}$ to $1.69 \cdot 10^{-8}$ $mol \cdot L^{-1}$ and $1.71 \cdot 10^{-5}$ to $2.18 \cdot 10^{-5}$ $mol \cdot L^{-1}$, respectively (Table III-6). The recharge temperature and excess air were estimated from the relationship between Ar and Ne (Figure III-13).

In May 2018, the estimated recharge temperature was similar in all waters of the study area with an average value of 10 °C. It should be noted that no recharge temperature information can be estimated at FBN4 due to a high value of excess air. In October 2018, the recharge temperature showed a spatial variability, with values ranging from 10 and 16 °C (with an average value of 13 °C), higher than that in May (Figure III-13). This is consistent with several months' winter recharge with relatively low temperatures, making the estimated recharge temperature in water samples in May lower than in October.

The estimated excess air in samples ranged from 0 to more than 8 $ml \cdot L^{-1}$ with an average value of about 3.4 ± 2 $ml \cdot L^{-1}$. No significant difference in excess air values was observed between the two sampling campaigns. At FPM1, negative excess air value was observed, which could probably due to the absorption by rubber tubes present at this borehole. The highest values of excess air were observed in water samples at FP1, FA, PP and FBN4, with the maximum value (> 8 $ml \cdot L^{-1}$) for water sample collected at FBN4 in May 2018 (Figure III-13).

Higher excess air values were measured in groundwater at FP1, FA, PP and FBN4. These 4 boreholes have a thin UZ (less than 5 m in 2018 high water period; Table III-3). The water level at pumping station PP is not measured, but historical data showed a UZ thickness of about 5 m (InfoTerre.brgm.fr). It is suggested that at these 4 shallow groundwater sites, recharge by preferential fracture flow is favored with more fractures developed near the surface, while the other deeper groundwater sites are dominated by matrix flow as fracturing of the chalk decreases with depth (Haria et al., 2003; Mathias et al., 2006). The preferential flow is guaranteed by water-filled small fractures and the capillary channels above the water table, resulting in a subsequent rapid rise of water table after rainfalls (Heaton and Vogel, 1981). These effects are supposed to favor the formation and entrapment of air bubbles, which could possibly explain the higher quantity of excess air in water samples collected at these points. Note that the borehole FAP also has a water table depth of less than 5 m. However, the excess air values in water were relatively low, similar to the mean value of the study (Figure III-13). This is consistent with the very developed fracturing network at FAP. Large fractures are less favorable for the air entrapment, resulting in relatively low excess air values than other shallow groundwater sites.

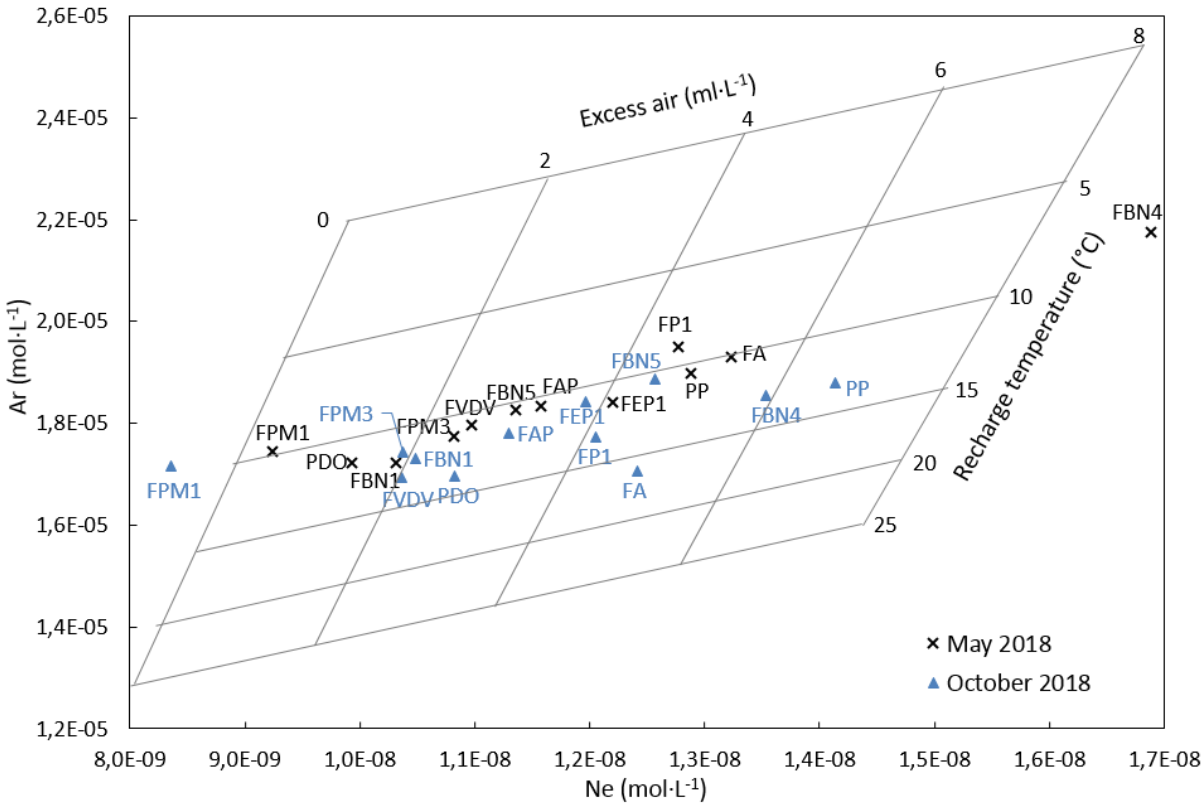

Figure III-13 : Dissolved gas concentration and estimated recharge temperature and excess air in groundwater samples collected in May and October 2018

Table III-6 : CFCs, SF_6, noble gases, dissolved O_2 saturation and estimated groundwater age by piston flow model, exponential mixing model (MRT = mean residence time) and binary mixing model (proportion and age of young and old water) in May and October 2018; the choices of the ideal model and estimated residence times are marked in bold; Cont.= contamination

Name	Sampling time	SF_6 (pptv)	CFC-12 (pptv)	CFC-11 (pptv)	CFC-113 (pptv)	Ar (10^{-5} mol·L^{-1})	Ne (10^{-8} mol·L^{-1})	O_2 (%)	Piston flow model				Exponential model (MRT years)				Binary mixing model			Comment
									SF_6	CFC-12	CFC-11	CFC-113	SF_6	CFC-12	CFC-11	CFC-113	% young water	young age	old age	
FA	May	9.7	522.7	205.5	56.6	1.93	1.32	84	6	24	34	31	0	7	25	27	**75**	**0**	**40**	
	Oct.	7.9	507.3	182.4	58.6	1.71	1.24	86	6	26	36	31	5	12	30	25	**80**	**0**	**>50**	
FAP	May	7.1	538.0	278.0	62.4	1.83	1.16	56	8	11	25	30	8	-	-	20	**70**	**0**	**35**	
	Oct.	6.2	504.9	237.9	58.5	1.78	1.13	59	11	27	31	31	12	13,5	12	25	**50**	**0**	**30**	
FBN1	May	5.1	cont.	cont.	66.4	1.72	1.03	68	16			30	**18**	-	-	**18**	40	0	30	
	Oct.	5.3	cont.	cont.	75.2	1.73	1.05	24	16			28	**18**	-	-	7	40	0	30	
FBN4	May	2.1	cont.	206.3	cont.	2.18	1.69	102	29		34		70	-	**25**	-	10	0	35	
	Oct.	5.4	472.7	188.1	cont.	1.85	1.35	92	15	29	36		17	17,5	**30**	-	50	0	35	
FBN5	May	5.1	cont.	cont.	cont.	1.83	1.16	55	16				18	-	-	-	-	-	-	Not datable
	Oct.	4.0	cont.	cont.	72.6	1.89	1.26	62	21			29	30	-	-	12	25	0	30	
FEP1	May	5.4	cont.	cont.	46.9	1.84	1.22	82	14			**33**	16	-	-	40	60	0	>30	
	Oct.	5.1	cont.	cont.	70.6	1.84	1.20	83	16			**29**	19	-	-	13,5	90	15	>60	
FP1	May	7.5	cont.	cont.	41.0	1.95	1.28	55	7			33	6	-	-	**40**	-	-	-	
	Oct.	3.6	376.1	cont.	46.2	1.77	1.21	48	23	34		33	**35**	**35**	-	**40**	30	0	40	
FPM1	May	cont.	cont.	cont.	46.7	1.75	0.92	66				33	-	-	-	40	-	-	-	Not datable
	Oct.	cont.	cont.	cont.	cont.	1.72	0.84	72					-	-	-	-	-	-	-	
FPM3	May	cont.	cont.	141.8	cont.	1.77	1.08	74			41		-	-	50	-	-	-	-	Not datable
	Oct.	cont.	cont.	95.9	cont.	1.74	1.04	67			45		-	-	100	-	-	-	-	
FVDV	May	4.5	cont.	258.1	cont.	1.80	1.10	64	19		15		22	-		-	**30**	**0**	**30**	
	Oct.	3.9	cont.	239.4	cont.	1.70	1.04	68	22		31		35		11	-	**25**	**0**	**30**	
PDO	May	5.1	504.5	163.9	49.9	1.72	0.99	76	16	26	38	32	18	12	40	35	**30-50**	**0**	**>40**	
	Oct.	6.1	416.7	162.0	44.0	1.70	1.08	80	12	32	39	33	13,5	27	40	45	**60**	**0**	**45**	
PP	May	6.4	449.7	147.4	80.7	1.90	1.29	74	10	30	**41**	27	11	20	50	-	-	-		
	Oct.	6.9	376.1	135.4	cont.	1.88	1.41	84	9	34	**42**		8,5	35	70	-	65	0	>60	

2.3.2.2. Contamination of CFCs and SF_6

The measured CFCs and SF_6 concentrations in water samples (in $pmol \cdot L^{-1}$) were transferred to atmospheric partial pressures (in pptv) according to Henry's law. The water samples were marked as contaminated when calculated concentrations were greater than atmospheric peak concentrations (Table III-6) and the data was rejected.

A frequent contamination of tracer gases was observed in the study area, especially for CFC-12 (8 points contaminated; Table III-6 and Figure III-14). The widespread contamination of European aquifers by CFCs has also been reported by previous studies (e.g., Höhener et al, 2003; Nativ et al., 1999; Oster et al., 1996). Although most SF_6 concentrations did not exceed atmospheric peak concentrations, apparent ages estimated by SF_6 were generally much younger than all the other tracers (Table III-6), suggesting some anthropogenic and/or natural addition of SF_6.

The studied aquifer is unconfined with fractures, making the soil and groundwater very vulnerable to contamination. The landfill site in middle of the study area (Figure III-14) appears to be a major source of contamination of CFCs and SF_6. A small waste deposit site located near the borehole FBN1 (Figure III-14) could also represent a local source of pollution for CFCs and SF_6. Furthermore, since the majority of the study area is used as farmland, the agricultural application of pesticides could also be a potential source of contamination for CFCs, especially CFC-11 (Plummer et al., 2000). Unlike CFCs, terrigenous source of SF_6 could be present in several different rock types including fluorite, granite, hydrothermal mineral deposits, halite and dolomite (cf. Part III.2.1.2.1). Therefore, the natural presence of SF_6 in Chalk cannot be excluded, as dolomite is commonly present in Chalk as impurity (Barhoum et al., 2014; Gillon et al., 2010).

It should be noted that water samples collected at FPM1 were contaminated by all the 4 trace gases. Indeed, FPM1 is a private well in a farm where a permanently pumping system is installed. Water samples were collected directly from the tap. Air contact with the pumped water may occur between the pump and the tap. Rubber water tubes connected with the tap could also present a potential source of contamination. As a result of frequent contamination, some water samples are not datable (FBN5, FPM1 and FPM3; Table III-6) as only one or two tracers are valid for calculation and estimated ages are not consistent for different tracer gases.

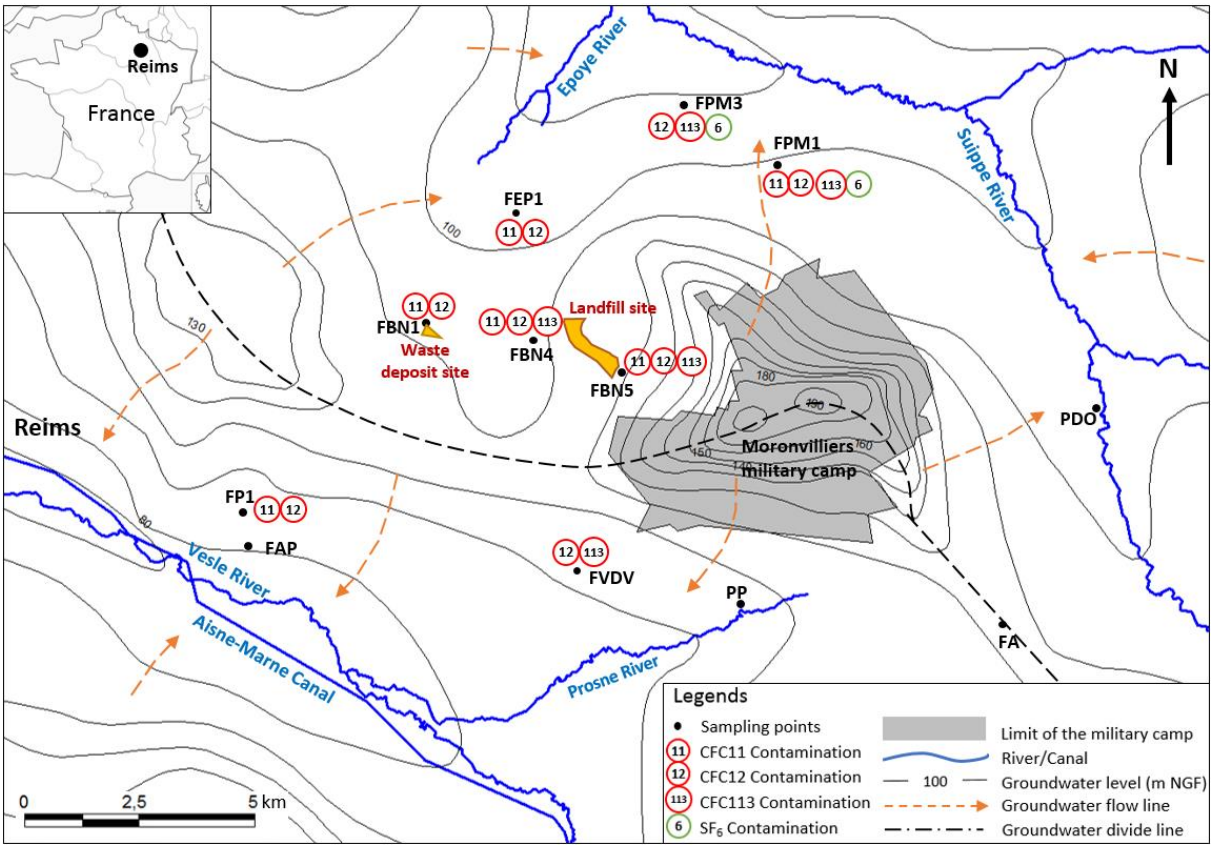

Figure III-14 : Contamination of CFCs and SF_6 in the study area

2.3.2.3. Groundwater apparent age

Cross-plots of concentrations of different tracer gases can be used to recognize contamination/degradation and to provide information for the selection of mixing models (Solomon et al., 2006) (Figure III-15). In general, areas of the diagrams bounded by curves representing different modelled tracer concentrations should include measured values of water samples if no other processes have affected them (Plummer et al., 2006b). Samples that plot far outside the bounded areas may be contaminated or degraded. A sample of water that is not a mixture should plot somewhere along the piston flow curves. Samples that do not plot on the piston flow curves are likely to represent mixtures. An exponential mixture should plot somewhere along the exponential mixing curves. Binary mixtures could plot anywhere within the bounded area depending on the ages of end members. Since the temporal variation of atmospheric concentrations of different tracers is different, it may be difficult to distinguish different models for some combinations. For example, as CFC-11 and CFC-12 have similar historical concentrations, curves of the three models are very similar (Figure III-15b). Also, the consistency of apparent ages estimated by different tracer gases and by different sampling campaigns can be used for the validation of models (Plummer et al., 2003). When different tracers did not give consistent apparent ages, values estimated by CFC-11 and CFC-113 were considered to be more reliable than CFC-12 and SF_6 as the latter two tracers were largely influenced by anthropogenic activities in the study area.

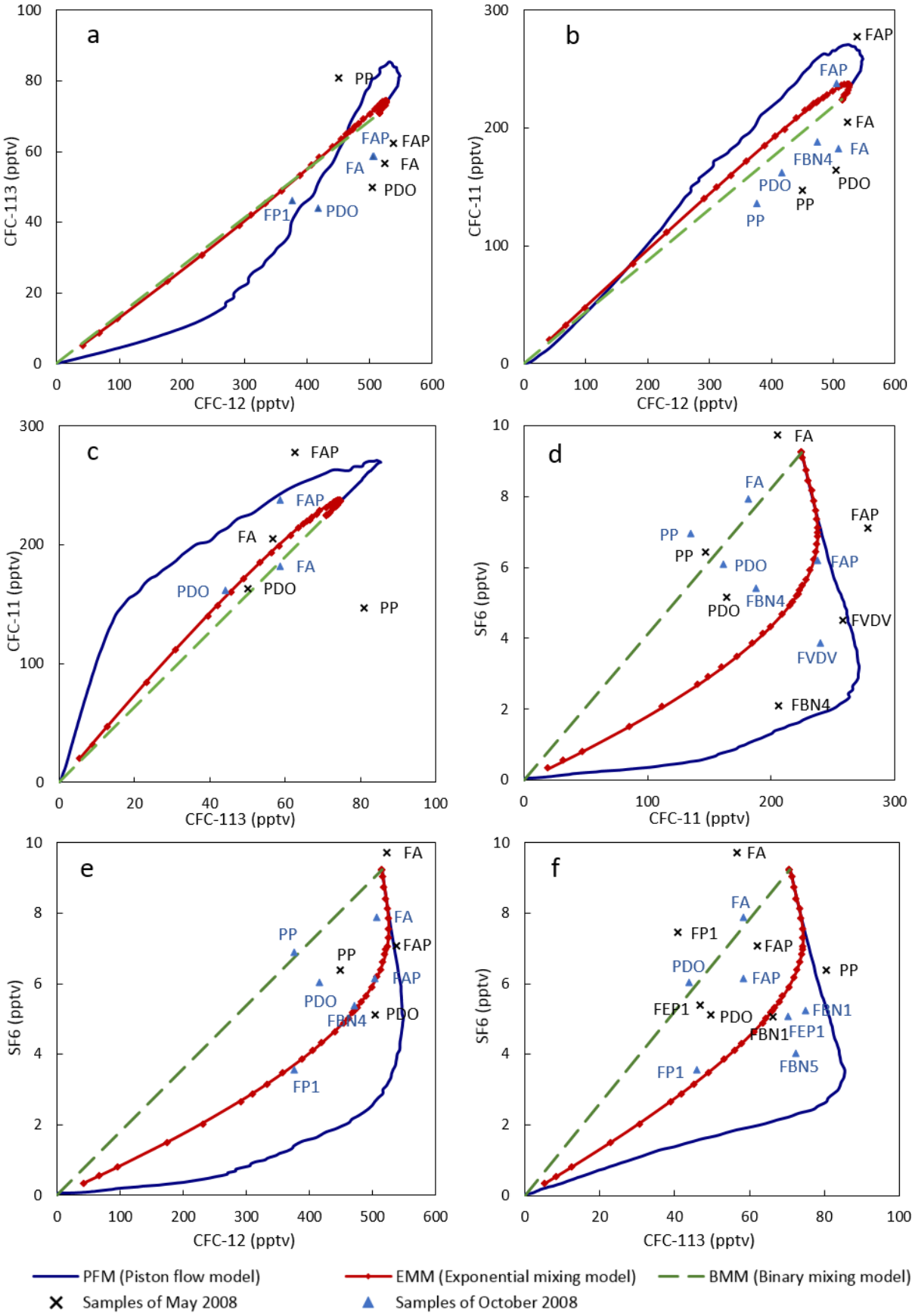

Figure III-15 : Tracer plots comparing CFC-11, CFC-12, CFC-113 and SF_6 atmospheric concentrations and plots of tracer gas concentrations in water samples collected in May and October 2018

The selected mixing models and estimated residence time are resumed in Table III-6. Groundwater residence time of the study area is rather heterogeneous, ranging from modern to about 50 years.

The piston flow model is more suitable for FEP1 and PP (30 to 40 years). The exponential mixing model is the best model for FBN1, FBN4 and FP1 (MRT from 18 to 40 years). The binary mixing model is more suitable for FA, FAP, FVDV and PDO (25% to 80% of modern water and an end member of old water ranging from 30 to about 50 years). Residence times estimated by piston flow and exponential mixing model at each point were similar between the sampling campaign of May 2018 (high water) and October 2018 (low water). For boreholes applying the binary mixing model, significant differences of residence time were observed between the two sampling campaigns. At FA, FAP and FVDV, estimated apparent ages for samples collected in May are younger than in October with higher proportions of modern water or younger ages of the old end member. At PDO, apparent ages for samples collected in May are older than in October with less proportions of modern water (Table III-6).

In general, the result of groundwater dating by ^{3}H and CFCs/SF_6 were consistent for the majority of water samples, with relatively young apparent ages estimated. Two exceptions existed for water samples collected at FBN1 and FEP1. Additional information (e.g., the $^{3}H/^{3}He$ ratio) is needed to explain the very low concentrations of ^{3}H at these two points. The apparent ages estimated by CFCs/SF_6 at these two points are used in the following sections as the results were consistent for different CFCs and SF_6 thus considered as reliable.

In conclusion, the unconfined Champagne Chalk aquifer is made up of waters of different ages ranging from modern to about 50 years, with piston flow, exponential or binary mixing models defined at each sampling site implying different flow pathways and mixing processes in the aquifer.

3. Groundwater geochemistry of the unconfined Champagne Chalk aquifer

3.1. Results of analysis on major and trace elements

3.1.1. Physicochemical parameters and major elements

Physicochemical parameters and concentrations of major ions measured in groundwater and surface water samples from June 2017 to June 2019 are summarized in Table III-7 and Table III-8. For each sampling point, the average value from monthly data is presented. The minimum, average and maximum values of each parameter were calculated for groundwater and surface water. The major-ion data was also shown as box plots.

- **Groundwater**

The mean values of EC at each site varied widely from 297 to 1,095 $\mu s \cdot cm^{-1}$, with an average value of 564 $\mu s \cdot cm^{-1}$ for all groundwater samples, implying a high spatial heterogeneity of mineralization degree in the study area. Water samples collected at FEP2 and FP2 were the least and the most mineralized, respectively. The pH values of the groundwater samples were relatively homogeneous, with average values at each sampling site ranging from 6.87 to 7.71 and a mean value of 7.36 for all groundwater samples (Table III-7).

The chemical composition of the monitored groundwater was typical of the Chalk groundwater, as Ca^{2+} and HCO_3^- were the dominant ions with average concentrations of 108.7 $mg \cdot L^{-1}$ and 239.9 $mg \cdot L^{-1}$ respectively, which were about an order of magnitude higher than the other major ions (Table III-7 and Figure III-16). Despite the Ca^{2+} - HCO_3^- chemical facies, significant heterogeneities were observed on concentrations of major ions in groundwater. Average concentrations of Ca^{2+} and HCO_3^- at each sampling site from June 2017 to June 2019 ranged from 61.7 to 171.4 $mg \cdot L^{-1}$ and from 170.0 to 402.6 $mg \cdot L^{-1}$, with a 25 – 75 percentile range of 95.1 to 116.3 $mg \cdot L^{-1}$ and 208.6 to 258.9 $mg \cdot L^{-1}$ respectively.

Measured concentrations of Cl^-, NO_3^- and SO_4^{2-} ions were lower than that of Ca^{2+} and HCO_3^-, with average concentrations of 29.7, 27.8 and 19.0 $mg \cdot L^{-1}$, respectively (Table III-7). The 25 – 75 percentile ranges were 18.4 - 31.6 $mg \cdot L^{-1}$, 22.1 - 36.7 $mg \cdot L^{-1}$ and 6.6 - 24.8 $mg \cdot L^{-1}$ for Cl^-, NO_3^- and SO_4^{2-} respectively. Extreme values far away from the ranges above could occur at some points (Figure III-16).

Concentrations of Na^+, K^+ and Mg^{2+} were also variable but much lower, with average concentrations of 7.9, 2.2 and 1.7 $mg \cdot L^{-1}$, respectively (Table III-7 and Figure III-16). Concentrations of these ions have 25 – 75 percentile ranges of 4.7 – 8.4 $mg \cdot L^{-1}$, 0.6 – 2.3 $mg \cdot L^{-1}$ and 1.0 – 2.3 $mg \cdot L^{-1}$ for Na^+, K^+ and Mg^{2+} respectively.

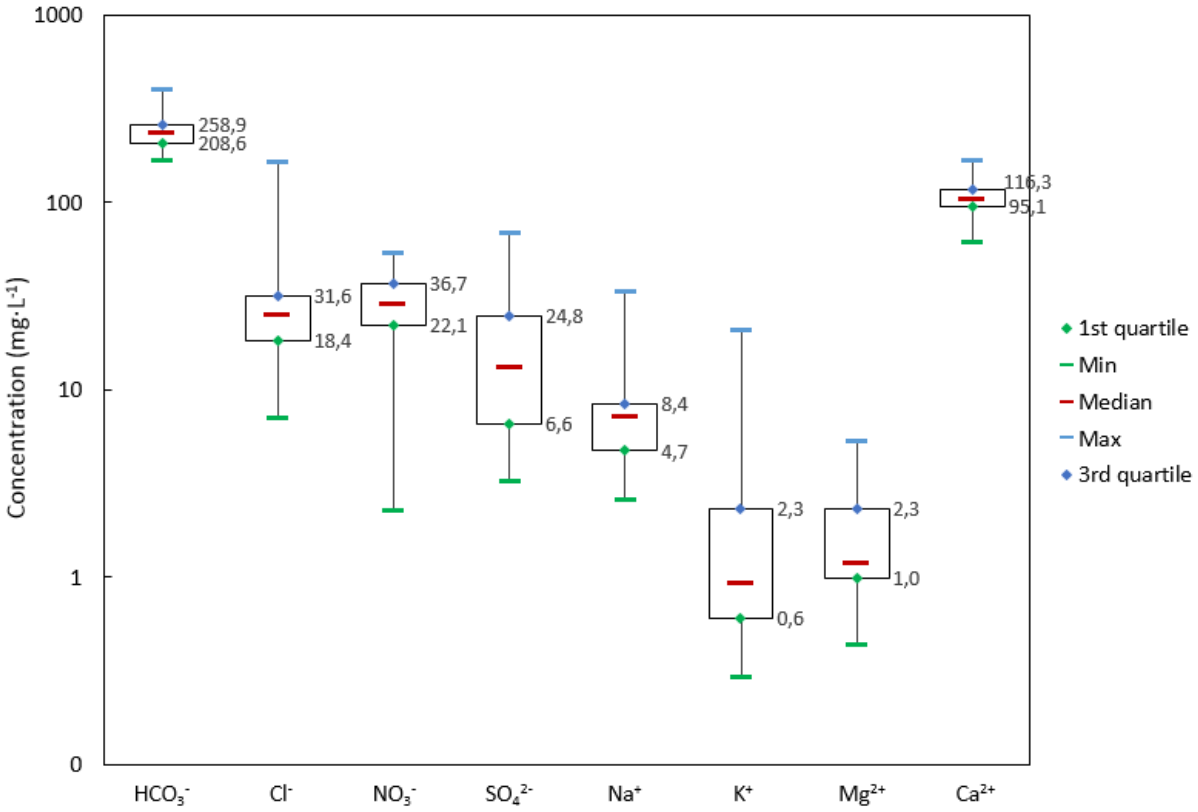

Figure III-16 : Box plots for major ions in groundwater of the Champagne Chalk aquifer in the study area

- **Surface water**

The pH values ranged from 7.12 to 8.20 in surface water samples with an average value of 7.91, which were higher than those measured in groundwater. This could probably be explained by the activities of plants, organisms and biodegradation processes in surface waters and the equilibrium with atmospheric CO_2. The EC mean values at each site ranged from 412 to 568 $\mu s \cdot cm^{-1}$ with an average value of 497 $\mu s \cdot cm^{-1}$, with relatively lower variabilities at the different sampling points compared to those measured in groundwater (Table III-8).

Surface water samples had the same Ca^{2+} - HCO_3^- chemical facies as groundwater samples (average concentrations of 96.0 and 216.0 $mg \cdot L^{-1}$ respectively; Table III-8 and Figure III-17), as river water in the study area comes mainly from drainage of the Chalk aquifer. Unlike the significant spatial heterogeneities observed in groundwater, the concentrations in surface water were rather homogenous with very low variabilities (Figure III-17).

The Concentrations of major ions in surface water were similar to the average concentrations of groundwater, except for samples collected in the Canal Aisne-Marne (C1 and C2) (Table III-8). At these two sites, water samples showed lower concentrations of Ca^{2+}, HCO_3^-, Cl^- and NO_3^- but higher concentrations of Na^+ and K^+ than those of other surface water samples and the average values of groundwater.

The spatial and temporal heterogeneities on concentrations of major ions and physicochemical parameters will be discussed in detail in the following sections.

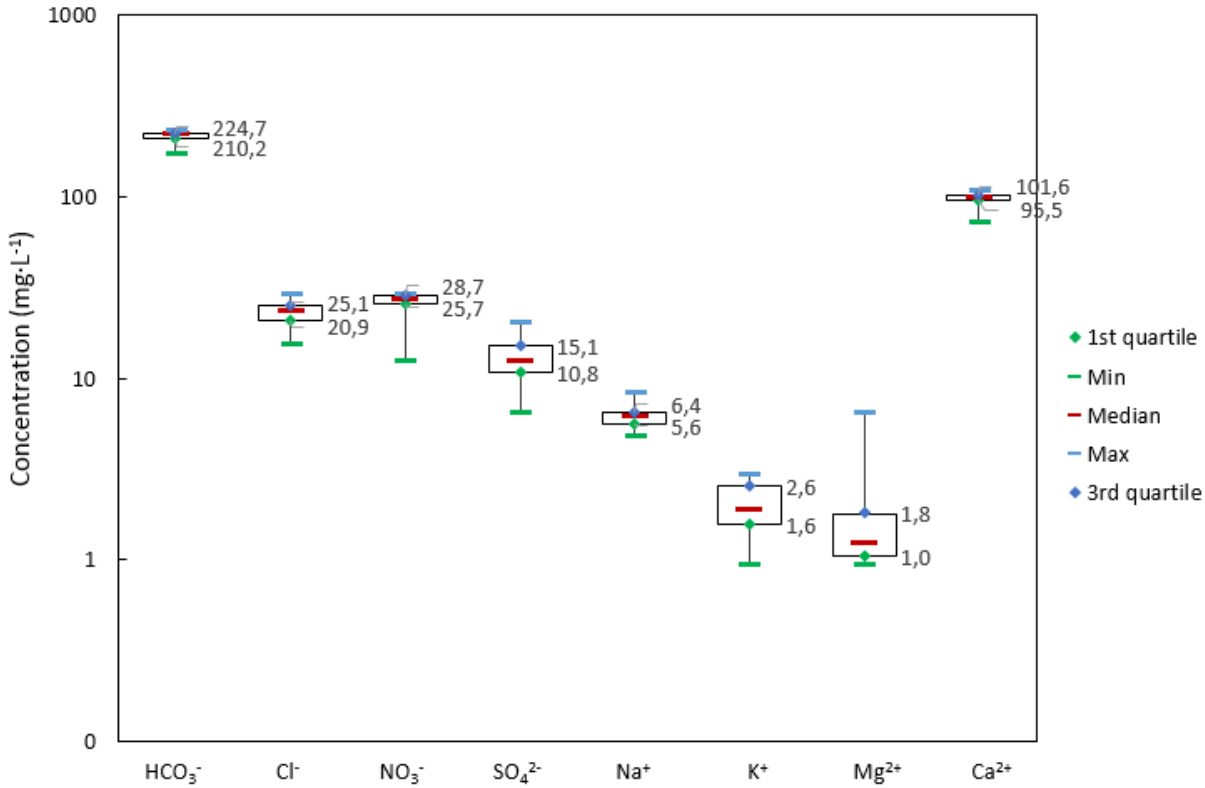

Figure III-17 : Box plots for major ions in surface water of the Champagne Chalk aquifer in the study area

Table III-7 : Major ion concentrations and physicochemical parameters of Chalk groundwater from June 2017 to June 2019 (average values from monthly data) with the temporal variation coefficient (%) at each sampling point in brackets; N = Number of samples; EC = electric conductivity.

	Name	N	pH	EC	HCO_3^-	Cl^-	NO_3^-	SO_4^{2-}	Na^+	K^+	Mg^{2+}	Ca^{2+}	HCO_3^-	Cl^-	NO_3^-	SO_4^{2-}	Na^+	K^+	Mg^{2+}	Ca^{2+}
				($\mu s \cdot cm^{-1}$)	($mg \cdot L^{-1}$)								($meq \cdot L^{-1}$)							
Groundwater	FA	21	7.41 (2.5)	533 (8.3)	208.6	35.4	39.7	9.2	4.4	0.3	0.6	103.9	3.42 (13.7)	1.00 (17.9)	0.64 (15.2)	0.19 (20.8)	0.19 (10.2)	0.01 (36.3)	0.05 (9.9)	5,19 (8,4)
	FAP	21	7.17 (3.3)	613 (14.7)	265.4	30.7	28.4	20.9	11.8	4.1	2.7	112.6	4.35 (17.3)	0.87 (30.8)	0.46 (23.4)	0.44 (18.4)	0.51 (54.3)	0.10 (20.0)	0.22 (22.6)	5,62 (16,8)
	FBN1	21	7.38 (4.5)	511 (9.6)	225.9	25.0	28.9	13.9	7.5	0.9	1.2	97.3	3.70 (6.2)	0.71 (35.1)	0.47 (26.2)	0.29 (62.2)	0.32 (41.9)	0.02 (26.9)	0.10 (23.0)	4,86 (4,5)
	FBN4	21	7.07 (2.6)	770 (3.7)	292.1	52.9	54.3	18.7	8.4	5.9	2.9	143.8	4.79 (6.7)	1.49 (5.0)	0.88 (4.8)	0.39 (8.4)	0.37 (8.9)	0.15 (5.8)	0.24 (10.6)	7,18 (3,0)
	FBN5	21	7.29 (4.0)	504 (19.6)	251.4	15.0	31.6	3.8	5.9	3.1	1.3	98.4	4.12 (15.3)	0.42 (61.4)	0.51 (35.7)	0.08 (37.9)	0.26 (87.6)	0.08 (23.0)	0.11 (24.5)	4,91 (20,2)
	FEP1	21	7.42 (6.8)	541 (1.1)	235.1	35.2	36.7	4.2	6.1	0.6	1.2	104.1	3.80 (7.62)	0.99 (2.7)	0.59 (3.8)	0.09 (20.1)	0.26 (7.0)	0.02 (14.4)	0.09 (8.8)	5,19 (3,7)
	FP1	21	7.23 (2.7)	592 (4.4)	258.0	28.0	29.9	19.4	6.4	3.0	2.3	115.9	4.23 (5.4)	0.79 (10.2)	0.48 (13.1)	0.40 (5.8)	0.28 (9.8)	0.08 (9.5)	0.19 (9.8)	5,78 (5,3)
	FPM1	21	7.48 (3.6)	410 (3.0)	206.6	7.6	19.0	5.8	3.6	0.9	1.2	83.0	3.39 (3.7)	0.21 (9.1)	0.31 (4.4)	0.12 (13.8)	0.15 (7.7)	0.02 (8.4)	0.10 (8.7)	4,14 (3,5)
	FPM3	21	7.48 (2.9)	412 (8.1)	183.9	18.6	24.0	5.7	4.1	0.5	0.7	80.9	3.01 (9.1)	0.52 (27.0)	0.39 (23.8)	0.12 (11.8)	0.18 (9.4)	0.01 (16.5)	0.06 (10.7)	4,04 (7,8)
	FVDV	21	7.28 (3.2)	602 (2.3)	239.9	39.0	40.0	10.0	7.9	2.9	1.1	113.6	3.94 (4.9)	1.10 (4.2)	0.64 (5.6)	0.21 (13.5)	0.34 (10.8)	0.07 (14.8)	0.09 (10.1)	5,67 (3,3)
	PDO	21	7.34 (2.9)	562 (1.8)	214.7	33.9	42.1	13.1	4.9	0.8	0.9	109.3	3.52 (5.9)	0.96 (3.8)	0.68 (4.8)	0.27 (5.2)	0.21 (7.0)	0.02 (18.2)	0.07 (8.8)	5,45 (3,5)
	PP	21	7.38 (2.0)	459 (3.1)	203.8	21.8	25.8	6.6	4.3	0.6	0.7	90.8	3.34 (7.0)	0.61 (5.2)	0.42 (3.3)	0.14 (12.6)	0.19 (7.7)	0.02 (31.2)	0.06 (8.9)	4,53 (3,5)
	FCE	1	7.72	477	231.8	7.2	3.1	29.9	4.2	1.0	1.8	95.1	3.80	0.20	0.05	0.62	0.18	0.03	0.15	4,74
	FNA	1	7.45	736	312.3	20.0	24.3	60.1	8.2	1.4	2.3	152.7	5.12	0.56	0.39	1.25	0.36	0.04	0.19	7,62
	FBN3	3	7.41 (2.6)	435 (9.1)	222.0	13.4	15.2	9.1	4.0	0.5	1.0	89.7	3.64 (11.6)	0.38 (18.2)	0.25 (14.5)	0.19 (19.3)	0.18 (13.9)	0.01 (16.8)	0.08 (12.9)	4,48 (9,8)
	FBN2	4	7.23 (0.7)	587 (7.1)	258.9	31.6	18.2	24.8	9.6	1.9	1.5	116.3	4.24 (4.2)	0.89 (12.8)	0.29 (68.4)	0.52 (56.7)	0.42 (14.4)	0.05 (15.8)	0.12 (5.2)	5,80 (5,8)
	FEP2	6	7.67 (1.0)	297 (1.6)	170.0	8.8	9.5	3.3	2.6	0.3	0.4	61.7	2.79 (14.6)	0.25 (6.7)	0.15 (7.9)	0.07 (16.5)	0.11 (9.2)	0.01 (20.8)	0.04 (5.7)	3,08 (5,7)
	FPM2	5	7.65 (4.2)	417 (6.9)	205.0	16.2	22.1	5.1	4.7	0.8	1.8	82.8	3.36 (8.6)	0.46 (31.4)	0.36 (23.4)	0.11 (76.3)	0.21 (29.6)	0.02 (34.4)	0.15 (22.0)	4,13 (5,6)
	FP2	4	7.15 (1.2)	1095 (0.7)	288.2	165.8	38.0	29.5	34.1	21.2	5.4	167.6	4.72 (2.4)	4.68 (11.4)	0.61 (8.7)	0.61 (3.9)	1.48 (12.2)	0.54 (4.0)	0.45 (5.5)	8,36 (3,0)
	FP	4	7.69 (4.8)	512 (7.0)	185.1	39.0	45.0	5.0	7.8	0.3	0.8	96.9	3.03 (5.4)	1.10 (8.6)	0.73 (11.0)	0.10 (2.1)	0.34 (1.3)	0.01 (14.8)	0.07 (14.0)	4,84 (7,4)
	FB	1	7.35	581	241.6	28.0	36.6	13.0	7.2	0.5	0.8	116.5	3.96	0.79	0.59	0.27	0.31	0.01	0.07	5,81
	PS	4	7.39 (0.5)	502 (3.2)	213.8	23.6	32.4	7.8	6.0	0.9	1.0	99.1	3.50 (14.1)	0.67 (5.9)	0.52 (8.2)	0.16 (17.2)	0.26 (4.5)	0.02 (12.8)	0.08 (3.9)	4,94 (4,6)
	P1	3	7.30 (0.8)	664 (5.1)	290.0	31.3	27.5	32.4	10.4	4.3	2.5	120.8	4.75 (4.7)	0.88 (10.6)	0.44 (13.3)	0.67 (11.6)	0.45 (6.3)	0.11 (49.0)	0.21 (8.8)	6,03 (3,6)
	P5	6	7.28 (0.6)	595 (1.9)	260.3	26.0	27.9	28.5	9.9	2.3	2.4	117.9	4.27 (4.9)	0.73 (4.9)	0.45 (2.8)	0.59 (5.5)	0.43 (10.7)	0.06 (10.0)	0.20 (7.3)	5,88 (3,2)
	P6	9	7.55 (3.3)	534 (2.9)	253.9	20.6	22.6	16.7	7.5	1.6	2.0	107.5	4.16 (9.4)	0.58 (7.1)	0.36 (4.7)	0.35 (7.7)	0.32 (11.2)	0.04 (10.9)	0.16 (7.2)	5,37 (3,4)
	SEP	7	7.44 (4.9)	523 (6.2)	226.3	23.5	33.1	12.1	5.7	1.4	1.0	101.6	3.71 (4.8)	0.66 (24.4)	0.53 (19.9)	0.25 (27.6)	0.25 (24.5)	0.04 (18.3)	0.09 (8.7)	5,07 (5,7)
	SCG	2	7.19 (3.2)	559 (0.9)	232.4	28.5	40.7	11.3	7.4	0.5	1.1	106.4	3.81 (1.1)	0.80 (0.6)	0.66 (0.4)	0.23 (3.2)	0.32 (5.3)	0.01 (13.9)	0.09 (5.8)	5,31 (2,0)
	SB1	1	6.87	502	176.9	16.5	7.8	62.0	10.2	0.9	2.7	93.9	2.90	0.47	0.13	1.29	0.44	0.02	0.22	4,69
	SB2	1	7.05	845	402.6	18.4	2.3	70.1	13.0	1.3	4.8	171.4	6.60	0.52	0.04	1.46	0.56	0.03	0.39	8,55
	Minimum		6.87	297	170.0	7.2	2.3	3.3	2.6	0.3	0.4	61.7	2.79	0.20	0.04	0.07	0.11	0.01	0.04	3.08
	Mean		7.36	564	239.9	29.7	27.8	19.0	7.9	2.2	1.7	108.7	3.93	0.84	0.45	0.40	0.34	0.06	0.14	5.42
	Maximum		7.72	1095	402.6	165.8	54.3	70.1	34.1	21.2	5.4	171.4	6.60	4.68	0.88	1.46	1.48	0.54	0.45	8.55
	Variation coefficient (%)		2.68	26.9	19.8	94.8	45.1	93.6	72.0	174.9	67.8	22.7	19.8	94.9	45.1	93.6	72.1	174.2	68.1	22.7

Table III-8 : Major ion concentrations and physicochemical parameters of surface water from June 2017 to June 2019 (average values from monthly data) with the temporal variation coefficient (%) at each sampling point in brackets; N = Number of samples; EC = electric conductivity.

	Name	N	pH	EC ($\mu s \cdot cm^{-1}$)	HCO_3^-	Cl^-	NO_3^-	SO_4^{2-}	Na^+	K^+	Mg^{2+}	Ca^{2+}	HCO_3^-	Cl^-	NO_3^-	SO_4^{2-}	Na^+	K^+	Mg^{2+}	Ca^{2+}
					($mg \cdot L^{-1}$)								($meq \cdot L^{-1}$)							
Surface water	RS1	21	8.04 (3.3)	517 (4.5)	218.6	25.8	29.3	12.0	5.8	1.9	1.0	101.3	3.58 (7.5)	0.73 (6.6)	0.47 (6.2)	0.25 (20.5)	0.25 (11.3)	0.05 (24.5)	0.08 (9.6)	5,06 (4,6)
	RPY	21	7.94 (3.4)	488 (5.8)	222.6	20.7	28.5	6.5	5.1	0.9	1.0	97.4	3.65 (8.0)	0.58 (7.8)	0.46 (5.7)	0.14 (27.1)	0.22 (12.9)	0.02 (12.9)	0.08 (8.3)	4,86 (3,1)
	RS2	21	8.07 (2.8)	510 (4.9)	221.2	24.3	29.6	10.5	5.6	1.6	1.0	100.9	3.63 (7.3)	0.69 (5.3)	0.48 (6.1)	0.22 (20.6)	0.24 (8.1)	0.04 (17.8)	0.08 (9.8)	5,03 (4,1)
	RA	4	7.81 (1.0)	489 (3.4)	225.4	22.1	26.1	7.8	4.8	1.3	1.3	98.3	3.69 (4.8)	0.62 (4.6)	0.42 (4.6)	0.16 (10.5)	0.21 (12.0)	0.03 (13.0)	0.11 (8.6)	4,90 (4,0)
	RS3	4	8.07 (1.9)	520 (2.6)	225.4	25.2	28.8	11.7	6.4	1.9	1.3	102.1	3.69 (0.3)	0.71 (1.6)	0.46 (2.8)	0.24 (5.8)	0.28 (9.7)	0.05 (12.5)	0.11 (11.7)	5,10 (3,2)
	RV1	3	7.83 (1.1)	568 (2.4)	238.3	29.3	25.9	20.5	8.4	2.9	2.0	109.8	3.91 (2.6)	0.83 (3.8)	0.42 (14.4)	0.43 (6.3)	0.37 (14.0)	0.07 (13.1)	0.16 (23.3)	5,48 (4,8)
	RV2	3	7.95 (2.7)	469 (12.4)	222.4	25.0	28.5	12.5	6.4	1.8	1.1	101.7	3.65 (3.3)	0.71 (7.7)	0.46 (9.9)	0.26 (11.5)	0.28 (13.2)	0.05 (10.2)	0.09 (2.6)	5,08 (5,1)
	RP	1	8.10	512	201.3	21.3	25.6	13.9	5.9	1.6	1.1	94.8	3.30	0.60	0.41	0.29	0.26	0.04	0.09	4,73
	C1	1	8.20	412	176.9	18.3	12.7	15.6	6.4	2.8	4.9	73.0	2.90	0.52	0.20	0.32	0.28	0.07	0.41	3,64
	C2	1	7.12	480	207.4	15.5	13.1	15.8	6.6	3.0	6.6	80.4	3.40	0.44	0.21	0.33	0.29	0.08	0.54	4,01
	Minimum		7.12	412	176.9	15.5	12.7	6.5	4.8	0.9	1.0	73.0	2.90	0.44	0.20	0.14	0.21	0.02	0.08	3.64
	Mean		7.91	497	216.0	22.7	24.8	12.7	6.2	2.0	2.1	96.0	3.54	0.64	0.40	0.26	0.27	0.05	0.17	4.79
	Maximum		8.20	568	238.3	29.3	29.6	20.5	8.4	3.0	6.6	109.8	3.91	0.83	0.48	0.43	0.37	0.08	0.54	5.48
	Variation coefficient (%)		3.8	8.2	7.9	17.6	26.0	32.0	16.3	34.7	92.9	11.5	7.9	17.9	25.9	32.1	16.8	36.8	93.4	11.5

3.1.2. Trace elements

The statistical data of the trace elements measured concentrations are summarized in Table III-9. Some values below the limit of quantification (1 µg·L^{-1}) were retained if the coefficient of variation of the 3 measured values were below 10% (cf. Part II.2.3.4.2). However, these values should be used with caution as they were considered less reliable compared with the values above the detection limit.

Cu, Fe, Zn and Mn were the most detected trace elements in groundwater, with detected values representing 26.7%, 48.1%, 82.9% and 29.5% of the total number of analysis and average detectable values of 2.4, 10.7, 11.7 and 1.5 µg·L^{-1}, respectively (Table III-9). High concentrations of these elements were observed in water samples collected at pumping stations (PP and PDO) and private exploited boreholes equipped with pumps and pipework (FPM1 and FNA). This could possibly be explained by the common source of these elements originated from metal pipework and fittings in the water distribution systems or on boreholes (Stuart and Smedley, 2009). Specifically, of these four frequently detected elements, Zn was the most detected with concentrations varying over two orders of magnitude from 1 to 147.6 µg·L^{-1}. In fact, Zn could occur as a trace element in clays and in calcite and is typically present in higher concentrations than other trace elements under neutral pH conditions (Stuart and Smedley, 2009). Fe, Zn and Mn were also the most detected trace elements in surface water with detected values representing 78.8%, 80.0% and 100% of the total number of analysis. However, unlike in groundwater, Cu was less detected in surface water representing only 10% of the total number of analysis.

Concentrations of Pb were generally low in the ground- and surface waters, with detected values representing only 6.2% and 5% of the total number of analysis and average detectable concentrations of 2.1 and 1.7 µg·L^{-1}, respectively (Table III-9). The only samples with concentrations > 5 µg·L^{-1} was collected in FCE, an exploited boreholes equipped with pumps and pipes in an equestrian center on the Berru Mount (Figure II-8).

Detectable concentrations of Al represented 21.1% and 11.3% of the total number of analysis in ground- and surface waters, with average detectable concentrations of 5.4 and 3.8 µg·L^{-1}, respectively. Potential sources of Al include clay and silt minerals (Gillon et al., 2010), which is consistent with high concentrations (up to 21.6 µg·L^{-1}) observed on areas covered by superficial formations (FBN5, FEP1, PPM1 and FPM3; Figure II-8).

Concentrations of As and Sb were universally low in all water samples with no values > 5 µg·L^{-1}. Measured Cr concentrations were also low with average detectable values of 1.3 and 0.3 µg·L^{-1} in ground- and surface waters. The only samples with concentrations > 5 µg·L^{-1} were collected in borehole FP1 (Figure II-8). Cd, Co and Ni were not detected (<1 µg·L^{-1}) in ground- and surface water.

Table III-9 : Concentrations of trace elements in groundwater and surface water measured from June 2017 to June 2019 (average of detectable values) with N = Number of samples; N/D = not detected.

	Name	N	Cu	Fe	Zn	Mn	Pb	Al	As	Cd	Co	Cr	Ni	Sb
			($\mu g \cdot L^{-1}$)											
Groundwater	FA	21	0.8	4.3	1.9	0.5	1.4	3.4	2.5	N/D	N/D	0.6	N/D	2,6
	FAP	21	1.1	1.6	5.1	0.6	1.0	3.3	1.9	N/D	N/D	3.9	N/D	3,6
	FBN1	21	0.9	4.0	3.0	0.6	N/D	2.7	2.0	N/D	N/D	0.9	N/D	0,9
	FBN4	21	1.2	2.7	2.6	0.5	N/D	2.5	2.2	N/D	N/D	1.3	N/D	2,7
	FBN5	21	1.8	8.9	18.4	1.3	1.4	10.9	2.1	N/D	N/D	1.5	N/D	1,9
	FEP1	21	1.3	4.0	2.2	0.3	N/D	19.5	2.1	N/D	N/D	0.4	N/D	2,5
	FP1	21	N/D	4.9	2.8	0.6	0.7	3.5	N/D	N/D	N/D	7.3	N/D	1,6
	FPM1	21	8.0	9.8	147.6	1.2	1.7	10.7	3.0	N/D	N/D	0.3	N/D	2,6
	FPM3	21	1.5	5.0	3.3	2.3	N/D	8.8	N/D	N/D	N/D	0.6	N/D	N/D
	FVDV	21	0.6	4.0	1.9	0.4	N/D	N/D	0.3	N/D	N/D	0.3	N/D	N/D
	PDO	21	4.4	11.7	12.3	0.4	N/D	2.3	3.2	N/D	N/D	N/D	N/D	2,2
	PP	21	1.9	13.0	6.9	0.6	1.7	2.6	3.1	N/D	N/D	0.7	N/D	N/D
	FCE	1	3.5	N/D	5.1	N/D	7.2	N/D	N/D	N/D	N/D	N/D	N/D	N/D
	FNA	1	9.7	19.5	41.8	3.3	N/D	N/D	N/D	N/D	N/D	N/D	N/D	N/D
	FBN3	3	N/D	6.6	1.0	N/D	N/D	1.9	N/D	N/D	N/D	N/D	N/D	N/D
	FBN2	4	0.5	3.0	3.5	1.3	N/D	2.3	3.0	N/D	N/D	0.9	N/D	N/D
	FEP2	6	N/D	3.0	2.6	0.3	N/D	3.0	3.4	N/D	N/D	0.6	N/D	2,5
	FPM2	5	N/D	2.6	2.2	1.0	1.3	3.6	N/D	N/D	N/D	N/D	N/D	1,1
	FP2	4	1.5	10.9	4.5	0.4	1.7	2.2	N/D	N/D	N/D	N/D	N/D	1,1
	FP	4	N/D	4.2	2.7	N/D	N/D	2.5	N/D	N/D	N/D	0.5	N/D	N/D
	FB	1	N/D	N/D	N/D	N/D	N/D	N/D	N/D	N/D	N/D	N/D	N/D	N/D
	PS	4	N/D	4.3	3.2	0.4	N/D	3.6	2.7	N/D	N/D	0.4	N/D	N/D
	P1	3	1.4	4.0	7.0	1.8	N/D	2.9	3.0	N/D	N/D	N/D	N/D	N/D
	P5	6	2.3	1.9	4.4	N/D	N/D	21.6	2.4	N/D	N/D	N/D	N/D	N/D
	P6	9	1.7	1.8	4.7	0.3	N/D	3.5	N/D	N/D	N/D	N/D	N/D	N/D
	SEP	12	N/D	3.5	2.8	1.1	N/D	1.5	2.9	N/D	N/D	0.3	N/D	1,7
	SCG	2	N/D	N/D	N/D	N/D	N/D	N/D	N/D	N/D	N/D	N/D	N/D	N/D
	SB1	1	N/D	90.1	N/D	9.1	2.8	N/D	N/D	N/D	N/D	N/D	N/D	2,1
	SB2	1	N/D	48.5	N/D	5.4	2.1	N/D	2.5	N/D	N/D	N/D	N/D	1,5
	% of detectable values		26.7	48.1	82.9	29.5	6.2	21.1	8.4	N/D	N/D	14.0	N/D	5.6
	Minimum		0.5	1.6	1.0	0.3	0.7	1.5	0.3	N/D	N/D	0.3	N/D	0.9
	Mean		2.4	10.7	11.7	1.5	2.1	5.4	2.5	N/D	N/D	1.3	N/D	2.0
	Maximum		9.7	90.1	147.6	9.1	7.2	21.6	3.4	N/D	N/D	7.3	N/D	3.6
Surface water	RS1	21	1.5	4.7	6.3	2.2	2.5	6.0	4.2	N/D	N/D	0.1	N/D	1,9
	RPY	21	N/D	4.3	2.6	1.7	1.1	3.1	1.9	N/D	N/D	0.1	N/D	N/D
	RS2	21	0.6	4.5	2.2	1.6	1.5	2.1	3.3	N/D	N/D	0.2	N/D	1,6
	RA	4	N/D	3.5	1.6	2.2	N/D	N/D	N/D	N/D	N/D	0.2	N/D	1,8
	RS3	4	N/D	2.4	2.4	1.5	N/D	N/D	4.8	N/D	N/D	0.7	N/D	N/D
	RV1	3	N/D	9.0	3.0	3.6	N/D	N/D	1.9	N/D	N/D	N/D	N/D	2,1
	RV2	3	N/D	2.5	1.6	1.7	N/D	N/D	N/D	N/D	N/D	N/D	N/D	N/D
	RP	1	N/D	N/D	1.7	0.4	N/D	N/D	4.3	N/D	N/D	N/D	N/D	1,4
	C1	1	N/D	N/D	0.6	0.6	N/D	N/D	2.9	N/D	N/D	N/D	N/D	1,4
	C2	1	N/D	3.3	N/D	1.7	N/D	N/D	N/D	N/D	N/D	N/D	N/D	N/D
	% of detectable values		10.0	78.8	80.0	100	5.0	11.3	12.5	N/D	N/D	6.3	N/D	8.8
	Minimum		0.6	2.4	0.6	0.4	1.1	2.1	1.9	N/D	N/D	0.1	N/D	1.4
	Mean		1.0	4.3	2.4	1.7	1.7	3.8	3.3	N/D	N/D	0.3	N/D	1.7
	Maximum		1.5	9.0	6.3	3.6	2.5	6.0	4.8	N/D	N/D	0.7	N/D	2.1

3.2. Origin of major ions

The correlation relationship between major ions were calculated by using an approach based on a semi-parametric regression model. More precisely, a generalized additive model with cubic splines accounting for autocorrelation of data through a first order autoregressive model (AR1) was used. Each generalized additive model was carried out using the Akaike information criterion score and the likelihood ratio (Cao et al., 2020). The corresponding adjustment coefficient of determination (Adj. R^2) associated with a significance test at a P-value < 0.01 was used to characterize correlations between response variable and the explicative one. The detailed results are presented in Appendix 4.

The correlation matrix of major ions and relationships between ions were used to study the origin of major ions (Appendix 4 and Figure III-18). Concentrations of Ca^{2+} and HCO_3^- ions are significantly correlated (Figure III-18a and Appendix 4), which is consistent with the typical chemistry of Chalk groundwater. However, Ca^{2+} / HCO_3^- plots (Figure III-18a) are not aligned to the 1:1 line (Edmunds et al., 1987) with an enrichment of Ca^{2+} compared with HCO_3^-, indicating a secondary origin of Ca^{2+} in addition to Chalk dissolution (Barhoum et al., 2014).

Ca^{2+} excess compared with HCO_3^- was then plotted with the sum of Cl^-, NO_3^- and SO_4^{2-} (Figure III-18b). Most data points are plotted along the 1:1 line, implying that Ca^{2+} excess may be due to an agricultural source as Cl^-, NO_3^- and SO_4^{2-}. Indeed, a common agriculture source of Cl^-, NO_3^- and SO_4^{2-} is also indicated by a significant correlation between these ions (Appendix 4). In fact, lime (CaO) can be used in agricultural to optimize field pH (Aquilina et al., 2012; Bolan et al., 2003) and some fertilizers could contain CaO or Ca^{2+} as secondary or minor component (such as *TSP-SUPER 45*® used in the Champagne region).

According to the Cl^- *versus* Na^+ graph (Figure III-18c), a high enrichment of Cl^- is observed with respect to the meteoric water line (Edmunds et al., 1987; Kloppmann et al., 1994), which confirms the Cl^- source due to anthropogenic activities. Indeed, chlorine salt is used by sugar factories on the study area for the sugar beet extractions. The discharge water of these sugar factories containing high concentrations of Cl^- is spread directly on the surface of farmlands to be used as agricultural fertilizer, which could explain then enrichment of Cl^- in Chalk groundwater of the study area (Cristal Union, 2018).

Also, the correlation is observed between Mg^{2+}, K^+ and SO_4^{2-} ions (Appendix 4). These correlation relations imply that Mg^{2+}, K^+ and a part of SO_4^{2-} may have a common terrigenous source. In fact, Chalk impurities and clay minerals in superficial formations (mainly colluvium and alluvium in the study area) may provide Mg^{2+}, K^+ as well as SO_4^{2-} to groundwater (Gillon et al., 2010; Stuart and Smedley, 2009).

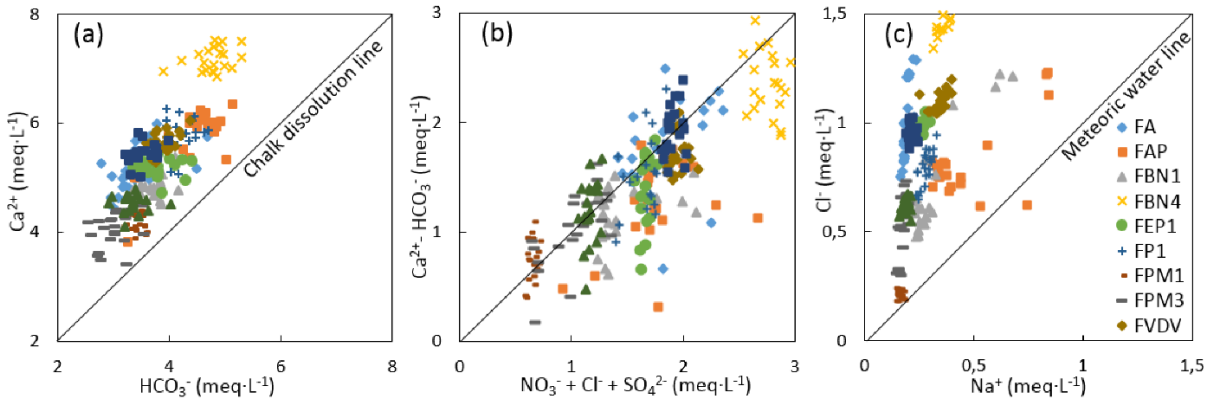

Figure III-18 : (a) Ca^{2+} versus HCO_3^- (solid line 1:1 represents the Chalk dissolution line); (b) [Ca^{2+} - HCO_3^-] versus [NO_3^- + Cl^- + SO_4^{2-}]; (c) Cl^- versus Na^+ (solid line 1:1 represents the meteoric water line).

3.3. Spatio-temporal variations of Chalk groundwater geochemistry under effects of hydrogeological setting and residence time

3.3.1. Spatial variation of Chalk groundwater geochemistry

In order to study the spatial distribution of Chalk groundwater geochemistry, the Piper plot of major ions was realized (Figure III-19), with the aim to clarify the chemical facies of surface and groundwater in the study area.

For the majority of ground- and surface water samples, a similar Ca^{2+} - HCO_3^- chemical facies is observed. However, several water samples show significant different chemical facies as the others, which is the case for one groundwater sampling site in the Chalk aquifer (FP2) and all the sampling sites in the Berru Mount area (SB1, SB2, FCE and FNA) and the Aisne-Marne Canal (C1 and C2) (Figure III-19).

The values of EC of groundwater samples collected at FP2 are the highest of all water samples collected in the study area, with high concentrations of almost all major ions (Table III-7). At the two other sampling sites located close to FP2 (FAP and FP1; Figure II-8), the values of EC and concentrations of major ions are much lower than those of FP2. This could probably be explained by the pollution caused by improper manipulations during drilling or by the presence of localized source of contamination (industrial and/or agricultural) at the borehole FP2.

For groundwater samples collected in the Berru Mount area (SB1, SB2, FCE and FNA), the Piper plot shows higher concentrations of SO_4^{2-} (Figure III-19). Higher concentrations of Na^+, Mg^{2+} and K^+ at these points are also observed (Table III-7). This could possibly be explained by the tertiary formations covered on the Chalk at the Berru Mount (cf. Part II.1.2.2), as these ions are presented in higher concentrations in clay, marl and gypsum minerals of tertiary formations (Gillon et al., 2010; Lambert, 1858).

Surface water samples collected in the canal (C1 and C2) show also different chemical facies, with significantly higher concentrations of Mg^{2+} than the other water samples (Figure III-19). This implied that the canal is not directly related to the Chalk aquifer of the study area. In fact, the canal water originates mainly from the the Vesle River far upstream and the Marne River, whose watershed areas have different hydrogeological contexts from the unconfined Chalk aquifer in the study area.

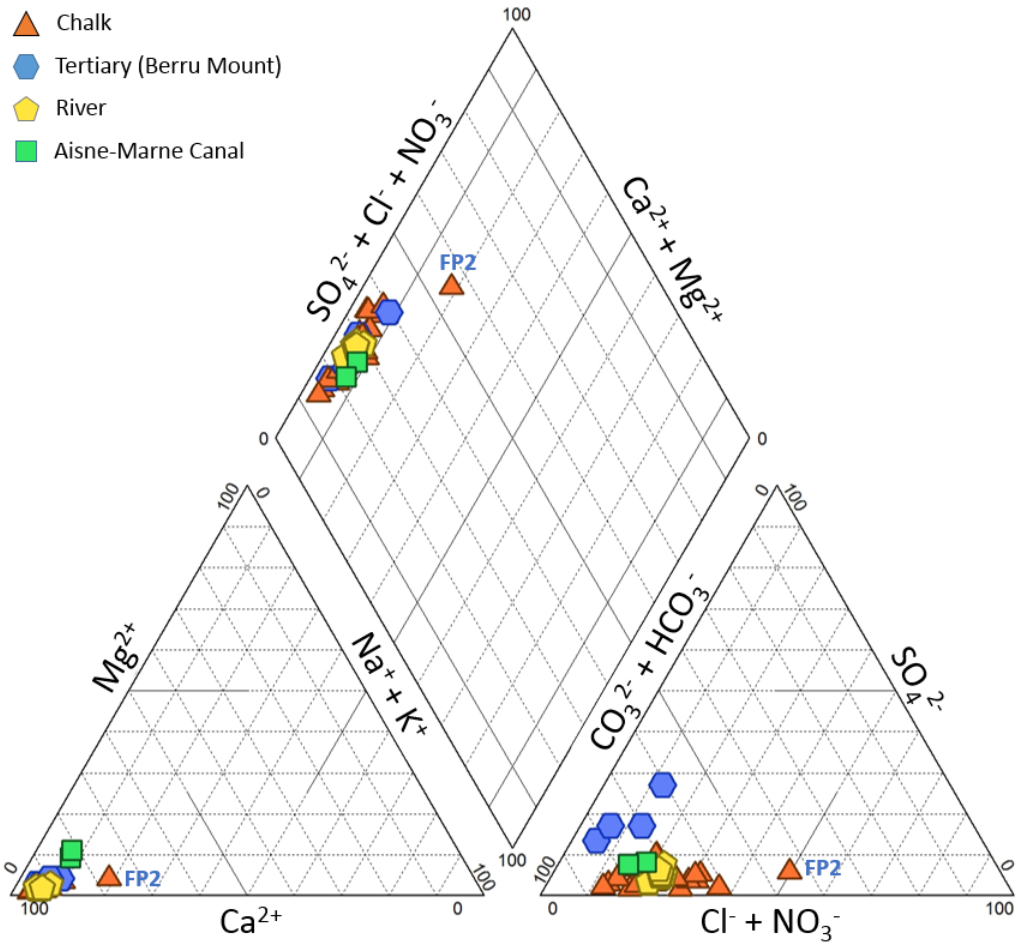

Figure III-19 : Piper plot of major ions in groundwater and surface water

The Piper plot allowed to provide a global visualization of the spatial distribution of geochemistry and to distinguish sites with different chemical facies than the majority of sampling points (especially Berru Mount and the Aisne-Marne Canal). However, for the majority part of the Chalk aquifer presenting a very similar Ca^{2+} - HCO_3^- chemical facies, the spatial distribution was not yet clarified. To achieve this, a principal component analysis (PCA) of major ion concentrations on the 15 monthly monitored sampling points was performed (Figure III-20).

All monthly monitoring data for major ion concentrations at each sampling site are used in order to take into account the temporal variation in concentrations. In the PCA graph, each site is plotted using the center of the monthly data clustering for a better visualization of the spatial distribution of geochemistry. The first two principal components (F1 and F2) justified together 78% of the variance. F1 was positively weighted on the allochthonous agricultural ions (NO_3^- and Cl^-) and on Ca^{2+} (more weakly) and negatively weighted on Na^+, Mg^{2+}, SO_4^{2-}, K^+ and HCO_3^-, which were interpreted as autochthonous ions. F2 was positively weighted on all the major ions but the most strongly on Ca^{2+} and HCO_3^-, which correspond to the typical geochemistry of Chalk groundwater dominated by these two ions.

Hierarchical clustering of PCA shows a vast spatial heterogeneity of major ion concentrations the study area and distinguishes six water-type groups (Figure III-20). RS1, RS2 and RPY (river waters) are plotted near the center zone of PCA graph, implying that the geochemistry of river water is similar to the average condition of groundwater, which is justified by the drainage of the whole aquifer by the rivers. Relatively low concentrations of agricultural ions (NO_3^-, Cl^- and Ca^{2+}) are observed at FBN1 and FBN5, which could be explained by the large UZ thickness (> 20 m; Table III-3), whereby the aquifer tends to be less influenced by agriculture activities (e.g., fertilizer applications). In contrast, higher concentrations of agricultural ions are observed at FVDV, PDO, FA and FEP1 because of smaller UZ thickness (< 10 m; Table III-3). Extremely high major ion concentrations at FBN4 are supposed to be related to the landfill located upstream (Figure II-6), representing an important point source of pollution. FP1 and FAP have a similar chemical composition with high concentrations on autochthonous ions especially Na^+. At these two points, the Chalk is covered by a large surface of colluvium, which represents a possibly source of Na^+ in groundwater (Gillon et al., 2010). Low concentrations of major ions are observed at FPM1, FPM3 and PP, which could be explained by the presence of superficial formations (graveluche and alluvium) limiting the transfer of water and solute from surface to the aquifer (Linoir, 2014). The impact of superficial formations overlying the Chalk on groundwater geochemistry are further discussed in the following section.

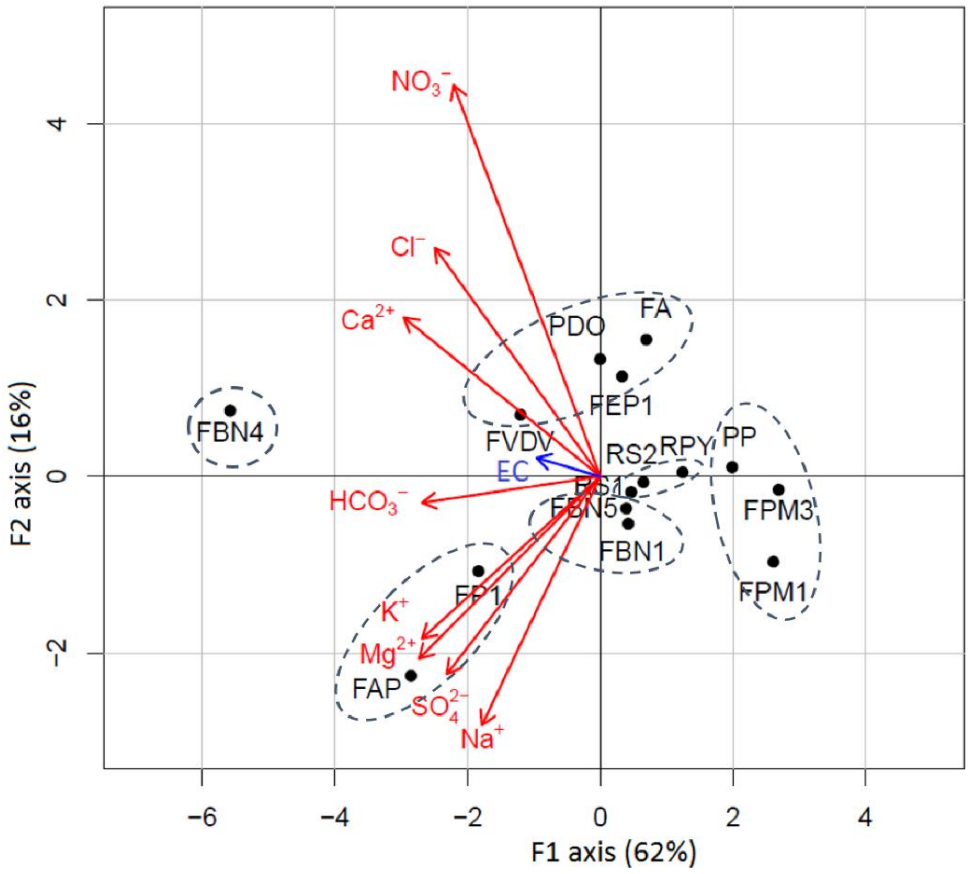

Figure III-20 : PCA of major ion concentration in groundwater and surface water (mean values of monthly data at each sampling point from June 2017 to June 2019; dotted circles evidences the six water-type groups discussed in the text)

3.3.2. Temporal variation of chalk groundwater geochemistry

The temporal variation of groundwater geochemistry was explored by analyzing the chronicle of EC and major ion concentrations compared with groundwater level time series. Different correlation relationships between the EC time series and groundwater level fluctuations were observed: correlated, anti-correlated or independent (Figure III-21).

The variation of EC could mostly be attributed to the variation of concentrations of NO_3^- and Cl^-, as the curves of NO_3^- and Cl^- showed very similar tendencies as that of EC (Figure III-21 and Figure III-22). As the two dominant ions in Chalk groundwater, concentrations of Ca^{2+} and HCO_3^- were relatively stable with time (Figure III-23). Nevertheless, the temporal variability of Ca^{2+} was slightly higher than that of HCO_3^-, which could probably be explained by the secondary (agricultural) source of Ca^{2+} in addition to Chalk dissolution (see Part III.3.2). As to Na^+, Mg^{2+} and K^+, which were interpreted as mostly autochthonous ions, the concentrations were generally independent on the groundwater level fluctuation and stable over time (Figure III-24). Several exceptions were observed for the concentration of Na^+: relatively high variabilities were observed for groundwater samples collected at FBN1 and river water samples (RS1, RPY and RS2). Indeed, a waste deposit site is located close to FBN1 (Figure II-6) and the infiltration of leachate from the site could contain high concentrations of Na^+ (Medalie, 2013), which could probably explain the abnormality of Na^+ at FBN1. In river samples, increases on Na^+ concentrations were observed during winter period, which could be due to the contamination of river water by road salt in winter (Medalie, 2013).

In order to study more precisely the geochemistry of Chalk groundwater in the study area, the temporal variations of EC and major ions concentrations were analyzed at each sampling site. A combination of hydrogeological setting, residence time and land use information were used to explain the temporal variations of Chalk geochemistry.

3.3.2.1. Area with large fluctuation in water level

Large fluctuation in water level was observed at FBN1 and FBN5 (> 12 m; Table III-3). EC time series were highly correlated with water level fluctuations (Figure III-21 and Table III-10). During high water level period in 2018, water level increased substantially following intensive recharge, resulting in an increase in EC of about 150 and 300 $\mu s \cdot cm^{-1}$ at FBN1and FBN5 respectively. However, no significant variation of EC was observed during high water level period in 2019, as water level was much lower under dry climate conditions. Significant correlation relationship was also observed between time series of NO_3^-, Cl^-, Ca^{2+} concentrations and water level fluctuation (Figure III-22, Figure III-23 and Table III-10).

According to groundwater dating, the groundwater flow was described by the exponential mixing model and a mean residence time (MRT) of 18 years was estimated at FBN1 (no accurate age was deduced for FBN5), indicating a spatially uniform recharge and a mixture of different flows (Table III-6). In this context, contaminants concentrated near the land surface area (e.g. agricultural ions including NO_3^-, Cl^- and Ca^{2+}) infiltrated progressively across the UZ following recharge. Under low water level conditions, the contamination front was disconnected with the SZ. It transferred slowly downward through the unsaturated Chalk matrix. Meanwhile, solutes in the SZ were diluted by the mixing process of groundwater, so that a low EC was observed. As water level rose and reached the contamination front, the contamination source was re-activated and contaminants concentrations increased rapidly in the SZ so that a high EC was observed (Brouyère et al., 2004).

At FBN4, a high correlation between EC and large water level fluctuation (15.5m; Table III-3) was also observed in a context of exponential mixing (MRT = 17 years; Table III-6). However, the temporal variation of EC followed that of water level during the whole monitoring period (2017-2019) while EC remained stable at low water levels at FBN1 and FBN5. This could be explained by the thin UZ at FBN4 (2.5m; Table III-3), whereby the contaminated area was always partially submerged by groundwater level even during low water level period.

At FVDV, the water level fluctuation was smaller (8 m; Table III-3), resulting in a lower correlation between EC and water level times series (r = 0.69; Table III-10) compared to FBN1, FBN4 and FBN5. Groundwater consisted mainly of 30-year-old water mixed with 25-30% of modern water, suggesting small contributions of rapid recharge through fractures.

3.3.2.2. Area with developed fracture network and low UZ thickness

EC time series were inversely related to water level fluctuation at FAP and FA (Figure III-5 and Figure III-21), suggesting that the dilution effect was the most important factor that influences the geochemistry. At these two sites, the UZ thickness was low (< 3 m; Table III-3) and fractures were supposed to be developed near surface area. Groundwater dating showed 50-70% and 75-80% of modern water at FAP and FA respectively by the binary mixing model (Table III-6), indicating an aquifer constituted mainly by freshly percolated rainwater that favors the process of dilution. Larger proportion of modern water at FA could be explained by its location close to groundwater divide line, receiving few lateral flow. It should be noted that, even during high water level period, the groundwater at FAP and FA was composed of 20% to 50% of old water aged over 30 years. This older end-member is linked to the lateral flow originated from upstream recharge areas.

3.3.2.3. Area with superficial formation

EC values as well as concentrations of major ions were stable in time at FPM1 and FEP1 (Figure III-21 to Figure III-24). Groundwater dating showed a residence time of > 30 years at FEP1 in a piston flow context, indicating a small recharge area away from the site (no accurate age was deduced for FPM1; Table III-6).

These two wells are situated in the north of the study area, where large surfaces of the Chalk are covered by graveluche (Figure II-8). The graveluche layers rich in clayey minerals are less permeable with an infiltration rate about 3 to 4 times slower than in the Chalk, therefore could constitute a barrier or buffer zone that limits rapid transport of water and solute from surface to the SZ (Linoir, 2014). Consequently, the aquifer received recharge mainly from the upstream graveluche covered area (near the Champagne mounts; Figure II-8). Water traveled laterally in the SZ during more than 30 years, resulting in a stable geochemistry independent on water level fluctuation.

At FPM3 (downstream the borehole FPM1; Figure II-8), a time lag was observed between EC and water level time series, as a result of delayed solute transfer by the discontinuous graveluche formations. At PP, EC was also stable with a residence time of about 40 years estimated by a piston flow model (Table III-6). With a high proportion of clayey minerals, the alluvium can play the same role as graveluche as a flow barrier on the Chalk. Moreover, the deep screen position of PP (23-80 m; Table III-3) allowed pumping of deep groundwater with longer residence time. Previous studies have shown that other superficial formations such as flint clay layers can have similar impacts on Chalk aquifers (e.g., Barhoum et al. 2014; El Janyani et al. 2012).

3.3.2.4. Area along riverside

PDO is a pumping station used for drinking water supply located close to the Suippe River (Figure II-8). The drawdown of groundwater level due to intensive exploitation could result in a recharge of aquifer by river water, as testified by a higher proportion of modern water in October than in May 2018 (Table III-6). Indeed, the groundwater level was lower in October resulting in increased flow from the river to the aquifer. The EC and concentrations of major ions of river water was relatively stable, making the EC and concentrations of major ions at PDO stable over time.

FP1 is a non-exploited borehole located in the Vesle River valley (Figure II-8). No correlation relationship between EC and water level was observed. Located far from the groundwater divide line, FP1 has a very large recharge area, receiving groundwater of different residence times (a mean residence time of 35-40 years was estimated in an exponential mixing context; Table III-6). As a result, groundwater chemistry was greatly buffered, and EC was poorly related to water level fluctuation.

*Table III-10 : Correlation coefficient (r^2) of electric conductivity and all major ions with groundwater level (statistically significant as the P-value < 0.05, related r^2 values when P-value < 0.05 are marked in bold; calculation details are presented in **Appendix 5**)*

	EC	HCO_3^-	Cl^-	NO_3^-	SO_4^{2-}	Na^+	K^+	Mg^{2+}	Ca^{2+}
FBN1	**0.95**	0.06	**0.95**	**0.58**	**0.51**	**0.95**	0.20	**0.88**	**0.57**
FBN4	**0.73**	**0.19**	0.15	0.05	**0.62**	0.04	0.32	0.32	**0.21**
FBN5	**0.89**	**0.86**	**0.40**	**0.37**	**0.29**	0.11	**0.46**	**0.76**	**0.72**
FVDV	**0.68**	-0.05	0.14	**0.22**	**0.47**	0.04	**0.27**	0.07	0.07
FEP1	-0.01	0.14	0.02	**0.3**	0.08	0.19	0.01	0.01	0.07
FP1	**0.2**	0.03	-0.04	**0.03**	**0.5**	0.08	0.25	0.29	0.02
FA	0.02	0.09	0.11	0.14	0.18	0.05	0.03	0.31	0.21
FAP	-0.05	-0.04	0.02	0.06	0.02	0.00	0.02	0.04	0.05
FPM3	**0.26**	0.01	0.00	0.02	**0.62**	0.09	0.05	0.08	0.01

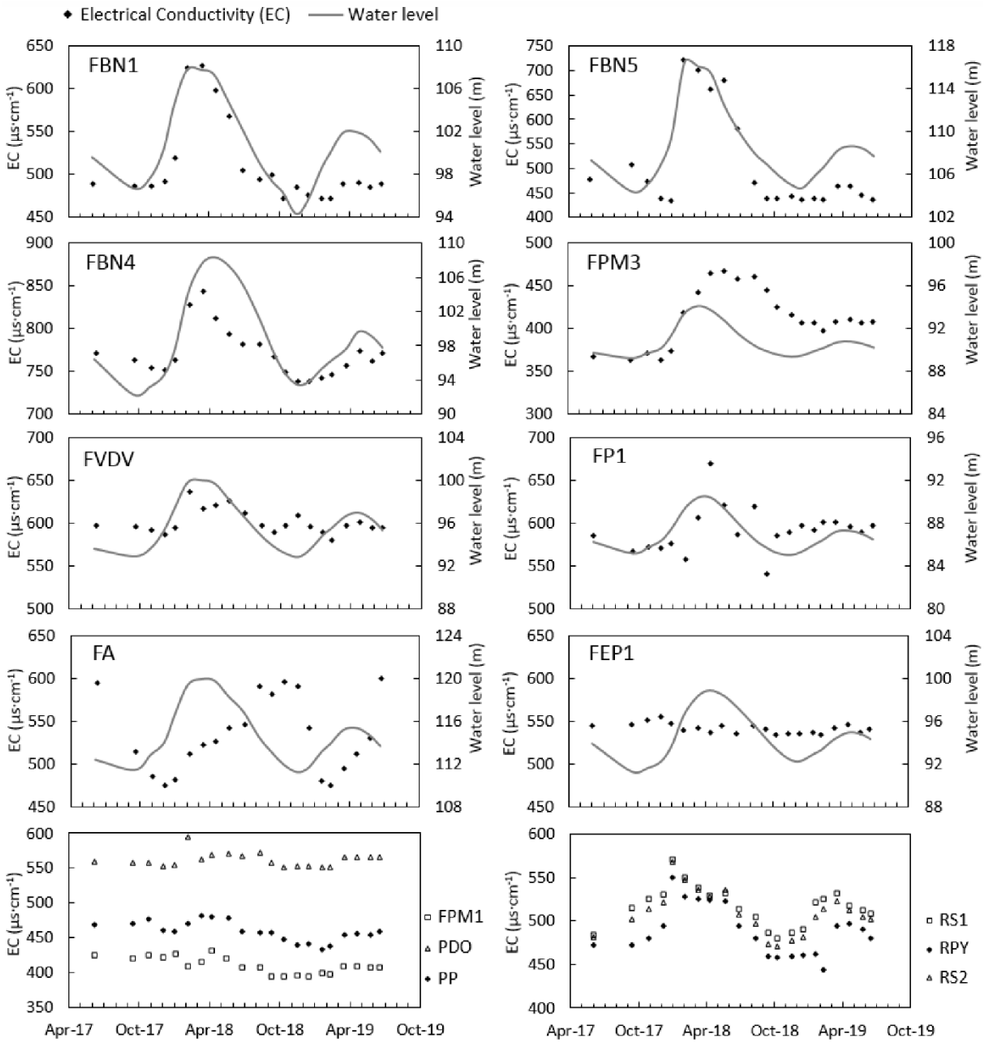

Figure III-21: Temporal variation of groundwater level and EC (monthly data from June 2017 to June 2019)

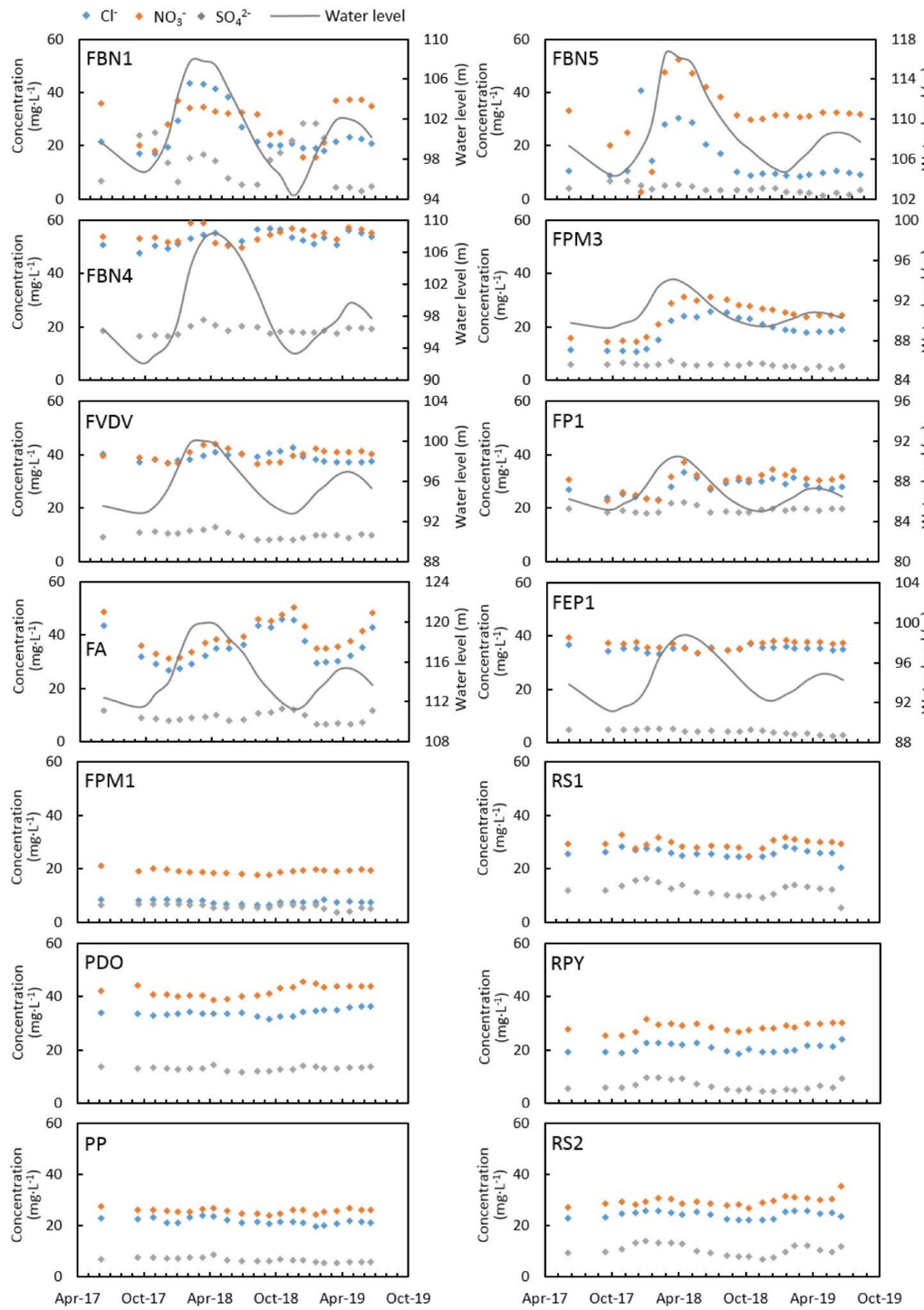

Figure III-22 : Temporal variation of Cl^-, NO_3^- and SO_4^{2-} (monthly data from June 2017 to June 2019)

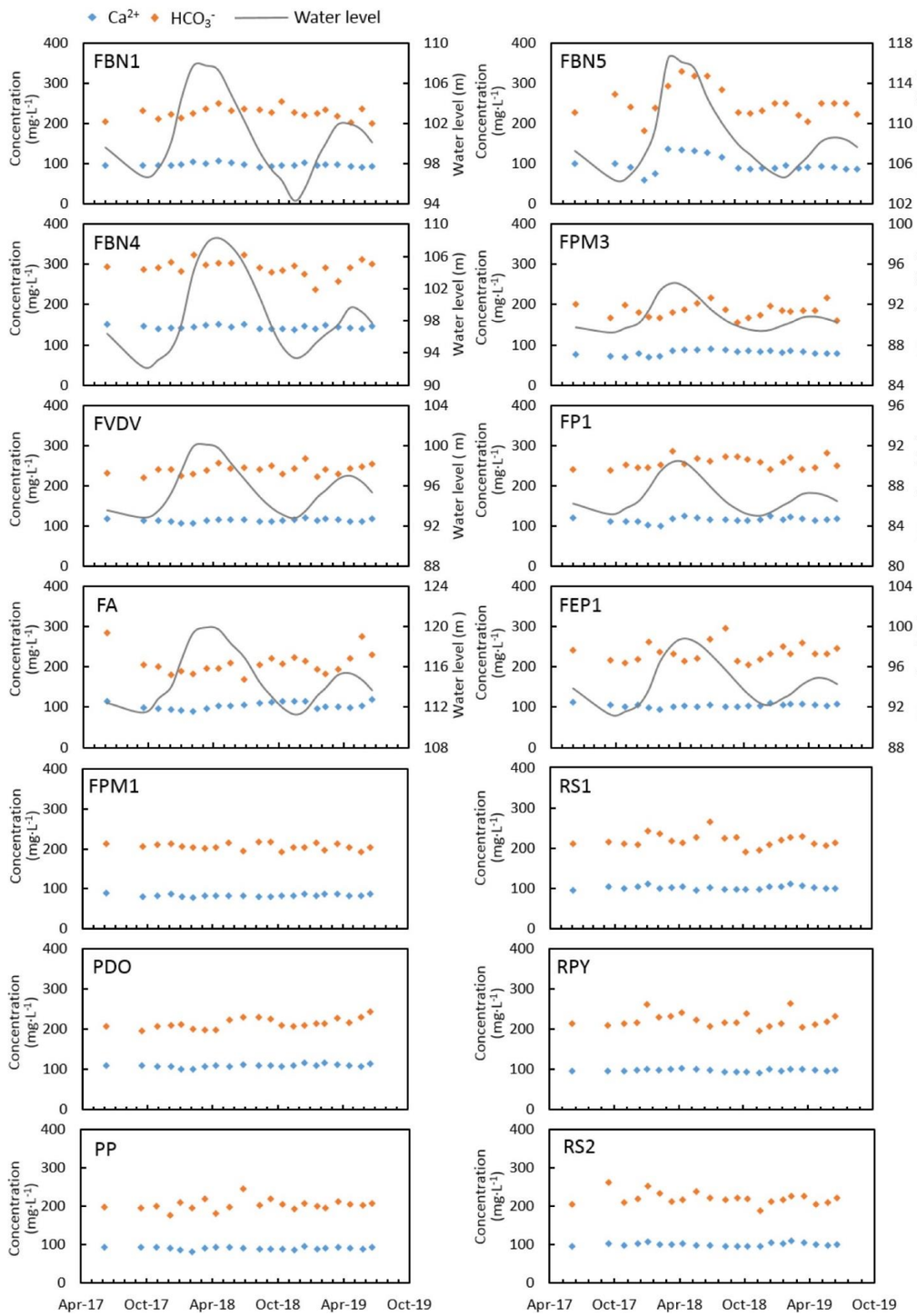

Figure III-23 : Temporal variation of Ca^{2+} and HCO_3^- (monthly data from June 2017 to June 2019)

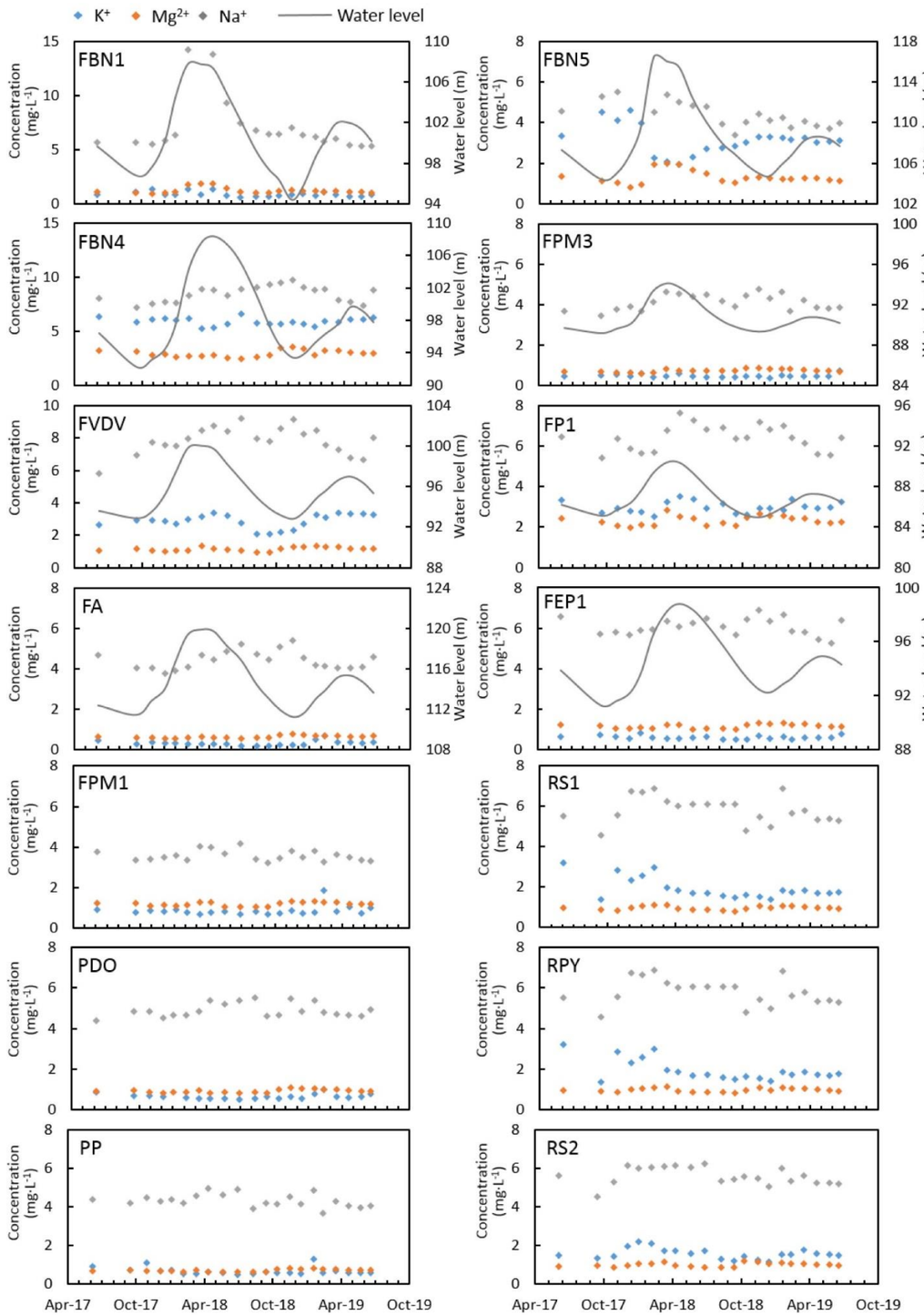

Figure III-24 : Temporal variation of K^+, Na^+ and Mg^{2+} (monthly data from June 2017 to June 2019)

4. Conclusion on hydrogeological functioning of the unconfined Champagne Chalk aquifer

A conceptual model of unconfined Chalk aquifer (Figure III-25) was established in order to explore how hydrogeological settings including fracture distribution, groundwater level depth, superficial formations and aquifer-river relationship can influence the hydrogeological functioning in terms of flow pathways, mixing process, residence time and groundwater geochemistry variation.

In general, under deep groundwater level conditions, the geochemistry of the aquifer tends to be less influenced by near surface contaminations with relatively low concentrations of agriculture ions. This situation usually occurs on interfluves, near the groundwater divide line (Figure III-25A). If no superficial formations overlay on the Chalk, the aquifer receives a spatially uniform recharge and an exponential mixing model could be applied with a relatively short residence time. As hydraulic conductivity is low on interfluve, groundwater level fluctuations are important, leading to levels of contamination positively correlated to water table dynamics.

At shallow groundwater sites, the thin UZ of Chalk aquifer is usually highly fractured (Figure III-25B). Rapid recharge through fractures is favored, making groundwater a mixture of freshly percolated water and old water coming from upstream recharge area, as demonstrated by a binary mixing model. The shallow groundwater sites with high proportion of modern water mainly locate in river valleys (where fracture networks are well developed) but could also present on interfluves. At these sites, groundwater geochemistry is mostly influenced by the dilution effects of infiltrated rain water, leading to mineralization degree of groundwater negatively correlated to water table dynamics.

Superficial formations overlaying on the Chalk such as graveluche, colluvium and alluvium have important effects on groundwater flow and geochemistry. These superficial formations are usually intermitted and constituted by high content of clayey minerals, presenting a lower permeability than the Chalk. They could consequently constitute a barrier limiting the rapid recharge of water and solute into the aquifer. At these sites, a piston flow model better describes the groundwater flow and relatively old groundwater ages are estimated, which could explain the stable or delayed groundwater geochemistry with respect to water table fluctuations (Figure III-25C and D).

For sites near rivers where groundwater is exploited, the exchange between groundwater and river water should be considered (Figure III-25E). The recharge of aquifer by rivers could occur, especially during low water level period, leading to groundwater geochemistry influenced by surface water.

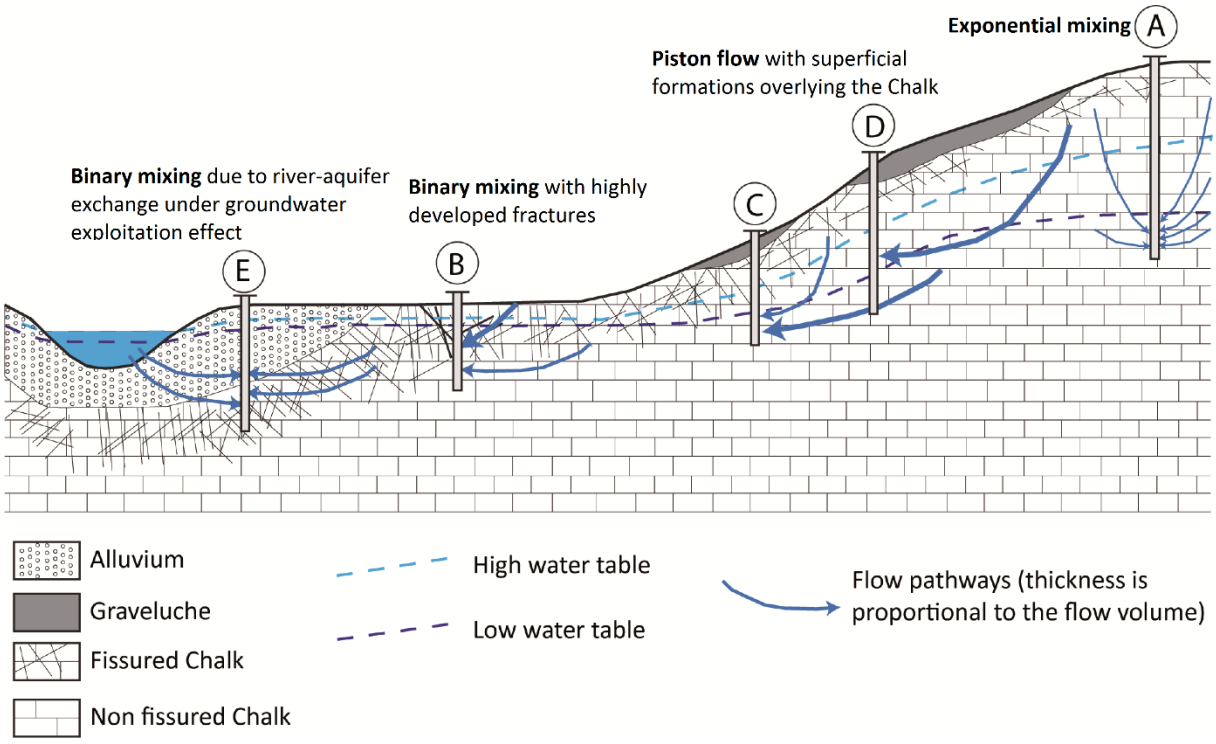

Figure III-25 : Schematized hydrogeological functioning of unconfined Chalk aquifers

In conclusion, seasonal and annual fluctuations of groundwater level were observed in the study area as a result of seasonal and annual variations in ER (aquifer recharge). Although the majority of the aquifer has an inertial behavior with respect to recharge, a rapid response following rainfalls can be observed locally by highly developed fractured network in the Chalk.

Groundwater dating using ^{3}H, CFCs and SF_6 showed that the aquifer is made up of waters of different ages ranging from modern to about 50 years, with piston flow, exponential or binary mixing models defined at each sampling site implying for different flow pathways and mixing processes in the aquifer.

Despite the Ca^{2+} - HCO_3^- chemical facies, a high spatial and temporal heterogeneity of groundwater geochemistry in the unconfined Chalk aquifer was highlighted. Different correlation relationships between the EC time series and groundwater level fluctuations were observed: correlated, anti-correlated or independent. These variabilities were explained by a combined effect of water level fluctuation, groundwater residence time, thickness of the UZ, superficial formations, distribution of fracturing network, aquifer-river relationships and human activities. The combination of different tools allowed the establishment of a conceptual model of chalk aquifer functioning, which could provide very useful information for a better management of this water resource under the context of intensive groundwater exploitation and water quality deterioration.

Part IV. Sources and behavior of perchlorate in the Champagne Chalk aquifer

Results and interpretations regarding the sources and evolution of perchlorate in the Champagne Chalk aquifer are presented in this part, based on a combination of continuously monitored ClO_4^- concentrations, isotopic analysis of ClO_4^- and NO_3^- as well as hydrologic and geochemical analysis accomplished in the previous parts.

This part is started by an introduction chapter, in which background of the study, objectives and methodology used are reiterated. Then, potential sources of perchlorate in the study area are presented, including former military activities/sites related to WWI, information regarding the former use of Chilean nitrates fertilizer as well as other industrial activities potentially emitting perchlorate into the environment. Next, measured concentrations of ClO_4^- and explosives are presented, with a detailed description of geographic distribution of ClO_4^- in the study area. According to the measured ClO_4^- concentrations and water flow rates in rivers, the mass flow rate of ClO_4^- is estimated with the aim to provide a quantitative vision of ClO_4^- contamination on a watershed scale. The results of isotopic analysis of ClO_4^- and NO_3^- are presented, allowing to provide evidence of ClO_4^- origin (synthetic and/or natural). Different tendencies of ClO_4^- variation are discussed, highlighting major sources of ClO_4^- and main factors governing the spatio-temporal variations of ClO_4^- in the Champagne Chalk aquifer. The results presented are discussed and summarized at last.

The results presented in Part IV has been published in "Journal of Hazardous Materials" in June 2020:

Cao, F., Sturchio, N.C., Ollivier, P., Devau, N., Heraty, L.J., Jaunat, J., 2020. Sources and behavior of perchlorate in a shallow Chalk aquifer under military (World War I) and agricultural influences. Journal of Hazardous Materials 123072. https://doi.org/10.1016/j.jhazmat.2020.123072.

The abstract of the article is presented below and complete version can be found in Appendix 6.

Abstract

Perchlorate (ClO_4^-) has been detected at concentrations of concern for human health on a large scale in groundwater used for drinking water supplies in NE France. Two sources are suspected: a military source related to World War I (WWI) and an agricultural source related to past use of Chilean nitrate fertilizers. The sources and behavior of ClO_4^- have been studied in groundwater and rivers near the Reims city, by monitoring monthly the major ions and ClO_4^- concentrations for two years (2017 – 2019), and by measuring the isotopic composition of ClO_4^- and NO_3^- in water samples. ClO_4^- was detected throughout the study area with high concentrations (> 4 $\mu g \cdot L^{-1}$) detected mainly downgradient of the Champagne Mounts, where large quantities of ammunition were used, stored and destroyed during and after WWI. A WWI military origin of ClO_4^- is inferred from isotopic analysis and groundwater ages. Different tendencies of ClO_4^- variation are observed and interpreted by a combination of ClO_4^- concentrations, aquifer functioning and historical investigations, revealing major sources of ClO_4^- (e.g., unexploded ordnance, ammunition destruction sites) and its transfer mechanisms in the aquifer. Finally, we show that concentrations of ClO_4^- in groundwater seems unlikely to decrease in the short- to medium-term.

1. Introduction

The large extent of ClO_4^- contamination in NE France (see Part I.1.2.2) is unlikely to have been caused by point sources related to industrial activities. Two potential sources are suspected: a military source related to WWI and an agricultural source related to the past use of Chilean nitrate fertilizer. For a better management of water resources in NE France, it is now necessary to clarify the source of ClO_4^- contamination (military and/or agricultural). In addition to hydrogeological and historical investigations, isotopic analysis of ClO_4^- can provide a direct approach for ClO_4^- source apportionment.

Measurements of stable isotope ratios of chlorine ($^{37}Cl/^{35}Cl$) and oxygen ($^{18}O/^{16}O$, $^{17}O/^{16}O$) and the fractional abundance of the radioactive isotope ^{36}Cl in ClO_4^- ions have shown that the primary source types of ClO_4^- (synthetic, Chilean (from Atacama Desert) and indigenous natural atmospheric deposition) can be clearly distinguished isotopically. Additional background information about the ranges of isotopic composition of ClO_4^- is detailed in Part I.1.1 (see also Cao et al., 2019).

The selected study area, located east of the Reims city in NE France, is a representative study area with two potential sources of ClO_4^- contamination (military and/or agricultural). In this agricultural and military (WWI) landscape, the primary objectives are 1) to assess the extent of ClO_4^- contamination and its spatial-temporal evolution in the Chalk aquifer, 2) to clarify the sources of ClO_4^- contamination (military and/or agricultural) and 3) to understand the mechanism of transport and predict the evolution of ClO_4^- in groundwater in the short- to medium- term.

To achieve these goals, the results hydrogeological investigations (groundwater dating along with hydrologic and geochemical analysis) presented in Part III are used, allowing to provide a solid background information for the study of ClO_4^- contamination. Historical investigations were realized, indicating sites/activities potentially emitting perchlorate into the environment in the study area. ClO_4^- concentrations were monitored monthly for two years based on the established sampling network (see Part II.2.2). In parallel, isotopic analysis of ClO_4^- and NO_3^- has been realized to better clarify the sources of ClO_4^-. This methodology could be further applied in other ClO_4^- contaminated areas.

2. Potential sources of perchlorate in the study area

2.1. Military activities related to WWI

The ancient region Champagne-Ardenne (now included in the new larger region Grand-Est) was intensively marked by events of World War I (WWI) (Facon, 2018; Laurent, 1988). Ammunition used during WWI can be loaded with explosives made up to 86% of ammonium perchlorate (Hubé, 2016). Large quantities of these ammunitions, exploded or not, are still buried underground since the end of the war (Robin des Bois, 2007). Potential sources of perchlorate include not only former battles sites and trench areas, but also the ammunitions storage / destruction sites used during and after WWI.

2.1.1. Trench areas and former battle sites during WWI

2.1.1.1. Trench areas

After the First Battle of the Marne (September 1914), the conflict got bogged down and a war of movement (mobile warfare) was then replaced by a war of position (trench warfare) for four years. Indeed, from September 1914 until October 1918, the front stabilized on an East-West line extending from Reims to Verdun and crossed the majority of the study area. The trench area extended from a few hundred meters to tens of kilometers wide (Allouc et al., 1995).

The spatial analysis and digitization of the defense networks by Taborelli (2018) based on the 1918 trenches maps of the "Groupes de Canevas de Tirs des Armées" allowed the mapping of German and Allied trenches in the study area (Figure IV-1). At the Champagne Mounts in middle of the study area, the defense networks were extremely intensive, with surface densities up to 5.6 km/km^2 of trenches. Theoretically, the number of shells fired was therefore very important in areas where the trench density is important, especially in the front line. In addition, bombs and trench mortars, used primarily in the first line, had a much higher explosive charge than artillery shells and therefore contained much more perchlorates (Taborelli, 2018).

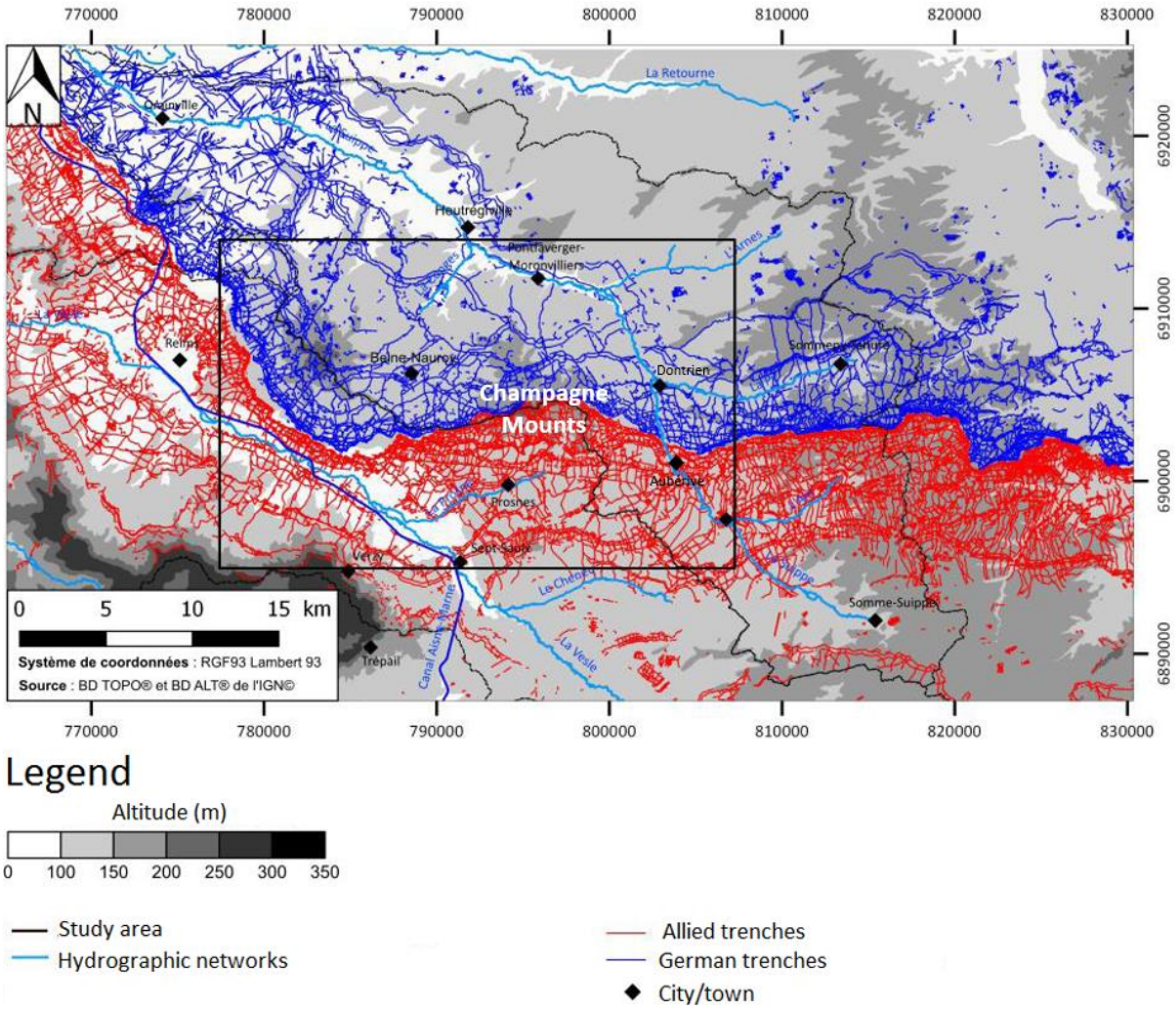

Figure IV-1 : Map of the WWI defense networks in the study area (adopted from Taborelli, 2018)

2.1.1.2. Former battle sites

During the 4-year of trench warfare, the trench area was the scene of intensive battles of WWI. Three major battles took place in the Champagne Region:

1) Second Battle of Champagne (September 1915 – October 1915)

It was a French offensive against the German army with a very limited French success, affecting mainly the eastern sector of the study area.

2) Battle of the Hills (April - May 1917)

The Battle of the Hills (Batailles des Monts de Champagne) was also known as the Third Battle of Champagne. The battle took place in the middle of the study area, along the Champagne Mounts which is formed by a group of connected hills (Figure IV-2). After the Battle, the French army took the Heights of Moronvilliers from the German army and about 6,000 German prisoners were taken (Front de Champagne 1914-1918, http://champagne1418.net/).

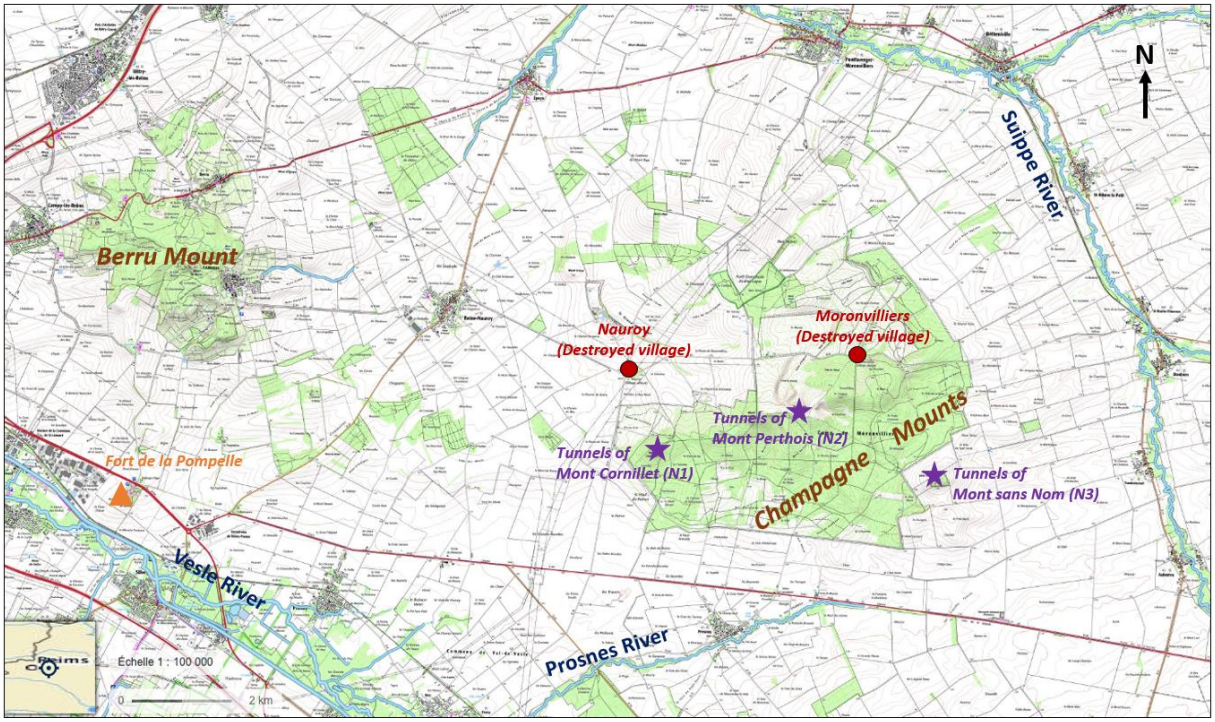

Figure IV-2 : Remarkable former military sites in the study area during the WWI

Several tunnels had been dug in the Chalk by the German army, such as tunnels of Mont Cornillet, Mont Perthois and Mont sans Nom (Figure IV-2). The tunnels of Mont Cornillet had three galleries, with light railways along two of the galleries, a transverse connecting tunnel and air shafts up to the top of the hill (Figure IV-3). These tunnels, equipped with quantities of ammunitions, were connected with the foremost German positions with the rear and allowed the German infantry to fire until the last moment. On May 20, 1917, a shell fired from the French army hit the Mont Cornillet and blocked an air shaft of one tunnel occupied by more than 600 German soldiers. The results of this French attack caused the death of all the occupants. After WWI, the tunnels of Mont Cornillet were forgotten until rediscovered in 1973. Countless ammunition and equipment were found, and more than 300 bodies of German soldiers were extracted (SOUTERRAINS & VESTIGES, http://souterrains.vestiges.free.fr/).

The tunnels of the Mont Perthois and Mont sans Nom were less elaborated than those of Mont Cornillet but also had many machine-gun posts, observatories and exits. Unfortunately, very limited information can be found today concerning these two tunnels. Indeed, other unknown tunnels could possibly exist, but it's difficult to find their traces as these tunnels were most likely destroyed by the French army after they had taken the sites so that the tunnels could not serve the enemy again (SOUTERRAINS & VESTIGES, http://souterrains.vestiges.free.fr/). It's very probably that quantities of ammunitions remain still underground at these sites until nowadays, representing potential sources of groundwater contamination on perchlorate and other pyrotechnic compounds.

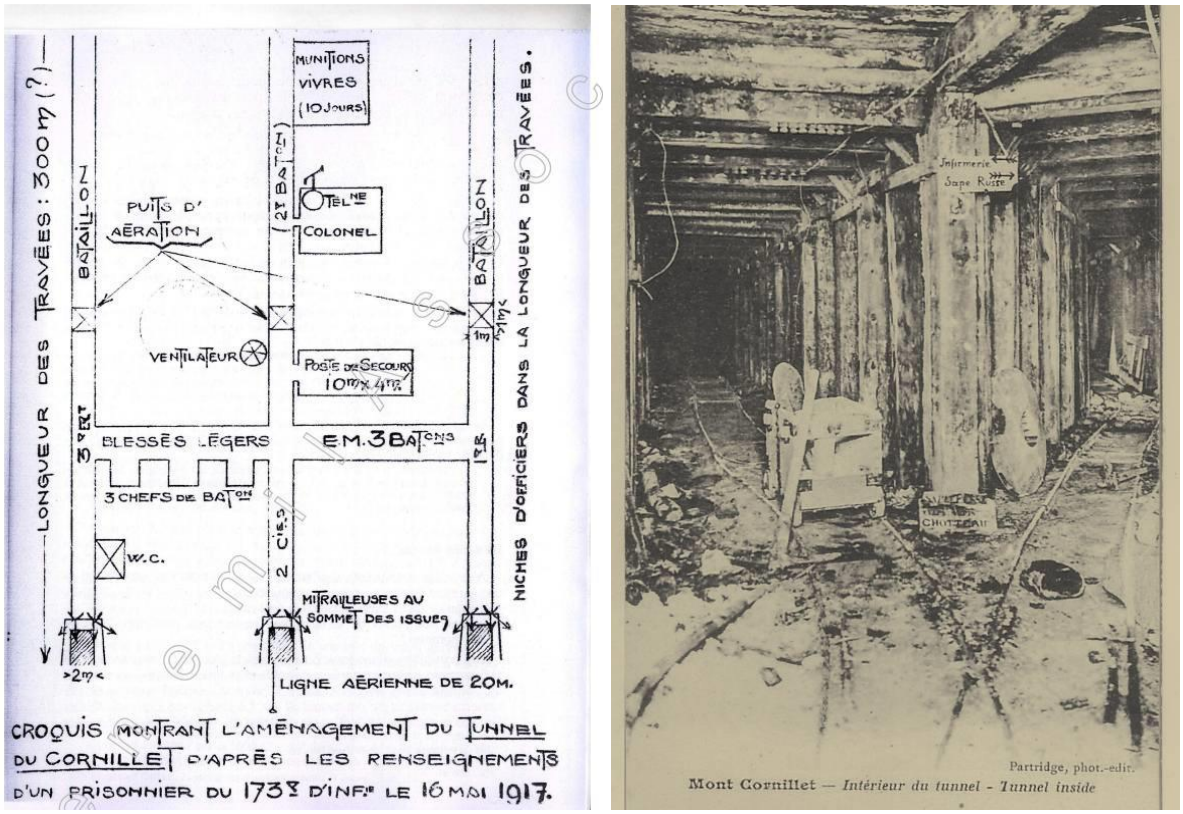

Figure IV-3 : Left: structure of tunnels of Mont Cornillet according to a German prisoner on 16 May 1917 (Moreau, 2007); right: photo of inside of tunnels of Mont Cornillet (Les amis de Nauroy et de l'église de Beine, http://www.lesamisdenauroy.fr)

Two villages, Nauroy and Moronvilliers (Figure IV-2), were completely destroyed during WWI. The German army occupied these two villages at the beginning of the war in 1914. On April 1917, the Battle of the Hills began, and the French army tried to conquer the hills between Nauroy and Moronvilliers. The shells continued to crush the houses and streets. After the battle, there were only ashes and ruins in the villages, impossible to identify the streets and paths. In 1950, Nauroy was attached to the neighboring town of Beine to form the town of Beine-Nauroy and Moronvilliers was attached to Pontfaverger to form the town of Pontfaverger-Moronvilliers.

3) Fourth battle of Champagne (July 1918)

This battle was part of the Second Battle of the Marne (Germany: Friedensturm) and also the last major Germain offensive on the Western Front. The German army aimed to maintain their positions on the Massifs de Moronvilliers but failed since the first day of the battle.

The Fort de la Pompelle, located in the south-western of the study area (Figure IV-2) was intensivly bombarded during this battle (Figure IV-4) and remains in a state of ruin. The fort is now a military museum: the Museum of Fort de la Pompelle.

Figure IV-4 : Military aerial photograph of the Fort de la Pompelle on 1918 (collection of the Museum of Fort de la Pompelle)

2.1.2. Ammunition storage/destruction site after WWI

After the end of WWI, large quantities of unused ammunitions were still present on the French land. Under the pressures of agricultural lobbies, it was necessary to clear the battlefield in order to make these lands habitable and cultivable on an industrial scale. Thus, unused ammunitions were dismantled to recycle valuable materials or destroyed by explosion.

The ammunition explosion sites were recognizable in aerial photographs by characteristics such as alignments of shell-holes, an access road and a storage area. Several explosion sites were identified in the study area (Figure IV-5) according to historical aerial photographs.

One of the ammunition destruction / recycling sites is located near the destroyed village of Nauroy (N4). The activities of ammunition deconstruction at the site were initially carried out by the LAROYE Company. Following a fatal accident on May 1996, the destruction activities were suspended by the government. It was not until 2009 that the demining department of the direction of civil security intervened on the site at the request of the prefecture of Marne. The results of this intervention included the removal of about 20,000 detonators, the transport of some of the ammunition to the Suippes Military Camp (103 T of ammunition) and the destruction *in-situ* of another part of the ammunition (6 T of explosives and 1 T of hand fires). On June 2010, an inspection was conducted, and it was pointed that the site represented an area of about 17 ha and the military waste was still present.

Today, according to the database BASOL (https://basol.developpement-durable.gouv.fr/recherche.php), the site N4 still presents a very important pyrotechnic risk related to WWI (presence of trenches and tunnels, front lines of WWI, possible presence of unexploded ammunitions…). A risk of soil pollution can be present, especially on those explosions or burning areas. Finally, the presence of buried ammunition generated by the LAROYE Company's activities is not excluded. This site has been always under restriction of use due to all these risks presented above.

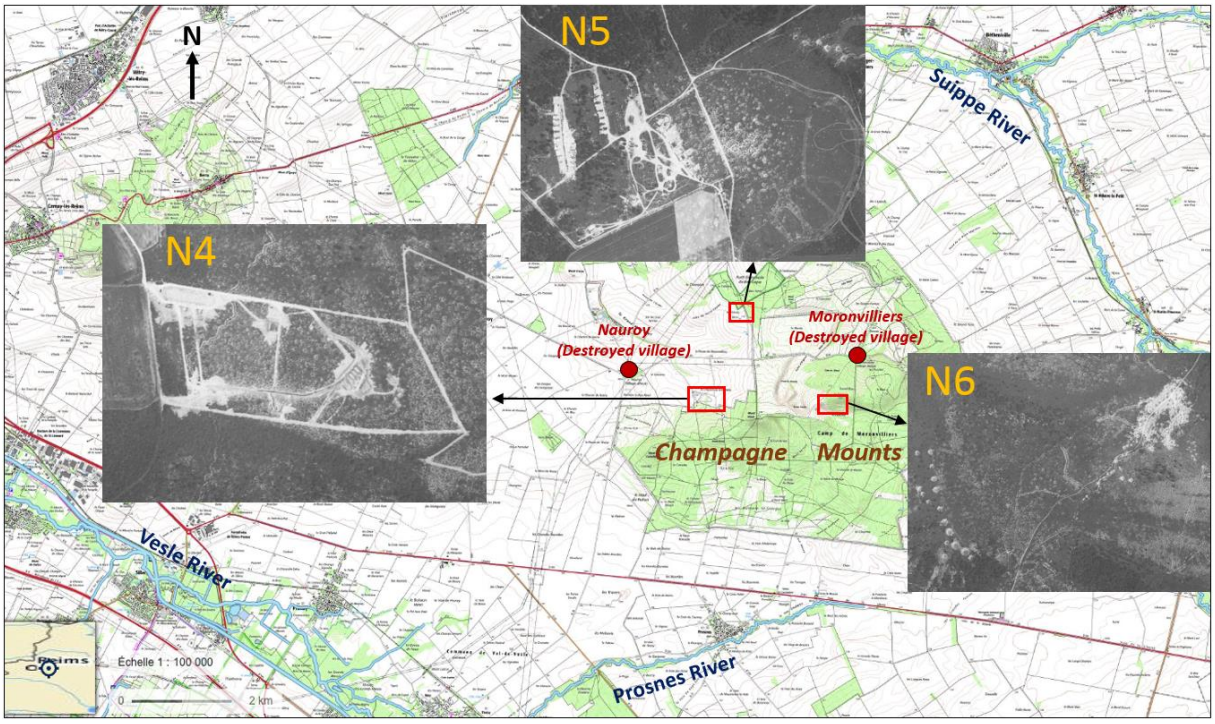

Figure IV-5 : Ammunition destruction sites on the study area after the WWI according to historical aerial photos on 1957 (https://remonterletemps.ign.fr)

2.1.3. Unexploded ammunitions subsisting in the subsoil

In addition to the exploded ammunition, large quantities of unexploded ammunition (about 30% of the total quantity of ammunition used) could still subsist in subsoil on the trench areas, representing a continuous and diffuse source of perchlorate contamination into the soil and groundwater (cf. Part I.1.2.3). In the region of Champagne-Ardenne, unexploded ammunitions were discovered on 22 sites from 2008 to 2011 (Robin des Bois, 2012). On 2018, during one of the sampling campaigns of this study, a shell was discovered on the Py riverside (Figure IV-6). The demining service was called for the remove of this ammunition in security. The existence of other ammunitions on this area cannot be ruled out.

Indeed, the accurate quantity of unexploded ammunitions subsisting in subsoil is difficult to estimate. Some areas covered by forests have not been cleared up after the WWI for agricultural use. At these sites, the possibility of the existence of unexploded ammunitions could be much higher than the farmlands.

Figure IV-6 : A shell discovered on the Py riverside during the sampling campaign on 2018

The information presented in this sector makes it possible to place the study area in a military-industrial context related to the WWI. The sites and activities listed are not exhaustive since the data compilation is based on existing data from historical archives and/or former aerial photography campaigns that did not cover the entire sector of the study area. In addition, traces of military activities could be quickly eased, making it difficult to identify all related sites. Any hot-spot of groundwater contamination highlighted by the results of analyzes could further be explained by the location of some of these sites. The "Impact 14-18" scientific project conducted by the GEGENAA laboratory at Reims University has proven that the airborne LIDAR (LIght Detection And Ranging) technology is an excellent way to evidence past landscape military activity traces (Taborelli et al. 2017) even in post-conflict agricultural context. Unfortunately, no LIDAR campaign has been deployed over the study area.

2.2. Former use of Chilean nitrates as fertilizer

In addition to the military sources related to the WWI, the former use of Chilean nitrates as fertilizer constitutes another potential source of perchlorate in the study area as this natural nitrate deposits contain perchlorate as impurity (cf. Part I.1.1.2.1). Between 1980 and 1950, France imported from Chile large quantities of natural nitrates ($NaNO_3$) to amend the soils for wheat and beet cultivation. As a traditional agricultural area, the region of Champagne-Ardenne was much concerned with the use of Chilean nitrates.

At the end of the 19th century, there were already more than 20 beet sugar factories in the region Champagne-Ardenne (FRAB Champagne-Ardenne, 2015). The beet industry was then heavily affected by the war. From 1930 to 1945, a few less than 10,000 ha of beet were planted in Champagne-Ardenne. In 1950s, the regional beet cultivation surface had increased to 30,000 hectares. The increase in such a short period of time was due to the development of mechanization and the demand for sugar industry (Agreste Champagne-Ardenne, 2009).

In 1953, a study of the INSEE (National Institute of Statistics and Economic Studies) observed that the average annual consummation of nitrogen in Marne (the county of the ancient region Champagne-Ardenne in which the study area is located) was between 7,000 and 10,000 T (Figure IV-7, Lopez et al, 2014). Although the nitrates used after 1950 were already synthetic nitrates, this survey provided information concerning the historical quantity of nitrates used in the sector compared with other parts of France. The use by spreading and the storage of these Chilean nitrates could represent diffuse and punctual sources of groundwater contamination in perchlorate.

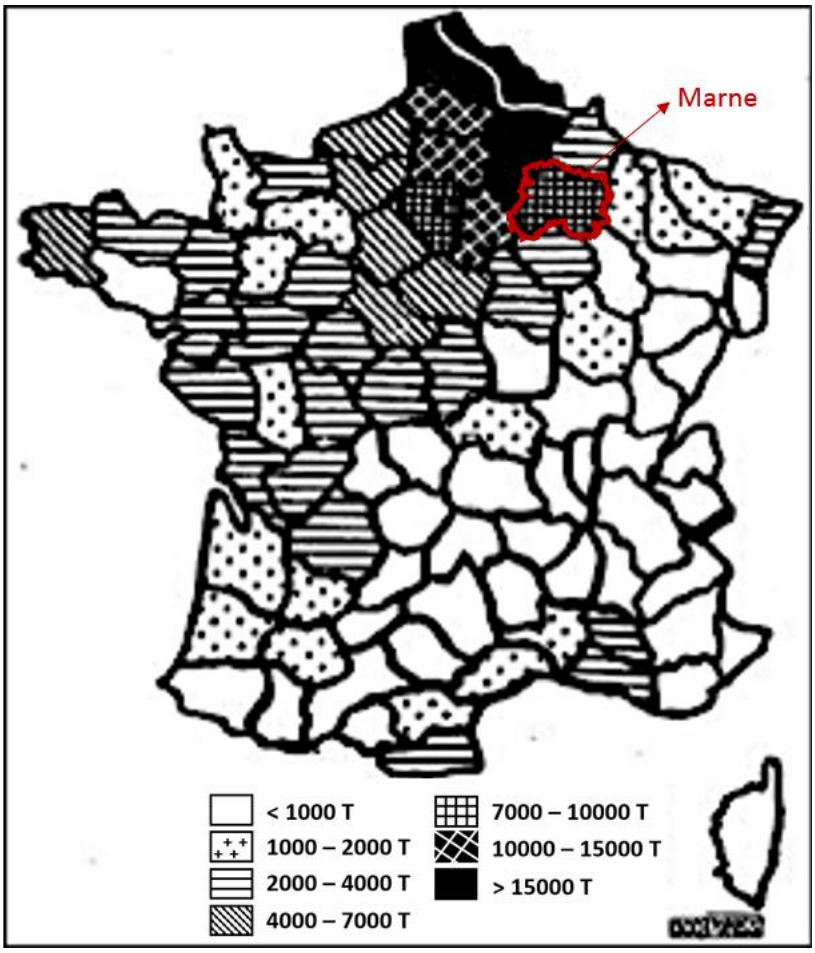

Figure IV-7 : Average annual use of nitrogen (campaigns 1950-1951 and 1951-1952 by the INSEE; Lopez et al. 2014)

2.3. Other activities potentially emitting perchlorate

The following databases were consulted in order to identify activities potentially emitting perchlorate:

- The BASIAS database (historical inventory of industrial sites and service activities): http://www.georisques.gouv.fr/dossiers/basias/donnees
- The BASOL database (database of polluted sites and soil): https://basol.developpement-durable.gouv.fr/recherche.php
- The Base des installations classées : http://www.installationsclassees.developpement-durable.gouv.fr/

Several sites, potentially concerned with the use or diffusion of perchlorates (cf. Part I.1.1.2.2) were identified in the study area (Figure IV-8) including:

- A water treatment plant (possible presence of perchlorate in waste water affluent)
- A Chalk rock quarry (possible usage of explosive during the rock exploitation)
- An automobile junkyard (presence of perchlorate in airbags)
- A factory which produces equipment of automobile (presence of perchlorate in airbags)

These sites are still in activity except for the automobile junkyard whose status of activity is unknown.

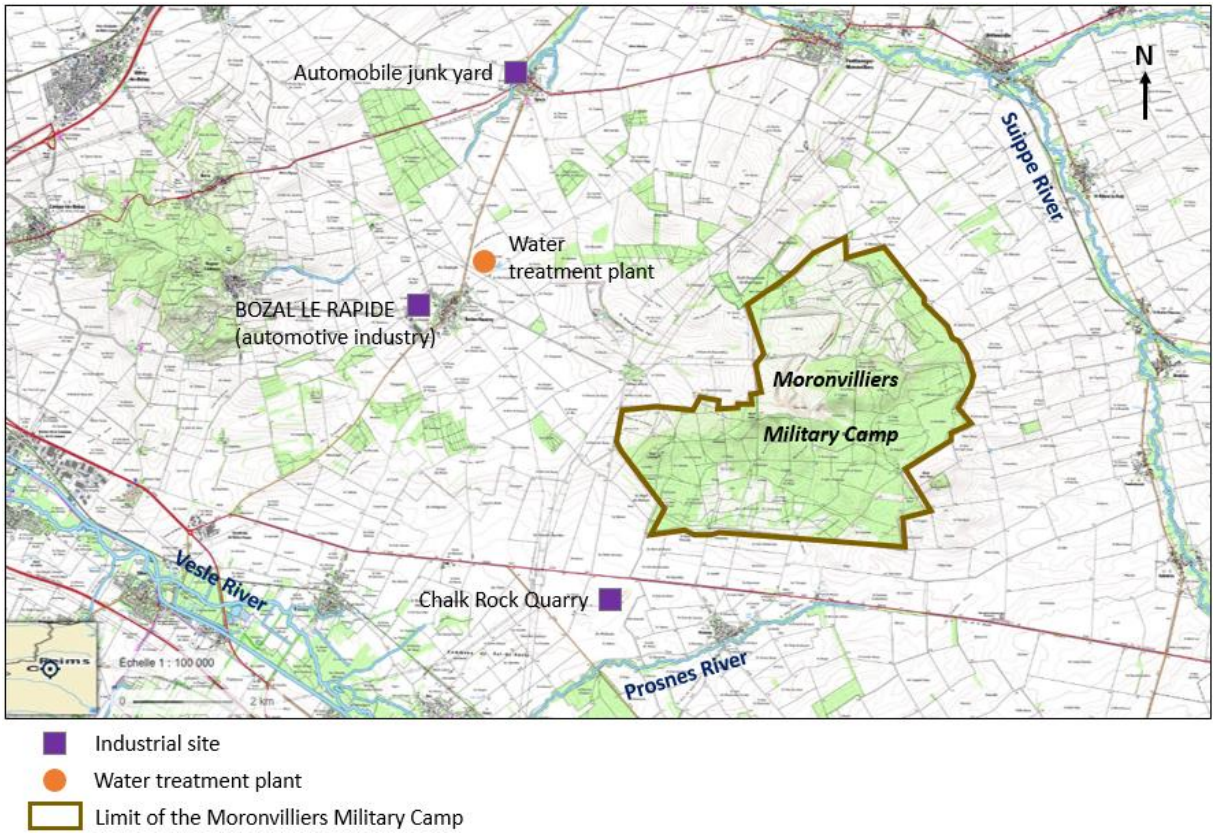

Figure IV-8 : Industrial sites potentially emitting perchlorates in the study area

In conclusion, although there are some industrial activities that can generate and release perchlorates into the environment, their impact seems limited compared to the potential military and agricultural sources described in the previous sections.

3. Occurrence of perchlorate contamination

3.1. Concentration of perchlorate and explosives

Perchlorate was detected at almost all sampling sites (33 out of 36), with concentrations ranging from < 0.5 µg·L^{-1} (limit of quantification) to 44.4 ± 4.9 µg·L^{-1} (Table IV-1). ClO_4^- concentrations > 4 µg·L^{-1} were measured at 17 sites, including two sites with concentrations > 15 µg·L^{-1}, representing 49% and 6% of the sampling sites respectively. Low concentrations (< 4 µg·L^{-1}) were measured at 19 sites, representing 51% of the sampling points.

Table IV-1 : Properties of sampling points, water table depth, concentrations of Cl^-, NO_3^- and ClO_4^- and isotopic compositions of NO_3^- in ground- and surface water samples (N: number of sampling; NA: not available. -: not applicable)

Name	Type	N	Depth (m)	Water table depth (m)	Cl^- (mg·L^{-1})	NO_3^- (mg·L^{-1})	ClO_4^- (µg·L^{-1})	NO_3^- $\delta^{18}O$ (‰)	NO_3^- $\delta^{15}N$ (‰)
FA	Borehole	21	35	2 - 6	35.4 ± 6.3	39.7 ± 6.0	3.1 ± 0.9	-1.4	-0.7
FAP	Borehole	21	15	3 - 12	30.7 ± 9.5	28.4 ± 6.7	5.4 ± 2.2	-1.9	1.7
FBN1	Borehole	21	48	26 - 40.5	25 ± 8.8	28.9 ± 7.6	3.6 ± 1.7	2.1	3.9
FBN4	Borehole	21	28	2.5 - 18	52.9 ± 2.6	54.3 ± 2.6	20.8 ± 3.2	-0.6	1.0
FBN5	Borehole	21	47	22.5 - 35	15 ± 9.2	31.6 ± 11.3	7.9 ± 3.7	-0.6	1.1
FEP1	Borehole	21	25	7.5 - 17	35.2 ± 1.0	36.7 ± 1.4	12.9 ± 2.4	-0.3	0.5
FP1	Borehole	21	19	4.5 - 13	28 ± 2.9	29.9 ± 3.9	6.6 ± 1.9	-1.3	1.1
FPM1	Borehole	21	24	NA	7.6 ± 0.7	19 ± 0.8	14.1 ± 2.0	-1.4	0.4
FPM3	Borehole	21	21	9 - 18	18.6 ± 5.0	24 ± 5.7	3.5 ± 0.8	-0.5	0.3
FVDV	Borehole	21	22	7 - 15	39 ± 1.6	40 ± 2.3	44.4 ± 6.9	-1.7	0.8
PDO	Pumping station	21	25	NA	33.9 ± 1.2	42.1 ± 2.0	11.5 ± 1.7	-1.8	0.6
PP	Pumping station	21	80	NA	21.8 ± 1.1	25.8 ± 0.9	9.2 ± 4.0	-1.5	0.0
PS	Pumping station	4	16	NA	23.6 ± 1.4	32.4 ± 2.7	4.1 ± 1.4	-0.2	1.6
FCE	Borehole	1	85	NA	7.2	3.1	0.5	NA	NA
FNA	Borehole	1	47	NA	20.0	24.3	1.3	NA	NA
FBN3	Borehole	3	56	16 - 22	13.4 ± 2.4	15.2 ± 2.2	1.3 ± 0.4	5.4	7.5
FBN2	Borehole	4	32	17 - 26	31.6 ± 4.1	18.2 ± 12.5	2 ± 1.7	6.6	10.3
FEP2	Borehole	6	23	15 - 18.5	8.8 ± 0.6	9.5 ± 0.8	2 ± 1.3	-0.3	-0.5
FPM2	Borehole	5	35	30 - 31	16.2 ± 5.1	22.1 ± 5.2	6.1 ± 0.6	-1.3	0.6
FP2	Borehole	4	21	8 - 13	165.8 ± 18.9	38 ± 3.3	1.2 ± 0.7	-0.9	3.6
FP	Borehole	4	23	12 - 17	39.0 ± 3.3	45 ± 5.0	5.9 ± 0.9	-1.7	0.6
FB	Borehole	1	33	12.8	28,0	36.6	2.2	NA	NA
SEP	Spring	12	-	-	23.5 ± 1.9	33.1 ± 2.6	5.5 ± 3.0	-1.5	1.8
SCG	Spring	2	-	-	28.5 ± 0.2	40.7 ± 0.1	4.7 ± 2.1	NA	NA
SB1	Spring	1	-	-	16.5	7.8	< 0.5	NA	NA
SB2	Spring	1	-	-	18.4	2.3	2.1	NA	NA
RS1	River	21	-	-	25.8 ± 1.2	29.3 ± 1.9	3.4 ± 0.8	1.0	3.7
RPY	River	21	-	-	20.7 ± 1.5	28.5 ± 1.6	11.6 ± 3.1	NA	NA
RS2	River	21	-	-	24.3 ± 1.3	29.6 ± 1.3	6.5 ± 2.1	0.8	2.6
RA	River	4	-	-	22.1 ± 1.0	26.1 ± 1.2	1.5 ± 1.0	0.4	3.1
RS3	River	4	-	-	25.2 ± 0.4	28.8 ± 0.8	5.1 ± 1.5	0.4	3.1
RV1	River	3	-	-	29.3 ± 1.1	25.9 ± 3.7	1.2 ± 0.5	0.7	5.9
RV2	River	3	-	-	25 ± 1.9	28.5 ± 2.8	0.9 ± 0.4	0.4	4.7
RP	River	1	-	-	21.3	25.6	3.6	NA	NA
C1	Canal	1	-	-	18.3	12.7	< 0.5	NA	NA
C2	Canal	1	-	-	15.5	13.1	< 0.5	NA	NA

An analysis of the geographic distribution of ClO_4^- is presented in Figure IV-9, revealing some major trends and potential sources of ClO_4^-. In order to better understand the distribution of ClO_4^- contamination in the study area, major military sites including military tunnels and ammunition destruction sites are also marked in Figure IV-9 (for more details of military sites N1 to N6 see Part IV.2.1.2).

Lower concentrations of ClO_4^- (< 4 $\mu g \cdot L^{-1}$) were mainly found on the Berru Mount, in the Vesle River and in the Aisne-Marne Canal. As mentioned in Part II.1.2.2, the Tertiary formation on the Berru Mount is represented by a succession of permeable and impermeable layers, which contains several small aquifers in which water could be renewed quickly by precipitation. As a result, low levels of ClO_4^- were detected in this area. In the Vesle River, ClO_4^- concentrations ranged from 0.9 ± 0.4 $\mu g \cdot L^{-1}$ to 1.2 ± 0.5 $\mu g \cdot L^{-1}$. The Vesle River originates far away upstream, receiving groundwater discharge from outside the study area that is little affected by ClO_4^- contamination. In the Aisne-Marne Canal, ClO_4^- was not detected (< 0.5 $\mu g \cdot L^{-1}$), indicating that the Aisne-Marne Canal has little or no input from the contaminated groundwater or river water (Vesle River) of the study area.

Most of the sampling sites with ClO_4^- concentrations exceeding 4 $\mu g \cdot L^{-1}$ were located downgradient of the Champagne Mounts (Figure IV-9), where large quantities of ammunitions were used, stored and destroyed during and after WWI (cf. Part IV.2.1). The highest concentrations of ClO_4^- were found at borehole FVDV, with a maximum of 62.5 $\mu g \cdot L^{-1}$ and an average of 44.4 ± 4.9 $\mu g \cdot L^{-1}$, indicating the presence of point source of ClO_4^- close to FVDV. Specifically, the military tunnel N1 (Tunnel of Mont Cornillet; Figure IV-9) was very likely responsible for the high concentrations of ClO_4^- measured at FVDV. Plume-like patterns of ClO_4^- were observed along the sections A – A' and B – B' (similar direction as the groundwater flow line; Figure IV-9). At FBN4, FEP1 and SEP (A – A'), ClO_4^- concentrations were 20.8 ± 3.2 $\mu g \cdot L^{-1}$, 12.9 ± 2.4 $\mu g \cdot L^{-1}$ and 5.5 ± 3.0 $\mu g \cdot L^{-1}$ respectively, indicating a progressive decrease. At FBN5 (located upstream the borehole FBN4), ClO_4^- concentration was much lower (7.9 ± 3.7 $\mu g \cdot L^{-1}$). Consequently, ClO_4^- contamination along the section A – A' could be related to the presence of point source of ClO_4^- between FBN4 and FBN5 or to the ammunition destruction site N4 (Figure IV-9). This could be furtherly confirmed by a more precise piezometric map and more information on historical activities in this area. A similar pattern was observed at FPM1, FPM2 and FPM3 (B – B') with concentrations of 14.1 ± 2.0 $\mu g \cdot L^{-1}$, 6.1 ± 0.6 $\mu g \cdot L^{-1}$ and 3.5 ± 0.8 $\mu g \cdot L^{-1}$ respectively, which indicated the presence of contamination source upstream the borehole FPM1, such as the ammunition destruction site N5 Figure IV-9.

Although ClO_4^- concentrations in river waters were generally lower than those of groundwater, some river sites had relatively high ClO_4^- concentrations (>10 µg·L^{-1}), such as RPY in the Py River (Figure IV-9). In the Suippe River upstream of the confluence with the Py River (RS1), low concentrations of ClO_4^- (3.4 ± 0.5 µg·L^{-1}) were detected; downstream of this confluence (RS2), higher concentrations (6.5 ± 2.1 µg·L^{-1}) were observed. Indeed, the Py River is downstream from the Suippes military camp (Figure I-4) that represents a potential source of ClO_4^- contamination to the Py river watershed.

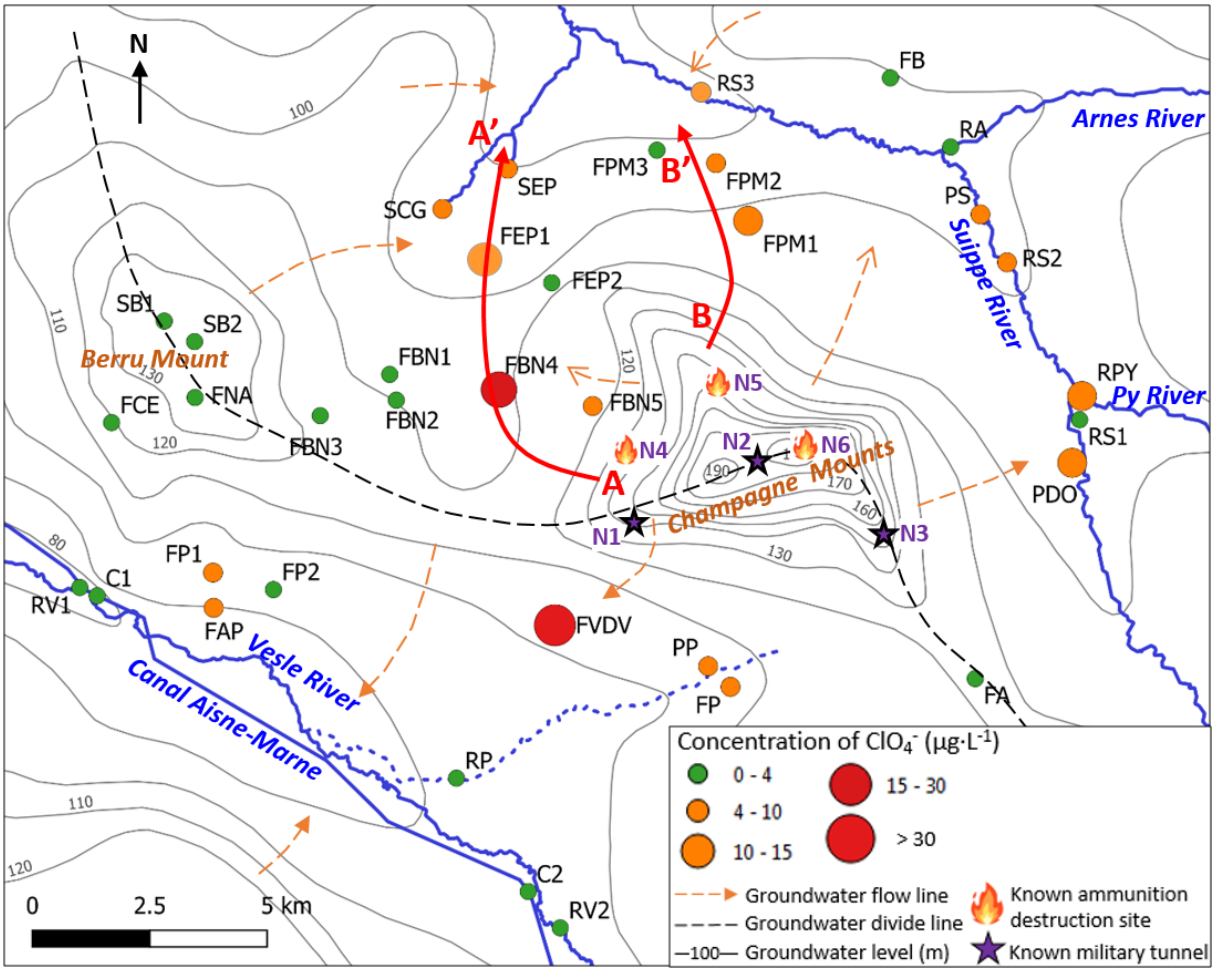

Figure IV-9 : Spatial distribution of ClO_4^- contamination in the study area and major military sites related to the WWI (for more details of military sites N1 to N6, see Figure IV-2 and Figure IV-5 in Part IV.2.1).

Unlike the widespread contamination of ClO_4^-, organic explosives have not been detected in surface and groundwater samples, which could be explained by their low persistence and mobility in soil and water (Clausen et al., 2006). During WWI, nitro group explosives such as TNT, nitroglycerine and nitrocellulose were largely used (see Part I.1.2.3). TNT can be rapidly degraded in most soil and aquifer systems and therefore, its presence is typically restricted to areas near its introduction to the environment. At most sites, TNT can be completely attenuated in the surface soil, thereby preventing contamination of the unsaturated zone (UZ) or groundwater (Clausen et al., 2006). Nitroglycerin is soluble when present alone and is subject to rapid biodegradation, but when present with nitrocellulose it is insoluble. Nitrocellulose is also insoluble, resulting in its low mobility in the environment (Quinn, 2015).

3.2. Mass flow rate of perchlorate

In the Suippe River and its tributaries where ClO_4^- concentrations were relatively high (Table IV-2), the mass flow rate of ClO_4^- (M) has been estimated according to the measured water flow rate (Q) and ClO_4^- concentrations (C):

$$M = C \times Q \quad (1)$$

The data of water flow rate and ClO_4^- concentration used for calculation was measured on October 2017. The estimated mass flow rate of ClO_4^- is 54 kg·yr^{-1} upstream the Suippe River (RS1) and 172 kg·yr^{-1} downstream of the Suippe River (RS3) (Table IV-2). The Py River, which joins the Suippe River between RS1 and RS2, contributes about 107 kg·yr^{-1} of ClO_4^- into the Suippe River while the Arnes Rivers only contains less than 1.8 kg·yr^{-1} of ClO_4^-. The increase of mass flow rate from RS2 to RS3 was due to the contribution of Chalk aquifer discharge.

This estimation could be quite conservative as water flow rates were measured during low water period (October) whereas ClO_4^- concentrations in rivers were relatively stable over time according to the low values of standard deviations presented in Table IV-1.

Table IV-2 : Mass flow rate of ClO_4^- in the Suippe River and its tributaries (data measured on October 2017)

Name	Location	Water flow rate (L·s^{-1})	ClO_4^- concentration (µg·L^{-1})	ClO_4^- mass flow rate (kg·yr^{-1})
RS1	Suippe River	401	4.3	54
RS2	Suippe River	752	6.7	159
RS3	Suippe River	1184	4.6	172
RPY	Py River	276	12.3	107
RA	Arnes River	110	< 0.5	< 1.8

4. Isotopic content of perchlorate and nitrate

In order to discriminate ClO_4^- sources (natural and/or synthetic), 4 sampling campaigns for isotopic analyzes of ClO_4^- was carried out in the study area at the following monitoring sites: FBN4 (on high water level and low water level), FVDV and PY (Py River). One sampling campaign was carried out outside the study area, near the Suippes Military camp (RM; Figure I-4) in order to obtain a "pure military isotopic signature" of ClO_4^-.

The results of Cl and O stable isotope analysis for ClO_4^- in water samples (Table IV-3) are presented by dual isotope plots in comparison to published data for synthetic, Atacama and selected US indigenous natural ClO_4^- occurrences (Figure IV-10). There is no evidence of ClO_4^- biodegradation, which is consistent with the typical oxic condition of the unconfined Chalk aquifer (Table III-6) (Barhoum et al., 2014; Cao et al., 2020; Edmunds et al., 1987); the isotopic composition of ClO_4^- could therefore reflect initial values of the sources.

Table IV-3 : Isotopic compositions of ClO_4^- in ground- and surface water samples (HW: high water; LW: low water)

Name	Sample date	$\delta^{18}O$ (‰)	$\Delta^{17}O$ (‰)	$\delta^{37}Cl$ (‰)
FVDV	04/05/18	-20.7	0.2	0.3
FBN4 (HW)	04/06/18	-21.8	0.2	0.2
FBN4 (LW)	01/18/19	-29.6	-0.3	-3.3
RPY	04/10/19	-22.9	1.3	-6.0
RM	02/22/19	-18.2	0.1	-0.2

The $\delta^{37}Cl$, $\delta^{18}O$ and $\Delta^{17}O$ values of ClO_4^- in water sample collected at the Suippe military camp (RM; pure military source), FVDV and FBN4 (high water) plotted exactly within the synthetic ClO_4^- ranges (Figure IV-10), proving similar military sources of ClO_4^- at these sites. However, the results for FBN4 (low water) was different, with a lower $\delta^{18}O$ value (-29.6‰) falling outside the published synthetic ClO_4^- ranges. Nevertheless, the $\Delta^{17}O$ and $\delta^{37}Cl$ values (-0.3‰ and -3.3‰, respectively) were typical of the measured synthetic ClO_4^-. Therefore, ClO_4^- at FBN4 (low water) was interpreted as of synthetic origin, different from other samples and currently reported synthetic ClO_4^- products. Indeed, the manufacturing processes of synthetic ClO_4^- and the materials used more than 100 years ago during WWI may be different from those of today. Even during WWI, different ClO_4^- salts (NH_4ClO_4 and/or $KClO_4$) were used in explosives (see Part I.1.2.3); they were produced in different facilities and the method could also have evolved during the WWI conflict. This could possibly explain why this "unusual" synthetic end-member was observed at FBN4 (low water). The different isotopic signatures observed at FBN4 on high and low water period indicated that sources of ClO_4^- at different depth could be different depending on different military activities (e.g. unexploded ammunitions persisting underground, unused ammunitions stored or blown up on the surface after WWI).

In the RPY sample, a component of Atacama ClO_4^- was supposed. The lower value of $\delta^{37}Cl$ (-6.0‰) and the higher value of $\Delta^{17}O$ (1.3‰) were both consistent with a mixture of the postulated synthetic end-member with the typical Atacama ClO_4^-. This could probably be explained by the nitrogen explosives of WWI (black powder and nitro group explosives) made with Chilean nitrate and/or the past use of Chilean nitrate as fertilizer. Indeed, the PY River water consists of aquifer discharge from the entire watershed, which is an agricultural area marked by military activities of WWI. Although synthetic (military) ClO_4^- is indicated by isotopic analysis at two sites with the highest ClO_4^- concentrations (FVDV and FBN4), Atacama ClO_4^- from Chilean nitrate fertilizer might be present, especially at sites related to diffuse sources with low ClO_4^- concentrations.

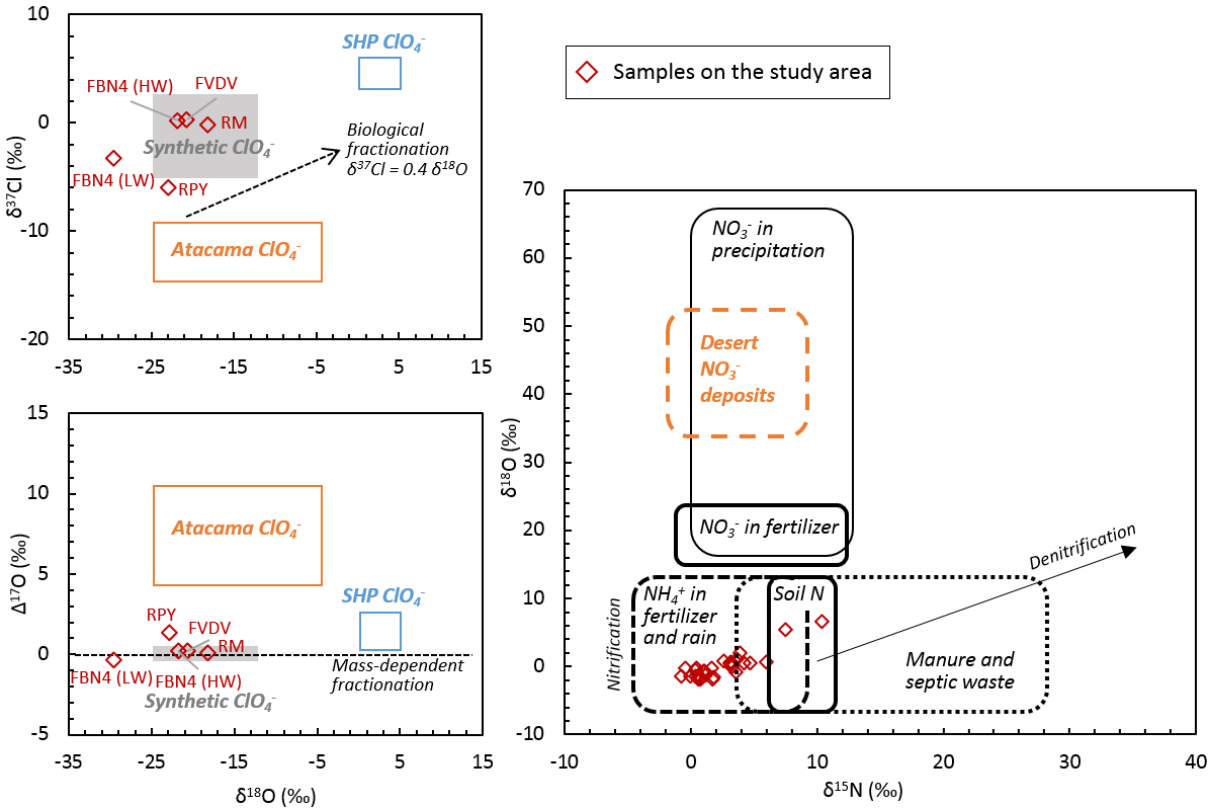

Figure IV-10: Summary of isotope data for ClO_4^- and NO_3^- in water samples of the study area, compared with major known ClO_4^- sources including synthetic, Atacama and indigenous natural ClO_4^- from the Southern High Plain (Texas) (SHP) (Ader et al., 2001 ; Bao and Gu, 2004 ; Böhlke et al., 2005, 2009 ; Jackson et al., 2005b, 2010 ; Parker et al., 2008 ; Plummer et al., 2006 ; Rajagopalan et al., 2006 ; Rao et al., 2007 ; Sturchio et al., 2007, 2011). Arrow in the $\delta^{37}Cl$ vs $\delta^{18}O$ graph represents the slope of biodegradation ($\delta^{37}Cl = 0.4\ \delta^{18}O$) and arrow in the $\Delta^{17}O$ vs $\delta^{18}O$ graph represents the direction of mass dependent fractionation.

The NO_3^- isotope data at all the sampling points did not show any evidence of an Atacama source for the NO_3^- (Figure IV-10). However, this cannot rule out the possibility of the existence of Atacama NO_3^- in groundwater samples, as Atacama NO_3^- could have been replaced and/or assimilated with the biogenic NO_3^- in the soil (Böhlke et al., 2009). Indeed, the distinctive isotopic composition of oxygen in atmospheric NO_3^- is preserved only in hyper-arid environments and lost in soils where higher biological activities exist (Böhlke et al., 1997; Michalski et al., 2015). Therefore, more information is needed to better evaluate the extent of ClO_4^- sources related to the past use of Chilean nitrates in the study area.

5. Temporal trends of perchlorate compared with groundwater level and major ions

The temporal variation of ClO_4^- concentrations measured from June 2017 to June 2019 was compared with groundwater level fluctuation and the temporal variation of NO_3^- and Cl^- (two major agriculture-derived ions, Cao et al., 2020), in order to explore the potential sources of ClO_4^- (point and/or diffuse), the mechanism of transport and the possible future evolution of ClO_4^- in the Chalk aquifer.

5.1. Temporal trends of perchlorate *vs* groundwater level

At most sites, annual variations of ClO_4^- concentrations were observed: the highest concentrations were observed in 2018, corresponding with the high groundwater level in 2018 (cf. Part III.1.2). At sites having relatively high levels of ClO_4^- (> 10 µg·L^{-1}) (FVDV, FBN4, FEP1 and FBN5; Figure IV-11), several peaks of ClO_4^- concentration were observed and the temporal variation of ClO_4^- was poorly correlated with groundwater level fluctuation (Table IV-4). The peaks could possibly be explained by localized flushing of ClO_4^- from the UZ by natural (rainfall) or artificial (irrigation) recharge processes, indicating the presence of point sources of ClO_4^- upstream of these sites. At FVDV and FBN4, the two most contaminated sites, the correlation coefficients between ClO_4^- and groundwater level were the lowest (Table IV-4 and Figure IV-11), as ClO_4^- concentrations here were mainly controlled by the ClO_4^- transfer waves following flushing rather than the groundwater level fluctuation.

At sites having low levels of ClO_4^- (< 10 µg·L^{-1}) (FA, FBN1, FP1 and FPM3; Figure IV-11), however, the temporal variation of ClO_4^- was positively correlated to the groundwater level fluctuation. The correlation relationship was stronger at FA and FBN1 (r = 0.42 and 0.54, respectively; Table IV-4) with larger groundwater level fluctuation; at FP1 and FPM3 where the groundwater level fluctuated less, the correlation relationship was weaker (r = 0.35 and 0.20, respectively; Table IV-4). Diffuse sources of ClO_4^- were presumed to be present at these sites. During low water level periods, most of the sources were apparently disconnected from the saturated zone (SZ). As water level rose, the contamination source was re-activated and more contaminants were dissolved and flushed into the UZ, resulting in the increase of ClO_4^- concentrations.

At RPY (Py River) and RS2 (Suippe River after the confluence of Py River), a decrease in ClO_4^- concentration was observed during high flow periods (May 2018 and May 2019; Figure IV-11), implying a dilution effect of water (from rainfall and aquifer discharge) on ClO_4^- concentration. A similar tendency was observed at PDO, the pumping station near RPY, which is consistent with a mixture of groundwater and surface water at this point, as implied by the groundwater dating results (30% to 60% of modern water and an end member of old water of about 40 years; Cao et al. (2020).

5.2. Temporal trends of perchlorate *vs* major agricultural ions

The temporal eveolution of ClO_4^- was compared with the chronicles of NO_3^- and Cl^-, the two major agriculture ions in groundwater of the Champagne Chalk aquifer (Cao et al., 2020). At most sites, the temporal evolution of ClO_4^- was different from that of NO_3^- and Cl^- (Figure IV-11), indicating different origins of ClO_4^- versus NO_3^- and Cl^-. At FEP1, FPM1 and PP, despite the temporal heterogeneity of ClO_4^- levels, the concentrations of NO_3^- and Cl^- were stable over time (Figure IV-11). As described in Part III.2.3.2.3, estimated groundwater ages at these points were > 30 years under a piston flow context, which is related to the superficial formations limiting rapid transport of water and solutes (NO_3^- and Cl^-) from surface (agricultural ions are distributed mainly in the soil area near the surface) to the SZ. Consequently, the aquifer receives recharge mainly from upstream of the superficial formation covered area. Water traveled laterally in the SZ during > 30 years and solute concentrations were greatly buffered, resulting in stable NO_3^- and Cl^- levels independent of water level fluctuation. The large variation of ClO_4^- concentrations, in contrast to the temporal stability of NO_3^- and Cl^-, could be interpreted by the location of ClO_4^- sources much deeper than those of agricultural ions (mainly in the soil area). As groundwater level rose, the contamination front of ClO_4^- was soon reached, generating changes in ClO_4^- levels, despite the fact that flush from the soil towards the aqufier was larged limited by superfacial formations. At FPM3 (downstream the borehole FPM1; Figure IV-9), a time lag was observed between groundwater level and concentrations of NO_3^- and Cl^-, as a result of delayed effect by the discontinuous graveluche formations. However, ClO_4^- levels varied with groundwater level without time lag, implying again that deeper ClO_4^- sources were more quickly activated by the rise of water table.

At FA, unlike the highly correlated relationship between ClO_4^- and groundwater level, NO_3^- and Cl^- were negatively correlated with groundwater level (Figure IV-11 and Table IV-4), indicating a dilution effect. At this site, groundwater dating showed 75-80% of modern water by the binary mixing model, indicating an aquifer constituted mainly by freshly percolated rainwater that favors the process of dilution (Cao et al., 2020). During the rapid flow process following precipitation, the low mineralized rainwater entered the aquifer resulting in decrease of NO_3^- and Cl^- concentrations. As to ClO_4^-, it seemed that the dissolution of potential ClO_4^- sources in the UZ following the rise of groundwater level was more important than the contribution of dilution process, resulting in ClO_4^- increased with groundwater level.

At FBN1 and FBN5, the temporal variabilities of ClO_4^-, NO_3^- and Cl^- were positively correlated (Figure IV-11 and Table IV-4). Indeed, located near the groundwater divide line (Figure IV-9), deep water table levels were observed (> 22 m; Table III-3) and low permeability were suggested at these two sites (Cao et al., 2020). According to groundwater dating, the groundwater flow was described by the exponential mixing model (mean residence time of < 20 years), indicating a spatially uniform recharge. Under this context, ClO_4^-, NO_3^- and Cl^- were flushed from the potential sources located in the UZ following recharge, showing a similar temporal variation.

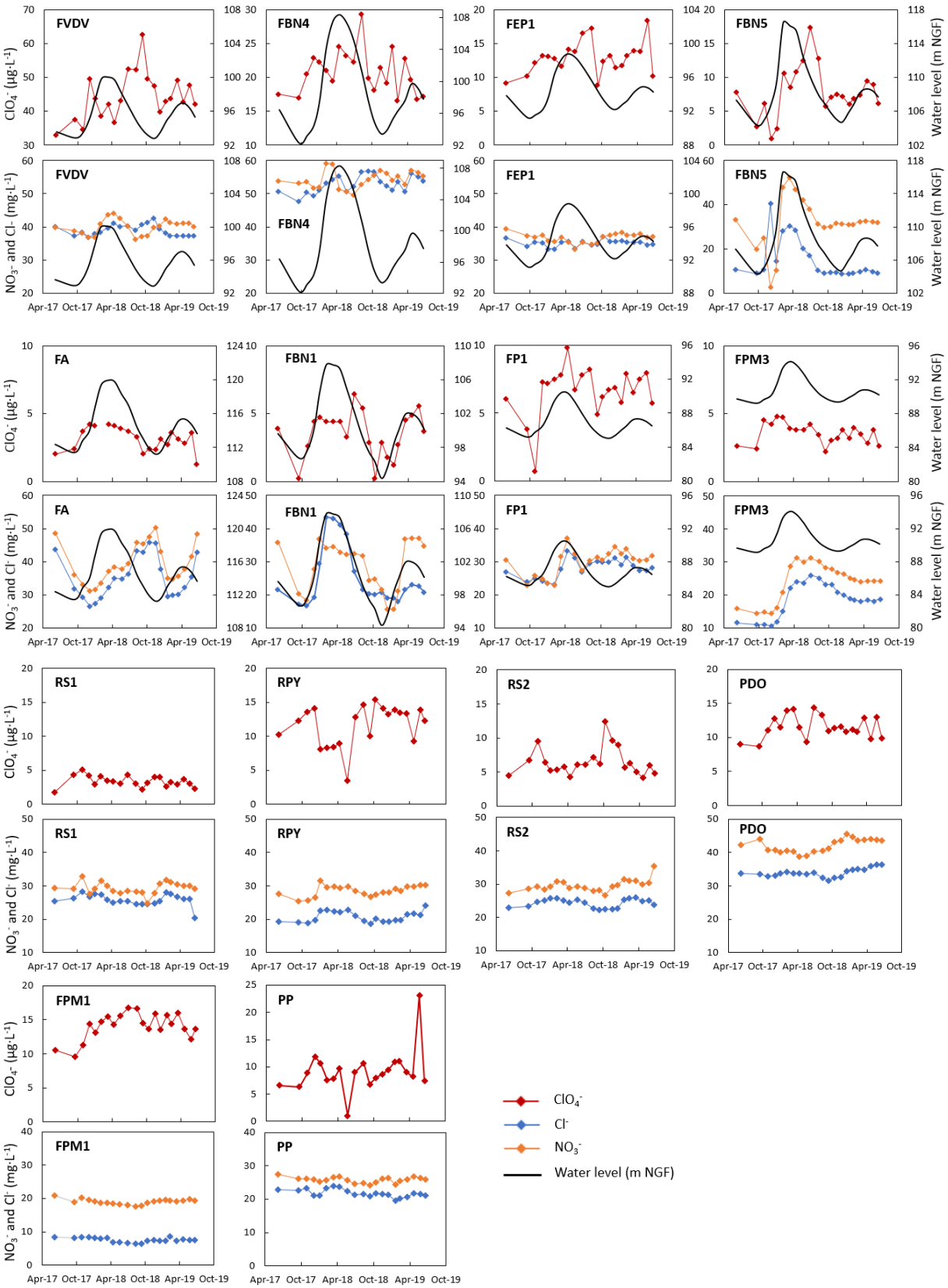

Figure IV-11 : Temporal variation of perchlorate concentration compared with groundwater level fluctuation from June 2017 to June 2019

Table IV-4 : Correlation coefficients (r) of ClO_4^- with groundwater level and major ion concentrations (statistically significant as the P-value < 0.05, related r values when P-value < 0.05 are marked in bold; NA: not available)

Name	Water level	Cl^-	NO_3^-	SO_4^{2-}	Na^+	K^+	Mg^{2+}	Ca^{2+}
FA	**0.42**	**0.54**	**0.56**	**0.68**	0.04	0.29	**0.24**	**0.64**
FBN1	**0.54**	**0.53**	**0.67**	**0.55**	-0.02	**0.62**	0.35	-0.02
FP1	**0.35**	0.17	0.25	0.23	0.28	**0.48**	-0.05	0.05
FPM3	**0.20**	-0.03	-0.04	-0.05	-0.04	0.17	**0.46**	0.18
FBN5	**0.22**	**0.71**	**0.64**	0.02	**0.28**	**0.67**	**0.41**	**0.61**
FEP1	0.08	0.00	0.08	0.05	**0.32**	-0.02	-0.03	0.03
FBN4	0.07	0.03	**0.32**	0.24	0.03	0.18	**0.31**	0.01
FVDV	0.07	-0.04	**0.21**	**0.37**	0.15	**0.53**	**0.41**	0.08
FPM1	NA	**0.28**	**0.51**	-0.02	**0.10**	**0.33**	0.22	0.11
PDO	NA	-0.05	0.06	0.01	-0.03	**0.16**	-0.03	0.19
PP	NA	0.29	**0.02**	-0.05	0.16	0.03	0.08	-0.06
RS1	NA	**0.61**	**0.13**	**0.53**	**0.49**	**0.37**	-0.06	0.05
RPY	NA	**0.10**	0.06	-0.01	-0.03	-0.06	-0.06	0.13
RS2	NA	**0.51**	**0.11**	**0.36**	0.02	**0.17**	**0.53**	0.13

6. Discussion and conclusion on sources and behavior of perchlorate in the Champagne Chalk aquifer

This study examined the sources and evolution of ClO_4^- contamination in groundwater of NE France. The NE region of France is suspected to have multiple sources of ClO_4^- related to military activities of WWI and/or the past use of Chilean nitrate as fertilizer in agriculture. An intensive sampling network was established on a study area of a representative watershed, where ClO_4^- concentrations were monitored monthly for two years (2017-2019). A combination of isotopic analysis of ClO_4^-, groundwater dating, as well as hydrologic and geochemical analysis has been applied to clarify the sources of ClO_4^- and to understand its evolution in groundwater.

This work produced the first precise ClO_4^- contamination mapping in the study area east of Reims city with groundwater ClO_4^- concentrations ranging from < 0.5 to 62.5 $\mu g \cdot L^{-1}$. About half of the sampling sites showed ClO_4^- concentrations > 4 $\mu g \cdot L^{-1}$ and most of these sites were located downgradient of the Champagne Mounts area, where huge quantities of ClO_4^- were used, stored or destroyed during and after WWI. The isotopic signature of ClO_4^- showed a synthetic origin (except for a minor component of Atacama ClO_4^- at one site), proving the military source of ClO_4^- contamination in the study area. In addition, groundwater dating using CFCs, SF_6 and ^3H indicated an average residence time of < 50 years, implying that **ClO_4^- contamination is related to sources that may still persist in the subsoil long after the end of WWI (e.g. unexploded ammunition and ammunition destruction sites) rather than sources being emitted by military activities during the conflict.**

Annual variations of ClO_4^- concentration were observed, indicating the influence of recharge processes and groundwater levels on ClO_4^- contamination. Two major temporal trends of ClO_4^- concentration were observed: 1) ClO_4^- concentrations poorly correlated to groundwater level with peaks of contamination due to flushing at sites having high levels of ClO_4^- (> 10 $\mu g \cdot L^{-1}$), implying the presence of point sources; 2) ClO_4^- concentrations highly correlated to groundwater level at sites having low levels of ClO_4^- (< 10 $\mu g \cdot L^{-1}$), where diffuse sources were suggested. In addition, the rapid response of ClO_4^- concentration following the rise of groundwater level compared with relatively stable concentrations of agricultural ions at some sites indicated that the location of ClO_4^- sources could be much deeper than those of agricultural ions (mainly in the soil area).

The potential sources of ClO_4^- located deeper than agricultural ions in the UZ refer most probably to unexploded ammunitions still present underground after WWI. Indeed, some shells fired during the war could reach more than 10 meters underground without exploding. Unused ammunitions could also still be present underground in military tunnels of WWI. In addition, in the Champagne Mounts area, some unused ammunitions on the surface could have been cleaned up by buring directly in specified boreholes (Debant, 2019). Over time, the release of the explosive charge occurs as a result of the general corrosion of the envelope and / or its perforation. The time required for perforation was estimated between 250 and 450 years, at a rate of 1 mm / year on average (Parker et al., 2004). These unexploded ammunitions can be difficult to locate and clean up due to their number and their deep underground location.

Contamination plumes observed at some sites indicate that the ammunition destruction sites may be the main point sources of ClO_4^-, as repeated detonation causes an accumulation of residual ClO_4^- at these sites. The residue of ammunition destroyed by detonation can persist for more than 100 years in soils (Hubé, 2014). Despite the huge quantities of fully exploded ammunition, their residue is estimated at around 0.01% and can only persist for a short time underground, representing a relatively small contribution to the ClO_4^- contamination of groundwater. Considering that most of the potential sources of ClO_4^- have long persistence times, the ClO_4^- contamination in groundwater of the study area may not decline in the short to medium term.

Considered the long persistence time of the explosive residues related to unexploded ammunitions and ammunition destruction activities, the ClO_4^- contamination in groundwater of the study area seems unlikely to decrease in the short- to medium-term.

Part V. A case study: perchlorate contamination in the water catchment of Couraux

The water catchment of Couraux is an intensive groundwater exploitation site with rather complex hydrogeological properties on a small scale. The measurement campaigns carried out by Grand Reims in 2012, 2013 and 2017 showed high concentrations of ClO_4^- (> 15 µg·L^{-1}) in groundwater at this site.

The methodology used and the sources-and-behavior concepts of ClO_4^- developped in the previous sections is also applicable in other ClO_4^- contaminated areas. This is why a case study of ClO_4^- contamination in the drinking water catchment of Couraux is realized. In chapter 1, general characteristics of the water catchment is summarized, especially the geological and hydrogeological context. In chapter 2, the analysis results of concentrations and isotopic composition of ClO_4^- in groundwater are presented. In chapter 3, the observed spatial and temporal variation of ClO_4^- concentrations is shown and interpreted by a combination of isotopic contents and hydrogeological setting information, providing information regarding the sources and evolution of ClO_4^-. According to presented results, recommendations for a better management of water resource in the water catchment of Couraux are proposed in chapter 4.

1. General characteristics of the water catchment of Couraux

The drinking water catchment of Couraux is located on the territory of the communes of Puisieulx and Taissy, on the left and right bank of the Vesle River (Figure V-1). It was created in 1955 (8 wells on the left bank of the Vesle River, N° 1 to 8) and then extended in 1957 (2 wells on the right bank of the Vesle River, N° 9 and 10) (Mondain et al., 2006). According to data from 2003 to 2006, the water catchment of Couraux allowed to provide about a third of drinking water for the metropole of Reims, with an average production of 15 000 $m^3 \cdot d^{-1}$ (Banton et al., 2008).

The groundwater of the water catchment of Couraux is of bicarbonate-calcium type, which is typical of the Chalk aquifer. Within the water catchment, groundwater pumped from different wells showed a high heterogeneity in water quality, especially in terms of nitrate and phytosanitary products (Banton et al., 2008). For this reason, since 1997, the four wells with the best water quality (P1, P2, P5 and P6; Figure V-1) represent each about 20% of the total production of the water catchment. The remaining 20% of production is provided by the other 6 wells, which are of poorer water quality and are used in turn (Mondain et al., 2006).

According to the geological cross-section proposed by Castany (1977), the stratigraphic series of the water catchment of Couraux are:

- 0 – 3 m: recent alluvium (peat and clay),
- 3 – 6 m: old alluvium (graveluche),
- 6 – 20 m: fractured Chalk,
- > 20 m: compact Chalk.

On the water catchment of Couraux, all the wells were all drilled in the same way. With a depth of 30 m, they were cemented to the base of alluvium and then equipped with a 15 m steel tube screen of 600 mm diameter. Long-term pumping tests were realized on different wells which allowed to estimate the hydrodynamic properties of the aquifer (Berger et al., 1977). These tests indicated a radius of influence of about 420 m, an average hydraulic conductivity of about 0.02 $m \cdot s^{-1}$ and a storage coefficient of less than 1% (minimum value of 0.1%). The high permeability indicates that highly developed fractures are present in the aquifer of the water catchment. The storage coefficient is much lower than the average value on river valley areas of the Champagne Chalk aquifer (3% - 5%; Table II-2), indicating that the aquifer could be locally semi-captive on the water catchment of Couraux due to the presence of alluvium layer (Mondain et al., 2006).

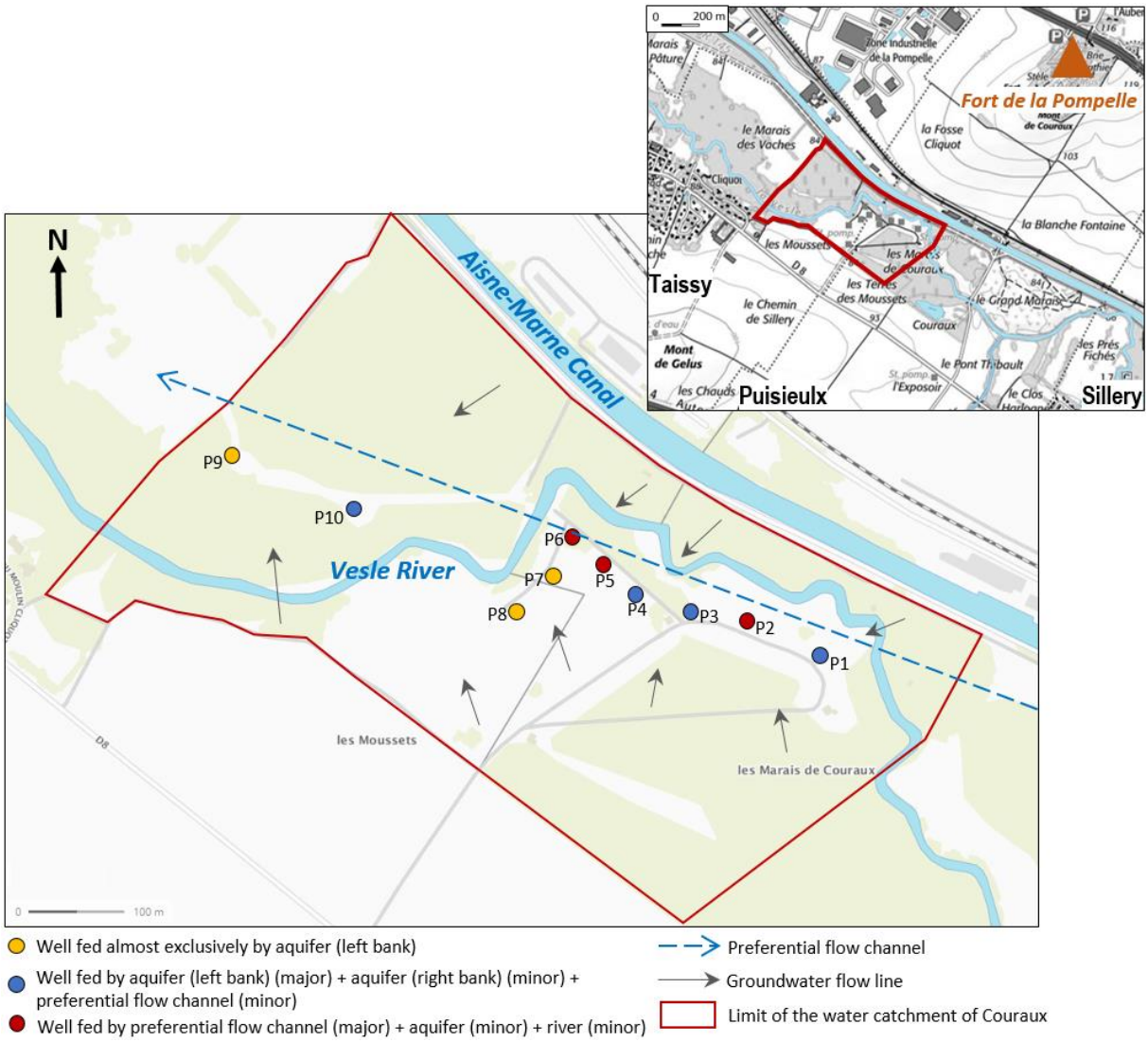

Figure V-1 : Location, wells and groundwater flow of the water catchment of Couraux.

In 2006, the SIABAVE (Syndicat Mixte Intercommunal d'Aménagement du Bassin de la Vesle) has entrusted the GALLIGEE-HYDRIAD group to carry out a study of the water catchment of Couraux. Geophysical, hydrological and geochemical investigations have been realized, providing information on the hydrogeological functioning of the water catchment (Banton et al., 2008, 2007; Mondain et al., 2006).

According to piezometric surveys, pumping tests and tracings, the exchange between the aquifer and the Vesle River on the water catchment of Couraux is very limited. At most of the wells (P1, P3, P4, P7, P8, P9 and P10), the exchange aquifer-river is almost absent. Nevertheless, recharge of groundwater by the Vesle River water has been observed in the sections of the wells P2, P5 and P6. This weak connection involves underground flows from the right bank of the Vesle River, passing under the Aisne-Marne Canal and the Vesle River (Banton et al., 2008).

Geophysical investigations and physicochemical characteristics have also shown that the recharge of the water catchment is largely supported by water flows through a preferential channel probably related

to the paleochannel of the Vesle River (Banton et al., 2007). It is estimated that this preferential channel crosses the permeable part of the alluvium layer and the upper part of the fractured Chalk and passes north of the wells P9 and P10, through the well P6 and north of the well P1 (Figure V-1).

According to the contribution of groundwater from different flow pathways, the wells of the water catchment of Couraux can be classified as following (Figure V-1):

- wells fed almost exclusively by the aquifer of left bank of the Vesle River (P7, P8 and P9),
- wells fed mainly by the aquifer of left bank of the Vesle River with a few mixture of water from the aquifer of right bank of the Vesle River and / or the preferential flow channel (P1, P3, P4 and P10),
- wells fed mainly by water though the preferential channel with some contribution from the aquifer and the Vesle River (P2, P5 and P6).

2. Perchlorate in groundwater of water catchment of Couraux

The data of ClO_4^- concentration of 2012-2013 and 2017 was provided by Grand Reims, with limits of quantification of 2 $\mu g \cdot L^{-1}$ and 0.5 $\mu g \cdot L^{-1}$ respectively. ClO_4^- concentration of 2018-2019 was measured in water samples collected in P1, P5 and P6 as part of the thesis research, with a limit of quantification of 0.5 $\mu g \cdot L^{-1}$. The isotopic composition of ClO_4^- was analyzed once in water sample collected at P6 on April 2019 and the isotopic composition of NO_3^- was analyzed once in water samples collected at P5 and P6 on October 2018 (for details of the analysis method see Part II.2.3)

2.1. Concentration of perchlorate

ClO_4^- was detected in all the 10 wells, with concentrations ranging from < 0.5 $\mu g \cdot L^{-1}$ to 71.4 $\mu g \cdot L^{-1}$ (Table V-1). From 2012 to 2013, the water samples collected at P4, P5 and P6 were the most concentrated in ClO_4^-, with average concentrations of 18 ± 9.7 $\mu g \cdot L^{-1}$ (n = 6), 18 ± 9.7 $\mu g \cdot L^{-1}$ (n = 5) and 21 ± 9.5 $\mu g \cdot L^{-1}$ (n = 6), respectively. In other wells, much lower concentrations of ClO_4^- were measured with average concentrations below 10 $\mu g \cdot L^{-1}$. In 2017, measured ClO_4^- concentrations in different wells were generally similar or lower than the 2012-2013 average concentrations, with the exception of much higher concentration measured at P1 (13.2 $\mu g \cdot L^{-1}$). From 2018 to 2019, the concentrations measured at P5 and P6 were much higher than those measured in 2012, 2013 and 2017, with average concentrations of 20.4 ± 5.8 $\mu g \cdot L^{-1}$ and 53.2 ± 9.4 $\mu g \cdot L^{-1}$, respectively. The average concentration in water samples at P1 was 2.8 ±0.7 $\mu g \cdot L^{-1}$, similar to measured concentrations from 2012 to 2013.

Table V-1 : ClO_4^- concentrations in groundwater of the water catchment of Couraux

	Sampling date	P1	P2	P3	P4	P5	P6	P7	P8	P9	P10
2012-2013	25/07/2012	3	8	5	7	11	30	-	4	5	5
	27/08/2012	2	7	7	5	21	18	5	4	4	4
	25/09/2012	3	6	9	22	5	3	5	4	4	4
	25/10/2012	3	5	8	29	-	-	4	-	-	-
	29/11/2012	2	5	13	-	-	-	-	4	-	-
	06/12/2012	2	-	9	24	-	24	-	-	-	-
	13/12/2012	-	-	8	-	22	24	-	3	-	-
	20/12/2012	-	4	-	20	29	26	4	-	-	-
	31/01/2013	3	9	-	-	-	-	7	5	-	-
	07/02/2013	3	11	-	-	-	-	8	-	4	-
	14/02/2013	-	11	-	-	-	-	10	5	-	6
	Mean	**3 ± 0.5**	**7 ± 2.7**	**8 ± 2.4**	**18 ± 9.7**	**18 ± 9.7**	**21 ± 9.5**	**6 ± 2.3**	**4 ± 0.6**	**4 ± 0.5**	**5 ± 1.1**
2017	19/09/2017	13.2	-	<0.5	-	11.2	-	2.6	-	-	-
	26/09/2017	-	10.4	-	<0.5	-	5.2	-	6.7	-	<0.5
	Mean	**13.2**	**10.4**	**<0.5**	**<0.5**	**11.2**	**5.2**	**2.6**	**6.7**	**-**	**<0.5**
2018-2019	15/10/2018	-	-	-	-	20.6	58.4	-	-	-	-
	20/11/2018	-	-	-	-	15.1	37.2	-	-	-	-
	19/12/2018	-	-	-	-	15.4	48	-	-	-	-
	23/01/2019	-	-	-	-	21.6	46.6	-	-	-	-
	14/02/2019	-	-	-	-	17.5	56.8	-	-	-	-
	21/03/2019	-	-	-	-	32.2	71.4	-	-	-	-
	25/04/2019	2.3	-	-	-	-	51.5	-	-	-	-
	28/05/2019	3.3	-	-	-	-	54.8	-	-	-	-
	27/06/2019	-	-	-	-	20.4	54.1	-	-	-	-
	Mean	**2.8 ± 0.7**	-	-	-	**20.4 ± 5.8**	**53.2 ± 9.4**	-	-	-	-

2.2. Isotopic composition of perchlorate

The results of Cl and O stable isotope analysis for ClO_4^- in water sample collected at P6 are presented by dual isotope plots in comparison to results for collected samples of this study and published data in litterature for synthetic, Atacama and selected US indigenous natural ClO_4^- occurrences (Figure V-2).

The isotopic composition of ClO_4^- at P6 was very similar to that of FBN4 (low water) (see PartV.Part IV.4), with a low $\delta^{18}O$ value (-30.4‰) falling outside the published synthetic ClO_4^- ranges and the $\Delta^{17}O$ and $\delta^{37}Cl$ values (0.5‰ and -4‰, respectively) typical of the measured synthetic ClO_4^-. Therefore, ClO_4^- at P6 was interpreted as of the same synthetic origin as FBN4 (low water), which is different from other samples and currently reported as synthetic ClO_4^- products. The different manufacturing processes of synthetic ClO_4^- during WWI could possible explain the “unusual” synthetic end-member observed at P6 and FBN4 (low water) (see Part IV.4).

The NO_3^- isotope data at P5 and P6 did not show any evidence of Atacama source for the NO_3^-, as showed by samples of the study area (Figure V-2). However, the possibility of the existence of Atacama NO_3^- cannot be ruled out as Atacama NO_3^- could have been replaced and/or assimilated with the soil NO_3^-. The ClO_4^- isotope data, which was apparently not modified during the recharge process, is a more reliable indicator of ClO_4^- origin (see Part IV.4).

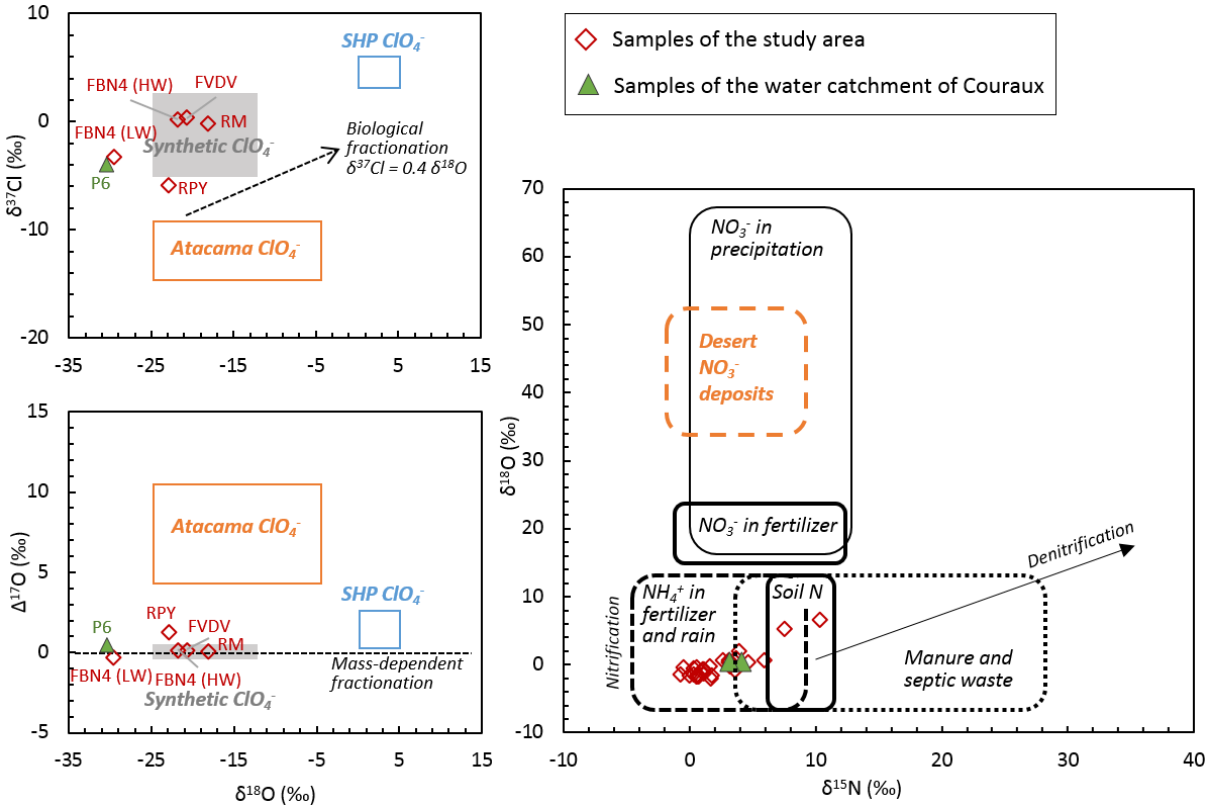

Figure V-2 : Summary of isotope data for ClO_4^- and NO_3^- in samples of the water catchment of Couraux and the study area, compared with major known ClO_4^- sources including synthetic, Atacama and indigenous natural ClO_4^- from the Southern High Plain (Texas) (SHP) (Ader et al., 2001 ; Bao and Gu, 2004 ; Böhlke et al., 2005, 2009 ; Jackson et al., 2005b, 2010 ; Parker et al., 2008 ; Plummer et al., 2006 ; Rajagopalan et al., 2006 ; Rao et al., 2007 ; Sturchio et al., 2007, 2011). Arrow in the $\delta^{37}Cl$ vs $\delta^{18}O$ graph represents the slope of biodegradation ($\delta^{37}Cl = 0.4\ \delta^{18}O$) and arrow in the $\Delta^{17}O$ vs $\delta^{18}O$ graph represents the direction of mass dependent fractionation.

3. Discussion and summary on sources and evolution of ClO_4^- contamination

The measured isotopic composition of ClO_4^- showed pure synthetic ClO_4^-, indicating a military source of ClO_4^- in groundwater of the water catchment of Couraux. ClO_4^- has been detected in all the wells, indicating the presence of extended ClO_4^- source on the water catchment.

Indeed, trenches of WWI also crossed the left bank area of the Vesle River, even though the density were much lower than the right bank (Figure V-3). Military sources of ClO_4^- related to WWI (battle-fields, ammunitions storage/destruction sites and unexploded ammunitions persisting underground) could possibly be present on and/or around the water catchment, leading to ClO_4^- contamination of groundwater. The Fort de la Pompelle located upstream the water catchment (Figure V-3), could be a potential point source of ClO_4^- contamination.

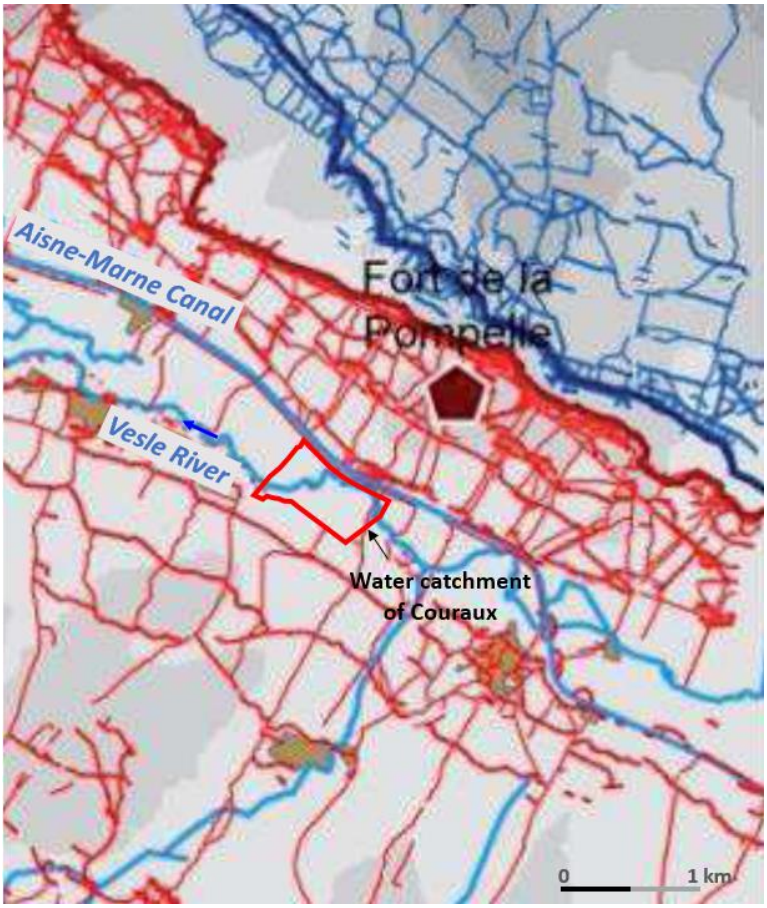

Figure V-3 : Map of the WWI defense networks around the water catchment of Couraux (adopted from Taborelli, 2018)

Groundwater collected in different wells of the water catchment showed a high spatial heterogeneity in ClO_4^- concentrations. In wells fed almost exclusively by the aquifer of left bank of the Vesle River (P7, P8 and P9; Figure V-1), relatively low concentrations of ClO_4^- were measured (Table V-1), indicating low levels of ClO_4^- in the aquifer of left bank. This was consistent with similar low concentrations of ClO_4^- measured in the wells of P1, P3 and P10 (Table V-1), which were mainly fed by the aquifer of left bank with only a few mixture of water from right bank and/or the preferential flow channel. However, in the well of P4 (same flow pattern as P1, P3 and P10; Figure V-1), much higher concentrations of ClO_4^- were measured (Table V-1), suggesting local sources of ClO_4^- in the aquifer of left bank at P4 radius of influence. The temporal evolution of ClO_4^- concentration at P4 was different from that of P5 and P6 (Figure V-4), implying different sources of ClO_4^-, which was consistent with the different flow patterns at P4 and P5/P6.

Indeed, the wells of P5 and P6, which were located very close to each other (Figure V-1), were fed mainly by the preferential flow channel, with some contribution of the Vesle River and the aquifer. The similar temporal variation of ClO_4^- concentrations at P5 and P6 (Figure V-4) indicated probably same sources of ClO_4^- for the two wells. However, in the well of P2 (same flow pattern as P5 and P6), much lower concentrations of ClO_4^- were measured (Table V-1). The contribution of ClO_4^- from the Vesle River can be excluded as the ClO_4^- concentrations measured in the Vesle River were quite low (< 2 $\mu g \cdot L^{-1}$; Table IV-1). Although the Canal Aisne-Marne also contributes to the recharge of the aquifer and the Vesle River (cf. Part II.1.3.2), the contribution of ClO_4^- is from the canal water is unlikely as ClO_4^- was not detected in the canal (< 0.5 $\mu g \cdot L^{-1}$; Table IV-1). Therefore, two possibilities have been suggested for the source of ClO_4^- at these sites: 1) local sources near the well of P6 or 2) sources upstream the water catchment connected with the preferential flow channel. The lower concentration of ClO_4^- at P5 and P2 could be explained by their longer distance to the potential sources than P6 in the first case or by the weaker connection with the preferential flow channel at P5 and P2 than P6.

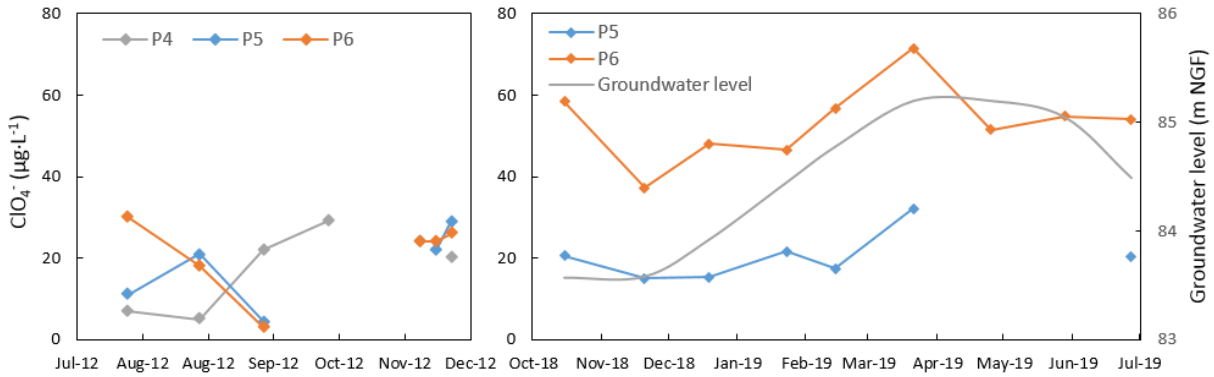

Figure V-4 : Temporal evolution of ClO_4^- concentration in water samples collected at P4, P5 and P6 in 2012, 2018 and 2019. The groundwater level data is from FAP, the closest borehole to the water catchment of Couraux in the study area (Figure II-8).

Annual variations of ClO_4^- concentrations were observed in groundwater of the water catchment of Couraux. Generally, the lowest and highest concentrations of ClO_4^- were observed in 2017 and 2018/2019 respectively, while the concentrations measured in 2012/2013 were moderate (Table V-1). The annual variations of ClO_4^- concentrations were consistent with the annual variations of groundwater level in the Champagne Chalk aquifer (**Appendix 3**): the water level in autumn 2017 was much lower than the average level while it was much higher in 2018.

Seasonal variations were also observed, mainly at P4, P5 and P6 where high ClO_4^- concentrations were observed. In other wells, ClO_4^- concentrations were relatively stable over time as shown by the low values of standard deviation (Table V-1). At P5 and P6 (wells with the longest observation record), lower concentrations were observed in summer/autumn while higher concentrations were observed in winter/spring (Figure V-4), which is consistent with the seasonal variation of groundwater level (cf. Part III.1.2.1).

4. Recommendations to improve water resource management in the water catchment of Couraux

Currently in the water catchment of Couraux, the wells of P1, P2, P5 and P6 represent each about 20% of the total production of the water catchment. However, in two of these permanently used wells (P5 and P6), high concentrations of ClO_4^- were observed (average concentrations > 15 $\mu g \cdot L^{-1}$). Groundwater pumped from P6 contained ClO_4^- with concentrations up to 71.5 $\mu g \cdot L^{-1}$, which is much higher than the advisory level of ClO_4^- in drinking water in France (5 $\mu g \cdot L^{-1}$; ANSES, 2018). **In order to ensure the drinking water safety in terms of ClO_4^-, more attention should be paid concerning the utilization of P5 and P6, especially the well P6.**

The influence of groundwater level on ClO_4^- concentration was highlighted according to the annual and seasonal variation of ClO_4^- concentrations observed in the water catchment of Couraux. ClO_4^- concentrations in groundwater seem to be higher during high water period than low water period. **Therefore, the water catchment is more vulnerable to ClO_4^- contamination during winter/spring seasons or years with abnormally intensive precipitations. Under such conditions, ClO_4^- concentrations in different wells should be more frequently monitored and the production of wells can be adjusted according to rainfall events and/or groundwater levels.**

Although interesting implications have been made from the current research, some limits still exist and can be furtherly improved. ClO_4^- concentrations have been measured several times from 2012 to 2019, however none of these measurement campaign allows to provide long-term continuous data to better observe the seasonal and annual variation of ClO_4^- concentrations under different climate conditions. **The measurement of ClO_4^- concentrations here should be continued to extend the data base of ClO_4^- contamination in the water catchment of Couraux. Groundwater dating using CFCs, SF_6 and /or ^3H could be a relevant complementary research to better understand the river-aquifer relations, groundwater flow patterns (especially the role of the preferential channel) and ClO_4^- evolution at this site.** In addition, a hydrodynamic and geochemical numerical model could be a useful tool to better understand the hydrogeological functioning of the Chalk aquifer and the transport of ClO_4^- in groundwater.

Part VI. Conclusions and perspectives

1. Results summary

The objectives of this thesis research are to: 1) describe the hydrogeological function of the unconfined Chalk aquifer; 2) identify the sources and understand the transfer mechanisms of perchlorate in the unconfined Champagne Chalk aquifer. The knowledge of aquifer function provides fundamental prerequisites for understanding the sources and behavior of ClO_4^- ions. A summary of the results on these two aspects are presented below.

- **<u>Hydrogeological functioning of the unconfined Chalk aquifer</u>**

  - **Aquifer response to recharge**

On the unconfined Champagne Chalk aquifer, the effective rainfall (ER) is considered equivalent to the aquifer recharge as zero runoff is assumed due to the high porosity of the Chalk. In this study, the ER from 2016 to 2019 is estimated using a water balance method.

According to the estimated ER (average annual value of 137.2 mm), two periods can be distinguished during a hydrological cycle: 1) aquifer recharge period from November to March, when large quantities of ER are produced due to excess of rainfall compared to evapotranspiration; 2) aquifer discharge period from April to October, when low to zero ER are produced due to evapotranspiration excess compared to rainfall. This recharge mode is consistent with the observed groundwater level fluctuations in the study area, whereby the highest water level was reached in March/April and the lowest level reached in October/November. Annual variations of ER were also observed and consistent with the observed annual variations of groundwater level: the water level in March/April 2018 was much higher than that of the same period in 2017 and 2019 due to the higher ER in winter/spring 2017-2018.

The unconfined Chalk aquifer possesses highly heterogeneous hydrological characteristics. Generally, the aquifer on interfluves shows poor permeability as evidenced by the low productivity of boreholes and large fluctuation of groundwater level. Conversely, in river valleys, high density of active fractures are consistently developed resulting in high permeability of the aquifer. Although the majority of the aquifer has an inertial behavior with respect to recharge, a rapid response following rainfalls can be achieved locally by the highly developed fractured network in the Chalk, as evidenced by the observed temporal evolutions of groundwater level, temperature, and electrical conductivity.

  - **Groundwater dating and hydrochemistry**

Groundwater dating using ^3H, CFCs and SF_6 was realized here for the first time in the unconfined Champagne Chalk aquifer. Low levels of ^3H (< 5 UT) were observed and compared directly with historical ^3H concentrations in rainwater, suggesting relatively young groundwater ages since the late 1980s (Clark and Fritz, 1997).

In order to estimate groundwater age with CFCs and SF_6, the measured CFCs/SF_6 concentrations in water were transformed to air mixing ratios and then compared to historical CFCs/SF_6 concentrations in local air using different models of underground water circulation (piston flow model, exponential mixing model, and binary mixing model). Despite the frequent contamination of CFCs and SF_6 detected in the study area, relevant information on residence times and mixing processes of the Chalk groundwater was obtained at the majority of sites. The unconfined Champagne Chalk aquifer is made up of waters of different ages ranging from modern to about 50 years, with mixing models defined at each sampling site implying different flow pathways and mixing processes in the aquifer.

The chemical composition of the monitored groundwater was typical of the Chalk groundwater, as Ca^{2+} and HCO_3^- were the two dominant solute ions due to Chalk dissolution. The origins of the major solute ions were studied: Cl^-, NO_3^-, SO_4^{2-} and some Ca^{2+} were interpreted as having an agricultural source, whereas Mg^{2+}, K^+ and a part of SO_4^{2-} are interpreted as mostly attributed from a terrigenous source related to Chalk impurities and clay minerals in the superficial formations (colluvium and alluvium).

Despite the Ca^{2+} - HCO_3^- chemical facies, spatial and temporal heterogeneities of groundwater geochemistry were observed in the unconfined Chalk aquifer. The variation of EC was mostly attributed to the variation of NO_3^- and Cl^- concentrations, as EC, NO_3^- and Cl^- showed similar spatial and temporal tendencies. Different correlations between EC time series and groundwater level fluctuations were observed: correlated, anti-correlated or independent. The geochemical heterogeneities of Chalk groundwater were interpreted to be caused by a combination of hydrogeological setting, residence time, and land use, highlighting the main factors governing the Chalk groundwater geochemistry including water level fluctuation, thickness of the Unsaturated Zone (UZ), the types of superficial formations, distribution of fracture networks, aquifer-river relations, and human activities.

- **Conceptual model of aquifer functioning**

A conceptual model of the hydrogeological function of the unconfined Chalk aquifer was established by combining the results of aquifer recharge, groundwater dating, and hydrogeochemistry (Figure VI-1).

In general, under deep groundwater level conditions, the geochemistry of the aquifer tends to be less influenced by near surface contamination, with relatively low agricultural inputs. Where no superficial formations overlie the Chalk, an exponential mixing model could be applied with a relatively short residence time. At these sites, contaminations related to agricultural inputs are positively correlated to water table dynamics due to the large groundwater level fluctuations. At shallow groundwater sites, the Chalk aquifer is usually highly fractured. Rapid recharge through fractures is favored, making groundwater a mixture of freshly percolated water and old water coming from upstream recharge areas (binary mixing). Therefore, groundwater geochemistry is mostly influenced by the dilution effects of rainfall, leading to a degree of mineralization that is negatively correlated to water table level.

Superficial formations over the Chalk present a lower permeability than the Chalk, and thus may constitute a barrier limiting the rapid recharge of water and solutes into the aquifer. At these sites, a piston flow model better describes the groundwater flow and relatively old groundwater ages are estimated, which explains the stable or delayed response of groundwater geochemistry to water table fluctuations. For groundwater exploitation sites near rivers, recharge of the aquifer by rivers could occur especially during low water period, leading to groundwater geochemistry being influenced by surface water.

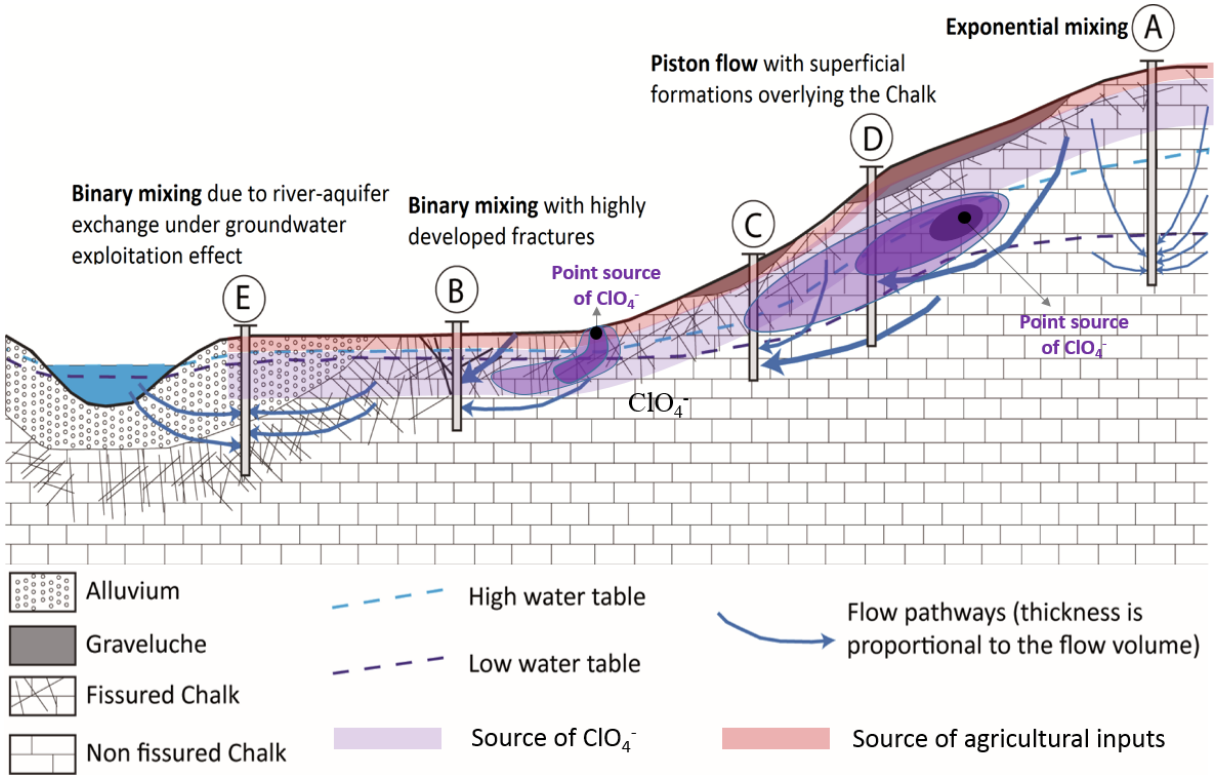

Figure VI-1 : Schematized hydrogeological functioning of unconfined Chalk aquifers and sources and transfer of ClO_4^- and agricultural ions

- **<u>Sources and behavior of perchlorate in the unconfined Chalk aquifer</u>**

In the unconfined Champagne Chalk aquifer, two potential sources of ClO_4^- are suspected: a military source related to WWI and an agricultural source related to the past use of Chilean nitrate fertilizer. In order to clarify the sources and understand the transfer mechanisms of ClO_4^-, a combination of continuously monitored ClO_4^- concentrations, isotopic analyses of ClO_4^- and NO_3^- as well as historical and hydrogeological investigations were used.

- **Occurrence of ClO_4^- contamination**

Perchlorate was detected at almost all sampling sites in the study area, with concentrations ranging from < 0.5 to 62.5 $\mu g \cdot L^{-1}$. About half of the sampling sites showed ClO_4^- concentrations > 4 $\mu g \cdot L^{-1}$ and most of these sites were located downgradient of the Champagne Mounts area, where huge quantities of ClO_4^- were used, stored, or destroyed during and after WWI. The high ClO_4^- levels at some sites and the observed plume-like patterns indicated that potential point-sources of ClO_4^- could be present.

Unlike the widespread contamination of ClO_4^- in the study area, organic explosives have not been detected in surface and groundwater samples, which could be explained by their low persistence and mobility in soil and water.

- **Post-WWI military origin of ClO_4^- inferred from isotopic analysis and groundwater ages**

The results of isotopic analyses showed synthetic ClO_4^- at most sites except for the small mixture of Atacama ClO_4^- in the Py River originated from the Suippe military camp outside the study area. This minor component of Atacama ClO_4^- is unlikely to have been caused by contribution from the agricultural use of Chilean nitrate (ended by the year 1950), since the estimated groundwater ages in the study area were less than 50 years and the time of transfer in the UZ were relatively short under the shallow groundwater context. It could be mostly explained by the nitrogen explosives of WWI (black powder and nitro group explosives) made with Chilean nitrate. Therefore, sources of ClO_4^- contamination in the study area were most likely related exclusively to military activities occurring after WWI rather than during the war. As only a small contribution of Atacama ClO_4^- was observed, ClO_4^- contamination was thereby mainly attributed by synthetic ClO_4^--based explosives rather than nitrate-based explosives produced with Chilean nitrate.

- **Sources and behavior of ClO_4^- in the Champagne Chalk aquifer**

Annual variations of ClO_4^- concentration were observed, indicating the influence of meteorological conditions and groundwater levels on ClO_4^- contamination. The Champagne Chalk aquifer seems to be more vulnerable to ClO_4^- contamination during winter/spring seasons or years with abnormally large amounts of precipitation. Two major temporal trends of ClO_4^- concentration were observed: 1) ClO_4^- concentrations poorly correlated to groundwater level with peaks of contamination due to flushing at sites having high levels of ClO_4^- (> 10 $\mu g \cdot L^{-1}$), implying the presence of point sources related mainly to old military tunnels and ammunition destruction sites; 2) ClO_4^- concentrations highly correlated to groundwater level at sites having low levels of ClO_4^- (< 10 $\mu g \cdot L^{-1}$), where diffuse sources were suggested.

The temporal evolution of ClO_4^- was also compared with the chronicles of NO_3^- and Cl^-, the two major agriculture-derived ions in groundwater of the Chalk aquifer. At most sites, the temporal evolution of ClO_4^- was different from that of NO_3^- and Cl^-, indicating different origins of ClO_4^- *versus* NO_3^- and Cl^-. The different temporal trends were interpreted with reference to the historical investigations and the conceptual model of aquifer function, as summarized in Figure VI-1.

At sites with superficial formations that overlie the Chalk, while concentrations of NO_3^- and Cl^- were stable over time due to the permeability barrier effect of superficial formations limiting rapid recharge and agricultural inputs from surface to the saturated zone (SZ), high temporal variations of ClO_4^- levels were observed. This implied that the location of ClO_4^- sources were much deeper than those of agriculture-derived ions which are contained mainly in the soil (Figure VI-1). As groundwater level rose, the contamination front of ClO_4^- was soon reached, generating changes in ClO_4^- levels, despite the fact that flush from the soil towards the aquifer was largely limited by the superficial formations. At sites with deep groundwater table levels, the temporal variabilities of ClO_4^-, NO_3^- and Cl^- were positively correlated, as the sources of ClO_4^-, NO_3^- and Cl^- were all located mostly in UZ and were flushed downgradient into the aquifer following recharge, showing a similar temporal variation (Figure VI-1).

The potential sources of ClO_4^- located deeper than those of agricultural-derived ions in the UZ refer most probably to: 1) unexploded ammunition that persists underground (down to more than 10 m depth) after WWI; 2) unused ammunition stocks present underground in old military tunnels of WWI or buried in specific boreholes after WWI. Over time, the release of the explosive material occurs as a result of the general corrosion of the envelope and/or its perforation, which could last for at most 250-450 years. Potential sources of ClO_4^- could also be located on the surface (Figure VI-1), which is mostly the case at ammunition destruction sites. At these sites, repeated detonations have caused accumulation of residual ClO_4^- which could persist for more than 100 years in soils. In addition, storage of unused ammunition could still exist at these sites, thereby representing a continuous source of ClO_4^- contamination.

Considered the long persistence time of the explosive residues related to unexploded ammunition and ammunition destruction activities, the ClO_4^- contamination in groundwater of the study area seems unlikely to decrease in the short- to medium-term.

2. Limits and perspectives

The combination of different tools has allowed the development of a conceptual model of Chalk aquifer function. The multi-tool methodology developed in this study and the established conceptual model might be used elsewhere in Chalk aquifers or other multi-porosity mediums for the prediction of spatial and temporal variations of groundwater mineralization and solute transport (natural or anthropogenic) and for the evaluation of aquifer vulnerability. However, these methods still have some limitations. This research can be improved and developed in several different aspects in the future.

- **Continuous monitoring of the Champagne Chalk aquifer**

The two-year long time series of groundwater level, geochemical parameters, and ClO_4^- concentrations are relatively short to interpret a general and comprehensive mechanism of aquifer function and the evolution pattern of ClO_4^- contamination in the Chalk aquifer. The continuous monitoring of the above parameters should be continued to obtain longer time series, with the aim to study the influence of different meteorological conditions on the Chalk aquifer function and evolution of ClO_4^- contamination.

- Indeed, under the global climate change context, extreme meteorological conditions (e.g. drought and flood) tend to occur more frequently (e.g., Haden et al., 2012; Ogunbode et al., 2019; Spence et al., 2011), thereby leading to changes of aquifer function and groundwater quality. The continuous monitoring of the aquifer could extend the data base of hydrogeological parameters, which is essential for a comprehensive understanding of the aquifer function and pollutant transfer. **Groundwater dating**

The groundwater dating using CFCs and SF_6 was disturbed by contamination of tracer gases in the study area, especially for CFC-12 and SF_6, resulting in missing groundwater flow and residence time information at some sites. Although tritium analysis was realized as a complement to CFCs and SF_6, only qualitative age information was obtained with the simple quantitative interpretation method applied. Despite the general consistency of groundwater apparent ages estimated by ^3H and CFCs/SF_6 for the majority of water samples, exceptions were found at two sites having very low concentrations of ^3H.

In order to better explain these abnormal results and to provide more information about groundwater flow for sites contaminated by CFCs/SF_6 tracers, $^3H/^3He$ ratio analyses could provide a good alternative dating method.

- **Geophysical investigations**

Geophysical investigations could provide additional perspectives for this study, allowing better characterization of the geometry (extension and thickness) and the structure (presence of fissures and faults) of the aquifer. Electromagnetic methods and electrical techniques (electrical resistivity tomography) have been successfully used in the drinking water catchment of Couraux in the Champagne region, which allowed to estimate the porosity of the rock, to clarify the extension and thickness of different geological formations as well as the position of potential drainage axes of groundwater (Banton et al., 2008, 2007). The same methods can be applied locally in the study area for a better understanding of groundwater flow and contaminant transport. Other techniques such as shallow seismic methods and remote sensing techniques could also be used for a non-destructive characterization of the hydrodynamic properties of the unconfined Champagne Chalk aquifer (Mussett and Khan, 2000).

- **Historical investigations**

The Moronvilliers military camp located on the Champagne Mounts was the scene of intensive battles during WWI and was also used as ammunition destruction grounds after the WWI. In the study area, high ClO_4^- concentrations were detected mainly downgradient this site. This sector has become a military restricted area since 1957 with the establishment of a nuclear experimental center attached to the Atomic Energy Comision (CEA). Therefore, historical information concerning the location of ammunition destruction sites and other military activities realized on this military camp is very limited. Investigations need to be continued in military archives with the aim to precisely locate a maximum of potential point sources of ClO_4^-. In addition, the LIDAR (LIght Detection And Ranging) technology has been successfully used in the Champagne region to evidence past landscape military activity traces (Taborelli et al. 2017). Its use in the study area could make it possible to detect potential sources of ClO_4^-.

- **Isotopic analysis of perchlorate**

In this study, isotopic analysis of ClO_4^- has only been realized at several sites with high concentrations of ClO_4^-. This analysis should also be performed at sites having low concentrations of ClO_4^- to further confirm whether traces of Atacama ClO_4^- exist on these less-contaminated sites related to diffuse sources.

The results of analysis in the study area have showed a synthetic "end-member" of ClO_4^- presenting somewhat different isotopic composition from the published synthetic ClO_4^- ranges. Further isotopic measurements should be realized for ClO_4^- in different types of WWI ammunitions, to extend the data base of synthetic ClO_4^- ranges and facilitate the use of isotopic method for ClO_4^- source apportionment.

In addition, isotopic analysis of ClO_4^- should also be done on sites with exclusively agricultural sources of ClO_4^- (past use of Chilean nitrate fertilizer). This purely agricultural isotopic signature of ClO_4^- would provide good complementary information for this study and also for future studies on ClO_4^- contamination in other areas of NE France.

- **Piezometric map**

The piezometric map (high water) produced by BRGM in 2002 (Rouxel-David et al., 2002b) is used throughout this study, as the number of continuous monitored boreholes in the study area is not sufficient to produce a new piezometric map. However, this map is not accurate enough on the watershed scale of the study area. A more accurate piezometric map of the study area on low and high water should be realized, which is necessary for a better understanding of groundwater flow and sources and transfer of contaminant on local scales and is also essential for further numerical modeling.

- **Numerical modeling**

The methods employed in this study focus mostly on a qualitative rather than a quantitative perspective, which could limit applications on contaminant transport prediction. A hydrodynamic and geochemical numerical model, based on the conceptual model established in this study, could be a useful tool to better understand the transport of ClO_4^- in the Chalk groundwater.

Part VII. Résumé substantiel en Français

1. Table des matières

1. Réponse de la nappe par rapport à la recharge

1.1. Recharge de la nappe : estimation de la pluie efficace

1.1.1. Méthode du bilan hydrique

1.1.2. Pluie efficace calculée

1.2. Chroniques piézométriques, de températures et de conductivité électriques

1.2.1. Variations saisonnières et annuelles des niveaux piézométriques

1.2.2. Comportement de la nappe par rapport aux évènements pluvieux

1.2.2.1 Situation générale

1.2.2.2 Cas particulier : FAP

1.2.2.3 Cas particulier : FBN1 et FBN5

1.2.3. Comparaison avec la carte piézométrique historique

1.3. Discussion autour de la recharge et des caractéristiques hydrologiques de la nappe

2. Datation des eaux souterraines par les CFCs, SF_6 et ^3H

2.1. Principe de la datation

2.1.1. Datation avec le ^3H

2.1.1.1 Origines et concentrations atmosphériques

2.1.1.2 Méthode de datation

2.1.2. Datation avec les CFCs et SF_6

2.1.2.1 Origines et concentrations atmosphériques

2.1.2.2 Méthode de datation

2.1.2.3 Facteurs pouvant influencer la datation

2.2. Modèles d'interprétation

2.2.1. Modèle piston

2.2.2. Modèle exponentiel

2.2.3. Modèle du mélange binaire

2.3. Résultats et interprétations

2.3.1. Résultats de datation avec le ^3H

2.3.2. Résultats de datation avec les CFCs et SF_6

2. Introduction

2.1. Contexte général

L'intérêt croissant porté sur les ions perchlorates (ClO_4^-) est lié à leur effet néfaste sur la santé en tant que perturbateur endocrinien (e.g., Brabant et al., 1992 ; Braverman et al., 2005 ; Greer et al., 2002). L'ion ClO_4^- est un anion inorganique et oxydant, très soluble et mobile dans l'eau. En milieu non-réducteur et dans les conditions environnementales classiques des eaux de surfaces et souterraines, les ions ClO_4^- peuvent persister pendant de nombreuses années, voire plusieurs décennies dans l'environnement aquatique (Sturchio et al., 2014). Les sels de ClO_4^- sont utilisés dans de nombreuses industries modernes, par exemple comme propulseurs de fusées et comburant des explosifs (Urbansky, 1998). Naturellement, les ClO_4^- peuvent se former dans l'atmosphère et s'accumuler par dépôts secs et humides dans les sols des environnement arides et semi-arides tels ceux du désert d'Atacama (Chili) et du sud-ouest des États-Unis (Jackson et al., 2015, 2016 ; Lybrand et al., 2016 ; Rao et al., 2007). Les dépôts de nitrate géogéniques présents dans le désert d'Atacama (nitrate chilien), qui sont accompagnés de traces de ClO_4^-, ont été raffinés et distribués dans le monde entier pour être utilisés comme engrais au cours de la première moitié du XXe siècle, ce qui représente une source potentielle de contamination en ClO_4^- (Ericksen, 1983 ; Rajagopalan et al., 2006).

L'eau potable est probablement la plus grande source d'exposition humaine au ClO_4^- (Steinmaus, 2016). Au cours des deux dernières décennies, la contamination des eaux par le ClO_4^- a été signalée dans de nombreux pays, tels que les États-Unis, le Canada, le Chili, la Chine, l'Inde, le Royaume-Uni et la France, avec des origines diverses (e.g., Cao et al., 2019a, 2018 ; Furdui et al., 2018 ; Jackson et al., 2005 ; Kannan et al., 2009 ; McLaughlin et al., 2011; Qin et al., 2014 ; Sturchio et al., 2014 ; Vega et al., 2018).

En France, l'intérêt porté aux ClO_4^- s'est accru depuis 2011 en raison de la découverte d'une contamination de plusieurs ressources en eau brutes destinées à la consommation humaine dans des régions du sud-ouest de la France, du Bassin Parisien et du nord-est de la France (Lopez et al., 2015). Des valeurs de recommandation concernant les ClO_4^- dans l'eau potable ont été proposées en 2011 par l'Agence Nationale de Sécurité Sanitaire (ANSES) : 15 $\mu g \cdot L^{-1}$ pour les adultes et 4 $\mu g \cdot L^{-1}$ pour les nourrissons de moins de 6 mois.

En Champagne-Ardenne, les campagnes de mesures menées par l'Agence Régionale de Santé (ARS) en 2014 ont mis en évidence des concentrations élevées en ClO_4^- (> 15 $\mu g \cdot L^{-1}$) dans des captages d'eau potable. Deux sources potentielles dans les eaux sont suspectées en Champagne-Ardenne : militaire et agricole.

En effet, la région Champagne-Ardenne a été durablement marquée par les évènements de la Grande Guerre. Ces activités militaires peuvent avoir émis de grande quantité de ClO_4^- dans l'environnement, les ClO_4^- synthétiques et les nitrates chiliens ayant été utilisés pour la fabrication de munitions pendant la Première Guerre Mondiale. Ainsi, il existe un lien géographique entre les concentrations élevées en ClO_4^- dans les eaux souterraines et les positions des lignes de fronts entre 1914 et 1918. Une source agricole est également suspectée, car une grande quantité de nitrates chilien a été utilisée comme engrais naturel en France (notamment en région Champagne-Ardenne) entre 1880 et 1950 (Lopez et al., 2015). Afin d'améliorer la gestion des ressources en eau de la région Champagne-Ardenne (appartement aujourd'hui à la grande région Grand-Est), il s'avère nécessaire de clarifier les sources de ClO_4^- (militaire et/ou agricole) et de comprendre leur comportement dans les eaux souterraines.

La zone d'étude sélectionnée avec de multi-sources potentielles en ions ClO_4^- est située à l'est de Reims. Comme le transfert de ClO_4^- dans la nappe suit essentiellement l'écoulement des eaux souterraines en raison de leur solubilité et de leur stabilité dans l'eau, les connaissances concernant le fonctionnement de l'aquifère sont fondamentales pour mieux comprendre les sources et le comportement des ClO_4^- dans l'environnement.

L'aquifère étudié est celui de la craie de Champagne au sein duquel s'écoule la nappe libre de la craie, une ressource en eau cruciale de la région. En effet, l'aquifère de la craie est l'un des aquifères les plus importants en Europe. Il est intensivement exploité avec une grande proportion réservée à l'eau potable. En France, la nappe de la craie couvre environ 20% du territoire métropolitain et fournit environ 12 milliards de m^3 d'eau par an, ce qui représente 70% de l'eau potable consommée dans le nord de la France (Lallahem, 2002). Les propriétés hydrauliques de la craie sont complexes du fait d'une d'une double porosité de matrice et de fracture (Allen et al., 1997). La recharge de la nappe peut être très rapide à travers le réseau de fractures et lente à travers la matrice. Par conséquent, la nappe de la craie peut être très vulnérable aux contaminations en particulier sur ses zones d'affleurement. Au cours des dernières décennies, la détérioration de la qualité des eaux souterraines de la nappe de la craie due aux activités humaines a été fréquemment reportée (e.g., Baran et al., 2008 ; Barhoum, 2014 ; Chen et al., 2019 ; Longstaff et al., 1992). De ce fait, des connaissances approfondies sur le fonctionnement hydrogéologique de la nappe de la craie de Champagne s'avèrent indispensables, non seulement pour l'étude de la contamination des eaux en ClO_4^- mais aussi pour une meilleure protection et gestion de cette ressource.

2.2. Objectifs de l'étude

Dans le contexte présenté ci-dessus, les travaux de cette étude sont réalisés selon deux axes : la contamination en ClO_4^- d'une part et le fonctionnement de la nappe de la craie d'autre part. Les objectifs principaux du premier axe sont :

- d'évaluer l'étendue de la contamination et l'évolution spatio-temporelle des ions ClO_4^- dans la nappe de la craie sur la zone d'étude ;
- d'identifier les sources de ClO_4^- (diffuses et/ou ponctuelles) et d'établir des liens entre la présence de ClO_4^- et le type d'activité humaine (militaire et/ou agricole) ;
- de comprendre les mécanismes de transferts et de prévoir le devenir des ions ClO_4^- dans les eaux souterraines de la craie de Champagne à court et moyen termes.

Les objectifs principaux du second axe sont :

- de préciser les modalités d'écoulements et de minéralisation des eaux souterraines de l'aquifère de la craie de Champagne ;
- d'expliquer les hétérogénéités observées dans la qualité des eaux souterraines.

Afin d'approfondir les connaissances sur le fonctionnement de la nappe de la craie, une méthodologie combinant des outils hydrodynamiques, hydrogéochimiques et de datation des eaux souterraines a été développée. Des recherches dans les archives historiques ont été effectuées afin d'identifier, dans la zone d'étude sélectionnée, les sites civils, industriels et militaires susceptibles d'émettre et/ou d'avoir émis des ions ClO_4^-. De plus, l'analyse isotopique des chlorures et de l'oxygène des ions ClO_4^- a été réalisée, afin de discriminer les sources de ClO_4^- (naturel ou synthétique). La surveillance continue des concentrations en ClO_4^-, et les investigations hydrogéologiques et historiques ont été combinées afin de préciser les sources et le comportement des ClO_4^- dans les eaux souterraines de la craie de Champagne.

2.3. Structure de la thèse

La première partie présente une synthèse des connaissances actuelles sur les ClO_4^- dans l'eau et les caractéristiques générales de la nappe de la craie. Tout d'abord, l'occurrence et l'origine des perchlorates dans l'eau à l'échelle mondiale sont présentées. Ces travaux ont fait l'objet d'un article publié dans la revue Science of the Total Environment (*Cao, F., Jaunat, J., Sturchio, N., Cancès, B., Morvan, X., Devos, A., Barbin, V., Ollivier, P., 2019. Worldwide occurrence and origin of perchlorate ion in waters: A review. Sci. Total Environ. 661, 737–749. https://doi.org/10.1016/j.scitotenv.2019.01.107*). Les technologies de traitement des eaux contaminées par les ClO_4^- sont ensuite brièvement décrites. Enfin, les caractéristiques générales de la formation du crétacé et les propriétés de l'aquifère de la craie sont introduites.

La deuxième partie présente en détail la la méthodologie utilisée dans cette étude. La zone d'étude est tout d'abord décrite, y compris la localisation, la topographie, le contexte géologique et hydrogéologique, le contexte climatique, l'occupation du sol et les sources potentielles de ClO_4^-. Ensuite, la stratégie de l'étude et les différentes approches et outils utilisés sont décrits. Les points de prélèvements, la fréquence d'échantillonnage et les analyses effectuées sont enfin présentés.

La troisième partie s'intéresse au fonctionnement hydrogéologique de la nappe de la craie de Champagne. Cette partie a fait objet d'un article publié dans la revue Journal of Hydrology (*Cao, F., Jaunat, J., Vergnaud-Ayraud, V., Devau, N., Labasque, T., Guillou, A., Guillaneuf, A., Hubert, J., Aquilina, L., Ollivier, P., 2020. Heterogeneous behavior of unconfined Chalk aquifers infer from combination of groundwater residence time, hydrochemistry and hydrodynamic tools. Journal of Hydrology 581, 124433. https://doi.org/10.1016/j.jhydrol.2019.124433*). Les modalités de recharge et la réponse de la nappe par rapport à la recharge sont tout d'abord présentées, ces connaissances étant essentielles pour étudier l'écoulement et la géochimie des eaux souterraines. Ensuite, les principes et les résultats de la datation des eaux souterraines par le ^3H, les CFCs et SF_6 sont détaillés. Enfin, la géochimie des eaux souterraines étudiées est décrite en détail. Les origines des ions majeurs sont discutées et validées. Les variations spatio-temporelles de la géochimie des eaux souterraines sont présentées et interprétées au regard du contexte hydrogéologique, du temps de résidence de l'eau dans le sous-sol et de l'occupation du sol. Un modèle conceptuel est finalement proposé, celui-ci résumant le fonctionnement hydrogéologique de la nappe libre de la craie mis en évidence au cours de ces travaux.

Dans la quatrième partie, les résultats concernant les sources et l'évolution des ions ClO_4^- dans l'aquifère de la craie de Champagne sont présentés et discutés. Dans un premier temps, l'étendue de la contamination en ClO_4^- sur la zone d'étude est présentée. Les résultats des analyses isotopiques des chlorures et de l'oxygène des ClO_4^- et de l'azote et de l'oxygène des NO_3^- sont ensuite détaillés, afin de préciser les sources synthétiques et/ou naturelles. Enfin, l'évolution temporelle des ClO_4^- au cours de la période d'étude est discutée et comparée avec la fluctuation des niveaux piézométriques et les concentrations en ions majeurs, mettant en évidence les sources principales de ClO_4^- et les facteurs régissant le transfert des ions ClO_4^- dans la nappe de la craie.

La cinquième partie est une étude de cas basée sur la contamination en ClO_4^- observé au sein du champ captant de Couraux (l'une des ressources en eau potable de la communauté urbaine du Grand-Reims), en appliquant la méthodologie développée sur la zone d'étude de la thèse. Les caractéristiques générales du champ captant de Couraux sont présentées dans un premier temps. Ensuite, les concentrations en ClO_4^- et les résultats d'analyse isotopique sont détaillés. Les sources de ClO_4^- et l'évolution des concentrations sont enfin discutées. Ce travail permet d'une part d'apporter des recommandations afin d'améliorer la gestion de la ressource en eau de ce site et d'autre part de démontrer l'applicabilité des travaux menées au cours de cette thèse.

La conclusion générale de la thèse synthétise les résultats obtenus sur le fonctionnement hydrogéologique de la nappe de la craie ainsi que sur les sources et le comportement des ions ClO_4^- dans l'aquifère de la craie de Champagne. Les limites de l'étude ainsi que les perspectives de recherche ouvertes par ces travaux viennent conclure cette partie.

3. Résumé de chaque partie de la thèse

3.1. Étude bibliographique

3.1.1. Perchlorate dans l'eau

La première partie de la thèse résume les connaissances scientifiques disponibles dans la littérature concernant les ions ClO_4^- dans l'eau et les caractéristiques générales de la nappe de la craie, afin de fournir une base solide pour les investigations ultérieures à ce travail.

L'ion ClO_4^- est un oxydant très stable et soluble dans l'eau. Cette forte solubilité et la faible adsorption des ions ClO_4^- par les sols rendent ce composé très mobile dans l'environnement, en particulier dans les eaux de surfaces et les eaux souterraines (Sturchio et al., 2014). Il est considéré comme un contaminant d'importance du fait de son effet néfaste sur la santé en tant que perturbateur endocrinien (e.g., Brabant et al., 1992 ; Braverman et al., 2005). L'origine du ClO_4^- dans l'environnement peut être synthétique ou naturelle. Naturellement, les ClO_4^- peuvent se former dans l'atmosphère et s'accumuler par dépôt sec et humide dans les sols arides et semi-arides tels que ceux du désert d'Atacama (Chili) et du sud-ouest des États-Unis (Jackson et al., 2015, 2016 ; Lybrand et al., 2016 ; Rao et al., 2007). Les dépôts de nitrates naturels du Chili ont été intensivement exploités jusqu'au milieu du 20^{ième} siècle pour amender les sols agricoles, ces caliches contenant des ClO_4^- en tant qu'impuretés. Les ClO_4^- synthétiques sont utilisés dans de nombreuses industries à forts enjeux économiques comme l'aérospatiale, l'armement et l'industrie pyrotechnique, ce qui conduit à la diffusion ce cette molécule dans l'environnement.

L'eau potable est probablement la plus grande source d'exposition humaine au ClO_4^- (Steinmaus, 2016). Au cours des deux dernières décennies, la présence de ClO_4^- dans l'eau a été signalée dans de nombreux pays avec des origines diverses. L'occurrence de ClO_4^- due aux dépôts atmosphériques a été reportée aux États-Unis, au Canada, en Chine et en Irlande avec des concentrations dans l'eau de pluie comprises entre < 5 ng·L^{-1} et 27.3 µg·L^{-1} (e.g., Dasgupta et al., 2006 ; Parker et al., 2008 ; Qin et al., 2014). L'occurrence de ClO_4^- dans les milieux aquatiques liée aux sels de perchlorates présents dans les déserts arides et semi-arides a été signalée principalement aux Etats Unis et au Chili, avec des concentrations détectées dans les eaux naturelles jusqu'à 10 mg·L^{-1} (e.g., Jackson et al., 2010 ; Plummer et al., 2006 ; Vega et al., 2018). Des contaminations des eaux par les ClO_4^- due aux activités anthropiques ont été également observées. Elles sont liées à l'utilisation des nitrates chiliens comme engrais agricole, à la fabrication et/ou l'utilisation de propulseurs de fusées et comburant d'explosifs (e.g., munitions, feu d'artifice), ou encore à la gestion des eaux usées domestiques et aux usines de fabrication de ClO_4^-.

L'analyse de la composition isotopique des chlorures ($\delta^{37}Cl$) et de l'oxygène ($\delta^{18}O$) dans les ions ClO_4^- peut permettre de discriminer les ions ClO_4^- issus de différentes sources. Les ClO_4^- naturels (e.g. provenant du désert Atacama ou du sud-ouest des États-Unis) et synthétiques possèdent en effet des signatures isotopiques distinctes l'un de l'autre. Un fractionnement isotopique lors du processus de biodégradation a également été mise en évidence, avec un rapport $\varepsilon^{18}O/\varepsilon^{37}Cl$ d'environ 2.5 (Sturchio et al., 2007 ; Hatzinger et al., 2009). Enfin, des développements méthodologiques prometteurs permettent d'envisager également l'utilisation de l'isotope radioactif du chlorure ^{36}Cl comme un traceur supplémentaire pour l'identification des sources de ClO_4^-.

Par suite de cette synthèse sur l'occurrence et l'origine des ClO_4^- dans l'eau à l'échelle mondiale, la situation en France est détaillée. Les concentrations en ClO_4^- mesurées dans l'eau à l'échelle nationale sont présentées, démontrant que la majorité des sites avec teneurs élevées en ClO_4^- (> 4 $\mu g \cdot L^{-1}$) sont situées dans le Nord de la France. Cette contamination a deux sources potentielles suspectées : une source militaire liée à la Première Guerre Mondiale et une source agricole liée à l'utilisation passée des nitrates chiliens comme engrais naturel.

3.1.2. Aquifère de la craie

L'aquifère de la craie est l'un des aquifères les plus importants en Europe du fait de l'exploitation intensive de cette ressource, notamment pour la consommation humaine. Les connaissances concernant le fonctionnement de la nappe de la craie de Champagne sont fondamentales à une gestion raisonnée de cette ressource mais également pour mieux comprendre les sources et le comportement des ClO_4^- dans les eaux souterraines. La craie est une roche carbonatée avec une double voire tripe porosité : de matrice, fissurée et karstique. La distribution des fractures dans la craie est très hétérogène : la densité des fractures diminue avec la profondeur et la distance aux axes de drainage. Dans la majorité des zones non saturées, la recharge se fait principalement à travers la matrice. Lorsqu'il existe un réseau de fracture développé, un écoulement préférentiel à travers des fissures peut être initié si le taux d'infiltration dépasse la conductivité hydraulique de la matrice (Price et al., 2000). Trois types de recharge peuvent être distinguées : recharge lente à travers la matrice (~ $m \cdot an^{-1}$), recharge intermédiaire à rapide à travers le réseau de fracturation (~ $m \cdot jr^{-1}$) et recharge très rapide en cas de karstification (~ $km \cdot jr^{-1}$) (Maurice, 2009). L'écoulement dans la zone saturée peut être décrit par la loi de Darcy. Dans les milieux à porosité multiple comme la craie, le transport des solutés dans la zone saturée peut être influencé par plusieurs processus, en particulier l'advection, la diffusion, l'adsorption et la dispersion.

Les eaux de la nappe de la craie sont typiquement bicarbonatées-calciques. La plupart des caractéristiques géochimique sont acquises lors de la percolation initiale à travers le sol et la zone non saturée (Edmunds et al., 1987). La géochimie des eaux souterraines peut également être influencée par plusieurs processus, notamment la signale d'entrée (précipitation), les interactions eau-roche, les processus de mélanges des eaux souterraines, les réactions rédox et les activités humaines.

3.2. Zone d'étude, matériels et méthodes

La zone d'étude sélectionnée est située à l'est de Reims dans le département de la Marne (Région Grand-Est). C'est une zone agricole concernée par les activités militaires liés à la Première Guerre Mondiale mais également par l'utilisation passée des nitrates chiliens en agriculture. La zone couvre environ 500 km^2 entre la Suippe (limites nord et ouest) et la Vesle (limite sud). Les Monts de Champagne et le Mont de Berru constituent les principaux reliefs de la zone d'étude.

La zone d'étude se situe sur la nappe libre de la craie qui constitue une ressource en eau cruciale pour la région. Les 10 à 20 premiers mètres de la craie de Champagne sont significativement fracturés et la fracturation diminue avec la profondeur (Mangeret et al., 2012 ; Vachier et al., 1987). La craie est partiellement recouverte de formations Tertiaires et Quaternaires (graveluche, colluvion et alluvion). La zone d'étude est divisée en deux parties par une ligne de partage des eaux souterraines qui traverse le sommet du Mont de Berru et les Monts de Champagne, en délimitant le bassin versant de la Vesle au sud et le bassin versant de la Suippe au nord. Selon les données piézométriques de la zone d'étude (Rouxel-David et al., 2002), la nappe de la craie est naturellement drainée par les rivières et les vallées sèches. Cependant, l'exploitation des eaux souterraines peut modifier localement la direction d'écoulement, en particulier pour les stations de pompage implantées le long des rivières, notamment en périodes de basses eaux. L'occupation du sol de la zone d'étude est majoritairement agricole et le climat de la région est de type tempéré océanique humide à tendance continentale.

Sur la zone d'étude sélectionnée, un réseau d'échantillonnage comprenant 36 points de prélèvements a été établi, avec 22 forages, 4 sources et 10 points d'eau de surface. Afin d'acquérir les connaissances nécessaires sur le fonctionnement de la nappe de la craie, les niveaux piézométriques, les paramètres physico-chimiques et les teneurs en éléments majeures et traces ont été suivis mensuellement pendant deux cycles hydrologiques (2017-2019) au sein du réseau d'échantillonnage établi. Les temps de résidence des eaux souterraines ont également été estimé à l'aide des gaz dissous CFCs, SF_6 et ^3H. Les concentrations en ClO_4^- ont aussi été suivis mensuellement pendant 2 ans, afin d'observer leurs évolutions temporelles et spatiales dans l'aquifère. Des explosifs organiques, qui pourrait éventuellement coexister avec les ClO_4^- ont également analysés. En parallèle, des analyses isotopiques des chlorures et de l'oxygène des ClO_4^- et de l'azote et l'oxygène des NO_3^- ont été réalisées, permettant de distinguer les origines de contamination.

3.3. Caractérisation du fonctionnement de la nappe de la craie de Champagne

3.3.1. Réponse de la nappe par rapport à la recharge

La pluie efficace est la part des précipitations qui donne lieu au ruissellement et à la recharge de la nappe. Un ruissellement nul est supposé sur l'aquifère de la craie de Champagne, la pluie efficace est donc équivalente à la recharge de la nappe. Dans cette étude, la pluie efficace de 2016 à 2019 est estimée par la méthode du bilan hydrique.

Selon la pluie efficace estimée, deux périodes peuvent être distinguées au cours d'une année hydrologique : 1) la période de recharge de la nappe de novembre à mars ; 2) une période de vidange d'avril à octobre, lorsque les pluies efficaces sont faibles à nulles. Ces modalités de recharge sont cohérentes avec les fluctuations des niveaux piézométriques observées sur la zone d'étude : le niveau d'eau le plus élevé est atteint en mars/avril et celui le plus bas est atteint en octobre/novembre. Des variations interannuelles de la pluie efficace sont également observées et cohérentes avec les variations interannuelles des niveaux piézométriques : le niveau d'eau en mars/avril 2018 était beaucoup plus élevé que celui de la même période en 2017 et 2019, comme la pluie efficace plus élevée en hiver/printemps 2017-2018.

La nappe libre de la craie possède des caractéristiques hydrologiques très hétérogènes. La fluctuation des niveaux d'eau observée est plus élevée aux niveaux des reliefs que dans les vallées, indiquant des différences de transmissivité et de coefficient d'emmagasinement. Bien que la majorité de la nappe possède un comportement inertiel par rapport à la recharge, des réponses rapides suites aux évènements pluvieux peuvent être observées, mettant en évidence la présence localement des réseaux de fracture très développé dans la nappe de la craie.

3.3.2. Temps de résidence et géochimie des eaux souterraines

La datation des eaux souterraines par le ^{3}H, les CFCs et les SF_6 a été réalisée pour la première fois dans la l'aquifère de la craie de Champagne. De faibles concentrations de ^{3}H (< 5 UT) ont été observées et comparés avec les concentrations historiques de ^{3}H dans les eaux de pluie, indiquant des temps de résidence relativement faibles (Clark et Fritz, 1997). Les concentrations en CFCs et SF_6 mesurées dans les eaux souterraines ont été converties en concentrations atmosphériques puis comparées avec les concentrations atmosphériques historiques locales en utilisant différents modèles de mélange simplifiés (modèle piston, modèle exponentiel et modèle mélange binaire).

Malgré des contaminations fréquentes en CFCs et SF_6 détectées dans la zone d'étude, des informations importantes sur le temps de séjour et les processus de mélanges des eaux souterraines ont été obtenues. L'aquifère de la craie de Champagne est composé d'eaux d'âges différents de moderne jusqu'à environ 50 ans, avec des modèles de mélange définis pour chaque point de prélèvement impliquant différentes modalités d'écoulement et processus de mélanges dans la nappe.

La composition chimique des eaux souterraines est typique d'une nappe crayeuse avec les ions Ca^{2+} et HCO_3^- dominants, tous deux issus de la dissolution de la craie. Les origines des ions majeurs sont étudiées : les ions Cl^-, NO_3^-, SO_4^{2-} et une partie du Ca^{2+} sont interprétés comme des ions d'origine agricole, tandis que les ions Mg^{2+}, K^+ et une partie des SO_4^{2-} sont interprétés comme ayant une source terrigène liée aux impuretés de la craie et aux minéraux constitutifs des formations superficielles (colluvions et alluvions).

Malgré le faciès chimique Ca^{2+} - HCO_3^-, des hétérogénéités spatiales et temporelles de la géochimie des eaux souterraines sont observés dans la nappe. La variation de la conductivité électrique est principalement attribuée à la variation des concentrations en Cl^- et NO_3^-, car ces paramètres possèdent des tendances spatiales et temporelles similaires. Différentes relations de corrélations entre les chroniques de conductivité électrique et les fluctuations des niveaux piézométriques sont observées : corrélées, anti-corrélées et indépendantes. Les hétérogénéités de la géochimie des eaux souterraines sont expliqués par une combinaison de facteurs hydrogéologiques, de temps de résidence et d'utilisation du sol, mettant en évidence les principaux facteurs régissant la géochimie des eaux souterraines de la nappe de la craie, à savoir la fluctuation du niveau piézométrique, l'épaisseur de la zone non saturée, la présence et le type des formations superficielles, la distribution des réseaux de fracture, les relations nappe-rivière et les activités humaines.

3.3.3. Modèle conceptuel du fonctionnement de la nappe

Un modèle conceptuel du fonctionnement hydrogéologique de la nappe libre de la craie est établi en combinant les résultats sur la recharge de l'aquifère, sur la datation des eaux souterraines et sur l'hydrogéochimie (Figure VII-1).

En général, dans les zones avec de grandes épaisseurs de la zone non saturée, la géochimie des eaux souterraines est moins influencée par les activités agricoles avec des concentrations en ions agricoles relativement faible. Lorsque la craie n'est pas couverte par les formations superficielles, un modèle exponentiel peut être appliqué avec un âge de l'eau relativement jeune. La contamination liée aux ions agricoles est donc positivement corrélée à l'hydrodynamique de l'aquifère due à la forte fluctuation des niveaux piézométriques.

Dans les zones avec une faible épaisseur de zone non saturée, la craie est généralement très fracturée. La recharge rapide à travers les fractures est privilégiée, les eaux souterraines sont donc issues d'un mélange d'eaux de pluies infiltrées récemment et d'eaux anciennes provenant de l'amont (modèle du mélange binaire). Dans ce cas-là, la géochimie des eaux souterraines est principalement influencée par l'effet de dilution de la pluie et le degré de minéralisation est négativement corrélé avec les niveaux piézométriques de la nappe.

Les formations superficielles sous-jacentes à la craie possèdent une perméabilité plus faible que celle de la craie. Elles peuvent donc constituer une barrière limitant la recharge rapide de l'eau et de soluté vers la nappe. Sur ces sites, un modèle de type piston décrit le mieux l'écoulement des eaux souterraines et des âges d'eau relativement anciens sont estimés, ce qui explique la stabilité de la géochimie des eaux dans ce contexte, indépendante de la fluctuation des niveaux piézométriques.

Pour les sites d'exploitation des eaux souterraines à proximité des rivières, une réalimentation de la nappe par la rivière peut se produire, particulièrement en période de basses eaux. La géochimie des eaux souterraines peut alors être influencée par les eaux de surface.

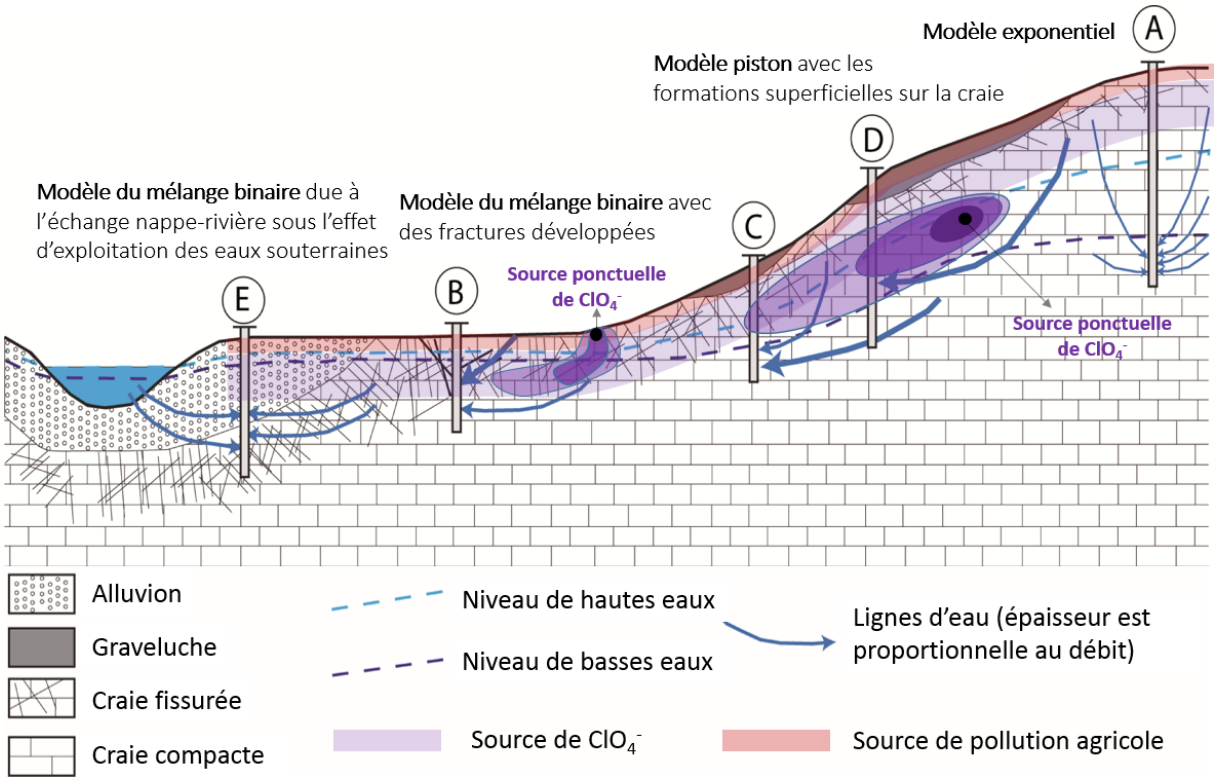

Figure VII-1 : Modèle conceptuel du fonctionnement hydrogéologique de la nappe libre de la craie et sources et modalités de transfert des ions ClO_4^- et des ions d'origine agricole

3.4. Sources et devenir des perchlorates dans l'aquifère de la craie de Champagne

Dans la nappe libre de la craie de Champagne, deux sources potentielles de ClO_4^- sont suspectées : une source militaire liée à la Première Guerre Mondiale et une source agricole liée à l'utilisation passée des nitrates chiliens comme engrais naturel. Afin de mieux contraindre les sources et les mécanismes de transfert des ions ClO_4^- dans les eaux souterraines, le suivi en continu des concentrations de ClO_4^- est combiné à des analyses isotopiques des chlorures et de l'oxygène des ClO_4^- et de l'azote des NO_3^- et à des investigations historiques et hydrogéologiques.

3.4.1. Occurrence des perchlorates

Les ions ClO_4^- sont détectés dans la quasi-totalité des points de prélèvement sur la zone d'étude, avec des concentrations allant de < 0,5 à 62,5 $\mu g \cdot L^{-1}$. Les concentrations > 4 $\mu g \cdot L^{-1}$ sont détectées sur environ la moitié des points d'échantillonnage et la plupart se situent en aval hydrogéologique des Monts de Champagne, où de grandes quantités de munitions ont été utilisées, stockées et détruites pendant et après la Première Guerre Mondiale. Les niveaux élevés de ClO_4^- sur certains sites et les panaches de contamination observés indiquent que des sources ponctuelles de ClO_4^- pourraient être présentes. En revanche, aucun explosif organique n'est détecté dans les échantillons d'eau de surface et souterraine, ce qui pourrait s'expliquer par leur faible persistance et mobilité dans le sol et l'eau.

3.4.2. Une origine militaire indiquée par l'analyse isotopique et l'âge des eaux souterraines

Les résultats des analyses isotopiques mettent en évidence la présence de ClO_4^- synthétique sur la plupart des sites d'échantillonnage, à l'exception d'un faible mélange avec des ClO_4^- d'Atacama sur un site. Il est peu probable que cette faible proportion de ClO_4^- d'Atacama soit liée à l'utilisation agricole des nitrates chiliens (terminée dans les années 1950s), puisque le temps de résidence des eaux estimée dans la zone d'étude est inférieur à 50 ans et que le temps de transit dans la zone non saturée est relativement faible (< 30 ans). La présence des ClO_4^- d'Atacama pourrait donc s'expliquer par l'utilisation des explosifs azotés de la Première Guerre Mondiale (poudre noire et explosifs du groupe nitroaromatiques) fabriqués avec des nitrates chiliens et toujours présents après le conflit. Par conséquent, les sources de contamination en ClO_4^- sur la zone d'étude sont probablement liées exclusivement aux activités militaires post-Première Guerre Mondiale plutôt que contemporaines du conflit. Comme seulement une faible contribution de ClO_4^- d'Atacama est observée, la contamination en ClO_4^- est principalement attribuée aux explosifs à base de ClO_4^- synthétiques plutôt qu'aux explosifs fabriqués avec des nitrates chiliens.

3.4.3. Sources et comportement des ClO_4^- dans l'aquifère de la craie de Champagne

Des variations annuelles des concentrations en ClO_4^- sont observées, indiquant l'influence des conditions climatiques et des niveaux d'eau souterraine sur la contamination. L'aquifère de la craie de Champagne semble être plus vulnérable à la contamination en ClO_4^- pendant les saisons d'hiver/printemps et durant les années humides. Deux types de tendances temporelles des concentrations en ClO_4^- sont observées : 1) sur les sites avec des teneurs élevées en ClO_4^- (> 10 µg·L^{-1}), les concentrations en ClO_4^- sont faiblement corrélées aux niveaux piézométriques avec des pics de contamination suivant les évènements de recharge, indiquant la présence des sources ponctuelles liées principalement aux activités de la Première Guerre Mondiale et aux sites de destruction des munitions ; 2) sur les sites avec des teneurs faibles en ClO_4^- (< 10 µg·L^{-1}), les concentrations de ClO_4^- sont fortement corrélées aux niveaux piézométriques et des sources diffuses sont supposées.

L'évolution temporelle des concentrations en ClO_4^- est également comparée aux chroniques de concentrations en Cl^- et NO_3^-, les deux principaux ions agricoles dans les eaux souterraines de la nappe de la craie de Champagne. Sur la plupart des sites, l'évolution temporelle des concentrations en ClO_4^- est différente de celle des Cl^- et NO_3^-, indiquant des origines différentes. Ces différentes tendances temporelles sont interprétées au regard des investigations historiques et du modèle conceptuel du fonctionnement de la nappe, synthétisé dans la Figure VII-1.

Dans les zones où la craie est recouverte par des formations superficielles, alors que les concentrations en Cl^- et NO_3^- sont stables au cours du temps du fait de l'effet de barrière engendré par les formations superficielles qui limitent le transfert rapide des ions agricoles depuis la surface vers la nappe, de fortes variations temporelles des concentrations en ClO_4^- sont observées. Cela indique que la position des sources de ClO_4^- est plus profonde que celle des ions agricoles qui sont situées principalement dans le sol proche de la surface (Figure VII-1). Avec l'augmentation du niveau d'eau souterraine, le front de la contamination en ClO_4^- est rapidement atteint, générant des variations dans les concentrations en ClO_4^-, malgré le fait que l'infiltration vers la nappe soit limitée par les formations superficielles. Dans les zones avec une zone non saturée épaisse, les évolutions temporelles des concentrations en ClO_4^-, NO_3^- et Cl^- sont positivement corrélées, car les sources de ces ions sont toutes situées principalement dans la zone non saturée et sont transférées vers la zone saturée pendant la phase de la recharge. Par conséquent, des variations temporelles similaires sont observées (Figure VII-1).

Les sources potentielles de ClO_4^- situées plus profondes que les ions agricoles sont probablement liés à : 1) des munitions non explosées persistant dans le sous-sol (jusqu'à plus de 10 m de profondeur) après la Première Guerre Mondiale ; 2) des munitions non utilisées présentes dans les anciens tunnels militaires de la Première Guerre Mondiale ; 3) des munitions non utilisées potentiellement enterrées dans des ouvrages spécifiques après la guerre. Au cours du temps, les enveloppes de ces munitions se corrodent lentement (jusqu'à 450 ans ; Parker et al., 2004), ce qui entraine une libération progressive des ClO_4^- dans les sols et les eaux. Des sources potentielles de ClO_4^- peuvent également être situées proche de la surface (Figure VII-1), ce qui correspond principalement à des sites de destruction des munitions. Sur ces sites, les détonations répétées ont provoqué des accumulations de ClO_4^- qui pourraient persister pendant plus de 100 ans dans les sous-sols. De plus, le stockage des munitions non utilisées pourrait encore exister sur ces sites, représentant ainsi des sources continues de contamination en ClO_4^-.

Compte tenu de la forte persistance des résidus d'explosifs liés aux munitions non explosées et aux activités de destruction des munitions, la contamination en ClO_4^- dans les eaux souterraines de la zone d'étude ne semble pas tendre vers une diminution à court ou moyen termes.

3.5. Étude de cas : contamination en perchlorate au champ captant de Couraux

Le Champ captant de Couraux est un site d'exploitation d'eaux souterraines qui alimente la métropole de Reims. Les campagnes de mesures menées par Grand Reims depuis 2012 ont montré des concentrations élevées de ClO_4^- dans les eaux souterraines de ce site. La méthodologie développée et les concepts sur les sources et le transfert du ClO_4^- développés au cours de cette étude sont applicables sur d'autres zones contaminées en ClO_4^-. C'est pourquoi une étude de cas sur la contamination en ClO_4^- au champ captant de Couraux est réalisée.

Les caractéristiques générales du champ captant de Couraux étudiées dans de précédents travaux montrent que les eaux souterraines pompées depuis les différents forages possèdent une grande hétérogénéité en termes de qualité d'eau, notamment vis-à-vis des nitrates et des produits phytosanitaires, en raison de relations nappe-rivière complexes, d'une distribution hétérogène des fractures et de la présence d'un paléo chenal traversant le site induisant des écoulements préférentiels (Banton et al., 2007, 2008 ; Mondain et al., 2006).

Selon les résultats fournis par Grand Reims et les analyses réalisées dans le cadre du projet de la thèse, les ions ClO_4^- ont été détectés dans tous les 10 forages du champ captant de Couraux, avec des concentrations très hétérogènes de < 0,5 à 71,4 $\mu g \cdot L^{-1}$. Sur le Champ captant de Couraux, les puits P1, P2, P5 et P6 représentent chacun environ 20% de la production totale du champ captant. Dans deux de ces puits utilisés en permanence (P5 et P6), des concentrations élevées en ClO_4^- ont été observées (concentrations moyennes > 15 $\mu g \cdot L^{-1}$).

L'influence de la fluctuation des niveaux piézométriques sur les concentrations en ClO_4^- a été mise en évidence par les variations annuelles et saisonnières des concentrations observées dans les eaux souterraines. Les concentrations en ClO_4^- sont plus élevées en périodes de hautes eaux qu'en périodes de basses eaux. Par conséquent, le bassin versant est plus vulnérable à la contamination en ClO_4^- pendant les saisons d'hiver / printemps et les années avec des précipitations intenses.

La signature isotopique des ClO_4^- mesurée la présence de ClO_4^- exclusivement synthétiques, indiquant une source militaire des ClO_4^- présents dans les eaux souterraines de champ captant du Couraux. Les ClO_4^- retrouvés ici peuvent être originaires non seulement des aquifères crayeux des rives gauche et droite de la Vesle mais aussi de l'amont du site à travers le chenal d'écoulement préférentiel.

Selon les résultats présentés, des recommandations pour une meilleure gestion des ressources en eau du champ captant de Couraux sont proposées. Afin d'assurer la qualité des eaux vis à vis du paramètre ClO_4^-, une plus grande attention devrait être accordée à l'utilisation des puits P5 et P6. Les concentrations en ClO_4^- devraient être surveillées plus fréquemment pendant les périodes de hautes eaux et la production des puits pourrait être ajustée en fonction des niveaux d'‘eaux souterraine et/ou les évènements de recharge. Enfin, le suivi des concentrations en ClO_4^- devrait être poursuivi pour obtenir des chroniques plus longues, afin de mieux comprendre l'évolution de la contamination en ClO_4^- sur le site. La datation des eaux souterraines en utilisant les CFCs, SF6 et ^3H pourrait être une donnée complémentaire pertinente pour préciser les relations nappe-rivière, les modalités d'écoulement des eaux souterraines (en particulier le rôle du chenal préférentiel) et l'évolution de la contamination en ClO_4^- sur ce site.

4. Conclusion et perspectives

4.1. Conclusion générale

Les objectifs de cette étude sont : 1) de préciser le fonctionnement hydrogéologique de la nappe libre de la craie ; 2) de mieux contraindre les sources et les mécanismes de transfert des ions ClO_4^- dans l'aquifère de la craie de Champagne. Les connaissances du fonctionnement de la nappe sont fondamentales pour comprendre les sources et le comportement des ions ClO_4^-.

La zone d'étude sélectionnée avec multi-sources potentielles de ClO_4^- (militaire et agricole) est située à l'est de Reims dans le département de la Marne (région Grand-Est), où la qualité de l'eau captée pour l'alimentation en eau potable est fortement impactée par la contamination en ClO_4^-. La zone d'étude se situe sur la nappe libre de la craie qui constitue une ressource en eau cruciale pour la région. Sur la zone d'étude sélectionnée, un réseau d'échantillonnage comprenant 36 points de prélèvement a été établi, avec 22 forages, 4 sources et 10 points d'eau de surface. Au sein du réseau d'échantillonnage établi, les niveaux piézométriques, les paramètres physico-chimiques et les teneurs en éléments majeures et traces ont été suivis mensuellement pendant deux cycles hydrologiques (2017-2019). Les temps de résidence des eaux souterraines ont également été estimé à l'aide des gaz dissous CFCs, SF_6 et ^3H. Les concentrations en ClO_4^- ont aussi été suivis mensuellement pendant 2 ans, afin d'observer leurs évolutions temporelles et spatiales dans l'aquifère. En parallèle, des analyses isotopiques des chlorures et de l'oxygène des ClO_4^- et de l'azote des NO_3^- ont été réalisées, permettant de distinguer les origines de contamination.

Des variations saisonnières et annuelles des niveaux piézométriques ont été observées en lien avec les variations saisonnières et annuelles de la précipitation efficace (recharge de la nappe). Globalement, la nappe de la craie possède un comportement inertiel par rapport à la recharge. Néanmoins, des réponses rapides de la nappe ont été observées sur un site, suggérant la présence d'un réseau de fractures très développé à l'échelle locale.

La datation des eaux souterraines par la méthode des CFCs, SF_6 et du ^3H indique que la nappe de la craie est composée d'eaux souterraines présentant des temps de séjour hétérogènes, de moderne jusqu'à environ 50 ans, avec des modèles de mélange différents (modèle piston, modèle exponentiel et modèle du mélange binaire), définis pour chaque site de prélèvement et impliquant des modalités d'écoulements variables au sein l'aquifère.

Malgré un faciès chimique bicarbonaté-calcique homogène, de fortes hétérogénéités spatiales et temporelles de la géochimie des eaux souterraines sont observées dans la nappe libre de la craie. Ces hétérogénéités sont interprétées par la combinaison de paramètres hydrogéologiques, de temps de résidence et d'informations sur l'occupation du sol, mettant en évidence les principaux facteurs régissant la géochimie des eaux souterraines de la craie, à savoir la fluctuation des niveaux piézométriques, l'épaisseur de la zone non saturée, la présence des formations superficielles, la distribution des réseaux de fractures, les relations nappe-rivière et les activités humaines. Un modèle conceptuel a été proposé pour clarifier le fonctionnement hydrogéologique des nappes libres en milieu crayeux, ce qui fournira des informations très utiles pour la recherche de l'origine et la compréhension du comportement des perchlorates dans cet aquifère. Ce modèle conceptuel sera également un outil précieux à destination des gestionnaires de la ressource.

Les ions ClO_4^- ont été détectés dans la quasi-totalité des points de prélèvement sur la zone d'étude (33 sur 36) avec une valeur maximale de 62,5 $\mu g \cdot L^{-1}$. Des concentrations supérieures à 4 $\mu g \cdot L^{-1}$ (valeurs de recommandation) ont été détectée principalement en aval hydrogéologique des Monts de Champagne, où de grandes quantités de munitions ont été utilisées, stockées et détruites pendant et après la Première Guerre Mondiale.

Une origine synthétique des ClO_4^- a été mise en évidence par les analyses isotopiques des chlorures et de l'oxygène des ions ClO_4^-, confirmant pour la première fois dans le secteur une source militaire de la contamination. Les temps de résidence des eaux souterraines estimés de moins de 50 ans indiquent que la contamination en ClO_4^- est liée à des sources qui persistent dans le sous-sol après la Première Guerre Mondiale (e.g., munitions non explosées) plutôt qu'aux activités militaires pendant le conflit. Des variations annuelles des concentrations en ClO_4^- sont observées, indiquant l'influence des conditions climatiques et des niveaux d'eau souterraine sur la contamination en ClO_4^-. L'aquifère de la craie de Champagne semble être plus vulnérable à la contamination en ClO_4^- pendant les saisons d'hiver/printemps et pendant les années humides. Sur les sites avec des teneurs élevées en ClO_4^- (> 10 $\mu g \cdot L^{-1}$), les concentrations sont principalement contrôlées par la distance aux sources ponctuelles en ClO_4^- et par les évènements de recharge avec une faible corrélation entre les niveaux d'eau et les concentrations de ClO_4^-. En revanche, sur les sites avec des teneurs faibles en ClO_4^- (< 10 $\mu g \cdot L^{-1}$), les concentrations sont contrôlées par la fluctuation des niveaux piézométriques avec une forte corrélation entre les niveaux d'eau et les concentrations en ClO_4^-, des sources diffuses sont alors supposées. Compte tenu de la forte persistance des résidus d'explosifs liés aux munitions non explosées et aux activités de destruction des munitions, les concentrations en ClO_4^- dans les eaux souterraines ne semblent pas montrer de tendance à la diminution à court ou moyen terme.

4.2. Limites et perspectives

La combinaison des différents outils a permis le développent d'un modèle conceptuel du fonctionnement de la nappe de la craie. La méthodologie multidisciplinaire développée dans cette étude et le modèle conceptuel établi pourraient être utilisés dans les aquifères crayeux européens ou dans d'autres milieux avec une multi-porosité, pour la prédiction des variations spatiales et temporelles de la minéralisation des eaux souterraines et du transfert des solutés (naturels ou anthropiques) et pour l'évaluation de la vulnérabilité des aquifères par rapport à la pollution. Cependant, ces méthodes ont encore certaines limites. Ces travaux peuvent être améliorés et développés via différentes approches dans le futur.

4.2.1. Suivi en continu de l'aquifère de la craie de Champagne

Le suivi en continue des niveaux piézométriques, des paramètres géochimiques et des concentrations en ClO_4^- pendant 2 ans est relativement court pour obtenir un modèle général et complet du fonctionnement de l'aquifère et du mécanisme de l'évolution de la contamination en ClO_4^- dans la nappe de la craie. Ce suivi en continu devrait être poursuivi pour obtenir des chroniques plus longes, afin d'étudier notamment l'influence de conditions climatiques différents sur le fonctionnement de la nappe de la craie et sur l'évolution des concentrations en ClO_4^-.

En effet, dans le contexte actuel de changement climatique, les événements extrêmes (e.g., sécheresse et inondations) ont tendance à se produire plus fréquemment (e.g., Haden et al., 2012 ; Ogunbode et al., 2019 ; Spence et al., 2011), pouvant conduire à des changements sur le fonctionnement de l'aquifère et sur la qualité des eaux souterraines. Le suivi en continue de l'aquifère pourrait étendre la base de données des paramètres hydrogéologiques, ce qui est essentiel pour une bonne compréhension du fonctionnement de l'aquifère et du transfert de polluants.

4.2.2. Datation des eaux souterraines

La datation des eaux souterraines par les CFCs et SF_6 a été perturbée par une contamination des gaz dissous dans la zone d'étude, surtout pour les CFC-12 et SF_6, entraînant un manque d'informations sur l'écoulement et le temps de résidence des eaux souterraines sur certains sites. Bien que la datation par le ^3H ait été réalisée en complément des CFCs et SF_6, seules des informations qualitatives sur l'âge des eaux ont été obtenues sur ces points. Malgré la cohérence des âges apparents estimés par le ^3H, les CFCs et le SF_6 sur la majorité des échantillons d'eau, des exceptions sont constatées sur deux sites avec de très faibles concentrations en ^3H. Afin de mieux comprendre ces résultats étonnants et de fournir plus d'informations sur l'écoulement des eaux souterraines pour les sites contaminés par des traceurs CFCs / SF_6, les analyses du ratio ^3H / ^3He pourraient être une méthode complémentaire intéressante.

4.2.3. Investigations géophysiques

L'outil géophysique semble être une perspective intéressante permettant de préciser les caractéristiques géométriques (extension et épaisseur) et la structure (présence de fissures et de failles) de l'aquifère. Des méthodes électromagnétiques et des techniques électriques (tomographie de résistivité électrique) ont été utilisée avec succès au champ captant du Couraux , ce qui a permis d'estimer la porosité de la roche, de clarifier l'extension et l'épaisseur de différentes formations géologiques ainsi que la position des axes potentiels de drainage des eaux souterraines (Banton et al., 2007, 2008). Les mêmes méthodes pourraient être appliquées localement sur la zone d'étude pour une meilleur compréhension de l'écoulement des eaux souterraines et du transfert des contaminants. D'autres techniques telles que les méthodes sismiques peu profondes et les techniques de télédétection semble également être prometteuse pour la caractérisation non destructive des propriétés hydrodynamiques de l'aquifère de la craie de Champagne (Mussett et Khan, 2000).

4.2.4. Investigations historiques

Le camp militaire de Moronvilliers situé sur les Monts de Champagne a été le lieu de batailles intenses pendant la Première Guerre Mondiale et a également été utilisé comme terrain de destruction de munitions à l'issue du conflit. Dans la zone d'étude, des concentrations élevées en ClO_4^- ont été détectées principalement en aval hydrogéologique de ce site. Ce secteur est devenu une zone militaire restreinte depuis 1957 avec la création d'un centre expérimental nucléaire rattaché au Commissariat à l'Energie Atomique et aux énergies alternatives (CEA). Par conséquent, les informations historiques concernant la localisation des sites de destruction de munitions et d'autres activités militaires réalisées sur ce camp militaire sont très limitées. Des enquêtes historiques doivent être poursuivies dans les archives militaires afin de localiser précisément un maximum de sources ponctuelles potentielles de ClO_4^-, sur le camp militaire mais également en dehors. Au-delà des travaux sur les archives historiques, l'outil LIDAR (Light detection and ranging) utilisé par exemple par Taborelli et al. (2017) a prouvé son intérêt dans la mise en évidence de polémoformes. Son utilisation sur le site d'étude pourrait permettre de détecter certaines zones sources éventuelles.

4.2.5. Analyse isotopique des perchlorates

Dans cette étude, l'analyse isotopique des ions ClO_4^- n'a été réalisée que sur les sites avec de fortes concentrations en ClO_4^-. Cette analyse devrait également être effectuée sur des sites avec de faibles concentrations afin de vérifier la présence des ClO_4^- d'Atacama sur ces sites moins contaminés liés à des sources diffuses.

Les résultats d'analyse sur la zone d'étude ont mis en évidence la présence de ClO_4^- synthétique avec une composition isotopique légèrement différente de celles des ClO_4^- synthétiques jusqu'alors publiées dans la littérature. D'autres mesures isotopiques devraient être réalisées pour les ClO_4^- dans différents types de munitions de la Première Guerre Mondiale, afin d'étendre la base de données des signatures isotopiques synthétiques et de faciliter la future utilisation de la méthode isotopique pour distinguer les origines des ClO_4^-.

Enfin, l'analyse isotopique du ClO_4^- devrait également être réalisée sur les sites avec exclusivement des sources agricoles (utilisation passée des nitrates chiliens comme engrais). Cette signature pure agricole pourrait apporter des informations complémentaires pour cette étude ainsi que pour les futures études sur la contamination en ClO_4^- dans d'autres régions de France.

4.2.6. Carte piézométrique

La carte piézométrique (hautes eaux) produite par le BRGM en 2002 (Rouxel-David et al., 2002b) est utilisée dans cette étude, car le nombre de forages surveillés en continu sur la zone d'étude n'est pas suffisant pour réaliser une nouvelle carte piézométrique. Cependant, cette carte n'est pas suffisamment précise à l'échelle du bassin versant de la zone d'étude. Une carte piézométrique plus précise de la zone d'étude en hautes eaux et basses eaux devrait être réalisée, ce qui est nécessaire pour une meilleure compréhension de l'écoulement des eaux souterraines ainsi que des sources et du transfert des contaminants à l'échelle locale. Il est également essentiel pour une future modélisation numérique.

4.2.7. Modélisation numérique

Les méthodes utilisées dans cette étude se concentrent principalement sur une vision qualitative plutôt que quantitative, ce qui pourrait limiter les applications sur la prédiction du transfert des contaminants. Une modélisation numérique hydrodynamique et géochimique, basée sur le modèle conceptuel établi dans cette étude, pourrait être un outil utile pour mieux comprendre le transfert de ClO_4^- dans les eaux souterraines de la nappe de la craie.

References

~~~~~~~~~~~~~~~~~ A ~~~~~~~~~~~~~~~~~

Ader, M., Chaudhuri, S., Coates, J.D., Coleman, M., 2008. Microbial perchlorate reduction: A precise laboratory determination of the chlorine isotope fractionation and its possible biochemical basis. Earth and Planetary Science Letters 269, 605–613. https://doi.org/10.1016/j.epsl.2008.03.023

Ader, M., Coleman, M.L., Doyle, S.P., Stroud, M., Wakelin, D., 2001. Methods for the Stable Isotopic Analysis of Chlorine in Chlorate and Perchlorate Compounds. Anal. Chem. 73, 4946–4950. https://doi.org/10.1021/ac010489u

ADES Database, 2019. ADES: le portail national d'Accès aux Données sur les Eaux Souterraines pour la France métropolitaine et les départements d'outre-mer. https://ades.eaufrance.fr/. Accessed date: 22 July 2019

Ahlvin, R.G., Smoots, V.A., 1988. Construction Guide for Soils and Foundations. John Wiley & Sons. 310 p.

Allen, D.J., Brewerton, L.J., Coleby, L.M., Gibbs, B.R., Lewis, M.A., MacDonald, A.M., Wagstaff, S.J., Williams, A.T., 1997. The physical properties of major aquifers in England and Wales. British Geological Survey, Technical Report No. WD/97/34, 312 p.

Allouc, J., Le Roux, J., 1995. Carte géol. France (1/50 000) feuile Mourmelon-le-Grand (133). Orléans : BRGM. Notice explicative par Allouc, J., Le Roux, J., Monciardini, C., Ravaux, J.P, Morfaux, P., 1995, 65 p.

Allshorn, S.J.L., Bottrell, S.H., West, L.J., Odling, N.E., 2007. Rapid karstic bypass flow in the unsaturated zone of the Yorkshire chalk aquifer and implications for contaminant transport. Geological Society, London, Special Publications 279, 111–122. https://doi.org/10.1144/SP279.10

Andraski, B.J., Jackson, W., Welborn, T., Bohlke, J., Sevanthi Dilipan, R., Stonestrom, D.A., 2014. Soil, Plant, and Terrain Effects on Natural Perchlorate Distribution in a Desert Landscape. Journal of environmental quality 43, 980–94. https://doi.org/10.2134/jeq2013.11.0453

Andrews, J.N., Lee, D.J., 1979. Inert gases in groundwater from the Bunter Sandstone of England as indicators of age and palaeoclimatic trends. Journal of Hydrology 41, 233–252. https://doi.org/10.1016/0022-1694(79)90064-7

ANSES, 2018. Avis de l'ANSES relatif à la « Pertinence de la ré-évaluation de la valeur guide pour les ions perchlorate dans l'eau destinée à la consommation humaine ». Maison-Alfort, Anses - Agence nationale de sécurité sanitaire de l'alimentation, de l'environnement et du travail, 42 p.

ANSES, 2014. Avis de l'Anses relatif à la présence d'ions perchlorate dans le lait infantile et dans l'eau destinée à la consommation humaine en France. Maison-Alfort, Anses - Agence nationale de sécurité sanitaire de l'alimentation, de l'environnement et du travail, 55 p.

ANSES, 2013. Campagne nationale d'occurrence de polluants émergents dans les eaux destinées à la consommation humaine. Maison-Alfort, Anses - Agence nationale de sécurité sanitaire de l'alimentation, de l'environnement et du travail, 56 p.

ANSES, 2012. Avis de l'Anses relatif aux études épidémiologiques portant sur les associations entre une exposition aux ions perchlorate dans l'eau de boisson et la fonction thyroïdienne dans des populations spécifiques. Maison-Alfort, Anses - Agence nationale de sécurité sanitaire de l'alimentation, de l'environnement et du travail, 16 p.

ANSES, 2011. Avis de l'Anses relatif à l'évaluation des risques sanitaires liés à la présence d'ions perchlorate dans les eaux destinées à la consommation humaine. Anses - Agence nationale de sécurité sanitaire de l'alimentation, de l'environnement et du travail, saisine n°2011-SA-0024. Maison-Alfort, Anses, 22 p.

Anupama, V.N., Kannan, K., V. G. Prajeesh, P., Rugmini, S., Bhaskaran, K., 2012. Perchlorate, Chlorate and Bromate in water samples from the South-West coast of India. Water Science & Technology Water Supply 12. https://doi.org/10.2166/ws.2012.033

Appelo, C.A.J., Postma, D., 2004. Geochemistry, Groundwater and Pollution, Second Edition. CRC Press, 678 p.

Aquilina, L., Ayraud, V., Labasque, T., Le Corre, P., 2006. Dosage des composés chlorofluorocarbonés et du tétrachlorure de carbone dans les eaux souterraines. Application à la datation des eaux, 51 p.

Aquilina, L., Poszwa, A., Walter, C., Vergnaud, V., Pierson-Wickmann, A.-C., Ruiz, L., 2012. Long-Term Effects of High Nitrogen Loads on Cation and Carbon Riverine Export in Agricultural Catchments. Environ. Sci. Technol. 46, 9447–9455. https://doi.org/10.1021/es301715t

Aranda-Rodriguez, R., Lemieux, F., Jin, Z., Hnatiw, J., Tugulea, A.-M., 2017. (Yet more) challenges for water treatment plants: potential contribution of hypochlorite solutions to bromate, chlorate, chlorite and perchlorate in drinking water. Journal of Water Supply: Research and Technology - AQUA 66, 621–631. https://doi.org/10.2166/aqua.2017.147

ARIA Database. The ARIA Database: La référence du retour d'expérience sur accidents technologiques. http://www.aria.developpement-durable.gouv.fr/the-barpi/the-aria-database/?lang=en. Accessed date: 13 november 2018.

Asami, M., Kosaka, K., Yoshida, N., 2009. Occurrence of Chlorate and Perchlorate in Bottled Beverages in Japan. Journal of Health Science 55, 549–553. https://doi.org/10.1248/jhs.55.549

Atkinson, T.C., Smith, D.I., 1974. Rapid groundwater flow in fissures in the chalk: an example from south Hampshire. Quarterly Journal of Engineering Geology and Hydrogeology 7, 197–205. https://doi.org/10.1144/GSL.QJEG.1974.007.02.05

Attaway, H., Smith, M., 1993. Reduction of perchlorate by an anaerobic enrichment culture. Journal of Industrial Microbiology 12, 408–412. https://doi.org/10.1007/BF01569673

Ayraud, V., 2005. Détermination du temps de résidence des eaux souterraines : application au transfert d'azote dans les aquifères fracturés hétérogènes. PhD thesis, Université Rennes 1, 313 p.

Azeez, N.H., 2017. Hydrology of the Chalk Aquifer in East Yorkshire from Spring Recession Analysis. PhD thesis, University of Leeds, 379 p.

Aziz, C., Borch, R., Nicholson, P., Cox, E., 2006. Alternative Causes of Wide-Spread, Low Concentration Perchlorate Impacts to Groundwater, in: Perchlorate: Environmental Occurrence, Interactions and Treatment. Springer, Boston, MA, pp. 71–91. https://doi.org/10.1007/0-387-31113-0_4

~~~~~~~~~~~~~~~~ B ~~~~~~~~~~~~~~~~

Backus, S.M., Klawuun, P., Brown, S., D'sa, I., Sharp, S., Surette, C., Williams, D.J., 2005. Determination of perchlorate in selected surface waters in the Great Lakes Basin by HPLC/MS/MS. Chemosphere 61, 834–843. https://doi.org/10.1016/j.chemosphere.2005.04.054

Bakalowicz, M., 2018. De l'évolution historique du concept d'aquifère de la craie. Géologues 199, 4–6.

Banton, O., Comte, J.C., Mondain, P.H., Pillet, M.A., 2008. Etude du fonctionnemnt du bassin d'alimentation du Champ Captant de Couraux, Rapport de synthèse. Rapport Calligée-Hydriad N° 06-51113 D, 50 p.

Banton, O., Comte, J.C., Mondain, P.H., Pillet, M.A., 2007. Etude du fonctionnemnt du bassin d'alimentation du Champ Captant de Couraux, Phase 2. Rapport Calligée-Hydriad N° 06-51113 B, 192 p.

Bao, H., Gu, B., 2004. Natural perchlorate has a unique oxygen isotope signature. Environ. Sci. Technol. 38, 5073–5077.

Baran, N., Lepiller, M., Mouvet, C., 2008. Agricultural diffuse pollution in a chalk aquifer (Trois Fontaines, France): Influence of pesticide properties and hydrodynamic constraints. Journal of Hydrology 358, 56–69. https://doi.org/10.1016/j.jhydrol.2008.05.031

Bardiya, N., Bae, J.-H., 2011. Dissimilatory perchlorate reduction: A review. Microbiological Research 166, 237–254. https://doi.org/10.1016/j.micres.2010.11.005

Barhoum, S., 2014. Transferts dans la craie : approche régionale : le Nord-Ouest du Bassin de Paris : approche locale : la carrière de Saint-Martin-le-Nœud. PhD thesis, Université Pierre et Marie Curie - Paris VI, 334 p.

Barhoum, S., Valdès, D., Guérin, R., Marlin, C., Vitale, Q., Benmamar, J., Gombert, P., 2014. Spatial heterogeneity of high-resolution Chalk groundwater geochemistry – Underground quarry at Saint Martin-le-Noeud, France. Journal of Hydrology 519, 756–768. https://doi.org/10.1016/j.jhydrol.2014.08.001

Barker, J.A., Foster, S.S.D., 1981. A diffusion exchange model for solute movement in fissured porous rock. Quarterly Journal of Engineering Geology and Hydrogeology 14, 17–24. https://doi.org/10.1144/GSL.QJEG.1981.014.01.02

Barraclough, D., Gardner, C.M.K., Wellings, S.R., Cooper, J.D., 1994. A tracer investigation into the importance of fissure flow in the unsaturated zone of the British Upper Chalk. Journal of Hydrology 156, 459–469. https://doi.org/10.1016/0022-1694(94)90090-6

Barron, L., Nesterenko, P.N., Paull, B., 2006. Rapid on-line preconcentration and suppressed micro-bore ion chromatography of part per trillion levels of perchlorate in rainwater samples. Analytica Chimica Acta, Perchlorate: an Enigma for the New Millennium 567, 127–134. https://doi.org/10.1016/j.aca.2006.01.038

Batista, J.R., McGarvey, F.X., Vieira, A.R., 2000. The Removal of Perchlorate from Waters Using Ion-Exchange Resins, in: Urbansky, E.T. (Ed.), Perchlorate in the Environment, Environmental Science Research. Springer US, Boston, MA, pp. 135–145. https://doi.org/10.1007/978-1-4615-4303-9_13

Bausinger, T., Bonnaire, E., Preuß, J., 2007. Exposure assessment of a burning ground for chemical ammunition on the Great War battlefields of Verdun. Science of The Total Environment 382, 259–271. https://doi.org/10.1016/j.scitotenv.2007.04.029

Bender, K.S., Shang, C., Chakraborty, R., Belchik, S.M., Coates, J.D., Achenbach, L.A., 2005. Identification, Characterization, and Classification of Genes Encoding Perchlorate Reductase. J Bacteriol 187, 5090–5096. https://doi.org/10.1128/JB.187.15.5090-5096.2005

Bennett, P., 2015. Comments on "Isotopic tracing of perchlorate sources in groundwater from Pomona, California" by Neil C. Sturchio, Abelardo Beloso Jr., Linnea J. Heraty, Stephen Wheatcraft, Rina Schumer. Applied Geochemistry 52, 191–194. https://doi.org/10.1016/j.apgeochem.2014.11.022

Berger, G., Lemaresquier, H., Marquet, G., 1977. Alimentation en eau potable du district de Reims (Marne) - Etude hydrogéologique des Champs Captants de fléchalbault et de Couraux. Rapport BRGM, 77 SGN 006 BDP, 32 p.

Bloomfield, J., 1997. The role of diagenisis in the hydrogeological stratification of carbonate aquifers: an example from the chalk at Fair Cross, Berkshire, UK. Hydrology and Earth System Sciences 1, 19–33. https://doi.org/10.5194/hess-1-19-1997

Bloomfield, J., 1996. Characterisation of hydrogeologically significant fracture distributions in the Chalk: an example from the Upper Chalk of southern England. Journal of Hydrology 184, 355–379. https://doi.org/10.1016/0022-1694(95)02954-0

Bloomfield, J.P., Brewerton, L.J., Allen, D.J., 1995. Regional trends in matrix porosity and dry density of the Chalk of England. Quarterly Journal of Engineering Geology and Hydrogeology 28, S131–S142. https://doi.org/10.1144/GSL.QJEGH.1995.028.S2.04

Böhlke, J.K., Ericksen, G.E., Revesz, K., 1997. Stable isotope evidence for an atmospheric origin of desert nitrate deposits in northern Chile and southern California, U.S.A. Chemical Geology 136, 135152. https://doi.org/10.1016/S0009-2541(96)00124-6

Böhlke, J.K., Hatzinger, P.B., Sturchio, N.C., Gu, B., Abbene, I., Mroczkowski, S.J., 2009. Atacama perchlorate as an agricultural contaminant in groundwater: isotopic and chronologic evidence from Long Island, New York. Environ. Sci. Technol. 43, 5619–5625.

Böhlke, J.K., Mroczkowski, S.J., Sturchio, N.C., Heraty, L.J., Richman, K.W., Sullivan, D.B., Griffith, K.N., Gu, B., Hatzinger, P.B., 2017. Stable isotope analyses of oxygen (18O:17O:16O) and chlorine (37Cl:35Cl) in perchlorate: reference materials, calibrations, methods, and interferences. Rapid Communications in Mass Spectrometry 31, 85–110. https://doi.org/10.1002/rcm.7751

Böhlke, J.K., Sturchio, N.C., Gu, B., Horita, J., Brown, G.M., Jackson, W.A., Batista, J., Hatzinger, P.B., 2005. Perchlorate Isotope Forensics. Anal. Chem. 77, 7838–7842. https://doi.org/10.1021/ac051360d

Bolan, N.S., Adriano, D.C., Curtin, D., 2003. Soil acidification and liming interactions with nutrientand heavy metal transformationand bioavailability, in: Advances in Agronomy, Advances in Agronomy. Academic Press, pp. 215–272. https://doi.org/10.1016/S0065-2113(02)78006-1

Borczak, S., Motyka, J., Pulido-Bosch, A., 1990. The hydrogeological properties of the matrix of the chalk in the Lublin coal basin (southeast Poland). Hydrological Sciences Journal 35, 523–534. https://doi.org/10.1080/02626669009492456

Bourdon, B., Bureau, S., Andersen, M.B., Pili, E., Hubert, A., 2009. Weathering rates from top to bottom in a carbonate environment. Chemical Geology 258, 275–287. https://doi.org/10.1016/j.chemgeo.2008.10.026

Brabant, G., Bergmann, P., Kirsch, C.M., Köhrle, J., Hesch, R.D., von zur Mühlen, A., 1992. Early adaptation of thyrotropin and thyroglobulin secretion to experimentally decreased iodine supply in man. Metabolism 41, 1093–1096. https://doi.org/10.1016/0026-0495(92)90291-H

Braverman, L.E., He, X., Pino, S., Cross, M., Magnani, B., Lamm, S.H., Kruse, M.B., Engel, A., Crump, K.S., Gibbs, J.P., 2005. The effect of perchlorate, thiocyanate, and nitrate on thyroid function in workers exposed to perchlorate long-term. J. Clin. Endocrinol. Metab. 90, 700–706. https://doi.org/10.1210/jc.2004-1821

Brouyère, S., Dassargues, A., Hallet, V., 2004. Migration of contaminants through the unsaturated zone overlying the Hesbaye chalky aquifer in Belgium: a field investigation. Journal of Contaminant Hydrology 72, 135–164. https://doi.org/10.1016/j.jconhyd.2003.10.009

Brown, G.M., Gu, B., 2006. The Chemistry of Perchlorate in the Environment, in: Perchlorate: Environmental Occurence, Interactions and Treatment. Springer, Boston, MA, pp. 17–47. https://doi.org/10.1007/0-387-31113-0_2

Bu, X., Warner, M.J., 1995. Solubility of chlorofluorocarbon 113 in water and seawater. Deep Sea Research Part I: Oceanographic Research Papers 42, 1151–1161. https://doi.org/10.1016/0967-0637(95)00052-8

Bullister, J.L., Wisegarver, D.P., Menzia, F.A., 2002. The solubility of sulfur hexafluoride in water and seawater. Deep Sea Research Part I: Oceanographic Research Papers 49, 175–187. https://doi.org/10.1016/S0967-0637(01)00051-6

Burgess, W., Barker, J., Watson, S., Fretwell, B., 2005. Contaminant retardation by double-porosity diffusive exchange in the Chalk: Implications for monitoring. in Bringing Groundwater Quality Research to the Watershed scale. Proceedings of the 4th International Groundwater Quality Conference. IAH, Waterloo, Canada.

Burns, D.T., Dunford, M.D., Sutthivaiyakit, P., 1997. Spectrophotometric determination of perchlorate after extraction as protriptylinium perchlorate. Analytica Chimica Acta 356, 141–143. https://doi.org/10.1016/S0003-2670(97)00445-5

Busenberg, E., Plummer, L.N., 2000. Dating young groundwater with sulfur hexafluoride: Natural and anthropogenic sources of sulfur hexafluoride. Water Resources Research 36, 3011–3030. https://doi.org/10.1029/2000WR900151

Busenberg, E., Plummer, L.N., 1992. Use of chlorofluorocarbons (CCl3F and CCl2F2) as hydrologic tracers and age-dating tools: The alluvium and terrace system of central Oklahoma. Water Resources Research 28, 2257–2283. https://doi.org/10.1029/92WR01263

Busenberg, E., Weeks, E.P., Plummer, N., Bartholomay, R.C., 1993. Age dating ground water by use of chlorofluorocarbons (CCl3F and CCl2F2) and distribution of chlorofluorocarbons in the unsaturated zone, Snake River Plain Aquifer, Idaho National Engineering Laboratory, Idaho (No. 93–4054). U.S. Geological Survey. https://doi.org/10.3133/wri934054

~~~~~~~~~~~~~~~~ C ~~~~~~~~~~~~~~~~

Calba, F., 1980. Hydrogéologie du karst crayeux du Pays de Caux (France), PhD thesis. Université Pièrre et Marie Curie - Paris VI, 231 p.

Calderón, R., Palma, P., Parker, D., Molina, M., Godoy, F.A., Escudey, M., 2014. Perchlorate Levels in Soil and Waters from the Atacama Desert. Arch Environ Contam Toxicol 66, 155–161. https://doi.org/10.1007/s00244-013-9960-y

Cao, F., Jaunat, J., Ollivier, P., Cancès, B., Morvan, X., Hubé, D., Devos, A., Devau, N., Barbin, V., Pannet, P., 2018. Sources and behavior of perchlorate ions (ClO4-) in chalk aquifer of Champagne-Ardenne, France: preliminary results, in: Proceedings of the International Association of Hydrological Sciences. Presented at the Innovative water resources management – understanding and balancing interactions between humankind and nature - 8th International Water Resources Management Conference of ICWRS, Beijing, China, 13–15 June 2018, Copernicus GmbH, pp. 113–117. https://doi.org/10.5194/piahs-379-113-2018

Cao, F., Jaunat, J., Sturchio, N., Cancès, B., Morvan, X., Devos, A., Barbin, V., Ollivier, P., 2019. Worldwide occurrence and origin of perchlorate ion in waters: A review. Science of The Total Environment 661, 737–749. https://doi.org/10.1016/j.scitotenv.2019.01.107

Cao, F., Jaunat, J., Vergnaud-Ayraud, V., Devau, N., Labasque, T., Guillou, A., Guillaneuf, A., Hubert, J., Aquilina, L., Ollivier, P., 2020. Heterogeneous behavior of unconfined Chalk aquifers infer from combination of groundwater residence time, hydrochemistry and hydrodynamic tools. Journal of Hydrology 581, 124433. https://doi.org/10.1016/j.jhydrol.2019.124433

Cao, F., Sturchio, N.C., Ollivier, P., Devau, N., Heraty, L.J., Jaunat, J., 2020. Sources and behavior of perchlorate in a shallow Chalk aquifer under military (World War I) and agricultural influences. Journal of Hazardous Materials 123072. https://doi.org/10.1016/j.jhazmat.2020.123072

Carrega, P., 2013. Geographical Information and Climatology. John Wiley & Sons, 303 p.

Castany, G., 1982. Principes et méthodes de l'hydrogéologie. Bordas : Dunod, Paris, 238 p.

Castany, G., 1977. Distinct de Reims - Définition des périmètres de protection du champ captant de Couraux. Rapport BRGM, 77 GA 18BDP, 9 p.

Celle, H., 2000. Caractérisation des précipitations sur le pourtour de la Méditerranée occidentale : approche isotopique et chimique. PhD thesis, Université d'Avignon, 265 p.

CEPA (2005). Canadian Environmental Protection Act Annual Report for Periode April 2004 to March 2005. http://www.ec.gc.ca/lcpe-cepa/default.asp?lang=En&n=443CAC37-1. Accessed date: 5 January 2019

Chen, D.P., Yu, C., Chang, C.-Y., Wan, Y., Frechet, J.M.J., Goddard, W.A., Diallo, M.S., 2012. Branched polymeric media: perchlorate-selective resins from hyperbranched polyethyleneimine. Environ. Sci. Technol. 46, 10718–10726. https://doi.org/10.1021/es301418j

Chen, N., Valdes, D., Marlin, C., Blanchoud, H., Guerin, R., Rouelle, M., Ribstein, P., 2019. Water, nitrate and atrazine transfer through the unsaturated zone of the Chalk aquifer in northern France.

Science of The Total Environment 652, 927–938. https://doi.org/10.1016/j.scitotenv.2018.10.286

Chen, W., Cannon, F.S., Rangel-Mendez, J.R., 2005. Ammonia-tailoring of GAC to enhance perchlorate removal. II: Perchlorate adsorption. Carbon 43, 581–590. https://doi.org/10.1016/j.carbon.2004.10.025

Chiesi, F., 1993. Transfert et epuration dans la zone non saturee de la craie en champagne : etude de quelques cas concernant les nitrates et l'atrazine. PhD thesis, Reims, 197 p.

Choi, Y.C., Li, X., Raskin, L., Morgenroth, E., 2008. Chemisorption of oxygen onto activated carbon can enhance the stability of biological perchlorate reduction in fixed bed biofilm reactors. Water Res. 42, 3425–3434. https://doi.org/10.1016/j.watres.2008.05.004

Chung Jinwook, Nerenberg Robert, Rittmann Bruce E., 2007. Evaluation for Biological Reduction of Nitrate and Perchlorate in Brine Water Using the Hydrogen-Based Membrane Biofilm Reactor. Journal of Environmental Engineering 133, 157–164. https://doi.org/10.1061/(ASCE)0733-9372(2007)133:2(157)

Cicerone, R.J., Stolarski, R.S., Walters, S., 1974. Stratospheric Ozone Destruction by Man-Made Chlorofluoromethanes. Science 185, 1165–1167.

Clark, I.D., Fritz, P., 1997. Environmental Isotopes in Hydrogeology. Lewis Publishers, New York, USA. 342 p.

Clark, J.J.J., 2000. Toxicology of Perchlorate, in: Perchlorate in the Environment, Environmental Science Research. Springer, Boston, MA, pp. 15–29. https://doi.org/10.1007/978-1-4615-4303-9_3

Clausen, J., Robb, J., Curry, D., Korte, N., 2004. A case study of contaminants on military ranges: Camp Edwards, Massachusetts, USA. Environmental Pollution 129, 13–21. https://doi.org/10.1016/j.envpol.2003.10.002

Clausen, J.L., Korte, N., Dodson, M., Robb, J., Rieven, S., 2006. Conceptual Model for the Transport of Energetic Residues from Surface Soil to Groundwater by Range Activities. Cold regions research and engineering lab, Final report, ERDC/CRREL-TR-06-18, 169 p.

Coates, J.D., Achenbach, L.A., 2004. Microbial perchlorate reduction: rocket-fueled metabolism. Nat. Rev. Microbiol. 2, 569–580. https://doi.org/10.1038/nrmicro926

Coates, J.D., Michaelidou, U., Bruce, R.A., O'Connor, S.M., Crespi, J.N., Achenbach, L.A., 1999. Ubiquity and Diversity of Dissimilatory (Per)chlorate-Reducing Bacteria. Appl Environ Microbiol 65, 5234–5241.

Coleman, M.L., Ader, M., Chaudhuri, S., Coates, J.D., 2003. Microbial Isotopic Fractionation of Perchlorate Chlorine. Appl Environ Microbiol 69, 4997–5000. https://doi.org/10.1128/AEM.69.8.4997-5000.2003

Cook, P.G., Plummer, L.N., Busenberg, E., Solomon, D.K., Han, L.F., 2006. Chapter 4. Effects and processes that can modify apparent CFC age, in: Use of Chlorofluorocarbons in Hydrology: A Guidebook, pp 31 - 56.

Cook, P.G., Solomon, D.K., 1995. Transport of Atmospheric Trace Gases to the Water Table: Implications for Groundwater Dating with Chlorofluorocarbons and Krypton 85. Water Resources Research 31, 263–270. https://doi.org/10.1029/94WR02232

Crampon, N., Custodio, E., Downing, R.A., 1996. The hydrogeology of Western Europe: a basic framework. Quarterly Journal of Engineering Geology and Hydrogeology 29, 163–180. https://doi.org/10.1144/GSL.QJEGH.1996.029.P2.05

Crampon, N., Roux, J.C., Bracq, P., 1993. Hydrogeology of the chalk in France, in The Hydrogeology of the Chalk of North-West Europe, edited by R. A. Downing, M. Price, and G. P. Jones, Oxford Univ. Press, New York, pp. 81–123.

Cristal Union, 2018. Sucrerie de Sillery – Surveillance de la qualité des eaux souterraines sous les périmètres d'épandage des eaux résiduaires. Report A95171/A, 153 p.

Crump, C., Michaud, P., Téllez, R., Reyes, C., Gonzalez, G., Montgomery, E.L., Crump, K.S., Lobo, G., Becerra, C., Gibbs, J.P., 2000. Does Perchlorate in Drinking Water Affect Thyroid Function in Newborns or School-Age Children? Journal of Occupational and Environmental Medicine 42, 603.

~~~~~~~~~~~~~~~~ D ~~~~~~~~~~~~~~~~

Darling, W.G., Gooddy, D.C., MacDonald, A.M., Morris, B.L., 2012. The practicalities of using CFCs and SF6 for groundwater dating and tracing. Applied Geochemistry, 13th International Symposium on Water-Rock Interaction (WRI -13) 27, 1688–1697. https://doi.org/10.1016/j.apgeochem.2012.02.005

Darling, W.G., Morris, B., Stuart, M.E., Gooddy, D.C., 2005. Groundwater Age Indicators from Public Supplies Tapping the Chalk Aquifer of Southern England. Water and Environment Journal 19, 30–40. https://doi.org/10.1111/j.1747-6593.2005.tb00546.x

Dasgupta, P.K., Dyke, J.V., Kirk, A.B., Jackson, W.A., 2006. Perchlorate in the United States. Analysis of relative source contributions to the food chain. Environ. Sci. Technol. 40, 6608–6614.

Dasgupta, P.K., Martinelango, P.K., Jackson, W.A., Anderson, T.A., Tian, K., Tock, R.W., Rajagopalan, S., 2005. The origin of naturally occurring perchlorate: the role of atmospheric processes. Environ. Sci. Technol. 39, 1569–1575.

Debant, J., 2019. La lente dépollution du CEA de Moronvilliers. L'hebdo du vendredi. http://www.lhebdoduvendredi.com/article/36274/la-lente-depollution-du-cea-de-moronvilliers. Accessed date : December 5, 2019.

Deconinck, J.F., Amédro, F., Baudin, F., Godet, A., Pellenard, P., Robaszynski, F., Zimmerlin, I., 2005. Late Cretaceous palaeoenvironments expressed by the clay mineralogy of Cenomanian–Campanian chalks from the east of the Paris Basin. Cretaceous Research 26, 171–179. https://doi.org/10.1016/j.cretres.2004.10.002

Desailloud, R., Wemeau, J.-L., 2016. Faut-il craindre les ions perchlorate dans l'environnement ? La Presse Médicale, Médecine et environnement 45, 107–116. https://doi.org/10.1016/j.lpm.2015.10.002

Devos, A., Lejeune, O., Chopin, E., 2007. Dynamiques d'infiltration karstique et spatialisation de la vidange aquifère en milieu crayeux : exemple du bassin de la vesle en amont de Reims

(Champagne Sèche/France). Eur. j. water qual. 38, 23–37. https://doi.org/10.1051/wqual/2007009

Devos, A., O, L., Butaeye, D., Barbin, V., 2006. Front de karstification et spatialisation des écoulements en pays calcaire : l'exemple du bassin de la Vesle (Marne/France), rapport d'activité Piren-Seine 2005, www.sisyphe.jussieu.fr/internet\piren, 17 p.

Dingman, S.L., 2002. Physical Hydrology. 575 p. Waveland Press, 2nd edition, ISBN: 978-1-57766-561-8

Downing, R.A., Price, M., Jones, G.P. (Eds.), 1993. The Hydrogeology of the Chalk of north-west Europe, Oxford science publications. Clarendon Press ; Oxford University Press, Oxford : New York. 300 p.

Dunkle, S.A., Plummer, L.N., Busenberg, E., Phillips, P.J., Denver, J.M., Hamilton, P.A., Michel, R.L., Coplen, T.B., 1993. Chlorofluorocarbons (CCl3F and CCl2F2) as dating tools and hydrologic tracers in shallow groundwater of the Delmarva Peninsula, Atlantic Coastal Plain, United States. Water Resources Research 29, 3837–3860. https://doi.org/10.1029/93WR02073

~~~~~~~~~~~~~~~~ E ~~~~~~~~~~~~~~~~

Edmonds, C.N., 1983. Towards the prediction of subsidence risk upon the Chalk outcrop. Quarterly Journal of Engineering Geology and Hydrogeology 16, 261–266. https://doi.org/10.1144/GSL.QJEG.1983.016.04.03

Edmunds, W.M., Cook, J.M., Darling, W.G., Kinniburgh, D.G., Miles, D.L., Bath, A.H., Morgan-Jones, M., Andrews, J.N., 1987. Baseline geochemical conditions in the Chalk aquifer, Berkshire, U.K.: a basis for groundwater quality management. Applied Geochemistry 2, 251–274. https://doi.org/10.1016/0883-2927(87)90042-4

El Janyani, S., Dupont, J.-P., Massei, N., Slimani, S., Dörfliger, N., 2014. Hydrological role of karst in the Chalk aquifer of Upper Normandy, France. Hydrogeol J 22, 663–677. https://doi.org/10.1007/s10040-013-1083-z

EFSA Panel on Contaminants in the Food Chain (EFSA CONTAM Panel), 2014. Scientific opinion on the risks to public health related to the presence of perchlorate in food, in particular fruits and vegetables. EFSA J. 12, 3869. https://doi.org/10.2903/j. efsa.2014.3869

Ericksen, G.E., 1983. The Chilean nitrate deposits. American Scientist 71, 366–374.

Ericksen, G.E., 1981. Geology and origin of the Chilean nitrate deposits. USGS Numbered Series No. 1188, Professional Paper. U.S. G.P.O., 42 p.

Etcheverry, D., 2002. Valorisation des méthodes isotopiques pour la question pratique liée aux eaux souterraines - Isotopes de l'oxygène et de l'hydrogène. Rapport de l'OFEG, Série Géologie, Berne, 71p.

~~~~~~~~~~~~~~~~~ F ~~~~~~~~~~~~~~~~~

Fabian, P., Borchers, R., Penkett, S.A., Prosser, N.J.D., 1981. Halocarbons in the stratosphere. Nature 294, 733–735. https://doi.org/10.1038/294733a0

Facon, P., 2018. Les batailles des monts de Champagne 1914-1918. Editions Tranchées, Paris : Louviers, 239 p.

Fagg, C.C., 1958. Swallow Holes in the Mole Gap. Field Studies Council. 13 p.

Fitzpatrick, C.M., 2011. The hydrogeology of bromate contamination in the Hertfordshire Chalk: double-porosity effects on catchment-scale evolution. PhD thesis, University College London, 371 p.

Flowers, T.C., Hunt, J.R., 2007. Viscous and gravitational contributions to mixing during vertical brine transport in water-saturated porous media. Water resources research 43, W01407.1.

Foster, S.S.D., 1975. The Chalk groundwater tritium anomaly — A possible explanation. Journal of Hydrology 25, 159–165. https://doi.org/10.1016/0022-1694(75)90045-1

Fram, M.S., Belitz, K., 2011. Probability of Detecting Perchlorate under Natural Conditions in Deep Groundwater in California and the Southwestern United States. Environ. Sci. Technol. 45, 1271–1277. https://doi.org/10.1021/es103103p

Furdui, V.I., Zheng, J., Furdui, A., 2018. Anthropogenic Perchlorate Increases since 1980 in the Canadian High Arctic. Environ. Sci. Technol. 52, 972–981. https://doi.org/10.1021/acs.est.7b03132

~~~~~~~~~~~~~~~~~ G ~~~~~~~~~~~~~~~~~

Gal, H., Weisbrod, N., Dahan, O., Ronen, Z., Nativ, R., 2009. Perchlorate accumulation and migration in the deep vadose zone in a semiarid region. Journal of Hydrology 378, 142–149. https://doi.org/10.1016/j.jhydrol.2009.09.018

Geller, L.S., Elkins, J.W., Lobert, J.M., Clarke, A.D., Hurst, D.F., Butler, J.H., Myers, R.C., 1997. Tropospheric SF6: Observed latitudinal distribution and trends, derived emissions and interhemispheric exchange time. Geophysical Research Letters 24, 675–678. https://doi.org/10.1029/97GL00523

Gély, J.-P., Hanot, F., 2014. Coupe géologique du Bassin parisien et du Fossé rhénan. Bull. Inf. Géol. Bass. Paris, Mémoire hors-série n° 9, 1 p.

Gillon, M., Crançon, P., Aupiais, J., 2010. Modelling the baseline geochemistry of groundwater in a Chalk aquifer considering solid solutions for carbonate phases. Applied Geochemistry 25, 1564–1574. https://doi.org/10.1016/j.apgeochem.2010.08.006

Greer, M.A., Goodman, G., Pleus, R.C., Greer, S.E., 2002. Health effects assessment for environmental perchlorate contamination: the dose response for inhibition of thyroidal radioiodine uptake in humans. Environ Health Perspect 110, 927–937.

Grisak, G.E., Pickens, J.F., 1981. An analytical solution for solute transport through fractured media with matrix diffusion. Journal of Hydrology 52, 47–57. https://doi.org/10.1016/0022-1694(81)90095-0

Grisak, G.E., Pickens, J.F., 1980. Solute transport through fractured media: 1. The effect of matrix diffusion. Water Resources Research 16, 719–730. https://doi.org/10.1029/WR016i004p00719

Gu, B., Böhlke, J.K., Sturchio, N.C., Hatzinger, P.B., Jackson, W.A., Beloso Jr., A.D., Heraty, L.J., Bian, Y., Jiang, X., Brown, G.M., 2011. Removal, Recovery and Fingerprinting of Perchlorate by Ion Exchange Processes in Ion Exchange And Solvent Extraction: a Series of Advances, twentieth ed. Taylor and Francis Group, New York, pp. 117–144.

Gu, B., Brown, G.M., 2006. Recent Advances in Ion Exchange for Perchlorate Treatment, Recovery and Destruction, in: Gu, B., Coates, J.D. (Eds.), Perchlorate: Environmental Occurrence, Interactions and Treatment. Springer US, Boston, MA, pp. 209–251. https://doi.org/10.1007/0-387-31113-0_10

Gu, B., Brown, G.M., Chiang, C.-C., 2007. Treatment of Perchlorate-Contaminated Groundwater Using Highly Selective, Regenerable Ion-Exchange Technologies. Environ. Sci. Technol. 41, 6277–6282. https://doi.org/10.1021/es0706910

Gu, B., Brown, G.M., Maya, L., Lance, M.J., Moyer, B.A., 2001. Regeneration of Perchlorate (ClO4-)-Loaded Anion Exchange Resins by a Novel Tetrachloroferrate (FeCl4-) Displacement Technique. Environ. Sci. Technol. 35, 3363–3368. https://doi.org/10.1021/es010604i

~~~~~~~~~~~~~~~~ H ~~~~~~~~~~~~~~~~

Haden, V.R., Niles, M.T., Lubell, M., Perlman, J., Jackson, L.E., 2012. Global and Local Concerns: What Attitudes and Beliefs Motivate Farmers to Mitigate and Adapt to Climate Change? PLOS ONE 7, e52882. https://doi.org/10.1371/journal.pone.0052882

Hakoun, V., Orban, P., Dassargues, A., Brouyère, S., 2017. Factors controlling spatial and temporal patterns of multiple pesticide compounds in groundwater (Hesbaye chalk aquifer, Belgium). Environmental Pollution 223, 185–199. https://doi.org/10.1016/j.envpol.2017.01.012

Hancock, J.M., 1975. The petrology of the Chalk. Proceedings of the Geologists' Association 86, 499–535. https://doi.org/10.1016/S0016-7878(75)80061-7

Haria, A.H., Hodnett, M.G., Johnson, A.C., 2003. Mechanisms of groundwater recharge and pesticide penetration to a chalk aquifer in southern England. Journal of Hydrology 275, 122–137. https://doi.org/10.1016/S0022-1694(03)00017-9

Harnisch, J., Eisenhauer, A., 1998. Natural CF4 and SF6 on Earth. Geophysical Research Letters 25, 2401–2404. https://doi.org/10.1029/98GL01779

Hatzinger, P.B., Böhlke, J.K., Sturchio, N.C., Izbicki, J., Teague, N., 2018. Four-dimensional isotopic approach to identify perchlorate sources in groundwater: Application to the Rialto-Colton and Chino subbasins, southern California (USA). Applied Geochemistry 97, 213–225. https://doi.org/10.1016/j.apgeochem.2018.08.020

Hatzinger, P.B., Böhlke, J.K., Sturchio, N.C., Gu, B., 2011. Validation of chlorine and oxygen isotope ratio analysis to differentiate perchlorate sources and to document perchlorate biodegradation. U.S. Department of Defense, ESTCP Project ER-200509, 107 p.

Hatzinger, P.B., Böhlke, J.K., Sturchio, N.C., Gu, B., Heraty, L.J., Borden, R.C., 2009. Fractionation of stable isotopes in perchlorate and nitrate during in situ biodegradation in a sandy aquifer. Environmental Chemistry 6, 9. https://doi.org/10.1071/EN09008

Hauser, P.C., Renner, N.D., Hong, A.P.C., 1994. Anion detection in capillary electrophoresis with ion-selective microelectrodes. Analytica Chimica Acta 295, 181–186. https://doi.org/10.1016/0003-2670(94)80349-8

Headworth, H.G., Keating, T., Packman, M.J., 1982. Evidence for a shallow highly-permeable zone in the Chalk of Hampshire, U.K. Journal of Hydrology 55, 93–112. https://doi.org/10.1016/0022-1694(82)90122-6

Heaton, T.H.E., Vogel, J.C., 1981. "Excess air" in groundwater. Journal of Hydrology 50, 201–216. https://doi.org/10.1016/0022-1694(81)90070-6

Her, N., Jeong, H., Kim, J., Yoon, Y., 2011. Occurrence of Perchlorate in Drinking Water and Seawater in South Korea. Arch Environ Contam Toxicol 61, 166–172. https://doi.org/10.1007/s00244-010-9616-0

Herzberg, O., Mazor, E., 1979. Hydrological applications of noble gases and temperature measurements in underground water systems: Examples from Israel. Journal of Hydrology 41, 217–231. https://doi.org/10.1016/0022-1694(79)90063-5

Hinsby, K., Højberg, A.L., Engesgaard, P., Jensen, K.H., Larsen, F., Plummer, L.N., Busenberg, E., 2007. Transport and degradation of chlorofluorocarbons (CFCs) in the pyritic Rabis Creek aquifer, Denmark. Water Resources Research 43. https://doi.org/10.1029/2006WR005854

Hiscock, K.M., 2009. Hydrogeology: Principles and Practice. John Wiley & Sons. 406 p.

Höhener, P., Werner, D., Balsiger, C., Pasteris, G., 2003. Worldwide Occurrence and Fate of Chlorofluorocarbons in Groundwater. Critical Reviews in Environmental Science and Technology 33, 1–29. https://doi.org/10.1080/10643380390814433

Horneman, A., Stute, M., Schlosser, P., Smethie, W., Santella, N., Ho, D.T., Mailloux, B., Gorman, E., Zheng, Y., van Geen, A., 2008. Degradation rates of CFC-11, CFC-12 and CFC-113 in anoxic shallow aquifers of Araihazar, Bangladesh. J. Contam. Hydrol. 97, 27–41. https://doi.org/10.1016/j.jconhyd.2007.12.001

Hristovski, K., Westerhoff, P., Möller, T., Sylvester, P., Condit, W., Mash, H., 2008. Simultaneous removal of perchlorate and arsenate by ion-exchange media modified with nanostructured iron (hydr)oxide. J Hazard Mater 152, 397–406. https://doi.org/10.1016/j.jhazmat.2007.07.016

Hubé, D., 2017. Industrial-scale destruction of old chemical ammunition near Verdun: a forgotten chapter of the Great War. https://doi.org/10.1080/19475020.2017.1393347

Hubé, D., 2016. Sur les traces d'un secret enfoui: Enquête sur l'héritage toxique de la Grande Guerre - Préface de Jean-Yves Le Naour. Editions Michalon, Paris. 288 p.

Hubé, D., 2014. Perchlorates : éléments historiques et d'expertise pour une évaluation de l'impact environnemental. https://centenaire.org/fr/print/5814. Accessed date: November 13, 2019.

Hubé, D., Bausinger, T., 2013. Marquage pyrotechnique : analyse de la problématique environnementale. Comparatif entre Allemagne et France. Géologues 179, 32–38.

Hubé, D., Urban, S., 2013. Préliminaire sur la présence des ions perchlorates dans les eaux souterraines en Alsace. Rapport BRGM/RP-62588-FR, 23 p.

Hubert, A., 2005. Déséquilibres des séries de l'uranium dans les aquifères : quantification des mécanismes de transport de l'uranium et de ses descendants : cas de l'aquifère de la craie (Champagne, France). Phd thesis, Institut de physique du globe (Paris), 251 p.

Hubert, A., Bourdon, B., Pili, E., Meynadier, L., 2006. Transport of radionuclides in an unconfined chalk aquifer inferred from U-series disequilibria. Geochimica et Cosmochimica Acta 70, 5437–5454. https://doi.org/10.1016/j.gca.2006.08.008

Hunter, W.J., 2001. Perchlorate is Not a Common Contaminant of Fertilizers. Journal of Agronomy and Crop Science 187, 203–206. https://doi.org/10.1046/j.1439-037x.2001.00519.x

~~~~~~~~~~~~~~~~~ I ~~~~~~~~~~~~~~~~~

IAEA, 2008. Isotopes de l'environnement dans le cycle hydrologique. International Atomic Energy Agency (IAEA), collection cours de formation. 590 p.

IAEA, 2006. Use of Chlorofluorocarbons in Hydrology. 277 p.

Iannece, P., Motta, O., Tedesco, R., Carotenuto, M., Proto, A., 2013. Determination of Perchlorate in Bottled Water from Italy. Water 5, 767–779. https://doi.org/10.3390/w5020767

INERIS, 2014. Données technico-économiques sur les substances chimiques en France : Perchlorate d'ammonium, DRC-13-126866-06964C, 71 p. https://rsde.ineris.fr/fiches_technico.php. Accessed date: November 13, 2018.

Ineson, J., 1962. A hydrogeological study of the permeability of the Chalk. Journal of the Institute of Water Engineers 449–463.

Ireson, A.M., Butler, A.P., 2011. Controls on preferential recharge to Chalk aquifers. Journal of Hydrology 398, 109–123. https://doi.org/10.1016/j.jhydrol.2010.12.015

Ireson, A.M., Wheater, H.S., Butler, A.P., Mathias, S.A., Finch, J., Cooper, J.D., 2006. Hydrological processes in the Chalk unsaturated zone – Insights from an intensive field monitoring programme. Journal of Hydrology, Hydro-ecological functioning of the Pang and Lambourn catchments, UK 330, 29–43. https://doi.org/10.1016/j.jhydrol.2006.04.021
~~~~~~~~~~~~~~~~~

Isobe, T., Ogawa, S.P., Sugimoto, R., Ramu, K., Sudaryanto, A., Malarvannan, G., Devanathan, G., Ramaswamy, B.R., Munuswamy, N., Ganesh, D.S., Sivakumar, J., Sethuraman, A., Parthasarathy, V., Subramanian, A., Field, J., Tanabe, S., 2013. Perchlorate contamination of groundwater from fireworks manufacturing area in South India. Environ Monit Assess 185, 5627–5637. https://doi.org/10.1007/s10661-012-2972-7

Izbicki, J.A., Teague, N.F., Hatzinger, P.B., Böhlke, J.K., Sturchio, N.C., 2014. Groundwater movement, recharge, and perchlorate occurrence in a faulted alluvial aquifer in California (USA). Hydrogeology Journal 23, 467–491.

~~~~~~~~~~~~~~~~ J ~~~~~~~~~~~~~~~~

Jackson, P.E., Gokhale, S., Streib, T., Rohrer, J.S., Pohl, C.A., 2000. Improved method for the determination of trace perchlorate in ground and drinking waters by ion chromatography. Journal of Chromatography A 888, 151–158. https://doi.org/10.1016/S0021-9673(00)00557-4

Jackson, W.A., Böhlke, J.K., Andraski, B.J., Fahlquist, L., Bexfield, L., Eckardt, F.D., Gates, J.B., Davila, A.F., McKay, C.P., Rao, B., Sevanthi, R., Rajagopalan, S., Estrada, N., Sturchio, N., Hatzinger, P.B., Anderson, T.A., Orris, G., Betancourt, J., Stonestrom, D., Latorre, C., Li, Y., Harvey, G.J., 2015. Global patterns and environmental controls of perchlorate and nitrate co-occurrence in arid and semi-arid environments. Geochimica et Cosmochimica Acta 164, 502–522. https://doi.org/10.1016/j.gca.2015.05.016

Jackson, W.A., Böhlke, J.K., Gu, B., Hatzinger, P.B., Sturchio, N.C., 2010. Isotopic composition and origin of indigenous natural perchlorate and co-occurring nitrate in the southwestern United States. Environ. Sci. Technol. 44, 4869–4876. https://doi.org/10.1021/es903802j

Jackson, W.A., Kumar Anandam, S., Anderson, T., Lehman, T., Rainwater, K., Rajagopalan, S., Ridley, M., Tock, R., 2005. Perchlorate occurrence in the Texas Southern High Plains Aquifer System. Ground Water Monitoring & Remediation 25, 137–149. https://doi.org/10.1111/j.1745-6592.2005.0009.x

Jaeglé, L., Yung, Y.L., Toon, G.C., Sen, B., Blavier, J.-F., 1996. Balloon observations of organic and inorganic chlorine in the stratosphere: The role of HClO4 production on sulfate aerosols. Geophysical Research Letters 23, 1749–1752. https://doi.org/10.1029/96GL01543

Jarvis, I., 1980. Geochemistry of phosphatic chalks and hardgrounds from the Santonian to early Campanian (Cretaceous) of northern France. Journal of the Geological Society 137, 705–721. https://doi.org/10.1144/gsjgs.137.6.0705

Jaunat, J., Taborelli, P., Devos, A., 2018. Les impacts de La Grande Guerre sur la qualité des eaux souterraines: les cas des perchlorates, in: « 14-18 La Terre et Le Feu Géologie et Géologues Sur Le Front Occidental », Bergerat, F. (Dir.), Co-Éd. AGBP – COFRHIGEO – SGN, Mém. Hors-Série N°10 de l'AGBP, 414- 417.

Johnson, A.C., Besien, T.J., Bhardwaj, C.L., Dixon, A., Gooddy, D.C., Haria, A.H., White, C., 2001. Penetration of herbicides to groundwater in an unconfined chalk aquifer following normal soil applications. Journal of Contaminant Hydrology 53, 101–117. https://doi.org/10.1016/S0169-7722(01)00139-5

Jurgens, B.C., Böhlke, J.K., Eberts, S.M., 2012. TracerLPM (Version 1): An Excel® workbook for interpreting groundwater age distributions from environmental tracer data: U.S. Geological Survey Techniques and Methods. Report 4-F3, 60 p.

~~~~~~~~~~~~~~~~~ K ~~~~~~~~~~~~~~~~~

Kannan, K., Praamsma, M.L., Oldi, J.F., Kunisue, T., Sinha, R.K., 2009. Occurrence of perchlorate in drinking water, groundwater, surface water and human saliva from India. Chemosphere 76, 22–26. https://doi.org/10.1016/j.chemosphere.2009.02.054

Katz, B.G., Lee, T.M., Plummer, L.N., Busenberg, E., 1995. Chemical Evolution of Groundwater Near a Sinkhole Lake, Northern Florida: 1. Flow Patterns, Age of Groundwater, and Influence of Lake Water Leakage. Water Resources Research 31, 1549–1564. https://doi.org/10.1029/95WR00221

Katz, B.G., McBride, W.S., Hunt, A.G., Crandall, C.A., Metz, P.A., Eberts, S.M., Berndt, M.P., 2009. Vulnerability of a Public Supply Well in a Karstic Aquifer to Contamination. Groundwater 47, 438–452. https://doi.org/10.1111/j.1745-6584.2008.00504.x

Kaufman, S., Libby, W.F., 1954. The Natural Distribution of Tritium. Phys. Rev. 93, 1337–1344. https://doi.org/10.1103/PhysRev.93.1337

Khalil, M. a. K., Rasmussen, R.A., 1989. The potential of soils as a sink of chlorofluorocarbons and other man-made chlorocarbons. Geophysical Research Letters 16, 679–682. https://doi.org/10.1029/GL016i007p00679

Kjeldsen, P., Christophersen, M., 2001. Composition of leachate from old landfills in Denmark. Waste Manag Res 19, 249–256. https://doi.org/10.1177/0734242X0101900306

Kjeldsen, P., Jensen, M.H., 2001. Release of CFC-11 from disposal of polyurethane foam waste. Environ. Sci. Technol. 35, 3055–3063.

Kloppmann, W., Dever, L., Edmouds, W.M., 1994. Isotopic and geochemical investigations of Chalk groundwater of the Champagne region, France. Z. Dt. Geol. Ges. 143–152.

Kloppmann, W., Dever, L., Edmunds, W.M., 1998. Residence time of Chalk groundwaters in the Paris Basin and the North German Basin: a geochemical approach. Applied Geochemistry 13, 593–606. https://doi.org/10.1016/S0883-2927(97)00110-8

Kosaka, K., Asami, M., Matsuoka, Y., Kamoshita, M., Kunikane, S., 2007. Occurrence of perchlorate in drinking water sources of metropolitan area in Japan. Water Res. 41, 3474–3482. https://doi.org/10.1016/j.watres.2007.05.011
~~~~~~~~~~~~~~~~~

~~~~~~~~~~~~~~~~ L ~~~~~~~~~~~~~~~~

Lacherez-Bastin, S., 2005. Contribution à l'étude de la migration des nitrates dans le sol et la zone non saturée de la nappe de la craie dans le Nord de la France : modélisation intégrée des nitrates dans le bassin versant de l'Escrebieux, PhD thesis, Université de Lille 1, 191 p.

Lallahem, S., 2002. Structure et modélisation hydrodynamique des eaux souterraines : application à l'aquifère crayeux de la bordure nord du Bassin de Paris. PhD thesis, Université de Lille 1, 219 p.

Lambert, E.D., 1858. Étude géologique sur le terrain tertiaire au nord du bassin de Paris, 8 p.

Lamm, S.H., Doemland, M., 1999. Has Perchlorate in Drinking Water Increased the Rate of Congenital Hypothyroidism? Journal of Occupational and Environmental Medicine 41, 409.

Lanini, S., Caballero, Y., Seguin, J.-J., Maréchal, J.-C., 2015. ESPERE—A Multiple-Method Microsoft Excel Application for Estimating Aquifer Recharge. Groundwater 54, 155–156. https://doi.org/10.1111/gwat.12390

Laurain, M., Guérin, H., Durand, R., Chertier, B., Louis, P., Morfaux, P., Neiss, R., 1981. Notive explicative, Carte géol. France (1/50 000) feuile Reims (132). Orléans : BRGM, 34 p. Carte géol. France par Laurain, M., Guérin, H., Barta, L., Monciardini, Ch., Durand, R., Neiss, R., 1981.

Laurent, A., 1988. La Grande Guerre en Champagne et la deuxième victoire de la Marne. Secrétariat d'État aux anciens combattants, Le Coteau, 157 p.

Lee, L.J.E., Lawrence, D.S.L., Price, M., 2006. Analysis of water-level response to rainfall and implications for recharge pathways in the Chalk aquifer, SE England. Journal of Hydrology 330, 604–620. https://doi.org/10.1016/j.jhydrol.2006.04.025

Lee, R.W., 1997. Effects of carbon dioxide variations in the unsaturated zone on water chemistry in a glacial-outwash aquifer. Applied Geochemistry 12, 347–366. https://doi.org/10.1016/S0883-2927(97)00001-2

Lehman, S.G., Badruzzaman, M., Adham, S., Roberts, D.J., Clifford, D.A., 2008. Perchlorate and nitrate treatment by ion exchange integrated with biological brine treatment. Water Res 42, 969–976. https://doi.org/10.1016/j.watres.2007.09.011

Lehmann, B.E., Davis, S.N., Fabryka-Martin, J.T., 1993. Atmospheric and subsurface sources of stable and radioactive nuclides used for groundwater dating. Water Resour. Res. 29, 2027–2040. https://doi.org/10.1029/93WR00543

Lewis, M.A., Jones, H.K., Macdonald, D.M.J., Price, M, Barker, J.A., Shearer, T.R., Wesselink, A.J., Evans, D.J., 1993. Groundwater storage in British aquifers: Chalk. R&D Note 169, National Rivers Authority, Bristol.

Li, F.X., Byrd, D.M., Deyhle, G.M., Sesser, D.E., Skeels, M.R., Katkowsky, S.R., Lamm, S.H., 2000. Neonatal thyroid-stimulating hormone level and perchlorate in drinking water. Teratology 62, 429–431. https://doi.org/10.1002/1096-9926(200012)62:6<429::AID-TERA10>3.0.CO;2-I

Linoir, D., 2014. Les horizons d'accumulations carbonatées (HAC) en Champagne-Ardenne ; répartition régionale, caractérisation et conséquences sur les transferts hydriques. PhD thesis, Université de Reims Champagne-Ardenne, 384 p.

List, R.J., 1949. Smithsonian meteorological tables, 6th edn. Smithsonian Institution Press, Washington DC. 114 p.

Liu, F., Jensen, C., Shahnazari, A., Andersen, M., Jacobsen, S.-E., 2005. ABA regulated stomatal control and photosynthetic water use efficiency of potato (Solanum tuberosum L.) during progressive soil drying. Plant Science 168, 831–836. https://doi.org/10.1016/j.plantsci.2004.10.016

Liu, G., Zong, G., Dhana, K., Hu, Y., Blount, B.C., Morel-Espinosa, M., Sun, Q., 2017. Exposure to perchlorate, nitrate and thiocyanate, and prevalence of diabetes mellitus. Int J Epidemiol 46, 1913–1923. https://doi.org/10.1093/ije/dyx188

Longstaff, S.L., Aldous, P.J., Clark, L., Flavin, R.J., Partington, J., 1992. Contamination of the Chalk Aquifer by Chlorinated Solvents: A Case Study of the Luton and Dunstable Area. Water and Environment Journal 6, 541–550. https://doi.org/10.1111/j.1747-6593.1992.tb00789.x

Lopez, B., Brugeron, A., Devau, N., Ollivier, P., 2014. Vulnérabilité des eaux souterraines de France métropolitaine vis-à-vis des ions perchlorates. Rapport final. BRGM/RP-63270-FR. 108 p.

Lopez, B., Vernoux, J.F., Neveux, A., Barrez, F., Brugeron, A., 2015. Recherche des origines de la pollution en perchlorate impactant des captages au sein des AAC de la région de Nemours et Bourron-Marlotte. Rapport BRGM/RP-64840-FR, 140 p.

Lybrand, R.A., Bockheim, J.G., Ge, W., Graham, R.C., Hlohowskyj, S.R., Michalski, G., Prellwitz, J.S., Rech, J.A., Wang, F., Parker, D.R., 2016. Nitrate, perchlorate, and iodate co-occur in coastal and inland deserts on Earth. Chemical Geology 442, 174–186. https://doi.org/10.1016/j.chemgeo.2016.05.023

~~~~~~~~~~~~~~~~~ M ~~~~~~~~~~~~~~~~

Ma, H., Bonnie, N.A., Yu, M., Che, S., Wang, Q., 2016. Biological treatment of ammonium perchlorate-contaminated wastewater: A review. Journal of Water Reuse and Desalination 6, 82–107. https://doi.org/10.2166/wrd.2015.016

MacDonald, A.M., Allen, D.J., 2001. Aquifer properties of the Chalk of England. Quarterly Journal of Engineering Geology and Hydrogeology 34, 371–384. https://doi.org/10.1144/qjegh.34.4.371

MacDonald, A.M., Brewerton, L.J., Allen, D.J., 1998a. Evidence for rapid groundwater flow and karst-type behavior in the Chalk of southern England, in: Robins, N.S. (Ed.), Groundwater Pollution, Aquifer Recharge and Vulnerability. Geological Society of London, pp. 95–106.

MacDonald, A.M., Brewerton, L.J., Allen, D.J., 1998b. Evidence for rapid groundwater flow and karst-type behavior in the Chalk of southern England. Geological Society, London, Special Publications 130, 95–106. https://doi.org/10.1144/GSL.SP.1998.130.01.09
~~~~~~~~~~~~~~~~~

Małoszewski, P., Zuber, A., 1982. Determining the turnover time of groundwater systems with the aid of environmental tracers: 1. Models and their applicability. Journal of Hydrology 57, 207–231. https://doi.org/10.1016/0022-1694(82)90147-0

Mangeret, A., De Windt, L., Crançon, P., 2012. Reactive transport modelling of groundwater chemistry in a chalk aquifer at the watershed scale. Journal of Contaminant Hydrology 138–139, 60–74. https://doi.org/10.1016/j.jconhyd.2012.06.004

Martel, R., Mailloux, M., Gabriel, U., Lefebvre, R., Thiboutot, S., Ampleman, G., 2009. Behavior of energetic materials in ground water at an anti-tank range. J. Environ. Qual. 38, 75–92. https://doi.org/10.2134/jeq2007.0606

Mass DEP, 2005. The occurence and sources of Perchlorate in Massachusetts. Massachusetts Departement of Environmental Protection, Boston, MA. https://www.mass.gov/dep/. 54 p.

Mastrocicco, M., Di, G., Vincenzi, F., Colombani, N., Castaldelli, G., 2017. Chlorate origin and fate in shallow groundwater below agricultural landscapes. Environmental Pollution 231, 1453–1462. https://doi.org/10.1016/j.envpol.2017.09.007

Mathias, S.A., Butler, A.P., Jackson, B.M., Wheater, H.S., 2006. Transient simulations of flow and transport in the Chalk unsaturated zone. Journal of Hydrology, Hydro-ecological functioning of the Pang and Lambourn catchments, UK 330, 10–28. https://doi.org/10.1016/j.jhydrol.2006.04.010

Matthess, G., 1982. The properties of Groundwater. Department of Environmental Science, John Wiley and Sons Inc., Nex York. 406 p.

Maurice, L., 2009. Investigations of rapid groundwater flow and karst in the Chalk (Doctoral). UCL (University College London), 453 p.

Maurice, L.D., Atkinson, T.C., Barker, J.A., Williams, A.T., Gallagher, A.J., 2012. The nature and distribution of flowing features in a weakly karstified porous limestone aquifer. Journal of Hydrology 438–439, 3–15. https://doi.org/10.1016/j.jhydrol.2011.11.050

Mazor, E., 1972. Paleotemperatures and other hydrological parameters deduced from noble gases dissolved in groundwaters; Jordan Rift Valley, Israel. Geochimica et Cosmochimica Acta 36, 1321–1336. https://doi.org/10.1016/0016-7037(72)90065-8

Mccarthy, R.L., Bower, F.A., Jesson, J.P., 1977. The fluorocarbon-ozone theory—I. Production and release—world production and release of CCl3F and CCl2F2 (fluorocarbons 11 and 12) through 1975. Atmospheric Environment (1967) 11, 491–497. https://doi.org/10.1016/0004-6981(77)90065-8

McCulloch, A., 1999. CFC and Halon replacements in the environment. Journal of Fluorine Chemistry 100, 163–173. https://doi.org/10.1016/S0022-1139(99)00198-0

McLaughlin, C.L., Blake, S., Hall, T., Harman, M., Kanda, R., Hunt, J., Rumsby, P.C., 2011. Perchlorate in raw and drinking water sources in England and Wales. Water and Environment Journal 25, 456–465. https://doi.org/10.1111/j.1747-6593.2010.00237.x

Medalie, L., 2013. Concentrations of chloride and sodium in groundwater in New Hampshire from 1960 through 2011 (USGS Numbered Series No. 2013–3011), Fact Sheet. U.S. Geological Survey, Reston, VA.

Mégnien, C., 1979. Hydrogéologie du centre du bassin de Paris : contribution à l'étude de quelques aquifères principaux. Mémoire du BRGM n°98. 532 p.

Mendiratta, S.K., Dotson, R.L., Brooker, R.T., 1996. Perchloric Acid and Perchlorates, in: Kirk-Othmer Encyclopedia of Chemical Technology. John Wiley & Sons, Inc., New York. https://doi.org/10.1002/0471238961.1605180313051404.a01.pub2

Michalski, G., Kolanowski, M., Riha, K.M., 2015. Oxygen and nitrogen isotopic composition of nitrate in commercial fertilizers, nitric acid, and reagent salts. Isotopes in Environmental and Health Studies 51, 382–391. https://doi.org/10.1080/10256016.2015.1054821

Michel, R.L., 2004. Tritium hydrology of the Mississippi River basin. Hydrological Processes 18, 15. https://doi.org/10.1002/hyp.1403

Mohr, T.K.G., 2007. Assessing perchlorate origins using stable isotopes. Southwest hydrology 22–23.

Molina, M.J., Rowland, F.S., 1974. Stratospheric sink for chlorofluoromethanes: chlorine atom-catalysed destruction of ozone. Nature 249, 810–812. https://doi.org/10.1038/249810a0

Mondain, P.H., Pillet, M.A., Banton, O., Comte, J.C., 2006. Etude du fonctionnemnt du bassin d'alimentation du Champ Captant de Couraux, Phase 1. Rpport Calligée-Hydrian N° 06-51113 A. 142 p.

Moreau, CF., Morfaux, P., Rambaud, D., Kerbaul, A., Pommenof, T., 1985. Etude hydrogéologique de la nappe de la craie et des alluvions dans le bassin versant de la Vesle en vue de sa modélisation. Rapport BRGM, 85 SGN 175 CHA, 287 p.

Morin, S., Savarino, J., Frey, M.M., Domine, F., Jacobi, H.-W., Kaleschke, L., Martins, J.M.F., 2009. Comprehensive isotopic composition of atmospheric nitrate in the Atlantic Ocean boundary layer from 65°S to 79°N. Journal of Geophysical Research: Atmospheres 114. https://doi.org/10.1029/2008JD010696

Morris, B., Stuart, M.E., Darling, W.G., Gooddy, D.C., 2005. Use of Groundwater Age Indicators in Risk Assessment to Aid Water Supply Operational Planning. Water and Environment Journal 19, 41–48. https://doi.org/10.1111/j.1747-6593.2005.tb00547.x

Morris, B.L., George Darling, W., Gooddy, D.C., Litvak, R.G., Neumann, I., Nemaltseva, E.J., Poddubnaia, I., 2006. Assessing the extent of induced leakage to an urban aquifer using environmental tracers: an example from Bishkek, capital of Kyrgyzstan, Central Asia. Hydrogeol J 14, 225–243. https://doi.org/10.1007/s10040-005-0441-x

Munster, J., Hanson, G.N., 2009. Perchlorate and ion chemistry of road runoff. Environ. Chem. 6, 28–35. https://doi.org/10.1071/EN08085

Munster, J., Hanson, G.N., Jackson, W.A., Rajagopalan, S., 2009. The Fallout from Fireworks: Perchlorate in Total Deposition. Water Air Soil Pollut 198, 149–153. https://doi.org/10.1007/s11270-008-9833-6

Munster, J.E., 2008. Non-point sources of nitrate and perchlorate in urban land use to groundwater, Suffolk County, NY. PhD. dissertation, Stony Brook University, 132 p.

Mussett, A.E., Khan, M.A., 2000. Looking Into the Earth: An Introduction to Geological Geophysics. Cambridge University Press. 506 p.

~~~~~~~~~~~~~~~~~ N ~~~~~~~~~~~~~~~~~

Na, C., Cannon, F.S., Hagerup, B., 2002. Perchlorate removal via IRON-PRELOADED GAC and BOROHYDRIDE REGENERATION. Journal - American Water Works Association 94, 90–102. https://doi.org/10.1002/j.1551-8833.2002.tb10233.x

Nadaraja, A.V., Puthiyaveettil, P.G., Bhaskaran, K., 2015. Surveillance of perchlorate in ground water, surface water and bottled water in Kerala, India. J Environ Health Sci Eng 13, 56. https://doi.org/10.1186/s40201-015-0213-z

Nann, A., Pretsch, E., 1994. Potentiometric detection of anions separated by capillary electrophoresis using an ion-selective microelectrode. Journal of Chromatography A 676, 437–442. https://doi.org/10.1016/0021-9673(94)80444-3

Nativ, R., Gunay, G., Hotzl, H., Reichert, B., Solomon, D.K., and Tezcan, L., Separation of groundwater-flow components in a karstified aquifer using environmental tracers. Applied Geochemistry. 14: 1001–1014, 1999

Negrel, P., Ollivier, P., Flehoc, C., Hube, D., 2017. An innovative application of stable isotopes (δ2H and δ18O) for tracing pollutant plumes in groundwater. Science of The Total Environment 578, 495–501. https://doi.org/10.1016/j.scitotenv.2016.10.214

Nguyen, H.D., 2009. Influence des interactions eau-roche sur le comportement à long terme de cavités souterraines dans la craie (phd thesis). Ecole des Ponts ParisTech. 212 p.

Noble, L.F., Mansfield, G.R., (1922). Nitrate deposits in the Amargosa Region southeastern California. United States Geological Survey, Bulletin 724, 1–99.

~~~~~~~~~~~~~~~~~ O ~~~~~~~~~~~~~~~~~

Ogunbode, C.A., Demski, C., Capstick, S.B., Sposato, R.G., 2019. Attribution matters: Revisiting the link between extreme weather experience and climate change mitigation responses. Global Environmental Change 54, 31–39. https://doi.org/10.1016/j.gloenvcha.2018.11.005

Oster, H., Sonntag, C., Münnich, K.O., 1996. Groundwater age dating with chlorofluorocarbons. Water Resources Research 32, 2989–3001. https://doi.org/10.1029/96WR01775

~~~~~~~~~~~~~~~~ P ~~~~~~~~~~~~~~~~

Parker, B., Chendorain, M., Stewart, L., 2004. UXO Corrosion - Potential Contamination Source. SERDP Project ER-1226, 95 p.

Parker, D.R., Seyfferth, A.L., Reese, B.K., 2008. Perchlorate in groundwater: a synoptic survey of "pristine" sites in the coterminous United States. Environ. Sci. Technol. 42, 1465–1471.

Phillips, F.M., 2000. Chlorine-36, in: Cook, P.G., Herczeg, A.L. (Eds.), Environmental Tracers in Subsurface Hydrology. Springer US, Boston, MA, pp. 299–348. https://doi.org/10.1007/978-1-4615-4557-6_10

Plummer, L., Bohlke, J., Busenberg, E., 2003. Water-Resources Investigations Report 03-4035, U.S. Geological Survey, 12-24.

Plummer, L. Niel, Böhlke, J.K., Doughten, M.W., 2006. Perchlorate in pleistocene and holocene groundwater in north-central New Mexico. Environ. Sci. Technol. 40, 1757–1763.

Plummer, L. N., Busenberg, E., Cook, P.G., 2006a. Chapter 3. Principles of chlorofluorocarbon dating, in: Use of Chlorofluorocarbons in Hydrology: A Guidebook. 277 p.

Plummer, L. N., Busenberg, E., Solomon, D.K., Han, L.F., 2006b. Chapter 5. CFCs in binary mixtures of young and old groundwater. Use of chlorofluorocarbons in hydrology: A guidebook. 277 p.

Plummer, L.N., Rupert, M.G., Busenberg, E., Schlosser, P., 2000. Age of Irrigation Water in Ground Water from the Eastern Snake River Plain Aquifer, South-Central Idaho. Groundwater 38, 264–283. https://doi.org/10.1111/j.1745-6584.2000.tb00338.x

Plummer, N., Busenberg, E., Bohlke, J.K., Carmody, R.W., Casile, G.C., Coplen, T.B., Doughten, M.W., Hannon, J.E., Kirkland, W., Michel, R.L., Nelms, D.L., Norton, B.C., Plummer, K.E., Qi, H., Revesz, K., Schlosser, P., Spitzer, S., Wayland, J.E., Widman, P.K., 2000. Chemical and isotopic composition of water from springs, wells, and streams in parts of Shenandoah National Park, Virginia, and vicinity, 1995-1999 (No. 2000–373). U.S. Dept. of the Interior, U.S. Geological Survey. https://doi.org/10.3133/ofr00373

Plummer, N., Busenberg, E., Böhlke, J.K., Nelms, D.L., Michel, R.L., Schlosser, P., 2001. Groundwater residence times in Shenandoah National Park, Blue Ridge Mountains, Virginia, USA: A multi-tracer approach. Chemical Geology 179, 19. https://doi.org/10.1016/S0009-2541(01)00317-5

Poghosyan, A., Sturchio, N.C., Morrison, C.G., Beloso, A.D., Guan, Y., Eiler, J.M., Jackson, W.A., Hatzinger, P.B., 2014. Perchlorate in the Great Lakes: isotopic composition and origin. Environ. Sci. Technol. 48, 11146–11153. https://doi.org/10.1021/es502796d

Pollard, D.D., Aydin, A., 1988. Progress in understanding jointing over the past century. GSA Bulletin 100, 1181–1204. https://doi.org/10.1130/0016-7606(1988)100<1181:PIUJOT>2.3.CO;2

Pontius, F.W., Damian, P., Eaton, A.D., 2000. Regulating Perchlorate in Drinking Water, in: Perchlorate in the Environment, Environmental Science Research. Springer, Boston, MA, pp. 31–36. https://doi.org/10.1007/978-1-4615-4303-9_4

Price, M., 1996. Introducing Groundwater. Psychology Press. 316 p.

Price, M., 1987. Fluid flow in the Chalk of England. Geological Society, London, Special Publications 34, 141–156. https://doi.org/10.1144/GSL.SP.1987.034.01.10

Price, M., Downing, R.A., Edmunds, W.M., 1993. The Chalk as an aquifer, in: Downing, R.A., Price, M., Jones, G.P. (Eds.), The Hydrogeology of the Chalk of North West Europe. Oxford, pp. 35–58.

Price, M., Low, R.G., McCann, C., 2000. Mechanisms of water storage and flow in the unsaturated zone of the Chalk aquifer. Journal of Hydrology 233, 54–71. https://doi.org/10.1016/S0022-1694(00)00222-5

~~~~~~~~~~~~~~~~~ Q ~~~~~~~~~~~~~~~~~

Qin, X., Zhang, T., Gan, Z., Sun, H., 2014. Spatial distribution of perchlorate, iodide and thiocyanate in the aquatic environment of Tianjin, China: environmental source analysis. Chemosphere 111, 201–208. https://doi.org/10.1016/j.chemosphere.2014.03.082

Quinn, M.J., 2015. Chapter 11 - Wildlife Toxicity Assessment for Nitrocellulose, in: Williams, M.A., Reddy, G., Quinn, M.J., Johnson, M.S. (Eds.), Wildlife Toxicity Assessments for Chemicals of Military Concern. Elsevier, pp. 217–226. https://doi.org/10.1016/B978-0-12-800020-5.00011-9

Quiñones, O., Oh, J.-E., Vanderford, B., Kim, J.H., Cho, J., Snyder, S.A., 2007. Perchlorate assessment of the Nakdong and Yeongsan watersheds, Republic of Korea. Environ. Toxicol. Chem. 26, 1349–1354.

~~~~~~~~~~~~~~~~~ R ~~~~~~~~~~~~~~~~~

Rajagopalan, S., Anderson, T., Cox, S., Harvey, G., Cheng, Q., Jackson, W.A., 2009. Perchlorate in Wet Deposition Across North America. Environ. Sci. Technol. 43, 616–622. https://doi.org/10.1021/es801737u

Rajagopalan, S., Anderson, T.A., Fahlquist, L., Rainwater, K.A., Ridley, M., Jackson, W.A., 2006. Widespread presence of naturally occurring perchlorate in high plains of Texas and New Mexico. Environ. Sci. Technol. 40, 3156–3162.

Rao, B., Anderson, T.A., Orris, G.J., Rainwater, K.A., Rajagopalan, S., Sandvig, R.M., Scanlon, B.R., Stonestrom, D.A., Walvoord, M.A., Jackson, W.A., 2007. Widespread natural perchlorate in unsaturated zones of the southwest United States. Environ. Sci. Technol. 41, 4522–4528.

Ravishankara, A.R., Solomon, S., Turnipseed, A.A., Warren, R.F., 1993. Atmospheric Lifetimes of Long-Lived Halogenated Species. Science 259, 194–199. https://doi.org/10.1126/science.259.5092.194

R Core Team, 2018. R: A Language and Environment for Statistical Computing. R Foundation for Statistical Computing, Vienna. https://www.R-project.org

Reardon, E.J., Allison, G.B., Fritz, P., 1979. Seasonal Chemical and Isotopic Variations of Soil Co2 at Trout Creek, Ontario, in: Back, W., Stephenson, D.A. (Eds.), Developments in Water Science, Contemporary Hydrogeology. Elsevier, pp. 355–371. https://doi.org/10.1016/S0167-5648(09)70026-7

Reardon, E.J., Mozeto, A.A., Fritz, P., 1980. Recharge in northern clime calcareous sandy soils: soil water chemical and carbon-14 evolution. Geochimica et Cosmochimica Acta 44, 1723–1735. https://doi.org/10.1016/0016-7037(80)90223-9

Renner, R., 1999. Study finding perchlorate in fertilizer rattles industry. Environ. Sci. Technol. 33, 394A–5A. https://doi.org/10.1021/es993030e

Richard, J., Sizun, J.-P., Machhour, L., 2005. Environmental and diagenetic records from a new reference section for the Boreal realm: the Campanian chalk of the Mons basin (Belgium). Sedimentary Geology 178, 99–111.

Ricour, J., 2013. Un exemple d'altération du fond géochimique naturel des sols et des eaux souterraines : les séquelles environnementales des grands conflits mondiaux en France. Géologues 179, 27–31.

Robin des Bois, 2012. En attendant les démineurs – Inventaires des déchets de guerre du 1er janvier 2008 au 31 décembre 2011 | Robin des Bois. URL http://www.robindesbois.org/en-attendant-les-demineurs-inventaires-des-dechets-de-guerre-du-1er-janvier-2008-au-31-decembre-2011/ (accessed 10.11.18).

Rodet, J., 1993. Le rôle des formations quaternaires dans le drainage karstique : l'exemple des craies du bassin de Paris. Quaternaire 4, 97–102. https://doi.org/10.3406/quate.1993.1998

Roux, J.C., 2018. Historique de l'hydrogéologie de la Craie en France. Géologues 199, 7–10.

Rouxel-David, E., Batkowski, D., Baudouin, V., Cordonnier, G., Cubizolles, J., Herrouin, J.P., Izac, J.L., Jegou, J.P., Kieffer, C., Mardhel, V., Paya, H., 2002a. Cartographie de la piézométrie de la nappe de la craie en Champagne-Ardenne, Rapport BRGM/RP-52332-FR, 29 p.

Rouxel-David, E., Cordonnier, G., 2002. Les échanges entre la nappe de la craie et les cours d'eau. Tableau de bord de la nappe de la craie, DREAL 38, 15–18.

Rouxel-David, E., Cordonnier, G., Dachy, S., 2002b. Synthèse des études menées sur le bassin versant du champ captant de Couraux (Marne). Rapport BRGM, RP-51739-FR, 159 p.

~~~~~~~~~~~~~~~~~ S ~~~~~~~~~~~~~~~~~

Sanchez, C.A., Krieger, R.I., Khandaker, N.R., Valentin-Blasini, L., Blount, B.C., 2006. Potential perchlorate exposure from Citrus sp. irrigated with contaminated water. Analytica Chimica Acta, Perchlorate: an Enigma for the New Millennium 567, 33–38. https://doi.org/10.1016/j.aca.2006.02.013

Santella, N., Ho, D.T., Schlosser, P., Stute, M., 2008. Widespread elevated atmospheric SF6 mixing ratios in the Northeastern United States: Implications for groundwater dating. Journal of Hydrology 349, 139–146. https://doi.org/10.1016/j.jhydrol.2007.10.031

Santoni, S., Huneau, F., Garel, E., Celle-Jeanton, H., 2018. Multiple recharge processes to heterogeneous Mediterranean coastal aquifers and implications on recharge rates evolution in time. Journal of Hydrology 559, 669–683. https://doi.org/10.1016/j.jhydrol.2018.02.068

Savarino, J., Morin, S., Erbland, J., Grannec, F., Patey, M.D., Vicars, W., Alexander, B., Achterberg, E.P., 2013. Isotopic composition of atmospheric nitrate in a tropical marine boundary layer. PNAS 110, 17668–17673. https://doi.org/10.1073/pnas.1216639110

Scanlon, B., B. Gates, J., Reedy, R., Jackson, W., Bordovsky, J., 2010. Effects of irrigated agroecosystems: 2. Quality of soil water and groundwater in the southern High Plains, Texas. Water Resources Research - WATER RESOUR RES 46. https://doi.org/10.1029/2009WR008428

Scheytt, T.J., Freywald, J., Ptacek, C.J., 2011. Study of selected soil, ground, and surface water samples on perchlorate in Germany: First results. Grundwasser 16, 37–43.

Schilt, A.A., 1979. Perchloric acid and perchlorates. G. F. Smith Chemical Co., Columbus, Ohio. 197 p.

Schumacher, J.C., 1960. Perchlorates: Their Properties, Manufacture and Uses. Edited by J.C. Schumacher. New York; Chapman & Hall: London, 257 p.

Sebol, L.A., Robertson, W.D., Busenberg, E., Plummer, N., Ryan, M.C., Schiff, S.L., 2007. Evidence of CFC degradation in groundwater under pyrite-oxidizing conditions. Journal of Hydrology 347, 12. https://doi.org/10.1016/j.jhydrol.2007.08.009

Sellers, K., Weeks, K., Alsop, W.R., Clough, S.R., Hoyt, M., Pugh, B., Robb, J., 2006. Perchlorate: Environmental Problems and Solutions. CRC Press, 258 p.

Serrano-Nascimento, C., Calil-Silveira, J., Dalbosco, R., Zorn, T.T., Nunes, M.T., 2018. Evaluation of hypothalamus-pituitary-thyroid axis function by chronic perchlorate exposure in male rats. Environmental Toxicology 33, 209–219. https://doi.org/10.1002/tox.22509

Shi, Y., Zhang, P., Wang, Y., Shi, J., Cai, Y., Mou, S., Jiang, G., 2007. Perchlorate in sewage sludge, rice, bottled water and milk collected from different areas in China. Environ Int 33, 955–962. https://doi.org/10.1016/j.envint.2007.05.007

Sijimol, M.R., Mohan, M., 2014. Environmental impacts of perchlorate with special reference to fireworks--a review. Environ Monit Assess 186, 7203–7210. https://doi.org/10.1007/s10661-014-3921-4
~~~~~~~~~~~~~~~~~

Silva, M.A., 2003. Safety flares threaten water quality with perchlorate. Santa Clara Valley Water District Publication. http://www.valleywater.org.

Smith, D.B., Richards, H.J., 1972. Selected environmental studies using radioactive tracers. Proceedings of IAEA Symposium on peaceful uses of atomic energy, IAEA, Vienna 467–480.

Smith, D.B., Wearn, P.L., Richards, H.J., Rowe, P.C., 1970. Water Movement in the Unsaturated Zone of High and Low Permeability Strata by Measuring Natural Tritium. Isotope Hydrology 1970. Proceedings of a Symposium on Use of Isotopes in Hydrology, pp 73 - 86.

Solomon, D.K., Plummer, L.N., Busenberg, E., Cook, P.G., 2006. Chapter 6. Models of groundwater ages and residence times, in: Use of Chlorofluorocarbons in Hydrology: A Guidebook. 277 p.

Spence, A., Poortinga, W., Butler, C., Pidgeon, N.F., 2011. Perceptions of climate change and willingness to save energy related to flood experience. Nature Clim Change 1, 46–49. https://doi.org/10.1038/nclimate1059

Sperling, C.H.B., Goudie, A.S., Stoddart, D.R., Poole, G.G., 1977. Dolines of the Dorset Chalklands and Other Areas in Southern Britain. Transactions of the Institute of British Geographers 2, 205–223. https://doi.org/10.2307/621858

Srinivasan, A., Viraraghavan, T., 2009. Perchlorate: Health Effects and Technologies for Its Removal from Water Resources. International Journal of Environmental Research and Public Health 6, 1418–1442. https://doi.org/10.3390/ijerph6041418

Srinivasan, R., Sorial, G.A., 2009. Treatment of perchlorate in drinking water: A critical review. Separation and Purification Technology 69, 7–21. https://doi.org/10.1016/j.seppur.2009.06.025

Stanford, B.D., Pisarenko, A.N., Snyder, S.A., Gordon, G., 2011. Perchlorate, bromate, and chlorate in hypochlorite solutions: Guidelines for utilities. American Water Works Association 103, 71–83.

Steinmaus, C.M., 2016. Perchlorate in Water Supplies: Sources, Exposures, and Health Effects. Current environmental health reports 3, 136–143. https://doi.org/10.1007/s40572-016-0087-y

Stroo, H.F., Loehr, R.C., Ward, C.H., 2009. In Situ Bioremediation Of Perchlorate In Groundwater: An Overview, in: In Situ Bioremediation of Perchlorate in Groundwater, SERDP/ESTCP Environmental Remediation Technology. Springer, New York, NY, pp. 1–13. https://doi.org/10.1007/978-0-387-84921-8_1

Stuart, M.E., Smedley, P.L., 2009. Baseline groundwater chemistry : the Chalk aquifer of Hampshire (Open report No. OR/09/052). British Geological Survey, 61 p.

Sturchio, N.C., 2015. Reply to the comments by P. Bennett on ``Isotopic tracing of perchlorate sources in groundwater of Pomona, California'' by N.C. Sturchio, A. Beloso Jr., L.J. Heraty, S. Wheatcraft, and R. Schumer. Applied Geochemistry, vol. 52, pp. 195-196 52, 195–196. https://doi.org/10.1016/j.apgeochem.2014.11.027

Sturchio, N.C., Beloso, A., Heraty, L.J., Wheatcraft, S., Schumer, R., 2014. Isotopic tracing of perchlorate sources in groundwater from Pomona, California. Applied Geochemistry 43, 80–87. https://doi.org/10.1016/j.apgeochem.2014.01.012

Sturchio, N.C., Böhlke, J.K., Beloso, A.D., Streger, S.H., Heraty, L.J., Hatzinger, P.B., 2007. Oxygen and chlorine isotopic fractionation during perchlorate biodegradation: laboratory results and implications for forensics and natural attenuation studies. Environ. Sci. Technol. 41, 2796–2802.

Sturchio, N.C., Böhlke, J.K., Gu, B., Hatzinger, P.B., Jackson, W.A., 2011. Isotopic Tracing of Perchlorate in the Environment, in: Handbook of Environmental Isotope Geochemistry, Advances in Isotope Geochemistry. Springer, Berlin, Heidelberg, pp. 437–452. https://doi.org/10.1007/978-3-642-10637-8_22

Sturchio, N.C., Böhlke, J.K., Gu, B., Horita, J., Brown, G.M., Beloso Jr., A.D., Patterson, L.J., Hatzinger, P.B., Jackson, W.A., Batista, J., 2006. Stable isotopic composition of chlorine and oxygen in synthetic and natural perchlorate, in: Perchlorate: Environmental Occurrence, Interactions and Treatment. pp. 93–109. https://doi.org/10.1007/0-387-31113-0_5

Sturchio, N.C., Caffee, M., Beloso, A.D., Heraty, L.J., Böhlke, J.K., Hatzinger, P.B., Jackson, W.A., Gu, B., Heikoop, J.M., Dale, M., 2009. Chlorine-36 as a tracer of perchlorate origin. Environ. Sci. Technol. 43, 6934–6938.

Sturchio, N.C., Hatzinger, P.B., Arkins, M.D., Suh, C., Heraty, L.J., 2003. Chlorine Isotope Fractionation during Microbial Reduction of Perchlorate. Environ. Sci. Technol. 37, 3859–3863. https://doi.org/10.1021/es034066g

Sturchio, N.C., Hoaglund, J.R., Marroquin, R.J., Beloso, A.D., Heraty, L.J., Bortz, S.E., Patterson, T.L., 2012. Isotopic mapping of groundwater perchlorate plumes. Ground Water 50, 94–102. https://doi.org/10.1111/j.1745-6584.2011.00802.x

Suckow, A., 2014. The age of groundwater – Definitions, models and why we do not need this term. Applied Geochemistry 50, 222–230. https://doi.org/10.1016/j.apgeochem.2014.04.016

Susarla, S., Collette, T.W., Garrison, A.W., Wolfe, N.L., McCutcheon, S.C., 1999. Perchlorate Identification in Fertilizers. Environ. Sci. Technol. 33, 3469–3472. https://doi.org/10.1021/es990577k

Sutton, P.M., 2006. Bioreactor Configurations for Ex-Situ Treatment of Perchlorate: A Review. Water Environment Research 78, 2417–2427. https://doi.org/10.2175/106143006X123067

~~~~~~~~~~~~~~~~ T ~~~~~~~~~~~~~~~~

Taborelli, P., 2018. Les conditions géographiques et l'organisation spatiale du front de la Grande Guerre : application à l'évaluation environnementale post-conflit en Champagne-Ardenne (France) Phd thesis, Reims, 427 p.

Taborelli, P., Devos, A., Setastien, L., Brenot, J., Bollot, N., Jean-Paul, D., Stichelbaut, B., 2017. Integrating GIS, trenches maps, LiDAR data processing and archaeological approach for the WWI landscapes survey of the Champagne front (France). Presented at 9th International Conference on Geomorpholgy at New-Dehli (India).

Tan, K., Anderson, T.A., Jackson, W.A., 2005a. Temporal and spatial variation of perchlorate in streambed sediments: results from in-situ dialysis samplers. Environmental Pollution 136, 283–291. https://doi.org/10.1016/j.envpol.2004.12.037
~~~~~~~~~~~~~~~~

Tan, K., Anderson, T.A., Jackson, W.A., 2005b. Temporal and spatial variation of perchlorate in streambed sediments: results from in-situ dialysis samplers. Environ. Pollut. 136, 283–291. https://doi.org/10.1016/j.envpol.2004.12.037

Téllez, R.T., Chacón, P.M., Abarca, C.R., Blount, B.C., Landingham, C.B.V., Crump, K.S., Gibbs, J.P., 2005. Long-Term Environmental Exposure to Perchlorate Through Drinking Water and Thyroid Function During Pregnancy and the Neonatal Period. Thyroid 15, 963–975. https://doi.org/10.1089/thy.2005.15.963

Thiéry, D., 1980. Prévision de grandeurs hydrologiques par les méthodes de convolution. Hydrological forecasting - Prévisions hydrologiques (Proceedings of the Oxford Symposium, April 1980; Actes du Colloque d'Oxford, avril 1980): IAHS-AISH Publ. no. 129. April 1980; Actes du Colloque d'Oxford, avril 1980): IAHS-AISH Publ. no. 129.

Thornthwaite, C.W., 1948. An Approach toward a Rational Classification of Climate. Geographical Review 38, 55–94. https://doi.org/10.2307/210739

Ting, D., Howd, R.A., Fan, A.M., Alexeeff, G.V., 2006. Development of a health-protective drinking water level for perchlorate. Environ. Health Perspect. 114, 881–886.

Tipton, D.K., Rolston, D.E., Scow, K.M., 2003. Transport and biodegradation of perchlorate in soils. J. Environ. Qual. 32, 40–46.

Trumpolt, C.W., Crain, M., Cullison, G.D., Flanagan, S.J.P., Siegel, L., Lathrop, S., 2005. Perchlorate: Sources, Uses, and Occurrences in the Environment. Remediation Journal 16, 65–89. https://doi.org/10.1002/rem.20071

Tsui, D.T., Clewell, R.A., Eldridge, J.E., Mattie, D.R., 2000. Perchlorate Analysis with the AS16 Separation Column, in: Perchlorate in the Environment, Environmental Science Research. Springer, Boston, MA, pp. 59–80. https://doi.org/10.1007/978-1-4615-4303-9_7

~~~~~~~~~~~~~~~~~ U ~~~~~~~~~~~~~~~~~

Unterweger, M.P., Coursey, B.M., Schima, F.J., Mann, W.B., 1980. Preparation and calibration of the 1978 National Bureau of Standards tritiated-water standards. The International Journal of Applied Radiation and Isotopes 31, 611–614. https://doi.org/10.1016/0020-708X(80)90017-4

Urbansky, E.T., 2002. Perchlorate as an environmental contaminant. Environ Sci & Potlut Res 9, 187–192. https://doi.org/10.1007/BF02987487

Urbansky, E.T., 2000. Quantitation of Perchlorate Ion: Practices and Advances Applied to the Analysis of Common Matrices 30. https://doi.org/10.1080/10408340008984163

Urbansky, E.T., 1998. Perchlorate Chemistry: Implications for Analysis and Remediation. Bioremediation Journal 2, 81–95. https://doi.org/10.1080/10889869891214231

Urbansky, E. T., Brown, S.K., Magnuson, M.L., Kelty, C.A., 2001. Perchlorate levels in samples of sodium nitrate fertilizer derived from Chilean caliche. Environmental Pollution 112, 299–302. https://doi.org/10.1016/S0269-7491(00)00132-9

Urbansky, E.T., Collette, T.W., Robarge, W.P., Hall, W.L., Skillen, J.M., Kane, P.F., 2001. Survey of fertilizers and related materials for Perchlorate (ClO_4^-): final report. 8 p. National Risk Management Research Laboratory, Office of Research and Development, U.S. Environmental Protection Agency, Cincinnati, OH.

US EPA, 2005. Perchlorate and perchlorate salts. Washington, DC: Integrated Risk Information System (IRIS). U.S. Environmental Protection Agency. 22 p.

USEPA 1998. Perchlorate Environmental Contamination: Toxicological Review and Risk Characterization Based on Emerging Information (External Review Draft). National Center for Environment Assessment, Office of Research and Development, U.S. Environmental Protection Agency, Washington.

USEPA 2006. Assessment Guidance for Perchlorate. Memorandum to Regional Administrators. US EPA Office of Solid Waste and Emergency Response, Washington, DC.

USEPA 2009. Revised Assessment Guidance for Perchlorate. Memorandum to Regional Administrators. US EPA Office of Solid Waste and Emergency Response, Washington, DC.

~~~~~~~~~~~~~~~~~ V ~~~~~~~~~~~~~~~~~

Vachier, P., Cambier, P., Prost, J.C., 1987. Mouvements de l'eau dans la zone non sature´e et alimentation de la nappe de la craie de champagne (France). In: Isotope Techniques in Water Resources Development, Vienna, IAEA Conference, pp 367–379.

Valdes, D., Dupont, J.-P., Massei, N., Laignel, B., Rodet, J., 2005. Analysis of karst hydrodynamics through comparison of dissolved and suspended solids' transport. Comptes Rendus Geoscience 337, 1365–1374. https://doi.org/10.1016/j.crte.2005.07.011

Van den Daele, G.F.A., Barker, J.A., Connell, L.D., Atkinson, T.C., Darling, W.G., Cooper, J.D., 2007. Unsaturated flow and solute transport through the Chalk: Tracer test and dual permeability modelling. Journal of Hydrology 342, 157–172. https://doi.org/10.1016/j.jhydrol.2007.05.021

Vega, M., Nerenberg, R., Vargas, I., 2018. Perchlorate contamination in Chile: Legacy, challenges, and potential solutions. Environmental research 164, 316–326. https://doi.org/10.1016/j.envres.2018.02.034

Vella, A.J., Chircop, C., Micallef, T., Pace, C., 2015. Perchlorate in dust fall and indoor dust in Malta: An effect of fireworks. Science of The Total Environment 521–522, 46–51. https://doi.org/10.1016/j.scitotenv.2015.03.071

Vergnaud-Ayraud, V., Aquilina, L., Pauwels, H., Labasque, T., 2008. La datation des eaux souterraines par analyse des CFC : un outil de gestion durable de la ressource en eau. TSM 37–44. https://doi.org/10.1051/tsm/200801037

Vernhet, Y., 2007. Carte geologique harmonisée du département de la Marne. BRGM report, RP-55732-FR, 112 p.
~~~~~~~~~~~~~~~~~

Vigreux-Besret, C., Mahé, A., Ledoux, G., Garnier, A., Rosin, C., Baert, A., Joyeux, M., Badot, P.-M., Panetier, P., Rivière, G., 2015. Perchlorate: water and infant formulae contamination in France and risk assessment in infants. Food Addit Contam Part A Chem Anal Control Expo Risk Assess 32, 1148–1155. https://doi.org/10.1080/19440049.2015.1036382

Vittecoq, B., Gourcy, L., Baran, N., 2007. Datation des eaux souterraines de Martinique par l'analyse conjointe des CFC, SF6 et tritium et relation avec les concentrations en nitrates et produits phytosanitaires. BRGM report, RP-55844-FR, 57 p.

Von Clarmann, T., 2013. Chlorine in the stratosphere. Atmósfera 26, 415–458. https://doi.org/10.1016/S0187-6236(13)71086-5

~~~~~~~~~~~~~~~~~ W ~~~~~~~~~~~~~~~~

Wallace, W., Ward, T., Breen, A., Attaway, H., 1996. Identification of an anaerobic bacterium which reduces perchlorate and chlorate as Wolinella succinogenes. Journal of Industrial Microbiology 16, 68–72. https://doi.org/10.1007/BF01569924

Waller, A.S., Cox, E.E., Edwards, E.A., 2004. Perchlorate-reducing microorganisms isolated from contaminated sites. Environmental Microbiology 6, 517–527. https://doi.org/10.1111/j.1462-2920.2004.00598.x

Warner, M.J., Weiss, R.F., 1985. Solubilities of chlorofluorocarbons 11 and 12 in water and seawater. Deep Sea Research Part A. Oceanographic Research Papers 32, 1485–1497. https://doi.org/10.1016/0198-0149(85)90099-8

Weeks, E.P., Earp, D.E., Thompson, G.M., 1982. Use of atmospheric fluorocarbons F-11 and F-12 to determine the diffusion parameters of the unsaturated zone in the Southern High Plains of Texas. Water Resources Research 18, 1365–1378. https://doi.org/10.1029/WR018i005p01365

Weiss, R.F., 1970. The solubility of nitrogen, oxygen and argon in water and seawater. Deep Sea Research and Oceanographic Abstracts 17, 721–735. https://doi.org/10.1016/0011-7471(70)90037-9

Weiss, R.F., Price, B.A., 1980. Nitrous oxide solubility in water and seawater. Marine Chemistry 8, 347–359. https://doi.org/10.1016/0304-4203(80)90024-9

Wellings, S.R., 1984a. Recharge of the Upper Chalk aquifer at a site in Hampshire, England: 2. Solute movement. Journal of Hydrology 69, 275–285. https://doi.org/10.1016/0022-1694(84)90167-7

Wellings, S.R., 1984b. Recharge of the Upper Chalk aquifer at a site in Hampshire, England: 1. Water balance and unsaturated flow. Journal of Hydrology 69, 259–273. https://doi.org/10.1016/0022-1694(84)90166-5

Wellings, S.R., Bell, J.P., 1980. Movement of water and nitrate in the unsaturated zone of Upper Chalk near Winchester, Hants., England. Journal of Hydrology 48, 119–136. https://doi.org/10.1016/0022-1694(80)90070-0
~~~~~~~~~~~~~~~~~

Whitehead, E.J., Lawrence, A.R., 2006. The chalk aquifer system of Lincolnshire (No. RR/06/03). British Geological Survey, 74 p.

WHO (2017). Guidelines for drinking-water quality: fourth edition incorporating first addendum Geneva: World Health Organization. Licence: CC BY-NC-SA 3.0 IGO. 541 p.

Wilkin, R.T., Fine, D.D., Burnett, N.G., 2007. Perchlorate behavior in a municipal lake following fireworks displays. Environ. Sci. Technol. 41, 3966–3971.

Williams, G.P., Gold, L.W., 1976. Ground temperatures. Canadian Building Digest; no. CBD-180. https://doi.org/10.4224/40000712

Wilson, G.B., McNeill, G.W., 1997. Noble gas recharge temperatures and the excess air component. Applied Geochemistry 12, 747–762. https://doi.org/10.1016/S0883-2927(97)00035-8

Wisniak, J., Garcés, 2001. The Rise and Fall of the Salitre (Sodium Nitrate) Industry. Indian Journal of Chemical Technology 8, 427–438.

Wolff, J., 1998. Perchlorate and the Thyroid Gland. Pharmacol Rev 50, 89–106.

Worthington, S.R., 2003. A comprehensive strategy for understanding flow in carbonate aquifer. Speleogenesis and Evolution of Karst Aquifers 1–8.

Wu, J., Unz, R.F., Zhang, H., Logan, B.E., 2001. Persistence of Perchlorate and the Relative Numbers of Perchlorate- and Chlorate-Respiring Microorganisms in Natural Waters, Soils, and Wastewater. Bioremediation Journal 5, 119–130. https://doi.org/10.1080/20018891079230

Wu, Q., Oldi, J.F., Kannan, K., 2011. Fate of perchlorate in a man-made reflecting pond following a fireworks display in Albany, New York, USA. Environmental Toxicology and Chemistry 30, 2449–2455. https://doi.org/10.1002/etc.648

Wu, Q., Zhang, T., Sun, H., Kannan, K., 2010. Perchlorate in tap water, groundwater, surface waters, and bottled water from China and its association with other inorganic anions and with disinfection byproducts. Arch. Environ. Contam. Toxicol. 58, 543–550. https://doi.org/10.1007/s00244-010-9485-6

~~~~~~~~~~~~~~~~~ X ~~~~~~~~~~~~~~~~~

Xie, Y., Ren, L., Zhu, X., Gou, X., Chen, S., 2018. Physical and chemical treatments for removal of perchlorate from water–A review. Process Safety and Environmental Protection 116, 180–198. https://doi.org/10.1016/j.psep.2018.02.009

Xu, X., Gao, B., Jin, B., Zhen, H., Wang, X., Dai, M., 2015. Study of microbial perchlorate reduction: Considering of multiple pH, electron acceptors and donors. Journal of Hazardous Materials 285, 228–235. https://doi.org/10.1016/j.jhazmat.2014.10.061
~~~~~~~~~~~~~~~~~

~~~~~~~~~~~~~~~~~ Y ~~~~~~~~~~~~~~~~~

Ye, L., You, H., Yao, J., Kang, X., Tang, L., 2013. Seasonal variation and factors influencing perchlorate in water, snow, soil and corns in Northeastern China. Chemosphere 90, 2493–2498. https://doi.org/10.1016/j.chemosphere.2012.10.058

Ye, L., You, H., Yao, J., Su, H., 2012. Water treatment technologies for perchlorate: A review. Desalination 298, 1–12. https://doi.org/10.1016/j.desal.2012.05.006

Young, E., Galy, A., Nagahara, H., 2002. Kinetic and equilibrium mass-dependent isotope fractionation laws in Nature and their geochemical and cosmochemical significance. Geochimica et Cosmochimica Acta 66, 1095–1104. https://doi.org/10.1016/S0016-7037(01)00832-8

Yu, X., Amrhein, C., Deshusses, M.A., Matsumoto, M.R., 2007. Perchlorate reduction by autotrophic bacteria attached to zerovalent iron in a flow-through reactor. Environ. Sci. Technol. 41, 990–997.

~~~~~~~~~~~~~~~~~ Z ~~~~~~~~~~~~~~~~~

Zimmermann, M., 1917. Le nitrate du Chili. Annales de géographie 26, 237–238.

Appendices

Appendix 1 : Article published in Science of the Total Environment: Worldwide occurrence and origin of perchlorate ion in waters: A review.

Science of the Total Environment 661 (2019) 737–749

Contents lists available at ScienceDirect

Science of the Total Environment

journal homepage: www.elsevier.com/locate/scitotenv

Review

Worldwide occurrence and origin of perchlorate ion in waters: A review

Feifei Cao [a,*], Jessy Jaunat [a], Neil Sturchio [b], Benjamin Cancès [a], Xavier Morvan [a], Alain Devos [a], Vincent Barbin [a], Patrick Ollivier [c]

[a] Université de Reims Champagne-Ardenne – GEGENAA – EA 3795, 2 esplanade Roland Garros, 51100 Reims, France
[b] Department of Geological Sciences, University of Delaware, 255 Academy Street/103 Penny Hall, Newark, DE 19716, United States
[c] BRGM, 3 av. C. Guillemin, BP 36009, 45060 Orléans Cedex 2, France

HIGHLIGHTS

- ClO_4^- is a water contaminant of concern due to its toxicity and widespread presence.
- Both natural and anthropogenic process could contribute to ClO_4^- contamination.
- Stable and radiogenic isotopes analysis of ClO_4^- distinguishes different ClO_4^- origins.
- The French case illustrates the growing recognition of ClO_4^- contamination in water.

GRAPHICAL ABSTRACT

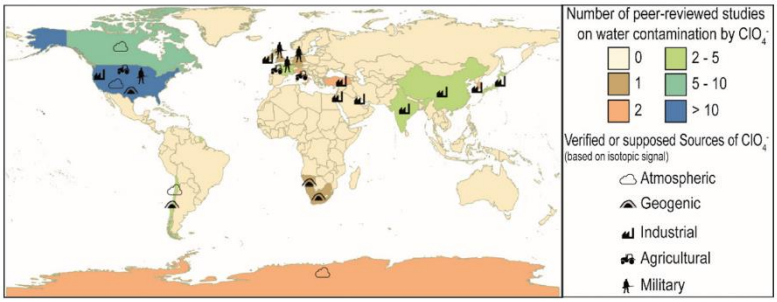

ARTICLE INFO

Article history:
Received 14 November 2018
Received in revised form 9 January 2019
Accepted 10 January 2019
Available online 14 January 2019

Editor: Damia Barcelo

Keywords:
ClO_4^-
Chilean nitrates
Military contamination
Isotope analysis
Forensics

ABSTRACT

Perchlorate (ClO_4^-) is a persistent water soluble oxyanion of growing environmental interest. Perchlorate contamination can be a health concern due to its ability to disrupt the use of iodine by the thyroid gland and the production of metabolic hormones. Its widespread presence in surface water and groundwater makes the aquatic environment a potential source of perchlorate exposure. However, the amount of published data on perchlorate origins and water contamination worldwide remains spatially limited. Here, we present an overview of research on perchlorate origins and occurrences in water, and the methodology to distinguish the different perchlorate sources based on isotope analysis. All published ranges of isotopic content in perchlorate from different sources are presented, including naturally occurring and man-made perchlorate source types, as well as the effects of isotope fractionation that accompanies biodegradation processes. An example of a case study in France is presented to emphasize the need for further research on this topic.

© 2019 Elsevier B.V. All rights reserved.

Contents

* Corresponding author.
E-mail address: feifei.cao@etudiant.univ-reims.fr (F. Cao).

https://doi.org/10.1016/j.scitotenv.2019.01.107
0048-9697/© 2019 Elsevier B.V. All rights reserved.

1. Introduction

Perchlorate (ClO_4^-) is a chemically stable anion and a powerful oxidizer, and inorganic perchlorate salts are extremely soluble in water (Urbansky, 1998). The high water solubility and the poor adsorption of ClO_4^- to typical soil minerals and organic carbon make this oxyanion highly mobile in the environment (Brown and Gu, 2006), especially in surface water and groundwater.

As the ClO_4^- ion is similar to iodine in both charge and ionic radius, it is known to disrupt the uptake of iodine in the thyroid, potentially affecting thyroid function (Clark, 2000; Urbansky, 2002; Wolff, 1998). The ingestion of ClO_4^- can alter birth outcomes and result in mental retardation and thyroid tumors (e.g., Brabant et al., 1992; Serrano-Nascimento et al., 2018). Also, independent of traditional risk factors, an increased prevalence of diabetes mellitus has been associated with high urinary ClO_4^- levels (Liu et al., 2017).

The concern of ClO_4^- in waters appeared in the second half of the 1990s, with the discovery of important concentrations in ground- and surface waters in several western states in the USA, including the Colorado River which is extensively used for irrigation and human consumption. Concentrations ranging from 8 $\mu g \cdot L^{-1}$ to 3.7 $g \cdot L^{-1}$ have been measured (Urbansky, 1998). Due to suspected toxicity of ClO_4^- and its presence in the environment, analytical techniques for determining low concentrations of ClO_4^- in water have been improved, particularly since the late 1990s. During the period between 1993 and 2005, the detection limit of ClO_4^- was reduced from approximately 400 $\mu g \cdot L^{-1}$ to 0.022 $\mu g \cdot L^{-1}$ (e.g., Burns et al., 1997; Hauser et al., 1994; Jackson et al., 2000; Nann and Pretsch, 1994; Pontius et al., 2000; Sellers et al., 2006; Trumpolt et al., 2005; Tsui et al., 2000; Urbansky, 2000). Today, the detection limit is as low as 5 $ng \cdot L^{-1}$ using LC-ESI-MS/MS method (liquid chromatography-electrospray ionization-tandem mass spectrometry) (Iannece et al., 2013). The current concern and the knowledge base regarding the environmental occurrences and sources of contamination have expanded as the ability to routinely measure low ClO_4^- concentrations in water has increased.

Drinking water is likely to be the largest source of ClO_4^- exposure (Steinmaus, 2016). The United States Environmental Protection Agency (USEPA, 1998) has placed ClO_4^- on the drinking water contaminant candidate list in 1998. Consequently, various states have implemented guidelines or goals ranging from 1 $\mu g \cdot L^{-1}$ (Maryland, Massachusetts and New Mexico) to 18 $\mu g \cdot L^{-1}$ (Nevada and Texas) for ClO_4^- in drinking water (Srinivasan and Viraraghavan, 2009). In 2009, the US EPA set a recommended value of 15 $\mu g \cdot L^{-1}$ for drinking water (USEPA, 2006, 2009). In Canada, according to the Canadian Environmental Protection Act (CEPA, 2005), a drinking water guidance value of 6 $\mu g \cdot L^{-1}$ for perchlorate has been developed. The European Food Safety Authority (EFSA) established a tolerable daily intake of 0.3 $\mu g \cdot L^{-1}$ of body weight and defined reference values for perchlorate in different foods (EFSA CONTAM Panel, 2014). However, in Europe, ClO_4^- is not yet on the list of priority water contaminants and is not routinely measured during sanitary inspection of drinking water. In France, high concentrations of ClO_4^- (>15 $\mu g \cdot L^{-1}$) have been measured in several drinking waters, leading authorities to issue related health recommendations: tap water should not be consumed by pregnant and nursing women or be used to prepare baby bottles if ClO_4^- concentrations are higher than 4 $\mu g \cdot L^{-1}$ and should not be consumed by adults if concentrations are higher than 15 $\mu g \cdot L^{-1}$ (ANSES, 2011). In 2017, the World Health Organization (WHO) issued an addendum to its fourth edition of the 2011 Guidelines for Drinking Water Quality (GDWQ), which includes a new guideline for ClO_4^- (0.07 $mg \cdot L^{-1}$; WHO, 2017).To our knowledge, there are no standards concerning ClO_4^- concentration in drinking water outside the North America and Europe. This can be explained by the paucity of studies conducted outside these areas.

During the last two decades, case studies on origins and occurrence of ClO_4^- in the environment have been published, focusing mainly on North America (e.g., Clausen et al., 2004; Dasgupta et al., 2005; Fram and Belitz, 2011; Izbicki et al., 2014; Jackson et al., 2005a, 2005b, 2010; Parker et al., 2008; Plummer et al., 2006; Rao et al., 2007; Susarla et al., 1999; Urbansky, 2002; Urbansky et al., 2001a). In recent years, increasing number of studies on ClO_4^- contamination in waters from China, South Korea, India, Japan, Italy, UK, Germany, France and Chile have been published (Anupama et al., 2012; Asami et al., 2009; Calderón et al., 2014; Iannece et al., 2013; Kosaka et al., 2007; McLaughlin et al., 2011; Nadaraja et al., 2015; Qin et al., 2014; Quiñones et al., 2007; Scheytt et al., 2011; Vega et al., 2018; Vigreux-Besret et al., 2015; Wu et al., 2010). A few review papers have been published, providing summaries of case studies on ClO_4^- occurrence in waters from different regions in the world (e.g., Calderón et al., 2017;

Kumarathilaka et al., 2016; Srinivasan and Viraraghavan, 2009; Xie et al., 2018; Ye et al., 2012). However, none of these studies provided a comprehensive and detailed review focusing on ClO_4^- contamination in waters on a worldwide scale.

Here we present a review of ClO_4^- occurrence measured in each compartment of the water cycle, including surface water, groundwater and rainwater in a worldwide scale. The natural and anthropogenic origins of ClO_4^- in the environment are described, including the theory of origin of natural ClO_4^-, accumulation mechanism in arid and semi-arid environments, the manufacturing and the use of synthetic ClO_4^-. Measured ClO_4^- concentrations related to natural and synthetic sources from different case studies are presented in detail, intending to provide a comprehensive perspective of research status on ClO_4^- occurrence in waters. The French case study is presented due to the high occurrence of ClO_4^- in waters at large scale and the potential multiple sources (e.g., military, agriculture, industrial). The methodology to distinguish these sources is discussed, which is mostly based on the isotopic composition of ClO_4^-. A summary of all published ranges of isotopic composition of ClO_4^- from different sources in the world including terrestrial ClO_4^- from different regions (e.g., Atacama, southwestern United States) and synthetic ClO_4^- is presented, aiming to provide a comprehensive perspective on isotopic signature of ClO_4^- and its use for future forensic studies.

2. Sources and uses of perchlorate

2.1. Natural perchlorate

2.1.1. The atmospheric origin of natural perchlorate

The atmospheric production of natural ClO_4^- is a well-known process. Photochemical reactions between inorganic chlorine and ozone can create ClO_4^- (Trumpolt et al., 2005). UV-mediated photo-oxidation may also play a role in the creation of ClO_4^- (Dasgupta et al., 2005; Jackson et al., 2010). Volcanic eruptions were proposed as another natural source of increased atmospheric ClO_4^- (Furdui et al., 2018; Jaeglé et al., 1996). Also, natural organic chlorine species such as methyl chlorine can be converted to inorganic species (e.g., HCl, $ClONO_2$, ClO) in the atmosphere and can thus contribute to the formation of ClO_4^- in stratosphere (Brown and Gu, 2006; Fabian et al., 1981; Von Clarmann, 2013). Production of ClO_4^- in the atmosphere may also be related to anthropogenic contaminants. Recently, Furdui et al. (2018) suggested that the atmospheric input of chlorinated solvents (e.g., methyl chloroform) from anthropogenic activities could contribute to ClO_4^- sources.

2.1.2. Arid and semi-arid deserts

Following atmospheric production, ClO_4^- is deposited at the earth's surface by dry and wet deposition (Andraski et al., 2014; Rajagopalan et al., 2009). However, given its high solubility and poor sorption properties, it is readily transported to surface water or groundwater through runoff and infiltration of precipitation (Rajagopalan et al., 2009; Rao et al., 2007). This may explain why most natural ClO_4^- occurrences are confined to arid and semi-arid environments, as the evapotranspiration is strong and the amount of atmospheric deposition exceeds the rate of dissolution by ongoing precipitation (Jackson et al., 2015; Rajagopalan et al., 2006; Rao et al., 2007).

Terrestrial soil ClO_4^- has been measured in the Atacama Desert (Chile), southwestern United States, southern Africa, United Arab Emirates, northwestern China and Antarctica at concentrations ranging from 10^{-1} to 10^6 $\mu g \cdot kg^{-1}$ (Jackson et al., 2015; Lybrand et al., 2016; Rao et al., 2007). The ClO_4^- accumulation in soils/caliche depends not only on its deposition rate but also on site-specific geologic, hydrologic and biogeochemical conditions.

Generally, the ClO_4^- concentration increases with aridity index and the duration of arid conditions (Jackson et al., 2015). The Atacama Desert is known as the driest desert in the world receiving <5 $mm \cdot yr^{-1}$ of rain. ClO_4^- has possibly accumulated in this region over 6–10 million years under such hyper-arid conditions (Lybrand et al., 2016; Rao et al., 2007). ClO_4^- concentrations were 1–2 orders of magnitude higher in the Atacama Desert (average concentration of 2×10^5 $\mu g \cdot kg^{-1}$) than in other arid and semi-arid deserts such as the southwestern United States (Death Valley) and the northwestern China (Kumtag Desert) with a shorter duration of arid conditions (Pleistocene and Holocene aged deposits) (Jackson et al., 2015; Lybrand et al., 2016; Qin et al., 2012; Rao et al., 2007).

Despite the shorter accumulation time, a "bottom-up" mechanism in contrast to the primarily "top-down" mechanism in Atacama Desert was proposed for the ClO_4^- accumulation in the Death Valley and the Kumtag Desert: salts were deposited in strata through geological time and have since been redistributed and eva-concentrated into the upper soil horizons by capillary rise (Lybrand et al., 2013; Lybrand et al., 2016; Qin et al., 2012). The type of soil may also play an important role in ClO_4^- accumulation. For example, in the Death Valley, the clay-rich soil that swell during episodic rain events prevents the leaching of underlying salts, including ClO_4^- (Noble and Mansfield, 1922; Ericksen et al., 1988).

Furthermore, site-specific biological activities (e.g., plants or bacteria) can also influence ClO_4^- accumulation. Despite its high persistence in oxic environments due to large activation energies (Urbansky, 1998), ClO_4^- could be used by microorganisms as an electron acceptor under anoxic conditions; such microorganisms are ubiquitous in the environment (Coates et al., 1999; Xu et al., 2003). Perchlorate-reducing microbes are mostly facultative anaerobes, many of which appear to preferentially reduce nitrate, which generally co-occurs with ClO_4^- in soil/caliche of arid and semi-arid regions (Nozawa-Inoue et al., 2005; Jackson et al., 2015). Perchlorate could also accumulate in some plants (Andraski et al., 2014; Jackson et al., 2005a). In Atacama Desert, vegetation is absent in the majority of the area and the microbes in soils are generally several orders of magnitude less than in soils of milder deserts (Ericksen, 1981). The very low level of biological activity could be neglected and has been essential to the preservation of nitrate and perchlorate in Atacama Desert. However, in regions with more active biological processes, their influence on natural ClO_4^- concentrations cannot be neglected. In unsaturated zones of the Death Valley, losses of natural ClO_4^- have been observed and attributed to bacteria reduction and plant accumulation (Rao et al., 2007). In 2014, Andraski et al. showed that in a desert-shrub landscape of southwestern United States (Amargosa Desert), selective plant uptake and bioaccumulation were evidenced by leaf ClO_4^- concentrations and Cl^-/ClO_4^- molar ratios that were respectively about 8000 times greater and 40 times less than soil values. The authors also proposed a ClO_4^- cycle which is hypothesized to include atmospheric deposition, selective plant uptake, leaf bioaccumulation and leaf drop to the soil surface resulting in soil ClO_4^- enrichment and recycling. The topography-soil-plant-water interactions can thus locally influence the distribution of natural ClO_4^- concentrations in a desert-shrub landscape (Andraski et al., 2014).

2.1.3. Environmental release of natural perchlorate by human activities

Paleogeochemical deposits of the Atacama Desert are a rich source of naturally occurring sodium nitrate and perchlorate. These deposits have been intensively mined and exported for agricultural and industrial use. As a result, ClO_4^- present in these deposits has been widely dispersed in the environment. The first recorded exports of Chilean nitrate took place in 1830 to the USA, France, and England. In 1900, Chile provided two thirds of the fertilizer nitrogen used around the world. Afterwards, the breakout of the First World War transformed the consumption of Chilean nitrate from agricultural use toward large-scale production of gunpowder and explosives. Consequently, the production of Chilean nitrate strongly increased, with a peak production of almost 3 million tons in 1916. During the war, European countries (especially Great Britain and Germany) and the USA accounted for >97% of the Chilean nitrate market (Ericksen, 1981; Wisniak and Garcés, 2001). In the early 1930s, with the development of industrial processes for nitrogen

fixation, the production of Chilean nitrate was greatly reduced and was surpassed by synthetic nitrogen compounds. By 1950 and 1980, Chilean nitrate accounted for only 15% and 0.14%, respectively, of the world market for fixed nitrogen (Ericksen, 1983; Fram and Belitz, 2011; Rajagopalan et al., 2006). Thus, ClO_4^- contamination related to the utilization of Chilean nitrate has declined in recent decades.

In 1960, damage to crops was attributed to the ClO_4^- naturally present in Chilean saltpeter (Schumacher, 1960). In fact, ClO_4^- levels in Chilean caliche are high enough to adversely affect sensitive crops (Hunter, 2001; Susarla et al., 1999; Urbansky, 2000). In 2001, measurements showed that sodium nitrate fertilizers derived from Chilean caliche commercialized in United States contained approximately 0.5 to 2 $mg \cdot g^{-1}$ of ClO_4^- (Urbansky et al., 2001b). In 2005, a median value about 1 $mg \cdot g^{-1}$ was proposed (Dasgupta et al., 2005). In the 1990s, the refining process of Atacama fertilizers was modified to reduce ClO_4^- concentrations in NO_3^- fertilizer product to 0.1 $mg \cdot g^{-1}$ (Renner, 1999; Urbansky et al., 2001a, 2001b). Nowadays, some Chilean nitrate is still imported to the United States for limited use in organic farming of cotton, tobacco, citrus, and some vegetable crops (Aziz et al., 2006; Sanchez et al., 2006; Urbansky et al., 2001a, 2001b).

Despite the agricultural and industrial use of Chilean nitrates, natural ClO_4^- accumulating in unsaturated area can be readily flushed and mobilized by introduced percolation, especially in arid and semi-arid regions with intensive agriculture. In southwestern United States, continuous irrigation has displaced accumulated salts to depth of several meters and flushed perchlorate from unsaturated zone to groundwater (Rao et al., 2007; Scanlon et al., 2008, 2010). The influence of irrigation on the ClO_4^- groundwater contamination is fully discussed in Section 3.2.

2.2. Synthetic perchlorate

Numerous industrial processes exist for synthetic ClO_4^- production, and among them the electrolytic method using sodium chloride as feedstock is the most used (Brown and Gu, 2006; Schilt, 1979). Synthetic ClO_4^- was firstly manufactured in commercial quantities in Masebo, Sweden in the 1890s (Trumpolt et al., 2005).

The production of synthetic ClO_4^- has been a substantial industry in the United States and Europe. This industry was linked to the emergence of solid rocket fuel using NH_4ClO_4 as a propellant (Mendiratta et al., 1996). Because of its useful properties, ClO_4^- is today widely used in solid propellants, fireworks, explosives, safety flares, matches, electroplating solutions, and a few medical applications. Fireworks used by both pyrotechnic professionals and individual customers contain up to 70% potassium or NH_4ClO_4. Safety flares are used in emergency situations such as road-side accidents. The Santa Clara Valley Water District in California (USA) analyzed the contents of an unburned safety flare and it contained 50,000 $mg \cdot kg^{-1}$ of ClO_4^- and 450,000 $mg \cdot kg^{-1}$ of nitrate (Silva, 2003). The number of industrial uses of ClO_4^- may continue to expand as our understanding and awareness of its usage matures (Trumpolt et al., 2005).

ClO_4^- can also be found in numerous products as impurities. For example, it is present in sodium hypochlorite as a breakdown product and in sodium chlorate as a manufacturing by-product (Aziz et al., 2006). Sodium hypochlorite (NaOCl) is used on a large scale for surface purification, bleaching, odor removal and water disinfection. Hypochlorite solutions contain trace amounts of ClO_4^- that forms during and after manufacture (Stanford et al., 2011). Asami et al. (2009) showed that ClO_4^- concentrations in purchased sodium hypochlorite solutions ranged from 0.17 to 33,000 $\mu g \cdot L^{-1}$. Dasgupta et al. (2006) measured that freshly bought 5% and 10% hypochlorite solutions contain low levels of ClO_4^-, around 10 $\mu g \cdot L^{-1}$. However, after 6 months of aging, ClO_4^- concentration of the 5% hypochlorite solution was 3000 $\mu g \cdot L^{-1}$ and that of the 10% hypochlorite solution was twice as high. Munster (2008) measured in a fresh container of household bleach a ClO_4^- concentration of 390 $\mu g \cdot L^{-1}$ and it increased to 8000 $\mu g \cdot L^{-1}$ after two years. Thus, the ClO_4^- concentration in bleach increases with age during storage and this depends on both the initial concentration of sodium hypochlorite and the storage temperature. It has been proposed that sodium hypochlorite breaks down to form ClO_4^- most probably by the formation of chlorate from hypochlorite and then by the formation of ClO_4^- from ClO_3^- (Stanford et al., 2011). Sodium chlorate is largely used in bleaching processes at pulp and paper mills and also as defoliant/herbicide. Electrochemical production of sodium chlorate can generate ClO_4^- impurities at 50–230 $mg \cdot kg^{-1}$ ClO_3^- (Aziz et al., 2006).

3. Behaviour of perchlorate in waters

Once the chemical element is released into natural water systems, its fate depends on both the chemical and physical properties of the aqueous system. Perchlorate salts are characterized by high solubility in water, and the ClO_4^- ion is commonly observed to be stable in the environment, although it may undergo biodegradation by perchlorate-degrading anaerobic bacteria in specific environments in which significant levels of organic carbon are present and electron donors such as oxygen and nitrate are depleted (Trumpolt et al., 2005).

The movement of ClO_4^- in soil is largely dependent on the presence and circulation of water. ClO_4^- does not bind to soil particles. If sufficient infiltration occurs, the ClO_4^- may be completely leached from the soil (Trumpolt et al., 2005). Otherwise, in arid and semi-arid regions, ClO_4^- may accumulate at various horizons in the soil due to evaporation of infiltrating rainfall that leached ClO_4^- from shallower depths.

In dilute concentrations typically found in groundwater, ClO_4^- ions will migrate along the groundwater gradient toward discharge points (Clausen et al., 2004). In addition, longitudinal dispersion results in a faster moving velocity of the contaminant front than the average groundwater velocity. These observations demonstrate that the knowledge about water flow paths and aquifer properties are essential prerequisites to understanding groundwater ClO_4^- contamination.

4. Occurrence of perchlorate in natural waters

4.1. Occurrence of perchlorate due to natural sources

4.1.1. Wet and dry deposition inputs

Concentrations of ClO_4^- in rainwater have been reported in a few studies. A total of 1578 precipitation samples were collected weekly at 16 NADP sites (National Atmospheric Deposition Program) across the United States over a 3-year period from October 2004 to October 2007, indicating a range of ClO_4^- concentration in precipitation from <5 to 102 $ng \cdot L^{-1}$ (Rajagopalan et al., 2009, Table 1). In 2004, 70% of 25 precipitation samples collected in Lubbock, Texas showed the presence of ClO_4^- (Dasgupta et al., 2005, Table 1). Extreme events, especially lightning, can lead to higher concentrations. (Parker et al., 2008, Table 1).

Various concentrations of ClO_4^- have also been detected in rain samples collected in Ireland and China (Barron et al., 2006; Qin et al., 2014; Table 1). In 2005, Qin et al. also showed that ClO_4^- concentrations observed at sampling sites of urban areas were higher than those observed in rural areas, possibly due to the air pollution which is more severe and more difficult to diffuse in urban areas than in rural areas. Furthermore, where the water in the surface environment is mostly contributed by precipitation, rainwater may be an important source of ClO_4^- in surface water (Qin et al., 2014).

Measurements by Backus et al. (2005) and Poghosyan et al. (2014) demonstrated that ClO_4^- is present throughout the water of all the Great Lakes (Canada and United Sates) at low concentrations. Isotopic measurements indicated that ClO_4^- in the Great Lakes is dominantly of atmospheric origin (Poghosyan et al., 2014).

Other studies have estimated long-term average concentrations of ClO_4^- in wet deposition. Plummer et al. (2006) predicted ClO_4^- concentrations in precipitation ranging from 19 to 93 $ng \cdot L^{-1}$ based on evapotranspiration-adjusted Holocene groundwater ClO_4^- levels. Rao

Table 1
Perchlorate occurrence in waters due to natural sources (ET = Evapotranspiration).

Water type	Location	Measured ClO_4^- concentrations	ClO_4^- source	References
Rainwater	USA	1578 samples (16 sites) from <5 to 102 ng·L^{-1} Mean value = 14.1 ng·L^{-1} Site mean value from 7.3 ng·L^{-1} to 21.9 ng·L^{-1}	Atmospheric deposition	Rajagopalan et al., 2009; Dasgupta et al., 2006
Rainwater	Texas, USA	25 samples 70% contained measurable ClO_4^- (>10 ng·L^{-1}) Max value = 1.6 μg·L^{-1}	Atmospheric deposition	Dasgupta et al., 2005
Rainwater (thunderstorms)	USA	Max value = 24.4 μg·L^{-1}	Atmospheric deposition	Parker et al., 2008
Rainwater	Ireland	10 samples from <250 ng·L^{-1} to 2.8 μg·L^{-1}	Atmospheric deposition	Barron et al., 2006
Rainwater	China	From 0.35 to 27.3 μg·L^{-1} Mean value = 6.37 μg·L^{-1}	Atmospheric deposition	Qin et al., 2014
Surface water	Great Lakes, USA and Canada	From 0.05 to 0.13 μg·L^{-1}	Atmospheric deposition	Backus et al., 2005; Poghosyan et al., 2014
Groundwater for industrial use	Atacama Desert, Chile	From 1 to 10 mg·L^{-1}	Arid and semi-arid deserts	Jackson et al., 2010
Groundwater for human consumption	Atacama Desert, Chile	From 50 to 150 μg·L^{-1}	Arid and semi-arid deserts	Jackson et al., 2010
Tap water	Taltal, Chile	From 110 to 120 μg·L^{-1}	Arid and semi-arid deserts	Crump et al., 2000; Vega et al., 2018
Surface water	Atacama Desert, Chile	From 744 to 1480 μg·L^{-1}	Arid and semi-arid deserts	Calderón et al., 2014
Groundwater	Middle Rio Grande Basin, New Mexico, USA	From 0.12 to 1.8 μg·L^{-1}	Arid and semi-arid deserts	Plummer et al., 2006
Groundwater	Southern High Plains, USA	Max value = 200 μg·L^{-1}	Atmospheric deposition and ET enrichment/irrigation	Böhlke et al., 2005; Jackson et al., 2005b; Rajagopalan et al., 2006; Rao et al., 2007; Scanlon et al., 2010

et al. (2007) estimated ClO_4^- concentrations in precipitation ranging from 3 to 23 ng·L^{-1} with an overall mean of 9 ng·L^{-1} based on natural ClO_4^- reservoirs present in unsaturated zones of the arid and semi-arid southwestern United States.

4.1.2. Arid and semi-arid deserts

The perchlorate-rich geological formations could lead to enrichment of ClO_4^- in surface water and in groundwater during infiltration. Crump et al. (2000) reported ClO_4^- concentrations in groundwater near nitrate deposits in the Atacama Desert at high concentrations up to 10 mg·L^{-1} (Table 1). ClO_4^- concentrations in tap water from several cities in Chile were also measured, indicating levels much higher than the US EPA or European recommendations for potable water (Crump et al., 2000; Vega et al., 2018; Table 1). In northern Chile (Atacama desert), high levels of ClO_4^- in surface water were attributed to natural nitrate deposits (Calderón et al., 2014, Table 1).

Unsaturated zones of the arid and semi-arid southwestern United States are an important source of ClO_4^- contamination in groundwater (Jackson et al., 2005b; Parker et al., 2008; Rajagopalan et al., 2006; Rao et al., 2007). ClO_4^- has been measured in pre-anthropogenic groundwater from upstream parts in the Middle Rio Grande Basin of North-Central New Mexico and attributed to be from natural deposition (Plummer et al., 2006; Table 1). Geographically extensive elevated ClO_4^- has also been reported in groundwater in the High Plains of Texas, New Mexico, which has been attributed mainly to atmospheric ClO_4^- accumulation in the unsaturated zone (Rajagopalan et al., 2006; Table 1). Natural occurrence of ClO_4^- has also been reported in some other parts of the Southwest United States (Rao et al., 2007; Table 1).

4.2. Water contamination by anthropogenic activities

4.2.1. Chilean nitrate fertilizer

As noted above, Chilean nitrate fertilizer can contain high quantities of ClO_4^-. It was intensively used in agriculture, leading to the dissemination of natural ClO_4^- in the environment. A metric ton of imported Chilean nitrate could yield as much as $150 \cdot 10^6$ to $1300 \cdot 10^6$ L of water with 6 μg·L^{-1} of ClO_4^- (Böhlke et al., 2005).

In 2005, ClO_4^- contamination detected in groundwater of southern California (up to 12 μg·L^{-1}) and northern New Jersey (25.9 μg·L^{-1}) with similar isotopic composition to Atacama ClO_4^- was suspected to be derived from the use of Chilean nitrate fertilizer (Böhlke et al., 2005). ClO_4^- in groundwater from the southern High Plains in west Texas was attributed to either a natural source that is isotopically distinct from Atacama ClO_4^-, or mixture of synthetic (~90%) and Atacama (~10%) ClO_4^- that had been substantially biodegraded (Böhlke et al., 2005). ClO_4^- contamination of groundwater from some agricultural areas in Long Island has also been attributed to Chilean fertilizer use (Böhlke et al., 2009). ClO_4^- contamination in groundwater of southeastern San Bernardino Basin in southern California, with concentrations ranging from 2.5 to 99 μg·L^{-1} was partly attributed to Chilean fertilizer along with a likely component of indigenous natural ClO_4^- (Sturchio et al., 2012). Evaluation of mixing proportions of ClO_4^- present in groundwater of Pomona, California (from 2.5 to 11 μg·L^{-1}) indicated that contamination is dominantly (85–89%) Atacama ClO_4^- derived from the past use of imported Chilean nitrate fertilizer in citrus cultivation (Sturchio et al., 2014).

Recent research carried out by Mastrocicco et al. (2017) indicates ClO_4^- contamination in groundwater of the Po River Delta plain in Italy, which the authors supposed to be derived from Chilean nitrate fertilizer. Moreover, chlorate detected in same water samples was suggested to be a result of ClO_4^- degradation by anaerobic bacteria under low oxygen reduction potential (ORP) conditions in groundwater.

4.2.2. Solid propellant and military usages

Water contamination from solid propellant is often linked with military activities. ClO_4^- diffusion in water from this usage can be related to the manufacturing of the products as well as their use in training sites or in conflict areas.

Camp Edwards located within the Massachusetts Military Reservation near Falmouth (USA) is a good example of ClO_4^- contamination owning to military activities (Table 2). Training activities at Camp

Table 2
Principal water contamination from anthropogenic activities.

Uses	Compounds	Reported risk	References
Chilean nitrates used as natural fertilizer in agriculture	$NaClO_4$ $KClO_4$	Use	Böhlke et al., 2005, 2009; Cao et al., 2018; Hatzinger et al., 2018; Jackson et al., 2005b; Mastrocicco et al., 2017; Sturchio et al., 2012, 2014
Solid propellant and military usages/aerospace industry/commercial explosives	$NaClO_4$, NH_4ClO_4, $KClO_4$	Manufacturing, disposal, missile recycling, historical buried rockets	Bausinger et al., 2007; Böhlke et al., 2005; Clausen et al., 2004; Hubé, 2014, 2017; Hatzinger et al., 2018; Hubé and Bausinger, 2013; Izbicki et al., 2014; Mass, 2005; Mohr, 2007; Ricour, 2013; Sturchio et al., 2012; Tan et al., 2005
Fireworks and emergency and signal flares	$KClO_4$, NH_4ClO_4	Manufacturing, use	Aziz et al., 2006; Backus et al., 2005; Isobe et al., 2013; Mass, 2005; Munster and Hanson, 2009; Munster et al., 2009; Sijimol and Mohan, 2014; Silva, 2003; Vella et al., 2015; Wilkin et al., 2007; Wu et al., 2011; Ye et al., 2013
Industrial manufacturing and uses (airbag inflators, additives in oils, electroplating, tuber manufacturing…)	$NaClO_4$, NH_4ClO_4, $KClO_4$, $HClO_4$	Manufacturing, disposal, use	Böhlke et al., 2005; Fram and Belitz, 2011; Gal et al., 2009; Izbicki et al., 2014
Water and wastewater treatment and domestic detergents	ClO_4 derived from NaOCl	Storage, use	Aranda-Rodriguez et al., 2017; Her et al., 2011; Mass, 2005; Qin et al., 2014; Shi et al., 2007

Edwards are typical of most military ranges, and it can be used as a model for future military ranges studies (Clausen et al., 2004). The impact area contains artillery and mortar targets that have been used for training activities since 1911, with the highest frequency of use during World War II. ClO_4^- is largely present at the site scale, with concentrations up to 174 $\mu g \cdot L^{-1}$. The conceptual model realized in the hydrological system of Camp Edwards shows that ClO_4^- is principally found at burn and detonation sites (Clausen et al., 2004). There is also evidence that the use of artillery and mortar spotting charges containing ClO_4^- can contribute to groundwater contamination.

The First World War battlefields of Verdun (France) served as the destruction site of German ammunition deposits in the 1920s. Groundwater at this site has elevated ClO_4^-, and concentrations up to 800 $\mu g \cdot L^{-1}$ have been measured in leachate samples (Bausinger et al., 2007; Ricour, 2013; Table 2). Widespread ClO_4^- contamination of groundwater related to the First World War is suspected in France at regional scale along or near the former front line, which is probably linked with perchlorate-bearing explosives left on battlefields and/or on ammunition destruction sites (Hubé, 2017). ClO_4^- present in ammunition during the First World War could be derived from either Chilean nitrate or synthetic ClO_4^-. Further research is being conducted to confirm the sources of ClO_4^- and to assess the related environmental and human health risks (Cao et al., 2018).

4.2.3. Fireworks and road flares

ClO_4^- salts of potassium and ammonium are the primary oxidants in pyrotechnic mixtures, and there have been numerous studies of the contamination of surface and groundwater by ClO_4^- residue from firework displays, especially those launched near or over surface waters (Table 2). ClO_4^- contamination in surface water samples in Harbour (Canada) was measured 4 days after a firework display (Backus et al., 2005). At the same site, ClO_4^- was not detected a week later. A fireworks display at a lake in Oklahoma (USA) led to ClO_4^- concentrations in surface water ranging from 24 to 1028 times the mean baseline value, with a maximum concentration of 44.2 $\mu g \cdot L^{-1}$ following the July 4th event in 2006 (Wilkin et al., 2007). Authors observed a rapid disappearance of ClO_4^- in the lake waters following the fireworks display, with return to the baseline value after 10 to over 70 days, due to biodegradation and flushing. From 2008 to 2010, the fate of ClO_4^- in a man-made reflecting pond in New York (USA) was monitored following a firework display. ClO_4^- levels in pond water increased significantly, with concentrations ranging from 0.11 to 519 $\mu g \cdot L^{-1}$ following the fireworks display. ClO_4^- concentrations in pond water then decreased with an average half-life of 29 days (Wu et al., 2011).

In addition to surface water contamination, Munster et al. (2009) showed that total atmospheric deposition can strongly increase following a fireworks display (Table 2), with measured concentrations of ClO_4^- in precipitation after the July 4th fireworks 18 times above the background level on Long Island in the United States. In China, a seasonal study of ClO_4^- concentrations in snow and surface soil concluded that the contamination comes mainly from the fireworks display of an annual festival (Ye et al., 2013; Table 2). In Malta, Vella et al. (2015) detected ClO_4^- in 108 of 153 samples of dust fall (71%) and in 28 of 37 indoor dust samples (76%) with concentrations ranging from 0.52 to 561 $\mu g \cdot L^{-1}$, derived exclusively from fireworks. A recent review of environmental ClO_4^- occurrence from fireworks identified the use of fireworks as one of the main contributors of ClO_4^- contamination and focused on the lack of knowledge on this issue (Sijimol and Mohan, 2014; Table 2).

Preliminary research on road flares of the Santa Clara Valley Water District (USA) suggested that each unburned and burned flare could leach 3.6 g and 1.9 mg of ClO_4^-, respectively (Silva, 2003). It is estimated that the ClO_4^- leached from a single unburned, damaged road flare can potentially contaminate approximately 2700 m^3 of drinking water with concentrations above 4 $\mu g \cdot L^{-1}$ (Silva, 2003). The role of road flares, especially partially burnt ones, in ClO_4^- contamination of water has also been highlighted by Munster and Hanson (2009). In areas with high occurrence of traffic incidents, 10% of the road runoff samples have ClO_4^- concentration above 5 $\mu g \cdot L^{-1}$ (Table 2).

4.2.4. Domestic detergents and water - wastewater treatment

Hypochlorite solutions are known to contain trace amounts of ClO_4^-, therefore when hypochlorite is used in the water treatment process ClO_4^- may subsequently be found in drinking water. Aranda-Rodriguez et al. (2017) detected ClO_4^- (between 0.06 and 5.7 $\mu g \cdot L^{-1}$) in treated water from Canadian drinking water treatment plants that use hypochlorite as a disinfectant.

Qin et al. (2014) observed ClO_4^- concentrations ranging from <0.09 to 1.05 $\mu g \cdot L^{-1}$ in treated wastewater effluent in China (Table 2). Shi et al. (2007) sampled 31 sewage sludges from different sewage plants in across China. ClO_4^- was detected in all samples with concentrations up to 379.9 $\mu g \cdot kg^{-1}$ and an average concentration about 21.7 $\mu g \cdot kg^{-1}$. Her et al. (2011) also measured ClO_4^- in coastal water samples in South Korea with concentrations up to 6.11 $\mu g \cdot L^{-1}$, attributed to runoff of wastewater effluents.

4.2.5. Manufacturing

The contamination of water linked to the use of ClO_4^- containing products is of high importance, but past and present manufacturing sites of these products are also sources of strong environmental risks. Tan et al. (2005) reported ClO_4^- contamination of groundwater, stream water (up to 400 $\mu g \cdot L^{-1}$), and sediment pore water (up to 30 $\mu g \cdot L^{-1}$) in Texas (USA), attributed to a solid fuel rocket motor manufacture that closed in 1995 (Table 2). Several streams far from this study site have been contaminated by groundwater or seepages containing ClO_4^- from the plant. In South India, ClO_4^- concentrations in groundwater, surface water, and tap water have been measured (up to 7.7 $\mu g \cdot L^{-1}$, 30.2 $\mu g \cdot L^{-1}$ and 0.4 $\mu g \cdot L^{-1}$, respectively) in and around a fireworks factory (Isobe et al., 2013; Table 2). These authors demonstrated that the fireworks industry is the principal source of the water contamination.

In China, Wu et al. (2010) measured ClO_4^- concentrations as high as 54.4 μg·L^{-1} in surface water samples around a fireworks manufacturing site.

Another example is a plant in Israel that has manufactured NH_4ClO_4 for 25 years (Gal et al., 2009). Untreated wastewater was disposed in four infiltration ponds, causing extensive contamination of the underlying aquifer with measured ClO_4^- concentrations up to 35,000 mg·L^{-1} for pore water and up to 412 mg·L^{-1} for groundwater. In France, Negrel et al. (2017) showed high concentrations of ClO_4^- (>400 mg·L^{-1}) in groundwater at an industrial site used for electrochemical production of ClO_3^- and ClO_4^-. Stable isotope analyses of water gave evidence of leakage from end-product storage and the accumulation and release of ClO_4^- from soil.

Although ClO_4^- is highly soluble and mobile in waters, Flowers and Hunt (2007) showed that a point source release of highly concentrated brine solutions can influence ClO_4^- concentrations in groundwater for a long period (>100 years). Indeed, because of the density of the brine, it may move vertically in groundwater. On the top of confining layers, ClO_4^- may physically migrate into low permeability layers from where it may be continuously released to the groundwater by diffusion. This type of release may occur at industrial sites where ClO_4^- is handled in concentrated brines.

4.2.6. Irrigation impact

The natural geochemical cycle of ClO_4^- can be strongly affected by irrigation activities, especially in agricultural areas located in semi-arid or arid regions. If there is substantial accumulation of natural ClO_4^- in the unsaturated zone, ClO_4^- concentration may rapidly increase in groundwater where artificial recharge from irrigation exceeds that from precipitation. This impact can be summarized in terms of three major components: 1) irrigation can lead to the flushing of atmospherically deposited ClO_4^- from the unsaturated zone into groundwater (Fram and Belitz, 2011; Rajagopalan et al., 2006); 2) in case of an intensively used aquifer, the volume of groundwater impacts the capacity to dilute or assimilate salts introduced from the unsaturated zone, with salinity increasing linearly as aquifer saturated thickness decreases (Scanlon et al., 2010); and 3) the evaporative concentration effect can be strongly increased due to multiple irrigation and return flow cycles which will heighten the annual enrichment factor (Rajagopalan et al., 2006; Rao et al., 2007).

In arid and semi-arid regions, in the case of a closed-basin aquifer used for irrigation, the groundwater quality is expected to degrade over time if the water inflows are mainly by irrigation pumping. For example, in the High Plains of Texas, total dissolved solids are projected to increase in coming decades by an additional 2200 mg·L^{-1}, SO_4^{2-} by 880 mg·L^{-1}, NO_3^- by 230 mg·L^{-1} and ClO_4^- by 21 μg·L^{-1} (Scanlon et al., 2010).

5. Assessment of perchlorate origin

5.1. Stable isotopic composition of perchlorate

Since the early 2000s, methods of stable isotope analysis have been developed to differentiate natural and synthetic ClO_4^-. ClO_4^- is a non-labile oxyanion and once formed, its oxygen atoms do not exchange with those of the ambient environment over many decades. Therefore, the isotopic composition obtained when the ClO_4^- ion forms is retained as it is transported through the environment. Oxygen isotope ratios are reported as follows:

$$\delta^{18}O\ (‰) = \left[\left(\frac{^{18}O}{^{16}O}\right)\text{sample} - \left(\frac{^{18}O}{^{16}O}\right)\text{VSMOW} - 1\right] \times 1000 \quad (1)$$

$$\delta^{17}O\ (‰) = \left[\left(\frac{^{17}O}{^{16}O}\right)\text{sample} - \left(\frac{^{17}O}{^{16}O}\right)\text{VSMOW} - 1\right] \times 1000 \quad (2)$$

where VSMOW is the Vienna Standard Mean Ocean Water isotopic reference material. For normal terrestrial oxygen, $\delta^{18}O$ and $\delta^{17}O$ values are correlated according to the following mass-dependent relationship (Young et al., 2002):

$$\delta^{17}O \approx 0.52 \times \delta^{18}O \quad (3)$$

Based on this relation, natural and synthetic ClO_4^- may be differentiated through the calculation of the deviation of $\delta^{17}O$ value from the terrestrial fractionation line (Eq. 3) by:

$$\Delta^{17}O = \delta^{17}O - 0.52 \times \delta^{18}O \quad (4)$$

Several authors have reported isotopic compositions of natural ClO_4^-, and all have significantly positive $\Delta^{17}O$ values. The first measurements of the isotopic composition of oxygen in synthetic and Atacama ClO_4^- were reported by Bao and Gu (2004), who found that $\delta^{18}O$ values of synthetic ClO_4^- were −18.4 ± 1.2‰, whereas those of Atacama Desert ClO_4^- ranged from −24.8‰ to −4.5‰, and Atacama ClO_4^- is enriched in ^{17}O (+4.2‰ < $\Delta^{17}O$ < +10.5‰, Fig. 1). The ^{17}O enrichment observed in Atacama ClO_4^- was attributed to its production in the upper atmosphere by reactions involving ozone (Bao and Gu, 2004). Other stable isotope data for oxygen in synthetic ClO_4^- have been published subsequently, showing that values of $\delta^{18}O$ in synthetic ClO_4^- range from −24.8‰ to −12.3‰ and its $\Delta^{17}O$ value is always 0.0 ± 0.2‰ (Böhlke et al., 2005; Sturchio et al., 2011; Fig. 1). Oxygen in synthetic ClO_4^- is derived from the water used in its production by an electrochemical process, which results in mass-dependent fractionation with $\Delta^{17}O \sim 0$ (Böhlke et al., 2017; Sturchio et al., 2006; Fig. 1).

Systematic differences in Cl stable isotope ratios of synthetic and natural ClO_4^- are also observed. The $\delta^{37}Cl$ values of synthetic ClO_4^- were first reported by Ader et al. (2001), Böhlke et al. (2005), and Sturchio et al. (2006), ranging from −5.0 to +2.3‰. In natural ClO_4^- from Chilean Atacama Desert, reported $\delta^{37}Cl$ values are extremely negative, ranging from −14.5‰ to −9.2‰ (Böhlke et al., 2005; Sturchio et al., 2006; Jackson et al., 2010).

Other than natural ClO_4^- from the Atacama Desert, which is as a well-known natural occurrence of this ion, other indigenous natural

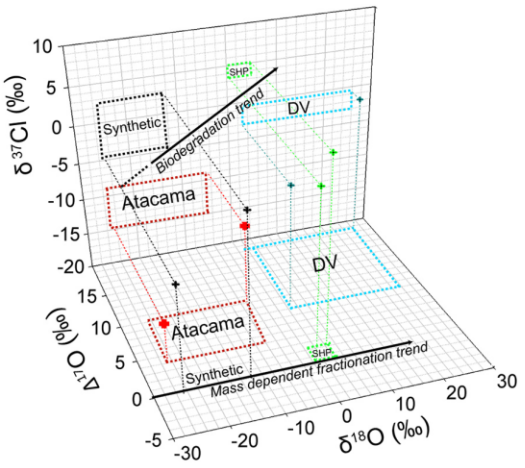

Fig. 1. Diagram showing the isotopic signature ($\delta^{37}Cl$, $\Delta^{17}O$ and $\delta^{18}O$) of ClO_4^- in synthetic, Atacama, Death Valley (California) (DV) and Southern High Plain (Texas) (SHP) samples from data published in peer-reviewed literature. Arrow in the $\delta^{37}Cl$ vs $\delta^{18}O$ graph represent the direction of biodegradation ($\delta^{37}Cl = 0.4\ \delta^{18}O$) and arrow in the $\Delta^{17}O$ vs $\delta^{18}O$ graph represent the direction of mass dependent fractionation. Dashed boxes represents the maximum range of isotopic signature of the different sources, established through all the data published. (Ader et al., 2001; Bao and Gu, 2004; Böhlke et al., 2005, 2009; Jackson et al., 2005b, 2010; Parker et al., 2008; Plummer et al., 2006; Rajagopalan et al., 2006; Rao et al., 2007; Sturchio et al., 2007, 2011)

deposits of ClO_4^- have been observed especially in the arid southwestern United States, including the Southern High Plains (Texas) and near Death Valley (California) (Jackson et al., 2005b; Plummer et al., 2006; Rajagopalan et al., 2006; Rao et al., 2007). While the Atacama Desert ClO_4^- has a relatively well documented isotopic composition, relatively few studies have been done to discriminate other indigenous natural ClO_4^- sources through isotopic measurements because of the difficulties involved in sample collection and processing (Sturchio et al., 2011). ClO_4^- from the Southern High Plains has $\Delta^{17}O$ values ranging from +0.2‰ to +2.6‰, $\delta^{18}O$ values from +0.5‰ to +5.1‰. The isotopic composition of the Death Valley ClO_4^- is somewhat different with $\Delta^{17}O$, $\delta^{18}O$ and $\delta^{37}Cl$ values ranging from +8.6‰ to +18.4‰, +2.9 to +26.1‰ and − 3.1‰ to −0.8‰ respectively (Fig. 1).

The reason for such a wide range values of $\delta^{37}Cl$ in natural ClO_4^- is still not well understood, but it may be related to regional or hemispheric differences in the source of atmospheric Cl^- or to the mechanism involved in ClO_4^- production. The range of $\Delta^{17}O$ values in natural ClO_4^- could be explained by regional differences in climate and the mode of ClO_4^- formation, as well as possible slow oxygen isotope exchange or abiotic degradation, as the values for Southern High Plains are mostly from groundwater samples and those from Death Valley are from unsaturated zone (Sturchio et al., 2011). Samples from the Great Lakes waters have similar ClO_4^- isotopic compositions to those of SW United States groundwaters, which may indicate that this is a typical isotopic composition of indigenous natural ClO_4^- across midcontinent North America. Despite such remaining uncertainty, forensics studies have successfully used ClO_4^- isotopic date to identify the sources of contamination and mixing fractions in mixed ClO_4^- plumes (Böhlke et al., 2005, 2009; Hatzinger et al., 2018; Jackson et al., 2010; Poghosyan et al., 2014; Sturchio et al., 2011, 2012, 2014).

5.2. Isotopic fractionation during biodegradation

Numerous studies have demonstrated that ClO_4^- can be metabolized by perchlorate-reducing bacteria (PCRB) (Ader et al., 2008; Attaway and Smith, 1993; Coates and Achenbach, 2004; Coates et al., 1999; Hatzinger et al., 2009; Stroo et al., 2009; Wallace et al., 1996; Xu et al., 2015). These organisms could be responsible for ClO_4^- degradation in natural waters using ClO_4^- as an electron acceptor in anoxic environments. They present a high potential for in situ bioremediation of ClO_4^- contaminated sites. Numerous laboratory and field studies show isotopic fractionation of ClO_4^- during its degradation. The first studies on the kinetic isotopic fractionation of Cl in ClO_4^- resulting from microbial respiration were those of Coleman et al. (2003) and Sturchio et al. (2003). Beside demonstrating temperature-dependent degradation kinetics (the ClO_4^- reduction was nearly complete in about 90 min at 37 °C and in 5.5 h to 18 days at 22 °C), they showed that $^{35}Cl_{ClO_4}$ reduction was faster than that of $^{37}Cl_{ClO_4}$. Reported isotopic fractionation factors for chloride relative to ClO_4^- were between −16.6‰ and −12.9‰ at 22 °C (Sturchio et al., 2003) and between −15.8 ± 0.4‰ and −14.8 ± 0.7‰ at 37 °C (Coleman et al., 2003). A statistical re-evaluation of the Coleman et al. (2003) experimental data set of $\delta^{37}Cl$ values of chloride gave a value of Cl isotopic fractionation factor of −14.94 ± 0.15‰ during biodegradation, with fractionation factor remaining constant during the reaction (Ader et al., 2008). These studies also indicate that fractionation is not sensitive to the ClO_4^- concentration in the basal medium, nor to the rate of ClO_4^- reduction. The relationship between chloride concentration and Cl isotope ratio follows a Rayleigh distillation model (Ader et al., 2008). Subsequent studies produced data on both oxygen and chlorine isotopic fractionation during ClO_4^- biodegradation, using two different bacterial genera in cultures at temperatures of 22 °C and 10 °C (Sturchio et al., 2007). The data obtained from these laboratory experiments showed Cl and O fractionation factors of −13.2 ± 0.5‰ and −33.1 ± 1.2‰ respectively, with no evidence of dependence on bacterial strain or temperature. This work also showed negligible O isotope exchange between ClO_4^- and water during microbial reduction and a fractionation factor ratio ($\varepsilon^{18}O/\varepsilon^{37}Cl$) with a constant value about 2.50 ± 0.04 (Fig. 1). This last result was confirmed in a field study where biodegradation of a groundwater ClO_4^- plume was enhanced by injection of emulsified soybean oil and the isotopic compositions of partly reduced ClO_4^- yielded a $\varepsilon^{18}O/\varepsilon^{37}Cl$ ratio of ~2.63 (Hatzinger et al., 2009). Knowledge of the isotope effects of ClO_4^- biodegradation is of primary importance in forensic studies of ClO_4^- origin and behavior in the environment, as it can provide a test of the microbial reduction hypothesis in field-based ClO_4^- isotopic data sets as well as setting a constraint on the initial isotopic composition of partially biodegraded ClO_4^- (Jackson et al., 2010; Poghosyan et al., 2014; Sturchio et al., 2014).

5.3. ^{36}Cl as an additional tracer

Radioactive ^{36}Cl (half-life = 301,000 years) is an additional tracer that can be used for distinguishing ClO_4^- sources. Natural atmospheric production of ^{36}Cl occurs due to activation of atmospheric Ar by cosmic-ray spallation reactions and is deposited at Earth's surface as dry fallout or in precipitation (Lehmann et al., 1993). It is also produced in situ by cosmic-ray induced reactions of ^{35}Cl, K and Ca within the upper few meters of the land surface (Clark and Fritz, 1997). Natural ^{36}Cl production and fallout varies with latitude from close to 20 atoms.m^{-2} at mid latitudes to <5 atoms.m^{-2} near the equator and poles (Clark and Fritz, 1997). Testing of thermonuclear bombs at oceanic sites in the 1950s also injected a large amount of ^{36}Cl into the stratosphere, resulting in worldwide fallout for several years after (Phillips, 2000). The presence of this bomb pulse ^{36}Cl in dissolved chloride of water may be identified from its anomalously high $^{36}Cl/Cl$ ratio and its association with relatively high ^{3}H activity. Consequently, ^{36}Cl isotopic abundance can be used to identify modern groundwater, analogous to the way elevated ^{3}H is used as an indicator of post-bomb recharge. The washing out of atmospheric Cl^- has brought $^{36}Cl/Cl$ ratios in precipitation back to near-natural levels since about 1980.

In 2009, ^{36}Cl abundance and $^{36}Cl/Cl$ ratio were measured in ClO_4^- of 35 samples chosen to represent the principal known sources of ClO_4^- in the environment: synthetic, natural from Atacama Desert and natural from southwestern United States (Sturchio et al., 2009). The ranges of $^{36}Cl/Cl$ ratio and $\delta^{37}Cl$ from this study are summarized in Table 3.

Synthetic ClO_4^- samples have the lowest $^{36}Cl/Cl$ ratios, reflecting the NaCl sources used in the manufacturing process. Conversely, SW United States samples have extremely high $^{36}Cl/Cl$ ratios. The presence of 1950s nuclear ^{36}Cl may be present in the ClO_4^- extracted from some of these groundwater samples. Nevertheless, the absence of tritium in most of these groundwaters indicates pre-bomb recharge. Thus, a largely stratospheric source of ClO_4^- was indicated (Sturchio et al., 2009), because there is no other viable explanation for the elevated ^{36}Cl abundance, and it is also consistent with the elevated ^{17}O abundance found in natural ClO_4^-. Atacama ClO_4^- samples have intermediate ranges of $^{36}Cl/Cl$ ratios, which may be interpreted as initially high $^{36}Cl/Cl$ ratios (similar to those from the SW United States) that decreased by radioactive decay (Sturchio et al., 2009).

Chlorine-36 as a tracer of the source of ClO_4^- in the environment has been applied in the waters of the Great Lakes (United States and Canada), as well as in groundwater around the large Rialto-Colton ClO_4^- plume in SE San Bernardino County, CA. In addition to $\delta^{18}O$,

Table 3
$^{36}Cl/Cl$ ratio and $\delta^{37}Cl$ in synthetic and natural (from Atacama and SW United States) perchlorates (Sturchio et al., 2009).

	$^{36}Cl/Cl$ ($\times 10^{-5}$)		$\delta^{37}Cl$ (‰)	
	Min	Max	Min	Max
Synthetic reagents ($n = 16$)	0	40	−5	2.3
Atacama ($n = 10$)	0.9	590	−14.5	−9.2
United States ($n = 8$)	3130	28800	−3.1	5.1

$\Delta^{17}O$ and $\delta^{37}Cl$, the ^{36}Cl abundances of ClO_4^- from Great Lakes water samples were used to trace ClO_4^- (0.05 $\mu g \cdot L^{-1}$ to 0.13 $\mu g \cdot L^{-1}$) origin in these hydrological systems (Poghosyan et al., 2014). This multitracer study indicated that the principal source of ClO_4^- in the Great Lakes is natural ClO_4^- origin from atmospheric deposition and identified a substantial fraction of ClO_4^- in these lakes was deposited during the peak of atmospheric ^{36}Cl abundance following the Pacific thermonuclear bomb tests in the 1950s.

Additional data are still needed and a better knowledge and comprehension of ^{36}Cl natural formation and behavior will be useful for the interpretation of $^{36}Cl/Cl$ ratios of ClO_4^-. Nevertheless, the isotopic abundance of ^{36}Cl in ClO_4^- appears to be a promising supplementary tracer than can greatly improve forensics studies on the origin of ClO_4^-. It is a particularly sensitive indicator of the presence of trace amounts of indigenous natural ClO_4^- in the case of mixed-source samples (e.g., Hatzinger et al., 2018).

5.4. Limits of perchlorate isotope forensics

Over the past few decades, the evolution of research on stable and radiogenic isotopes of ClO_4^- has provided important tools for studying ClO_4^- origin. Despite progress in methodology and increase in available data on the isotopic composition of ClO_4^-, some limits still need to be considered.

The first is related to the paucity of ClO_4^- isotope studies from different sources, including natural and synthetic ones. Due to the existence of natural ClO_4^- around the world, further studies on these occurrences and their isotopic compositions are recommended. The full range of natural ClO_4^- sources may not be represented in Fig. 1. Fractionation that occurs during biodegradation could lead to misinterpretation of analytical results. The article, comments, and reply published by Sturchio et al. (2014), Bennett (2015), and Sturchio (2015) illustrated the limitations of isotope forensics analysis for ClO_4^- origin determination. Based on isotopic analyses of ClO_4^-, hydrogeological background, numerical modeling, and aerial photography archives, Sturchio et al. (2014) and Sturchio (2015) explained the ClO_4^- occurrence in groundwater of Ponoma (California) to be a result mainly of the past use of imported Chilean nitrate fertilizer in citrus groves. However, Bennett (2015) argued that indigenous natural sources might explain the ClO_4^- concentration in Ponoma groundwater, and that more isotopic data on indigenous ClO_4^- of this region are needed to conclude whether the groundwater ClO_4^- is mainly from Chilean nitrate fertilizer or if it could be mainly indigenous natural ClO_4^-. Bennett (2015) specifically suggested measuring ^{36}Cl as a means by which to resolve the question in this case. In response, Sturchio (2015) presented archived ^{36}Cl data obtained for ClO_4^- from one of the Pomona wells, and from another well in the adjacent city, that were both consistent with a Chilean fertilizer source. This discussion emphasizes that in forensic analysis of ClO_4^- origin based on isotopic analysis, knowledge of hydrological settings and historical land-use data are necessary but not always sufficient to give indisputable conclusions. Multiple isotope ratio measurements of ClO_4^- are needed to best resolve its origin, geographic distribution, and possible mixing relationships or biodegradation. In the future, more geographically-widespread isotopic analyses of indigenous natural ClO_4^- may lead to more robust forensic results.

6. Perchlorate contamination of water: a worldwide phenomenon

6.1. Example of the French case

The French case illustrates the growing recognition of ClO_4^- contamination in groundwater. In 2009 and 2010, some aquifers of SW and NE France showed ClO_4^- contamination of municipal water supplies at concentrations exceeding 4 $\mu g \cdot L^{-1}$. Based on these observations, a national sampling campaign was conducted by the Regional Health Agencies (Agences Régionales pour la Santé; ARS), with 300 raw and treated water samples evenly distributed across France supplying 20 to 25% of the population. In addition, 87 supplementary sites were selected by the Professional Federation of Water Enterprises (Fédération Professionnelle des Entreprises de l'Eau, FP2E). These additional samples were selected for their vulnerability to ClO_4^- contamination considering nearby industrial activities, land use, and past military activities. Of these additional samples, 62% came from groundwater, 37% from surface water and 1% from sea water or mixed water (ANSES, 2013). Of the >300 water samples analyzed to date, 75% had ClO_4^- concentrations <0.5 $\mu g \cdot L^{-1}$ (limit of detection), 2% were between 4 $\mu g \cdot L^{-1}$ and 15 $\mu g \cdot L^{-1}$, and 1% had concentrations above 15 $\mu g \cdot L^{-1}$ with a maximum of about 22 $\mu g \cdot L^{-1}$.

In France, three potential sources of ClO_4^- contamination are suspected: industrial, military sources related to WWI and agricultural. First, 4000 t/y of NH_4ClO_4 are produced in southwestern France and numerous French plants use ClO_4^- in their manufacturing processes (fireworks manufacturing, armament material, car safety, construction activities; INERIS, 2014). Since 1977, 65 incidents involving ClO_4^- uses and release of hazardous materials have been recorded in metropolitan France (ARIA Database, 2018). Second, both Chilean nitrates and synthetic ClO_4^- were used for manufacturing of ammunition during the First World War. During the period from November 1915 to November 1916, 2,940,000 t of Chilean nitrate was used for military purposes throughout 140 manufacturing sites in NE France (Hubé, 2014). Thus, there is a potential link between high ClO_4^- concentrations in groundwater from NE France and the position of the front line in this area between 1914 and 1918. This hypothesis is supported by numerous French reports and national publications (Cao et al., 2018; Hubé, 2016; Hubé and Bausinger, 2013; Hubé and Urban, 2013; Lopez et al., 2014; Ricour, 2013). However, this hypothesis is only based on the geographical similarity between ClO_4^- plume occurrences and historical records of conflict areas. More hydrogeological investigations (hydrodynamic investigations, groundwater age data and numerical modeling) are necessary to confirm this hypothesis. Isotopic analysis on ClO_4^- could also afford a way to distinguish different sources of ClO_4^- present in groundwaters of NE France. Finally, between 1875 and 1920, large quantities of Chilean nitrates were used as fertilizers in France, which contributed another potential source of ClO_4^- contamination. In fact, France imported large quantities of Chilean nitrates for use both as fertilizer and for the production of ammunition. In 1899 and 1929, the consumption of Chilean nitrate was 150,000 t and 413,000 t respectively.

6.2. Evidence and perspectives

Interest in ClO_4^- has increased significantly since the discovery of ClO_4^- contamination in potable water supplies of 7 counties of California and Nevada at levels up to 16 $\mu g \cdot L^{-1}$ in 1997. Since the 1990s, 72 peer-reviewed case studies in the natural environment have been listed (Scopus research conducted in September 2018), including natural occurrences and anthropogenic contamination in waters all over the world. Significant geographic differences are observed (Fig. 2); 43% of these studies were conducted in the USA (51% in USA and Canada).

The lack of scientific research on ClO_4^- occurrence in many parts of the world does not mean that ClO_4^- is absent. Jackson et al. (2015) reported a global survey of ClO_4^- in water and soil samples that included data from Antarctica, Namibia, United Arab Emirates, and South Africa that were thought to be of natural origin based on their elevated concentrations and remote locations in hyper-arid desert environments. Arid environments like those of the Atacama Desert (hyper-arid), Death Valley and the southern High Plains (semi-arid) can be found on all continents and it seems likely that elevated concentrations of natural indigenous ClO_4^- will eventually be found at such locations.

In addition, the industrial production and use of ClO_4^- are expected to increase in decades to come. The current production of ClO_4^- is difficult to estimate because of its strategic status in military and aerospace applications. Regarding the results observed in USA and in Asia, systematic surveys seem essential in areas of past and current production and

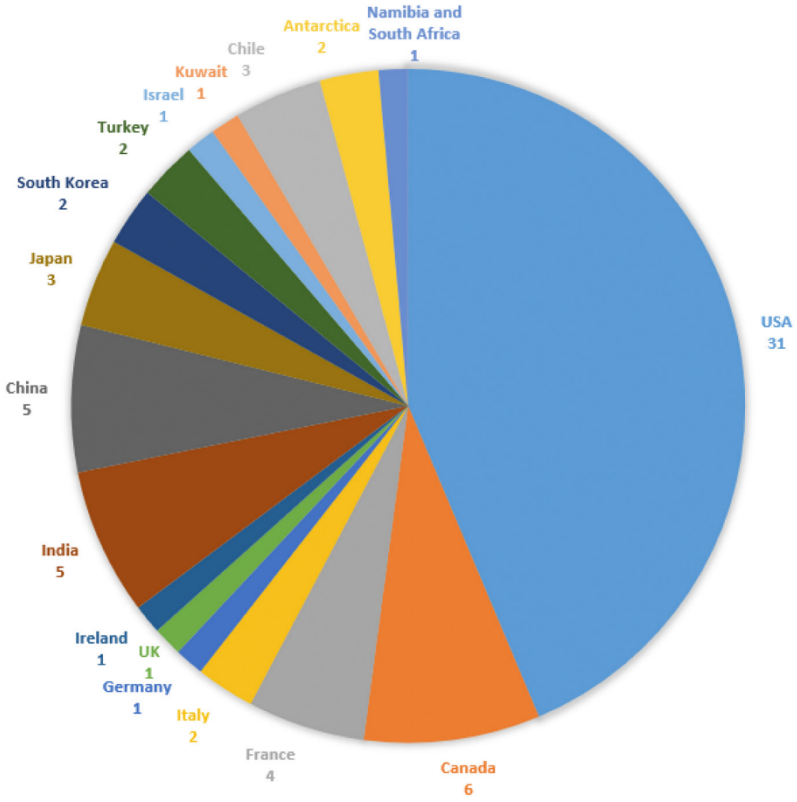

Fig. 2. Number of peer-reviewed publications (total = 72) dealing with perchlorate contamination of water (occurrence, natural biodegradation, source determination, field remediation) published in international journals, sorted according to the location of the study sites (number of articles is given; UK: United Kingdom).

use. ClO_4^- production plants, fireworks and airbag factories, aerospace testing and launch sites, weapons factories, military installations, and historic battlefields are places where ClO_4^- contamination may occur and should be monitored.

The usefulness of Cl and O perchlorate isotope analysis has been clearly demonstrated in a growing number of studies, primarily in the USA. Further improvement of the forensics methodology for the determination of ClO_4^- sources and their environmental distribution and behavior will benefit large populations in areas where water supplies may be impacted by ClO_4^- contamination. This will require the measurement of many more ClO_4^- isotopic compositions from worldwide sampling of synthetic and natural ClO_4^-.

Acknowledgments

This work was co-funded by the BRGM, the Agence de l'Eau Seine-Normandie, the Region Grand-Est, the Grand-Reims Metropole and ARS Grand-Est. The authors would also like to thank the two anonymous reviewers for their valuable comments that helped to improve the quality of the manuscript.

References

Ader, M., Coleman, M.L., Doyle, S.P., Stroud, M., Wakelin, D., 2001. Methods for the stable isotopic analysis of chlorine in chlorate and perchlorate compounds. Anal. Chem. 73, 4946–4950. https://doi.org/10.1021/ac010489u.

Ader, M., Chaudhuri, S., Coates, J.D., Coleman, M., 2008. Microbial perchlorate reduction: a precise laboratory determination of the chlorine isotope fractionation and its possible biochemical basis. Earth Planet. Sci. Lett. 269, 605–613. https://doi.org/10.1016/j.epsl.2008.03.023.

Andraski, B.J., Jackson, W., Welborn, T., Bohlke, J., Sevanthi Dilipan, R., Stonestrom, D.A., 2014. Soil, plant, and terrain effects on natural perchlorate distribution in a desert landscape. J. Environ. Qual. 43, 980–994. https://doi.org/10.2134/jeq2013.11.0453.

ANSES, 2011. Avis de l'Anses relatif à l'évaluation des risques sanitaires liés à la présence d'ions perchlorate dans les eaux destinées à la consommation humaine. Agence nationale de sécurité sanitaire de l'alimentation, de l'environnement et du travail, saisine n°2011-SA-0024 http://www.anses.fr/sites/default/files/documents/EAUX2012sa0119.pdf (Accessed date: 13 November 2018).

ANSES, 2013. Campagne nationale d'occurrence de polluants émergents dans les eaux destinées à la consommation humaine. Agence nationale de sécurité sanitaire de l'alimentation, de l'environnement et du travail https://www.anses.fr/fr/system/files/LABO-Ra-PolluantsEmergents-T01Ra.pdf (Accessed date: 13 November 2018).

Anupama, V.N., Kannan, K., Prajeesh, V.G., Rugmini, S., Bhaskaran, K., 2012. Perchlorate, chlorate and bromate in water samples from the south-west coast of India. Water Sci. Technol. Water Supply 12, 595–603. https://doi.org/10.2166/ws.2012.033.

Aranda-Rodriguez, R., Lemieux, F., Jin, Z., Hnatiw, J., Tugulea, A.-M., 2017. (Yet more) challenges for water treatment plants: potential contribution of hypochlorite solutions to bromate, chlorate, chlorite and perchlorate in drinking water. J. Water Supply Res. Technol. AQUA 66, 621–631. https://doi.org/10.2166/aqua.2017.147.

ARIA Database, 2018. The ARIA Database: La référence du Retour D"expérience sur Accidents Technologiques. http://www.aria.developpement-durable.gouv.fr/the-barpi/the-aria-database/?lang=en, Accessed date: 13 November 2018.

Asami, M., Kosaka, K., Yoshida, N., 2009. Occurrence of chlorate and perchlorate in bottled beverages in Japan. J. Health Sci. 55, 549–553. https://doi.org/10.1248/jhs.55.549.

Attaway, H., Smith, M., 1993. Reduction of perchlorate by an anaerobic enrichment culture. J. Ind. Microbiol. 12, 408–412. https://doi.org/10.1007/BF01569673.

Aziz, C., Borch, R., Nicholson, P., Cox, E., 2006. Alternative causes of wide-spread, low concentration perchlorate impacts to groundwater. Perchlorate: Environmental Occurrence, Interactions and Treatment. Springer US, Boston, MA, pp. 71–91.

Backus, S.M., Klawuun, P., Brown, S., D'sa, I., Sharp, S., Surette, C., Williams, D.J., 2005. Determination of perchlorate in selected surface waters in the Great Lakes Basin by HPLC/MS/MS. Chemosphere 61, 834–843. https://doi.org/10.1016/j.chemosphere.2005.04.054.

Bao, H., Gu, B., 2004. Natural perchlorate has a unique oxygen isotope signature. Environ. Sci. Technol. 38, 5073–5077. https://doi.org/10.1021/es049516z.

Barron, L., Nesterenko, P.N., Paull, B., 2006. Rapid on-line preconcentration and suppressed micro-bore ion chromatography of part per trillion levels of perchlorate in rainwater samples. Anal. Chim. Acta 567, 127–134. https://doi.org/10.1016/j.aca.2006.01.038.

Bausinger, T., Bonnaire, E., Preuß, J., 2007. Exposure assessment of a burning ground for chemical ammunition on the Great War battlefields of Verdun. Sci. Total Environ. 382, 259–271. https://doi.org/10.1016/j.scitotenv.2007.04.029.

Bennett, P., 2015. Comments on "isotopic tracing of perchlorate sources in groundwater from Pomona, California" by Neil C. Sturchio, Abelardo Beloso Jr., Linnea J. Heraty,

Stephen Wheatcraft, Rina Schumer. Appl. Geochem. 52, 191–194. https://doi.org/10.1016/j.apgeochem.2014.11.022.
Böhlke, J.K., Sturchio, N.C., Gu, B., Horita, J., Brown, G.M., Jackson, W.A., Batista, J., Hatzinger, P.B., 2005. Perchlorate isotope forensics. Anal. Chem. 77, 7838–7842. https://doi.org/10.1021/ac051360d.
Böhlke, J.K., Hatzinger, P.B., Sturchio, N.C., Gu, B., Abbene, I., Mroczkowski, S.J., 2009. Atacama perchlorate as an agricultural contaminant in groundwater: isotopic and chronologic evidence from Long Island, New York. Environ. Sci. Technol. 43, 5619–5625. https://doi.org/10.1021/es9006433.
Böhlke, J.K., Mroczkowski, S.J., Sturchio, N.C., Heraty, L.J., Richman, K.W., Sullivan, D.B., Griffith, K.N., Gu, B., Hatzinger, P.B., 2017. Stable isotope analyses of oxygen (^{18}O:^{17}O:^{16}O) and chlorine (^{37}Cl:^{35}Cl) in perchlorate: reference materials, calibrations, methods, and interferences. Rapid Commun. Mass Spectrom. 31, 85–110. https://doi.org/10.1002/rcm.7751.
Brabant, G., Bergmann, P., Kirsch, C.M., Köhrle, J., Hesch, R.D., von zur Mühlen, A., 1992. Early adaptation of thyrotropin and thyroglobulin secretion to experimentally decreased iodine supply in man. Metabolism 41, 1093–1096. https://doi.org/10.1016/0026-0495(92)90291-H.
Brown, G.M., Gu, B., 2006. The chemistry of perchlorate in the environment. Perchlorate: Environmental Occurence, Interactions and Treatment. Springer, Boston, MA, pp. 17–47.
Burns, D., Dunford, M., Sutthivaiyakit, P., 1997. Spectrophotometric determination of perchlorate after extraction as protriptylinium perchlorate. Anal. Chim. Acta 356, 141–143. https://doi.org/10.1016/S0003-2670(97)00445-5.
Calderón, R., Palma, P., Parker, D., Molina, M., Godoy, F.A., Escudey, M., 2014. Perchlorate levels in soil and waters from the Atacama Desert. Arch. Environ. Contam. Toxicol. 66, 155–161. https://doi.org/10.1007/s00244-013-9960-y.
Calderón, R., Godoy, F., Escudey, M., Palma, P., 2017. A review of perchlorate (ClO_4^-) occurrence in fruits and vegetables. Environ. Monit. Assess. 189. https://doi.org/10.1007/s10661-017-5793-x.
Cao, F., Jaunat, J., Ollivier, P., Cancès, B., Morvan, X., Hubé, D., Devos, A., Devau, N., Barbin, V., Pannet, P., 2018. Sources and behavior of perchlorate ions (ClO4-) in chalk aquifer of Champagne-Ardenne, France: preliminary results. Proceedings of the International Association of Hydrological Sciences, Copernicus GmbH, pp. 113–117.
CEPA, 2005. Canadian Environmental Protection Act Annual Report for Periode April 2004 to March 2005. http://www.ec.gc.ca/lcpe-cepa/default.asp?lang=En&n=443CAC37-1, Accessed date: 5 January 2019.
Clark, J.J.J., 2000. Toxicology of perchlorate. Perchlorate in the Environment. Springer, Boston, MA, pp. 15–29.
Clark, I.D., Fritz, P., 1997. Environmental Isotopes in Hydrogeology. Lewis Publishers, New York, USA.
Clausen, J., Robb, J., Curry, D., Korte, N., 2004. A case study of contaminants on military ranges: Camp Edwards, Massachusetts, USA. Environ. Pollut. 129, 13–21. https://doi.org/10.1016/j.envpol.2003.10.002.
Coates, J.D., Achenbach, L.A., 2004. Microbial perchlorate reduction: rocket-fueled metabolism. Nat. Rev. Microbiol. 2, 569–580. https://doi.org/10.1038/nrmicro926.
Coates, J.D., Michaelidou, U., Bruce, R.A., O'Connor, S.M., Crespi, J.N., Achenbach, L.A., 1999. Ubiquity and diversity of dissimilatory (per)chlorate-reducing bacteria. Appl. Environ. Microbiol. 65, 5234–5241.
Coleman, M.L., Ader, M., Chaudhuri, S., Coates, J.D., 2003. Microbial isotopic fractionation of perchlorate chlorine. Appl. Environ. Microbiol. 69, 4997–5000. https://doi.org/10.1128/AEM.69.8.4997-5000.2003.
Crump, C., Michaud, P., Téllez, R., Reyes, C., Gonzalez, G., Montgomery, E.L., Crump, K.S., Lobo, G., Becerra, C., Gibbs, J.P., 2000. Does perchlorate in drinking water affect thyroid function in newborns or school-age children? J. Occup. Environ. Med. 42, 603. https://doi.org/10.1097/00043764-200006000-00009.
Dasgupta, P.K., Martinelango, P.K., Jackson, W.A., Anderson, T.A., Tian, K., Tock, R.W., Rajagopalan, S., 2005. The origin of naturally occurring perchlorate: the role of atmospheric processes. Environ. Sci. Technol. 39, 1569–1575. https://doi.org/10.1021/es048612x.
Dasgupta, P.K., Dyke, J.V., Kirk, A.B., Jackson, W.A., 2006. Perchlorate in the United States. Analysis of relative source contributions to the food chain. Environ. Sci. Technol. 40, 6608–6614. https://doi.org/10.1021/es061321z.
EFSA Panel on Contaminants in the Food Chain (EFSA CONTAM Panel), 2014. Scientific opinion on the risks to public health related to the presence of perchlorate in food, in particular fruits and vegetables. EFSA J. 12, 3869. https://doi.org/10.2903/j.efsa.2014.3869.
Ericksen, G.E., 1981. Geology and Origin of the Chilean Nitrate Deposits. United States Government printing Office, Washington https://doi.org/10.3133/pp1188 37 p.
Ericksen, G.E., 1983. The Chilean nitrate deposits: the origin of the Chilean nitrate deposits, which contain a unique group of saline minerals, has provoked lively discussion for more than 100 years. Am. Sci. 71, 366–374 Retrieved from. http://www.jstor.org/stable/27852136.
Ericksen, G.E., Hosterman, J.W., St. Amand, P., 1988. Chemistry, mineralogy and origin of the clay-hill nitrate deposits, Amargosa River valley, Death Valley region, California, U.S.A. Chem. Geol. 67, 85–102. https://doi.org/10.1016/0009-2541(88)90008-3.
Fabian, P., Borchers, R., Penkett, S.A., Prosser, N.J.D., 1981. Halocarbons in the stratosphere. Nature 294, 733–735. https://doi.org/10.1038/294733a0.
Flowers, T.C., Hunt, J.R., 2007. Viscous and gravitational contributions to mixing during vertical brine transport in water-saturated porous media. Water Resour. Res. 43, W01407.1. https://doi.org/10.1029/2005WR004773.
Fram, M.S., Belitz, K., 2011. Probability of detecting perchlorate under natural conditions in deep groundwater in California and the southwestern United States. Environ. Sci. Technol. 45, 1271–1277. https://doi.org/10.1021/es103103p.
Furdui, V.I., Zheng, J., Furdui, A., 2018. Anthropogenic perchlorate increases since 1980 in the Canadian high Arctic. Environ. Sci. Technol. 52, 972–981. https://doi.org/10.1021/acs.est.7b03132.
Gal, H., Weisbrod, N., Dahan, O., Ronen, Z., Nativ, R., 2009. Perchlorate accumulation and migration in the deep vadose zone in a semiarid region. J. Hydrol. 378, 142–149. https://doi.org/10.1016/j.jhydrol.2009.09.018.
Hatzinger, P.B., Böhlke, J.K., Sturchio, N.C., Gu, B., Heraty, L.J., Borden, R.C., 2009. Fractionation of stable isotopes in perchlorate and nitrate during in situ biodegradation in a sandy aquifer. Environ. Chem. 6, 9. https://doi.org/10.1071/EN09008.
Hatzinger, P.B., Böhlke, J.K., Sturchio, N.C., Izbicki, J., Teague, N., 2018. Four-dimensional isotopic approach to identify perchlorate sources in groundwater: application to the Rialto-Colton and Chino subbasins, southern California (USA). Appl. Geochem. 97, 213–225. https://doi.org/10.1016/j.apgeochem.2018.08.020.
Hauser, P.C., Renner, N.D., Hong, A.P.C., 1994. Anion detection in capillary electrophoresis with ion-selective microelectrodes. Anal. Chim. Acta 295, 181–186. https://doi.org/10.1016/0003-2670(94)80349-8.
Her, N., Jeong, H., Kim, J., Yoon, Y., 2011. Occurrence of perchlorate in drinking water and seawater in South Korea. Arch. Environ. Contam. Toxicol. 61, 166–172. https://doi.org/10.1007/s00244-010-9616-0.
Hubé, D., 2014. Perchlorates: éléments historiques et d'expertise pour une évaluation de l'impact environnemental. https://centenaire.org/fr/print/5814 Accessed date: 13 november 2018.
Hubé, D., 2016. Sur les traces d'un secret enfoui: Enquête sur l'héritage toxique de la Grande Guerre - Préface de Jean-Yves Le Naour, Michalon, Paris.
Hubé, D., 2017. Industrial-scale destruction of old chemical ammunition near Verdun: a forgotten chapter of the Great War. First World War Studies. 8:2–3, pp. 205–234. https://doi.org/10.1080/19475020.2017.1393347.
Hubé, D., Bausinger, T., 2013. Marquage pyrotechnique: analyse de la problématique environnementale. Comparatif entre Allemagne et France. Géologues. pp. 32–38.
Hubé, D., Urban, S., 2013. Préliminaire sur la présence des ions perchlorates dans les eaux souterraines en Alsace. Rapport BRGM/RP-62588-FR, 23 p, 5 fig.
Hunter, W.J., 2001. Perchlorate is not a common contaminant of fertilizers. J. Agron. Crop Sci. 187, 203–206. https://doi.org/10.1046/j.1439-037x.2001.00519.x.
Iannece, P., Motta, O., Tedesco, R., Carotenuto, M., Proto, A., 2013. Determination of perchlorate in bottled water from Italy. Water 5, 767–779. https://doi.org/10.3390/w5020767.
INERIS, 2014. Données technico-économiques sur les substances chimiques en France: Perchlorate d'ammonium, DRC-13-126866-06964C. (71 p.). https://rsde.ineris.fr/fiches_technico.php Accessed date: 13 November 2018.
Isobe, T., Ogawa, S.P., Sugimoto, R., Ramu, K., Sudaryanto, A., Malarvannan, G., Devanathan, G., Ramaswamy, B.R., Munuswamy, N., Ganesh, D.S., et al., 2013. Perchlorate contamination of groundwater from fireworks manufacturing area in South India. Environ. Monit. Assess. 185, 5627–5637. https://doi.org/10.1007/s10661-012-2972-7.
Izbicki, J.A., Teague, N.F., Hatzinger, P.B., Böhlke, J.K., Sturchio, N.C., 2014. Groundwater movement, recharge, and perchlorate occurrence in a faulted alluvial aquifer in California (USA). Hydrogeol. J. 23, 467–491. https://doi.org/10.1007/s10040-014-1217-y.
Jackson, P.E., Gokhale, S., Streib, T., Rohrer, J.S., Pohl, C.A., 2000. Improved method for the determination of trace perchlorate in ground and drinking waters by ion chromatography. J. Chromatogr. A 888, 151–158. https://doi.org/10.1016/S0021-9673(00)00557-4.
Jackson, W.A., Joseph, P., Laxman, P., Tan, K., Smith, P.N., Yu, L., Anderson, T.A., 2005a. Perchlorate accumulation in foliage and edible vegetation. J. Agric. Food Chem. 53, 369–373. https://doi.org/10.1021/jf0493021.
Jackson, W.A., Kumar Anandam, S., Anderson, T., Lehman, T., Rainwater, K., Rajagopalan, S., Ridley, M., Tock, R., 2005b. Perchlorate occurrence in the Texas southern High Plains aquifer system. Ground Water Monit. Remediat. 25, 137–149. https://doi.org/10.1111/j.1745-6592.2005.0009.x.
Jackson, W.A., Böhlke, J.K., Gu, B., Hatzinger, P.B., Sturchio, N.C., 2010. Isotopic composition and origin of indigenous natural perchlorate and co-occurring nitrate in the southwestern United States. Environ. Sci. Technol. 44, 4869–4876. https://doi.org/10.1021/es903802j.
Jackson, W.A., Böhlke, J.K., Andraski, B.J., Fahlquist, L., Bexfield, L., Eckardt, F.D., Gates, J.B., Davila, A.F., McKay, C.P., Rao, B., et al., 2015. Global patterns and environmental controls of perchlorate and nitrate co-occurrence in arid and semi-arid environments. Geochim. Cosmochim. Acta 164, 502–522. https://doi.org/10.1016/j.gca.2015.05.016.
Jaeglé, L., Yung, Y.L., Toon, G.C., Sen, B., Blavier, J.-F., 1996. Balloon observations of organic and inorganic chlorine in the stratosphere: the role of HClO4 production on sulfate aerosols. Geophys. Res. Lett. 23, 1749–1752. https://doi.org/10.1029/96GL01543.
Kosaka, K., Asami, M., Matsuoka, Y., Kamoshita, M., Kunikane, S., 2007. Occurrence of perchlorate in drinking water sources of metropolitan area in Japan. Water Res. 41, 3474–3482. https://doi.org/10.1016/j.watres.2007.05.011.
Kumarathilaka, P., Oze, C., Indraratne, S.P., Vithanage, M., 2016. Perchlorate as an emerging contaminant in soil, water and food. Chemosphere 150, 667–677. https://doi.org/10.1016/j.chemosphere.2016.01.109.
Lehmann, B.E., Davis, S.N., Fabryka-Martin, J.T., 1993. Atmospheric and subsurface sources of stable and radioactive nuclides used for groundwater dating. Water Resour. Res. 29, 2027–2040. https://doi.org/10.1029/93WR00543.
Liu, G., Zong, G., Dhana, K., Hu, Y., Blount, B.C., Morel-Espinosa, M., Sun, Q., 2017. Exposure to perchlorate, nitrate and thiocyanate, and prevalence of diabetes mellitus. Int. J. Epidemiol. 46, 1913–1923. https://doi.org/10.1093/ije/dyx188.
Lopez, B., Brugeron, A., Devau, N., Ollivier, P., 2014. Vulnérabilité des eaux souterraines de France métropolitaine vis-à-vis des ions perchlorates. Rapport final. BRGM/RP-63270-FR (108 p.).
Lybrand, R.A., Michalski, G., Graham, R.C., Parker, D.R., 2013. The geochemical associations of nitrate and naturally formed perchlorate in the Mojave Desert, California, USA. Geochim. Cosmochim. Acta 104, 136–147. https://doi.org/10.1016/j.gca.2012.10.028.
Lybrand, R.A., Bockheim, J.G., Ge, W., Graham, R.C., Hlohowskyj, S.R., Michalski, G., Prellwitz, J.S., Rech, J.A., Wang, F., Parker, D.R., 2016. Nitrate, perchlorate, and iodate

co-occur in coastal and inland deserts on Earth. Chem. Geol. 442, 174–186. https://doi.org/10.1016/j.chemgeo.2016.05.023.
Mass, D.E.P., 2005. The occurence and sources of Perchlorate in Massachusetts. Draft Report. Massachusetts Department of Environmental Protection, Boston, MA https://www.mass.gov/dep/.
Mastrocicco, M., Di, G., Vincenzi, F., Colombani, N., Castaldelli, G., 2017. Chlorate origin and fate in shallow groundwater below agricultural landscapes. Environ. Pollut. 231, 1453–1462. https://doi.org/10.1016/j.envpol.2017.09.007.
McLaughlin, C.L., Blake, S., Hall, T., Harman, M., Kanda, R., Hunt, J., Rumsby, P.C., 2011. Perchlorate in raw and drinking water sources in England and Wales. Water Environ. J. 25, 456–465. https://doi.org/10.1111/j.1747-6593.2010.00237.x.
Mendiratta, S.K., Dotson, R.L., Brooker, R.T., 1996. Perchloric Acid and Perchlorates, in: Kirk-Othmer Encyclopedia of Chemical Technology. John Wiley & Sons, Inc., New York.
Mohr, T.K.G., 2007. Assessing perchlorate origins using stable isotopes. Southwest Hydrol. 22–23.
Munster, J.E., 2008. Non-point Sources of Nitrate and Perchlorate in Urban Land Use to Groundwater, Suffolk County, NY. PhD. Dissertation. Stony Brook University (132 p.).
Munster, J., Hanson, G.N., 2009. Perchlorate and ion chemistry of road runoff. Environ. Chem. 6, 28–35. https://doi.org/10.1071/EN08085.
Munster, J., Hanson, G.N., Jackson, W.A., Rajagopalan, S., 2009. The fallout from fireworks: perchlorate in total deposition. Water Air Soil Pollut. 198, 149–153. https://doi.org/10.1007/s11270-008-9833-6.
Nadaraja, A.V., Puthiyaveettil, P.G., Bhaskaran, K., 2015. Surveillance of perchlorate in ground water, surface water and bottled water in Kerala, India. J. Environ. Health Sci. Eng. 13, 56. https://doi.org/10.1186/s40201-015-0213-z.
Nann, A., Pretsch, E., 1994. Potentiometric detection of anions separated by capillary electrophoresis using an ion-selective microelectrode. J. Chromatogr. A 676, 437–442. https://doi.org/10.1016/0021-9673(94)80444-3.
Negrel, P., Ollivier, P., Flehoc, C., Hube, D., 2017. An innovative application of stable isotopes (62H and 618O) for tracing pollutant plumes in groundwater. Sci. Total Environ. 578, 495–501. https://doi.org/10.1016/j.scitotenv.2016.10.214.
Noble, L.F., Mansfield, G.R., 1922. Nitrate deposits in the Amargosa region southeastern California. United States Geological Survey, Bulletin. 724, pp. 1–99.
Nozawa-Inoue, M., Scow, K.M., Rolston, D.E., 2005. Reduction of perchlorate and nitrate by microbial communities in vadose soil. Appl. Environ. Microbiol. 71, 3928–3934. https://doi.org/10.1128/AEM.71.7.3928-3934.2005.
Parker, D.R., Seyfferth, A.L., Reese, B.K., 2008. Perchlorate in groundwater: a synoptic survey of "pristine" sites in the coterminous United States. Environ. Sci. Technol. 42, 1465–1471. https://doi.org/10.1021/es7021957.
Phillips, F.M., 2000. Chlorine-36. In: Cook, P.G., Herczeg, A.L. (Eds.), Environmental Tracers in Subsurface Hydrology. Boston, MA, Springer US, pp. 299–348.
Plummer, L.N., Böhlke, J.K., Doughten, M.W., 2006. Perchlorate in pleistocene and holocene groundwater in north-central New Mexico. Environ. Sci. Technol. 40, 1757–1763. https://doi.org/10.1021/es051739h.
Poghosyan, A., Sturchio, N.C., Morrison, C.G., Beloso, A.D., Guan, Y., Eiler, J.M., Jackson, W.A., Hatzinger, P.B., 2014. Perchlorate in the Great Lakes: isotopic composition and origin. Environ. Sci. Technol. 48, 11146–11153. https://doi.org/10.1021/es502796d.
Pontius, F.W., Damian, P., Eaton, A.D., 2000. Regulating perchlorate in drinking water. Perchlorate in the Environment. Springer, Boston, MA, pp. 31–36.
Qin, Y., Li, Y., Bao, H., Liu, F., Hou, K., Wan, D., Zhang, C., 2012. Massive atmospheric nitrate accumulation in a continental interior desert, northwestern China. Geology 40, 623–626.
Qin, X., Zhang, T., Gan, Z., Sun, H., 2014. Spatial distribution of perchlorate, iodide and thiocyanate in the aquatic environment of Tianjin, China: environmental source analysis. Chemosphere 111, 201–208. https://doi.org/10.1016/j.chemosphere.2014.03.082.
Quiñones, O., Oh, J.-E., Vanderford, B., Kim, J.H., Cho, J., Snyder, S.A., 2007. Perchlorate assessment of the Nakdong and Yeongsan watersheds, Republic of Korea. Environ. Toxicol. Chem. 26, 1349–1354. https://doi.org/10.1897/06-469R.1.
Rajagopalan, S., Anderson, T.A., Fahlquist, L., Rainwater, K.A., Ridley, M., Jackson, W.A., 2006. Widespread presence of naturally occurring perchlorate in high plains of Texas and New Mexico. Environ. Sci. Technol. 40, 3156–3162. https://doi.org/10.1021/es052155i.
Rajagopalan, S., Anderson, T., Cox, S., Harvey, G., Cheng, Q., Jackson, W.A., 2009. Perchlorate in wet deposition across North America. Environ. Sci. Technol. 43, 616–622. https://doi.org/10.1021/es801737u.
Rao, B., Anderson, T.A., Orris, G.J., Rainwater, K.A., Rajagopalan, S., Sandvig, R.M., Scanlon, B.R., Stonestrom, D.A., Walvoord, M.A., Jackson, W.A., 2007. Widespread natural perchlorate in unsaturated zones of the Southwest United States. Environ. Sci. Technol. 41, 4522–4528. https://doi.org/10.1021/es062853i.
Renner, R., 1999. Study finding perchlorate in fertilizer rattles industry. Environ. Sci. Technol. 33, 394A–395A. https://doi.org/10.1021/es993030e.
Ricour, J., 2013. Un exemple d'altération du fond géochimique naturel des sols et des eaux souterraines: les séquelles environnementales des grands conflits mondiaux en France. Géologues 179, 27–31.
Sanchez, C.A., Krieger, R.I., Khandaker, N.R., Valentin-Blasini, L., Blount, B.C., 2006. Potential perchlorate exposure from Citrus sp. irrigated with contaminated water. Anal. Chim. Acta 567, 33–38. https://doi.org/10.1016/j.aca.2006.02.013.
Scanlon, B.R., Reedy, R.C., Jackson, W.A., Rao, B., 2008. Mobilization of naturally occurring perchlorate related to land-use change in the southern High Plains, Texas. Environ. Sci. Technol. 42, 8648–8653. https://doi.org/10.1021/es800361h.
Scanlon, B.R., Gates, J.B., Reedy, R.C., Jackson, W.A., Bordovsky, J.P., 2010. Effects of irrigated agroecosystems: 2. Quality of soil water and groundwater in the southern High Plains, Texas. Water Resour. Res. 46, W09538. https://doi.org/10.1029/2009WR008428.
Scheytt, T.J., Freywald, J., Ptacek, C.J., 2011. Study of selected soil, ground, and surface water samples on perchlorate in Germany: first results. Grundwasser 16, 37–43. https://doi.org/10.1007/s00767-010-0159-0.
Schilt, A.A., 1979. Perchloric Acid and Perchlorates. G. F. Smith Chemical Co., Columbus, Ohio.
Schumacher, J.C., 1960. Perchlorates: Their Properties, Manufacture and Uses. Chapman & Hall, London (257 p.).
Sellers, K., Weeks, K., Alsop, W.R., Clough, S.R., Hoyt, M., Pugh, B., Robb, J., 2006. Perchlorate: Environmental Problems and Solutions. CRC Press (258 p.).
Serrano-Nascimento, C., Calil-Silveira, J., Dalbosco, R., Zorn, T.T., Nunes, M.T., 2018. Evaluation of hypothalamus-pituitary-thyroid axis function by chronic perchlorate exposure in male rats. Environ. Toxicol. 33, 209–219. https://doi.org/10.1002/tox.22509.
Shi, Y., Zhang, P., Wang, Y., Shi, J., Cai, Y., Mou, S., Jiang, G., 2007. Perchlorate in sewage sludge, rice, bottled water and milk collected from different areas in China. Environ. Int. 33, 955–962. https://doi.org/10.1016/j.envint.2007.05.007.
Sijimol, M.R., Mohan, M., 2014. Environmental impacts of perchlorate with special reference to fireworks–a review. Environ. Monit. Assess. 186, 7203–7210. https://doi.org/10.1007/s10661-014-3921-4.
Silva, M.A., 2003. Safety Flares Threaten Water Quality with Perchlorate. Santa Clara Valley Water District Publication http://www.valleywater.org.
Srinivasan, A., Viraraghavan, T., 2009. Perchlorate: health effects and technologies for its removal from water resources. Int. J. Environ. Res. Public Health 6, 1418–1442. https://doi.org/10.3390/ijerph6041418.
Stanford, B.D., Pisarenko, A.N., Snyder, S.A., Gordon, G., 2011. Perchlorate, bromate, and chlorate in hypochlorite solutions: guidelines for utilities. J. Am. Water Works Assoc. 103, 71–83. https://doi.org/10.1002/j.1551-8833.2011.tb11474.x.
Steinmaus, C.M., 2016. Perchlorate in water supplies: sources, exposures, and health effects. Curr. Environ. Health Rep. 3, 136–143. https://doi.org/10.1007/s40572-016-0087-y.
Stroo, H.F., Loehr, R.C., Ward, C.H., 2009. In situ bioremediation of perchlorate in groundwater: an overview. In Situ Bioremediation of Perchlorate in Groundwater. Springer, New York, NY, pp. 1–13.
Sturchio, N.C., 2015. Reply to the comments by P. Bennett on "isotopic tracing of perchlorate sources in groundwater of Pomona, California" by N.C. Sturchio, A. Beloso Jr., L.J. Heraty, S. Wheatcraft, and R. Schumer. Appl. Geochem. 52, 195–196. https://doi.org/10.1016/j.apgeochem.2014.11.027.
Sturchio, N.C., Hatzinger, P.B., Arkins, M.D., Suh, C., Heraty, L.J., 2003. Chlorine isotope fractionation during microbial reduction of perchlorate. Environ. Sci. Technol. 37, 3859–3863. https://doi.org/10.1021/es034066g.
Sturchio, N.C., Böhlke, J.K., Gu, B., Horita, J., Brown, G.M., Beloso, A.D., Patterson, L.J., Hatzinger, P.B., Jackson, W.A., Batista, J., 2006. Stable isotopic composition of chlorine and oxygen in synthetic and natural perchlorate. Perchlorate: Environmental Occurrence, Interactions and Treatment. 411. Springer, New York, pp. 93–109.
Sturchio, N.C., Böhlke, J.K., Beloso, A.D., Streger, S.H., Heraty, L.J., Hatzinger, P.B., 2007. Oxygen and chlorine isotopic fractionation during perchlorate biodegradation: laboratory results and implications for forensics and natural attenuation studies. Environ. Sci. Technol. 41, 2796–2802. https://doi.org/10.1021/es0621849.
Sturchio, N.C., Caffee, M., Beloso, A.D., Heraty, L.J., Böhlke, J.K., Hatzinger, P.B., Jackson, W.A., Gu, B., Heikoop, J.M., Dale, M., 2009. Chlorine-36 as a tracer of perchlorate origin. Environ. Sci. Technol. 43, 6934–6938. https://doi.org/10.1021/es9012195.
Sturchio, N.C., Böhlke, J.K., Gu, B., Hatzinger, P.B., Jackson, W.A., 2011. Isotopic tracing of perchlorate in the environment. Handbook of Environmental Isotope Geochemistry. Springer, Berlin, Heidelberg, pp. 437–452 https://doi.org/10.1007/978-3-642-10637-8_22.
Sturchio, N.C., Hoaglund, J.R., Marroquin, R.J., Beloso, A.D., Heraty, L.J., Bortz, S.E., Patterson, T.L., 2012. Isotopic mapping of groundwater perchlorate plumes. Ground Water 50, 94–102. https://doi.org/10.1111/j.1745-6584.2011.00802.x.
Sturchio, N.C., Beloso, A., Heraty, L.J., Wheatcraft, S., Schumer, R., 2014. Isotopic tracing of perchlorate sources in groundwater from Pomona, California. Appl. Geochem. 43, 80–87. https://doi.org/10.1016/j.apgeochem.2014.01.012.
Susarla, S., Collette, T.W., Garrison, A.W., Wolfe, N.L., McCutcheon, S.C., 1999. Perchlorate identification in fertilizers. Environ. Sci. Technol. 33, 3469–3472. https://doi.org/10.1021/es990577k.
Tan, K., Anderson, T.A., Jackson, W.A., 2005. Temporal and spatial variation of perchlorate in streambed sediments: results from in-situ dialysis samplers. Environ. Pollut. 136, 283–291. https://doi.org/10.1016/j.envpol.2004.12.037.
Trumpolt, C.W., Crain, M., Cullison, G.D., Flanagan, S.J.P., Siegel, L., Lathrop, S., 2005. Perchlorate: sources, uses, and occurrences in the environment. Remediat. J. 16, 65–89. https://doi.org/10.1002/rem.20071.
Tsui, D.T., Clewell, R.A., Eldridge, J.E., Mattie, D.R., 2000. Perchlorate analysis with the AS16 separation column. Perchlorate in the Environment. Springer, Boston, MA, pp. 59–80.
Urbansky, E.T., 1998. Perchlorate chemistry: implications for analysis and remediation. Bioremediation J. 2, 81–95. https://doi.org/10.1080/10889869891214231.
Urbansky, E.T., 2000. Quantitation of perchlorate ion: practices and advances applied to the analysis of common matrices. Crit. Rev. Anal. Chem. 30, 311–343. https://doi.org/10.1080/10408340008984163.
Urbansky, E.T., 2002. Perchlorate as an environmental contaminant. Environ. Sci. Pollut. Res. 9, 187–192. https://doi.org/10.1007/BF02987487.
Urbansky, E.T., Collette, T.W., Robarge, W.P., Hall, W.L., Skillen, J.M., Kane, P.F., 2001a. Survey of Fertilizers and Related Materials for Perchlorate (ClO_4^-): Final Report. National Risk Management Research Laboratory, Office of Research and Development, U.S. Environmental Protection Agency, Cincinnati OH (26 p.).
Urbansky, E.T., Brown, S.K., Magnuson, M.L., Kelty, C.A., 2001b. Perchlorate levels in samples of sodium nitrate fertilizer derived from Chilean caliche. Environ. Pollut. 112, 299–302. https://doi.org/10.1016/S0269-7491(00)00132-9.
USEPA, 1998. Perchlorate Environmental Contamination: Toxicological Review and Risk Characterization Based on Emerging Information (External Review Draft). National

Center for Environment Assessment, Office of Research and Development, U.S. Environmental Protection Agency, Washington.
USEPA, 2006. Assessment guidance for perchlorate. Memorandum to Regional Administrators. US EPA Office of Solid Waste and Emergency Response, Washington, DC.
USEPA, 2009. Revised assessment guidance for perchlorate. Memorandum to Regional Administrators. US EPA Office of Solid Waste and Emergency Response, Washington, DC.
Vega, M., Nerenberg, R., Vargas, I., 2018. Perchlorate contamination in Chile: legacy, challenges, and potential solutions. Environ. Res. 164, 316–326. https://doi.org/10.1016/j.envres.2018.02.034.
Vella, A.J., Chircop, C., Micallef, T., Pace, C., 2015. Perchlorate in dust fall and indoor dust in Malta: an effect of fireworks. Sci. Total Environ. 521–522, 46–51. https://doi.org/10.1016/j.scitotenv.2015.03.071.
Vigreux-Besret, C., Mahé, A., Ledoux, G., Garnier, A., Rosin, C., Baert, A., Joyeux, M., Badot, P.-M., Panetier, P., Rivière, G., 2015. Perchlorate: water and infant formulae contamination in France and risk assessment in infants. Food Addit. Contam. Part Chem. Anal. Control Expo. Risk Assess. 32, 1148–1155. https://doi.org/10.1080/19440049.2015.1036382.
Von Clarmann, T., 2013. Chlorine in the stratosphere. Atmosfera 26, 415–458. https://doi.org/10.1016/S0187-6236(13)71086-5.
Wallace, W., Ward, T., Breen, A., Attaway, H., 1996. Identification of an anaerobic bacterium which reduces perchlorate and chlorate as Wolinella succinogenes. J. Ind. Microbiol. 16, 68–72. https://doi.org/10.1007/BF01569924.
WHO, 2017. Guidelines for Drinking-water Quality: Fourth Edition Incorporating First Addendum Geneva: World Health Organization. Licence: CC BY-NC-SA 3.0 IGO.
Wilkin, R.T., Fine, D.D., Burnett, N.G., 2007. Perchlorate behavior in a municipal lake following fireworks displays. Environ. Sci. Technol. 41, 3966–3971. https://doi.org/10.1021/es0700698.
Wisniak, J., Garcés, 2001. The rise and fall of the Salitre (sodium nitrate) industry. Indian J. Chem. Technol. 8, 427–438.
Wolff, J., 1998. Perchlorate and the thyroid gland. Pharmacol. Rev. 50, 89–106.
Wu, Q., Zhang, T., Sun, H., Kannan, K., 2010. Perchlorate in tap water, groundwater, surface waters, and bottled water from China and its association with other inorganic anions and with disinfection byproducts. Arch. Environ. Contam. Toxicol. 58, 543–550. https://doi.org/10.1007/s00244-010-9485-6.
Wu, Q., Oldi, J.F., Kannan, K., 2011. Fate of perchlorate in a man-made reflecting pond following a fireworks display in Albany, New York, USA. Environ. Toxicol. Chem. 30, 2449–2455. https://doi.org/10.1002/etc.648.
Xie, Y., Ren, L., Zhu, X., Gou, X., Chen, S., 2018. Physical and chemical treatments for removal of perchlorate from water–a review. Process. Saf. Environ. Prot. 116, 180–198.
Xu, J., Song, Y., Min, M., Steinberg, L., Logan, B.E., 2003. Microbial degradation of perchlorate: principles and applications. Environ. Eng. Sci. 20, 405–422. https://doi.org/10.1089/109287503768335904.
Xu, X., Gao, B., Jin, B., Zhen, H., Wang, X., Dai, M., 2015. Study of microbial perchlorate reduction: considering of multiple pH, electron acceptors and donors. J. Hazard. Mater. 285, 228–235. https://doi.org/10.1016/j.jhazmat.2014.10.061.
Ye, L., You, H., Yao, J., Su, H., 2012. Water treatment technologies for perchlorate: a review. Desalination 298, 1–12. https://doi.org/10.1016/j.desal.2012.05.006.
Ye, L., You, H., Yao, J., Kang, X., Tang, L., 2013. Seasonal variation and factors influencing perchlorate in water, snow, soil and corns in northeastern China. Chemosphere 90, 2493–2498. https://doi.org/10.1016/j.chemosphere.2012.10.058.
Young, E., Galy, A., Nagahara, H., 2002. Kinetic and equilibrium mass-dependent isotope fractionation laws in nature and their geochemical and cosmochemical significance. Geochim. Cosmochim. Acta 66, 1095–1104. https://doi.org/10.1016/S0016-7037(01)00832-8.

Appendix 2 : Article published in Journal of Hydrology: Heterogeneous behavior of unconfined Chalk aquifers infer from combination of groundwater residence time, hydrochemistry and hydrodynamic tools.

Journal of Hydrology 581 (2020) 124433

Contents lists available at ScienceDirect

Journal of Hydrology

journal homepage: www.elsevier.com/locate/jhydrol

Research papers

Heterogeneous behaviour of unconfined Chalk aquifers infer from combination of groundwater residence time, hydrochemistry and hydrodynamic tools

Feifei Cao[a,*], Jessy Jaunat[a], Virginie Vergnaud-Ayraud[b], Nicolas Devau[c], Thierry Labasque[b], Aurélie Guillou[b], Alexandra Guillaneuf[a], Julien Hubert[a], Luc Aquilina[b], Patrick Ollivier[c]

[a] Université de Reims Champagne-Ardenne – GEGENAA – EA 3795, 2 esplanade Roland Garros, 51100 Reims, France
[b] OSUR, Géosciences Rennes, UMR 6118, CNRS/Université Rennes-1, F-35042 Rennes, France
[c] BRGM, 3 av. C. Guillemin, BP 36009, 45060 Orléans Cedex 2, France

ARTICLE INFO

This manuscript was handled by Huaming Guo, Editor-in-Chief

Keywords:
Chalk aquifer
Groundwater age
Water level
Geochemistry variability
Water resource
Unsaturated zone

ABSTRACT

Chalk groundwater is an important aquifer resource. It is intensively exploited for human use, with a large proportion utilized for drinking water. The improvement of the knowledge on Chalk aquifer hydrogeological functioning is essential for the management of this resource. Here, we developed a methodology based on a combination of hydrodynamic, hydrochemistry and groundwater dating tools. A study site with Chalk outcrops was selected in NE France where groundwater geochemistry and water level were monitored continuously for 2 years from 2017 to 2019 and groundwater residence time was estimated using CFCs and SF_6. Overall, the aquifer has an inertial behaviour with respect to recharge. Nevertheless, a rapid water level response following rainfall events was observed at one site, suggesting the presence of highly developed fracture network at the local scale. According to the mixing process (piston flow, exponential or binary mixing) defined at each sampling site, groundwater dating indicated rather heterogeneous ages ranging from modern to about 50 years. High spatial and temporal heterogeneities were observed and interpreted by a combination of hydrogeological setting, residence time and land use information, highlighting main factors governing the Chalk groundwater geochemistry including water level fluctuation, thickness of the Unsaturated Zone (UZ), superficial formations, distribution of fracture network, aquifer-river relations and human activities. A conceptual model was proposed accordingly to explain the hydrogeological functioning of unconfined Chalk aquifers.

1. Introduction

The Chalk formation is widespread in northwestern Europe covering large areas between the Paris Basin, the London Basin, Denmark and the North West of Germany (Bakalowicz, 2018). Groundwater of the Chalk Aquifer is intensively exploited for human use, making it one of the most important aquifers over much of Northern Europe. In France, the Chalk aquifer covers about 20% of the metropolitan territory with a total area of 110,000 km^2 (Crampon et al., 1996; Roux, 2018) and provides approximately 12 billion $m^3 \cdot year^{-1}$ of water, which accounts for 70% of the drinking water consumed in the north of France (Lallahem, 2002). However, in recent decades, there is a growing evidence of the deterioration of the European Chalk groundwater quality due to human activities (Baran et al., 2008; Barhoum, 2014; Chen et al., 2019; Hakoun et al., 2017; Johnson et al., 2001; Longstaff et al., 1992). Aquifer protection requires a sound knowledge of the Chalk hydrogeology and groundwater geochemistry.

The Chalk is recognized as possessing possibly triple porosity: matrix, fracture and conduit (karst) porosity (Headworth et al., 1982; MacDonald et al., 1998; Price et al., 1993; Worthington, 2003), but the most common models describe this carbonate rocks as a double-porosity medium with a capacious porous space of low permeability and high permeable fissures of low volume (e.g., Brouyère, 2006; Fitzpatrick, 2011; Van den Daele et al., 2007). Fracture distribution in the Chalk is highly heterogeneous. Vertically, fractures are generally only developed towards the top of the aquifer (Allen et al., 1997). Laterally, fractures are more developed in river valleys than on interfluves as the structural weaknesses followed by valleys are more fractured and erosion along valleys favors the opening of horizontal fractures (Allen et al., 1997; Price, 1987; Price et al., 1993).

* Corresponding author.
E-mail address: feifei.cao@etudiant.univ-reims.fr (F. Cao).

https://doi.org/10.1016/j.jhydrol.2019.124433
Received 26 September 2019; Received in revised form 2 December 2019; Accepted 3 December 2019
Available online 06 December 2019
0022-1694/ © 2019 Published by Elsevier B.V.

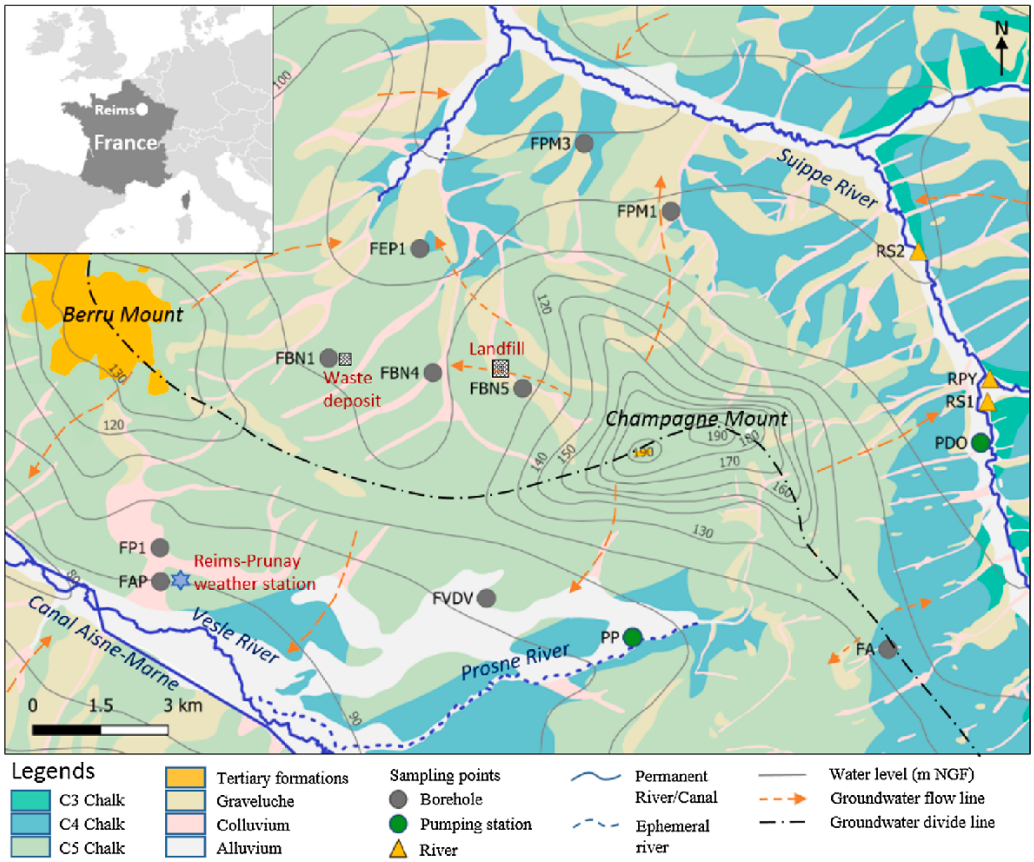

Fig. 1. Hydrogeological map of the study area recorded at high water level with the location of sampling points (source of geological map: Laurain et al., 1981, Allouc and Le Roux, 1995; source of water level data: Rouxel-David et al., 2002a).

Recharge through the UZ can occur very rapidly through fractures or slowly within the matrix (Allen et al., 1997). Most studies consider that in the UZ, recharge is predominately through the Chalk matrix with a mean downward rate of about 1 m·year^{-1} (Barraclough et al., 1994; Brouyère et al., 2004; Chen et al., 2019; Haria et al., 2003; Vachier et al., 1987; Van den Daele et al., 2007; Wellings, 1984). Recharge through fractures is faster but smaller in volume. It occurs episodically when the infiltration rate exceeds the hydraulic conductivity of the matrix (Ireson and Butler, 2011; Mathias et al., 2006; Price et al., 2000). Rapid flow could also temporally or locally be dominant, especially in zones where karstic systems are developed (Ireson et al., 2006; Mathias et al., 2006; Maurice, 2009). Flow rates have been estimated with values ranging from 1 to 20 km·day^{-1} in karstic systems and up to 1 m·h^{-1} in fissures (Allshorn et al., 2007; Baran et al., 2008; Calba, 1980; Devos et al., 2006; Ireson et al., 2006; Katz et al., 2009; MacDonald et al., 1998). It should be noted that karst flow has usually a small contribution to the recharge of Chalk aquifer but can cause punctual problems on groundwater quality such as nitrate and bacterial contaminations (Barhoum, 2014).

Chemical composition of the Chalk groundwater is mainly controlled by water–rock interactions due to the dissolution of primary rock minerals and the precipitation of second phases (Gillon et al., 2010). Most of the chemical characteristics of Chalk groundwater are acquired during initial percolation through the soil and upper Saturated Zone (SZ). As the Chalk matrix is dominated by carbonate minerals, a fast homogeneity of the baseline geochemistry is expected (Edmunds et al., 1987). However, spatial and temporal heterogeneities of the groundwater chemistry can be observed due to internal and external factors such as local variations of the rock mineralogy (e.g., presence of dolomitic bodies, clay-rich, phosphatic layers; Deconinck et al., 2005; Jarvis, 1980; Richard et al., 2005), the incongruent dissolution of Chalk and dolomitic impurities (Aquilina et al., 2003; Edmunds et al., 1987; Gillon et al., 2010; Kloppmann et al., 1998), pollution caused by human activities (e.g., NO_3^-, Cl^-, atrazine), especially agricultural application of fertilizer and pesticide (Barhoum, 2014; Kloppmann et al., 1994) and the mixing between waters of different residence times and origins including rapidly percolated water, fissure water and matrix pore water (Gillon et al. 2010). The mixing process depends on water level fluctuation (Brouyère et al., 2004; Hakoun et al., 2017), structure of the superficial formation (Barhoum et al., 2014; El Janyani et al., 2014; Valdes et al., 2014), climate conditions and topography.

A better understanding of the mixing process and flow mechanisms within aquifers could be achieved by groundwater dating using natural or anthropogenic age tracers (Cook et al., 1995; Darling et al., 2012a; Jaunat et al., 2012; Santoni et al., 2016; Suckow, 2014). In case of young groundwater with residence times ranging from 0 to 60 years, atmospheric trace gases such as CFCs (chlorofluorocarbons) and SF_6 (sulphur hexafluoride) could be used (e.g., Aeschbach-Hertig et al., 1999; Busenberg and Plummer, 1992; Cook and Solomon, 1995; Dunkle et al., 1993; Plummer et al., 2001; Vergnaud-Ayraud et al., 2008). An average age and a distribution of residence times of groundwater can be estimated considering various mixing models (the most commonly used are the piston flow, the binary or exponential mixing), providing information on aquifer functioning (Appelo and Postma, 2004; Cook et al., 2005; Małoszewski and Zuber, 1982). To date, only a few studies have been undertaken using CFCs and/or SF_6 to understand

groundwater flow in Chalk aquifers (Cary et al., 2014; Darling et al., 2012b, 2005; Gooddy et al., 2006). Furthermore, no studies have combined geological characterization, hydrodynamic conditions (water level fluctuations and recharge process), residence time determination and groundwater geochemistry within a Chalk aquifer. A methodology that combines these different approaches could provide a comprehensive understanding of the Chalk aquifer functioning.

Indeed, spatial and temporal heterogeneities of hydrogeological and geochemical properties could exist, resulting in a complex aquifer system even on a small scale. The aim of this work is to establish a conceptual model of the unconfined Chalk aquifer on a water catchment scale in terms of groundwater flow paths, mixings and geochemistry for a better understanding of the hydrogeological functioning of the aquifer.

2. Materials and methods

2.1. Site description

The study area is located at the East of the city of Reims in the Champagne region (NE of France; Fig. 1) and covers approximately 500 km^2 between the Suippe River (as the northern and western boundary) and the Vesle River (as the southern boundary). Both the two rivers have several tributaries; the Prosne River (tributary of the Vesle River) is dry for most of the time while others are permanent watercourses (Fig. 1).

The Cretaceous formations outcropping on the surface of the study area are constituted by: Coniacian (C3), Santonian (C4) and Campanian (C5) Chalks (Fig. 1). Despite the different age of formation, the three Chalks present a similar lithology. The first 10–20 m of the Champagne Chalk are significantly fractured and the fracturing decreases with depth (Mangeret et al., 2012; Vachier et al., 1987). The Chalk formation is partially covered by Tertiary formations (10–50 m; Laurain et al., 1981) at the Berru Mount and by Quaternary formations including graveluche, colluvium and alluvium (Fig. 1). Graveluche (also called grèze) refers to a periglacial formation with a maximum thickness of 6–10 m (Rouxel-David et al., 2002b). During the Quaternary, the long period of freeze - thaw alternation produced movement in the terrain. Graveluches, resulting from this gelification process of the chalk, are very variable in particle size and composition with more or less content on clay and silt (Vernhet, 2007). The graveluche formation is more widely spread in the north (the catchment area of the Suippe River) than in the south of the study area. Colluvium is present mainly in dry valleys, with a thickness of about 1–3 m. They have substantially the same composition as the soils from which they formed, but a higher silt and clay content. Alluvium deposits are located in river valleys, composed mainly by sand, clay and gravel (Vernhet, 2007). Their thickness could reach about 10 m in maximum, with locally accumulated clay layers up to 5 m (Rouxel-David et al., 2002b).

The unconfined Champagne chalk aquifer is a crucial water resource of the region. It is the only resource used for drinking water and is also largely exploited for agricultural and industrial uses. The total porosity of the Chalk is about 40% (Crampon et al., 1993), with only 1% related to the effective porosity (Vachier et al., 1987). The Champagne Mounts constitute the main reliefs where the transmissivity ranges from 10^{-6} $m^2 \cdot s^{-1}$ to 10^{-5} $m^2 \cdot s^{-1}$, whereas in the valleys these values are much higher, ranging from 10^{-2} $m^2 \cdot s^{-1}$ to 0.3 $m^2 \cdot s^{-1}$ (Rouxel-David et al., 2002b). The study area is divided into two parts by the groundwater divide line across the summit of Berru Mount and the Champagne Mounts, which delimits the Vesle River watershed in the south and the Suippe River watershed in the north. According to water levels, the chalk aquifer of the study area is generally drained by rivers (Rouxel-David et al., 2002a; Fig. 1). The precipitation constitutes the only recharge of the Champagne chalk aquifer. The climate of the region is temperate oceanic with an average temperature of 11.2 °C and average annual precipitation of 566 mm (values from MeteoFrance for 2012–2018 period at Reims-Prunay station; Fig. 1). The annual effective rainfall ranges generally from 100 to 150 mm (mainly in winter/spring), with the rest of the total precipitation being taken by evapotranspiration (Baran et al., 2006).

Land use of the study area can be divided into three major types: 1) agricultural: this type occupies the majority of the study area with the main crops of wheat, barley, sugar beet and alfalfa (Laurain et al. 1981); 2) forest: this is the second major type of land use which covers in particular the Berru and Champagne Mounts, representing about 15% of the surface of the study area; 3) anthropogenic: this category mainly includes cities and villages and represents about only 3% of the area of the sector, with a landfill situated in middle of the study area (Fig. 1).

2.2. Sampling and analytical methods

Water samples were collected monthly, from June 2017 to June 2019, at 15 sampling points (Fig. 1), including 10 boreholes, 2 pumping stations used for drinking water supply and 3 points in rivers, in order to take into account the groundwater/surface water exchanges. The sampling points are well distributed in the study area, allowing different geological contexts to be observed (properties of sampling points are presented in Table 1). In situ video inspection was done to examine the condition of boreholes. No abnormalities such as deterioration or cracks were found, except for FBN5. Inside the borehole FBN5, the casing set inside the borehole consists of a successive of short PVC pipes. However, these PVC pipes are not well connected and gaps between every two pipes were observed, allowing rainwater to seep into

Table 1
Properties of sampling points (N/A: no available data; \: not applicable; Y = Yes; N = No).

Name	Type	Latitude (°N)	Longitude (°E)	Altitude (m)	Depth (m)	Screen depth (m)	Equipped with water level loggers
FAP	Borehole	49.20634	4.15561	90	15	7–15	Y
FP1	Borehole	49.21308	4.15558	95	19	9–15	Y
FBN1	Borehole	49.25048	4.20809	134	48	4–48	Y
FBN4	Borehole	49.24725	4.23997	111	28	16–28	Y
FBN5	Borehole	49.24383	4.26732	140	47	24–43	Y
FEP1	Borehole	49.27210	4.23658	107	25	7–25	Y
FPM1	Borehole	49.27875	4.31364	107	24	N/A	N
FPM3	Borehole	49.29255	4.28730	103	21	7–21	Y
FVDV	Borehole	49.20202	4.25525	107	22	13–21	Y
FA	Borehole	49.19046	4.37777	123	35	4–29	Y
PP	Pumping station	49.19371	4.29981	111	80	23–80	N
PDO	Pumping station	49.23141	4.40722	110	25	7–25	N
RS1	River	49.23697	4.40956	108	\	\	\
RPY	River	49.24423	4.41038	107	\	\	\
RS2	River	49.27000	4.38921	102	\	\	\

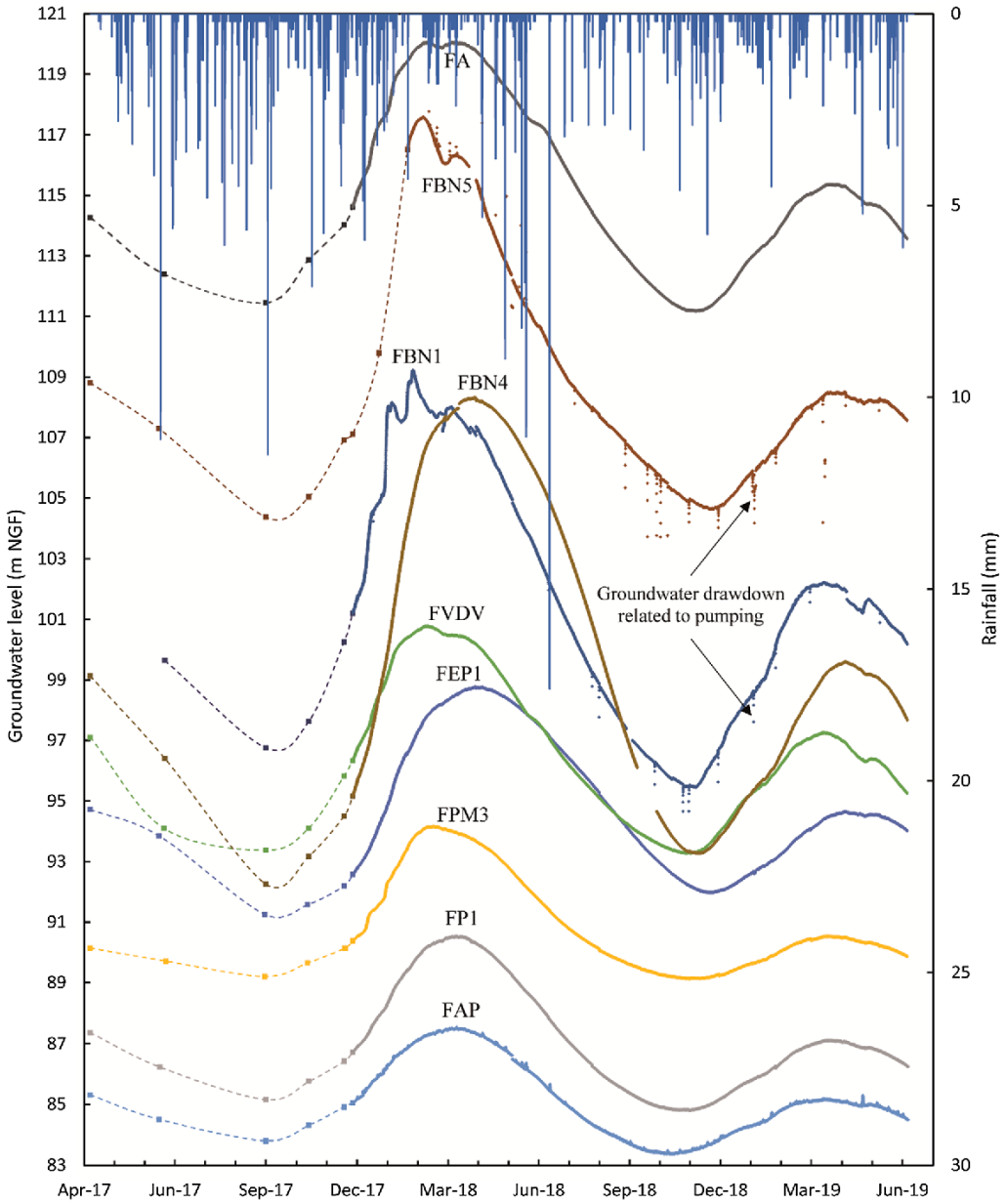

Fig. 2. Rainfall (hourly data) and groundwater level from April 2017 to June 2019 (solid line: hourly data measured by water-level loggers; dashed line: water level curve drawn by monthly data).

the borehole.

Groundwater levels were measured monthly. From December 2017, the water level and temperature were recorded hourly in the 9 non-exploited boreholes using pressure sensors (In-Situ Rugged TROLL 100 Water Level Logger; Table 1). In addition, a CTD-Diver water logger (Schlumberger Water Services) was installed in the borehole FAP to monitor hourly electrical conductivity (EC), as the water level here reacted much faster than the other boreholes following rainfall events.

In situ parameters were measured monthly at each site. Temperature, pH and EC were measured using a WTW 3320 pH meter and a WTW 3320 Conductivity meter. Alkalinity was determined using a HACH digital titrimeter. Water samples for analysis of major ions (Ca^{2+}, Mg^{2+}, Na^{+}, K^{+}, NO_3^{-}, SO_4^{2-}, Cl^{-}) were collected in two 50 ml polyethylene bottles after filtration through 0.45 µm membranes and the samples for cation analyses were acidified with HNO_3, the samples were then stored at 4 °C before analysis. Two sampling campaigns for groundwater dating using CFCs and SF_6 were carried out in May 2018 (high water level) and October 2018 (low water level). Waters for CFCs and SF_6 analysis were collected in stainless-steel ampoules after washing through at least three volumes of the ampoule, without any atmospheric contact during sampling. Waters for noble gases analysis were sampled in 500 ml glass flasks. The bottles were submerged in flowing water, flushed, and capped without headspace to avoid air bubbles.

Analyses of major cations and anions were done by ICP Optical Emission Spectrometry (ICAP 6300, THERMO) and Ion

Table 2
Summary of groundwater temperature and water table fluctuation from December 2017 to June 2019 (hourly data) measured by water-level loggers installed in unexploited boreholes and the minimum UZ thickness (derived from the water level in high water period in 2018).

Name	Temperature (°C)					Water level fluctuation (m)	Min thickness of the UZ (m)
	Number of data	Min	Mean	Max	Standard deviation		
FAP	11,703	8.7	11.5	14.2	0.59	4.0	2.0
FP1	11,703	10.9	11.1	11.3	0.03	8.5	4.5
FBN1	11,554	10.6	10.9	11.2	0.07	14.5	26.0
FBN4	11,192	10.2	10.5	10.8	0.09	15.5	2.5
FBN5	7041	11.2	11.3	11.6	0.02	12.5	22.5
FEP1	11,702	10.4	10.6	10.8	0.04	9.5	7.5
FPM3	11,695	11.0	11.2	11.4	0.04	9.0	9.0
FVDV	11,657	10.8	11.1	11.3	0.05	8.0	7.0
FA	11,699	10.7	11.0	11.3	0.05	9.0	3.0

Chromatography system (DIONEX ICS 2000) respectively. CFCs and SF_6 concentrations in water samples were measured by gas chromatography with an electron capture detector after pre-concentration by a "purge and trap" method, described by Aquilina et al. (2006) and Vergnaud-Ayraud et al. (2008). The analytical uncertainty is about 1–3% for CFCs and 5% for SF_6. Noble gases (Ar, Ne) were measured using a micro-gas chromatograph (GC 3000, SRA instruments) with an uncertainty of about 3% for Ne and less than 2% for Ar (Aquilina et al., 2006).

2.3. Estimation of recharge temperature, excess air and apparent age

The concentrations of noble gases were used to estimate recharge temperature and excess air contribution (Busenberg and Plummer, 1992; Heaton and Vogel, 1981). The estimation of the recharge temperature, defined as the temperature in the UZ above the water table where air–water equilibrium is carried out (Dunkle et al., 1993), is essential for determining the solubility of CFCs and SF_6 in Henry's law. Excess air refers to dissolution of air bubbles trapped by infiltrating water in the UZ (Heaton and Vogel, 1981). It is used to correct SF_6 data, which could be greatly influenced by this parameter in contrast to CFCs (Ayraud et al., 2008; Plummer et al., 2001; Vittecoq et al., 2007). The measured CFCs and SF_6 concentrations in water samples (in $pmol{\cdot}L^{-1}$) were converted to atmospheric partial pressures (in pptv) according to the estimated recharge temperature and then compared to the atmospheric evolution curve (available on USGS web site: https://water.usgs.gov/lab/software/air_curve/index.html) to determine the apparent age.

Groundwater is usually a contribution of water from different flow pathways according to aquifer properties. As a result, conceptual mixing models have to be used to interpret CFCs and SF_6 concentration as groundwater apparent ages. Three models are used in this study for the calculation of apparent ages: piston flow model (PFM), exponential mixing model (EMM) and binary mixing model (BMM). The piston flow model assumes that a tracer travels from the inlet position (recharge area) to the outlet position (e.g., a well or spring) without any dispersion or mixing (Jurgens et al., 2012; Etcheverry, 2002; Małoszewski and Zuber, 1982). The exponential mixing model describes an exponential distribution of transit times, with a transit time of zero for the shortest flow line and a transit time of infinity for the longest line. It is applicable for unconfined aquifers of constant thickness with uniform areal recharge (Cook et al., 2006). The apparent age calculated from EMM are expressed by the mean residence time (MRT), which corresponds to the transit time that is longer than that of 2/3 of the flow lines. Binary mixing model considers a mixing of young and old water masses, which represents the simplest mixing process. The proportion of the two components and the apparent age of one of the two components can be calculated. This model can be appropriate for aquifers with short-circuit pathways, karstic aquifers or watershed with transmissivity contrasts (Jurgens et al., 2012; Katz et al., 2009; Michel, 2004).

3. Results

3.1. Groundwater level fluctuation

Chalk groundwater level showed seasonal variations (Fig. 2). The highest water level was reached in March/April following the winter/spring recharge, due to excess of rainfall compared to evapotranspiration. Then the water level declined due to evapotranspiration excess and drainage by rivers. It reached the lowest level in October/November (Fig. 2). Annual variations were also observed. The water level in March/April 2018 was much higher than that of the same period in 2017 and 2019, as the winter of 2017 and the spring of 2018 were extremely wet with intensive precipitation. The water level during high water season of 2018 was the highest since the last ten years, as demonstrated by piezometric chronicles of two boreholes in Chalk aquifer near the study area monitored since 2008 (ADES database, 2019; SI 1).

Seasonal water level fluctuations were highly variable on the study area (Table 2). The changes in water level between high and low water conditions in 2018 were down to < 5 m near river valley (FAP) but could reach up to 15 m on interfluve (FBN1, FBN4 and FBN5), with the thickness of UZ varying from 2 m (FAP) to 26 m (FBN1) (Table 2). The rise of water level was not simultaneous in different boreholes (Fig. 2). In 2018, 4 boreholes (FBN4, FEP1, FP1 and FAP) reached their maximum levels in April, 4 boreholes (FA, FBN5, FVDV and FPM3) reached their maximum levels in March and 1 borehole (FBN1) reached its maximum level in February. Moreover, the rise of water level during recharge period was more rapid than the decline of water level during discharge period. This asymmetry was less obvious for boreholes near river valleys (FAP, FP1; Fig. 2).

The Chalk aquifer exhibits a very inertial behavior, whereby the temporal variation curves of groundwater levels are smooth with rather gentle slopes except for FBN1, FBN5 and FAP (Fig. 2). At FBN1 and FBN5, rapid drawdown was observed following pumping for water sampling during low water period (Fig. 2). Large fluctuations in water levels were also observed during high water level period, probably related to nearby groundwater exploitation for industrial and agricultural purposes. In addition, at FBN5, rapid increases in water level were observed following rainfall events, particularly during high water level period in 2018. This could be explained by a direct infiltration of rainwater into the borehole due to bad conditions of the casing as reported by video observations during period of high soil moisture and intensive precipitation. At FAP, water level also rapidly increased following the rainfall events (Figs. 2 and 3) but with a low range (several decimeters). It increased about 1 h after the rainfall and reaches a maximum value after 4 h. Then it stabilizes gradually to its pre-disturbance level in the following tens of hours (Fig. 3). The evolution of groundwater temperature and EC in this borehole follow the same pattern (Fig. 3). The video observations show that the tube is in good condition, a direct intrusion of rainwater into this borehole is unlikely.

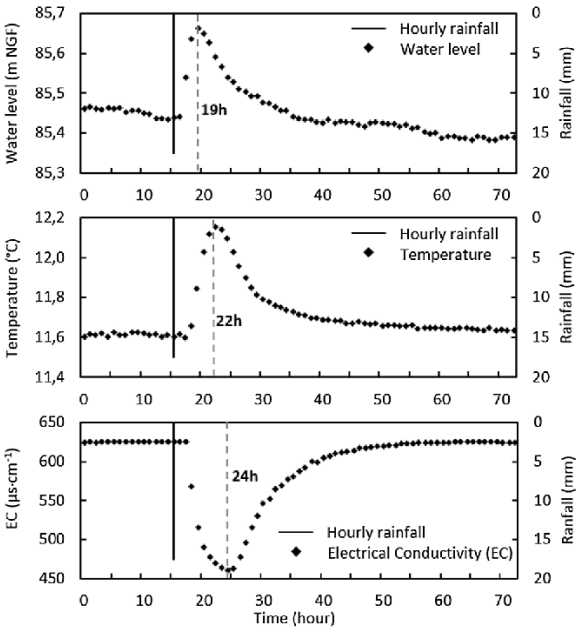

Fig. 3. Response of groundwater level (hourly data), temperature (hourly data) and EC (hourly data) to a rainfall event (17 mm at the 15th hour) at FAP from 5 July to 8 July 2018.

3.2. Chalk groundwater geochemistry

The chemical composition of the monitored groundwater is typical of the Chalk groundwater, with Ca^{2+} and HCO_3^- being the dominant ions (Table 3). However, significant spatial and temporal variations in groundwater geochemistry were observed, as shown by the variability of major ions concentrations and EC values. Average concentrations of Ca^{2+} and HCO_3^- at each sampling site ranged from 4.04 to 7.18 meq·L^{-1} and from 3.01 to 4.79 meq·L^{-1}, respectively. For Cl^- and NO_3^- ions, the average concentrations at each site ranged from 0.21 to 1.49 meq·L^{-1} and from 0.31 to 0.88 meq·L^{-1}, respectively. Concentrations of Mg^{2+}, Na^+, K^+ and SO_4^{2-} were also variable but much lower than those of other ions (Table 3). Temporal variations in concentrations were different for each major ion from one site to another.

Due to the high variability of the major ions concentrations, the mean values of EC at each site varied widely from 410 to 770 µs·cm^{-1}. Water samples collected at FBN4 were the most mineralized with the highest conductivity and high concentrations of almost all major ions. Water samples collected at FPM1 and FPM3 were the least mineralized with the lowest values of EC and low concentrations of major ions. The pH values of the groundwater samples were relatively homogeneous, with average values at each sampling site ranging from 7.07 to 7.48 (Table 3).

Surface water samples had the same Ca^{2+}–HCO_3^- chemical facies as groundwater samples, as river water in the study area comes mainly from drainage of the Chalk aquifer. The pH values (7.94–8.07) were higher than those measured in groundwater (7.07–7.48). The EC mean values at each site ranged from 488 to 517 µs·cm^{-1}, with relatively low spatial and temporal variabilities.

3.3. Groundwater dating by CFCs and SF_6

3.3.1. Recharge temperature and excess air

In groundwater samples, Ne and Ar concentrations ranged from $0.84{\cdot}10^{-8}$ to $1.69{\cdot}10^{-8}$ mol·L^{-1} and $1.71{\cdot}10^{-5}$ to $2.18{\cdot}10^{-5}$ mol·L^{-1}, respectively (Table 4). The recharge temperature and excess air were estimated from the relationship between Ar and Ne (SI 2).

In May 2018, the estimated recharge temperature was similar in all waters of the study area with an average value of 10 °C. No recharge temperature information can be estimated at FBN4 due to a high value of excess air. In October 2018, the recharge temperature showed a spatial variability, with values ranging from 10 and 16 °C (with an average value of 13 °C), higher than that in May. This is consistent with several months' winter recharge with relatively low temperatures, making the estimated recharge temperature in water samples in May lower than in October when samples were collected at the low water level with very few recharge in summer.

The estimated excess air in samples ranged from 0 to more than 8 ml·L^{-1} with an average value of about 3.4 ± 2 ml·L^{-1}. No significant difference in excess air values was observed between the two sampling

Table 3
Major ion concentrations and physicochemical parameters of Chalk groundwater from June 2017 to June 2019 (average values from monthly data) with the temporal variation coefficient (%) at each sampling point in blankets (N = Number of samples).

	Name	N	pH	EC	HCO_3^-	Cl^-	NO_3^-	SO_4^{2-}	Na^+	K^+	Mg^{2+}	Ca^{2+}
				(µs·cm^{-1})	(meq·L^{-1})							
Surface water	RS1	21	8.04 (3.3)	517 (4.5)	3.58 (7.5)	0.73 (6.6)	0.47 (6.2)	0.25 (20.5)	0.25 (11.3)	0.05 (24.5)	0.08 (9.6)	5.06 (4.6)
	RPY	21	7.94 (3.4)	488 (5.8)	3.65 (8.0)	0.58 (7.8)	0.46 (5.7)	0.14 (27.1)	0.22 (12.9)	0.02 (12.9)	0.08 (8.3)	4.86 (3.1)
	RS2	21	8.07 (2.8)	510 (4.9)	3.63 (7.3)	0.69 (5.3)	0.48 (6.1)	0.22 (20.6)	0.24 (8.1)	0.04 (17.8)	0.08 (9.8)	5.03 (4.1)
Groundwater	FA	21	7.41 (2.5)	533 (8.3)	3.42 (13.7)	1.00 (17.9)	0.64 (15.2)	0.19 (20.8)	0.19 (10.2)	0.01 (36.3)	0.05 (9.9)	5.19 (8.4)
	FAP	21	7.17 (3.3)	613 (14.7)	4.35 (17.3)	0.87 (30.8)	0.46 (23.4)	0.44 (18.4)	0.51 (54.3)	0.10 (20.0)	0.22 (22.6)	5.62 (16.8)
	FBN1	21	7.38 (4.5)	511 (9.6)	3.70 (6.2)	0.71 (35.1)	0.47 (26.2)	0.29 (62.2)	0.32 (41.9)	0.02 (26.9)	0.10 (23.0)	4.86 (4.5)
	FBN4	21	7.07 (2.6)	770 (3.7)	4.79 (6.7)	1.49 (5.0)	0.88 (4.8)	0.39 (8.4)	0.37 (8.9)	0.15 (5.8)	0.24 (10.6)	7.18 (3.0)
	FBN5	21	7.29 (4.0)	504 (19.6)	4.12 (15.3)	0.42 (61.4)	0.51 (35.7)	0.08 (37.9)	0.26 (87.6)	0.08 (23.0)	0.11 (24.5)	4.91 (20.2)
	FEP1	21	7.42 (6.8)	541 (1.1)	3.80 (7.62)	0.99 (2.7)	0.59 (3.8)	0.09 (20.1)	0.26 (7.0)	0.02 (14.4)	0.09 (8.8)	5.19 (3.7)
	FP1	21	7.23 (2.7)	592 (4.4)	4.23 (5.4)	0.79 (10.2)	0.48 (13.1)	0.40 (5.8)	0.28 (9.8)	0.08 (9.5)	0.19 (9.8)	5.78 (5.3)
	FPM1	21	7.48 (3.6)	410 (3.0)	3.39 (3.7)	0.21 (9.1)	0.31 (4.4)	0.12 (13.8)	0.15 (7.7)	0.02 (8.4)	0.10 (8.7)	4.14 (3.5)
	FPM3	21	7.48 (2.9)	412 (8.1)	3.01 (9.1)	0.52 (27.0)	0.39 (23.8)	0.12 (11.8)	0.18 (9.4)	0.01 (16.5)	0.06 (10.7)	4.04 (7.8)
	FVDV	21	7.28 (3.2)	602 (2.3)	3.94 (4.9)	1.10 (4.2)	0.64 (5.6)	0.21 (13.5)	0.34 (10.8)	0.07 (14.8)	0.09 (10.1)	5.67 (3.3)
	PDO	21	7.34 (2.9)	562 (1.8)	3.52 (5.9)	0.96 (3.8)	0.68 (4.8)	0.27 (5.2)	0.21 (7.0)	0.02 (18.2)	0.07 (8.8)	5.45 (3.5)
	PP	21	7.38 (2.0)	459 (3.1)	3.34 (7.0)	0.61 (5.2)	0.42 (3.3)	0.14 (12.6)	0.19 (7.7)	0.02 (31.2)	0.06 (8.9)	4.53 (3.5)
	Minimum		7.07	410	3.01	0.21	0.31	0.08	0.15	0.01	0.05	4.04
	Mean		7.33	542	3.80	0.81	0.54	0.23	0.27	0.05	0.12	5.21
	Maximum		7.48	770	4.79	1.49	0.88	0.44	0.51	0.15	0.24	7.18
	Variation coefficient (%)		4.2	16.4	12.0	38.3	26.1	51.1	33.7	83.5	51.3	14.5

Table 4
CFCs, SF_6, noble gases and estimated groundwater age by piston flow model, exponential mixing model (MRT = mean residence time) and binary mixing model (proportion of young and old water) in May and October 2018 (the choices of the ideal model and estimated residence times are marked in bold; Cont. = contamination: \ = not applicable).

Name	Sampling time	SF_6 (pptv)	CFC-12 (pptv)	CFC-11 (pptv)	CFC-113 (pptv)	Ar (10^{-5} mol·L^{-1})	Ne (10^{-8} mol·L^{-1})	SF_6	Piston flow model			Exponential model (MRT years)				Binary mixing model			Comment
									CFC-12	CFC-11	CFC-113	SF_6	CFC-12	CFC-11	CFC-113	% young water	young age	old age	
FA	May	9.7	522.7	205.5	56.6	1.93	1.32	6	24	34	31	0	7	25	27	75	0	40	
	Oct.	7.9	507.3	182.4	58.6	1.71	1.24	6	26	36	31	5	12	30	25	80	0	>50	
FAP	May	7.1	538.0	278.0	62.4	1.83	1.16	8	11	25	30	8	\	\	20	70	0	35	
	Oct.	6.2	504.9	237.9	58.5	1.78	1.13	11	27	31	31	12	13.5	12	25	50	0	30	
FBN1	May	5.1	cont.	cont.	66.4	1.72	1.03	16	\	\	30	18	\	\	18	40	0	30	
	Oct.	5.3	cont.	cont.	75.2	1.73	1.05	16	\	\	28	18	\	\	7	40	0	30	
FBN4	May	2.1	cont.	206.3	cont.	2.18	1.69	29	\	34	\	70	\	25	\	10	0	35	
	Oct.	5.4	472.7	188.1	cont.	1.85	1.35	15	29	36	\	17	17.5	30	\	50	0	35	
FBN5	May	5.1	cont.	cont.	cont.	1.83	1.16	16	\	\	\	18	\	\	\	\	\	\	Not datable
	Oct.	4.0	cont.	cont.	72.6	1.89	1.26	21	\	\	29	30	\	\	12	25	0	30	
FEP1	May	5.4	cont.	cont.	46.9	1.84	1.22	14	\	\	33	16	\	\	40	60	0	>30	
	Oct.	5.1	cont.	cont.	70.6	1.84	1.20	16	\	\	29	19	\	\	13.5	90	15	>60	
FP1	May	7.5	cont.	cont.	41.0	1.95	1.28	7	\	\	33	6	\	\	40	\	\	\	
	Oct.	3.6	376.1	cont.	46.2	1.77	1.21	23	34	\	33	35	35	\	40	30	0	40	
FPM1	May	cont.	cont.	cont.	46.7	1.75	0.92	\	\	\	33	\	\	\	40	\	\	\	Not datable
	Oct.	cont.	cont.	cont.	cont.	1.72	0.84	\	\	\	\	\	\	\	\	\	\	\	
FPM3	May	cont.	cont.	141.8	cont.	1.77	1.08	\	\	41	\	\	\	50	\	\	\	\	Not datable
	Oct.	cont.	cont.	95.9	cont.	1.74	1.04	\	\	45	\	\	\	100	\	\	\	\	
FVDV	May	4.5	cont.	258.1	cont.	1.80	1.10	19	\	15	\	22	\	\	\	30	0	30	
	Oct.	3.9	cont.	239.4	cont.	1.70	1.04	22	\	31	\	35	\	11	\	25	0	30	
PDO	May	5.1	504.5	163.9	49.9	1.72	0.99	16	26	38	32	18	12	40	35	30-50	0	>40	
	Oct.	6.1	416.7	162.0	44.0	1.70	1.08	12	32	39	33	13.5	27	40	45	60	0	45	
PP	May	6.4	449.7	147.4	80.7	1.90	1.29	10	30	41	27	11	20	50	\	\	\	\	
	Oct.	6.9	376.1	135.4	cont.	1.88	1.41	9	34	42	\	8.5	35	70	\	65	0	>60	

campaigns. At FPM1, negative excess air value was observed, which could probably due to the absorption by rubber tubes present at this borehole. The highest values of excess air were observed in water samples at FP1, FA, PP and FBN4, with the maximum value (> 8 ml·L^{-1}) for water sample collected at FBN4 in May 2018.

3.3.2. Groundwater apparent ages

The measured CFCs and SF_6 concentrations in water samples (in pmol·L^{-1}) were transferred to atmospheric partial pressures (in pptv) according to Henry's law. The data was rejected when calculated concentrations were greater than atmospheric peak concentrations (marked as contamination; Table 4).

A frequent contamination of tracer gases was observed on the study area, especially for CFC-12. Commonly recognized sources of CFCs contamination include seepage from septic tanks, landfills (Kjeldsen and Christophersen, 2001), release from polyurethane foam waste (Kjeldsen and Jensen, 2001), leaky sewer lines, leakage from underground storage tanks, infiltration or disposal of industrial wastes and recharge from rivers contaminated with CFCs (Cook et al., 2006). CFCs contamination could also result from agricultural activities. Agricultural application of pesticides may introduce CFCs, particularly CFC-11 to unsaturated air, as CFCs are allowed as inert ingredients in pesticide formulations (Plummer et al., 2000). In addition, CFCs can sorb into rubber and polymers; therefore water samples can also be contaminated with CFCs from contact with these materials such as permanently installed submersible pumps in wells with rubber parts (Cook et al., 2006; Dunkle et al., 1993). Although most SF_6 concentrations did not exceed atmospheric peak concentrations, apparent ages estimated by SF_6 were generally much younger than all the other tracers, suggesting some anthropogenic and/or natural addition of SF_6. Anthropogenic sources of SF_6 include high-voltage electricity supply equipment, Mg and Al melting and landfills (Darling et al., 2012a; Santella et al., 2008). Unlike CFCs, which come exclusively from anthropogenic sources, SF_6 can also be present naturally in rocks. The major known source of terrigenous SF_6 is found in fluorite and granite; however, significant concentrations of SF_6 is also reported in other mineral and rock types such as hydrothermal mineral deposits, halite and dolomite (Busenberg and Plummer, 2000; Harnisch and Eisenhauer, 1998). The natural presence of SF_6 in Chalk cannot be excluded, as dolomite is commonly present in Chalk as impurity (Barhoum et al., 2014; Gillon et al., 2010).

The studied aquifer is unconfined with fractures, making the soil and groundwater very vulnerable to contamination. The landfill site in middle of the study area (Fig. 1) appears to be a major source of contamination of CFCs and SF_6. A small waste deposit site located near the borehole FBN1 (Fig. 1) could also represent a local source of pollution. Furthermore, since the majority of the study area is used as farmland, the agricultural application of pesticides could also be a potential source of contamination for CFCs, especially CFC-11 (Plummer et al., 2000). It should be noted that water samples collected at FPM1 were contaminated by all the 4 trace gases. Indeed, FPM1 is a private well in a farm where a permanently pumping system is installed. Water samples were collected directly from the tap. Air contact with the pumped water may occur between the pump and the tap. Rubber water tubes connected with the tap could also present a potential source of contamination. As a result of frequent contamination, some water samples are not datable (FBN5, FPM1 and FPM3) as only one or two tracers are valid for calculation and estimated ages are not consistent for different tracer gases.

Cross-plots of concentrations for CFC-11 vs CFC-113 and SF_6 vs CFC-113 super imposed on the mixing models have been realized (SI 3). CFC-12 is not used for cross-plot due to its frequent contamination. Also, not all water samples were plotted as some of them were concerned by contamination of related tracers with concentrations surpassing the range of axis. The plot position of sampling points compared to PFM, EMM and BMM curves allowed to provide information for the selection of models. Also, the consistency of apparent ages between different tracer gases and between the two sampling campaigns is used for the validation of models. When different tracers did not give consistent apparent ages, values estimated by CFC-11 and CFC-113 were considered to be more reliable than CFC-12 and SF_6 as the latter two tracers were largely influenced by anthropogenic activities on the study area.

The selected mixing models and estimated residence time are resumed in Table 4. Groundwater residence time of the study area is rather heterogeneous, ranging from modern to about 50 years. This result is comparable with previously published data on the Champagne Mount area, with an average residence time of about 25 years (Mangeret et al., 2012). The piston flow model is more suitable for FEP1 and PP (30–40 years). The exponential mixing model is the best model for FBN1, FBN4 and FP1 (MRT from 18 to 40 years). The binary mixing model is more suitable for FA, FAP, FVDV and PDO (25% to 80% of modern water and an end member of old water ranging from 30 to more than 50 years). Residence times estimated by piston flow and

exponential mixing model at each point were similar between the sampling campaign of May 2018 (high water) and October 2018 (low water). For boreholes applying the binary mixing model, significant differences of residence time were observed between the two sampling campaigns. At FA, FAP and FVDV, estimated apparent ages for samples collected in May are younger than in October with higher proportions of modern water or younger ages of the old end member. At PDO, apparent ages for samples collected in May are older than in October with less proportions of modern water (age < 10 years) (Table 4).

4. Discussion

4.1. Hydrodynamic characteristics

The unconfined Chalk aquifer of the study area possesses highly heterogeneous hydrological characteristics. A higher variation in water levels was observed on interfluves than in river valleys (Fig. 2) attesting differences in transmissivity and storage yield. In river valleys, high density of active fractures are consistently developed, resulting in high permeability of the aquifer (Haria et al., 2003; Ineson, 1962; Price, 1987; Price et al., 1993). Water is discharged quickly through the fractures toward the valleys at times of high recharge, thus not allowing the water levels to rise significantly (Allen et al., 1997; Whitehead and Lawrence, 2006). Conversely, on interfluves, the low permeability and storage yield make the Chalk aquifer more sensitive to recharge and discharge, resulting in greater and faster water level fluctuations between low water and high water periods (Allen et al., 1997). In general, groundwater reached the maximum level earlier on interfluves than in river valleys, which is reasonable as on interfluves the distance to the groundwater divide line is closer and the time of lateral flow from the recharge zones towards the borehole is shorter.

Rapid drawdown of groundwater level observed at FBN1 and FBN5 implied a low productivity of these two boreholes, which could be explained by the thick UZ (> 20 m) and low permeability of the aquifer. The Chalk aquifer of the study area exhibits a very inertial behavior with respect to recharge, as evidenced by the slow and progressive temporal variations of the water levels and high stability of water temperature (standard deviations < 0.1 °C; Table 2). No impact of individual rainfall events was observed, suggesting a dominant recharge through the Chalk matrix, as demonstrated by numerous studies in Chalk aquifers (e.g., Barhoum, 2014; Haria et al., 2003; Ireson et al., 2006; Mathias et al., 2006; Smith et al., 1970; Wellings and Bell, 1980). However, differences are observed at FAP. Sharp increases in water level after rainfall events were observed, followed by equally rapid declines. Fig. 3 shows an example of this trend in July 2018. Water level started to increase about 1 h after the rainfall event and reached its maximum value about 4 h later (85.45–85.67 m NGF). Similar rapid responses within 24 h of rainfall were observed in a few previous investigations (Allen et al., 1997; Lee et al., 2006). Allen et al. (1997) suggested that this would be expected only if the large fractures had been replenished (rapid transfer initiated) and subsequently drained during recharge period. At FAP, hourly temperature and EC were also measured and compared with rainfall time series. Water temperature increased about 2 h after the rainfall and reached its maximum value about 7 h later (11.6–12.2 °C). EC decreased about 2 h after precipitation and reached the minimum value about 9 h later (625–460 $\mu S.cm^{-1}$). In July (summer), the increase in temperature may be easily explained by a higher atmospheric temperature in July compared with groundwater temperature. EC decreased due to the dilution by rainwater. The variation of temperature and EC combining with that of water level confirms that the aquifer at FAP testifies to rapid transfers *via* a well-developed fracturing network thus exhibits no longer an inertial behavior. Note that the response of water level was faster than that of temperature and EC, as the water pressure transfer process was faster than the mixing between rainwater and groundwater. Rapid flows through fractures are added to matrix flows that are still effective as evidenced by the evolution of groundwater levels on an annual scale (Fig. 2).

Excess air in groundwater provides also useful information on flow pathways and recharge processes. Higher excess air values were measured in groundwater at FP1, FA, PP and FBN4. These 4 boreholes have a thin UZ (less than 5 m in 2018 high water period; Table 2). The water level at pumping station PP is not measured, but historical data showed a UZ thickness of about 5 m (data source: InfoTerre.brgm.fr). It is suggested that at these 4 shallow groundwater sites, recharge by preferential fracture flow is favored with more fractures developed near the surface, while the other deeper groundwater sites are dominated by matrix flow as fracturing of the chalk decreases with depth (Haria et al., 2003; Mathias et al., 2006). The preferential flow is guaranteed by water-filled small fractures and the capillary channels above the water table, resulting in a subsequent rapid rise of water table after rainfalls (Heaton and Vogel, 1981). These effects are supposed to favor the formation and entrapment of air bubbles, which could possibly explain the higher quantity of excess air in water samples collected at these points. Note that the borehole FAP also has a water table depth of less than 5 m. However, the excess air values in water were relatively low, similar to the mean value of the study (SI 2). This is consistent with the very developed fracturing network at FAP. Large fractures are less favorable for the air entrapment, resulting in relatively low excess air values than other shallow groundwater sites.

4.2. Origin of major ions

The correlation matrix of major ions (details of the calculation method and results can be found in SI 4 and 5) and relationships between ions (Fig. 4) were used to study the origin of major ions.

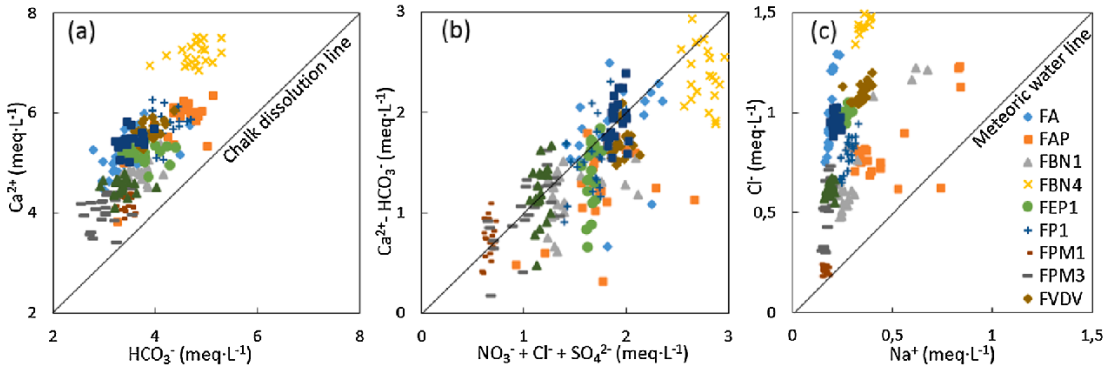

Fig. 4. (a) Ca^{2+} versus HCO_3^- (solid line 1:1 represents the Chalk dissolution line); (b) [Ca^{2+} - HCO_3^-] versus [NO_3^- + Cl^- + SO_4^{2-}]; (c) Cl^- versus Na^+ (solid line 1:1 represents the meteoric water line).

Concentrations of Ca^{2+} and HCO_3^- ions are significantly correlated (Fig. 4a and SI 5), which is consistent with the typical chemistry of Chalk groundwater. However, Ca^{2+} / HCO_3^- plots (Fig. 4a) are not aligned to the 1:1 line (Edmunds et al., 1987) with an enrichment of Ca^{2+} compared with HCO_3^-, indicating a secondary origin of Ca^{2+} in addition to Chalk dissolution (Barhoum et al., 2014). Ca^{2+} excess compared with HCO_3^- was then plotted with the sum of Cl^-, NO_3^- and SO_4^{2-} (Fig. 4b). Most data points are plotted along the 1:1 line, implying that Ca^{2+} excess may be due to an agricultural source as Cl^-, NO_3^- and SO_4^{2-}. Indeed, a common agriculture source of Cl^-, NO_3^- and SO_4^{2-} is also indicated by a significant correlation between these ions (SI 5). In fact, lime (CaO) can be used in agricultural to optimize field pH (Aquilina et al., 2012; Bolan et al., 2003) and some fertilizers could contain CaO or Ca^{2+} as secondary or minor component (such as *TSP-SUPER 45* used in the Champagne region). According to the Cl^- versus Na^+ graph (Fig. 4c), a high enrichment of Cl^- is observed with respect to the meteoric water line (Edmunds et al., 1987; Kloppmann et al., 1994), which confirms the Cl^- source due to anthropogenic activities.

Also, the correlation is observed between Mg^{2+}, K^+ and SO_4^{2-} ions (SI 5). These correlation relations imply that Mg^{2+}, K^+ and a part of SO_4^{2-} may have a common terrigenous source. In fact, Chalk impurities and clay minerals in superficial formations (mainly colluvium and alluvium in the study area) may provide Mg^{2+}, K^+ as well as SO_4^{2-} to groundwater (Gillon et al., 2010; Stuart and Smedley, 2009).

4.3. Spatial and temporal variations of Chalk groundwater geochemistry under effects of hydrogeological setting and residence time

4.3.1. Spatial analyses

To interpret the spatial distribution of Chalk groundwater geochemistry, a principal component analysis (PCA) of major ion concentrations and EC was performed (details of the method can be found in SI 4) (Fig. 5). The first two principal components (F1 and F2) justified together 78% of the variance. F1 is positively weighted on the allochthonous agricultural ions (NO_3^- and Cl^-) and on Ca^{2+} (more weakly) and negatively weighted on Na^+, Mg^{2+}, SO_4^{2-}, K^+ and HCO_3^-, which are interpreted as autochthonous ions. F2 is positively weighted on EC and all the major ions but the most strongly on Ca^{2+} and HCO_3^-, which correspond to the typical geochemistry of Chalk groundwater dominated by these two ions.

Hierarchical clustering of PCA shows a vast spatial heterogeneity of major ion concentrations on the study area and distinguishes six water-type groups (Fig. 5). RS1, RS2 and RPY (river waters) were plotted near the center zone of PCA graph, implying that the geochemistry of river water was similar to the average condition of groundwater, which is justified by the drainage of the whole aquifer by the rivers. Relatively low concentrations of agricultural ions (NO_3^-, Cl^- and Ca^{2+}) were observed at FBN1 and FBN5, which could be explained by the large UZ thickness (> 20 m; Table 2), whereby the aquifer tended to be less influenced by agriculture activities (e.g., fertilizer applications). In contrast, higher concentrations of agricultural ions were observed at FVDV, PDO, FA and FEP1 because of smaller UZ thickness (< 10 m; Table 2). Extremely high major ion concentrations at FBN4 were supposed to be related to the landfill located upstream, representing an important point source of pollution. FP1 and FAP have a similar chemical composition with high concentrations on Na^+, Mg^{2+}, SO_4^{2-} and K^+ ions especially. At these two points, the Chalk is covered by a large surface of colluvium with relatively high content on clay minerals (Fig. 1), which represents a possibly source of these ions in groundwater. Low concentrations of major ions were observed at FPM1, FPM3 and PP, which could be explained by the presence of superficial formations (graveluche and alluvium) limiting the transfer of water and solute from surface to the aquifer (Linoir, 2014). The impact of

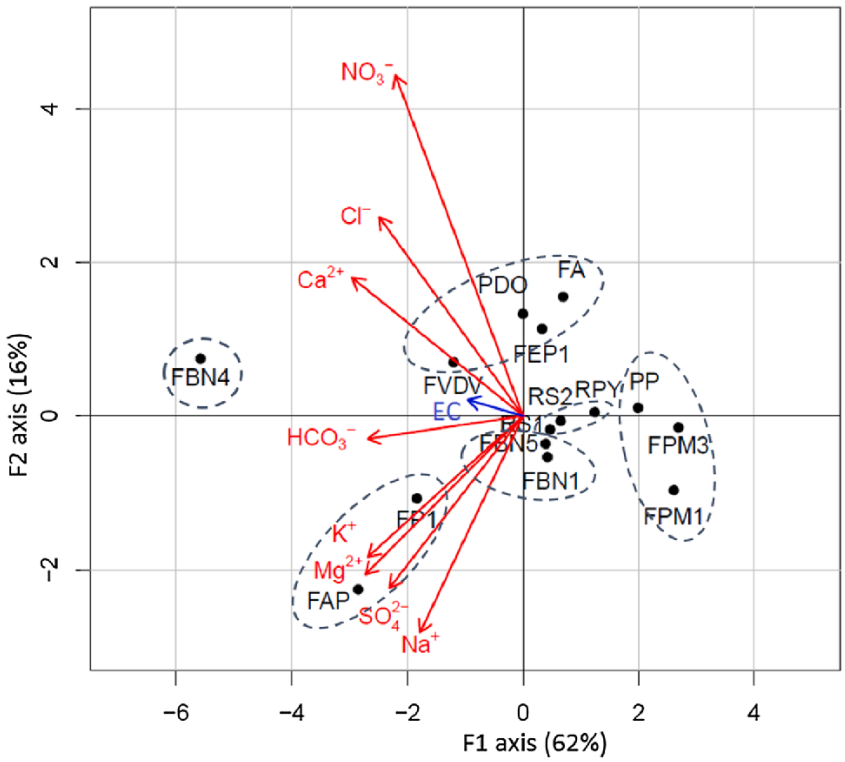

Fig. 5. PCA of major ion concentration in groundwater and surface water (mean values of monthly data at each sampling point from June 2017 to June 2019; dotted circles evidences the six water-type groups discussed in the text).

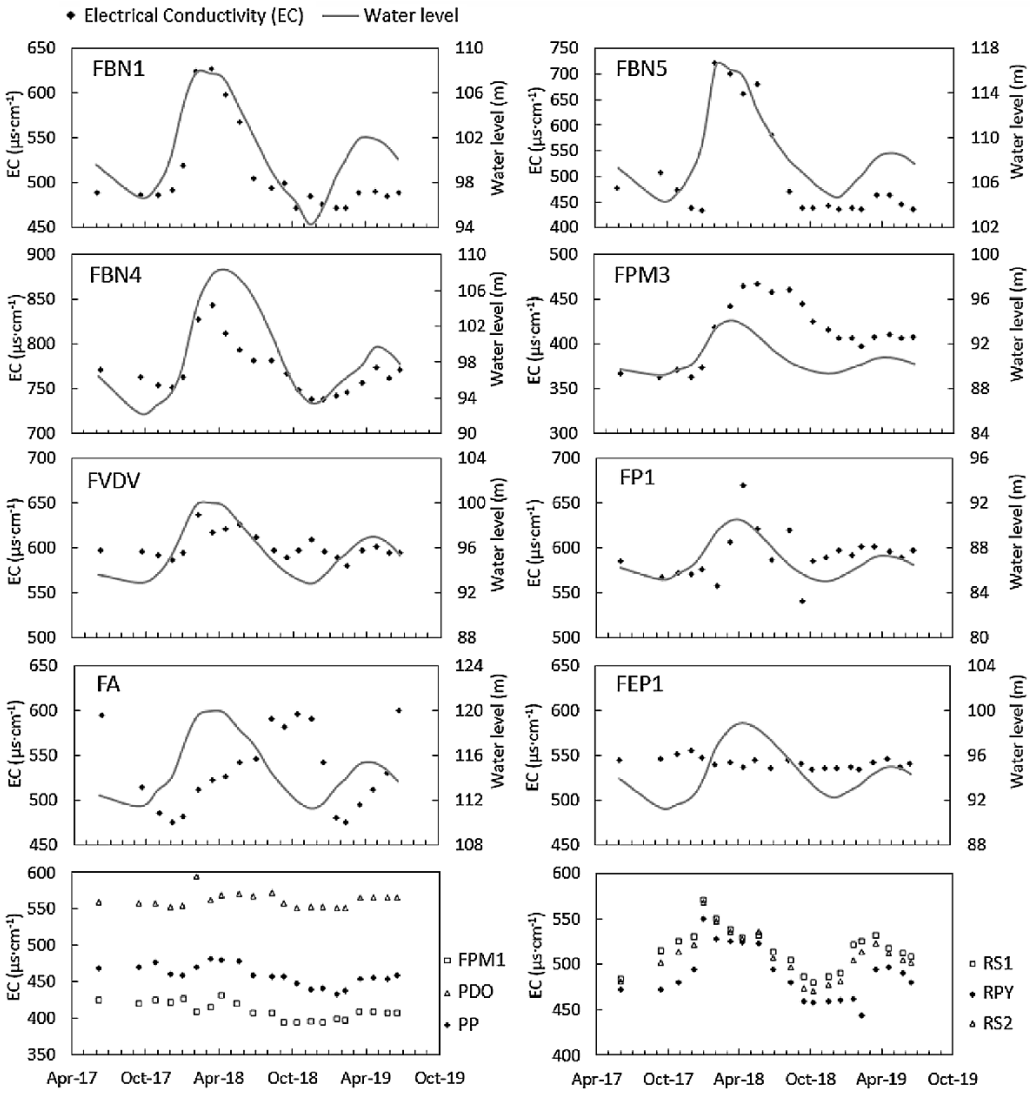

Fig. 6. Temporal variation of groundwater level and EC (monthly data from June 2017 to June 2019).

superficial formations overlying the Chalk on groundwater geochemistry are further discussed in the following section.

4.3.2. Temporal variations

The temporal variation of geochemistry was explored by analyzing the EC chronicle compared with groundwater level time series (Fig. 6). A combination of hydrogeological setting, residence time and land use information was used to explain the temporal variations of Chalk geochemistry on the study area.

- Area with large fluctuation in water level

Large fluctuation in water level was observed at FBN1 and FBN5 (> 12 m; Table 2). EC time series were highly correlated with water level fluctuations (Fig. 6 and Table 5). During high water level period in 2018, water level increased substantially following intensive recharge, resulting in an increase in EC of about 150 and 300 µs·cm^{-1} at FBN1and FBN5 respectively. However, no significant variation of EC was observed during high water level period in 2019, as water level was much lower under dry climate conditions. According to groundwater dating, the groundwater flow was described by the exponential mixing model and a MRT of 18 years was estimated at FBN1 (no accurate age was deduced for FBN5), indicating a spatially uniform recharge and a mixture of different flows. In this context, contaminants concentrated

Table 5
Correlation coefficient (r^2) of EC and all major ions with groundwater level (statistically significant as the P-value < 0.05, related r^2 values when P-value < 0.05 are marked in bold; calculation details are presented in SI 4 and 6).

	EC	HCO_3^-	Cl^-	NO_3^-	SO_4^{2-}	Na^+	K^+	Mg^{2+}	Ca^{2+}
FBN1	0,95	0,06	0,95	0,58	0,51	0,95	0,20	0,88	0,57
FBN4	0,73	0,19	0,15	0,05	0,62	0,04	0,32	0,32	0,21
FBN5	0,89	0,86	0,40	0,37	0,29	0,11	0,46	0,76	0,72
FVDV	0,68	−0,05	0,14	0,22	0,47	0,04	0,27	0,07	0,07
FEP1	−0,01	0,14	0,02	0,30	0,08	0,19	0,01	0,01	0,07
FP1	0,20	0,03	−0,04	0,03	0,50	0,08	0,25	0,29	0,02
FA	0,02	0,09	0,11	0,14	0,18	0,05	0,03	0,31	0,21
FAP	−0,05	−0,04	0,02	0,06	0,02	0,00	0,02	0,04	0,05
FPM3	0,26	0,01	0,00	0,02	0,62	0,09	0,05	0,08	0,01

near the land surface area infiltrated progressively across the UZ following recharge. Under low water level conditions, the contamination front was disconnected with the SZ. It transferred slowly downward through the unsaturated Chalk matrix. Meanwhile, solutes in the SZ were diluted by the mixing process of groundwater, so that a low EC was observed. As water level rose and reached the contamination front, the contamination source was re-activated and contaminants concentrations increased rapidly in the SZ so that a high EC was observed. Similar pollutant remobilization processes were previously suggested by Brouyère et al. (2004), Hakoun et al. (2017) and Orban et al. (2010). The highly correlation between time series of NO_3^-, Cl^-, SO_4^{2-}, Ca^{2+} concentrations and water level fluctuation (Table 5) confirms this mechanism.

At FBN4, a high correlation between EC and large water level fluctuation (15.5 m; Table 2) was also observed in a context of exponential mixing (MRT = 17 years; Table 4). However, the temporal variation of EC followed that of water level during the whole monitoring period (2017–2019) while EC remained stable at low water levels at FBN1 and FBN5. This could be explained by the thin UZ at FBN4 (2.5 m; Table 2), whereby the contaminated area was always partially submerged by groundwater level even during low water level period.

At FVDV, the water level fluctuation was smaller (8 m; Table 2), resulting in a lower correlation between EC and water level times series ($r = 0.69$; Table 5) compared to FBN1, FBN4 and FBN5. Groundwater consisted mainly of 30-year-old water mixed with 25–30% of modern water, suggesting small contributions of rapid recharge through fractures.

- Area with developed fracture network and low UZ thickness

EC time series were inversely related to water level fluctuation at FAP and FA (Figs. 3 and 6), suggesting that the dilution effect was the most important factor that influences the geochemistry. At these two sites, the UZ thickness was low (< 3 m; Table 2) and fractures were supposed to be developed near surface area. Groundwater dating showed 50–70% and 75–80% of modern water at FAP and FA respectively by the binary mixing model (Table 4), indicating an aquifer constituted mainly by freshly percolated rainwater that favors the process of dilution. Larger proportion of modern water at FA could be explained by its location close to groundwater divide line, receiving few lateral flow. It should be noted that, even during high water level period, the groundwater at FAP and FA was composed of 20% to 50% of old water aged over 30 years. This older end-member is linked to the lateral flow originated from upstream recharge areas.

- Area with superficial formation

EC values were stable in time at FPM1 and FEP1 (Fig. 6). Groundwater dating showed a residence time of > 30 years at FEP1 in a piston flow context, indicating a small recharge area away from the site (no accurate age was deduced for FPM1; Table 4). These two wells are situated in the north of the study area, where large surfaces of the Chalk are covered by graveluche (Fig. 1). The graveluche layers rich in clayey minerals are less permeable with an infiltration rate about 3 to 4 times slower than in the Chalk, therefore could constitute a barrier or buffer zone which limits rapid transport of water and solute from surface to the SZ (Linoir, 2014). Consequently, the aquifer received recharge mainly from upstream the graveluche covered area (near the Champagne mounts; Fig. 1). Water traveled laterally in the SZ during more than 30 years, resulting in a stable geochemistry independent on water level fluctuation. At FPM3 (downstream the borehole FPM1; Fig. 1), a time lag was observed between EC and water level time series, as a result of delayed solute transfer by the discontinuous graveluche formations. At PP, EC was also stable with a residence time of about 40 years estimated by a piston flow model (Table 4). With a high proportion of clayey minerals, the alluvium can play the same role as graveluche as a flow barrier on the Chalk. Moreover, the deep screen position of PP (23–80 m; Table 1) allowed pumping of deep groundwater with longer residence time. Previous studies (e.g., Barhoum et al. 2014; El Janyani et al. 2012) have shown that other superficial formations such as flint clay layers can have similar impacts on Chalk aquifers.

- Area along riverside

PDO is a pumping station used for drinking water supply located close to the Suippe River (Fig. 1). The drawdown of groundwater level due to intensive exploitation could result in a recharge of aquifer by river water, as testified by a higher proportion of modern water in October than in May 2018 (Table 4). Indeed, the groundwater level was lower in October resulting in increased flow from the river to the aquifer. The EC of river water was relatively stable, making the EC at PDO stable over time (Fig. 6).

FP1 is a non-exploited borehole located in the Vesle River valley (Fig. 1). No correlation relationship between EC and water level was observed. Located far from the groundwater divide line, FP1 has a very large recharge area, receiving groundwater of different residence times (a mean residence time of 35–40 years was estimated in an exponential mixing context; Table 4). As a result, groundwater chemistry was greatly buffered and EC was poorly related to water level fluctuation (Fig. 6).

4.4. A conceptual model of aquifer functioning

A conceptual model of unconfined Chalk aquifer (Fig. 7) was established in order to explore how hydrogeological settings including fracture distribution, groundwater level depth, superficial formations and aquifer-river relationship can influence the hydrogeological functioning of the aquifer in terms of flow pathways, mixing process, residence time and groundwater geochemistry variation.

In general, under deep groundwater level conditions, the geochemistry of the aquifer tends to be less influenced by near surface contaminations with relatively low concentrations of agriculture ions. This situation usually occurs on interfluves, near the groundwater divide line (Fig. 7A). If no superficial formations overlay on the Chalk, the aquifer receives a spatially uniform recharge and an exponential mixing model could be applied with a relatively short residence time. As transmissivity and storage yield are low on interfluve with a thick UZ, groundwater level fluctuations are important, leading to levels of contamination positively correlated to water table dynamics.

At shallow groundwater sites, the thin UZ of Chalk aquifer is usually highly fractured (Fig. 7B). Rapid recharge through fractures is favored, making groundwater a mixture of freshly percolated water and old water coming from upstream recharge area, as demonstrated by a binary mixing model. The shallow groundwater sites with high proportion of modern water mainly locate in river valleys (where fracture networks are well developed) but could also present on interfluves. At these sites, groundwater geochemistry is mostly influenced by the dilution effects of rainfall, leading to mineralization degree of groundwater negatively correlated to water table dynamics.

Superficial formations overlaying on the Chalk such as graveluche, colluvium and alluvium have important effects on groundwater flow and geochemistry. These superficial formations are usually intermitted and constituted by high content of clayey minerals, presenting a lower permeability than the Chalk. They could consequently constitute a barrier limiting the rapid recharge of water and solute into the aquifer. At these sites, a piston flow model better describes the groundwater flow and relatively old groundwater ages are estimated, which could explain the stable or delayed groundwater geochemistry with respect to water table fluctuations (Fig. 7C and D).

For sites near rivers where groundwater is exploited, the exchange between groundwater and river water should be considered (Fig. 7E).

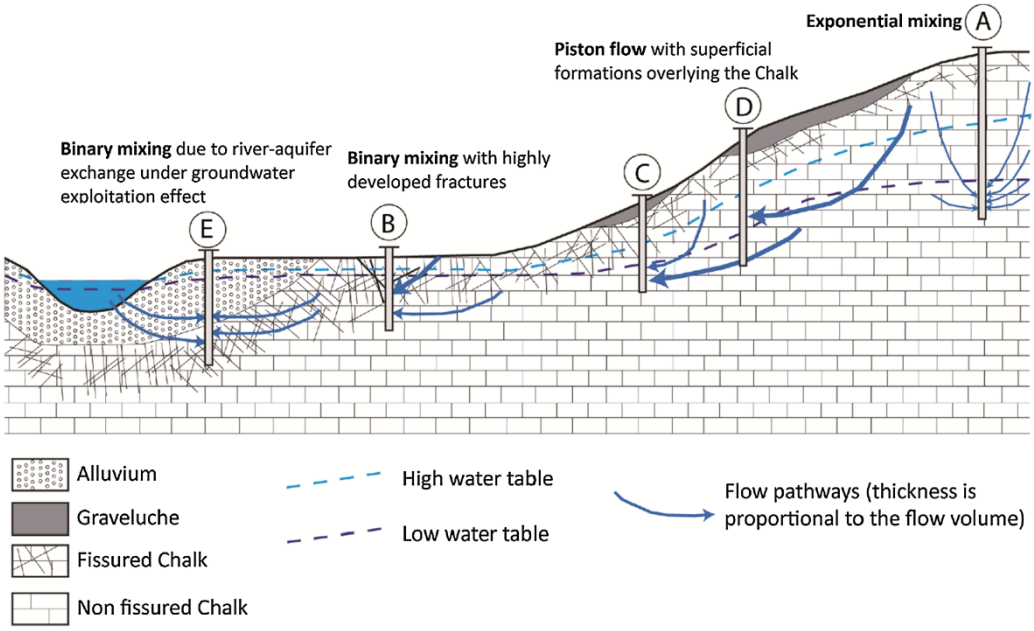

Fig. 7. Schematized hydrogeological functioning of unconfined Chalk aquifers.

The recharge of aquifer by rivers could occur, especially during low water level period, leading to groundwater geochemistry influenced by surface water.

5. Conclusion

The present study brings out interesting implications for the hydrogeological functioning of unconfined Chalk aquifers, by an approach combining hydrodynamic, geochemical and groundwater dating tools. Based on an intensive sampling network on a watershed scale, groundwater level fluctuations and chemical compositions (major ions concentrations) were monitored continuously during two years (2017–2019).

Seasonal and annual fluctuations of groundwater level were observed on the study area. The hourly data allowed to study precisely the response of aquifer following exploitation activities (pumping) and rainfalls. Although the majority of the aquifer has an inertial behavior with respect to recharge, a rapid response following rainfalls can be allowed locally by highly developed fractured network in the Chalk.

Groundwater dating using CFCs and SF_6 was also realized for the first time in this unconfined Chalk aquifer. Despite the frequent contaminations of CFCs and SF_6 detected on the study area, relevant information on residence times and mixing processes of the Chalk groundwater was obtained at the majority of sites. The aquifer is made up of waters of different ages ranging from less than 20 years to more than 50 years, with piston flow, exponential or binary mixing models defined at each sampling site implying for different flow pathways and mixing processes in the aquifer.

Despite the Ca^{2+}–HCO_3^- chemical facies, a high spatial and temporal heterogeneity of groundwater geochemistry in the unconfined Chalk aquifer was highlighted on the study area. Different correlation relationships between the EC time series and groundwater level fluctuations were observed: correlated, anti-correlated or independent. These variabilities were explained by a combined effect of water level fluctuation, groundwater residence time, thickness of the UZ, superficial formations, distribution of fracturing network, aquifer-river relationships and human activities.

The combination of different tools allowed the establishment of a conceptual model of chalk aquifer functioning. The multi-tool methodology developed in this study and the established conceptual model might be used in Chalk aquifers or other multi-porosity mediums for the prediction of spatial and temporal variations of groundwater mineralization and solutes transport (natural or anthropogenic) and for the evaluation of aquifer vulnerability. However, the used methods still have some limitations. Firstly, the two-year long time series of groundwater level and geochemical parameters are relatively short to interpret a general and comprehensive mechanism of aquifer functioning. Then, the age-dating was disturbed by the contamination of tracers, resulting in the missing of groundwater flow information at some sites. Also, the methods focus mostly on a qualitative rather than a quantitative perspective, which could limit its application on contaminant transport prediction. Therefore, further investigations would be necessary. The monitoring of groundwater level fluctuations and geochemistry can be continued to obtain longer times series, with the aim to study the influence of different climate conditions on the Chalk aquifer functioning in a climate change context. With respect to groundwater dating, tritium analysis could be a good complement for CFCs and SF_6, especially for sites contaminated by several tracers. At last, the hydrodynamic and geochemical numerical modeling tool, based on the conceptual model established in the study, could be a relevant complement.

CRediT authorship contribution statement

Feifei Cao: Conceptualization, Formal analysis, Investigation, Writing - original draft, Writing - review & editing, Visualization. **Jessy Jaunat:** Conceptualization, Validation, Investigation, Resources, Writing - review & editing, Visualization, Supervision, Project administration, Funding acquisition. **Virginie Vergnaud-Ayraud:** Conceptualization, Formal analysis, Resources. **Nicolas Devau:** Conceptualization, Formal analysis, Writing - review & editing, Visualization. **Thierry Labasque:** Conceptualization, Formal analysis, Resources. **Aurélie Guillou:** Conceptualization, Formal analysis, Resources. **Alexandra Guillaneuf:** Investigation, Resources. **Julien Hubert:** Investigation, Resources. **Luc Aquilina:** Conceptualization, Formal analysis, Resources, Writing - review & editing. **Patrick**

Ollivier: Conceptualization, Validation, Resources, Writing - review & editing, Supervision, Project administration, Funding acquisition.

Declaration of Competing Interest

The authors declare that they have no known competing financial interests or personal relationships that could have appeared to influence the work reported in this paper.

Acknowledgements

This work was co-funded by the BRGM, the Agence de l'Eau Seine-Normandie, the Region Grand-Est, the Grand-Reims Metropole and ARS Grand-Est. Authors would also like to thank the owners and operators for access to their boreholes. We also thank the associate editor and the three anonymous reviewers for their valuable comments that helped to improve the quality of the manuscript.

Appendix A. Supplementary data

Supplementary data to this article can be found online at https://doi.org/10.1016/j.jhydrol.2019.124433.

References

ADES Database, 2019. ADES: le portail national d'Accès aux Données sur les Eaux Souterraines pour la France métropolitaine et les départements d'outre-mer. https://ades.eaufrance.fr/. Accessed date: 22 July 2019.

Aeschbach-Hertig, W., Peeters, F., Beyerle, U., Kipfer, R., 1999. Interpretation of dissolved atmospheric noble gases in natural waters. Water Resour. Res. 35, 2779–2792. https://doi.org/10.1029/1999WR900130.

Allen, D.J., Brewerton, L.J., Coleby, L.M., Gibbs, B.R., Lewis, M.A., MacDonald, A.M., Wagstaff, S.J., Williams, A.T., 1997. The physical properties of major aquifers in England and Wales (Technical Report No. WD/97/34). British Geological Survey.

Allshorn, S.J.L., Bottrell, S.H., West, L.J., Odling, N.E., 2007. Rapid karstic bypass flow in the unsaturated zone of the Yorkshire chalk aquifer and implications for contaminant transport. Geol. Soc., London, Special Publications 279, 111–122. https://doi.org/10.1144/SP279.10.

Allouc, J., Le Roux, J., 1995. Carte géol. France (1/50 000) feuile Mourmelon-le-Grand (133). Orléans : BRGM. Notice explicative par Allouc, J., Le Roux, J., Monciardini, C., Ravaux, J.P, Morfaux, P., 1995, 65 p.

Appelo, C.A.J., Postma, D., 2004. Geochemistry, Groundwater and Pollution, Second ed. CRC Press, pp. 678.

Aquilina, L., Ayraud, V., Labasque, T., Le Corre, P., 2006. Dosage des composés chlorofluorocarbonés et du tétrachlorure de carbone dans les eaux souterraines. Application à la datation des eaux, 51 p.

Aquilina, L., Ladouche, B., Doerfliger, N., Bakalowicz, M., 2003. Deep water circulation, residence time, and chemistry in a karst complex. Groundwater 41, 790–805. https://doi.org/10.1111/j.1745-6584.2003.tb02420.x.

Aquilina, L., Poszwa, A., Walter, C., Vergnaud, V., Pierson-Wickmann, A.-C., Ruiz, L., 2012. Long-term effects of high nitrogen loads on cation and carbon riverine export in agricultural catchments. Environ. Sci. Technol. 46, 9447–9455. https://doi.org/10.1021/es301715t.

Ayraud, V., Aquilina, L., Labasque, T., Pauwels, H., Molenat, J., Pierson-Wickmann, A.-C., Durand, V., Bour, O., Tarits, C., Le Corre, P., Fourre, E., Merot, P., Davy, P., 2008. Compartmentalization of physical and chemical properties in hard-rock aquifers deduced from chemical and groundwater age analyses. Appl. Geochem. 23, 2686–2707. https://doi.org/10.1016/j.apgeochem.2008.06.001.

Bakalowicz, M., 2018. De l'évolution historique du concept d'aquifère de la craie. Géologues 199, 4–6.

Baran, N., Chabart, M., Braibant, G., Joublin, F., Pannet, P., Perceval, W., Schimidt, C., 2006. Détermination de la vitèsse de transfert des nitrates en zone crayeuse sur 2 bassin versants à enjeux : La retourne (08) et la Superbe (51). Rapport BRGM/RP-54985-FR, 109 p.

Baran, N., Lepiller, M., Mouvet, C., 2008. Agricultural diffuse pollution in a chalk aquifer (Trois Fontaines, France): influence of pesticide properties and hydrodynamic constraints. J. Hydrol. 358, 56–69. https://doi.org/10.1016/j.jhydrol.2008.05.031.

Barhoum, S., 2014. Transferts dans la craie : approche régionale : le Nord-Ouest du Bassin de Paris : approche locale : la carrière de Saint-Martin-le-Noeud (phdthesis). Université Pierre et Marie Curie - Paris VI, pp. 334.

Barhoum, S., Valdès, D., Guérin, R., Marlin, C., Vitale, Q., Benmamar, J., Gombert, P., 2014. Spatial heterogeneity of high-resolution Chalk groundwater geochemistry – underground quarry at Saint Martin-le-Noeud, France. J. Hydrol. 519, 756–768. https://doi.org/10.1016/j.jhydrol.2014.08.001.

Barraclough, D., Gardner, C.M.K., Wellings, S.R., Cooper, J.D., 1994. A tracer investigation into the importance of fissure flow in the unsaturated zone of the British Upper Chalk. J. Hydrol. 156, 459–469. https://doi.org/10.1016/0022-1694(94)90090-6.

Bolan, N.S., Adriano, D.C., Curtin, D., 2003. Soil acidification and liming interactions with nutrientand heavy metal transformationand bioavailability. In: Advances in Agronomy. Academic Press, pp. 215–272 https://doi.org/10.1016/S0065-2113(02)78006-1.

Brouyère, S., 2006. Modelling the migration of contaminants through variably saturated dual-porosity, dual-permeability chalk. J. Contaminant Hydrol. 82, 195–219. https://doi.org/10.1016/j.jconhyd.2005.10.004.

Brouyère, S., Dassargues, A., Hallet, V., 2004. Migration of contaminants through the unsaturated zone overlying the Hesbaye chalky aquifer in Belgium: a field investigation. J. Contam. Hydrol. 72, 135–164. https://doi.org/10.1016/j.jconhyd.2003.10.009.

Busenberg, E., Plummer, L.N., 2000. Dating young groundwater with sulfur hexafluoride: natural and anthropogenic sources of sulfur hexafluoride. Water Resour. Res. 36, 3011–3030. https://doi.org/10.1029/2000WR900151.

Busenberg, E., Plummer, L.N., 1992. Use of chlorofluorocarbons (CCl3F and CCl2F2) as hydrologic tracers and age-dating tools: the alluvium and terrace system of central Oklahoma. Water Resour. Res. 28, 2257–2283. https://doi.org/10.1029/92WR01263.

Calba, F., 1980. Hydrogéologie du karst crayeux du Pays de Caux (France), phd thesis. Université Pierre et Marie Curie - Paris VI, pp. 231.

Cary, L., Benabderraziq, H., Elkhattabi, J., Gourcy, L., Parmentier, M., Picot, J., Khaska, M., Laurent, A., Négrel, Ph., 2014. Tracking selenium in the Chalk aquifer of northern France: Sr isotope constraints. Appl. Geochem. 48, 70–82. https://doi.org/10.1016/j.apgeochem.2014.07.014.

Chen, N., Valdes, D., Marlin, C., Blanchoud, H., Guerin, R., Rouelle, M., Ribstein, P., 2019. Water, nitrate and atrazine transfer through the unsaturated zone of the Chalk aquifer in northern France. Sci. Total Environ. 652, 927–938. https://doi.org/10.1016/j.scitotenv.2018.10.286.

Cook, P.G., Love, A.J., Robinson, N.I., Simmons, C.T., 2005. Groundwater ages in fractured rock aquifers. J. Hydrol. 308, 284–301. https://doi.org/10.1016/j.jhydrol.2004.11.005.

Cook, P.G., Plummer, L.N., Busenberg, E., Solomon, D.K., Han, L.F., 2006. Chapter 4. Effects and processes that can modify apparent CFC age. In Use of chlorofluorocarbons in hydrology: A guidebook, pp 31–56.

Cook, P.G., Solomon, D.K., 1995. Transport of atmospheric trace gases to the water table: implications for groundwater dating with chlorofluorocarbons and krypton 85. Water Resour. Res. 31, 263–270. https://doi.org/10.1029/94WR02232.

Cook, P.G., Solomon, D.K., Plummer, L.N., Busenberg, E., Schiff, S.L., 1995. Chlorofluorocarbons as tracers of groundwater transport processes in a shallow, silty sand aquifer. Water Resour. Res. 31, 425–434. https://doi.org/10.1029/94WR02528.

Crampon, N., Custodio, E., Downing, R.A., 1996. The hydrogeology of Western Europe: a basic framework. Q. J. Eng. Geol. Hydrogeol. 29, 163–180. https://doi.org/10.1144/GSL.QJEGH.1996.029.P2.05.

Crampon, N., Roux, J.C., Bracq, P., 1993. Hydrogeology of the chalk in France. In: Downing, R.A., Price, M., Jones, G.P. (Eds.), The Hydrogeology of the Chalk of North-West Europe. Oxford Univ. Press, New York, pp. 81–123.

Darling, W.G., Gooddy, D.C., MacDonald, A.M., Morris, B.L., 2012a. The practicalities of using CFCs and SF6 for groundwater dating and tracing. Applied Geochemistry, 13th International Symposium on Water-Rock Interaction (WRI -13) 27, 1688–1697. https://doi.org/10.1016/j.apgeochem.2012.02.005.

Darling, W.G., Gooddy, D.C., Morris, B.L., Peach, D.W., 2012b. The hydrochemistry of a Chalk aquifer during recovery from drought. Q. J. Eng. Geol. Hydrogeol. 45, 473–486. https://doi.org/10.1144/qjegh2012-022.

Darling, W.G., Morris, B., Stuart, M.E., Gooddy, D.C., 2005. Groundwater age indicators from public supplies tapping the chalk aquifer of Southern England. Water Environ. J. 19, 30–40. https://doi.org/10.1111/j.1747-6593.2005.tb00546.x.

Deconinck, J.-F., Amédro, F., Baudin, F., Godet, A., Pellenard, P., Robaszynski, F., Zimmerlin, I., 2005. Late Cretaceous palaeoenvironments expressed by the clay mineralogy of Cenomanian-Campanian chalks from the east of the Paris Basin. Cretac. Res. 26, 171–179. https://doi.org/10.1016/j.cretres.2004.10.002.

Devos, A., O, L., Butaeye, D., Barbin, V., 2006. Front de karstification et spatialisation des écoulements en pays calcaire : l'exemple du bassin de la Vesle (Marne/France), rapport d'activité Piren-Seine 2005, www.sisyphe.jussieu.fr/internet\piren, 17 p.

Dunkle, S.A., Plummer, L.N., Busenberg, E., Phillips, P.J., Denver, J.M., Hamilton, P.A., Michel, R.L., Coplen, T.B., 1993. Chlorofluorocarbons (CCl3F and CCl2F2) as dating tools and hydrologic tracers in shallow groundwater of the Delmarva Peninsula, Atlantic Coastal Plain, United States. Water Resour. Res. 29, 3837–3860. https://doi.org/10.1029/93WR02073.

Edmunds, W.M., Cook, J.M., Darling, W.G., Kinniburgh, D.G., Miles, D.L., Bath, A.H., Morgan-Jones, M., Andrews, J.N., 1987. Baseline geochemical conditions in the Chalk aquifer, Berkshire, U.K.: a basis for groundwater quality management. Appl. Geochem. 2, 251–274. https://doi.org/10.1016/0883-2927(87)90042-4.

El Janyani, S., Dupont, J.-P., Massei, N., Slimani, S., Dörfliger, N., 2014. Hydrological role of karst in the Chalk aquifer of Upper Normandy, France. Hydrogeol. J. 22, 663–677. https://doi.org/10.1007/s10040-013-1083-z.

Etcheverry, D., 2002. Valorisation des méthodes isotopiques pour les questions pratiques liées aux eaux souterraines - Isotopes de l'oxygène et de l'hydrogène. Rapport de l'OFEG, Série Géologie, Berne, 71p.

Fitzpatrick, C.M., 2011. The Hydrogeology of Bromate Contamination in the Hertfordshire Chalk: Double-porosity Effects on Catchment-scale Evolution (Doctoral). UCL (University College, London), pp. 371p.

Gillon, M., Crançon, P., Aupiais, J., 2010. Modelling the baseline geochemistry of groundwater in a Chalk aquifer considering solid solutions for carbonate phases. Appl. Geochem. 25, 1564–1574. https://doi.org/10.1016/j.apgeochem.2010.08.006.

Gooddy, D.C., Darling, W.G., Abesser, C., Lapworth, D.J., 2006. Using chlorofluorocarbons (CFCs) and sulphur hexafluoride (SF6) to characterise groundwater

movement and residence time in a lowland Chalk catchment. Journal of Hydrology, Hydro-ecological functioning of the Pang and Lambourn catchments, UK 330, 44–52. https://doi.org/10.1016/j.jhydrol.2006.04.011.
Hakoun, V., Orban, P., Dassargues, A., Brouyère, S., 2017. Factors controlling spatial and temporal patterns of multiple pesticide compounds in groundwater (Hesbaye chalk aquifer, Belgium). Environ. Pollut. 223, 185–199. https://doi.org/10.1016/j.envpol.2017.01.012.
Haria, A.H., Hodnett, M.G., Johnson, A.C., 2003. Mechanisms of groundwater recharge and pesticide penetration to a chalk aquifer in southern England. J. Hydrol. 275, 122–137. https://doi.org/10.1016/S0022-1694(03)00017-9.
Harnisch, J., Eisenhauer, A., 1998. Natural CF4 and SF6 on Earth. Geophys. Res. Lett. 25, 2401–2404. https://doi.org/10.1029/98GL01779.
Headworth, H.G., Keating, T., Packman, M.J., 1982. Evidence for a shallow highly-permeable zone in the Chalk of Hampshire, U.K. J. Hydrol. 55, 93–112. https://doi.org/10.1016/0022-1694(82)90122-6.
Heaton, T.H.E., Vogel, J.C., 1981. "Excess air" in groundwater. J. Hydrol. 50, 201–216. https://doi.org/10.1016/0022-1694(81)90070-6.
Ineson, J., 1962. A hydrogeological study of the permeability of the Chalk. J. Inst. Water Eng. 449–463.
Ireson, A.M., Butler, A.P., 2011. Controls on preferential recharge to Chalk aquifers. J. Hydrol. 398, 109–123. https://doi.org/10.1016/j.jhydrol.2010.12.015.
Ireson, A.M., Wheater, H.S., Butler, A.P., Mathias, S.A., Finch, J., Cooper, J.D., 2006. Hydrological processes in the Chalk unsaturated zone – Insights from an intensive field monitoring programme. Journal of Hydrology, Hydro-ecological functioning of the Pang and Lambourn catchments, UK 330, 29–43. https://doi.org/10.1016/j.jhydrol.2006.04.021.
Jarvis, I., 1980. Geochemistry of phosphatic chalks and hardgrounds from the Santonian to early Campanian (Cretaceous) of northern France. J. Geol. Soc. 137, 705–721. https://doi.org/10.1144/gsjgs.137.6.0705.
Jaunat, J., Huneau, F., Dupuy, A., Celle-Jeanton, H., Vergnaud-Ayraud, V., Aquilina, L., Labasque, T., Le Coustumer, P., 2012. Hydrochemical data and groundwater dating to infer differential flowpaths through weathered profiles of a fractured aquifer. Appl. Geochem. 27, 2053–2067. https://doi.org/10.1016/j.apgeochem.2012.06.009.
Johnson, A.C., Besien, T.J., Bhardwaj, C.L., Dixon, A., Gooddy, D.C., Haria, A.H., White, C., 2001. Penetration of herbicides to groundwater in an unconfined chalk aquifer following normal soil applications. J. Contam. Hydrol. 53, 101–117. https://doi.org/10.1016/S0169-7722(01)00139-5.
Jurgens, B.C., Böhlke, J.K., Eberts, S.M., 2012. TracerLPM (Version 1): An Excel® workbook for interpreting groundwater age distributions from environmental tracer data: U.S. Geological Survey Techniques and Methods. Report 4-F3, 60 p.
Katz, B.G., McBride, W.S., Hunt, A.G., Crandall, C.A., Metz, P.A., Eberts, S.M., Berndt, M.P., 2009. Vulnerability of a public supply well in a karstic aquifer to contamination. Groundwater 47, 438–452. https://doi.org/10.1111/j.1745-6584.2008.00504.x.
Kjeldsen, P., Christophersen, M., 2001. Composition of leachate from old landfills in Denmark. Waste Manag Res 19, 249–256. https://doi.org/10.1177/0734242X0101900306.
Kjeldsen, P., Jensen, M.H., 2001. Release of CFC-11 from disposal of polyurethane foam waste. Environ. Sci. Technol. 35, 3055–3063.
Kloppmann, W., Dever, L., Edmouds, W.M., 1994. Isotopic and geochemical investigations of Chalk groundwater of the Champagne region, France. Z. Dt. Geol. Ges. 143–152.
Kloppmann, W., Dever, L., Edmunds, W.M., 1998. Residence time of Chalk groundwaters in the Paris Basin and the North German Basin: a geochemical approach. Appl. Geochem. 13, 593–606. https://doi.org/10.1016/S0883-2927(97)00110-8.
Lallahem, S., 2002. Structure et modélisation hydrodynamique des eaux souterraines : application à l'aquifère crayeux de la bordure nord du Bassin de Paris (thesis). Lille 1, 219 p.
Laurain, M., Guérin, H., Barta, L., Monciardini, C., Durand, R., Neiss, R., 1981. Carte géol. France (1/50 000) feuile Reims (132). Orléans : BRGM. Notice explicative par Laurain, M., Guérin, H., Durand, R., Chertier, B., Louis, P., Morfaux, P., Neiss, R., 34 p.
Lee, L.J.E., Lawrence, D.S.L., Price, M., 2006. Analysis of water-level response to rainfall and implications for recharge pathways in the Chalk aquifer, SE England. J. Hydrol. 330, 604–620. https://doi.org/10.1016/j.jhydrol.2006.04.025.
Linoir, D., 2014. Les horizons d'accumulations carbonatées (HAC) en Champagne-Ardenne; répartition régionale, caractérisation et conséquences sur les transferts hydriques, phd thesis. Université de Reims Champagne-Ardenne 384, p.
Longstaff, S.L., Aldous, P.J., Clark, L., Flavin, R.J., Partington, J., 1992. Contamination of the chalk aquifer by chlorinated solvents: a case study of the luton and dunstable area. Water Environ. J. 6, 541–550. https://doi.org/10.1111/j.1747-6593.1992.tb00789.x.
MacDonald, A.M., Brewerton, L.J., Allen, D.J., 1998. Evidence for rapid groundwater flow and karst-type behaviour in the Chalk of southern England. In: Robins, N.S. (Ed.), Groundwater Pollution, Aquifer Recharge and Vulnerability. Geological Society of London, pp. 95–106.
Małoszewski, P., Zuber, A., 1982. Determining the turnover time of groundwater systems with the aid of environmental tracers: 1. Models and their applicability. J. Hydrol. 57, 207–231. https://doi.org/10.1016/0022-1694(82)90147-0.
Mangeret, A., De Windt, L., Crançon, P., 2012. Reactive transport modelling of groundwater chemistry in a chalk aquifer at the watershed scale. J. Contam. Hydrol. 138–139, 60–74. https://doi.org/10.1016/j.jconhyd.2012.06.004.
Mathias, S.A., Butler, A.P., Jackson, B.M., Wheater, H.S., 2006. Transient simulations of flow and transport in the Chalk unsaturated zone. Journal of Hydrology, Hydro-ecological functioning of the Pang and Lambourn catchments, UK 330, 10–28. https://doi.org/10.1016/j.jhydrol.2006.04.010.
Maurice, L., 2009. Investigations of Rapid Groundwater Flow and Karst in the Chalk (Doctoral). UCL (University College London), pp. 453.
Michel, R.L., 2004. Tritium hydrology of the Mississippi River basin. Hydrol. Process. 18, 15. https://doi.org/10.1002/hyp.1403.
Plummer, L.N., Rupert, M.G., Busenberg, E., Schlosser, P., 2000. Age of irrigation water in ground water from the eastern snake river plain aquifer, South-Central Idaho. Groundwater 38, 264–283. https://doi.org/10.1111/j.1745-6584.2000.tb00338.x.
Plummer, N., Busenberg, E., Böhlke, J.K., Nelms, D.L., Michel, R.L., Schlosser, P., 2001. Groundwater residence times in Shenandoah National Park, Blue Ridge Mountains, Virginia, USA: a multi-tracer approach. Chem. Geol. 179, 19. https://doi.org/10.1016/S0009-2541(01)00317-5.
Orban, P., Brouyère, S., Batlle-Aguilar, J., Couturier, J., Goderniaux, P., Leroy, M., Maloszewski, P., Dassargues, A., 2010. Regional transport modelling for nitrate trend assessment and forecasting in a chalk aquifer. J. Contam. Hydrol. 118, 79–93. https://doi.org/10.1016/j.jconhyd.2010.08.008.
Price, M., 1987. Fluid flow in the Chalk of England. Geol. Soc., London, Special Publications 34, 141–156. https://doi.org/10.1144/GSL.SP.1987.034.01.10.
Price, M., Downing, R.A., Edmunds, W.M., 1993. The Chalk as an aquifer. In: Downing, R.A., Price, M., Jones, G.P. (Eds.), The Hydrogeology of the Chalk of North West Europe. Oxford, pp. 35–58.
Price, M., Low, R.G., McCann, C., 2000. Mechanisms of water storage and flow in the unsaturated zone of the Chalk aquifer. J. Hydrol. 233, 54–71. https://doi.org/10.1016/S0022-1694(00)00222-5.
Richard, J., Sizun, J.-P., Machhour, L., 2005. Environmental and diagenetic records from a new reference section for the Boreal realm: the Campanian chalk of the Mons basin (Belgium). Sed. Geol. 178, 99–111.
Roux, J.-C., 2018. Historique de l'hydrogéologie de la Craie en France. Géologues 199, 7–10.
Rouxel-David, E., Batkowski, D., Baudouin, V., Cordonnier, G., Cubizolles, J., Herrouin, J. P., Izac, J.L., Jegou, J.P., Kieffer, C., Mardhel, V., Paya, H., 2002. Cartographie de la piézométrie de la nappe de la craie en Champagne-Ardenne, Rapport BRGM/RP-52332-FR, 29p.
Rouxel-David, E., Cordonnier, G., Dachy, S., 2002. Synthèse des études menées sur le bassin versant du champ captant de Couraux (Marne), Rapport BRGM/RP-51739-FR, 97p.
Santella, N., Ho, D.T., Schlosser, P., Stute, M., 2008. Widespread elevated atmospheric SF6 mixing ratios in the Northeastern United States: Implications for groundwater dating. J. Hydrol. 349, 139–146. https://doi.org/10.1016/j.jhydrol.2007.10.031.
Santoni, S., Huneau, F., Garel, E., Vergnaud-Ayraud, V., Labasque, T., Aquilina, L., Jaunat, J., Celle-Jeanton, H., 2016. Residence time, mineralization processes and groundwater origin within a carbonate coastal aquifer with a thick unsaturated zone. J. Hydrol. 540, 50–63. https://doi.org/10.1016/j.jhydrol.2016.06.001.
Smith, D.B., Wearn, P.L., Richards, H.J., Rowe, P.C., 1970. Water Movement in the Unsaturated Zone of High and Low Permeability Strata by Measuring Natural Tritium. Isotope Hydrology 1970. Proceedings of a Symposium on Use of Isotopes in Hydrology, pp 73–86.
Stuart, M.E., Smedley, P.L., 2009. Baseline groundwater chemistry : the Chalk aquifer of Hampshire (Open report No. OR/09/052). British Geological Survey, 61 p.
Suckow, A., 2014. The age of groundwater – definitions, models and why we do not need this term. Appl. Geochem. 50, 222–230. https://doi.org/10.1016/j.apgeochem.2014.04.016.
Vachier, P., Cambier, P., Prost, J.C., 1987. Mouvements de l'eau dans la zone non saturée et alimentation de la nappe de la craie de champagne (France). In: Isotope Techniques in Water Resources Development, Vienna, IAEA Conference pp 367–379.
Valdes, D., Dupont, J.-P., Laignel, B., Slimani, S., Delbart, C., 2014. Infiltration processes in karstic chalk investigated through a spatial analysis of the geochemical properties of the groundwater: The effect of the superficial layer of clay-with-flints. J. Hydrol. 519, 23–33. https://doi.org/10.1016/j.jhydrol.2014.07.002.
Van den Daele, G.F.A., Barker, J.A., Connell, L.D., Atkinson, T.C., Darling, W.G., Cooper, J.D., 2007. Unsaturated flow and solute transport through the Chalk: tracer test and dual permeability modelling. J. Hydrol. 342, 157–172. https://doi.org/10.1016/j.jhydrol.2007.05.021.
Vergnaud-Ayraud, V., Aquilina, L., Pauwels, H., Labasque, T., 2008. La datation des eaux souterraines par analyse des CFC : un outil de gestion durable de la ressource en eau. TSM 37–44. https://doi.org/10.1051/tsm/200801037.
Vernhet, Y., 2007. Carte geologique harmonisée du département de la Marne (No. RP-55732-FR). BRGM.
Vittecoq, B., Gourcy, L., Baran, N., 2007. Datation des eaux souterraines de Martinique par l'analyse conjointe des CFC, SF6 et tritium et relation avec les concentrations en nitrates et produits phytosanitaires (No. RP-55844-FR). BRGM, 57 p.
Wellings, S.R., 1984. Recharge of the Upper Chalk aquifer at a site in Hampshire, England: 2. Solute movement. J. Hydrol. 69, 275–285. https://doi.org/10.1016/0022-1694(84)90167-7.
Wellings, S.R., Bell, J.P., 1980. Movement of water and nitrate in the unsaturated zone of Upper Chalk near Winchester, Hants, England. J. Hydrol. 48, 119–136. https://doi.org/10.1016/0022-1694(80)90070-0.
Whitehead, E.J., Lawrence, A.R., 2006. The chalk aquifer system of Lincolnshire (No. RR/06/03). British Geological Survey, 74 p.
Worthington, S.R., 2003. A comprehensive strategy for understanding flow in carbonate aquifer. Speleogenesis and Evolution of Karst Aquifers 1, 1–8.

Appendix 3 : Piezometric chronic data of two boreholes in Chalk aquifer near the study area monitored since 2008.

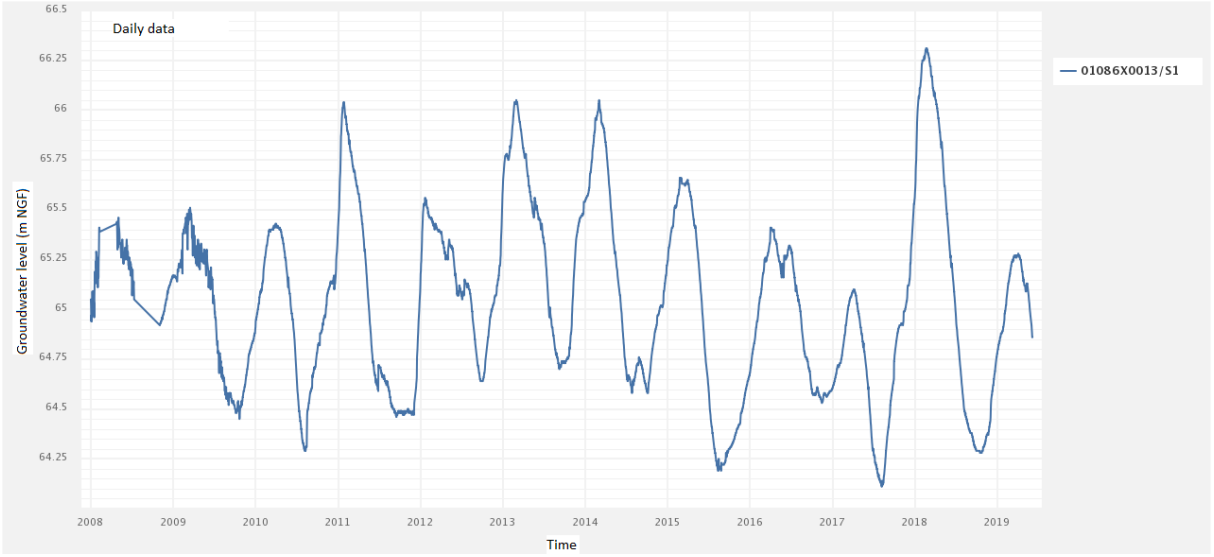

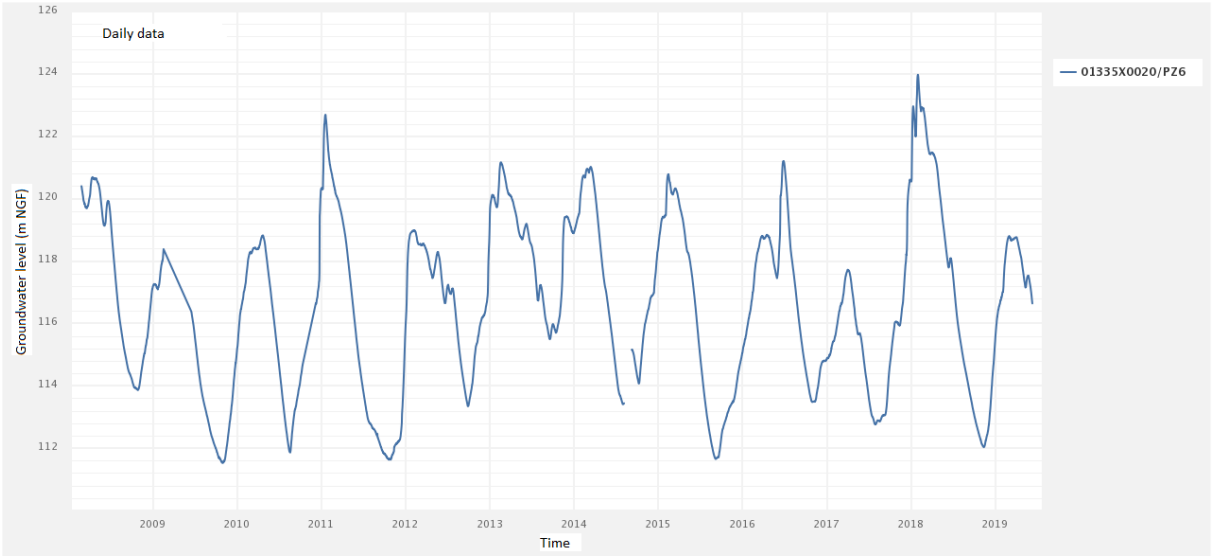

Appendix 4a: Correlation between HCO_3^- and other major ions (statistically significant as the P-value < 0.05, related r^2 values when P-value < 0.05 are marked in bold)

	r^2							P-value						
	Cl^-	NO_3^-	SO_4^{2-}	Na^+	K^+	Mg^{2+}	Ca^{2+}	Cl^-	NO_3^-	SO_4^{2-}	Na^+	K^+	Mg^{2+}	Ca^{2+}
FBN1	0,04	**0,20**	0,15	**0,19**	-0,05	**0,13**	0,06	0,147	0,027	0,096	0,013	0,678	0,048	0,106
FBN4	**-0,02**	**0,31**	**0,38**	-0,05	**0,16**	0,02	0,07	0,043	0,024	0,024	0,902	0,004	0,079	0,114
FBN5	**0,77**	**0,86**	-0,18	**0,40**	**0,64**	**0,73**	**0,82**	0,000	0,000	0,055	0,002	0,000	0,000	0,000
FVDV	0,01	0,00	0,11	0,04	-0,05	-0,06	**0,22**	0,348	0,326	0,261	0,226	0,890	0,855	0,030
FEP1	-0,06	-0,06	-0,02	-0,06	**0,14**	-0,05	-0,06	0,298	0,298	0,611	0,097	0,025	0,740	0,298
FP1	0,09	0,11	0,03	0,05	-0,01	0,08	0,05	0,100	0,198	0,204	0,128	0,356	0,293	0,426
FA	**0,24**	**0,35**	0,11	0,05	0,02	0,09	**0,26**	0,009	0,002	0,255	0,334	0,288	0,362	0,014
FAP	**0,22**	**0,88**	**0,81**	-0,04	**0,89**	**0,79**	**0,81**	0,024	0,000	0,000	0,081	0,000	0,000	0,000
FPM3	-0,03	-0,02	0,03	-0,01	0,02	0,07	**0,25**	0,509	0,439	0,207	0,386	0,163	0,326	0,000
FPM1	**0,05**	0,04	-0,06	0,14	0,04	0,00	-0,05	0,007	0,163	0,923	0,213	0,354	0,262	0,920
PDO	0,30	-0,10	**0,12**	-0,05	-0,05	-0,05	0,04	0,123	0,658	0,029	0,982	0,987	0,274	0,410
PP	-0,01	**0,07**	0,07	-0,04	**0,20**	0,11	-0,06	0,328	0,043	0,138	0,758	0,027	0,113	0,592
RPY	**0,14**	**0,11**	**0,27**	**0,61**	**0,21**	-0,02	**0,25**	0,029	0,041	0,011	0,000	0,020	0,354	0,041
RS1	0,01	0,05	0,00	**0,21**	-0,03	0,03	0,05	0,343	0,278	0,489	0,042	0,672	0,577	0,112
RS2	**0,27**	-0,05	0,09	**0,38**	**0,09**	-0,03	**0,19**	0,047	0,888	0,067	0,011	0,045	0,533	0,021

Appendix 4b: Correlation between Cl^- and other major ions (statistically significant as the P-value < 0.05, related r^2 values when P-value < 0.05 are marked in bold)

	r^2							P-value						
	HCO_3^-	NO_3^-	SO_4^{2-}	Na^+	K^+	Mg^{2+}	Ca^{2+}	HCO_3^-	NO_3^-	SO_4^{2-}	Na^+	K^+	Mg^{2+}	Ca^{2+}
FBN1	-0,04	0,12	0,04	**0,82**	-0,02	**0,70**	**0,32**	0,868	0,164	0,446	0,000	0,475	0,000	0,023
FBN4	-0,04	0,08	**0,30**	**0,26**	-0,66	-0,09	-0,01	0,272	0,053	0,005	0,026	0,093	0,691	0,464
FBN5	**0,91**	**0,99**	**0,77**	**0,31**	**0,64**	**0,99**	**0,98**	0,000	0,000	0,000	0,000	0,000	0,000	0,000
FVDV	-0,06	-0,10	0,16	**0,56**	0,28	-0,06	**0,03**	0,394	0,155	0,271	0,000	0,053	0,599	0,039
FEP1	-0,01	**0,24**	0,03	**0,46**	**0,31**	**0,29**	**0,41**	0,431	0,000	0,515	0,006	0,043	0,006	0,001
FP1	0,03	**0,89**	**0,30**	**0,53**	**0,25**	**0,38**	**0,64**	0,449	0,000	0,000	0,001	0,000	0,020	0,000
FA	**0,22**	**0,96**	**0,74**	**0,57**	-0,18	**0,16**	**0,85**	0,013	0,000	0,000	0,002	0,434	0,030	0,000
FAP	**-0,29**	**-0,34**	**-0,47**	**0,91**	**0,09**	**0,08**	**-0,47**	0,000	0,007	0,000	0,000	0,001	0,000	0,000
FPM3	-0,04	**0,99**	-0,06	0,18	-0,05	**0,33**	**0,54**	0,543	0,000	0,144	0,072	0,922	0,006	0,001
FPM1	**-0,01**	**0,47**	**0,18**	-0,03	0,06	0,23	0,08	0,029	0,000	0,025	0,650	0,374	0,194	0,136
PDO	-0,04	0,15	0,13	-0,03	**-0,37**	0,02	0,06	0,912	0,132	0,116	0,440	0,028	0,673	0,103
PP	-0,01	**0,28**	**0,62**	-0,09	0,09	0,11	-0,04	0,338	0,009	0,000	0,592	0,353	0,330	0,567
RPY	0,13	**0,71**	**0,69**	0,05	**0,59**	0,06	0,21	0,298	0,000	0,000	0,405	0,002	0,083	0,179
RS1	0,01	0,22	**0,77**	0,10	0,09	0,10	**0,16**	0,404	0,056	0,000	0,190	0,250	0,240	0,004
RS2	0,00	0,17	**0,71**	0,09	**0,44**	-0,05	0,07	0,425	0,150	0,000	0,144	0,008	0,707	0,464

Appendix 4c: Correlation between NO_3^- and other major ions (statistically significant as the P-value < 0.05, related r^2 values when P-value < 0.05 are marked in bold)

	r^2							P-value						
	HCO_3^-	Cl^-	SO_4^{2-}	Na^+	K^+	Mg^{2+}	Ca^{2+}	HCO_3^-	Cl^-	SO_4^{2-}	Na^+	K^+	Mg^{2+}	Ca^{2+}
FBN1	-0,03	**0,61**	**0,84**	-0,02	0,02	-0,01	-0,08	0,527	0,000	0,000	0,811	0,073	0,727	0,444
FBN4	-0,08	**0,13**	**0,01**	-0,03	-0,03	0,19	-0,03	0,342	0,034	0,017	0,248	0,631	0,129	0,662
FBN5	**0,61**	**0,74**	-0,09	**0,44**	**0,81**	**0,91**	**0,84**	0,000	0,000	0,713	0,000	0,000	0,000	0,000
FVDV	0,00	-0,10	**0,19**	0,00	**0,49**	**0,43**	0,09	0,293	0,142	0,044	0,352	0,000	0,008	0,078
FEP1	-0,06	**0,35**	-0,23	**0,12**	-0,07	**0,42**	**0,40**	0,094	0,000	0,490	0,030	0,700	0,002	0,001
FP1	0,04	**0,91**	**0,42**	**0,44**	**0,40**	**0,44**	**0,71**	0,322	0,000	0,000	0,000	0,000	0,006	0,000
FA	**0,32**	**0,96**	**0,74**	**0,52**	-0,22	**0,27**	**0,89**	0,004	0,000	0,000	0,003	0,559	0,011	0,000
FAP	**0,70**	**0,48**	**0,78**	**0,33**	**0,79**	**0,83**	**0,85**	0,000	0,000	0,000	0,024	0,000	0,000	0,000
FPM3	-0,03	**0,99**	-0,06	**0,21**	-0,04	**0,39**	**0,53**	0,288	0,000	0,369	0,045	0,777	0,001	0,001
FPM1	**0,44**	**0,48**	0,00	-0,12	**0,13**	0,02	0,20	0,047	0,000	0,320	0,363	0,048	0,610	0,095
PDO	-0,11	0,16	-0,06	-0,05	-0,22	**0,49**	0,15	0,466	0,121	0,931	0,668	0,245	0,003	0,217
PP	0,03	**0,28**	0,09	-0,05	0,19	0,31	**0,17**	0,371	0,008	0,143	0,944	0,156	0,111	0,045
RPY	-0,06	**0,60**	0,20	0,01	**0,33**	0,10	0,07	0,939	0,001	0,182	0,359	0,037	0,115	0,385
RS1	0,19	**0,49**	**0,39**	-0,01	0,25	0,10	**-0,21**	0,165	0,000	0,006	0,443	0,091	0,152	0,000
RS2	-0,05	0,07	0,27	-0,05	-0,11	-0,08	0,13	0,777	0,536	0,148	0,697	0,557	0,760	0,289

Appendix 4d: Correlation between SO_4^{2-} and other major (statistically significant as the P-value < 0.05, related r^2 values when P-value < 0.05 are marked in bold)

	r^2							P-value						
	HCO_3^-	Cl^-	NO_3^-	Na^+	K^+	Mg^{2+}	Ca^{2+}	HCO_3^-	Cl^-	NO_3^-	Na^+	K^+	Mg^{2+}	Ca^{2+}
FBN1	0,00	**0,60**	**0,82**	-0,11	**0,18**	-0,08	0,03	0,335	0,000	0,000	0,273	0,032	0,339	0,152
FBN4	**0,19**	**0,38**	**0,18**	0,02	0,31	0,01	0,14	0,028	0,005	0,035	0,073	0,092	0,617	0,117
FBN5	0,00	0,02	0,29	**0,58**	**0,48**	0,05	-0,01	0,151	0,605	0,055	0,013	0,030	0,294	0,183
FVDV	-0,07	-0,04	**0,30**	-0,06	**0,30**	-0,06	-0,05	0,600	0,759	0,043	0,203	0,001	0,339	0,994
FEP1	-0,08	-0,07	-0,17	**0,04**	-0,05	-0,11	-0,03	0,435	0,335	0,157	0,018	0,454	0,328	0,743
FP1	0,03	**0,03**	**0,34**	**0,32**	**0,67**	**0,38**	**0,39**	0,174	0,000	0,000	0,000	0,000	0,001	0,000
FA	0,04	**0,71**	**0,66**	**0,37**	-0,08	0,03	**0,62**	0,336	0,000	0,000	0,028	0,912	0,059	0,000
FAP	**0,60**	**0,04**	**0,59**	**0,54**	**0,53**	**0,73**	**0,75**	0,000	0,000	0,000	0,000	0,000	0,000	0,000
FPM3	0,03	**0,70**	**0,52**	0,11	-0,06	-0,07	-0,05	0,205	0,000	0,006	0,279	0,915	0,352	0,976
FPM1	-0,12	**0,18**	**0,00**	-0,01	0,03	-0,07	-0,06	0,097	0,026	0,311	0,407	0,140	0,664	0,454
PDO	0,17	**0,25**	0,24	-0,07	0,05	0,04	0,03	0,213	0,017	0,093	0,769	0,480	0,332	0,181
PP	0,10	**0,62**	0,08	0,05	-0,04	-0,03	-0,04	0,075	0,000	0,164	0,237	0,819	0,886	0,596
RPY	**0,23**	**0,70**	0,28	0,13	**0,72**	-0,01	0,13	0,031	0,000	0,081	0,192	0,000	0,434	0,192
RS1	-0,03	**0,73**	-0,06	0,22	**0,33**	0,02	0,22	0,769	0,000	0,982	0,056	0,002	0,483	0,068
RS2	0,00	**0,62**	0,03	0,07	**0,62**	-0,02	**0,34**	0,602	0,000	0,366	0,249	0,000	0,813	0,004

Appendix 4e: Correlation between Na^+ and other major ions (statistically significant as the P-value < 0.05, related r^2 values when P-value < 0.05 are marked in bold)

	r^2							P-value						
	HCO_3^-	Cl^-	NO_3^-	SO_4^{2-}	K^+	Mg^{2+}	Ca^{2+}	HCO_3^-	Cl^-	NO_3^-	SO_4^{2-}	K^+	Mg^{2+}	Ca^{2+}
FBN1	0,05	**0,95**	-0,04	0,11	0,06	**0,96**	**0,48**	0,290	0,000	0,892	0,105	0,111	0,000	0,006
FBN4	-0,08	**0,26**	-0,02	0,04	-0,06	-0,02	0,05	0,456	0,032	0,204	0,054	0,257	0,435	0,060
FBN5	**0,80**	**0,77**	**1,00**	0,03	**0,47**	**0,97**	**0,98**	0,000	0,000	0,000	0,052	0,002	0,000	0,000
FVDV	-0,04	0,26	-0,02	-0,09	-0,22	-0,05	-0,02	0,916	0,090	0,319	0,217	0,381	0,134	0,241
FEP1	-0,07	0,28	-0,11	0,12	-0,06	**0,26**	0,02	0,094	0,060	0,104	0,241	0,181	0,034	0,143
FP1	0,09	**0,49**	**0,42**	**0,21**	**0,26**	**0,27**	**0,34**	0,432	0,001	0,000	0,000	0,001	0,012	0,003
FA	-0,04	**0,59**	**0,53**	**0,34**	-0,03	**0,04**	**0,44**	0,721	0,000	0,002	0,012	0,890	0,004	0,003
FAP	**-0,33**	**0,86**	-0,32	**-0,46**	-0,13	**0,04**	**-0,57**	0,012	0,000	0,157	0,001	0,109	0,000	0,014
FPM3	-0,01	**0,48**	**0,51**	-0,02	0,02	**0,41**	**0,39**	0,312	0,000	0,000	0,723	0,417	0,001	0,002
FPM1	-0,05	0,34	-0,04	-0,02	0,03	0,03	0,01	0,788	0,125	0,782	0,226	0,288	0,324	0,254
PDO	-0,04	-0,03	0,10	0,16	-0,01	0,15	0,02	0,713	0,560	0,337	0,083	0,445	0,052	0,558
PP	**0,09**	0,06	-0,02	**0,10**	0,02	0,18	-0,05	0,012	0,201	0,745	0,044	0,072	0,187	0,945
RPY	-0,14	0,21	0,06	**0,23**	**0,44**	0,05	0,00	0,083	0,093	0,188	0,029	0,002	0,296	0,511
RS1	0,24	0,11	0,12	**0,31**	**0,37**	0,21	-0,11	0,061	0,134	0,243	0,037	0,020	0,090	0,543
RS2	-0,07	0,16	-0,05	0,15	**0,39**	-0,05	-0,07	0,183	0,052	0,693	0,068	0,002	0,933	0,811

Appendix 4f: Correlation between K^+ and other major ions (statistically significant as the P-value < 0.05, related r^2 values when P-value < 0.05 are marked in bold)

	r^2							P-value						
	HCO_3^-	Cl^-	NO_3^-	SO_4^{2-}	Na^+	Mg^{2+}	Ca^{2+}	HCO_3^-	Cl^-	NO_3^-	SO_4^{2-}	Na^+	Mg^{2+}	Ca^{2+}
FBN1	-0,05	**0,53**	0,02	**0,23**	**0,38**	0,23	**0,28**	0,637	0,000	0,206	0,043	0,006	0,070	0,006
FBN4	**0,17**	0,02	-0,02	0,30	0,07	0,13	-0,05	0,005	0,280	0,520	0,057	0,081	0,436	0,327
FBN5	**0,49**	**0,47**	**0,80**	-0,02	**0,12**	**0,65**	0,55	0,034	0,002	0,000	0,763	0,000	0,000	0,000
FVDV	-0,09	0,01	**0,48**	**0,33**	-0,15	0,21	**-0,04**	0,538	0,725	0,000	0,000	0,281	0,051	0,291
FEP1	**0,14**	0,08	-0,05	-0,04	-0,05	**0,34**	-0,05	0,028	0,110	0,814	0,876	0,262	0,017	0,953
FP1	-0,01	**0,47**	**0,36**	**0,71**	**0,25**	**0,16**	**0,70**	0,343	0,000	0,000	0,000	0,003	0,036	0,000
FA	-0,05	-0,09	-0,07	0,31	-0,01	-0,01	-0,17	0,420	0,863	0,733	0,100	0,807	0,519	0,421
FAP	**0,83**	**0,59**	**0,74**	**0,55**	0,08	**0,66**	**0,76**	0,000	0,000	0,000	0,000	0,214	0,000	0,000
FPM3	0,02	0,05	0,04	-0,05	0,04	0,13	0,10	0,128	0,119	0,148	0,756	0,170	0,053	0,078
FPM1	0,11	0,06	**0,12**	**0,17**	0,02	**0,17**	0,00	0,136	0,086	0,007	0,024	0,089	0,031	0,171
PDO	-0,05	0,03	0,23	0,04	-0,02	-0,01	0,09	0,974	0,424	0,198	0,672	0,514	0,706	0,151
PP	0,01	**0,47**	0,04	-0,05	**0,01**	**0,44**	-0,06	0,285	0,003	0,086	0,925	0,015	0,006	0,602
RPY	-0,14	**0,61**	**0,32**	**0,63**	**0,59**	0,09	-0,11	0,143	0,002	0,046	0,003	0,001	0,052	0,661
RS1	-0,03	0,17	0,09	**0,24**	**-0,45**	0,01	-0,13	0,572	0,085	0,143	0,001	0,000	0,320	0,170
RS2	0,01	**0,54**	-0,11	**0,79**	**0,38**	-0,02	0,10	0,555	0,000	0,528	0,000	0,002	0,269	0,310

Appendix 4g: Correlation between Mg^{2+} and other major ions (statistically significant as the P-value < 0.05, related r^2 values when P-value < 0.05 are marked in bold)

	r^2							P-value						
	HCO_3^-	Cl^-	NO_3^-	SO_4^{2-}	Na^+	K^+	Ca^{2+}	HCO_3^-	Cl^-	NO_3^-	SO_4^{2-}	Na^+	K^+	Ca^{2+}
FBN1	0,07	**0,88**	-0,02	0,07	**0,91**	0,07	**0,61**	0,160	0,000	0,763	0,173	0,000	0,080	0,000
FBN4	-0,08	-0,05	0,09	-0,07	-0,01	-0,04	-0,11	0,723	0,668	0,256	0,875	0,484	0,664	0,405
FBN5	**0,76**	**0,87**	**0,95**	-0,06	**0,06**	**0,84**	**0,91**	0,000	0,000	0,000	0,305	0,000	0,000	0,000
FVDV	-0,08	-0,07	**0,43**	-0,08	-0,06	**0,21**	**0,04**	0,491	0,628	0,002	0,395	0,147	0,033	0,030
FEP1	-0,05	**0,28**	**0,43**	-0,03	**0,17**	-0,05	**0,22**	0,645	0,007	0,001	0,818	0,045	0,983	0,027
FP1	0,01	**0,26**	**0,41**	**0,38**	**0,27**	**0,16**	**0,15**	0,309	0,012	0,001	0,001	0,010	0,032	0,010
FA	0,01	**0,28**	**0,27**	**0,49**	**0,06**	-0,01	**0,23**	0,442	0,024	0,010	0,024	0,002	0,547	0,042
FAP	**0,83**	**0,66**	**0,88**	**0,89**	0,21	**0,83**	**0,87**	0,000	0,000	0,000	0,000	0,091	0,000	0,000
FPM3	-0,05	**0,52**	**0,61**	**-0,09**	**0,40**	0,09	**0,62**	0,521	0,005	0,001	0,006	0,002	0,155	0,001
FPM1	-0,02	0,28	0,19	-0,07	-0,09	-0,06	0,11	0,467	0,180	0,315	0,720	0,152	0,543	0,165
PDO	-0,05	0,02	**0,56**	**0,09**	-0,03	-0,05	0,11	0,301	0,493	0,000	0,037	0,257	0,996	0,272
PP	-0,07	0,13	-0,05	0,00	-0,10	0,01	-0,09	0,602	0,263	0,819	0,726	0,269	0,447	0,532
RPY	0,19	0,02	0,15	0,00	0,21	0,13	-0,07	0,372	0,137	0,061	0,406	0,063	0,052	0,776
RS1	-0,06	0,07	-0,04	0,08	0,10	0,04	-0,01	0,730	0,300	0,932	0,339	0,099	0,511	0,775
RS2	-0,07	0,11	0,25	-0,04	-0,05	-0,02	0,01	0,763	0,392	0,193	0,763	0,937	0,338	0,483

Appendix 4h: Correlation between Ca^{2+} and other major ions (statistically significant as the P-value < 0.05, related r^2 values when P-value < 0.05 are marked in bold)

	r^2							P-value						
	HCO_3^-	Cl^-	NO_3^-	SO_4^{2-}	Na^+	K^+	Mg^{2+}	HCO_3^-	Cl^-	NO_3^-	SO_4^{2-}	Na^+	K^+	Mg^{2+}
FBN1	0,03	**0,58**	-0,07	0,15	**0,64**	**0,26**	**0,65**	0,389	0,001	0,472	0,176	0,001	0,004	0,000
FBN4	0,07	0,03	0,05	0,14	**0,29**	**0,35**	**0,02**	0,114	0,604	0,499	0,064	0,030	0,025	0,004
FBN5	**0,88**	**0,88**	**0,97**	-0,02	**0,20**	**0,71**	**0,95**	0,000	0,000	0,000	0,205	0,000	0,000	0,000
FVDV	**0,16**	0,01	0,08	0,21	-0,04	-0,05	**0,19**	0,018	0,259	0,078	0,178	0,556	0,472	0,040
FEP1	-0,07	**0,42**	**0,40**	0,21	0,02	-0,05	0,24	0,159	0,002	0,001	0,138	0,120	0,928	0,052
FP1	-0,03	**0,66**	**0,71**	**0,42**	**0,34**	**0,52**	**0,33**	0,511	0,000	0,000	0,000	0,003	0,000	0,020
FA	0,21	**0,87**	**0,89**	**0,54**	**0,52**	-0,21	0,21	0,061	0,000	0,000	0,000	0,002	0,191	0,072
FAP	**0,87**	**0,50**	**0,92**	**0,91**	**0,66**	**0,90**	**0,91**	0,000	0,000	0,000	0,000	0,000	0,000	0,000
FPM3	0,01	**0,79**	**0,82**	-0,06	0,24	0,04	**0,58**	0,323	0,000	0,000	0,838	0,140	0,325	0,003
FPM1	0,26	0,62	**0,27**	-0,01	-0,06	0,00	0,14	0,318	0,000	0,008	0,408	0,792	0,407	0,060
PDO	0,06	0,03	**0,28**	0,03	**0,06**	0,10	0,13	0,344	0,085	0,023	0,217	0,017	0,121	0,211
PP	-0,06	-0,04	**0,19**	-0,04	-0,05	-0,06	0,00	0,705	0,575	0,028	0,656	0,857	0,677	0,230
RPY	**0,18**	**0,31**	**0,25**	0,20	0,04	**0,57**	0,12	0,021	0,013	0,032	0,055	0,482	0,007	0,356
RS1	0,05	**0,24**	**-0,03**	**0,31**	-0,02	**0,30**	**0,22**	0,130	0,001	0,001	0,008	0,472	0,045	0,018
RS2	**0,19**	**0,39**	**0,18**	**0,44**	0,00	0,18	**0,50**	0,007	0,000	0,037	0,001	0,170	0,061	0,003

Appendix 5a: Correlation between EC and groundwater level calculated at each sampling point (statistically significant as the P-value < 0.05, related r2 values when P-value < 0.05 are marked in bold)

EC	Model	df	AIC	BIC	logLik	r^2	P-value
FBN1	1	5	175,248	180,4706	-82,62402	**0,95**	0,000
FBN4	2	5	174,8503	180,0729	-82,42516	**0,73**	0,000
FBN5	3	5	218,1791	223,4017	-104,08954	**0,89**	0,000
FVDV	4	5	157,808	163,0306	-73,90399	**0,68**	0,000
FEP1	5	5	139,5487	144,7713	-64,77432	-0,01	0,488
FP1	6	5	199,6934	204,9160	-94,84669	**0,20**	0,025
FA	7	5	215,4197	220,6423	-102,70983	0,02	0,383
FAP	8	5	256,5757	261,7983	-123,28785	-0,05	0,958
FPM3	9	5	178,0903	183,3129	-84,04513	**0,26**	0,006

Appendix 5b: Correlation between HCO_3^- and groundwater level calculated at each sampling point (statistically significant as the P-value < 0.05, related r^2 values when P-value < 0.05 are marked in bold)

HCO_3^-	Model	df	AIC	BIC	logLik	r^2	P-value
FBN1	1	5	5,67317	10,89579	2,163413	0,06	0,288
FBN4	2	5	15,14602	20,36863	-2,573011	**0,19**	0,018
FBN5	3	5	15,66432	20,88694	-2,832162	**0,86**	0,000
FVDV	4	5	-1,24328	3,97933	5,621639	-0,05	0,760
FEP1	5	5	13,82859	19,05120	-1,914295	0,14	0,202
FP1	6	5	5,09553	10,31814	2,452237	0,03	0,204
FA	7	5	32,71375	37,93636	-11,356874	0,09	0,175
FAP	8	5	53,55628	58,77889	-21,77814	-0,04	0,716
FPM3	9	5	13,48527	18,70789	-1,742637	0,01	0,552

Appendix 5c: Correlation between Cl^- and groundwater level calculated at each sampling point (statistically significant as the P-value < 0.05, related r^2 values when P-value < 0.05 are marked in bold)

Cl^-	Model	df	AIC	BIC	logLik	r^2	P-value
FBN1	1	5	-51,2591	-46,03648	30,62955	**0,95**	0,000
FBN4	2	5	-48,19265	-42,97004	29,09633	0,15	0,195
FBN5	3	5	-2,59505	2,62756	6,29752	**0,40**	0,005
FVDV	4	5	-71,77063	-66,54801	40,88531	0,14	0,333
FEP1	5	5	-83,94817	-78,72556	46,97409	0,02	0,244
FP1	6	5	-47,51732	-42,29471	28,75866	-0,04	0,145
FA	7	5	-19,13233	-13,90971	14,56616	0,11	0,180
FAP	8	5	10,94853	16,17114	-0,47426	0,02	0,323
FPM3	9	5	-47,86375	-42,64114	28,93188	0,00	0,194

Appendix 5d: Correlation between NO_3^- and groundwater level calculated at each sampling point (statistically significant as the P-value < 0.05, related r^2 values when P-value < 0.05 are marked in bold)

NO_3^-	Model	df	AIC	BIC	logLik	r^2	P-value
FBN1	1	5	-40,44599	-35,22337	25,22299	**0,58**	0,001
FBN4	2	5	-67,55514	-62,33253	38,77757	0,05	0,979
FBN5	3	5	-17,54607	-12,32346	13,77304	**0,37**	0,002
FVDV	4	5	-87,93982	-82,71721	48,96991	**0,22**	0,019
FEP1	5	5	-99,27917	-94,05656	54,63959	**0,30**	0,047
FP1	6	5	-57,0783	-51,85569	33,53915	**0,03**	0,020
FA	7	5	-42,45154	-37,22893	26,22577	0,14	0,181
FAP	8	5	-27,9766	-22,75399	18,9883	0,06	0,841
FPM3	9	5	-68,98692	-63,76431	39,49346	0,02	0,052

Appendix 5e: Correlation between SO_4^{2-} and groundwater level calculated at each sampling point (statistically significant as the P-value < 0.05, related r^2 values when P-value < 0.05 are marked in bold)

SO_4^{2-}	Model	df	AIC	BIC	logLik	r^2	P-value
FBN1	1	5	-22,68833	-17,46572	16,34417	**0,51**	0,001
FBN4	2	5	-97,15203	-91,92942	53,57601	**0,62**	0,000
FBN5	3	5	-101,82227	-96,59966	55,91113	**0,29**	0,003
FVDV	4	5	-102,37544	-97,15283	56,18772	**0,47**	0,021
FEP1	5	5	-130,91477	-125,69215	70,45738	0,08	0,576
FP1	6	5	-103,77999	-98,55738	56,89000	**0,50**	0,005
FA	7	5	-78,51531	-73,2927	44,25765	0,18	0,227
FAP	8	5	-37,64397	-32,42136	23,82199	0,02	0,650
FPM3	9	5	-125,24291	-120,02029	67,62145	**0,62**	0,000

Appendix 5f: Correlation between Na^+ and groundwater level calculated at each sampling point (statistically significant as the P-value < 0.05, related r^2 values when P-value < 0.05 are marked in bold)

Na^+	Model	df	AIC	BIC	logLik	r^2	P-value
FBN1	1	5	-76,06358	-70,84097	43,03179	**0,95**	0,000
FBN4	2	5	-86,27354	-81,05093	48,13677	0,04	0,564
FBN5	3	5	5,12144	10,34405	2,43928	0,11	0,348
FVDV	4	5	-77,51185	-72,28924	43,75593	0,04	0,942
FEP1	5	5	-98,99963	-93,77702	54,49982	0,19	0,431
FP1	6	5	-88,08122	-82,85861	49,04061	0,08	0,448
FA	7	5	-105,41041	-100,18779	57,7052	0,05	0,718
FAP	8	5	5,79685	11,01947	2,10157	0,00	0,472
FPM3	9	5	-109,65892	-104,43631	59,82946	0,09	0,172

Appendix 5g: Correlation between K^+ and groundwater level calculated at each sampling point (statistically significant as the P-value < 0.05, related r^2 values when P-value < 0.05 are marked in bold)

K^+	Model	df	AIC	BIC	logLik	r2	P-value
FBN1	1	5	-150,7951	-145,57253	80,39757	0,20	0,147
FBN4	2	5	-134,5918	-129,36919	72,29590	0,32	0,063
FBN5	3	5	-128,5816	-123,35899	69,29080	**0,46**	0,000
FVDV	4	5	-148,24	-143,01741	79,12001	**0,27**	0,016
FEP1	5	5	-187,4301	-182,20751	98,71506	0,01	0,271
FP1	6	5	-142,5825	-137,35989	76,29125	0,25	0,084
FA	7	5	-182,3889	-177,16626	96,19444	0,03	0,502
FAP	8	5	-95,1093	-89,88668	52,55465	0,02	0,372
FPM3	9	5	-193,6674	-188,44483	101,83372	0,05	0,954

Appendix 5h: Correlation between Mg^{2+} and groundwater level calculated at each sampling point (statistically significant as the P-value < 0.05, related r^2 values when P-value < 0.05 are marked in bold)

Mg^{2+}	Model	df	AIC	BIC	logLik	r2	P-value
FBN1	1	5	-141,05987	-135,83726	75,52993	**0,88**	0,000
FBN4	2	5	-100,29768	-95,07507	55,14884	0,32	0,071
FBN5	3	5	-119,49575	-114,27313	64,74787	**0,76**	0,000
FVDV	4	5	-133,70544	-128,48283	71,85272	0,07	0,615
FEP1	5	5	-138,33141	-133,1088	74,16571	0,01	0,581
FP1	6	5	-105,80423	-100,58162	57,90212	0,29	0,068
FA	7	5	-166,78326	-161,56065	88,39163	0,31	0,052
FAP	8	5	-58,44659	-53,22397	34,22329	0,04	0,773
FPM3	9	5	-155,87585	-150,65324	82,93793	0,08	0,134

Appendix 5i: Correlation between Ca^{2+} and groundwater level calculated at each sampling point (statistically significant as the P-value < 0.05, related r^2 values when P-value < 0.05 are marked in bold)

Ca^{2+}	Model	df	AIC	BIC	logLik	r2	P-value
FBN1	1	5	-11,91486	-6,69225	10,95743	**0,57**	0,002
FBN4	2	5	-1,58082	3,64179	5,79041	**0,21**	0,032
FBN5	3	5	41,38648	46,6091	-15,69324	**0,72**	0,000
FVDV	4	5	-133,70544	-128,48283	71,85272	0,07	0,615
FEP1	5	5	-5,27540	-0,05278	7,63770	0,07	0,275
FP1	6	5	13,87142	19,09403	-1,93571	0,02	0,255
FA	7	5	19,33873	24,56134	-4,66936	0,21	0,094
FAP	8	5	65,78043	71,00304	-27,89022	0,05	0,838
FPM3	9	5	4,11661	9,33922	2,9417	0,01	0,229

Sources and behavior of perchlorate in a shallow Chalk aquifer under military (World War I) and agricultural influences

Feifei Cao [(1)], Neil C. Sturchio [(2)], Patrick Ollivier [(3)], Nicolas Devau [(3)], Linnea J. Heraty [(2)], Jessy Jaunat [(1)]

[(1)] Université de Reims Champagne-Ardenne – GEGENAA – EA 3795, 2 Esplanade Roland Garros, 51100 Reims, France
[(2)] Department of Geological Sciences, University of Delaware, 255 Academy Street/103 Penny Hall, Newark, DE 19716, United States, Professor and Chair

[(3)] BRGM, 3 av. C. Guillemin, BP 36009, 45060 Orléans Cedex 2, France

**Corresponding author: Feifei Cao E-mail address: feifei.cao@etudiant.univ-reims.fr*

Abstract

Perchlorate (ClO_4^-) has been detected at concentrations of concern for human health on a large scale in groundwater used for drinking water supplies in NE France. Two sources are suspected: a military source related to World War I (WWI) and an agricultural source related to past use of Chilean nitrate fertilizers. The sources and behavior of ClO_4^- have been studied in groundwater and rivers near the Reims city, by monitoring monthly the major ions and ClO_4^- concentrations for two years (2017 – 2019), and by measuring the isotopic composition of ClO_4^- and NO_3^- in water samples. ClO_4^- was detected throughout the study area with high concentrations (> 4 $\mu g \cdot L^{-1}$) detected mainly downgradient of the Champagne Mounts, where large quantities of ammunition were used, stored, and destroyed during and after WWI. A WWI military origin of ClO_4^- is inferred from isotopic analysis and groundwater ages. Different tendencies of ClO_4^- variation are observed and interpreted by a combination of ClO_4^- concentrations, aquifer functioning and historical investigations, revealing major sources of ClO_4^- (e.g., unexploded ordnance, ammunition destruction sites) and its transfer mechanisms in the aquifer. Finally, we show that concentrations of ClO_4^- in groundwater seems unlikely to decrease in the short- to medium-term.

Keywords

Perchlorate; Isotope; Groundwater; France; World War I; Chilean nitrate fertilizer

Highlights

- High ClO_4^- concentrations are detected mainly downgradient of the Champagne mounts.
- ClO_4^- contamination of water comes mostly from WWI military sources.
- Factors governing ClO_4^- transfer in the Champagne Chalk aquifer are evidenced.
- ClO_4^- contamination seems unlikely to decline in the short- to medium-term.

1. Introduction

Perchlorate (ClO_4^-) is an environmental pollutant of growing concern due to its widespread occurrence in water and its adverse health effects by interfering with thyroid uptake of iodine and production of hormones (e.g., Brabant et al., 1992; Braverman et al., 2005; Greer et al., 2002). The high solubility and nonreactivity of ClO_4^- under typical geochemical conditions make it highly mobile in the aquatic environment (Brown and Gu, 2006; Urbansky, 1998). The origin of ClO_4^- in the environment can be synthetic or natural (Cao et al., 2019). ClO_4^- is widely used as an oxidant in solid rocket fuels and explosives (Urbansky, 1998). Therefore, the use and manufacture of these products may constitute an important source of ClO_4^- contamination. Other synthetic sources of ClO_4^- include fireworks, air bags, matches, road flares, chlorate herbicides and bleach products (Aziz et al., 2006; Trumpolt et al., 2005). In natural environments, ClO_4^- can form atmospherically and accumulate by dry and wet deposition in vadose soils in arid and semi-arid environments such as the Atacama Desert (Chile), the southwestern United States, northwestern China, and Antarctica (Jackson et al., 2015, 2016; Lybrand et al., 2016; Rao et al., 2007). The natural NO_3^--rich salt deposits in the Atacama Desert (Chilean nitrate), with ClO_4^- as a minor component (0.1-0.5 wt.%), have been refined and distributed worldwide for use as NO_3^- fertilizer, especially during the first half of the 19th century, thus representing a potential widespread source of ClO_4^- contamination in waters (Ericksen, 1983; Rajagopalan et al., 2006). Over the last two decades, ClO_4^- contamination has been reported from many countries including the USA, Canada, Chile, China, India, UK and France, related to various origins (e.g., Cao et al., 2019, 2018; Furdui et al., 2018; Jackson et al., 2005; Kannan et al., 2009; McLaughlin et al., 2011; Qin et al., 2014; Sturchio et al., 2014; Urbansky, 2002; Vega et al., 2018).

In France, recommended levels of ClO_4^- in drinking water were first issued in 2011 by the French Agency for Food, Environmental and Occupational Health & Safety (ANSES): 15 $\mu g \cdot L^{-1}$ for adults and 4 $\mu g \cdot L^{-1}$ for children under 6 months. The level was subsequently reduced from 15 to 5 $\mu g \cdot L^{-1}$ for adults

(ANSES, 2018). According to the national measurement campaign conducted by ANSES from 2011 to 2012, most of the sites having high concentrations of ClO_4^- (> 4 µg·L^{-1}) were located in NE France (ANSES, 2013).

The large extent of ClO_4^- contamination in NE France is unlikely to have been caused by point sources related to industrial activities (Figure 1). However, a potential link between the spatial distribution of high ClO_4^- concentrations and the position of the trench areas of WWI (1914 – 1918) was observed. Thus, a military source of ClO_4^- related to WWI seems likely (Hubé, 2016; Hubé and Bausinger, 2013; Ricour, 2013) but has never been clearly demonstrated. Indeed, synthetic ClO_4^- produced industrially by electrolysis was largely used in explosives manufacturing during WWI. According to Hubé (2014), ~131,000 T of (per)chlorate explosives (primarily composed of NH_4ClO_4 , $KClO_4$, or $NaClO_3$) were used during WWI, mainly in grenade and trench artillery. In addition, ClO_4^- could also be present in other explosives including black powder and nitro group explosives (e.g., TNT, nitroglycerine and nitrocellulose), as Chilean nitrate (with ClO_4^- impurity) was intensively used in the manufacturing of these explosives.

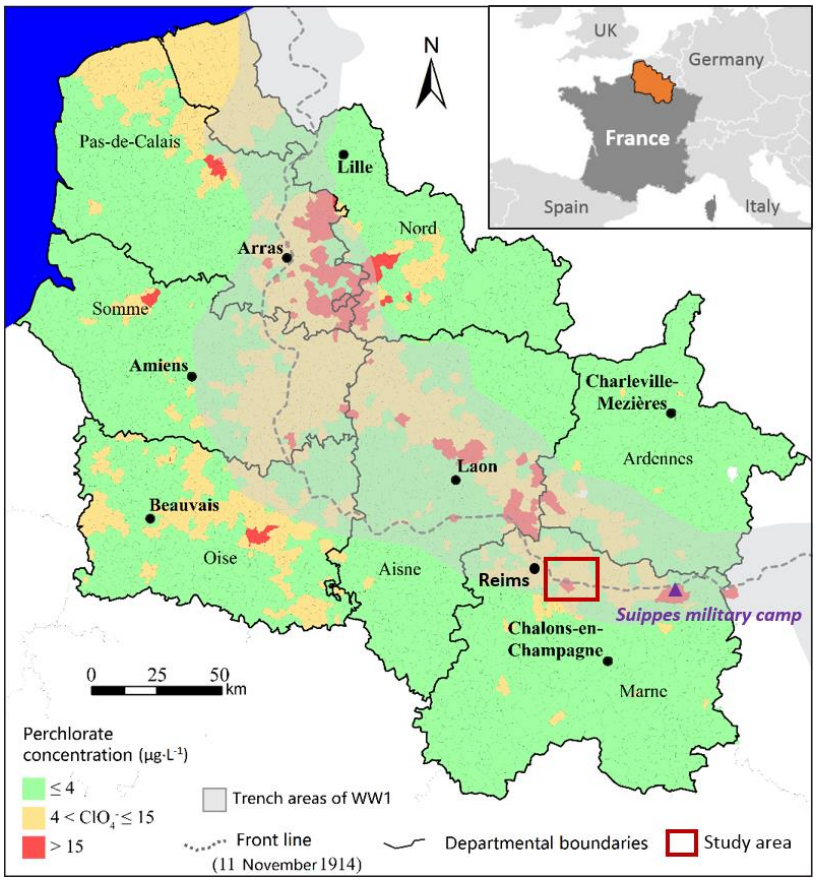

Figure 1: Distribution of ClO_4^- contamination in groundwater and the positions of the WWI trench areas in NE France (Jaunat et al., 2018)

High levels of ClO_4^- have also been detected in some regions outside the trench areas (e.g., Oise, Pas-de-Calais; Figure 1). An agricultural source was suspected, as large quantities of Chilean nitrate was

used as fertilizer in France between 1880 and 1950 (Lopez et al., 2015), especially for sugar beet and wheat cultivation (Zimmermann, 1917). Around the year 1928, the estimated amount of Chilean nitrate applied annually for wheat cultivation in France was between 150 and 400 $kg \cdot ha^{-1}$ and could exceed 800 $kg \cdot ha^{-1}$ for beet cultivation (Lopez et al., 2014). For a better management of water resources in NE France, it is now necessary to clarify the source of ClO_4^- contamination (military and/or agricultural). In addition to hydrogeological and historical investigations, isotopic analysis of ClO_4^- can provide a direct approach for ClO_4^- source apportionment.

Measurements of stable isotope ratios of chlorine ($^{37}Cl/^{35}Cl$) and oxygen ($^{18}O/^{16}O$, $^{17}O/^{16}O$) and the fractional abundance of the radioactive isotope ^{36}Cl in ClO_4^- ions have shown that three primary source types of ClO_4^- (synthetic; "Atacama" from nitrate salts mined in the Atacama Desert of Chile; and indigenous natural atmospheric deposition) can be clearly distinguished isotopically (Bao and Gu, 2004; Böhlke et al., 2017, 2009, 2005; Hatzinger et al., 2011; Jackson et al., 2010; Poghosyan et al., 2014; Sturchio et al., 2014, 2011, 2009, 2006). Additional background information about the ranges of isotopic composition of ClO_4^- is detailed in the references above and summarized in Cao et al. (2019).

In this study, a representative study area with two potential sources of ClO_4^- contamination (military and/or agricultural) was selected east of the Reims city in NE France (Figure 1). In this agricultural and military (WWI) context, the primary objectives of this study are to 1) assess the extent of ClO_4^- contamination and its spatio-temporal evolution in the Chalk aquifer, 2) clarify the sources of ClO_4^- contamination (military and/or agricultural) and 3) understand the mechanism of transport and predict the evolution of ClO_4^- in groundwater in the short- to medium- term. To achieve these goals, we used an approach combining continuous monitoring of ClO_4^- concentrations, isotopic composition measurements, historical and hydrogeological investigations, which could be further applied in other ClO_4^- contaminated areas.

2. Material and methods

2.1 Description of the study area

2.1.1. Location and land use

The study area is situated east of the city of Reims, in the Champagne region in NE France (Figure 1 and Figure 2). It covers about 500 km^2 between the Vesle River (as the southern boundary) and the Suippe River (as the northern and eastern boundaries; Figure 2). Land use in this area is largely agricultural (> 80%) with wheat, barley, sugar beet, and alfalfa as major crops. Forest covers about 15% of the study area, mainly on the Berru and Champagne Mounts and the riparian areas. Urban lands including towns, villages, and industrial sites represent only about 3% of the study area (CORINE Land Cover geographic database).

2.1.2. Geological and hydrogeological context

A detailed geological and hydrogeological description of the study area is given by Cao et al. (2020). The Chalk formation (Upper Cretaceous, 66 – 100 Ma) constitutes almost the entire surface of the study area, with only a limited exposure of Tertiary formation at Berru Mount (Figure 2). The Tertiary formation includes a succession of permeable (sand and coarse limestone) and impermeable deposits (clay and marl) where only a few thin aquifers of limited extent are developed with some springs flowing from the sand layers (Laurain et al., 1981). These aquifers are insufficiently productive to be used as drinking water supplies. The Chalk formation of the study area includes Coniacian (C3), Santonian (C4) and Campanian (C5) Chalks (Figure 2), which have similar lithology and hydrodynamic properties despite their different ages of formation. It is a pure, fine-grained carbonate rock, characterized by dual porosity (matrix and fracture) providing both slow and rapid flowpaths for groundwater (e.g., Foster, 1975; Headworth et al., 1982; Price, 1987). The total porosity of the Chalk is about 40% (Crampon et al., 1993) with only 1% effective porosity (Vachier et al., 1987). The first 10-20 m of the Chalk is significantly fractured; the density of fractures decreases with depth and distance to river valleys (Allen et al., 1997; Mangeret et al., 2012; Vachier et al., 1987). In addition, the Chalk formation is partially covered by superficial (Quaternary) formations including graveluche (a periglacial formation up to 10 m thick), colluvium (1-3 m thick) and alluvium (up to 10 m thick) with relatively high content of clay and silt (Allouc et al., 2000; Vernhet, 2007) (Figure 2).

The chalk aquifer is an important groundwater resource of the region. Precipitation is the only recharge source of the aquifer, mainly from November to March, due to the excess of rainfall compared to evapotranspiration (Cao et al., 2020; Chiesi, 1993). The surface runoff is usually considered as very low or absent for the Champagne Chalk aquifer (Chiesi, 1993; Foster, 1975; Mathias et al., 2006). The study area is divided into two parts by the groundwater divide line across the summit of Berru Mount and the Champagne Mounts, which delimits the Vesle River watershed in the south and the Suippe River watershed in the north (Figure 2).

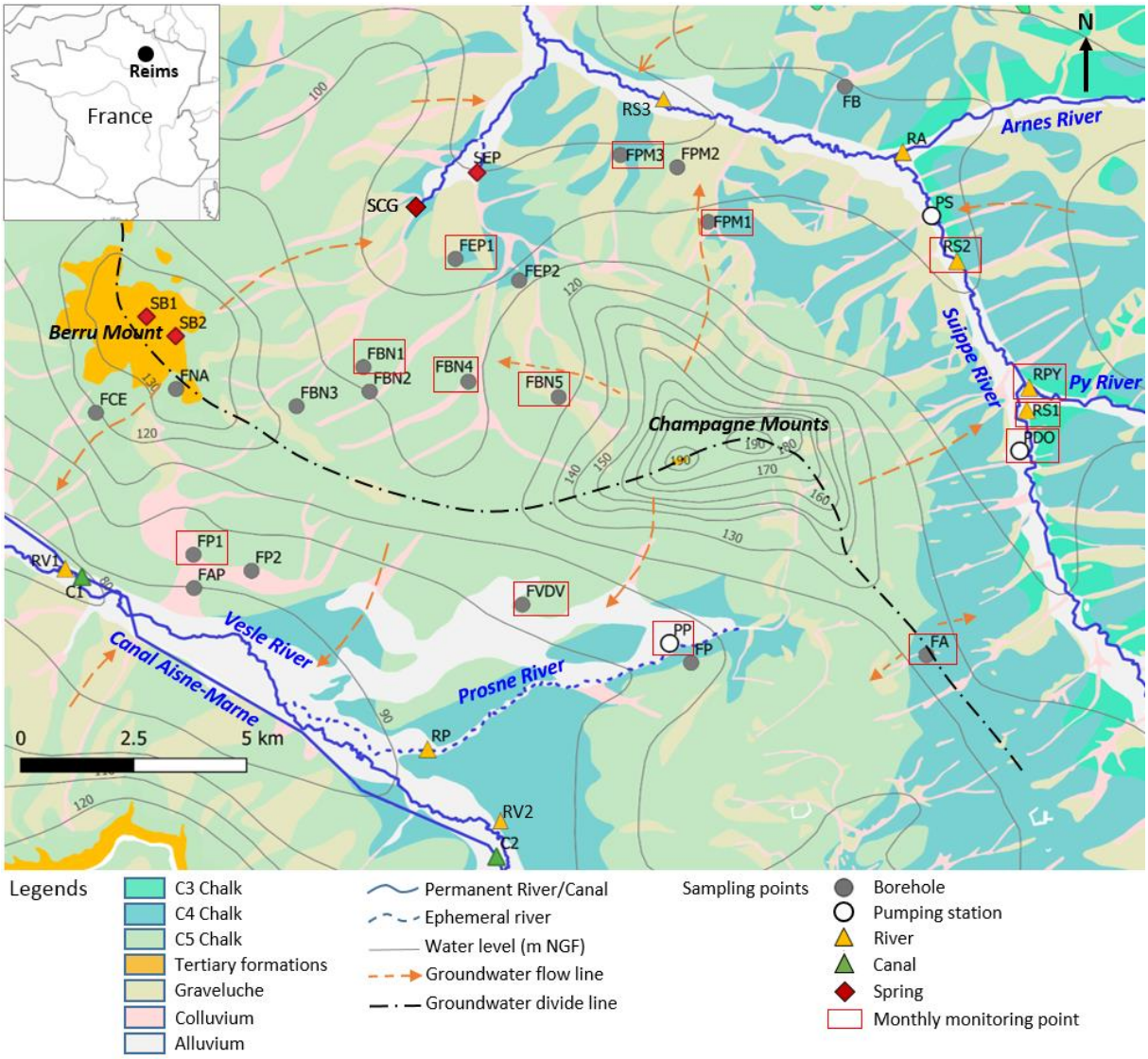

Figure 2: Geological and hydrogeological map of the study area recorded at high water level with the location of sampling points (modified from Cao et al., 2020). Source of geological map: Laurain et al. (1981), Allouc and Le Roux. (1995); source of water level data: Rouxel-David et al. (2002a).

2.1.3. Suspected sources of ClO_4^- contamination

Groundwater contamination by ClO_4^- in the study area is potentially caused by both the WWI-related military source and the agricultural source related to the past use of Chilean nitrate fertilizer. The study area was intensively marked by events of WWI (Facon, 2018; Laurent, 1988). As shown in Figure 3, almost the entire study area was crossed by trenches, particularly in the center of the area (Taborelli, 2018). From 1914 to 1918, these trench areas were the scenes of several intensive battles of WWI (e.g., the Battles of Champagne), especially on the Champagne Mounts. During WWI, military tunnels were dug by the German army, such as the tunnels of Mont Cornillet (N1), Mont Perthois (N2) and Mont sans Nom (N3) (Figure 3). These tunnels, usually equipped with quantities of ammunition, connected the German front positions with the rear and allowed the German army to fire until the last moment. It is highly probable that quantities of ammunition still remain underground at these sites, representing

potential sources of groundwater contamination of ClO_4^- and other pyrotechnic compounds. Furthermore, it is likely that the precise locations of some of these underground sites are unknown.

After WWI, large quantities of unused ammunition were still present on the French land and it was necessary to clear the battlefield in order to make these lands habitable and cultivable on a large scale. Thus, unused ammunitions were either dismantled to recycle valuable materials or destroyed by explosion. The ammunition explosion sites were recognizable in historical aerial photographs by anthropogenic forms such as alignments of shell-holes, an access road, and a storage area. Several explosion sites were identified in the study area from inspection of historical aerial photographs (IGN Remonter le temps database; Figure 3). While traces of N5 and N6 could no longer be recognized, the destruction activities on site N1 lasted until the 2000s and some military wastes are still present at this site (BASOL database). The sites and activities listed are not exhaustive since the compilation is based on existing data from historical archives and/or former aerial photographs that did not cover the entire study area. In addition, traces of military activities could have been quickly erased, making it difficult to identify all related sites. The ammunitions exploded on battlefields during WWI or destroyed after the war could have released ClO_4^- into the environment. In addition, large quantities of unexploded ammunitions (about 30% of the total quantity of ammunition used) could still persist in the subsoil (Desailloud and Wemeau, 2016), representing a continuous and diffuse source of ClO_4^-contamination.

As a traditional agricultural area for wheat and sugar beet, the study area was extensively cultivated with the use of Chilean nitrate fertilizer from 1880 to 1950. It was estimated that the average annual consumption of nitrogen in Marne (the department where the study area is located) was between 7,000 and 10,000 T in the 1950s (Lopez et al., 2014). The use by spreading and the storage of these Chilean nitrates could represent diffuse or point sources of ClO_4^- contamination in groundwater.

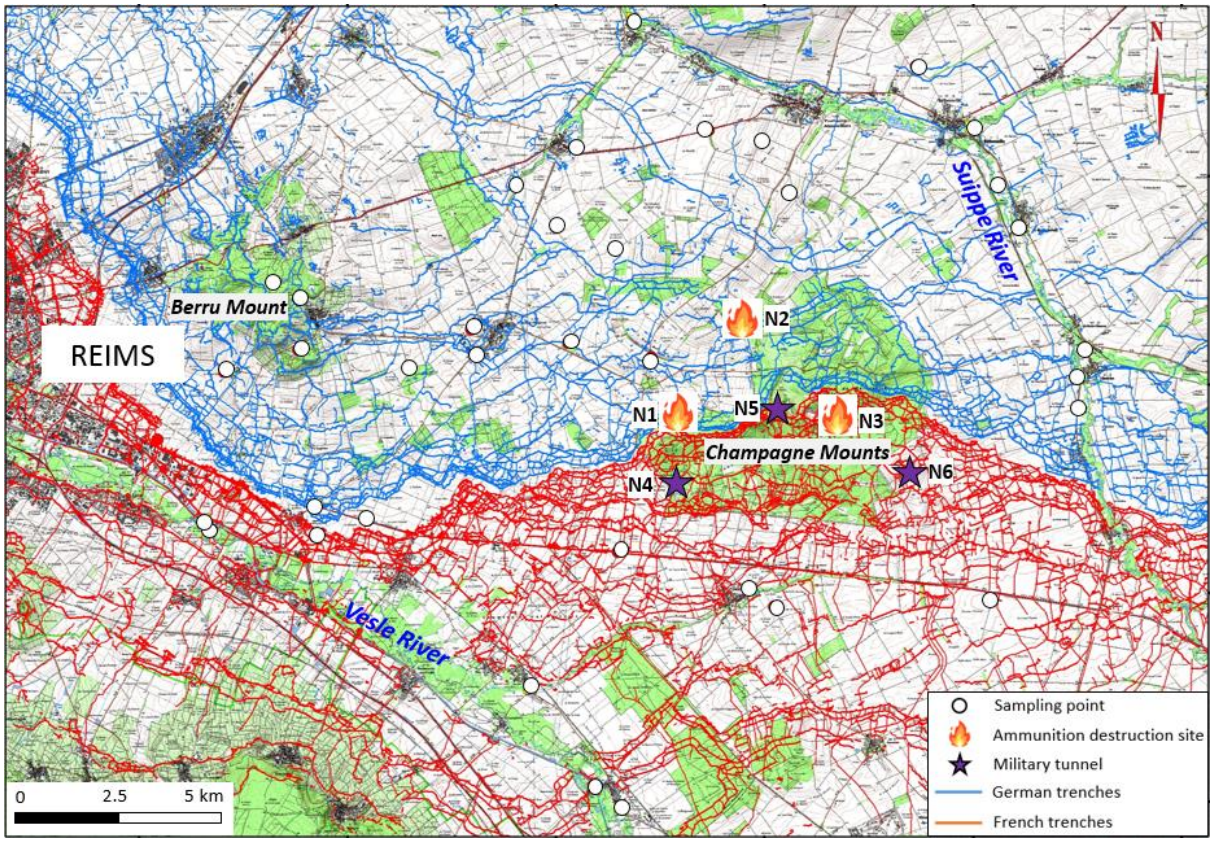

Figure 3: Trench areas, military tunnels and ammunition destruction sites related to the WWI in the study area

2.2. Sampling and analysis methods

An intensive sampling network was established in the study area with a total of 36 sampling points including 26 groundwater (19 boreholes, 3 pumping stations and 4 springs) and 10 surface water (2 in the Aisne-Marne Canal, 2 in the Vesle River, 3 in the Suippe River and 3 in their tributaries) (Figure 2), as surface water is here closely related to groundwater of the Chalk aquifer. The boreholes and pumping stations have long screen depths which cover at least half of the well depths (Table 1), thus providing a weighted average of groundwater. A first screening campaign was carried out in June 2017, which yielded a chemical map of the study area and the extent of ClO_4^- contamination. Fourteen sampling points (primarily points with high concentrations of ClO_4^-, well distributed in the study area; Figure 2) were then selected for monthly monitoring for 2 years to observe the spatio-temporal evolution of groundwater geochemistry and ClO_4^- concentrations. In addition, groundwater ages, water flow rate in rivers, explosive concentrations, and isotopic compositions of ClO_4^- and NO_3^- were measured.

The measurement methods and results of groundwater level, physico-chemical parameters, major ions and groundwater dating using CFCs and SF_6 have been fully described and interpreted previously in Cao et al. (2020). These results are directly used in this study.

Water discharge of rivers was measured by the cross-section method using an OTT C2 Small Current Meter. ClO_4^- was analyzed by ion chromatography at BRGM (Orléans, France) with a quantification

limit of 0.5 µg·L^{-1}. Thirty-nine explosives (see SI.1) were analyzed in waters with an RPHPLC-DAD system by the company Envilytix GmbH (Wiesbaden, Germany), as described by Bausinger et al. (2007).

Isotopic analyses of ClO_4^- were carried out in water samples collected from 3 sites in the study area: FBN4 (at high and low water levels), FVDV (at high water level) and PY (at high water level; Figure 2). In order to obtain a pure military isotopic signature of ClO_4^-, a water sample was also collected at the limit of the Suippes Military camp (outside the study area; Figure 1), as the only source of ClO_4^- here that is related to WWI without any potential agricultural influence. Water samples were collected using PVC columns containing ClO_4^- specific ion exchange resin (IX resin) and then purified and analyzed as described previously by Gu et al. (2011), Hatzinger et al. (2011, 2018), and Böhlke et al. (2017). The extraction and purification of ClO_4^- was done in the Department of Civil and Environmental Engineering of Texas Tech University (USA) and the key steps can be summarized as follows: 1) the resin was washed by deionized water and flushed with 4M HCl to remove NO_3^-, SO_4^{2-}, HCO_3^- and organics; 2) the absorbed ClO_4^- was eluted from the IX resin using a solution of 1M $FeCl_3$ and 4M HCl (Gu et al., 2007, 2001; Gu and Brown, 2006); 3) eluted ClO_4^- was purified by a series of precipitation, liquid-liquid extraction, evaporation, and cation exchange processes, then crystallized as a ClO_4^- salt for isotopic analysis. The relative abundances of stable isotopes of chlorine (^{37}Cl and ^{35}Cl) and oxygen (^{18}O, ^{17}O and ^{16}O) in ClO_4^- were measured using isotope-ratio mass spectrometry (IRMS) at the Environmental Isotope Geochemistry Laboratory of the University of Delaware (USA).

For isotopic analysis of NO_3^-, water samples were collected in 100-mL polyethylene bottles after filtration through 0.45 µm membranes. Nitrogen and oxygen isotope ratios were measured using an automated denitrifier method as described in Morin et al. (2009) and Savarino et al. (2013). This technique uses *Pseudomonas aureofaciens* bacteria to convert NO_3^- to N_2O, which is then analyzed for its isotopic composition after thermal decomposition to O_2 and N_2. Isotopic analysis was performed on a Thermo Finnigan MAT253 equipped with a gas-bench interface at the Laboratoire de Glaciologie et Géophysique de l'Environnement at the University of Joseph Fourier Grenoble (France).

2.3. Statistical analysis methods

Interactions between ClO_4^- concentrations and groundwater level as well as major ions were calculated by using an approach based on a semi-parametric regression model. More precisely, a generalized additive model (GAM) with cubic splines accounting for autocorrelation of data through a first order autoregressive model (AR1) was used. Each GAM was carried out using the Akaike information criterion (AIC) score and the likelihood ratio. The corresponding adjustment coefficient of determination (Adj. R^2) associated with a significance test at a P-value < 0.05 was used to characterize correlations between response variable and the explicative one.

The GAM was also adopted to decipher time-dependent changes in perchlorate concentrations. A model was built for each of the 14 sampling points, which were monitored monthly. Each of these GAM was

built considering a Gamma distribution of perchlorate concentration and the log link function was used as it was the most appropriate for this kind of distribution. Two time-dependent smooth functions were used to build each model. Seasonal changes in perchlorate concentrations are represented by the first term taking into account days of year. The penalized cubic regression spline was used for this smooth function to allow a nonlinear response of perchlorate to time during a calendar year. The second term was constructed to filter out the long-term trends (inter-annual variations). For convenient output, we have redefined the time-scale for this term as a continuous variable. For this second term, the thin plate regression spline was used.

For the two smooth functions, the smoothness was controlled by the number of knots and the associated effective number of degrees of freedom. The optimal number of knots was estimated through cross-validation. In consequence, the basis dimension for the two smooth functions was adapted to have enough degrees of freedom to fit the data while these values remained small enough to maintain reasonable computational efficiency and avoided over-fitting the data. For the two smooth functions, the method of the finite difference was used to calculate the first derivative of the function and the associated confidence interval. This first derivative was used to estimate the rate of change to identify periods of statistically significant change (either increase or decrease in perchlorate concentration).

The underlying assumption of homogeneity for model residuals has been checked by plotting deviance residuals against fitted values. QQ plots (sample quantiles against theoretical quantiles) and Shapiro tests were used to assess normality of the model residuals. We have examined autocorrelation of the model residuals; the autocorrelation function values showed that the model residuals were not correlated as they dropped to small values within a couple of days. Validity of the model was also assessed through AIC score and Adj.R^2. Analysis of deviance was used to assess the significance of the null hypothesis for the two smooth functions. All statistical tests were carried out using R-software (R core Team, 2018).

3. Results and discussion

3.1. Occurrence of ClO_4^- and explosives

Perchlorate was detected at almost all sampling sites (33 out of 36) (Table 1). Mean ClO_4^- concentrations measured during the two years monitoring were > 4 $\mu g \cdot L^{-1}$ at 17 sites, including two sites with mean concentrations > 15 $\mu g \cdot L^{-1}$, representing 49% and 6% of the sampling sites, respectively. Low concentrations (< 4 $\mu g \cdot L^{-1}$) were measured at 19 sites, representing 51% of the sampling points.

Table 1: Properties of sampling points, water table depth, concentrations of Cl^-, NO_3^- and ClO_4^- and isotopic compositions of NO_3^- in ground- and surface water samples (N: number of sampling; NA: not available. -: not applicable)

Name	Type	N	Depth (m)	Water table depth (m)	Cl^- ($mg \cdot L^{-1}$)	NO_3^- ($mg \cdot L^{-1}$)	ClO_4^- ($\mu g \cdot L^{-1}$)	NO_3^- $\delta^{18}O$ (‰)	NO_3^- $\delta^{15}N$ (‰)
FA	Borehole	21	35	2 - 6	35.4 ± 6.3	39.7 ± 6.0	3.1 ± 0.9	-1.4	-0.7
FAP	Borehole	21	15	3 - 12	30.7 ± 9.5	28.4 ± 6.7	5.4 ± 2.2	-1.9	1.7
FBN1	Borehole	21	48	26 - 40.5	25 ± 8.8	28.9 ± 7.6	3.6 ± 1.7	2.1	3.9
FBN4	Borehole	21	28	2.5 - 18	52.9 ± 2.6	54.3 ± 2.6	20.8 ± 3.2	-0.6	1.0
FBN5	Borehole	21	47	22.5 - 35	15 ± 9.2	31.6 ± 11.3	7.9 ± 3.7	-0.6	1.1
FEP1	Borehole	21	25	7.5 - 17	35.2 ± 1.0	36.7 ± 1.4	12.9 ± 2.4	-0.3	0.5
FP1	Borehole	21	19	4.5 - 13	28 ± 2.9	29.9 ± 3.9	6.6 ± 1.9	-1.3	1.1
FPM1	Borehole	21	24	NA	7.6 ± 0.7	19 ± 0.8	14.1 ± 2.0	-1.4	0.4
FPM3	Borehole	21	21	9 - 18	18.6 ± 5.0	24 ± 5.7	3.5 ± 0.8	-0.5	0.3
FVDV	Borehole	21	22	7 - 15	39 ± 1.6	40 ± 2.3	44.4 ± 6.9	-1.7	0.8
PDO	Pumping station	21	25	NA	33.9 ± 1.2	42.1 ± 2.0	11.5 ± 1.7	-1.8	0.6
PP	Pumping station	21	80	NA	21.8 ± 1.1	25.8 ± 0.9	9.2 ± 4.0	-1.5	0.0
PS	Pumping station	4	16	NA	23.6 ± 1.4	32.4 ± 2.7	4.1 ± 1.4	-0.2	1.6
FCE	Borehole	1	85	NA	7.2	3.1	0.5	NA	NA
FNA	Borehole	1	47	NA	20.0	24.3	1.3	NA	NA
FBN3	Borehole	3	56	16 - 22	13.4 ± 2.4	15.2 ± 2.2	1.3 ± 0.4	5.4	7.5
FBN2	Borehole	4	32	17 - 26	31.6 ± 4.1	18.2 ± 12.5	2 ± 1.7	6.6	10.3
FEP2	Borehole	6	23	15 - 18.5	8.8 ± 0.6	9.5 ± 0.8	2 ± 1.3	-0.3	-0.5
FPM2	Borehole	5	35	30 - 31	16.2 ± 5.1	22.1 ± 5.2	6.1 ± 0.6	-1.3	0.6
FP2	Borehole	4	21	8 - 13	165.8 ± 18.9	38 ± 3.3	1.2 ± 0.7	-0.9	3.6
FP	Borehole	4	23	12 - 17	39.0 ± 3.3	45 ± 5.0	5.9 ± 0.9	-1.7	0.6
FB	Borehole	1	33	12.8	28,0	36.6	2.2	NA	NA
SEP	Spring	12	-	-	23.5 ± 1.9	33.1 ± 2.6	5.5 ± 3.0	-1.5	1.8
SCG	Spring	2	-	-	28.5 ± 0.2	40.7 ± 0.1	4.7 ± 2.1	NA	NA
SB1	Spring	1	-	-	16.5	7.8	< 0.5	NA	NA
SB2	Spring	1	-	-	18.4	2.3	2.1	NA	NA
RS1	River	21	-	-	25.8 ± 1.2	29.3 ± 1.9	3.4 ± 0.8	1.0	3.7
RPY	River	21	-	-	20.7 ± 1.5	28.5 ± 1.6	11.6 ± 3.1	NA	NA
RS2	River	21	-	-	24.3 ± 1.3	29.6 ± 1.3	6.5 ± 2.1	0.8	2.6
RA	River	4	-	-	22.1 ± 1.0	26.1 ± 1.2	1.5 ± 1.0	0.4	3.1
RS3	River	4	-	-	25.2 ± 0.4	28.8 ± 0.8	5.1 ± 1.5	0.4	3.1
RV1	River	3	-	-	29.3 ± 1.1	25.9 ± 3.7	1.2 ± 0.5	0.7	5.9
RV2	River	3	-	-	25 ± 1.9	28.5 ± 2.8	0.9 ± 0.4	0.4	4.7
RP	River	1	-	-	21.3	25.6	3.6	NA	NA
C1	Canal	1	-	-	18.3	12.7	< 0.5	NA	NA
C2	Canal	1	-	-	15.5	13.1	< 0.5	NA	NA

An analysis of the geographic distribution of ClO_4^- is presented in Figure 4, revealing some major trends and potential sources of ClO_4^-. Lower concentrations of ClO_4^- (< 4 $\mu g \cdot L^{-1}$) were mainly found on the Berru Mount, in the Vesle River and in the Aisne-Marne Canal. As mentioned above, the Tertiary formation on the Berru Mount is represented by a succession of permeable and impermeable layers, which contains several small aquifers in which water could be renewed quickly by precipitation. As a result, low levels of ClO_4^- were detected in this area. In the Vesle River, ClO_4^- concentrations ranged from 0.9 ± 0.4 $\mu g \cdot L^{-1}$ to 1.2 ± 0.5 $\mu g \cdot L^{-1}$. The Vesle River originates far away upstream, receiving groundwater discharge from outside the study area that is little affected by ClO_4^- contamination. In the Aisne-Marne Canal, ClO_4^- was not detected (< 0.5 $\mu g \cdot L^{-1}$), indicating that the canal has little or no input from the contaminated groundwater or river water (Vesle River) of the study area.

Most of the sampling sites with ClO_4^- concentrations exceeding 4 $\mu g \cdot L^{-1}$ were located downgradient of the Champagne Mounts (Figure 4), where large quantities of ammunitions were used, stored, and destroyed during and after WWI. The highest concentrations of ClO_4^- were found at borehole FVDV, with a maximum of 62.5 $\mu g \cdot L^{-1}$ (in September 2018) and an average of 44.4 ± 4.9 $\mu g \cdot L^{-1}$. Plume-like patterns of ClO_4^- were observed along the sections A – A' and B – B' (the same direction as the groundwater flow line; Figure 4). At FBN4, FEP1 and SEP (A – A'), mean ClO_4^- concentrations over the two years monitoring were 20.8 ± 3.2 $\mu g \cdot L^{-1}$, 12.9 ± 2.4 $\mu g \cdot L^{-1}$ and 5.5 ± 3.0 $\mu g \cdot L^{-1}$ respectively, indicating a progressive decrease with distance downgradient. A similar pattern was observed at FPM1, FPM2 and FPM3 (B – B') with concentrations of 14.1 ± 2.0 $\mu g \cdot L^{-1}$, 6.1 ± 0.6 $\mu g \cdot L^{-1}$ and 3.5 ± 0.8 $\mu g \cdot L^{-1}$ respectively. The high ClO_4^- levels and the observed plume-like patterns indicated that potential point-sources of ClO_4^- could be present upstream at FVDV, FBN4 and FPM1. Specifically, the military tunnel N1 and the ammunition destruction sites (N4 and N5) were likely responsible for the high concentrations of ClO_4^- measured at these sites (Figure 4).

Although ClO_4^- concentrations in river waters were generally lower than those of groundwater, some river sites had relatively high ClO_4^- concentrations (>10 $\mu g \cdot L^{-1}$), such as RPY in the Py River (Figure 4 and Table 1). The Py River is downstream from the Suippes military camp that represents a potential source of ClO_4^- contamination to the Py river watershed (Figure 1). In the Suippe River upstream of the confluence with the Py River (RS1), low ClO_4^- concentrations (3.4 ± 0.5 $\mu g \cdot L^{-1}$) were measured while, downstream of this confluence (RS2), higher concentrations (6.5 ± 2.1 $\mu g \cdot L^{-1}$) were found.

Unlike the widespread contamination of ClO_4^- on the study area, organic explosives have not been detected in surface and groundwater samples, which could be explained by their low persistence and mobility in soil and water (Clausen et al., 2006). During WWI, nitro group explosives such as TNT, nitroglycerine and nitrocellulose were largely used. TNT can be rapidly degraded in most soil and aquifer systems; therefore, its presence is typically restricted to areas near its introduction to the environment. At most sites, TNT can be completely attenuated in the surface soil, thereby preventing contamination of the unsaturated zone (UZ) or groundwater (Clausen et al., 2006). Nitroglycerin is soluble when present alone and is subject to rapid biodegradation, but when present with nitrocellulose it is insoluble. Nitrocellulose is also insoluble, resulting in its low mobility in the environment (Quinn, 2015).

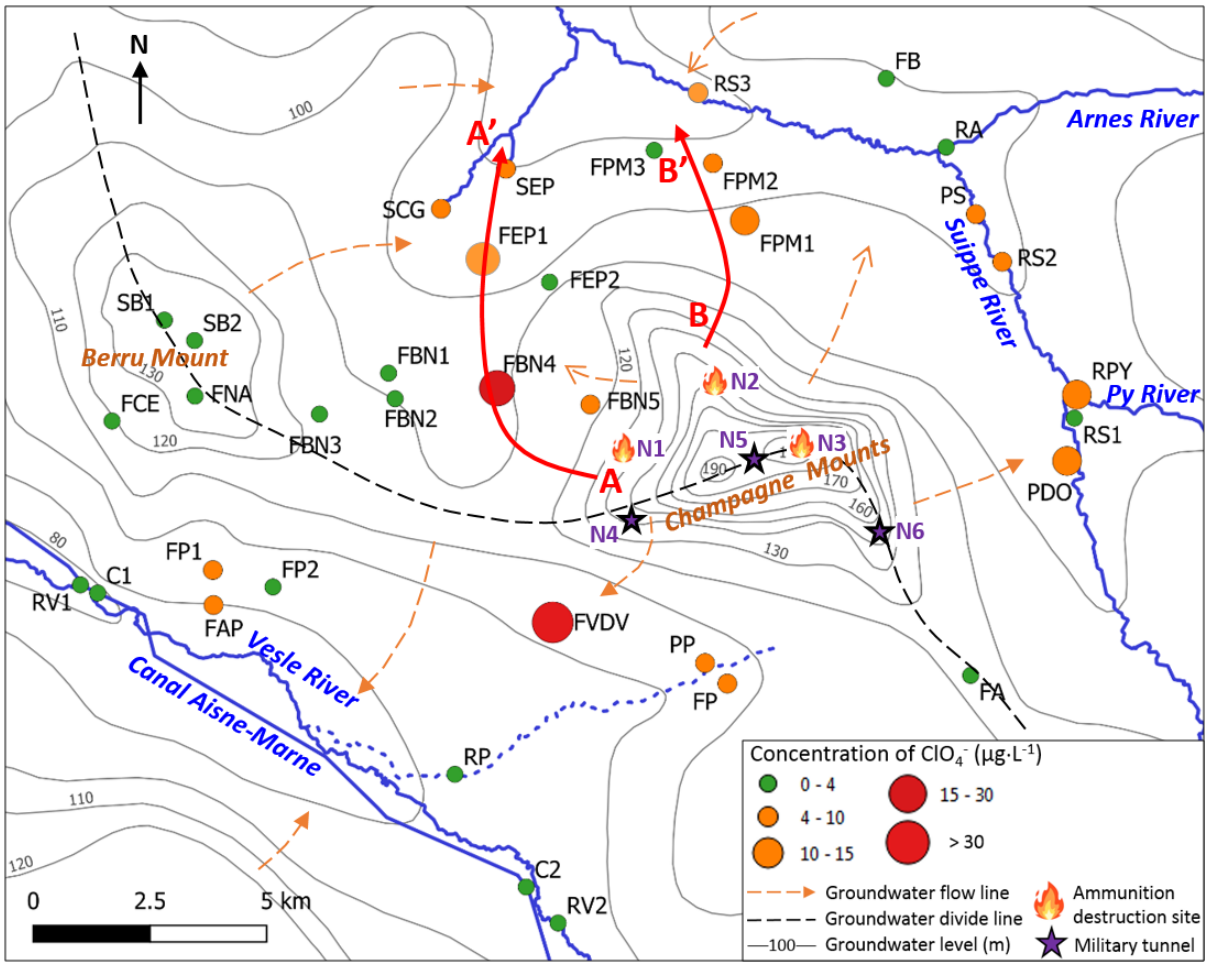

Figure 4: Spatial distribution of ClO_4^- contamination in the study area and military sites related to the WWI

3.2. Sources and fate of ClO_4^- in the Chalk aquifer

3.2.1. Isotopic composition of ClO_4^- and NO_3^-

The results of Cl and O stable isotope analysis for ClO_4^- in water samples are presented by dual isotope plots in comparison to published data for synthetic, Atacama and selected US indigenous natural ClO_4^- occurrences (Table 2 and Figure 5). There is no evidence of ClO_4^- biodegradation, which is consistent with the typical oxic condition of the unconfined Chalk aquifer (Barhoum et al., 2014; Edmunds et al., 1987); the isotopic composition of ClO_4^- could therefore reflect initial values of the sources.

Table 2 : Isotopic compositions of ClO_4^- in ground- and surface water samples (HW: high water; LW: low water)

Name	Sample date	$\delta^{18}O$ (‰)	$\Delta^{17}O$ (‰)	$\delta^{37}Cl$ (‰)
FVDV	04/05/18	-20,7	0,2	0,3
FBN4 (HW)	04/06/18	-21,8	0,2	0,2
FBN4 (LW)	01/18/19	-29,6	-0,3	-3,3
RPY	04/10/19	-22,9	1,3	-6.0
RM	02/22/19	-18,2	0,1	-0,2

The $\delta^{37}Cl$, $\delta^{18}O$ and $\Delta^{17}O$ values of ClO_4^- in water samples collected at the Suippe military camp (RM; pure military source), FVDV and FBN4 (at high water level) plotted exactly within the synthetic ClO_4^-

range, proving similar military sources of ClO_4^- at these sites (Figure 5). However, the results for FBN4 (at low water level) was different, with a lower $\delta^{18}O$ value (-29.6‰) falling outside the published synthetic ClO_4^- ranges. Nevertheless, the $\delta^{37}Cl$ and $\Delta^{17}O$ values (-3.3‰ and -0.3‰, respectively) were typical of synthetic ClO_4^-. Therefore, ClO_4^- at FBN4 (at low water level) was interpreted as of synthetic origin, but different from other samples and currently reported synthetic ClO_4^- products. Indeed, the manufacturing processes of synthetic ClO_4^- and the materials used more than 100 years ago during WWI may be different from those of today. Even during WWI, different ClO_4^- salts (NH_4ClO_4 and/or $KClO_4$) were used in explosives; they were produced in different facilities and the method could also have evolved during the WWI conflict. This could possibly explain why this "unusual" synthetic end-member was observed at FBN4 (at low water level). The different ClO_4^- isotopic compositions observed at FBN4 at high and low water levels suggest that there could be different sources of ClO_4^- at different depths. The estimated groundwater ages in the study area were less than 50 years (Cao et al., 2020). Moreover, because the thickness of UZ is less than 30 m (Table 1) and considering that the flow rate is about 1 $m \cdot year^{-1}$ through the Chalk matrix, the time of transfer in the UZ were less than 30 years (e.g., Barraclough et al., 1994; Brouyère et al., 2004; Chen et al., 2019; Wellings, 1984). Therefore, military sources of ClO_4^- contamination are most likely related to military activities after WWI (destruction of ammunitions) rather than during the conflict, or to the release of ClO_4^- from unexploded ordnance persisting in the subsoil (or unused ammunitions stored on the surface).

In the RPY sample, a substantial fraction of ClO_4^- with an Atacama-type isotopic composition is evident. The lower value of $\delta^{37}Cl$ (-6.0‰) and the higher value of $\Delta^{17}O$ (+1.3‰) are both consistent with a mixture of a synthetic end-member with typical Atacama ClO_4^-. This could probably be explained by the nitrogen explosives of WWI (black powder and nitro group explosives) made with Chilean nitrate and/or the past use of Chilean nitrate as fertilizer. Indeed, the PY River water consists of aquifer discharge from the entire watershed. Although synthetic (military) ClO_4^- is indicated by isotopic analysis at two sites with the highest ClO_4^- concentrations (FVDV and FBN4), Atacama ClO_4^- from Chilean nitrate fertilizer might be present, especially at sites with low ClO_4^- concentrations related to diffuse sources.

The NO_3^- isotope data at all the sampling points did not show any evidence of an Atacama source for the NO_3^- (Figure 5). However, this cannot rule out the possibility of the existence of Atacama NO_3^- in water samples, as Atacama NO_3^- could have been replaced and/or assimilated with the biogenic NO_3^- in the soil (Böhlke et al., 2009). Indeed, the distinctive isotopic composition of oxygen in atmospheric NO_3^- is preserved only in hyper-arid environments and is lost in moist soils where higher biological activity occurs (Böhlke et al., 1997; Michalski et al., 2015). Therefore, more information is needed to better evaluate the regional extent of ClO_4^- sources related to the past use of Chilean nitrate in the study area.

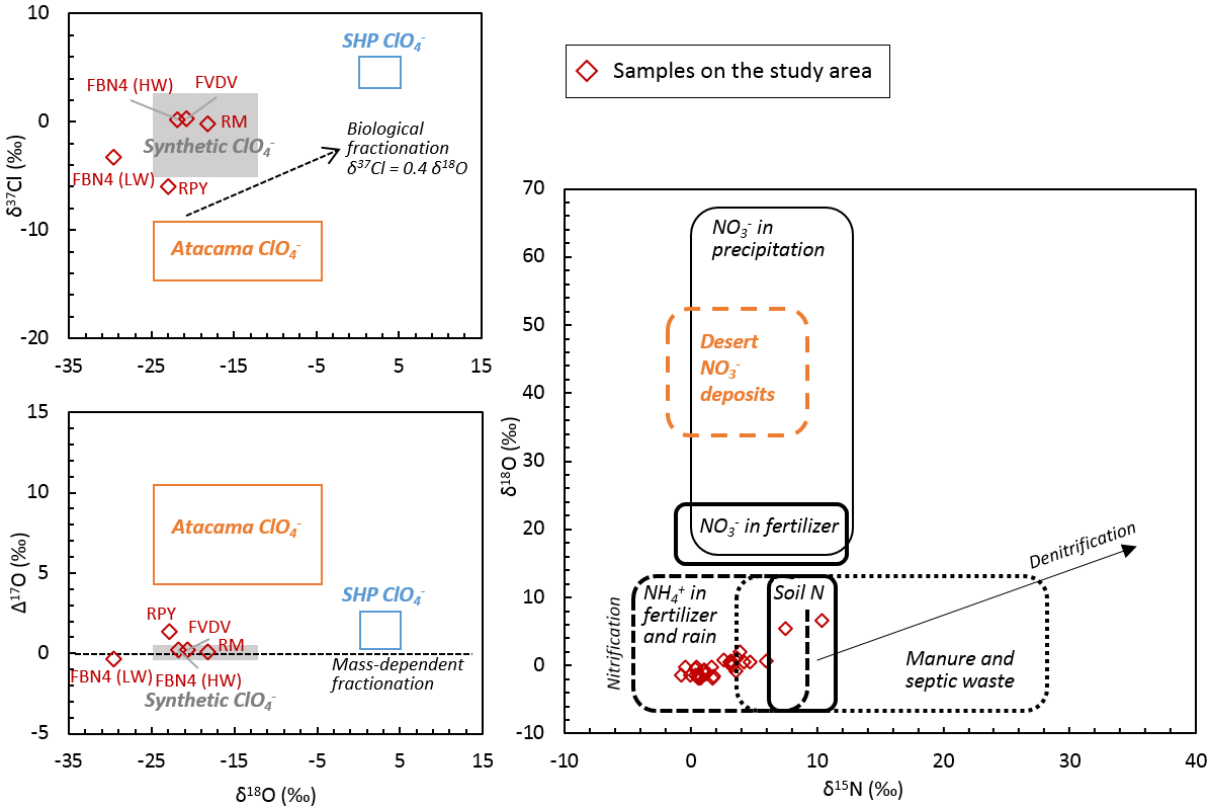

Figure 5: Summary of isotope data for ClO_4^- and NO_3^- in water samples of the study area, compared with major known ClO_4^- sources including synthetic, Atacama and indigenous natural ClO_4^- from the Southern High Plains (Texas) (SHP) (Ader et al., 2001 ; Bao and Gu, 2004 ; Böhlke et al., 2005, 2009 ; Jackson et al., 2005b, 2010 ; Parker et al., 2008 ; Plummer et al., 2006 ; Rajagopalan et al., 2006 ; Rao et al., 2007 ; Sturchio et al., 2007, 2011). Arrow in the $\delta^{37}Cl$ vs $\delta^{18}O$ graph represents the slope of biodegradation ($\delta^{37}Cl = 0.4\ \delta^{18}O$) and arrow in the $\Delta^{17}O$ vs $\delta^{18}O$ graph represents the direction of mass dependent fractionation.

3.2.2. Temporal variability of ClO_4^- compared with groundwater level and major ions

The temporal variation of ClO_4^- concentrations measured from June 2017 to June 2019 was compared with groundwater level fluctuation and the temporal variation of NO_3^- and Cl^- concentrations (two major agriculture-derived ions, Cao et al., 2020), in order to explore the potential sources of ClO_4^- (point and/or diffuse source), and the possible future evolution of ClO_4^- in the Chalk aquifer.

At most sites, inter-annual variations of ClO_4^- concentrations were observed and also revealed by the statistical trend analysis (Figure 6 and Table 3). The periods when ClO_4^- concentrations changed significantly under the seasonal and annual effects were estimated with the statistical methods presented in section 2.3 (results detailed in SI.2). Higher ClO_4^- concentrations were observed in 2018 (Figure 6 and SI.2), corresponding with the higher groundwater level in 2018.

Table 3 : Seasonal and annual effects on ClO_4^- concentrations (the effect is considered as statistically significant with P-value < 0.05, related values < 0.05 are marked in bold)

	Seasonal trend	Annual trend
FVDV	0,079	> **0.001**
FBN4	0,097	0,209
FEP1	0,052	0,291
FBN5	**0,003**	**0,007**
FA	0,176	**0,015**
FBN1	0.028	0,374
FP1	0,161	0,165
FPM3	0,067	**0,033**
RS1	0,053	0,767
RPY	**0,021**	**0,022**
RS2	**0,011**	0,240
PDO	0,624	0,135
FPM1	0,097	> **0.001**
PP	**0,012**	0,326

At sites having mean ClO_4^- concenrations > 10 µg·L^{-1} (FVDV, FBN4, FEP1 and FBN5; Figure 6), several peaks of ClO_4^- concentration were observed and the temporal variation of ClO_4^- was poorly correlated with the groundwater level fluctuation (Table 4). The peaks could possibly be explained by localized flushing of ClO_4^- from the UZ by natural (rainfall) or artificial (irrigation) recharge processes, indicating the presence of point sources of ClO_4^- contamination upstream of these sites. At FVDV and FBN4, the two most contaminated sites, the correlation coefficients between ClO_4^- and groundwater level were the lowest (Table 4 and Figure 6), as ClO_4^- concentrations here were mainly controlled by the ClO_4^- transfer waves following flushing rather than the groundwater level fluctuation.

In contrast, at sites showing ClO_4^- concentrations < 10 µg·L^{-1} (FA, FBN1, FP1 and FPM3; Figure 6), the temporal variation of ClO_4^- was significantly correlated to the groundwater level fluctuation (Table 4). The correlation relationship was stronger at FA and FBN1 (Adj. R^2 = 0.42 and 0.54, respectively; Table 4) with larger groundwater level fluctuation; at FP1 and FPM3 where the groundwater level fluctuated less, the correlation relationship was weaker (Adj. R^2 = 0.35 and 0.20, respectively; Table 4). Diffuse sources of ClO_4^- were presumed to be present at these sites. During low water level periods, most of the sources were apparently disconnected from the saturated zone. As water level rose, the contamination source was re-activated and more contaminants were released in water and flushed into the saturated zone, resulting in the increase of ClO_4^- concentrations.

Generally, a poor correlation was observed between ClO_4^- and major ions (Table 4). The temporal evolution of ClO_4^- was compared with the chronicles of NO_3^- and Cl^-, the two major agriculture-derived ions in groundwater of the Champagne Chalk aquifer (Cao et al., 2020). At most sites, the temporal evolution of ClO_4^- was different from that of NO_3^- and Cl^- (Figure 6), indicating different origins of ClO_4^- *versus* NO_3^- and Cl^-.

Table 4 : Correlation of ClO_4^- with groundwater levels and major ion concentrations. Values correspond to Adj. R^2 issued from the generalized additive model (statistically significant as the P-value < 0.05, related Adj. R^2 values when P-value < 0.05 are marked in bold; NA: not available)

Name	Water level	Cl^-	NO_3^-	SO_4^{2-}	Na^+	K^+	Mg^{2+}	Ca^{2+}
FVDV	0,07	-0,04	**0,21**	**0,37**	0,15	**0,53**	**0,41**	0,08
FBN4	0,07	0,03	**0,32**	0,24	0,03	0,18	**0,31**	0,01
FEP1	0,08	0,00	0,08	0,05	**0,32**	-0,02	-0,03	0,03
FBN5	**0,22**	**0,71**	**0,64**	0,02	**0,28**	**0,67**	**0,41**	**0,61**
FA	**0,42**	**0,54**	**0,56**	**0,68**	0,04	0,29	**0,24**	**0,64**
FBN1	**0,54**	**0,53**	**0,67**	**0,55**	-0,02	**0,62**	0,35	-0,02
FP1	**0,35**	0,17	0,25	0,23	0,28	**0,48**	-0,05	0,05
FPM3	**0,20**	-0,03	-0,04	-0,05	-0,04	0,17	**0,46**	0,18
RS1	NA	**0,61**	**0,13**	**0,53**	**0,49**	**0,37**	-0,06	0,05
RPY	NA	**0,10**	0,06	-0,01	-0,03	-0,06	-0,06	0,13
RS2	NA	**0,51**	**0,11**	**0,36**	0,02	**0,17**	**0,53**	0,13
PDO	NA	-0,05	0,06	0,01	-0,03	**0,16**	-0,03	0,19
FPM1	NA	**0,28**	**0,51**	-0,02	**0,10**	**0,33**	0,22	0,11
PP	NA	0,29	**0,02**	-0,05	0,16	0,03	0,08	-0,06

At FEP1, FPM1 and PP, despite the temporal heterogeneity of ClO_4^- levels, the concentrations of NO_3^- and Cl^- were stable over time (Figure 6). As described in Cao et al. (2020), estimated groundwater ages at these points were > 30 years in a piston flow model, which is related to the superficial formations limiting rapid transport of water and solutes (NO_3^- and Cl^-) from surface (agriculture-derived ions are distributed mainly in the soil area) to the saturated zone. Consequently, the aquifer receives recharge mainly from upstream of the superficial formation covered area. Water traveled laterally in the saturated zone during > 30 years and solute concentrations were greatly buffered, resulting in stable NO_3^- and Cl^- levels independent of water level fluctuation (Cao et al., 2020). The large variation of ClO_4^- concentrations, in contrast to the temporal stability of NO_3^- and Cl^-, could be interpreted as an indication that the location of ClO_4^- sources is much deeper than those of agriculture-derived ions. As groundwater levels rose, the contamination front of ClO_4^- was reached, generating changes in ClO_4^- levels, despite the fact that flushing from the soil was largely limited by superficial formations. At FPM3 (downstream from the borehole FPM1; Figure 2), a time lag was observed between groundwater levels and concentrations of NO_3^- and Cl^-, likely as a result of slow transport through the discontinuous graveluche formations. However, ClO_4^- levels varied with groundwater levels without time lag, implying again that deeper ClO_4^- sources were more quickly activated by the rise in water table.

At FA, unlike the positively correlated relationship between ClO_4^- and groundwater level, NO_3^- and Cl^- were negatively correlated with groundwater level (Figure 6 and Table 4), indicating a dilution effect. At this site, groundwater dating showed 75-80% of modern water by the binary mixing model, indicating a water table constituted mainly by freshly percolated rainwater that favors the process of dilution (Cao et al., 2020). During the rapid flow process following precipitation, the low mineralized rainwater entered the aquifer resulting in decrease of NO_3^- and Cl^- concentrations. For ClO_4^-, it seemed that the

inputs by the potential sources of ClO_4^- in the UZ following the rise of groundwater level was more important than the dilution process, which led to an increase in ClO_4^- with the groundwater level.

At FBN1 and FBN5, the temporal variabilities of ClO_4^-, NO_3^- and Cl^- were well correlated (Figure 6 and Table 4). Indeed, located near the groundwater divide line (Figure 2), deep water table levels were observed (> 22 m,Table 1) and low permeability was suggested at these two sites (Cao et al., 2020). According to groundwater dating, the groundwater flow was well described by the exponential mixing model (mean residence time of < 20 years), indicating a spatially uniform recharge (Cao et al., 2020). ClO_4^-, NO_3^- and Cl^- were thus flushed from the potential sources located in the UZ following recharge, showing a similar temporal variation.

At RPY (Py River) and RS2 (Suippe River after the confluence of Py River), a decrease in ClO_4^- concentration was observed during high flow period (May 2018 and May 2019; Figure 6), implying a dilution effect on ClO_4^- concentration. Indeed, the rivers are recharged by the Chalk aquifer with little surface runoff produced. In river valleys, the Chalk is usually highly fractured with shallow groundwater levels and preferential flow of rainwater is favored especially at high water level, resulting in dilution of the aquifer and the river water. A similar tendency was observed at PDO (pumping station near RPY), which is consistent with a mixture of groundwater and surface water as implied by groundwater dating (30% to 60% of modern water and an end-member of ~40-year old water; Cao et al., 2020).

The potential sources of ClO_4^- located deeper than the sources of agriculture-derived ions in the UZ refer most probably to unexploded ordnance still present underground after WWI. Indeed, some shells fired during the war could reach > 10 meters underground without exploding (UNMAS, 2015). Unused ammunitions could still be present underground in military tunnels of WWI. In addition, in the Champagne Mounts area, some unused ammunitions could have been cleaned up by burying in specified boreholes (Debant, 2019). Over time, the release of the explosive charge occurs as a result of the general corrosion of the envelope and/or its perforation. The time required for perforation was estimated between 250 and 450 years, at a rate of 1 mm/year on average (Parker et al., 2004). These unexploded ordnances can be difficult to locate and clean up due to their number and their deep underground location. Contamination plumes observed at some sites indicate that the ammunition destruction sites may be the main point sources of ClO_4^-, as repeated detonation causes an accumulation of residual ClO_4^- at these sites. The residue of ammunition destroyed by detonation can persist for more than 100 years in soils (Hubé, 2014). Despite the huge quantities of fully exploded ordnance, their residue is estimated at around 0.01% and can only persist for a short time underground, representing a relatively small contribution to the ClO_4^- contamination of groundwater. Considering that most of the potential sources of ClO_4^- have long persistence times, the ClO_4^- contamination in groundwater of the study area may not decline in the short to medium term.

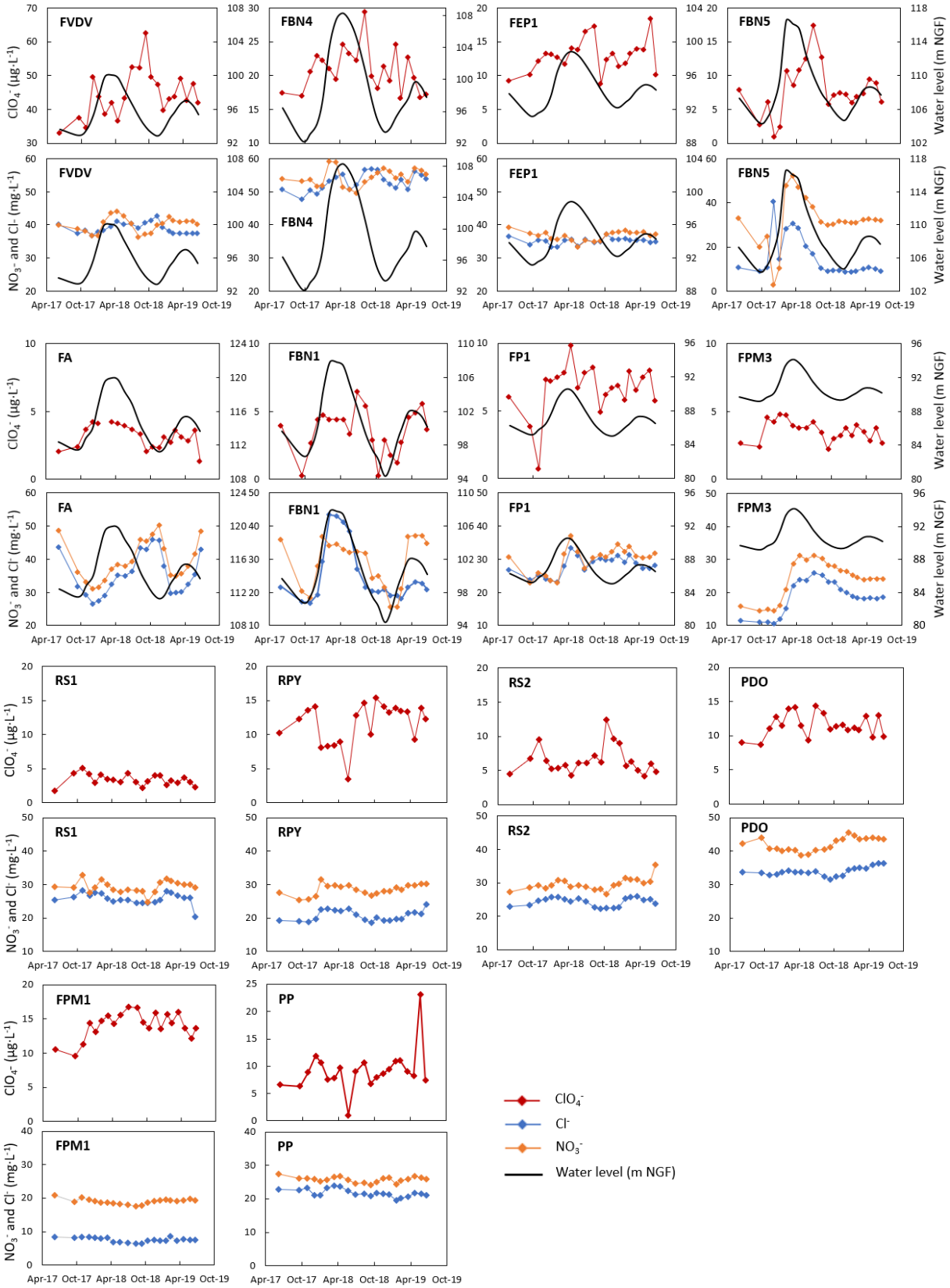

Figure 6: Temporal variation of perchlorate concentration compared with groundwater level fluctuation from June 2017 to June 2019

3.3. Mass flow rate of perchlorate

In the Suippe River and its tributaries (Figure 4), the mass flow rate of ClO_4^- (M) has been estimated according to the measured water flow rate (Q) and ClO_4^- concentrations (C):

$$M = C \times Q \quad (1)$$

The data of water flow rate and ClO_4^- concentration used for calculation was measured on October 2017. The estimated mass flow rate of ClO_4^- was 4.6 kg·month^{-1} upstream the Suippe River (RS1) and 13.5 kg·month^{-1} downstream of its confluence with the Py River (RS2) (Table 5). The increase of mass flow rate from RS1 to RS2 (8.9 kg·month^{-1}) was approximately equal to the contribution from Py River (9.6 kg·month^{-1}), implying that the contribution from the Chalk aquifer between RS1 and RS2 is negligible with low groundwater discharge and low ClO_4^- concentrations in the riparian aquifer.

The estimated mass flow rate of ClO_4^- downstream along the Suippe River (RS3) was 14.6 kg·month^{-1}. The Arnes River, which joins the Suippe River between RS2 and RS3, has a ClO_4^- flux less than 0.1 kg·month^{-1}. The increase of ClO_4^- mass flow rate from RS2 to RS3 (1.1 kg·month^{-1}) was due to the contribution of Chalk aquifer discharge (zero runoff is assumed on the Champagne Chalk). The groundwater discharge from RS2 to RS3 was 322 L·s^{-1}, estimated from the water flow rate at RS2, RS3 and RA. According to equation (1), a ClO_4^- concentration of 1.3 µg·L^{-1} in aquifer discharge on October 2017 was estimated, which represents the average concentration from the Chalk aquifer of left and right bank of the Suippe River.

Table 5 : Mass flow rate of ClO_4^- in the Suippe River and its tributaries (data measured on October 2017)

Name	Location	Water flow rate (L·s^{-1})	ClO_4^- concentration (µg·L^{-1})	ClO_4^- mass flow rate (kg·month^{-1})
RS1	Suippe River	401	4.3	4.6
RS2	Suippe River	752	6.7	13.5
RS3	Suippe River	1184	4.6	14.6
RPY	Py River	276	12.3	9.1
RA	Arnes River	110	< 0.5	< 0.1

The estimated monthly ClO_4^- flow rate on October 2017 represents approximately the minimum level in the Suippe River and its tributaries, as the water flow rate was measured during low discharge period, whereas ClO_4^- concentrations in rivers were relatively stable over time according to the low values of standard deviations presented in Table 1.

4. Conclusions and perspectives

This study examined sources and evolution of ClO_4^- contamination in groundwater of NE France. The NE region of France is suspected to have multiple sources of ClO_4^- related to military activities of WWI and/or the past use of Chilean nitrate as fertilizer in agriculture. An intensive sampling network was established on a study area of a representative watershed, where ClO_4^- concentrations were monitored monthly for two years (2017-2019). The measured concentrations and isotopic contents of ClO_4^- and the

historical investigations have been combined with previously published data on groundwater dating as well as hydrologic and geochemical characteristics of the Chalk aquifer (Cao et al. 2020), which allowed to clarify the sources of ClO_4^- and to understand its evolution in groundwater.

This work produced the first precise ClO_4^- contamination mapping in the study area east of Reims city with ClO_4^- concentrations in ground- and surface water ranging from < 0.5 to 62.5 $\mu g \cdot L^{-1}$. About half of the sampling sites showed ClO_4^- concentrations > 4 $\mu g \cdot L^{-1}$ and most of these sites were located downgradient of the Champagne Mounts area, where huge quantities of ClO_4^- were used, stored, or destroyed during and after WWI. Point sources of ClO_4^- were presumed to exist in the study area, as indicated by the plume-like patterns of contamination observed at some sites. The isotopic signature of ClO_4^- at the two most contaminated sites showed a synthetic origin, proving the military source of ClO_4^- contamination in the study area. In addition, the estimated groundwater ages in the study area were < 50 years, implying that ClO_4^- contamination is related to sources that may still persist in the subsoil long after the end of WWI (e.g., unexploded ammunition) or post-WWI military activities (e.g., destruction of ammunition). The isotopic analysis of ClO_4^- in river water showed a minor but distinct component of Atacama ClO_4^-, indicating the presence of some Chilean nitrate in the watershed.

Annual variations of ClO_4^- concentration were observed, indicating the influence of recharge processes and groundwater levels on ClO_4^- contamination. Two major temporal trends of ClO_4^- concentration were observed: 1) ClO_4^- concentrations poorly correlated to groundwater level with peaks of contamination due to flushing at sites having ClO_4^- concentrations > 10 $\mu g \cdot L^{-1}$, implying the presence of point sources; 2) ClO_4^- concentrations highly correlated to groundwater level at sites showing ClO_4^- concentrations < 10 $\mu g \cdot L^{-1}$, where diffuse sources were suggested. In addition, the rapid response of ClO_4^- concentration following the rise of groundwater level compared with relatively stable concentrations of agricultural ions at some sites indicated that the location of ClO_4^- sources could be much deeper than those of agricultural ions (mainly in the soil area). Considering the long persistence time of the explosive residues related to unexploded ammunitions and ammunition destruction activities, the ClO_4^- contamination in groundwater of the study area seems unlikely to decrease in the short- to medium-term.

The multi-tool methodology developed in the study area could furtherly be applied to other ClO_4^- contaminated sites in NE France with suspected military and agricultural sources, with the aim of making appropriate recommendations for a long-term management of groundwater resources. Moreover, this characterization methodology could more widely applicable elsewhere in Chalk aquifers or other multi-porosity mediums for the prediction of solute transport (natural or anthropogenic) and for the evaluation of aquifer vulnerability. However, this research can be improved and developed in several different aspects. The continuous monitoring of ClO_4^- concentrations and geochemistry can be continued to obtain longer time series, with the aim to confirm and specify our conclusions and also to study the evolution of ClO_4^- in the Chalk aquifer under different climate conditions. More measurements of water

flow rate in rivers can be realized (during low, medium and high discharge period) in order to better estimate the mass flow rate of ClO_4^-. In addition, groundwater sampling and analysis should also be realized at different depths of boreholes to obtain vertical profiles of ClO_4^- concentrations as well as other chemical characteristics, which allows to explore their relationships and to further confirm the position of potential ClO_4^- sources underground. In this study, isotopic analysis of ClO_4^- has only been realized at sites with high levels of ClO_4^-. This analysis should also be performed at sites having low concentrations of ClO_4^- to further confirm whether traces of Atacama ClO_4^- exist on these low contaminated sites related to diffuse sources. Finally, hydrogeochemical numerical modeling tools could be a relevant complement of this study to better understand the transfer mechanism of ClO_4^- in the Chalk groundwater.

Declaration of Competing Interest

The authors declare that they have no known competing financial interests or personal relationships that could have appeared to influence the work reported in this paper.

Acknowledgements

This work was co-funded by the BRGM, the Agence de l'Eau Seine-Normandie, the Region Grand-Est, the Grand-Reims Metropole and ARS Grand-Est. Authors want to thank Nicolas Caillon of University of Joseph Fourier Grenoble for the NO_3^- isotopic analysis; Alexandre Conreux and Julien Hubert of Gegenaa laboratory in University of Reims Champagne-Ardenne for their contribution in sampling campaigns and major ions analysis; and Alain Devos, Alexis Carlu, Thibaud Damien and Sarah Bambara for their participation in river flow measurement. Authors would also like to thank the owners and operators for access to their boreholes.

References

Allen, D.J., Brewerton, L.J., Coleby, L.M., Gibbs, B.R., Lewis, M.A., MacDonald, A.M., Wagstaff, S.J., Williams, A.T., 1997. The physical properties of major aquifers in England and Wales. British Geological Survey Technical Report WD/97/34, 312 p.

Allouc, J., Le Roux, J., Batkowski, D., Bourdillon, C., Catillon, J., Causero, L., Ménillet, F., Morfaux, P., Ravaux, P., 2000. Notice explicative, Carte géol. France (1/50 000), feuille Suippes (159).Orléans: BRGM, 73 p. Carte géologique par Allouc, J. et Le Roux, J. (2000)

ANSES, 2018. Avis de l'Anses relatif à la « Pertinence de la ré-évaluation de la valeur guide pour les ions perchlorate dans l'eau destinée à la consommation humaine ». Maison-Alfort, Anses, 42 p.

ANSES, 2013. Campagne nationale d'occurrence de polluants émergents dans les eaux destinées à la consommation humaine. Maison-Alfort, Anses, 56 p.

ANSES, 2011. Avis de l'Anses relatif à l'évaluation des risques sanitaires liés à la présence d'ions perchlorate dans les eaux destinées à la consommation humaine. Maison-Alfort, Anses, 22 p.

Aziz, C., Borch, R., Nicholson, P., Cox, E., 2006. Alternative Causes of Wide-Spread, Low Concentration Perchlorate Impacts to Groundwater, in: Perchlorate: Environmental Occurrence, Interactions and Treatment. Springer, Boston, MA, pp. 71–91. https://doi.org/10.1007/0-387-31113-0_4

Bao, H., Gu, B., 2004. Natural perchlorate has a unique oxygen isotope signature. Environ. Sci. Technol. 38, 5073–5077.

Barhoum, S., Valdès, D., Guérin, R., Marlin, C., Vitale, Q., Benmamar, J., Gombert, P., 2014. Spatial heterogeneity of high-resolution Chalk groundwater geochemistry – Underground quarry at Saint Martin-le-Noeud, France. Journal of Hydrology 519, 756–768. https://doi.org/10.1016/j.jhydrol.2014.08.001

Barraclough, D., Gardner, C.M.K., Wellings, S.R., Cooper, J.D., 1994. A tracer investigation into the importance of fissure flow in the unsaturated zone of the British Upper Chalk. Journal of Hydrology 156, 459–469. https://doi.org/10.1016/0022-1694(94)90090-6

BASOL database. https://basol.developpement-durable.gouv.fr/. Accessed date: October 2019.

Bausinger, T., Bonnaire, E., Preuß, J., 2007. Exposure assessment of a burning ground for chemical ammunition on the Great War battlefields of Verdun. Science of The Total Environment 382, 259–271. https://doi.org/10.1016/j.scitotenv.2007.04.029

Böhlke, J.K., Ericksen, G.E., Revesz, K., 1997. Stable isotope evidence for an atmospheric origin of desert nitrate deposits in northern Chile and southern California, U.S.A. Chem. Geol. 136, 135152. https://doi.org/10.1016/S0009-2541(96)00124-6

Böhlke, J.K., Hatzinger, P.B., Sturchio, N.C., Gu, B., Abbene, I., Mroczkowski, S.J., 2009. Atacama perchlorate as an agricultural contaminant in groundwater: isotopic and chronologic evidence from Long Island, New York. Environ. Sci. Technol. 43, 5619–5625.

Böhlke, J.K., Mroczkowski, S.J., Sturchio, N.C., Heraty, L.J., Richman, K.W., Sullivan, D.B., Griffith, K.N., Gu, B., Hatzinger, P.B., 2017. Stable isotope analyses of oxygen (18O:17O:16O) and chlorine (37Cl:35Cl) in perchlorate: reference materials, calibrations, methods, and interferences. Rapid Commun. Mass Spectrom. 31, 85–110. https://doi.org/10.1002/rcm.7751

Böhlke, J.K., Sturchio, N.C., Gu, B., Horita, J., Brown, G.M., Jackson, W.A., Batista, J., Hatzinger, P.B., 2005. Perchlorate Isotope Forensics. Anal. Chem. 77, 7838–7842. https://doi.org/10.1021/ac051360d

Brabant, G., Bergmann, P., Kirsch, C.M., Köhrle, J., Hesch, R.D., von zur Mühlen, A., 1992. Early adaptation of thyrotropin and thyroglobulin secretion to experimentally decreased iodine supply in man. Metabolism 41, 1093–1096. https://doi.org/10.1016/0026-0495(92)90291-H

Braverman, L.E., He, X., Pino, S., Cross, M., Magnani, B., Lamm, S.H., Kruse, M.B., Engel, A., Crump, K.S., Gibbs, J.P., 2005. The effect of perchlorate, thiocyanate, and nitrate on thyroid function in workers exposed to perchlorate long-term. J. Clin. Endocrinol. Metab. 90, 700–706. https://doi.org/10.1210/jc.2004-1821

Brouyère, S., Dassargues, A., Hallet, V., 2004. Migration of contaminants through the unsaturated zone overlying the Hesbaye chalky aquifer in Belgium: a field investigation. Journal of Contaminant Hydrology 72, 135–164. https://doi.org/10.1016/j.jconhyd.2003.10.009

Brown, G.M., Gu, B., 2006. The Chemistry of Perchlorate in the Environment, in: Perchlorate: Environmental Occurence, Interactions and Treatment. Springer, Boston, MA, pp. 17–47. https://doi.org/10.1007/0-387-31113-0_2

Cao, F., Jaunat, J., Ollivier, P., Cancès, B., Morvan, X., Hubé, D., Devos, A., Devau, N., Barbin, V., Pannet, P., 2018. Sources and behavior of perchlorate ions (ClO_4^-) in chalk aquifer of Champagne-Ardenne, France: preliminary results, in: IAHS-AISH Proceedings and Reports, 8th International Water Resources Management Conference of ICWRS, June 2018, Beijing (China). pp. 113–117. https://doi.org/10.5194/piahs-379-113-2018

Cao, F., Jaunat, J., Sturchio, N., Cancès, B., Morvan, X., Devos, A., Barbin, V., Ollivier, P., 2019. Worldwide occurrence and origin of perchlorate ion in waters: A review. Sci. Total Environ. 661, 737–749. https://doi.org/10.1016/j.scitotenv.2019.01.107

Cao, F., Jaunat, J., Vergnaud-Ayraud, V., Devau, N., Labasque, T., Guillou, A., Guillaneuf, A., Hubert, J., Aquilina, L., Ollivier, P., 2020. Heterogeneous behavior of unconfined Chalk aquifers infer from combination of groundwater residence time, hydrochemistry and hydrodynamic tools. Journal of Hydrology 581, 124433. https://doi.org/10.1016/j.jhydrol.2019.124433

Chen, N., Valdes, D., Marlin, C., Blanchoud, H., Guerin, R., Rouelle, M., Ribstein, P., 2019. Water, nitrate and atrazine transfer through the unsaturated zone of the Chalk aquifer in northern France. Science of The Total Environment 652, 927–938. https://doi.org/10.1016/j.scitotenv.2018.10.286

Chiesi, F., 1993. Transfert et epuration dans la zone non saturee de la craie en champagne : etude de quelques cas concernant les nitrates et l'atrazine. PhD thesis, Reims, 197 p.

Clausen, J.L., Korte, N., Dodson, M., Robb, J., Rieven, S., 2006. Conceptual Model for the Transport of Energetic Residues from Surface Soil to Groundwater by Range Activities. Cold regions research and engineering lab, Final report, ERDC/CRREL-TR-06-18, 169 p.

CORINE land cover database. https://www.geoportail.gouv.fr/donnees/corine-land-cover-2018. Accessed date: October 2019.

Crampon, N., J. C. Roux, Bracq, P., 1993, Hydrogeology of the chalk in France, in The Hydrogeology of the Chalk of North-West Europe, edited by R. A. Downing, M. Price, and G. P. Jones, Oxford Univ. Press, New York, pp. 81–123.

Debant, J., 2019. La lente dépollution du CEA de Moronvilliers. L'hebdo du vendredi. http://www.lhebdoduvendredi.com/article/36274/la-lente-depollution-du-cea-de-moronvilliers. Accessed date : December 5, 2019.

Desailloud, R., Wemeau, J.-L., 2016. Faut-il craindre les ions perchlorate dans l'environnement ? La Presse Médicale, Médecine et environnement 45, 107–116. https://doi.org/10.1016/j.lpm.2015.10.002

Edmunds, W.M., Cook, J.M., Darling, W.G., Kinniburgh, D.G., Miles, D.L., Bath, A.H., Morgan-Jones, M., Andrews, J.N., 1987. Baseline geochemical conditions in the Chalk aquifer, Berkshire, U.K.: a basis for groundwater quality management. Applied Geochemistry 2, 251–274. https://doi.org/10.1016/0883-2927(87)90042-4

Ericksen, G.E., 1983. The Chilean nitrate deposits. Am. Sci. 71, 366–374.

Facon, P., 2018. Les batailles des monts de Champagne 1914-1918. Editions Tranchées, Paris : Louviers, 239 p.

Foster, S.S.D., 1975. The Chalk groundwater tritium anomaly — A possible explanation. J. Hydrol. 25, 159–165. https://doi.org/10.1016/0022-1694(75)90045-1

Furdui, V.I., Zheng, J., Furdui, A., 2018. Anthropogenic Perchlorate Increases since 1980 in the Canadian High Arctic. Environ. Sci. Technol. 52, 972–981. https://doi.org/10.1021/acs.est.7b03132

Greer, M.A., Goodman, G., Pleus, R.C., Greer, S.E., 2002. Health effects assessment for environmental perchlorate contamination: the dose response for inhibition of thyroidal radioiodine uptake in humans. Environ. Health Perspect. 110, 927–937.

Gu, B., Böhlke, J.K., Sturchio, N.C., Hatzinger, P.B., Jackson, W.A., Beloso Jr., A.D., Heraty, L.J., Bian, Y., Jiang, X., Brown, G.M., 2011. Removal, Recovery and Fingerprinting of Perchlorate by Ion Exchange Processes in Ion Exchange And Solvent Extraction: a Series of Advances, twentieth ed. Taylor and Francis Group, New York, pp. 117–144.

Gu, B., Brown, G.M., 2006. Recent Advances in Ion Exchange for Perchlorate Treatment, Recovery and Destruction, in: Gu, B., Coates, J.D. (Eds.), Perchlorate: Environmental Occurrence, Interactions and Treatment. Springer US, Boston, MA, pp. 209–251. https://doi.org/10.1007/0-387-31113-0_10

Gu, B., Brown, G.M., Chiang, C.-C., 2007. Treatment of Perchlorate-Contaminated Groundwater Using Highly Selective, Regenerable Ion-Exchange Technologies. Environ. Sci. Technol. 41, 6277–6282. https://doi.org/10.1021/es0706910

Gu, B., Brown, G.M., Maya, L., Lance, M.J., Moyer, B.A., 2001. Regeneration of Perchlorate (ClO4-)-Loaded Anion Exchange Resins by a Novel Tetrachloroferrate (FeCl4-) Displacement Technique. Environ. Sci. Technol. 35, 3363–3368. https://doi.org/10.1021/es010604i

Hatzinger, P.B., Böhlke, J.K., Sturchio, N.C., Izbicki, J., Teague, N., 2018. Four-dimensional isotopic approach to identify perchlorate sources in groundwater: Application to the Rialto-Colton and Chino subbasins, southern California (USA). Applied Geochemistry 97, 213–225. https://doi.org/10.1016/j.apgeochem.2018.08.020

Hatzinger, P.B., Böhlke, J.K., Sturchio, N.C., Gu, B., 2011. Guidance Document: Validation of chlorine and oxygen isotope ratio analysis to differentiate perchlorate sources and to document perchlorate biodegradation U.S. Department of Defense, ESTCP Project ER-200509, 107 p. (available at https://www.serdp-estcp.org/Program-Areas/Environmental-

Restoration/Contaminated-Groundwater/Emerging-Issues/ER-200509/ER-200509/(language)/eng-US
Headworth, H.G., Keating, T., Packman, M.J., 1982. Evidence for a shallow highly-permeable zone in the Chalk of Hampshire, U.K. J. Hydrol. 55, 93–112. https://doi.org/10.1016/0022-1694(82)90122-6
Hubé, D., 2016. Sur les traces d'un secret enfoui: Enquête sur l'héritage toxique de la Grande Guerre - Préface de Jean-Yves Le Naour. Editions Michalon. 288 p.
Hubé, D., 2014. Perchlorates : éléments historiques et d'expertise pour une évaluation de l'impact environnemental. http://centenaire.org/fr/espace-scientifique/societe/perchlorates-elements-historiques-et-dexpertise-pour-une-evaluation-de (Accessed date: 15 October 2019).
Hubé, D., Bausinger, T., 2013. Marquage pyrotechnique : analyse de la problématique environnementale. Comparatif entre Allemagne et France. Géologues 32–38.
IGN Remonter le temps database. https://remonterletemps.ign.fr/. Accessed October 2019.
Jackson, W.A., Böhlke, J.K., Andraski, B.J., Fahlquist, L., Bexfield, L., Eckardt, F.D., Gates, J.B., Davila, A.F., McKay, C.P., Rao, B., Sevanthi, R., Rajagopalan, S., Estrada, N., Sturchio, N., Hatzinger, P.B., Anderson, T.A., Orris, G., Betancourt, J., Stonestrom, D., Latorre, C., Li, Y., Harvey, G.J., 2015. Global patterns and environmental controls of perchlorate and nitrate co-occurrence in arid and semi-arid environments. Geochim. Cosmochim. Acta 164, 502–522. https://doi.org/10.1016/j.gca.2015.05.016
Jackson, W.A., Böhlke, J.K., Gu, B., Hatzinger, P.B., Sturchio, N.C., 2010. Isotopic composition and origin of indigenous natural perchlorate and co-occurring nitrate in the southwestern United States. Environ. Sci. Technol. 44, 4869–4876. https://doi.org/10.1021/es903802j
Jackson, A., Davila, A.F., Böhlke, J.K., Sturchio, N.C., Sevanthi, R., Estrada, N., Brundrett, M., Lacelle, D., McKay, C.P., Poghosyan, A., Pollard, W., Zacny, K., 2016. Deposition, accumulation, and alteration of Cl^-, NO_3^-, ClO_4^- and ClO_3^- salts in a hyper-arid polar environment: Mass balance and isotopic constraints. Geochimica et Cosmochimica Acta 182, 197–215. https://doi.org/10.1016/j.gca.2016.03.012
Jackson, W.A., Kumar Anandam, S., Anderson, T., Lehman, T., Rainwater, K., Rajagopalan, S., Ridley, M., Tock, R., 2005. Perchlorate occurrence in the Texas Southern High Plains Aquifer System. Ground Water Monit. Remediat. 25, 137–149. https://doi.org/10.1111/j.1745-6592.2005.0009.x
Jaunat, J., Taborelli, P., Devos, A., 2018. Les impacts de La Grande Guerre sur la qualité des eaux souterraines: les cas des perchlorate, in: « 14-18 La Terre et Le Feu Géologie et Géologues Sur Le Front Occidental », Bergerat, F. (Dir.), Co-Éd. AGBP – COFRHIGEO – SGN, Mém. Hors-Série N°10 de l'AGBP, 414- 417.
Kannan, K., Praamsma, M.L., Oldi, J.F., Kunisue, T., Sinha, R.K., 2009. Occurrence of perchlorate in drinking water, groundwater, surface water and human saliva from India. Chemosphere 76, 22–26. https://doi.org/10.1016/j.chemosphere.2009.02.054
Laurain, M., Guérin, H., Durand, R., Chertier, B., Louis, P., Morfaux, P., Neiss, R., 1981. Notice explicative, Carte géol. France (1/50 000) feuile Reims (132). Orléans : BRGM, 34 p. Carte géol. France par Laurain, M., Guérin, H., Barta, L., Monciardini, Ch., Durand, R., Neiss, R., 1981.
Laurent, A., 1988. La Grande Guerre en Champagne et la deuxième victoire de la Marne. Secrétariat d'État aux anciens combattants, Le Coteau, 157 p.
Lopez, B., Brugeron, A., Devau, N., Ollivier, P., 2014. Vulnérabilité des eaux souterraines de France métropolitaine vis-à-vis des ions perchlorates. Rapport BRGM/RP-63270-FR, 108 p.
Lopez, B., Vernoux, J.F., Neveux, A., Barrez, F., Brugeron, A., 2015. Recherche des origines de la pollution en perchlorate impactant des captages au sein des AAC de la région de Nemours et Bourron-Marlotte. Rapport BRGM/RP-64840-FR, 140 p.
Lybrand, R.A., Bockheim, J.G., Ge, W., Graham, R.C., Hlohowskyj, S.R., Michalski, G., Prellwitz, J.S., Rech, J.A., Wang, F., Parker, D.R., 2016. Nitrate, perchlorate, and iodate co-occur in coastal and inland deserts on Earth. Chem. Geol. 442, 174–186. https://doi.org/10.1016/j.chemgeo.2016.05.023
Mangeret, A., De Windt, L., Crançon, P., 2012. Reactive transport modelling of groundwater chemistry in a chalk aquifer at the watershed scale. J. Contam. Hydrol. 138–139, 60–74. https://doi.org/10.1016/j.jconhyd.2012.06.004

Mathias, S.A., Butler, A.P., Jackson, B.M., Wheater, H.S., 2006. Transient simulations of flow and transport in the Chalk unsaturated zone. Journal of Hydrology, Hydro-ecological functioning of the Pang and Lambourn catchments, UK 330, 10–28. https://doi.org/10.1016/j.jhydrol.2006.04.010

McLaughlin, C.L., Blake, S., Hall, T., Harman, M., Kanda, R., Hunt, J., Rumsby, P.C., 2011. Perchlorate in raw and drinking water sources in England and Wales. Water Environ. J. 25, 456–465. https://doi.org/10.1111/j.1747-6593.2010.00237.x

Michalski, G., Kolanowski, M., Riha, K.M., 2015. Oxygen and nitrogen isotopic composition of nitrate in commercial fertilizers, nitric acid, and reagent salts. Isotopes Environ. Health Stud. 51, 382–391. https://doi.org/10.1080/10256016.2015.1054821

Morin, S., Savarino, J., Frey, M.M., Domine, F., Jacobi, H.-W., Kaleschke, L., Martins, J.M.F., 2009. Comprehensive isotopic composition of atmospheric nitrate in the Atlantic Ocean boundary layer from 65°S to 79°N. J. Geophys. Res. Atmospheres 114. https://doi.org/10.1029/2008JD010696

Parker, B., Chendorain, M., Stewart, L., 2004. UXO Corrosion - Potential Contamination Source. SERDP Project ER-1226, 95 p.

Poghosyan, A., Sturchio, N.C., Morrison, C.G., Beloso, A.D., Guan, Y., Eiler, J.M., Jackson, W.A., Hatzinger, P.B., 2014. Perchlorate in the Great Lakes: isotopic composition and origin. Environ. Sci. Technol. 48, 11146–11153. https://doi.org/10.1021/es502796d

Price, M., 1987. Fluid flow in the Chalk of England. Geol. Soc. Lond. Spec. Publ. 34, 141–156. https://doi.org/10.1144/GSL.SP.1987.034.01.10

Qin, X., Zhang, T., Gan, Z., Sun, H., 2014. Spatial distribution of perchlorate, iodide and thiocyanate in the aquatic environment of Tianjin, China: environmental source analysis. Chemosphere 111, 201–208. https://doi.org/10.1016/j.chemosphere.2014.03.082

Quinn, M.J., 2015. Chapter 11 - Wildlife Toxicity Assessment for Nitrocellulose, in: Williams, M.A., Reddy, G., Quinn, M.J., Johnson, M.S. (Eds.), Wildlife Toxicity Assessments for Chemicals of Military Concern. Elsevier, pp. 217–226. https://doi.org/10.1016/B978-0-12-800020-5.00011-9

Rajagopalan, S., Anderson, T.A., Fahlquist, L., Rainwater, K.A., Ridley, M., Jackson, W.A., 2006. Widespread presence of naturally occurring perchlorate in high plains of Texas and New Mexico. Environ. Sci. Technol. 40, 3156–3162.

Rao, B., Anderson, T.A., Orris, G.J., Rainwater, K.A., Rajagopalan, S., Sandvig, R.M., Scanlon, B.R., Stonestrom, D.A., Walvoord, M.A., Jackson, W.A., 2007. Widespread natural perchlorate in unsaturated zones of the southwest United States. Environ. Sci. Technol. 41, 4522–4528.

R Core Team, 2018. R: A Language and Environment for Statistical Computing. R Foundation for Statistical Computing, Vienna. https://www.R-project.org

Ricour, J., 2013. Un exemple d'altération du fond géochimique naturel des sols et des eaux souterraines : les séquelles environnementales des grands conflits mondiaux en France. Géologues 179, 27–31.

Rouxel-David, E., Batkowski, D., Baudouin, V., Cordonnier, G., Cubizolles, J., Herrouin, J.P., Izac, J.L., Jegou, J.P., Kieffer, C., Mardhel, V., Paya, H., 2002. Cartographie de la piézométrie de la nappe de la craie en Champagne-Ardenne, Rapport BRGM/RP-52332-FR, 29 p.

Savarino, J., Morin, S., Erbland, J., Grannec, F., Patey, M.D., Vicars, W., Alexander, B., Achterberg, E.P., 2013. Isotopic composition of atmospheric nitrate in a tropical marine boundary layer. Proc. Natl. Acad. Sci. 110, 17668–17673. https://doi.org/10.1073/pnas.1216639110

Serrano-Nascimento, C., Calil-Silveira, J., Dalbosco, R., Zorn, T.T., Nunes, M.T., 2018. Evaluation of hypothalamus-pituitary-thyroid axis function by chronic perchlorate exposure in male rats. Environ. Toxicol. 33, 209–219. https://doi.org/10.1002/tox.22509

Sturchio, N.C., Beloso, A., Heraty, L.J., Wheatcraft, S., Schumer, R., 2014. Isotopic tracing of perchlorate sources in groundwater from Pomona, California. Appl. Geochem. 43, 80–87. https://doi.org/10.1016/j.apgeochem.2014.01.012

Sturchio, N.C., Böhlke, J.K., Gu, B., Hatzinger, P.B., Jackson, W.A., 2011. Isotopic Tracing of Perchlorate in the Environment, in: Handbook of Environmental Isotope Geochemistry, Advances in Isotope Geochemistry. Springer, Berlin, Heidelberg, pp. 437–452. https://doi.org/10.1007/978-3-642-10637-8_22

Sturchio, N.C., Böhlke, J.K., Gu, B., Horita, J., Brown, G.M., Beloso Jr., A.D., Patterson, L.J., Hatzinger, P.B., Jackson, W.A., Batista, J., 2006. Stable isotopic composition of chlorine and oxygen in synthetic and natural perchlorate, in: Perchlorate: Environmental Occurrence, Interactions and Treatment. pp. 93–109. https://doi.org/10.1007/0-387-31113-0_5

Sturchio, N.C., Caffee, M., Beloso, A.D., Heraty, L.J., Böhlke, J.K., Hatzinger, P.B., Jackson, W.A., Gu, B., Heikoop, J.M., Dale, M., 2009. Chlorine-36 as a tracer of perchlorate origin. Environ. Sci. Technol. 43, 6934–6938.

Taborelli, P., 2018. Les conditions géographiques et l'organisation spatiale du front de la Grande Guerre : application à l'évaluation environnementale post-conflit en Champagne-Ardenne (France) Phd thesis, Reims, 427 p.

Trumpolt, C.W., Crain, M., Cullison, G.D., Flanagan, S.J.P., Siegel, L., Lathrop, S., 2005. Perchlorate: Sources, Uses, and Occurrences in the Environment. Remediat. J. 16, 65–89. https://doi.org/10.1002/rem.20071

Urbansky, E.T., 2002. Perchlorate as an environmental contaminant. Environ. Sci. Pollut. Res. 9, 187–192. https://doi.org/10.1007/BF02987487

Urbansky, E.T., 1998. Perchlorate Chemistry: Implications for Analysis and Remediation. Bioremediation J. 2, 81–95. https://doi.org/10.1080/10889869891214231

UNMAS, 2015. Mines terrestres, restes explosifs de guerre et engins explosifs improvisés - Manuel de sécurité, 3e édition. UNMAS - United Nations Mine Action Service, New York. 130 p.

Vachier, P., Cambier, P., Prost, J.C., 1987. Mouvements de l'eau dans la zone non sature´e et alimentation de la nappe de la craie de champagne (France). Isot. Tech. Water Resour. Dev. Vienna IAEA Conf. 367–379.

Vega, M., Nerenberg, R., Vargas, I., 2018. Perchlorate contamination in Chile: Legacy, challenges, and potential solutions. Environ. Res. 164, 316–326. https://doi.org/10.1016/j.envres.2018.02.034

Vergnaud-Ayraud, V., Aquilina, L., Pauwels, H., Labasque, T., 2008. La datation des eaux souterraines par analyse des CFC : un outil de gestion durable de la ressource en eau. Tech. Sci. Méthodes 37–44. https://doi.org/10.1051/tsm/200801037

Vernhet, Y., 2007. Carte geologique harmonisée du département de la Marne Rapport BRGM RP-55732-FR, 112 p.

Wellings, S.R., 1984. Recharge of the Upper Chalk aquifer at a site in Hampshire, England: 2. Solute movement. Journal of Hydrology 69, 275–285. https://doi.org/10.1016/0022-1694(84)90167-7

Zimmerm

Publications and conferences

Publications:

Cao, F., Jaunat, J., Ollivier, P., Cancès, B., Morvan, X., Hubé, D., Devos, A., Devau, N., Barbin, V., and Pannet, P., 2018. Sources and behavior of perchlorate ions (ClO_4^-) in chalk aquifer of Champagne-Ardenne, France: preliminary results. IAHS-AISH Proceedings and Reports, 8th International Water Resources Management Conference of ICWRS, juin 2018, Beijing (Chine).

Cao, F., Jaunat, J., Ollivier, P., 2018. Cartographie de la contamination de la nappe de la craie de Champagne en ions perchlorates. Géologues n°199, 95-100.

Cao, F., Jaunat, J., Sturchio, N., Cancès, B., Morvan, X., Devos, A., Barbin, V., Ollivier, P., 2019. Worldwide occurrence and origin of perchlorate ion in waters: A review. Science of The Total Environment 661, 737–749. https://.org/10.1016/j.sciv.2019.01.107

Cao, F., Jaunat, J., Vergnaud-Ayraud, V., Devau, N., Labasque, T., Guillou, A., Guillaneuf, A., Hubert, J., Aquilina, L., Ollivier, P., 2020. Heterogeneous behavior of unconfined Chalk aquifers infer from combination of groundwater residence time, hydrochemistry and hydrodynamic tools. Journal of Hydrology 581, 124433. https://doi.org/10.1016/j.jhydrol.2019.124433

Cao, F., Sturchio, N.C., Ollivier, P., Devau, N., Heraty, L.J., Jaunat, J., 2020. Sources and behavior of perchlorate in a shallow Chalk aquifer under military (World War I) and agricultural influences. Journal of Hazardous Materials 123072. https://doi.org/10.1016/j.jhazmat.2020.123072

Conferences attended:

Cao, F., Jaunat, J., Conreux, A., Hubert, J., Devau, N., Ollivier, P., 2019. Traces of World War I in groundwater: perchlorate contamination of the chalk aquifer in NE France. 46th IAH Congress – Groundwater management and governance coping with water scarcity, September 2019, Malaga, Spain.

Jaunat, J., **Cao, F.,** 2018. La qualité de l'eau souterraine durablement marquée par la Grande Guerre. Colloque impacts environnementaux et approches spatiales de la Grande Guerre, Septembre 2018, Reims, France.

Cao, F., Jaunat, J., Ollivier, P., Cancès, B., Morvan, X., Hubé, D., Devos, A., Devau, N., Barbin, V., Pannet, P., 2018. Sources and behavior of perchlorate ions (ClO_4^-) in chalk aquifer of Champagne-Ardenne, France: preliminary results. Conference IAHS 2018 - 8th International Water Resources Management Conference of ICWRS, June 2018, Beijing, China.

Cao, F., Jaunat, J., Ollivier, P., 2018. Cartographie de la contamination de la nappe de la craie en Champagne en ions perchlorates. 22émes journées techniques du Comité Français d'Hydrogéologie de l'Association Internationale des Hydrogéologues : Hydrologie de la Craie, Mai 2018, le Havre, France.

Cao, F., Jaunat, J., Ollivier, P., 2018. Perchlorates ions (ClO_4^-), explosives and nitrates in Chalk aquifer of Champagne-Ardenne, France. Goldschmidt conference, Août 2017, Paris, France.

Cao, F., Jaunat, J., Ollivier, P., Cancès, B., Morvan, X., Devos, A., Hubé, D., Chabar M., Devau, N., Barbin, V., Pannet, P., 2017. Perchlorates, explosifs et nitrates dans les eaux souterraines de la craie de Champagne : Origine et devenir. Les Journées Condorcet, Juin 2017, Lille, France.

Résumé:

Des analyses ont mis en évidence la présence de perchlorate (ClO_4^-, suspecté d'être un perturbateur endocrinien) dans des captages d'eau potable de Champagne-Ardenne. Deux sources sont suspectées : une source militaire liée à la Grande Guerre et une source agricole liée à l'utilisation passée de nitrates chiliens. Les objectifs de l'étude sont de déterminer l'origine et le comportement des ClO_4^- dans les eaux souterraines de la craie de Champagne et d'expliquer les hétérogénéités observées en précisant le fonctionnement de la nappe.

La zone d'étude se trouve à l'est de Reims, où une étude historique, hydrologique, géochimique et isotopique est réalisée. Une forte hétérogénéité géochimique des eaux de la nappe est observée. Un modèle conceptuel du fonctionnement de la nappe est proposé, mettant en évidence les facteurs contrôlant la géochimie des eaux souterraines. Les teneurs élevées en ClO_4^- (> 4 $\mu g \cdot L^{-1}$) sont détectées principalement en aval des Monts de Champagnes, où de grandes quantités de munitions ont été utilisées, stockées et détruites pendant et après la Grande Guerre. Une origine militaire post-conflit est mise en évidence par l'analyse isotopique des ClO_4^- et la détermination de l'âge des eaux. L'évolution spatio-temporelle des concentrations est discutée sur la base des teneurs en ClO_4^-, du fonctionnement de la nappe et des informations historiques, permettant de préciser les sources (e.g. munitions non explosés et sites de destruction des munitions) et les mécanismes de transfert des ClO_4^-. La contamination en ClO_4^- de l'aquifère de la craie de Champagne ne semble pas diminuer à court et moyen termes en raison de la forte persistance des sources de ClO_4^-.

Mots clés: Perchlorate, Nappe de la Craie, Isotope, Temps de séjour, Grand Guerre

Abstract:

Perchlorate (ClO_4^-) has frequently been detected in groundwater at concentrations relevant to human health. Analyzes in Champagne-Ardenne have highlighted the presence of ClO_4^- in groundwater for drinking water supply. The ClO_4^- has two suspected sources: a military source related to World War I (WWI) and an agricultural source related to past use of Chilean nitrate fertilizers. The objectives of the study are to determine the sources and behavior of ClO_4^- in the Champagne Chalk aquifer and to explain the heterogeneities observed by specifying the aquifer functioning.

The study area is located east of Reims. A methodology involving historical, hydrodynamic, geochemistry, groundwater dating and isotope analysis has been developed. High spatio-temporal heterogeneities are observed in the Chalk aquifer. A conceptual model of aquifer functioning is proposed, highlighting main factors governing the Chalk groundwater geochemistry. ClO_4^- is detected throughout the area with high concentrations (> 4 $\mu g \cdot L^{-1}$) detected mainly downgradient the Champagne Mounts, where large quantities of ammunition were used, stored and destroyed during and after WWI. A post-WWI military origin of ClO_4^- is inferred from isotopic analysis and groundwater ages. Different tendencies of ClO_4^- variation are observed and interpreted by a combination of ClO_4^- concentrations, aquifer functioning and historical investigations, revealing major sources of ClO_4^- (e.g., unexploded ammunitions, ammunition destruction sites) and its transfer mechanisms in the aquifer. ClO_4^- contamination in the Champagne Chalk seems unlikely to decrease in the short- to medium-term due to the long persistence time of major sources.

Keywords: Perchlorate, Chalk aquifer, Isotope analysis, Groundwater dating, World War I

Laboratoire : GEGENAA - Groupe d'Etude sur les Géomatériaux et Environnements Naturels, Anthropiques et Archéologiques - EA 3795